GEOCHEMICAL AND PETROLOGICAL TRENDS IN THE UG2-MERENSKY UNIT INTERVAL OF THE UPPER CRITICAL ZONE IN THE WESTERN BUSHVELD COMPLEX

THESIS
Submitted in fulfilment of the
Requirements for the Degree of
DOCTOR OF PHILOSOPHY
in the Department of Geology,
Rhodes University

by

WOLFGANG DEREK MAIER
(Hauptdiplom, Ludwig - Maximilians - Universität, München, Germany)

August 1991

ABSTRACT

One of the most remarkable features of the layered sequence of the Bushveld Complex is its lateral consistency in lithology. This work has established a geochemical and lithological correlation along 170 km of strike of the interval between the UG2 chromitite and the Merensky Reef within the Upper Critical zone of the western limb of the Bushveld Complex. The correlation is based on geochemical investigations of 10 borehole intersections and lithological comparisons of more than 20 borehole intersections around the western lobe of the complex. The basic data presented include 123 whole-rock analyses for major and 12 trace elements, 97 analyses for 12 trace elements, and ca. 5500 microprobe analyses of all major phases. Patterns of cryptic variation are established. Some layers (the UG2 chromitite and pyroxenite) show considerable consistency with regard to geochemistry and lithology. Others can be traced along most of the investigated strike length, such as the Lone Chrome Seam, the Footwall Marker anorthosite and the immediate anorthosite footwall to the Merensky Unit. Most of the distinguishable members within the study section, however, show great variation along strike (i.e., the Lower and Upper Pseudoreef Markers, the central noritic sequence in the southern arm of the western limb and parts of the immediate Merensky Reef footwall succession).

Several models have been evaluated to interpret the geochemical and lithological data. The author comes to the conclusion that the degree of lithological consistency depends on the variability of magmatic parameters within different parts of the chamber. The most important of these parameters are: (i) the size of fresh primitive influxes and consequently the heat flux, (ii) the composition of the residual liquid, and (iii) the frequency of the influxes. Fresh influxes of more or less similar composition thus spread out along the floor if the residual liquid was less dense than the fresh primitive liquid, but intruded the chamber as a plume where plagioclase had crystallized for some time and the residual liquid had become relatively dense. The

size of the influx may be regarded as a measure of the amount of heat flux from the feeder into the chamber. A large influx created uniform physicochemical conditions in the chamber whereas a smaller influx created a strong lateral gradient of physicochemical parameters in the chamber, with subsequent differences in viscosity, density, convection currents, yield strength and thus different mixing behaviour of different liquids. Furthermore, a persistent heat flux from the feeder may have delayed crystallization of successive phases in those parts of the chamber proximal to the feeder. Therefore, new influxes would have been deposited on a footwall of varying thickness and lithology in response to different degrees of crystallization and accumulation along strike. The development of a normal cyclic unit (chromitite-harzburgite-pyroxenite-norite (+anorthosite?)) may thus have been interrupted at various stages in different parts of the chamber.

The ability to correlate anorthosites over great strike distances implies that their formation did not follow entirely random processes but was dependent on specific magmatic conditions which prevailed over laterally extensive portions of the chamber at certain stages during the evolution of the crystallizing liquid.

ACKNOWLEDGEMENTS

This work has been supervised by Prof. H.V. Eales and I am sincerely grateful for the academic and technical guidance, and the time he spent with discussions, improvements, draft-reading, and encouragement as well as patiently improving my English.

My fellow research students B. Teigler, W.J. de Klerk, S. Haikney and R.H. Smithies contributed in various ways to this thesis. Additionally, W.J. de Klerk, M.Field and M. Ellis gratefully permitted to use parts of their data in this thesis. A.R. Butcher and A. Rice (University of Boulder, Colorado) contributed in the form of discussions and comments. Staff members J.S. Marsh, R. Harris, and R. Skae assisted in data processing, computing and the gathering of analytical data. B. Bongwana and W. Hashe are thanked for the preparation of thin sections.

The Geology Department at Rhodes University provided accommodation, analytical facilities and financial support for which I am truly indebted.

Messrs. Rand Mines, Genmin, J.C.I. and Golden Dumps helpfully provided the sample material and gave logistical as well as financial support. I would like to thank especially M. Bristow (Rand Mines), B. Walters (J.C.I.) and R. N. Scoon (Trojan Exploration) for their enthusiastic support. F.J. Kruger from the Bernard Price Institute executed the Sr isotope analyses.

A three year doctoral bursary from the FRD (Foundation for Research Development) provided financial support which is gratefully acknowledged.

I am grateful to my wife Sabine and my son Johannes Jarmo in Germany for their long distance encouragement.

DECLARATION

All work in this thesis is the original work of the author except where specific acknowledgement is made to the work of others.

Date: .....

Signed: .....
W. Maier

CONTENTS

CHAPTER 5: Whole-rock Geochemistry

CHAPTER 6: Geochemical Variations within Individual Sequences

CHAPTER 7: Correlation along Strike

LIST OF FIGURES

LIST OF TABLES

LIST OF PLATES

The text in this copy of the thesis has been changed somewhat from that in the original draft, submitted for examination. In order to avoid renumbering of all pages the convention is adopted here that one additional page inserted in the text will be numbered by the original page number (page 14) followed by the lettering "a".

CHAPTER 1: INTRODUCTION

1.1: The Problems Addressed

The Bushveld Complex (BC), situated in the western Transvaal (Republic of South Africa) and underlying an area of roughly 65,000 km^2 (Tankard et al. 1982) is by far the largest layered intrusion on earth (Fig. 1.1(a)). This work deals with a sequence of rocks within the layered sequence of the complex i.e., the interval between the Merensky Reef and the UG2 chromitite in the Upper Critical Zone (Fig. 1.2). For various reasons, this particular sequence has been of major interest, since the platiniferous Merensky Reef was discovered in 1929. It shows a great variety of rocks within a limited stratigraphic interval, ranging from chromitites, dunites, harzburgites, pyroxenites to norites, anorthosites, troctolites and pegmatoids. Furthermore, the sequence changes considerably in appearance and thickness along strike and a lateral correlation has not as yet been attempted for all units. Finally, the interval is defined by the two most important platiniferous deposits in the world, the UG2 chromitite and the Merensky Reef. An understanding of the processes that controlled the formation of the silicate rocks seems to be of prime importance in interpreting the platiniferous reefs.

The main geological problems which call for solution in this particular interval are:

1. How was the platinum concentrated in the two reefs? Are the two reefs genetically related and if so, in what way? How do high but erratic PGE concentrations in the Pseudoreefs and the Boulder Bed fit into the picture?

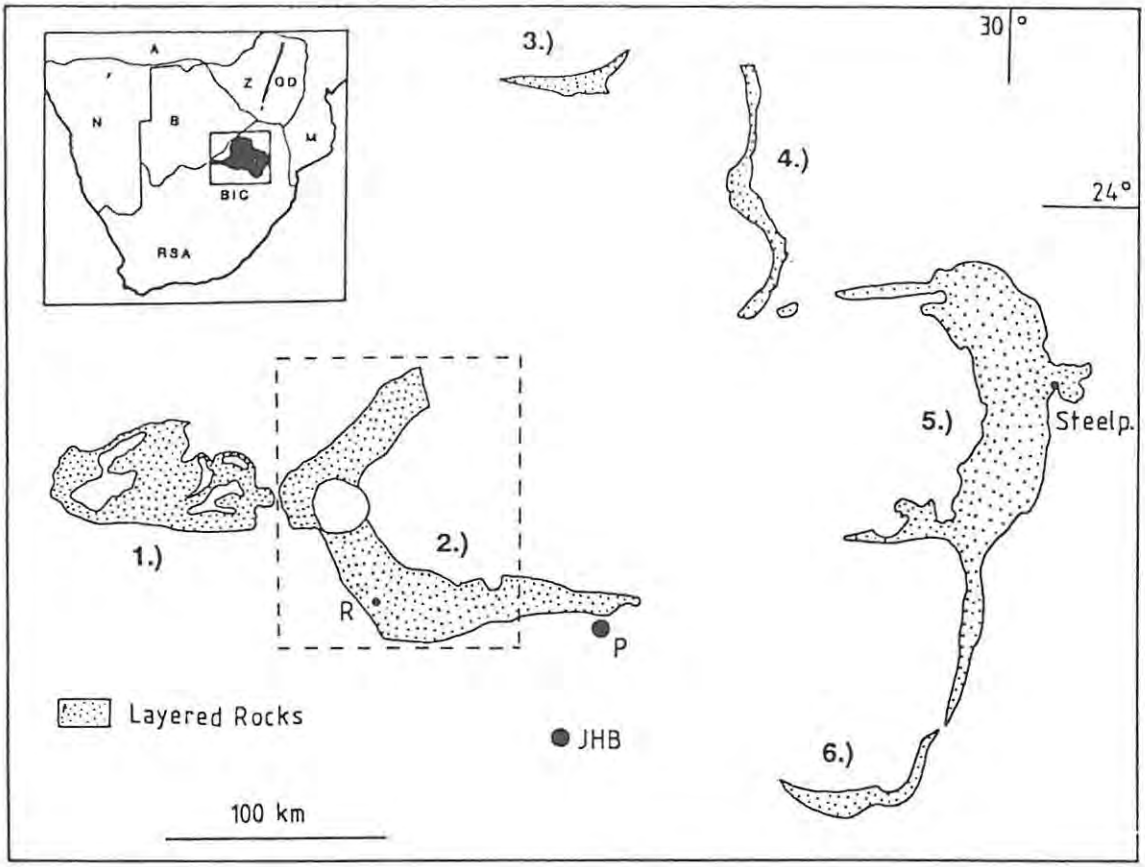

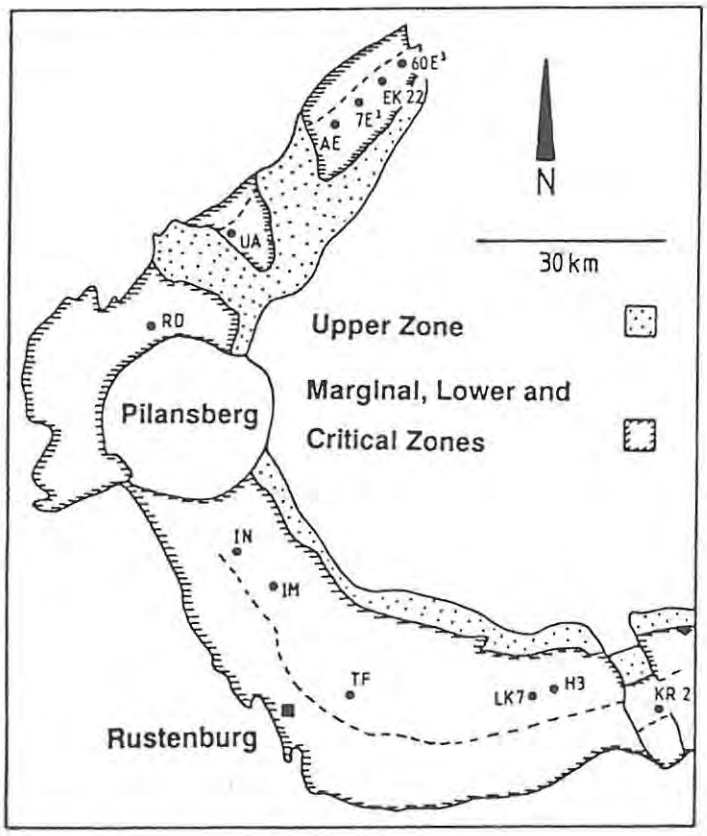

Fig. 1.1 (a) Simplified geological map of the Bushveld Complex. 1.) = Far-western lobe, 2.) = western lobe, 3.) = Villa Nora area, 4.) = Potgietersrus limb, 5.) = eastern lobe, 6.) = Bethal lobe. (b) The western lobe of the complex, with the locations of the investigated borehole cores. The dashed line indicates the suboutcrop position of the Merensky Reef. Cores AE, $7E^3$, EK22, $60E^3$: Amandelbult Section; UA: Union Section; RD: Rooderand; IN, IM: Impala Platinum Mines; TF: RPM Turffontein Shaft; LK7, H3: near Wolhuterskop; KR2: Crocodile River Mine.

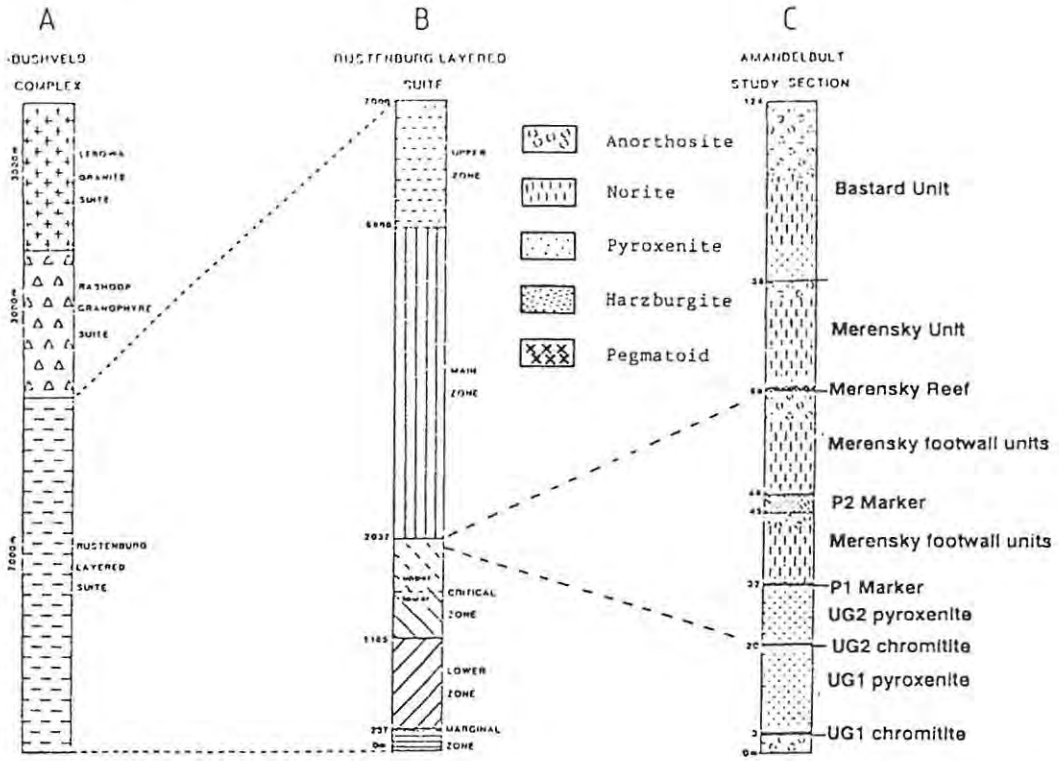

Fig. 1.2 Stratigraphic subdivision of (a) the Bushveld Complex, (b) the Rustenburg Layered Suite and (c) the study interval (at Amandelbult Section; modified after Field, 1987).

2. How could chromite concentrate at the base of the sequence to form a layer more than 1m thick? Mass balance calculations seem to require an unrealistically large magma volume to yield the total mass of chromium needed. Furthermore, phase relationships of stability fields of chromite suggest that mixing of two different types of magma is necessary for the liquid to enter the chromite stability field.

3. How do anorthosites form? In large complexes, where supercooling is unlikely, the anorthite - orthopyroxene cotectic of the An-Fo-Qz phase diagram is difficult to cross. Again, is a second, anorthositic magma type necessary to form anorthosites or does plagioclase accumulate by some fractionation mechanism?

4. How can sharp contacts between different rock types like anorthosites and pyroxenites be explained ?

5. By what mechanism did the rocks in the central part of the interval become gradually chemically more primitive upwards ?

6. How are lithological changes along strike of some units and, even more interesting, the remarkable continuity of other units to be explained? In this context, to what extent has thermal erosion been a significant process, and is there support for the concept of a proximal and distal facies in the western limb (Eales et al.,1988)?

7. Are there significant lithological changes down dip ?

The present work does not adress all these problems, but pays particular attention to points 2-6. No study of the platiniferous horizons was possible, because access to these layers was not granted by the mining companies concerned.

1.2: General Geology of the Bushveld Complex

According to Hall (1932) and Willemse (1969) the Bushveld Complex intruded in several stages, namely:

a) An early sill phase
b) An epicrustal phase: Rooiberg Felsite Group (2065 my, Rb/Sr method, Walraven et al., 1990)
c) A main plutonic phase: Rustenburg Layered Suite (2050 ± 22 my, Rb/Sr method, Sharpe, unpubl. data in von Gruenewaldt et al., 1985; 2025 ± 45 my, Rb/Sr method, Lee & Butcher, 1990)
d) A late plutonic phase: Lebowa Granite Suite (2050 ± 22 my, U/Pb method on the Nebo Granite, Retief, unpubl. data in von Gruenewaldt et al., 1985; 1670 ± 30 my, U/Pb method on the Makhutso Granite, Coertze et al., 1978)

An initial volcanic phase has been dated by the Rb/Sr method at 2224 ± 21 my (Burger & Coertze, 1973, on the Hekpoort Andesite Formation).

The mode of intrusion is still debated. Hypotheses favouring emplacement as a single lopolith (Hall, 1932; Irvine et al., 1983) are less favoured at the moment than theories which suggest that the complex intruded into a number of separate compartments (Truter, 1985; Lee & Sharpe, 1986; Meyer & de Beer, 1987). The same diversity of opinion exists on models concerning the trigger for intrusion. Hamilton (1977) and Rhodes (1975) suggested a meteorite impact origin, whereas van Biljon (1979) advocated intrusion from a spreading centre within a plate tectonic environment, with post-emplacement separation of western and eastern lobe. Cousins (1959) favoured crystallization from an open lava pool and observed a linear geographic pattern which includes the Great Dyke, the Vredefort structure, the Trompsburg Intrusion and the Brandfort gravity anomaly. Hunter (1976) envisaged an intrusive origin as a result of compressive stresses and Sharpe & Snyman (1980) related the trigger for intrusion to basin subsidence.

Geoelectrical and gravitational data by Meyer & de Beer (1987) indicate that the mafic sequence in both western and eastern compartments of the complex comprises segments of an inward-dipping sheet. This sheet apparently transgresses the layering of the sedimentary rocks of the Transvaal Group into which it intruded. Based on their data Meyer & de Beer (op. cit.) argued that the mafic rocks are absent from the central part of the complex.

Not much will be said here about the structure of the complex; for a review see Lee & Sharpe (1986). The layered rocks are generally little deformed and unmetamorphosed with an overall dip towards the centre of the complex of usually between 10 and 20°.

1.3: The Layered Sequence

The layered sequence of the Bushveld Complex (Rustenburg Layered Suite, hereafter RLS) transgressively intruded Rooiberg Felsites and sedimentary rocks of the Transvaal Supergroup. The Rooiberg Felsites were furthermore intruded by granophyric rocks (Rashop Granophyre). No agreement as to whether these granophyres predate or postdate the RLS has been reached as yet. The granites of the Lebowa Granite Suite which intruded close to the contact between the RLS and the roof of the complex represent the final magmatic phase of the complex.

The RLS, at various localities, is between 7000 and 9000 m thick and yields outcrop or suboutcrop in 6 areas (Fig. 1.1(a)), notably the far-western, western, and eastern lobes, the Potgietersrus limb, the Villa Nora area and the Bethal lobe. The RLS is stratigraphically subdivided into 5 major intervals or so-called "zones". These are the Marginal, Lower, Critical, Main and Upper Zones (Hall, 1932). The South African Committee for Stratigraphy (SACS) in 1980 recommended an alternative terminology which, however, will not be used in this work as frequent references to other workers would cause confusion.

The Marginal and Lower Zones

The Marginal Zone, normally between 100 and 250 m thick (Teigler, 1990) reaches up to 800 m west of the Pilansberg. It consists mostly of norites and pyroxenites with occasional sedimentary footwall xenoliths.

Descriptions of the Lower Zone can be found in Cameron (1978) for the eastern lobe, Teigler (1990) for the western lobe and Engelbrecht (1985) for the far-western lobe. The Lower Zone consists of roughly 1700 m of alternating dunite, harzburgite and bronzitite. Typically, the Lower Zone contains no chromitite layers, with the exception of the Potgietersrus limb where two massive chromitite seams of ca. 40 cm are mined south of Potgietersrus in the upper part of the Lower Zone (Hulbert & von Gruenewaldt, 1986).

The Critical Zone

The base of the Critical Zone, which is between 900 and 1500 m thick, is marked by the first occurrence of massive chromitite, the LG1 chromitite layer. In the western lobe the main chromitite layers of the Critical Zone have been subdivided into 8 Lower Group (LG), 4 Middle Group (MG) and 2 (3 in the eastern lobe) Upper Group (UG) chromitites. The dominant rock types of the Lower Critical Zone are pyroxenites and harzburgites, whereas the Upper Critical Zone consists mainly of pyroxenites, norites and anorthosites. The boundary between the Lower and Upper Critical Zone, by convention, is set between the MG2 and MG3 chromitites, where cumulus plagioclase appears for the first time (Cameron, 1980).

The Main and Upper Zones

Most authors place the base of the Main Zone at the top of the Bastard Unit (see de Klerk, 1991, for a detailed discussion). It is characterized by the appearance of cumulus clinopyroxene and the disappearance of chromite and olivine and consists of ca. 2700 - 4400 m of interlayered gabbronorite and anorthosite.

The approximately 2000 m thick anorthositic-noritic-dioritic Upper Zone is commonly subdivided into 3 subzones (SACS, 1980). The basal Subzone A is marked by the appearance of magnetite which is concentrated in 24 layers throughout the Upper Zone. Subzone B is characterized by the first occurrence of fayalitic olivine and towards the roof, in Subzone C, apatite becomes a cumulus phase.

Discordant pegmatitic bodies, which are frequently developed as topographic features, are described in detail by Scoon (1985) and Viljoen & Scoon (1985).

1.4: General Geology of the Study Area

The study area comprises a section of the layered rocks within the Upper Critical Zone of the western lobe of the complex (Fig. 1.1(b)), the interval between the Merensky Reef and the UG2 chromitite. The 10 geochemically and lithologically investigated intersections are regarded as representative, as judged by comparison with other cores and underground exposures examined during visits at numerous mines. The localities of the 10 investigated sections are shown in Fig. 1.1(b). Cores 60E[3], EK22 (39E[3]), 7E[3], and AE are situated at Amandelbult Section, Core UA in the south-western part of Union Section, cores IN (BH 1512) and IM (BH 1329; "Impala North" and "Impala Middle") at Impala Platinum Bafokeng and Wildebeestfontein Mines, respectively, intersection TF at RPM Turffontein Mine, cores LK7 and H3 (as well as LK5, which has not been investigated in detail) near Wolhuterskop and core KR2 in the Brits Graben. Core AE in the south-western part of Amandelbult has been geochemically investigated by Field (1987) and his analyses are incorporated into the data base. Core UA has been partly analysed (for whole-rock chemistry) by de Klerk (1988). All other cores have been investigated by the present author.

The dip of the layered rocks is variable in different parts of the western lobe. The approximate values at the separate localities are as follows: Union Section = 17°; Amandelbult Section = 20°; Impala = 10°; Wolhuterskop (cores LK7 and H3) = 12°; Brits Graben = 18°. For two reasons the relative thicknesses of the cores have not been recalculated into true thicknesses. Firstly, the ability to make comparisons with published data should be retained, and secondly, the relative differences in thickness of the cores would only change marginally and, hence, not affect the present author's interpretations.

The western lobe is regarded as a single lobe and gravity data suggest that a feeder zone is located between Union and Amandelbult Sections

(Sharpe et al., 1981; Fig. 1.3), with possible additional feeder zones near Rustenburg and Brits. Geochemical considerations led Eales et al. (1988) to the conclusion that a roughly linear increase in thickness of the UG2 - Merensky interval along strike is also connected to the distance from a feeder zone, located close to RPM Union Section.

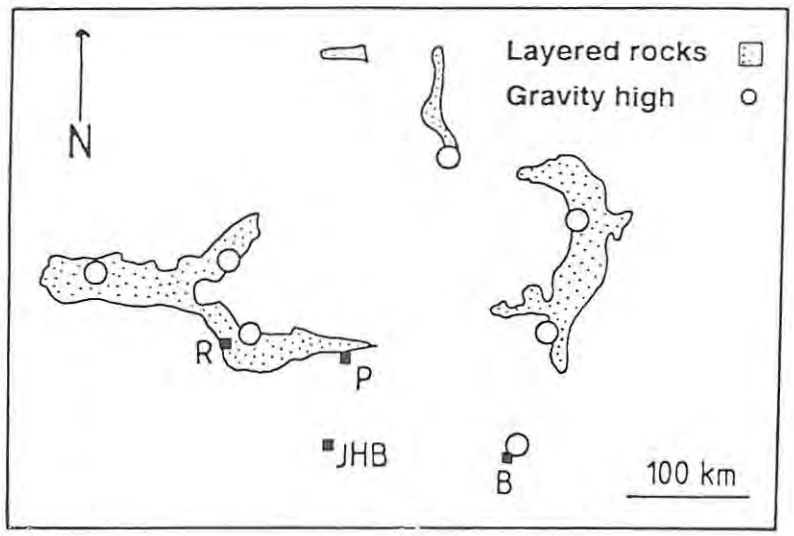

Fig. 1.3 Simplified geological map of the Bushveld Complex with locations of the most significant gravity highs (Fig. modified after Sharpe et al. 1981).

The KR2 core was drilled in the Brits Graben (Crocodile River Fault), a major feature of Karroo age. It is not certain whether this structure was already active during Bushveld times. In that case the reduction of thickness of that section in comparison with the cores next to the graben would gain special significance. Suggestions exist that the Crocodile River Fault is related to the Crocodile River Fragment (Lee & Sharpe, 1986).

In the north-western part of the western limb large sectors of the Lower, Critical and Main Zone succession are transgressed by Upper Zone rocks. The two areas north-east and south-west of Union Section are known as the northern and southern gap areas. Graben faulting was possibly one of the processes responsible for the transgressions (Viljoen & Feuchtwanger, 1977).

1.5: Nomenclature

The interval between the UG2 chromitite and the Merensky Reef has been subdivided in various ways depending on genetic and economic considerations. Kruger & Marsh (1985) used the terms UG2, Pseudoreef and Boulder Cyclic Units, thus following, in the main, the terminology used by J.C.I. Ltd. in the northern part of the western lobe. Eales et al. (1986) replaced the term "Boulder Cyclic Unit" by "Footwall Cyclic Unit". Impala Platinum Mines and Western Platinum Mine distinguish lithological members down from the mined Merensky Reef as Footwall 1 to 12 (Table 1.1), the latter of which is underlain by the UG2 pyroxenite and chromitite. Rand Mines (Crocodile River Mine) broadly follow the terminology of Western Platinum Mine. The present author has adopted the latter terminology in this work and Footwall 1-12 are hereafter abbreviated to FW 1-12. However, the FW layers 10 and 11 (Leeb-du Toit, 1986) could not be distinguished by the present author and are therefore treated as a single unit, i.e., FW 11 in this study.

Table 1.1: Terminology of FW layers in the southern part of the Western Bushveld Complex

Present authors classification				Leeb-du Toit (1986)	
FW 1	Footwall anorthosite to Merensky Reef plus underlying Leuconorite	up to	20 m	←	
FW 2	Mottled anorthosite	up to	1 m	←	
FW 3	Leuconorite	up to	5 m	←	
FW 4	Mottled anorthosite	up to	3 m	←	
FW 5	Leuconorite	up to	5 m	←	
FW 6	Mottled anorthosite plus "boulders"	up to	8 m	←	
FW 7	Norite/leuconorite	up to	120 m	←	
P2	Harzburgite/pyroxenite	up to	.2 m	FW 8 Leuconorite	up to 4m
FW 9	Mottled anorthosite/troctolite	up to	10 m	FW 9 Mottled anorthosite	up to 2m
P2	Harzburgite/pyroxenite	up to	.1 m	FW 10 Leuconorite	up to 20m
FW 11	Leuconorite	up to	30 m	FW 11 Leuconorite	up to 2m
FW 12	Mottled anorthosite	up to	20 m	FW 12 Mottled anorthosite	up to 20m

The term "cyclic unit", as defined by Eales et al. (1986) is not applicable for major parts of the interval under review as cycles are seldom complete and fractionation trends are often reversed. Furthermore, there does not exist any consensus yet about what should form the base of a cyclic unit (see Irvine et al., 1983; Eales et al., 1986).

For the above mentioned considerations the non-genetic mining terminology, used by Impala, seems to be the most practical approach when trying to correlate a genetically highly complicated interval over a strike length of 170 km, as subdivisions can easily be inserted. The terminology used by J.C.I. at Union and Amandelbult Sections cannot possibly be applied near Brits.

Throughout this work a limited number of abbreviations will be used in the figures and as subscripts in the text, namely opx, cpx, plag and ol for the minerals orthopyroxene, clinopyroxene, plagioclase and olivine, respectively. Furthermore, weight per cent and volume per cent will be abbreviated to wt% and vol%, respectively.

The most commonly used classification for gabbroic and ultramafic rocks is the IUGS system (Streckeisen, 1974; Fig. 1.4), which is based on the modal proportions of the various phases, irrespective of whether they are of cumulus or intercumulus nature. It seems sensible, however, to incorporate textural relationships into a classification, as this takes account of genetic implications as well. Therefore, Irvine (1982) proposed to consider cumulus phases only in classifying cumulus rocks. Hence, a rock consisting of 50 % cumulus orthopyroxene and 50 % intercumulus plagioclase would still be a pyroxenite.

Cumulus rocks are furthermore classified according to the amount of intercumulus phases present: orthocumulates, mesocumulates and adcumulates contain between 25 and 30 vol%, 7 and 25 vol%, and less than 7 vol% intercumulus material, respectively (Wager et al., 1960).

A purely chemical classification (Eales et al., 1988; Fig. 1.5) is difficult to apply in the field (a criticism which, to some degree, is applicable to all schemes) and sometimes obscures the genetic variations it aims to show. Quite frequently intercumulus orthopyroxene in a mottled anorthosite amounts to more than 15 vol%. This can lead to higher MgO contents than those encountered in some conventional leuconorites with around 10 % cumulus orthopyroxene (see Table 5.2).

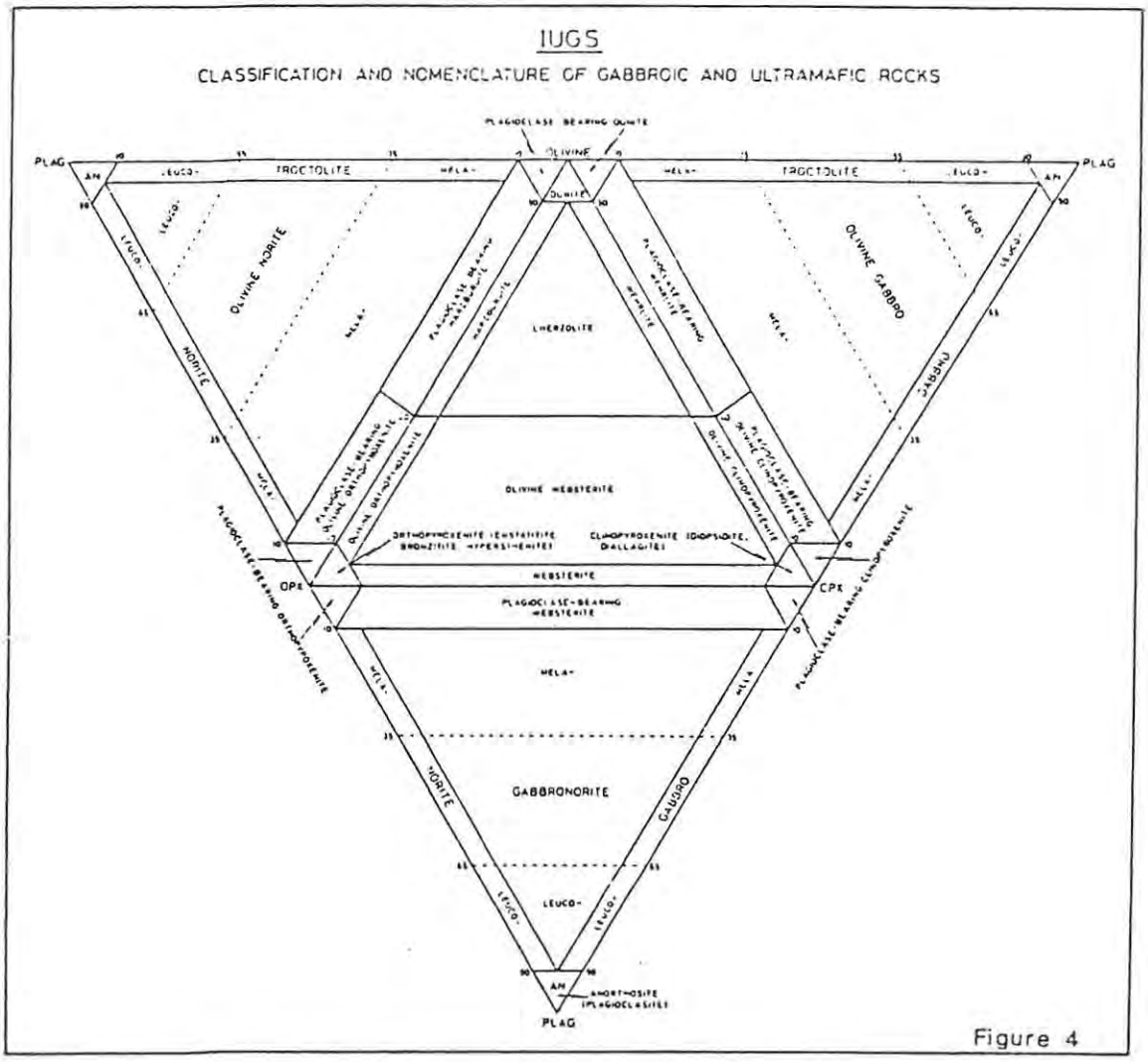

Fig. 1.4 The IUGS classification and nomenclature of gabbroic and ultramafic rocks (figure from de Klerk, 1981; modified after Streckeisen, 1974).

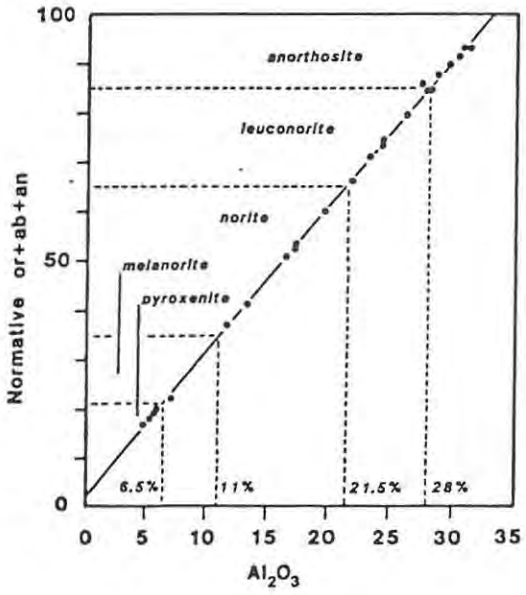

Fig. 1.5 Nomenclature of orthopyroxene-plagioclase rocks, based on plot of normative or + ab + an versus whole-rock Al_2O_3 (figure from Eales et al., 1988).

The terminology of igneous cumulates was originally based on the concept of crystal settling leading to the accumulation of rocks (Wager et al., 1960). Irvine (1982) proposed to use the term "cumulate" in a descriptive, textural way.

In the IUGS system the boundary between anorthosites and leuconorites is set at 10 vol% orthopyroxene content. This definition automatically includes two types of anorthosites in the study section, one bearing cumulus, and the other intercumulus orthopyroxene. In the mines the former type is commonly referred to as "spotted anorthosite" and the latter as "mottled anorthosite".

In the study section the amount of cumulus orthopyroxene may change in a gradational way between nearly pure plagioclase rocks and leuconorites. Furthermore, cumulus orthopyroxene usually shows different chemical characters than intercumulus orthopyroxene although the distinction between the two is not sharply defined. Hence, in the author's view, the arbitrary boundary at 10 % cumulus orthopyroxene does not make much sense. The classification leaves us with two types of anorthosites with markedly different compositions of orthopyroxene, with the "spotted" type having similar orthopyroxene compositions as leuconorite. On the other hand, it seems unconventional to call a plagioclase rock with only 2 % cumulus orthopyroxene a leuconorite. However, such a low proportion of orthopyroxene is rarely encountered in the interval under review. Only two out of ca. 260 samples have cumulus orthopyroxene contents between 0 and 3 %.

In view of these considerations, the present author has elected to call plagioclase rocks containing intercumulus orthopyroxene anorthosite and those containing cumulus orthopyroxene leuconorite. This represents an approach according to Irvine's suggestions (1982). It must be added that a further complication arises as intercumulus orthopyroxene "mottles" sometimes contain small cumulus cores which may be interconnected, enclosed and obscured by intercumulus orthopyroxene. These cumulus cores may become quite large (up to 1

mm). This coexistence of cumulus and intercumulus orthopyroxene within one grain may be responsible for the transitional character of the chemical boundary between the two varieties of orthopyroxene.

Anorthosites containing chromite as a major constituent (i.e., ≥ 5 vol%) are called chromitiferous anorthosites hereafter.

A specific problem is encountered when a large proportion of the rock consists of intercumulus phases, like the harzburgitic Pseudoreefs. Forty per cent cumulus olivine, 50 % poikilitic orthopyroxene and 10 % intercumulus plagioclase yield a dunite according to Irvine (1982). Jackson (1961), however, distinguished between granular and poikilitic harzburgites. The former consists of cumulus olivine and orthopyroxene plus intercumulus plagioclase, the latter of cumulus olivine, more than 40 % intercumulus orthopyroxene and intercumulus plagioclase. This nomenclature will be used in this work as well. A comparison of some schemes of classification is given in Table 1.2.

Table 1.2: Comparison of different schemes of terminology

Rock type	This study (vol% cum.plag)	IUGS (vol%plag)	Eales et al (1988) (% Al2O3)
Anorthosite	100	>90	> 28
Leuconorite	65-100	65-90	21.5 - 28
Norite	35-65	35-65	11 - 21.5
Melanorite	10-35	10-35	6.5 - 11
Pyroxenite	0-10	0-10	< 6.5
Harzburgite	0-10	0-10	not def.

1.6: Sampling Procedure

Half core samples of 9 boreholes around the western lobe of the Bushveld Complex were collected and analysed. The sampling interval depended wholly on lithological variability, thus ranging from 10 m down to 10 cm. Lithological contacts were always sampled where

obtainable. Two cores ($7E^3$ and $60E^3$) were sampled by B. Walters in 1981. Continuous 1 to 1.5 m sections of the latter had been crushed and analysed for whole-rock chemistry. For this reason no microprobe analyses could be executed on these two cores. Core UA was sampled by W.J. de Klerk. For the TF sequence only 14 sample chips, collected underground, were made available by Messrs. J.C.I. Ltd. and no whole-rock analyses could be executed. Furthermore, no detailed log of the shaft area could be obtained from the company. Core AE had been sampled and analysed by M. Field in 1986 and the results are incorporated into the data base (see Appendices). As in the case of intersection TF no detailed log could be obtained for this intersection.

Additional samples were collected during numerous underground visits at Lefkochrysos Platinum Mine (now Crocodile River Mine), Impala Platinum Mines, Western Platinum Mine, RPM Turffontein Section and Henry Gould and Millsell Chrome Mines.

CHAPTER 2: STRATIGRAPHY OF THE INTERVAL BETWEEN THE UG2 CHROMITITE AND THE MERENSKY REEF IN THE WESTERN BUSHVELD

2.1: Introduction

In the following chapter a detailed stratigraphic description of the ten intersections examined will be given. The borehole logs (underground log for intersection TF) are listed in Appendix I. The description will start with the most compressed succession at Union Section (core UA) and proceed towards Amandelbult Section in the north (cores $7E^3$, EK22, $60E^3$) and Impala Section (cores IN, IM), Rustenburg (TF sequence) and Brits (cores LK7, H3, KR2) in the south and south-east. The locations of the individual core intersections are indicated in Fig. 1.1(b). Profile RD (Rooderand), also shown in Fig. 1.1(b), will be referred to in a later chapter. This approach represents an order of study of increasing distance from Union Section. A simplified schematic picture of the interval in the different parts of the western limb is given in Fig. 2.1 and the author will refer to this figure frequently during the following description. The nomenclature used by mine geologists at Union and Amandelbult Sections is different from that at Impala Section and in the Brits area. A correlation of the two schemes will be attempted in Chapter 7. The individual profiles are presented in Fig. 2.2 and a detailed picture of the uppermost part of the interval under review is shown in Fig. 2.3.

2.2: The UA Sequence (RPM Union Section)

At Union Section the interval under review directly overlies the UG1 pyroxenite. It begins with 30 cm of pegmatoidal pyroxenite overlain by a chromitite layer which is 1.1 m thick, the UG2 chromitite. The latter consists of a main layer (ca. 80 cm thick) and a variable number of thin (ca. 10 cm) leader seams (not specified in the UA log). The chromitite is topped by 1.5 m of harzburgite which grades into a feldspathic pyroxenite (ca. 9.7 m thick).

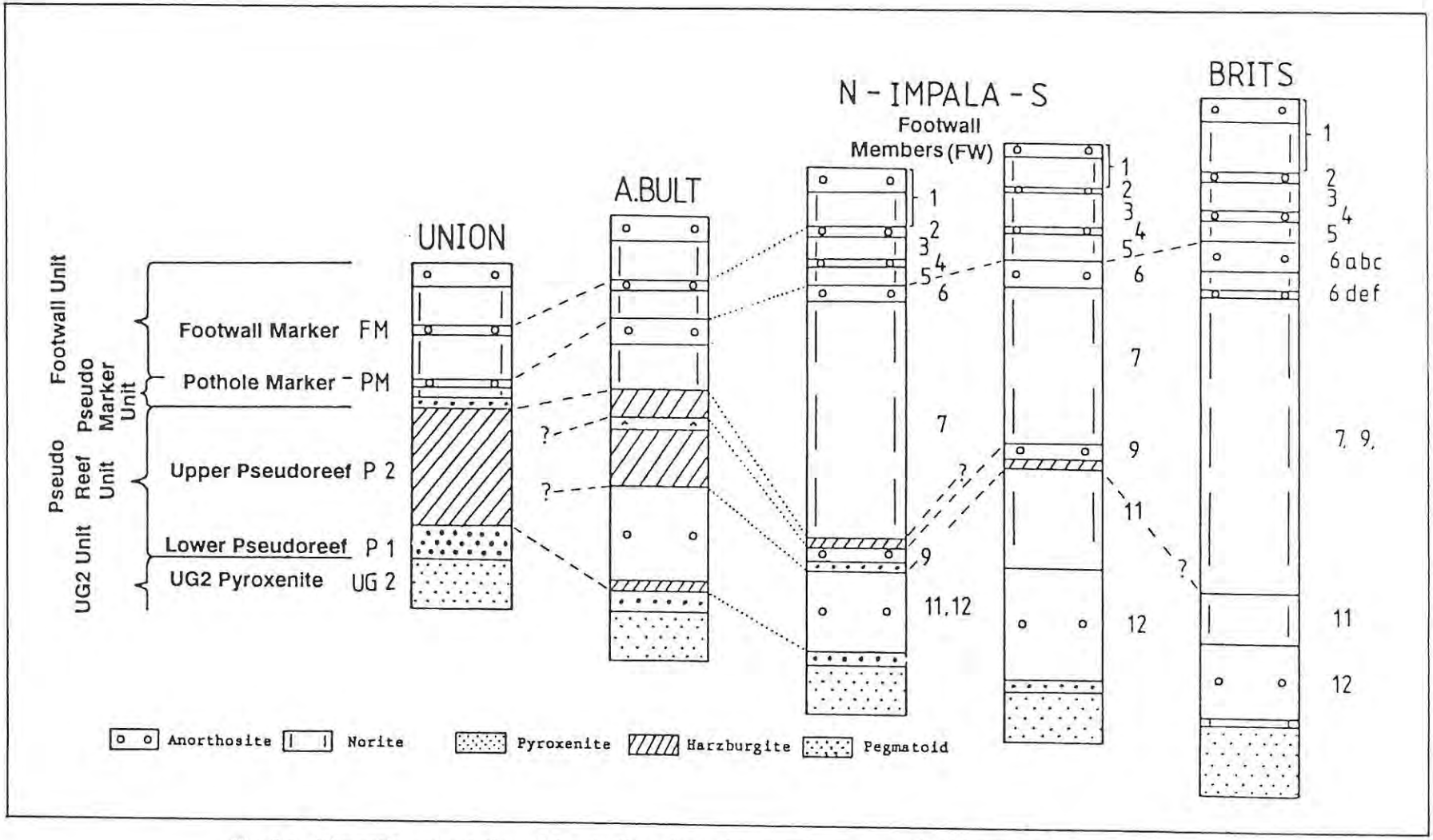

Fig. 2.1 Schematic presentation of the stratigraphy and nomenclature, used in this work, of the main distinguishable members in the interval between the UG2 pyroxenite and the Merensky Reef in the Western Bushveld Complex. Note the difference in nomenclature used at Union and Amandelbult Sections in the northern part of the western limb of the complex and that at Impala Section and the Brits area (Crocodile River Mine) in the southern part. Columns are not drawn to a fixed scale. The profile at Union Section spans ca. 30 m, and that for the Brits area ca 210 m.

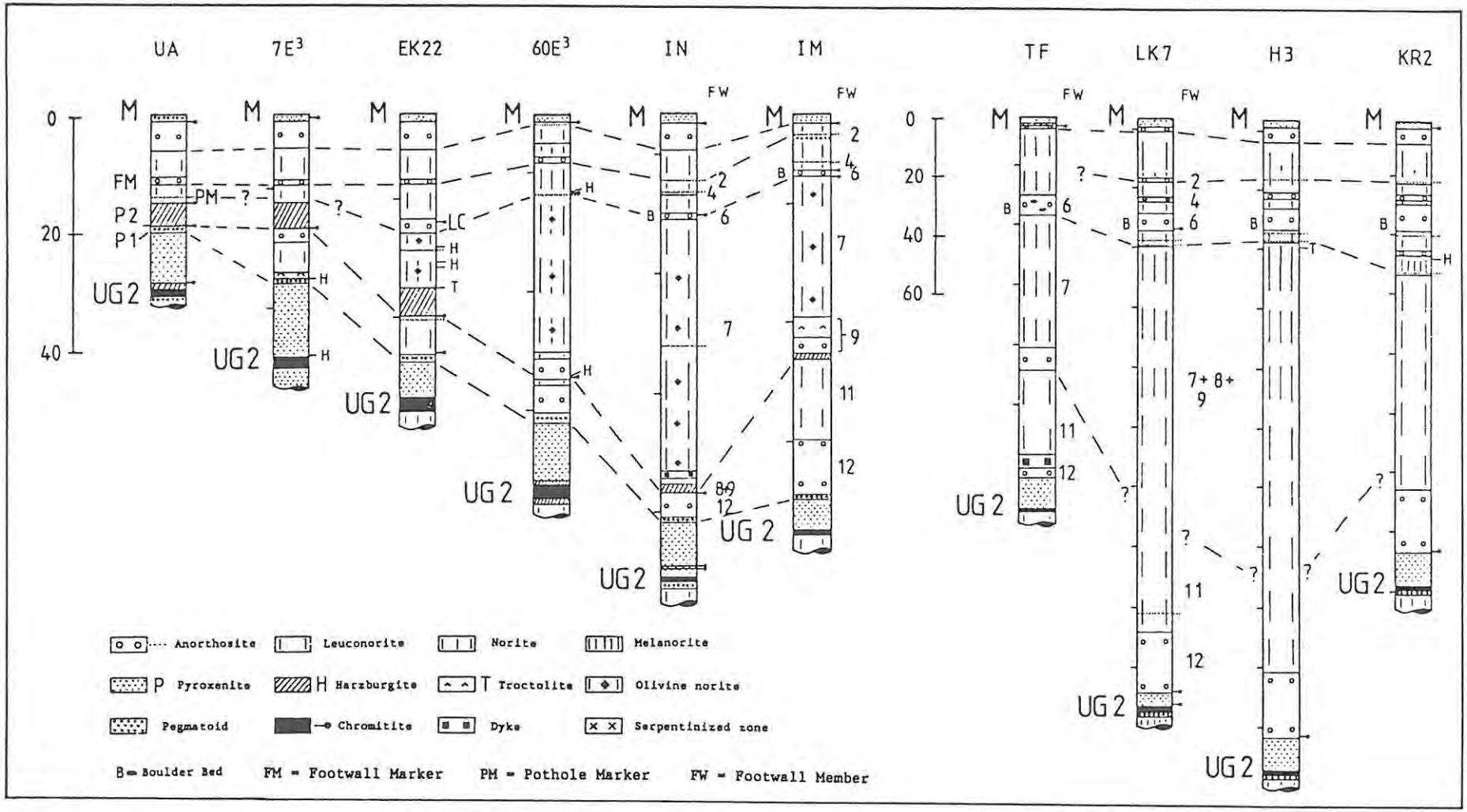

Fig. 2.2 Stratigraphy and provisional correlation of the interval under review in the investigated intersections. Note the change of scale between the 6 cores on the left-hand side and the 4 cores on the right-hand side of the diagram. The distance between marks (short lines on left side of profile) represents 20 m in each case. In some cases the thickness of thin layers is slightly exaggerated in order to show them more clearly. Question marks indicate that the correlation is tentative.

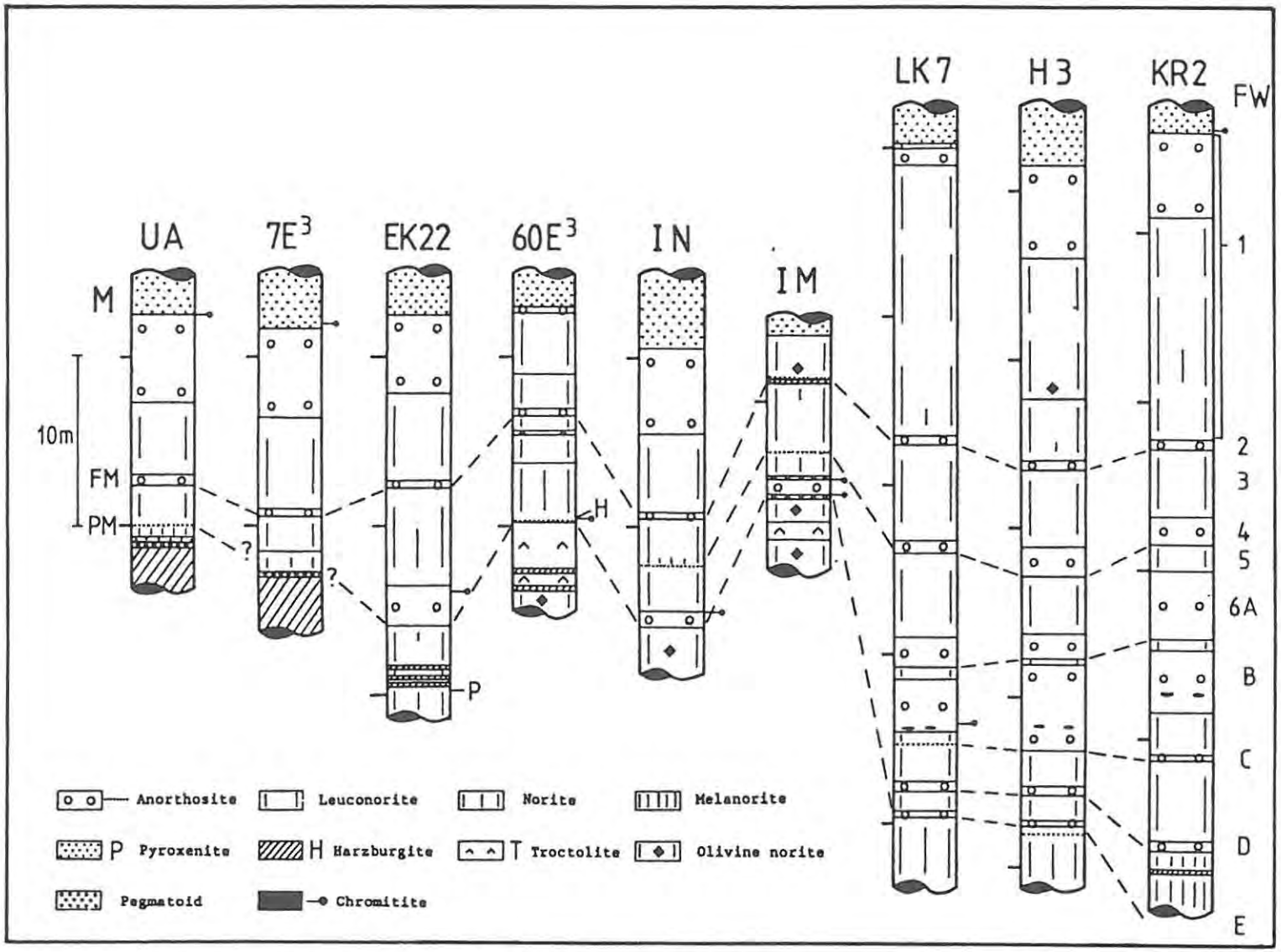

Fig. 2.3 Detailed stratigraphy and provisional correlation of the immediate footwall of the Merensky Reef. PM = Pothole Marker, FM = Footwall Marker, FW = Footwall Member.

This succession is usually called the UG2 Unit and shows great persistence all around the western limb.

There follows 1.1 m of pegmatoidal feldspathic harzburgite, the Lower Pseudoreef or P1 Marker. It is regarded as the base of the Pseudoreef Multicyclic Unit, as defined by Eales et al. (1988). The contact with the underlying pyroxenite is undulating. The next layer is a medium-grained harzburgite, ca. 4 m thick, the so-called Upper Pseudoreef or P2 Marker. At the upper and lower contacts of the P2 Marker, thin (1cm) chromitite stringers are usually present.

The following ca. 1 m thick succession of pegmatoidal harzburgite - pyroxenite - melanorite - anorthosite is known as the Pseudo Marker Unit (Viljoen et al., 1986a). The top anorthosite is 2 cm thick and is very persistent along strike at Union Section (Viljoen et al., 1986a). It is designated the Pothole Marker (PM) by mine geologists.

Above the Pothole Marker, one finds 7.7 m of leuconorite which at about mid-level is interrupted by 50 cm of mottled anorthosite. This anorthosite is known as the Footwall Marker at Amandelbult, and as FW 2 in the southern part of the western limb. It is not developed in all parts of Union Section. Nevertheless, in the present author's nomenclature, this anorthosite will be called Footwall Marker at Union Section as well. Immediately above and below the Footwall Marker inch-scale layering of orthopyroxene- and plagioclase-rich laminae is colloquially known as "streepies"-lamination. Also present in the leuconorite are so-called "corona structures", which are orthopyroxene clusters surrounded by anorthosite halos.

Forming the footwall of the Merensky Reef, is ca. 5 m of mottled anorthosite. The succession between the Footwall Marker and the Merensky Reef is called FW 1 at Impala Platinum Mines, a classification which will be adopted by the present author for Union Section as well. The Merensky pegmatoidal pyroxenite (ca. 2 m thick) at Union Section is often harzburgitic towards its base and shows the

development of bottom and top chromitite stringers. The bottom stringer normally has a "dimpled" (i.e., undulating) contact with the underlying anorthosite. A 1 to 4 cm zone of pure, white anorthosite, which also is discordant to the layering, is commonly developed beneath the bottom chromitite and follows its contours. This feature can be seen in all cores.

2.3: The $7E^3$ Sequence (RPM Amandelbult Section)

Within this intersection in the central part of Amandelbult Section, the UG2 chromitite lies on a fault zone with ca. 14 m displacement, so that its apparent 15 cm thickness in the borehole, and the 27 cm of overlying harzburgite, do not represent typical thicknesses. The basal harzburgite underlying the UG2 chromitite is missing, while the footwall beneath it consists of pyroxenite (UG1 pyroxenite). The UG2 feldspathic pyroxenite is 8.2 m thick.

The Lower Pseudoreef (P1 Marker, shown in coarse stipple immediately above the UG2 pyroxenite in Fig. 2.2) is built up of 40 cm of pegmatoidal pyroxenite. The Upper Pseudoreef (P2 Marker) at Amandelbult, according to Eales et al. 1988, can be subdivided into 3 members, namely Upper Pseudoreef A, B and C (hereafter P2-A, -B, and -C). The lowest member (P2-A), consisting of a thin chromitite stringer, 10 cm of harzburgite and another thin, irregular chromitite stringer, directly overlies the P1 Marker. The P2-B is separated from the P2-A at intersection $7E^3$ by a succession of 50 cm of olivine-bearing mottled anorthosite, 6 m of leuconorite and 2 m of mottled anorthosite which also is occasionally olivine-bearing. The P2-B Marker and the directly overlying P2-C Marker comprise 4 m of harzburgite underlain by a thin basal chromitite stringer. The P2-B and C Markers at south-western Amandelbult are usually separated by a thin troctolitic "Middling" (Fig. 2.1) although this is not developed at locality $7E^3$. The P2 Marker changes its appearance along strike at Amandelbult Section (see Chapter 7.5).

The P2 Marker is overlain by the Pseudo Marker which, in the central part of Amandelbult Section, is usually built up of 1 cm of chromitite, 10 cm of pegmatoidal harzburgite, and 70 cm of melanorite. This incomplete cyclic unit is capped by a very thin pyroxenite, followed by an equally thin anorthosite. The latter association is only 1 to 2 cm thick but is remarkably persistent along strike and is called the P2 Hangingwall Marker at Amandelbult. The anorthosite is likely to be correlated with the Pothole Marker at Union Section and, in this work, will be referred to under this name at Amandelbult as well. In the $7E^3$ intersection, however, the P2-B/-C harzburgite is directly overlain by melanorite which grades into leuconorite, which is in turn overlain by 40 cm of mottled anorthosite, the Footwall Marker. The P2 Hangingwall Marker is thus missing. The melanoritic-noritic sequence is 3.3 m thick.

The top part of the study interval at locality $7E^3$ (FW 1) is made up of 5.4 m of leuconorite, sharply overlain by 5.3 m of mottled anorthosite. The Merensky pegmatoidal pyroxenite at locality $7E^3$ is only 60 cm thick but has the usual basal and top chromitite stringers.

2.4: The EK22 Sequence (RPM Amandelbult Section)

Intersection EK22 is situated approximately 6 km north-east of intersection $7E^3$. The UG2 Unit at locality EK22 is composed of a basal 10 cm of pegmatoidal harzburgite overlain by 90 cm of massive chromitite, and about 7 m of feldspathic pyroxenite containing two 10 cm chromitite layers, grouped as "leaders" to the massive UG2 chromitite.

The succeeding P1 Marker consists of 90 cm of pegmatoidal pyroxenite. The top contact is defined by a thin chromitite stringer and 5 mm of harzburgite, possibly the P2-A Marker. The sequence up to the P2-B Marker consists of 6 m of leuconorite and 40 cm of anorthosite. Twenty cm above the base of the leuconorite, a 1 mm chromitite

stringer, capped by 1 cm of pyroxenite, forms a well defined layer (Plate 1). It is unclear if this is to be correlated with the top chromitite of the P2-A Marker at locality 7E3. The P2-B Marker comprises a thin basal chromitite and 20 cm of poikilitic harzburgite which grades into 4.5 m of granular harzburgite. The uppermost part of this harzburgite is, strictly speaking, a feldspathic dunite as cumulus orthopyroxene sinks below 10 modal per cent.

Plate 1: A 5 mm orthopyroxene orthocumulate layer within the FW 12/11 leuconorite underlain by a 1 mm chromitite stringer. Sample EK22 306.30, 15 cm above P1 pegmatoid. Field width 5.9 mm; crossed nicols.

The overlying 6.3 m of norite is olivine-bearing at the base. It is interrupted, in the core sampled, by two thin dykes and two thin harzburgite layers (ca. 10 cm thick), the latter showing sharp lower and gradational upper contacts. The following very variable zone begins with 10 cm of feldspathic pyroxenite and continues with 10 cm of leuconorite, 20 cm of harzburgite grading into troctolite, another thin harzburgite, 30 cm of leuconorite grading into anorthosite, and a 15 cm sequence of alternating harzburgite and pyroxenite (Fig. 2.4). This last sequence displays sharp lower and upper contacts and is overlain by 2.5 m of leuconorite which grades into a norite. The whole succession of harzburgites is regarded here as the P2-C Marker, now split apart into discrete laminae. The norite in turn is followed by 2.3 m of anorthosite, the Pothole Marker (P2 Hangingwall Marker, according to the nomenclature used by Viljoen et al., 1986b; FW 6 at Impala), the contact between the two being sharp. The anorthosite contains a chromitite stringer (1 cm thick) towards the top, which is usually called the Lone Chrome Seam (LC) in the mines and in the scanty literature (Viljoen et al., 1986b).

The succession continues with 6 m of norite, grading upwards into leuconorite which is capped by 12 cm of mottled anorthosite, the Footwall Marker (FW 2).

Another 5 m of leuconorite, followed by 5 m of anorthosite, form the footwall to the Merensky Reef (FW 1). The Merensky pegmatoid contains neither BMS nor PGMs in the EK22 intersection (RPM in-house log). There is also no basal or top chromitite stringer developed here.

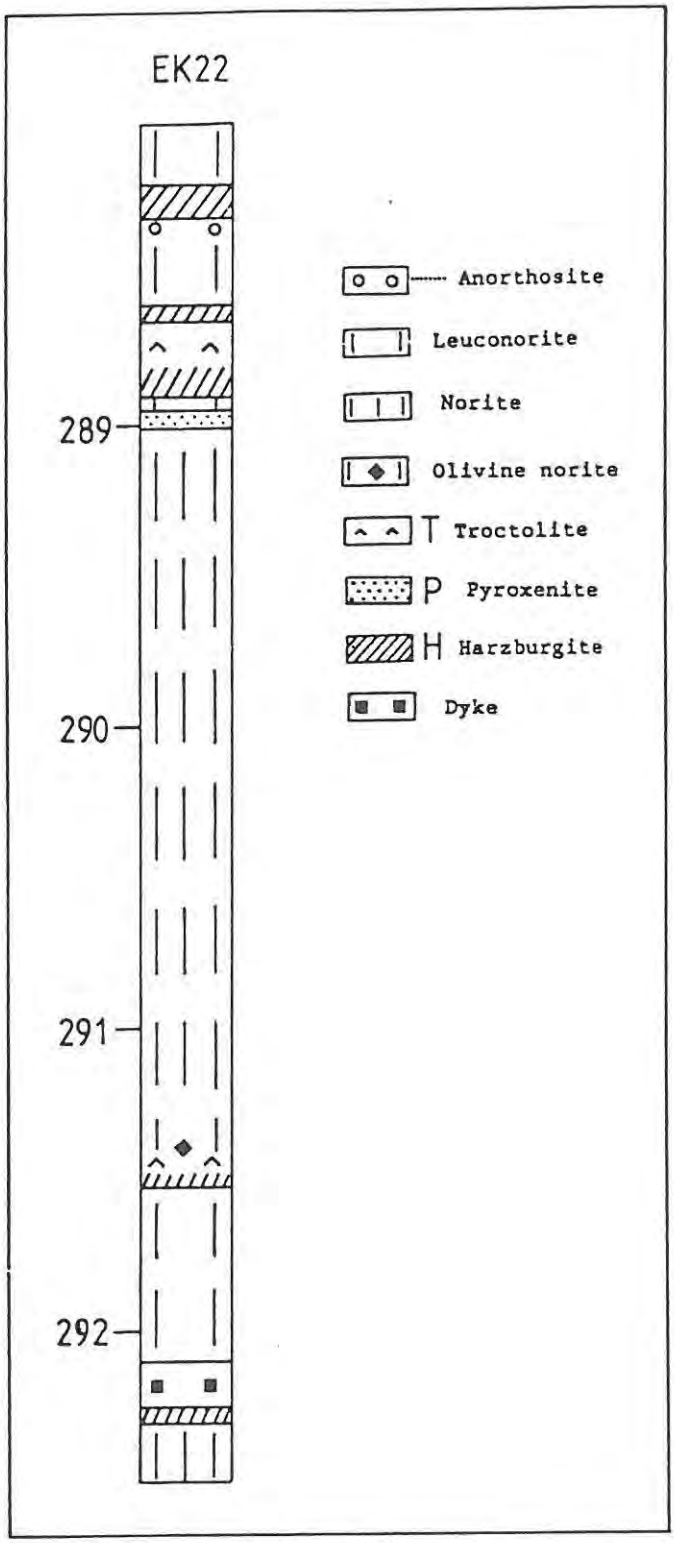

Fig. 2.4 Detailed stratigraphy of a section within the central part of the interval under review at intersection EK22 (see text for explanation).

2.5: The 60E^3 Sequence (RPM Amandelbult Section)

The complete UG2 Unit developed here consists of ca. 2 m of pegmatoidal harzburgite / pyroxenite, 20 cm of chromitite, followed by some 25 cm of pyroxenite containing a 16 cm leader chromitite, 44 cm of poikilitic harzburgite, and a ca. 10 m feldspathic pyroxenite.

The P1 Marker is formed by 1 m of harzburgitic pegmatoid with a disseminated chromite-rich zone towards the top being recorded. No clear development of the P2-A Marker can be observed. The overlying 5 m of mottled anorthosite grades into 80 cm of leuconorite. Another thin anorthosite is topped by an altered, serpentinized zone (ca. 50 cm thick) which displays a basal chromitite stringer (P2-B Marker ?). Two and a half metres of mottled anorthosite are then overlain by a thin troctolite and a relatively monotonous sequence of 27 m of olivine norite in which 5 - 6 thin harzburgites or dunites are developed (P2-C Marker ?). Towards the top of this medium-grained olivine norite, 3 zones of fine-grained, slightly laminated olivine norite or troctolite are prominent. The massive harzburgite of the Upper Pseudoreef B/C has thus given way to a thick sequence of olivine norite containing a number of thin harzburgites in the north-eastern exposures of Amandelbult Section.

The uppermost troctolite is capped by 4 cm of anorthosite, the Pothole Marker. Harzburgite (4 cm thick) with a basal chromitite stringer directly overlies the anorthosite. A 6 m succession of norite - leuconorite - troctolite - norite is then capped by the anorthositic Footwall Marker, which is 40 cm thick (FW 2 in the southern part of the western limb).

The top of the interval is formed by 2 m of norite which is olivine-bearing at the base, grading into 3.5 m of leuconorite and ending with 30 cm of mottled anorthosite (FW 1). The Merensky pegmatoid is only 40 cm thick and displays, as is normal, top and bottom chromitites.

2.6: The IN Sequence (Impala Platinum Mines, Bafokeng North Mine)

Fifty centimetres of UG2 chromitite is underlain by 90 cm of pegmatoidal pyroxenite in the IN intersection. The contact between the two is fairly irregular. Three leader chromitites, each about 5 to 10 cm thick, occur 2 - 3 m above the main chromitite: they are called the Leader Triplet. The UG2 pyroxenite is about 10 m thick and no harzburgite is developed at its base here. Fifteen cm of pegmatoidal pyroxenite, overlain by 30 cm of coarse-grained harzburgite, form the P1 and the P2-A Markers. The latter is capped by 5 m of mottled anorthosite (FW 12). In case the P1 and the P2-A Markers are missing, there is often a thin chromitite stringer developed at the contact between UG2 pyroxenite and overlying anorthosite (Leeb-du Toit, 1986).

A thin chromitite stringer followed by a pegmatoidal pyroxenite of some 3 cm thickness, 10 cm of norite, and 1 m of coarse-grained troctolite (FW 9) form the next distinguishable members. The troctolite may also be developed as a mottled anorthosite. The following 20 cm consist of a thin harzburgite, a chromitite stringer and 1 cm of pyroxenite overlain by an equally thick harzburgite. This entire package is correlated here with the P2-B Marker (pegmatoidal pyroxenite), the P2 Middling (troctolite) and the P2-C Marker (harzburgite), respectively, and is displayed in detail in Fig. 2.5.

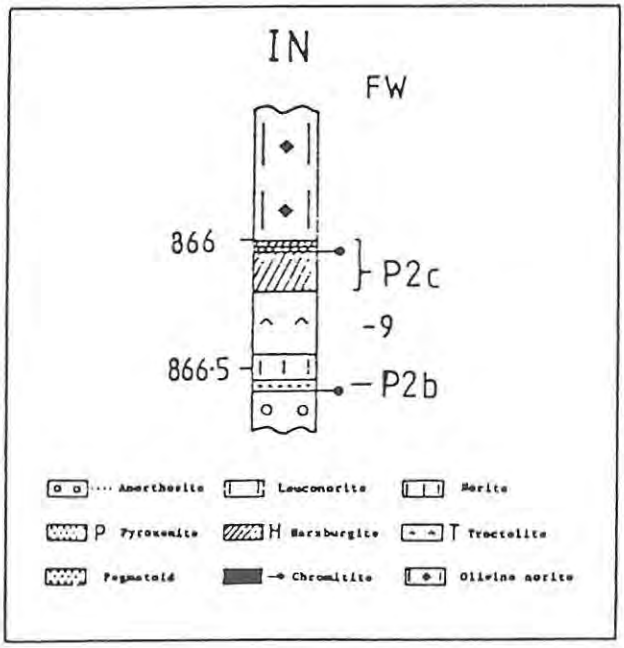

Fig. 2.5 Detailed profile of the sequence below and above FW 9 at locality IN (see text for explanation).

The hangingwall is formed by a monotonous sequence of 45 m of olivine norite (FW 7), interrupted only by 2 cm of anorthosite at about mid-level. Two metres of fine-grained olivine-noritic to troctolitic rock is found towards the top.

The overlying anorthosite (FW 6, ca. 1 m thick) normally hosts the so-called "boulders", pyroxenite or harzburgite spheroids of about 20 cm average diameter which usually occur towards the base of the layer. In borehole IN, however, no "boulder" was intersected by the core. The anorthosite becomes very thin in the far-northern part of the Impala lease area (Fig. 2.6). FW 6 is topped by the 5 mm Lone Chrome Seam, which is overlain by a 2 m succession of norite and anorthosite (FW 5 and 4). The latter disappears between 6 and 8 shaft area in the far-northern part of the lease area (Fig. 2.6). The following 80 cm sequence consists of melanorite (FW 3), grading into anorthosite (FW 2).

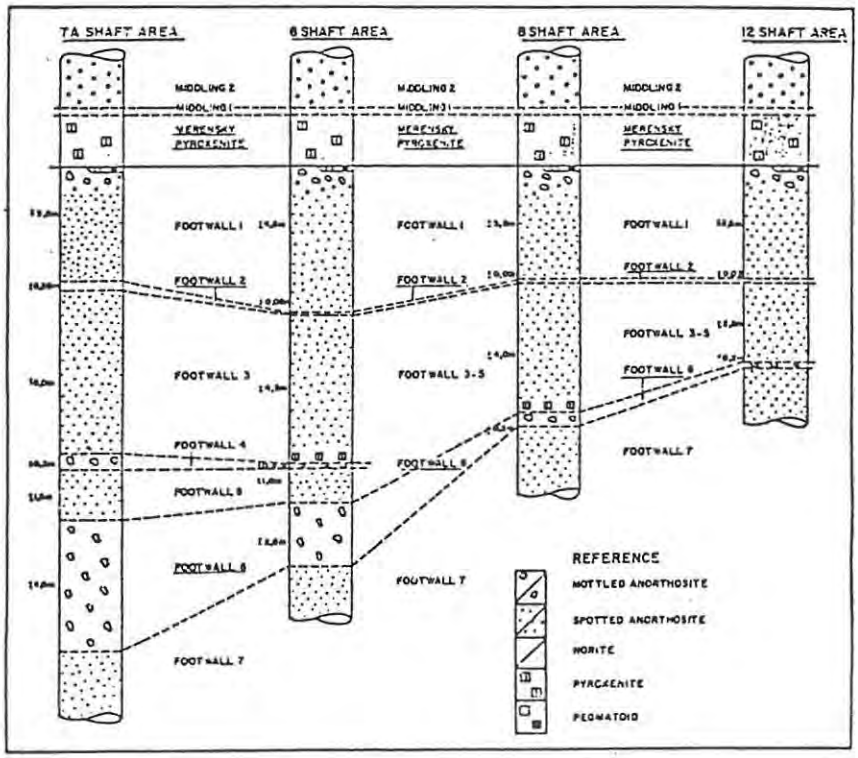

Fig. 2.6 Lithological variations along strike (from the south-east on the left, to the north-west on the right) in the Merensky footwall of the Bafokeng North lease area of Impala Platinum Mines (modified after Impala in-house logs).

FW 1 is 10 m thick and consists of leuconorite grading into anorthosite. The overlying Merensky pyroxenite (ca. 2 m thick) has a basal 2.5 cm chromitite. The Merensky pegmatoid, usually between 0 and 40 cm thick in the northern parts of Impala Section is missing at locality IN.

2.7: The IM Sequence (Impala Platinum Mines, Wildebeestfontein North Mine)

At this locality, 11 km south-east of the IN intersection, the UG2 chromitite is only 20 cm thick, and neither the basal pegmatoid nor leader chromitites are developed. Six metres of pyroxenite form the upper part of the UG2 Unit which is overlain by 50 cm of pegmatoidal pyroxenite, the P1 Marker. No P2-A Marker is developed. The reduced thickness of the sequence at locality IM, in comparison with the sequence at intersection IN, is thus already visible in the lowermost unit.

The following 10 m of mottled anorthosite (FW 12) is unusual insofar as towards its top the mottles consist of an olivine core and a rim zone of intercumulus orthopyroxene and fine-grained plagioclase. The overlying 12 m consist of leuconorite grading into norite (FW 11). A harzburgitic zone of 30 cm is developed at its top and this is probably to be correlated with the P2-B Marker. After another 20 cm of leuconorite, a 2 m package of mottled anorthosite grades into olivine-bearing mottled anorthosite and finally coarse-grained troctolite (FW 9 ?).

The next 24 m consist of olivine norite (FW 7). The harzburgitic-pyroxenitic succession, overlying the troctolite at intersection IN is thus missing here. The uppermost 3 m of the olivine norite are made up of fine-grained laminated troctolite which grades into a medium-grained leucotroctolite. The overlying 1 m of anorthosite represents FW 6 and shows thin chromitite stringers at the base and towards the

Chrome Seam ?). Within the following 6 m leuconorite grades into norite. One metre above the base, a doublet comprising two 5 cm layers of anorthosite is encountered (FW 4). This development of a doublet is common at that position at Impala Wildebeestfontein Mine. The norite is capped by a thin, irregular harzburgitic pegmatoid which forms the base of a 10 cm layer of anorthosite (FW 2). Sporadic pegmatoidal harzburgite is also developed at the top of the anorthosite.

The overlying FW 1 is 2 m thick and is built up of norite, grading into leuconorite. The lowermost 60 cm of the norite is olivine-bearing, the large anhedral crystals often being surrounded by plagioclase halos, strongly resembling the "corona structures" mentioned earlier. No anorthosite is developed at the top of FW 1 at locality IM. The Merensky Reef is a 10 cm PGE-bearing zone at the base of 1.4 m of Merensky pyroxenite which displays a basal chromitite. No pegmatoid or second chromitite is developed.

2.8: The TF Sequence (RPM Turffontein Mine)

For the TF intersection, only a generalized and simplified log accompanying small sample chips was made available by Messrs. J.C.I. Ltd. Therefore, only the most conspicuous features will be briefly outlined here. The sequence to the east of Rustenburg more or less resembles that at locality IM, but the total thickness of the UG2 - Merensky interval has increased to 130 m. The occurrence of olivine is restricted to the upper part of FW 7, and the Boulder Bed (FW 6) has become significantly thicker. The sequence between the Boulder Bed and the Merensky Reef seems to be very similar to that at locality IN, but footwall anorthosites are described by different names (Kruger, 1982). Thus, the FW 4 would be the Brakspruit Marker and a new anorthosite may be developed between the FW 4 and the Boulder Bed (FW 6b at locality LK7): the Pioneer Marker (FW 6a at LK7).

2.9: The LK7 Sequence (Core Supplied by Messrs. Rand Mines Ltd., Situated Near Wolhuterskop)

The sequence at locality LK7 begins with the normal succession of 1.5 m of harzburgitic pegmatoid underlying 1.5 m of main UG2 chromitite. One leader chromitite seam of 17 cm is situated about 1 m above the main seam. The overlying 5 m of pyroxenite contains a 7 cm harzburgite band close to the base.

The UG2 pyroxenite is sharply overlain by 7 cm of mottled anorthosite and 8 cm of pyroxenite with both a bottom and top chromitite stringer. This pyroxenite may elsewhere be situated up to 10 m above the UG2 pyroxenite (core LK5, 3 km to the east). The present author correlates this layer with the Upper Pseudoreef A. The succeeding 20 m of mottled anorthosite (FW 12) contain two 5 cm layers of very fine-grained norite towards the base. A leuconoritic section occurs at about mid-level in the anorthosite. The anorthosite is topped by nearly 130 m of leuconorite grading into norite which would be the equivalent of the FW 11-7 sequence at Impala. At locality LK5, this noritic sequence is intersected by two anorthosite layers, each ca. 1 m thick, at about mid-level.

In the highly variable FW 1-6 succession (Fig. 2.3) every layer appears to have thickened considerably compared to Impala and Rustenburg Sections and, as already mentioned in the description of the TF sequence, the FW 6 anorthosite splits up into a package of intercalated anorthosites and leuconorites which are labeled FW 6a - e, the Boulder Bed being FW 6b. Altogether, at locality LK7, one is dealing with 41 m of mostly leucocratic rocks, amongst them 8 anorthosite layers. FW 6b contains a chromitite stringer and a "boulder" was intersected towards the base of the layer. FW 6e consists of intercalated norite and anorthosite layers and is called the Norite Marker in the mines. The Merensky pyroxenite is 11 m thick and has a basal chromitite, but no pegmatoid or second chromitite stringer are developed. This feature can be observed in all cores east of Rustenburg.

2.10: The H3 Sequence (Supplied by Messrs. Golden Dumps Ltd., Situated ca. 7 km East of Intersection LK7)

At intersection H3, a pegmatoidal pyroxenite of 70 cm thickness underlies the 1.2 m main UG2 chromitite, which is interrupted by a thin pyroxenite parting towards the base. The UG2 pyroxenite is 11 m thick.

Fifteen cm of leuconorite, a 2 mm wide chromitite stringer with pure, anorthositic top and bottom zones (P2-A Marker?, Plate 2) and 21 m of mottled anorthosite (FW 12) form the immediate hangingwall succession of the UG2 Unit. Leuconoritic zones occur at 2 levels in the anorthosite. The central part of the interval is here made up of 140 m of leuconorite grading upwards into norite (FW 11-7).

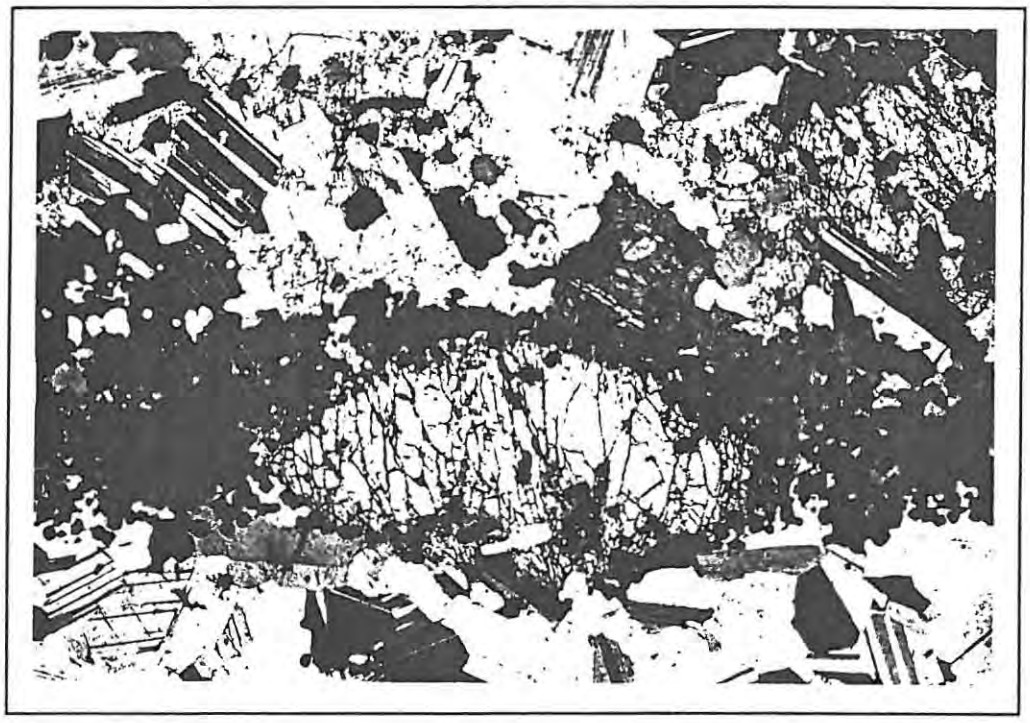

Plate 2: Chromitite stringer within leuconorite, underlain by a 5 mm zone of pure plagioclase. Sample H3 1253.3a, 15 cm above UG2 pyroxenite. Field width 8.7 mm; crossed nicols.

The top part of the interval is formed by the multicyclic Merensky footwall sequence, and a correlation with equivalent members in core LK7 is fairly certain. "Corona structures" occur at several levels. The Norite Marker (FW 6e) contains one 2 cm troctolite lens or layer and the FW 1 norite develops into two cycles, with a melanocratic, olivine-bearing zone at about mid-level.

2.11: The KR2 Sequence (Supplied by Messrs. Golden Dumps Ltd., Situated in the Brits Graben)

The most easterly intersection, provided by borehole KR2, is situated in the Brits Graben and does not continue the regular trend of thickness increase with distance from Union Section, established in the other profiles. It is not clear whether the reduced thickness is related to tectonic activity at the time of deposition, or if other factors like the possible presence of a minor feeder zone caused this sequence to be different.

The thickness of both UG2 chromitite and pyroxenite is nearly identical to that at intersection H3. Occasionally, minor olivine occurs at the base of the UG2 pyroxenite at Crocodile River Mine. The overlying 35 cm of leuconorite displays brecciated chromitite stringers towards the top (P2-A Marker ?). The thinning of the mottled anorthosite (FW 12) and the central leuconoritic part (FW 11-7) is responsible for the reduced total thickness of the interval, relative to intersections LK7 and H3.

In contrast to the reduction in thickness characterizing the central leuconoritic part of the sequence, the stratigraphic interval cut by the top section of the KR2 borehole is the thickest of all cores. The distance between the different anorthosites has increased, but a correlation still seems to be possible. Between FW 6d and 6e, 10 cm of pegmatoidal harzburgite has developed. The Merensky pyroxenite has increased in thickness from 11 m at locality LK7, to 12 m at H3, and 15 m at KR2.

2.12: Summary

It has become clear that, if the concept of cyclic units is to be applied, there are probably up to 9 such units at Amandelbult. These are (with increasing stratigraphic height) as follows:

(i) The UG2 Unit (chromitite-pyroxenite)
(ii) The P1 Marker Unit (chromitite - pegmatoidal pyroxenite)
(iii) The Upper Pseudoreef A Unit (chromitite - harzburgite - chromitite - coarse grained troctolite (olivine-bearing mottled anorthosite) -leuconorite - anorthosite)
(iv) The Upper Pseudoreef B Unit (chromitite -harzburgite - troctolitic Middling)
(v) The Upper Pseudoreef C Unit (chromitite - harzburgite)
(vi) The Pseudo Marker Unit (chromitite - pegmatoidal harzburgite - melanorite - leuconorite)
(vii) The P2 Hangingwall Marker Unit (pyroxenite - anorthosite)
(viii) The Footwall Marker Unit (leuconorite - anorthosite)
(ix) The Merensky Footwall Unit (norite - anorthosite)

Most of these units are in some way incomplete or beheaded. Towards Brits, a distinction of cyclic units becomes difficult as lithological (and geochemical) reversals become transitional in character and a number of additional anorthositic partings have developed in the upper part of the interval under review.

CHAPTER 3: PETROGRAPHY

3.1: Introduction

In the following chapter the petrography of the various rock types in the study section as investigated by means of: (a) microscopic and macroscopic rock descriptions, (b) grain size measurements on plagioclase and orthopyroxene, and (c) determination of rock modes by the point-counting technique will be discussed. Frequently, petrographic parameters such as grain size will be plotted versus geochemical parameters which in turn will be discussed in more detail in Chapter 4.

3.2: Anorthosites

As discussed in Chapter 1.5 the terminology used in this work differs slightly from the IUGS classification (Streckeisen, 1974). Anorthosites here are pure plagioclase cumulates with a varying amount of intercumulus material. The range of grain sizes of cumulus plagioclase in the anorthosites (as well as in the norites) is usually fairly wide ($\leq$ 0.5 to $\geq$ 3.5 mm^2, Fig. 3.1). The technique used for the measurements is described in Chapter 3.9. Usually, anorthosites are adcumulates with triple-point junctions and a more or less well developed foliation (Plate 3). In some cases, however, the grain boundaries are very irregular. Commonly this occurs in association with various strain features like bent grains and irregular twinning (Plate 4).

Intercumulus orthopyroxene and clinopyroxene, and in some cases olivine, may make up to 10% of the rock. Orthopyroxene and clinopyroxene may occur together; they are normally concentrated in the form of clusters, patches or "mottles" (in mining terminology). In that case they poikilitically enclose cumulus plagioclase.

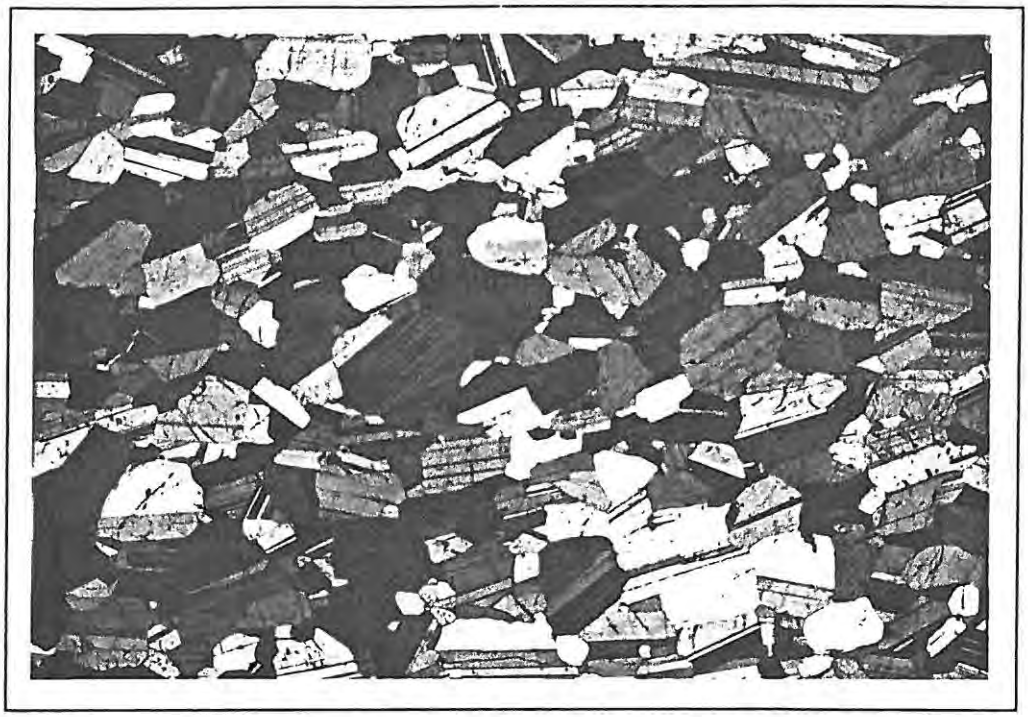

Plate 3: Plagioclase adcumulate showing triple-point junctions and foliation subparallel to the layering. Sample H3 1089.4b, anorthosite layer within Norite Marker. Field width 8.7 mm; crossed nicols.

Plate 4: Plagioclase adcumulate showing irregular grain boundaries, and irregular and bent twinning. Sample UA 642.8, Merensky footwall anorthosite. Field width 8.7 mm; crossed nicols.

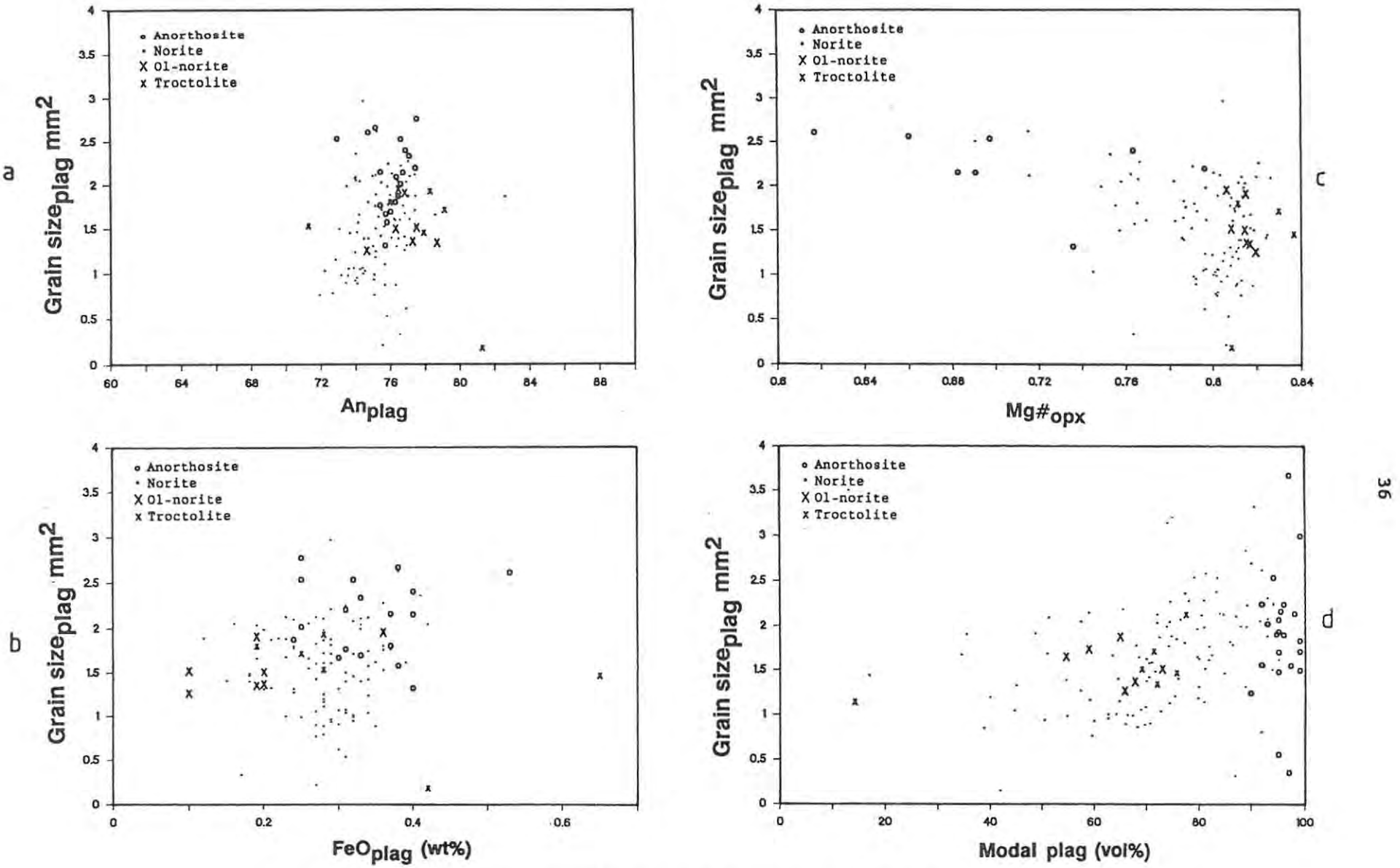

Fig. 3.1 Plots of grain size$_{plag}$ versus (a) An content of cumulus plagioclase, (b) FeO$_{plag}$, (c) Mg#$_{opx}$ (note that the number of anorthosites is smaller in this diagram because of the absence of orthopyroxene in many anorthosites), (d) modal proportion of cumulus plagioclase.

Occasionally, one may distinguish small, euhedral orthopyroxene crystals enclosed by intercumulus orthopyroxene. These euhedral crystals are, however, not chemically different from the intercumulus material. If one thus postulates that "mottles" grew around primary cumulus orthopyroxene, one must envisage equilibration as a process operating on a scale of several mm at least. These irregular patches or "mottles" may be orientated parallel to the layering, as illustrated in Plate 5.

Plate 5: Elongated "mottles" consisting of clinopyroxene poikilitically enclosing plagioclase chadacrysts. FW 6 anorthosite, Western Platinum Mine.

That plagioclase which is poikilitically enclosed shows a distinctively smaller average grain size and is usually not orientated parallel to the layering. Also, the grains are subrounded. The conclusion has been drawn before (Kruger, 1982) that these grains have been prevented from further growth (to form adcumulates) by the interstitial melt, which concentrated in certain areas through compaction of the semi-consolidated crystal pile. It is more likely that the intercumulus melt was expelled during crystal growth and concentrated in certain areas. The original grain sizes and shapes

have thus not been modified by inter-grain reactions or adcumulus processes, but possibly through resorption by the volatile-enriched intercumulus melt. Increased volatile fugacity leads to a depression of the plagioclase liquidus and solidus (Johannes, 1978).
Anorthosites, containing more than 5 vol% chromite, are referred to as chromitiferous anorthosites. This rock type, however, is very rare in the interval under review and is usually restricted to the immediate footwall of the Merensky Reef.

The zoning of plagioclase in anorthosites is not significantly different from zoning in norites and will be discussed in Chapter 4.9.

3.3 Norites and olivine norites

Norites and olivine norites are plagioclase-orthopyroxene-olivine-cumulates. Plagioclase rarely sinks below 50 modal per cent, thus remaining within cotectic proportions. This limits the frequency of occurrence of melanorites.

Grain sizes and textures in norites may be very variable. Plagioclase appears in the same way as in the anorthosites. Orthopyroxene is subhedral or anhedral. In the latter case, a rim of intercumulus overgrowth usually has developed around the grain, which totally obscures the original grain shape. In core LK7, two very fine-grained norite layers (orthopyroxene and plagioclase ca. 0.1 mm) occur in the FW 12 anorthosite (LK7 1575.95B, 1577.45). In respect of geochemical parameters, however, these norites are similar to other norites in the study section.

Olivine is usually mantled by a thin rim of orthopyroxene (Plate 6). The chemistry indicates that this rim is a reaction replacement feature (see Chapter 4.3 and 4.4). In this way, such olivine cores were effectively protected from further reaction with the melt.

Plate 6: Subhedral olivine mantled by orthopyroxene. A well-rounded plagioclase inclusion is situated in the center of the grain. Note the typically close association of biotite and olivine. Sample IN 865.52, FW 7 olivine norite. Field width 8.7 mm; crossed nicols.

Plate 7: Optically continuous clinopyroxene oikocryst poikilitically enclosing subhedral orthopyroxene and rounded, resorbed plagioclase chadacrysts. Note that orthopyroxene itself encloses plagioclase inclusions. Note also the plagioclase-free zone surrounding some of the orthopyroxene crystals. Sample H3 1118.5, FW 7 norite. Field width 8.7 mm; crossed nicols.

Chromite and biotite occur as accessory phases, the latter often being notably enriched in the olivine-rich rocks. Clinopyroxene occurs in the same way as in the anorthosites, as large, optically continuous oikocrysts (Plate 7).

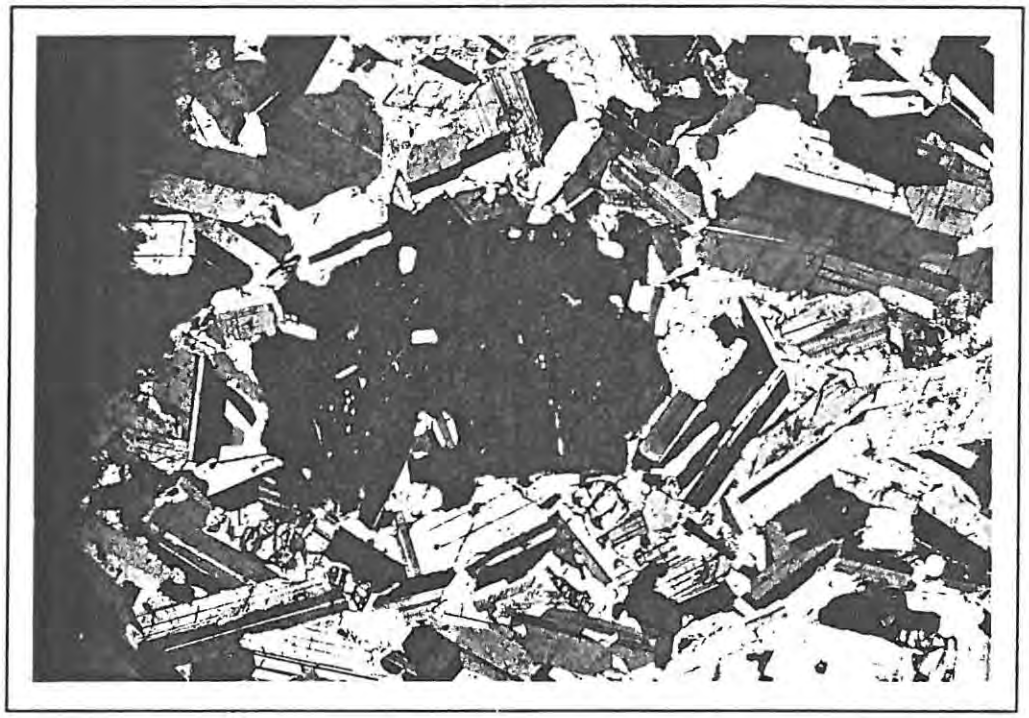

Plate 8: Orthopyroxene, hosting numerous well-rounded plagioclase inclusions. Note the highly resorbed plagioclase within the clinopyroxene rim zone of the orthopyroxene. Sample H3 1246.65, FW 7 leuconorite. Field width 8.7 mm; crossed nicols.

Both orthopyroxene and olivine often host numerous (up to 20) small (0.1-0.3 mm) and well-rounded plagioclase inclusions (Plate 6 and 8). In coexisting olivine and orthopyroxene, the inclusions tend to be smaller in olivine. Also, the number and size of inclusions seem to decrease with increasing modal amount of orthopyroxene. In pyroxenites and the P2 harzburgites they do not occur at all. It seems thus possible that orthopyroxene and olivine of norites crystallized from a liquid in which cumulus plagioclase was already present and subsequently became included in the ferromagnesian phases. However, it

is difficult to assess whether this plagioclase was on the liquidus or essentially out of equilibrium. In other words, did the liquid evolve from an anorthositic original composition or is it the mixing product of a residual plagioclase-bearing melt and a primitive influx ? Slight differences in composition between the inclusions and normal cumulus grains (see Chapter 4.2) as well as the rounded or embayed shapes (suggesting partial resorption) seem to support the second possibility at this stage.

3.4: Troctolites

Four types of troctolites occur in the study section. In Type 1 fine-grained subhedral olivine and plagioclase of ca. 1 mm^2 size occur in a ratio of 20% : 70% with the remaining 10% being orthopyroxene replacement-rims around olivine. As in all types of troctolites, numerous well-rounded plagioclase inclusions are dispersed throughout the olivine grain. A gradual change into olivine norite can be observed to occur. This variety of troctolite occurs towards the top of the central noritic part in profiles IM and $60E^3$ and contains a large amount of interstitial chromite as well as mica (Plate 9). The large amount of mica in olivine-bearing rocks has also been noted by McCallum et al. (1980) and Boudreau (1988) in the Stillwater Complex and by Teigler (1990) for the dunites of the Lower Zone of the Bushveld Complex.

The second variety (Type 2, Plate 10), which forms the FW 9 at locality IN, contains much larger olivine grains (up to 3.5 mm^2) and is also enriched in chromite and mica. The modal proportion of olivine to plagioclase has increased to 27% : 61%. The anhedral olivine grains are elongated subparallel to the layering and the outer zones of the grains develop an interstitial habit between surrounding cumulus plagioclase grains (Plate 11).

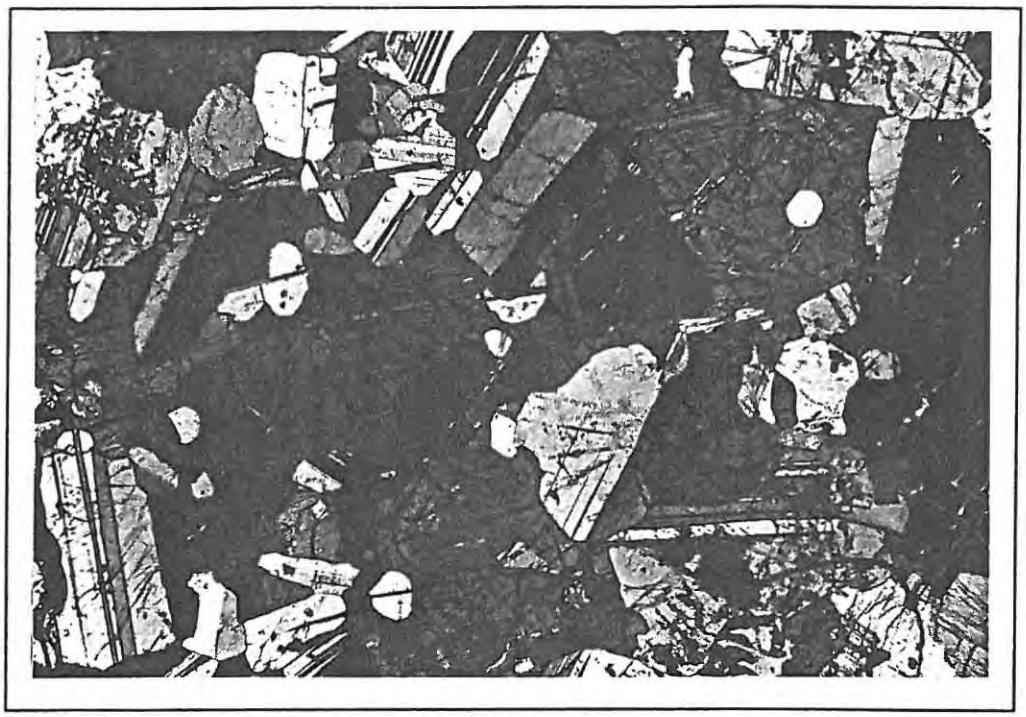

Plate 9: Olivine and plagioclase chadacrysts poikilitically enclosed by an orthopyroxene oikocryst. Note the extremely well-rounded plagioclase inclusions within olivine and the more irregularly resorbed inclusions within orthopyroxene. Note also the abundant mica with its preferred orientation. Sample IM 798.0, FW 7 Type 1 - troctolite. Field width 3.5 mm; crossed nicols.

Plate 10: Olivine crystal elongated subparallel to the layering, with numerous plagioclase inclusions. Note the orientated mica flakes distributed across the entire field perpendicular to the layering. Sample IM 819.85, FW 8 Type 2 - troctolite. Field width 8.7 mm; crossed nicols.

Plate 11: Olivine containing numerous plagioclase inclusions. The rim zone of the grain develops an interstitial habit. Sample IN 866.4, FW 9 Type 2 - troctolite. Field width 8.7 mm; crossed nicols.

The third variety of troctolite (Type 3, Plate 12) is very similar to the second in its texture. The anhedral character of the olivine grains has become more pronounced and a rim of interstitial orthopyroxene, poikilitically enclosing small plagioclase grains, has developed around the core. The plagioclase inclusions within the olivine core are markedly less rounded than those in the other types of troctolite. The macroscopic appearance is very much that of a mottled anorthosite and textural and geochemical properties possibly suggest the olivine to be postcumulus. The two-dimensional concentration of the olivine-orthopyroxene mottles usually is about one per 10 cm^2.

Finally, a fourth extremely fine-grained variety of troctolite (Type 4, plagioclase and olivine of up to 0.2 mm^2 size) occurs only as a thin (2 cm) layer in the Norite Marker at locality H3. It shows extremely high An values of plagioclase (An_{81}). Similarly high values were also found in one Type 1 troctolite at intersection EK22.

Plate 12: Olivine-bearing "mottle" with sub-rounded plagioclase inclusions enclosed by the olivine in the core. Note the selvage of poikilitic orthopyroxene. Sample IM 841.66, FW 12 Type 3 - troctolite. Field width 8.7 mm; crossed nicols.

3.5: Pyroxenites

Invariably, pyroxenites in the study section are orthopyroxenites. The prefix "feldspathic" as per definition implies that the rock contains more than 20 % interstitial plagioclase (Plate 13). The majority of pyroxenites in the study section are meso- or orthocumulates, adcumulates being less common (Plate 14). As will be argued in Chapter 4.9.1, what appears to be intercumulus plagioclase may occasionally consist of a cumulus core and an intercumulus overgrowth zone, by which the original grain boundaries have been obscured. Besides orthopyroxene and plagioclase, pyroxenites in the study section contain varying amounts of intercumulus clinopyroxene, biotite, chromite and sulphides. In one case (the UG2 pyroxenite in profile IM) oxyhornblende forms a major component of the rock (Plate 15).

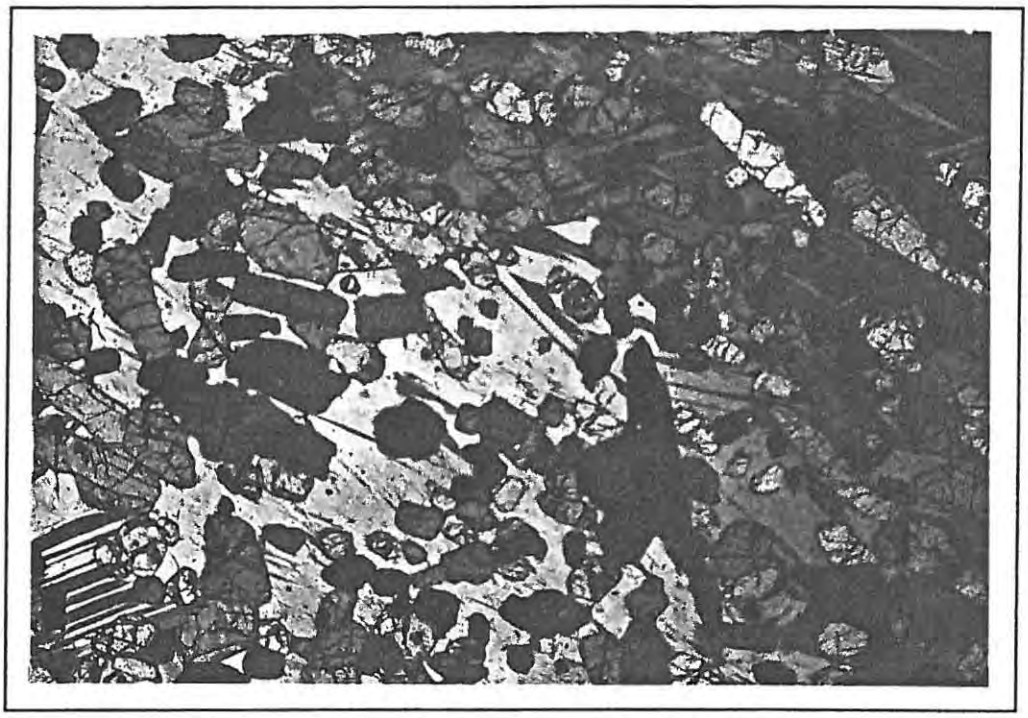

Plate 13: Foliated orthopyroxene orthocumulate. Sample LK7 1584.23b, UG2 pyroxenite. Field width 8.7 mm; crossed nicols.

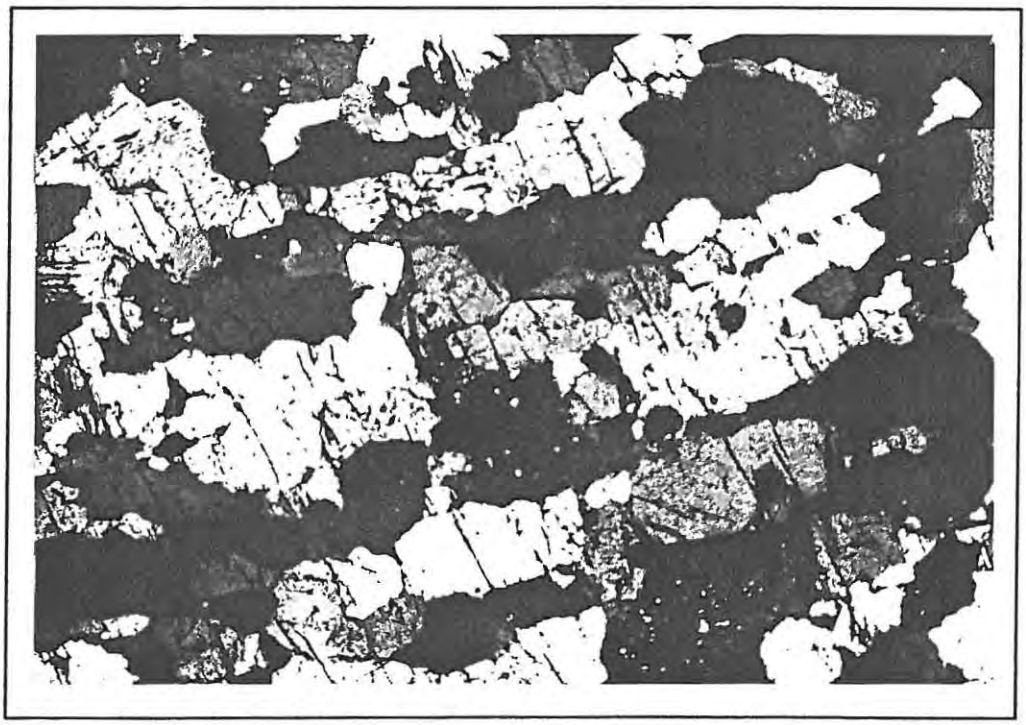

Plate 14: Foliated orthopyroxene adcumulate. Sample IN 871.93, UG2 pyroxenite. Field width 8.7 mm; crossed nicols.

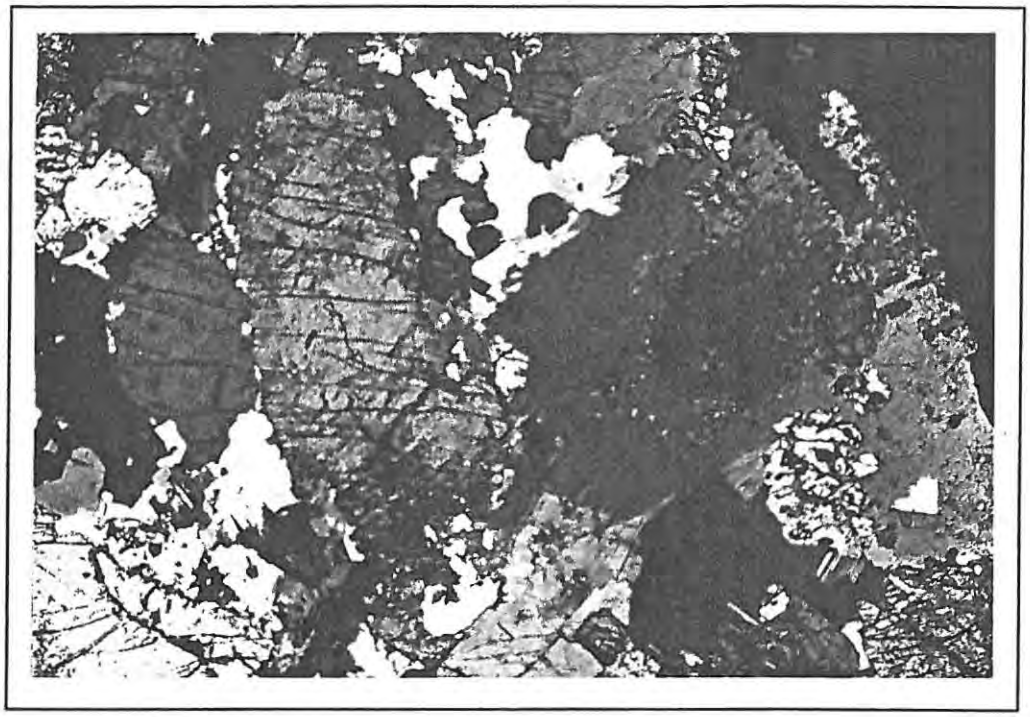

Plate 15: Oxyhornblende replacing clinopyroxene (centre right). Sample IM 851.9, UG2 pyroxenite. Field width 8.7 mm; crossed nicols.

The UG2 pyroxenite at locality H3 displays near perfect upwards-gradation in grain size, degree of lamination, and amount of intercumulus plagioclase and interstitial chromite, as well as cryptic variation in the composition of orthopyroxene (Fig. 3.2(a)). Over approximately 8 m, the grain size of orthopyroxene increases from ca. 1 mm^2 to more than 10 mm^2 upwards. Perfect lamination of euhedral orthopyroxene at the base gradually deteriorates into random orientation of subhedral to anhedral grains towards the top. The amount of intercumulus plagioclase increases from 8 vol% to 16 vol% and chromite decreases from 7 to zero vol%. Observation of these trends, however, requires careful sample preparation as the orientation of the slide determines the apparent amount of foliation and hence the proportion of intercumulus plagioclase. A similar trend in grain size can be observed at intersection UA (Fig. 3.2(b)).

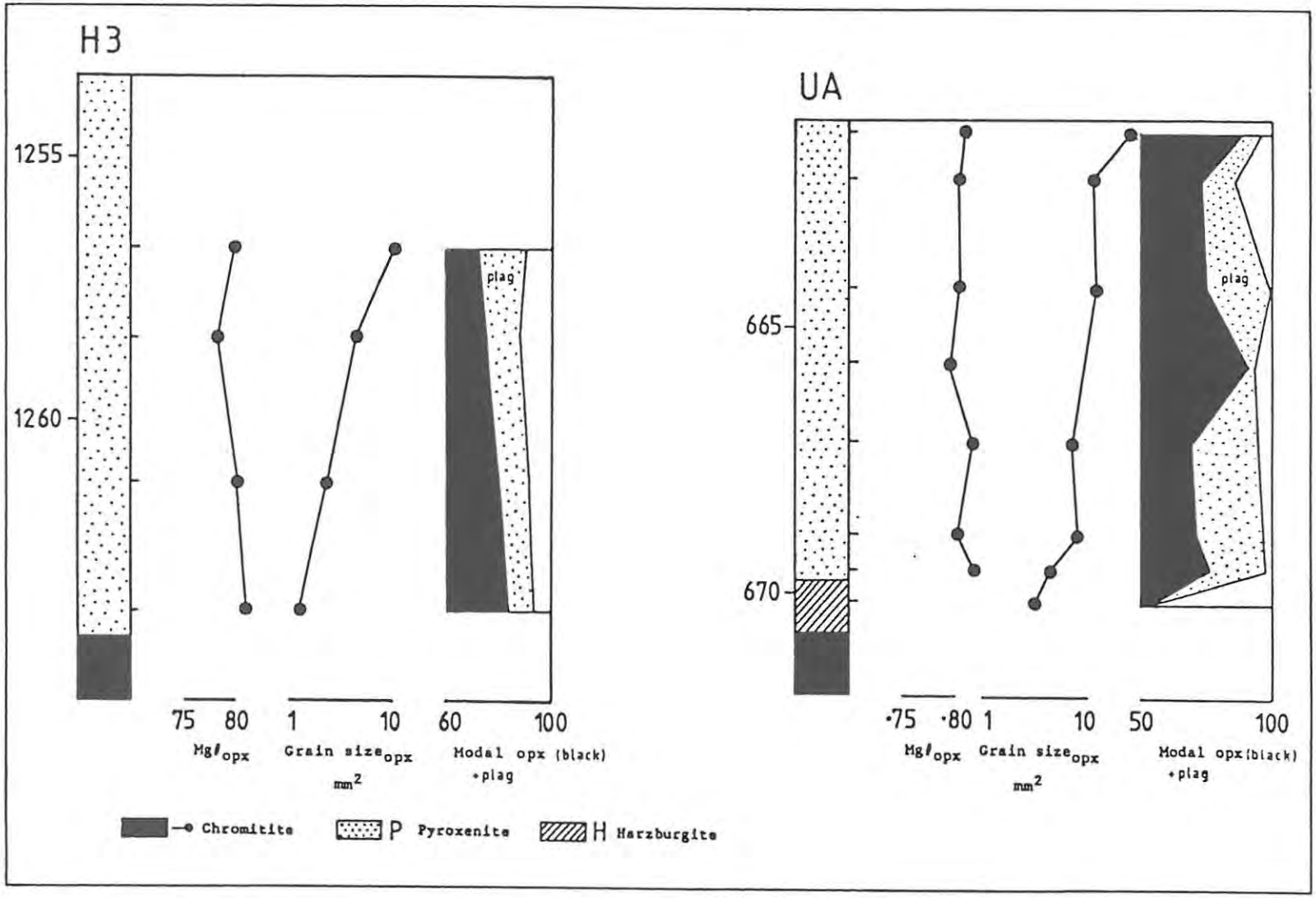

Fig. 3.2 Variations in composition, grain size and modal percentage of orthopyroxene in the UG2 pyroxenite at (a) intersection H3, and (b) intersection UA.

Besides its usual appearance as an interstitial phase, rims around plagioclase and exsolution lamellae in orthopyroxene, clinopyroxene in pyroxenites occasionally occurs as large oikocrysts of up to 2 cm diameter, poikilitically enclosing small (ca. 1 mm^2) rounded orthopyroxene inclusions.

3.6: Harzburgites

Harzburgites are relatively rare in the study section. Two types of harzburgites can be distinguished, poikilitic and granular harzburgites, as defined originally by Jackson (1961). Olivine is the only cumulus phase in the poikilitic variety (Plate 16), where orthopyroxene poikilitically encloses it and may constitute up to 50 vol% of the rock. The granular variety of harzburgite consists of cumulus olivine and orthopyroxene and is relatively uncommon in the Upper Critical Zone.

Plate 16: Serpentinized olivine mantled by optically continuous orthopyroxene. The original shape of the olivine crystals prior to reaction replacement is outlined by chromite. Sample BM 277.3a, P1 Marker, poikilitic harzburgite + top chromitite stringer. Field width 8.7 mm; crossed nicols.

Poikilitic textures are characteristic of a system which is cooled slowly (Lofgren, 1980) or, in other words, they are conceivably related to deferred crystallization. This may be envisaged in an intercumulus environment when late-stage components like H_2O and other volatiles become enriched and liquidus relationships are depressed.

Both types of harzburgites occasionally contain cuspate, sub-rounded, strongly resorbed plagioclase grains (Plate 16). They are often characterized by anomalously high An contents. The alteration products magnetite and serpentine are common phases in harzburgites, and biotite and chromite also appear to be above the average modal value for pyroxenites. Occasionally, orthopyroxene is completely absent from the rock, especially in parts of the P2 Marker (Plate 17). In this case, the rock must be classified as a dunite (Streckeisen, 1974).

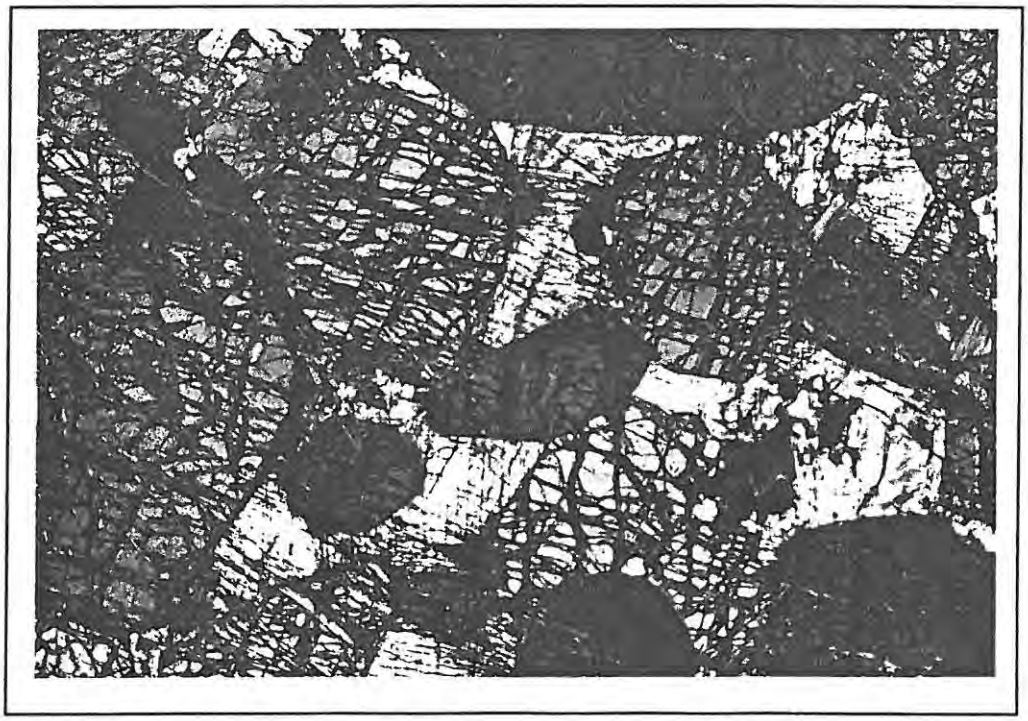

Plate 17: Subhedral olivine chadacrysts enclosed by poikilitic plagioclase. Minor poikilitic orthopyroxene can be seen in upper left corner. Sample AM 8b, P2 Marker dunite. Field width 8.7 mm; crossed nicols.

3.7: Ultramafic Pegmatoids

Ultramafic pegmatoids mainly occur sporadically beneath, within or directly above mafic layers or lenses such as chromitites, harzburgites and pyroxenites. Exceptions are the "boulders" of the Boulder Bed, which are hosted by anorthosite, and the rare occurrence of thin (ca.15 cm) layers or lenses of ultramafic pegmatoid in the central noritic part of intersection LK5 and in the melanorite of the Norite Marker at intersection KR2.

Ultramafic pegmatoids in the study section are more usually pyroxenites, olivine pyroxenites or harzburgites, showing grain sizes of the cumulus phases of up to 3 cm. Upward migration of volatiles and other late-stage fluids which led to recrystallization has been proposed to explain them (Barnes & Campbell, 1988).

The pegmatoids usually show elevated proportions of mica, clinopyroxene, quartz, graphite, sulphides and the chloride ion (Schiffries, 1984; Ballhaus & Stumpfl, 1985 a,b,c; Boudreau, 1988). Graphite plates up to 1m size have been recorded in the Merensky pegmatoid (de Klerk, 1989, pers.com.). Thin chromitite stringers (1 mm - 1 cm wide) are commonly associated with pegmatoids at their bottom and top contacts and it is believed by some authors that such chromitites are of secondary nature (Lee & Viljoen, 1983; Boudreau, 1988).

3.8: Chromitites

Chromitites in the interval under review can be subdivided into 3 varieties: (i) massive chromitites (the UG2 chromitite in intersection LK7), (ii) thin isolated chromitite stringers which are loosely packed and usually unannealed (the Lone Chrome Seam, Plate 18), and (iii) thin stringers of highly annealed chromite which are possibly secondary or reaction chromitites and which are usually associated

with ultramafic rocks (e.g., the Merensky Reef, P2-A and -B Marker top and bottom chromitites).

Plate 18: Chromitite stringer in anorthosite. Chromite grains are mostly euhedral and unannealed. Note the undulating lower contact of the stringer. Sample LK7 1424.28a, Lone Chrome Seam. Field height 8.7 mm; crossed nicols.

In the first two varieties, euhedral to subhedral chromite grains of varying size are usually unannealed and separated from each other by cumulus plagioclase or orthopyroxene. Different grain sizes are commonly arranged in distinguishable layers. This mode of occurrence, however, is not necessarily typical of the UG2 chromitite in general (Eales, 1991, pers. com.).

The third variety ((iii) above) consists of totally annealed chromite stringers. The grains have coalesced to yield clusters of lobate and cuspate forms which may or may not be concentrated to form more or less massive chromitite stringers. It is unlikely that these stringers represent a more compacted variety of chromitite, as one would expect the massive chromitites to be the most compacted. Models of Boudreau (1988) and Lee & Viljoen (1983) suggest that this type of chromitite is a reaction chromitite.

3.9: Grain Size Measurements

Grain size measurements on cumulus plagioclase have been performed on 180 samples from 6 cores (EK22, IN, IM, LK7, H3, KR2, see Appendix III). A method of measurement was chosen in which the long and short axes of the 20 largest cumulus grains of each slide were used to calculate an average size representative for each slide. Grains which are more than 30% larger than the average value of chosen grains were excluded as they could represent phenocrysts. The relatively small number of measurements has been chosen to keep the modal effect small, i.e., the smaller the modal proportion of plagioclase within the area of a slide of normal size, the more small grains will fall into the category of the 20 largest grains. On the other hand, this method obviously limits the statistical reliability of the measured average value and introduces some subjectivity. The study of grain sizes that follows is thus to be regarded as no better than semi-quantitative.

Remeasurements of the same slide 3 months after the initial measurement (listed below) have shown a relatively small difference in computed averages:

LK7 1562.25	First result:	2.61 mm^2	
	Second result:	2.45 mm^2	6% deviation
LK7 1446.20	First result:	0.94 mm^2	
	Second result:	1.03 mm^2	9% deviation

Standard deviations have been calculated for all measurements in one representative core (Fig. 3.3). A positive correlation between mean grain size and standard deviation can be observed illustrating that the larger grain sizes show a higher standard deviation. This result was to be expected, as the maximum average grain sizes usually represent a wider range of grain sizes measured.

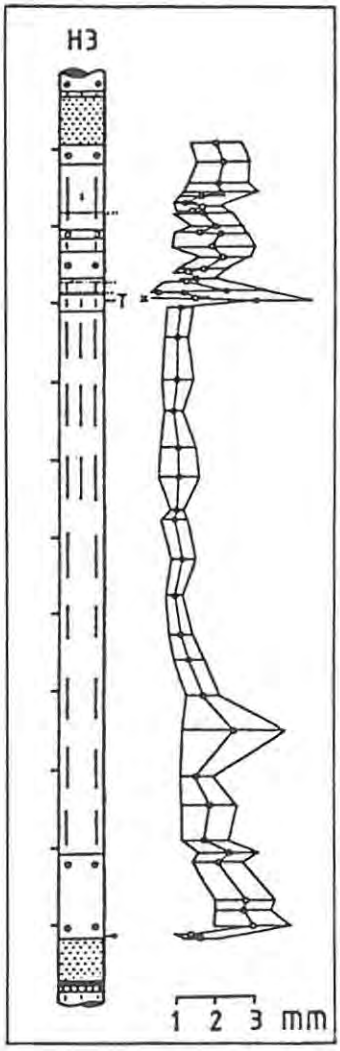

Fig. 3.3 Standard deviation (1σ) of grain size of plagioclase, displayed for one representative core

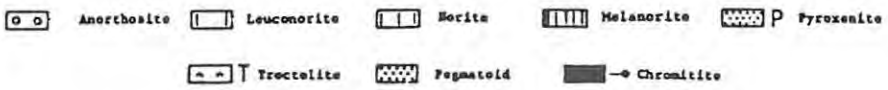

Fig. 3.1c shows a plot of grain size of cumulus plagioclase against $Mg\#_{opx}$ (determined by microprobe methods to be described later). A weak negative correlation can be detected in that low $Mg\#_{opx}$ (mostly anorthosites) is correlated with slightly larger grain sizes. Grain sizes are decoupled from both An and FeO contents of plagioclase (Fig. 3.1(a) and (b)). It is of interest to note that An contents of plagioclase are entirely decoupled from $Mg\#_{opx}$ (Fig. 4.3(c)). In summary, the composition of cumulus plagioclase seems to be decoupled from variations in the chemistry of orthopyroxene but small grain sizes of cumulus plagioclase are associated with more primitive compositions of orthopyroxene.

In Fig. 3.4 grain sizes of plagioclase are plotted against $Mg\#_{opx}$ for individual cores. Apparently in contradiction to the observations above, the diagrams show that the intersections which are located proximally to the presumed feeder zone at Union Section (cores EK22, IN, IM) seem to show a larger mean grain size than the south-eastern intersections (LK7, H3, KR2), i.e., they lack the smaller grain sizes. The present author believes this to be related to adcumulus enlargement of grain sizes due to a more prolonged and more intense heat flux in the areas proximal to the feeder, which leads to more complete textural equilibration. According to Maaløe (1976) and Hunter (1987) a process could be envisaged where larger grains grew at the expense of smaller grains in a postcumulus environment, thus reducing the ratio of surface area to volume and, hence, the free energy of the melt-crystal interface. This possibly renders the general correlation between grain size of plagioclase and $Mg\#_{opx}$ weak but, as can be seen in Fig. 3.4(a), the individual cores still show the above-mentioned pattern of smaller grain sizes with higher $Mg\#_{opx}$.

A weakly positive correlation is established between grain size and modal proportion of plagioclase (Fig. 3.1(d)): anorthosites on average display slightly larger grain sizes than other rock types.

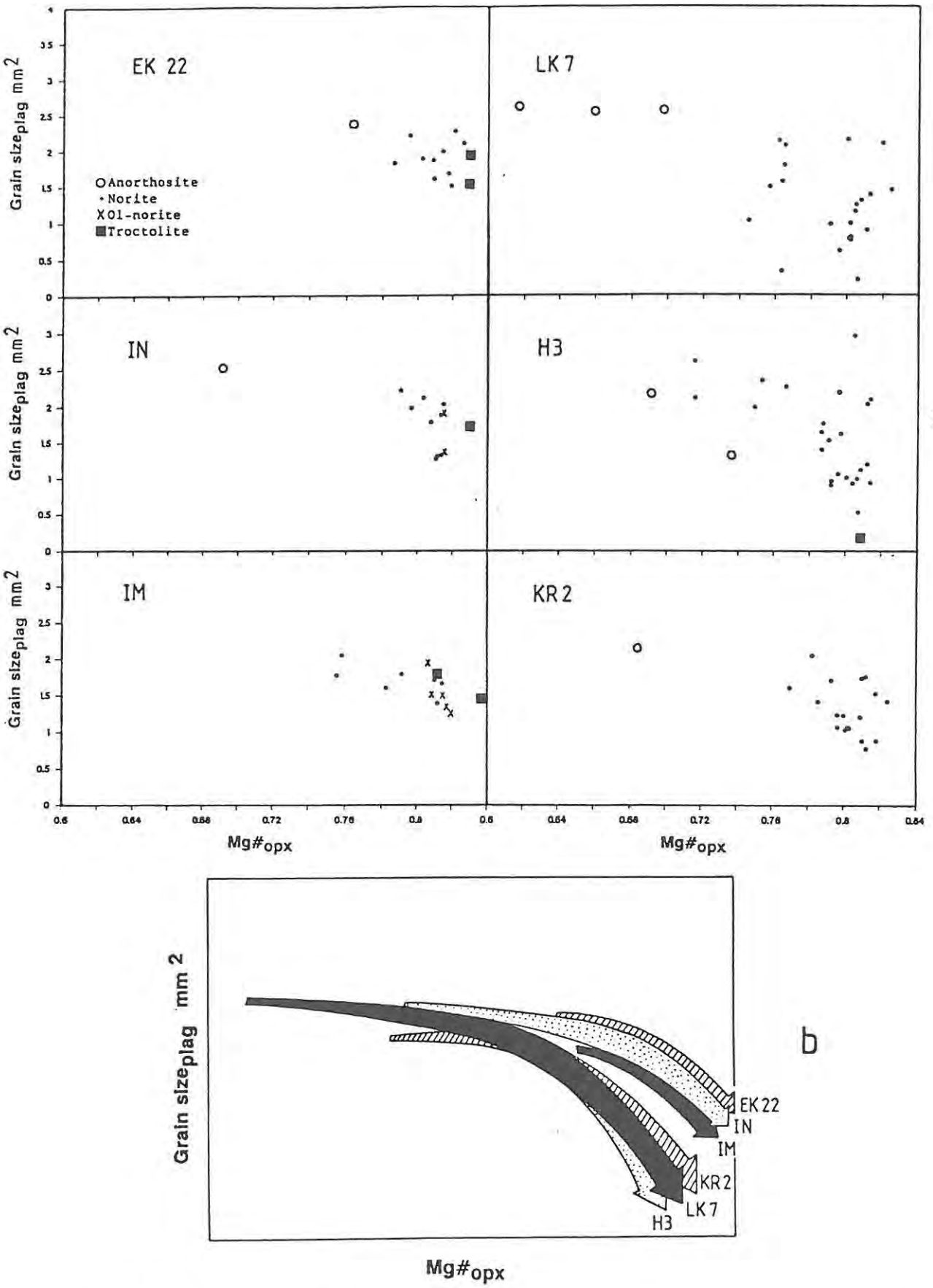

Fig. 3.4 (a) The data of Fig. 3.1(c) are separately plotted for the individual cores here, and (b) generalized trends drawn from the data.

The distribution of grain sizes has been investigated in one pure unfoliated anorthosite (EK22 267.7). It is difficult to interpret the result (Fig. 3.5), which shows an exponential distribution of grain sizes. The importance of factors like modification of primary grain sizes through textural equilibration, i.e., adcumulus growth (Morse, 1980, 1986), sintering (Reynolds, 1979), growth of larger grains at the expense of small grains (Maaloe, 1976; Hunter, 1987)) and the "cut effect" (orientation and positioning of the slice cut from the borehole core sample) is not possible to evaluate in the scope of the present study.

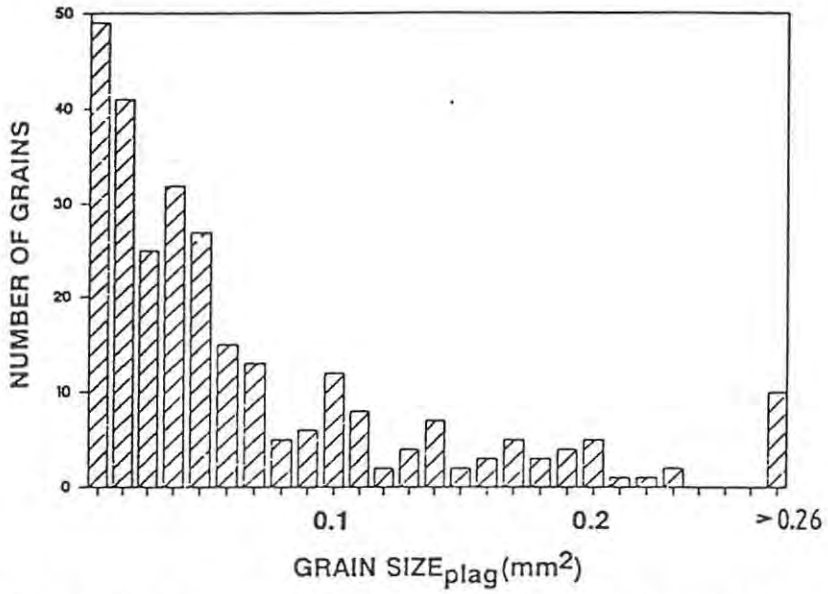

Fig. 3.5 Grain size distribution in an unlaminated anorthosite (sample EK22 267.7).

Grain size variations with stratigraphic height in layered intrusions have been described by a number of authors (Jackson, 1961; McDonald, 1967; Cameron, 1969; Irvine, 1974; McBirney & Noyes, 1979; Botha, 1987; Teigler, 1990). Both upwards-increasing and -decreasing grain size of various minerals have been observed in individual cyclic units (see Teigler, 1990). In the study section, grain sizes of orthopyroxene have been measured in the UG2 pyroxenite and show increasing size with stratigraphic height in some of the cores (UA, IN, TF, LK7, H3, see Fig. 3.2(a) and (b)). This trend correlates with

upwards-decreasing $Mg\#_{opx}$. No systematic trend could be detected in the central noritic part, with orthopyroxene showing the same grain size over ca. 125 m of norite in profile LK7. Grain size variations of plagioclase with stratigraphic height are discussed in more detail in Chapter 7.11.

Bowen (1915), Irvine (1974), and McDonald (1967) explained grain size variations by different processes of gravitative accumulation. Teigler (1990) favoured control of grain sizes of orthopyroxene by the nucleation rate. Thus, a high rate of nucleation should lead to small grain sizes and meso- to adcumulate textures. Similarly, a low rate of nucleation should lead to large grain sizes, more pore space and the formation of orthocumulates. This, however, is not the case in the UG2 pyroxenite, where the smallest grain sizes are frequently developed in orthocumulates with up to 40% pore space. Perfect orthopyroxene adcumulates within the measured profiles usually display the largest grain sizes (see also Naldrett & Wilson, 1990).

3.10: Rock modes

A total of 180 slides from 5 cores have been point-counted with an average point density of between 300 and 400 points per slide (see Appendix II). The results for the modal proportion of combined cumulus orthopyroxene and olivine are plotted against $Mg\#_{opx}$ in Fig. 3.6. The most important point to note is that the modal proportion of cumulus orthopyroxene and olivine increases with increasing $Mg\#_{opx}$ in norites and pyroxenites. Furthermore, pyroxenites and norites define two discrete compositional fields.

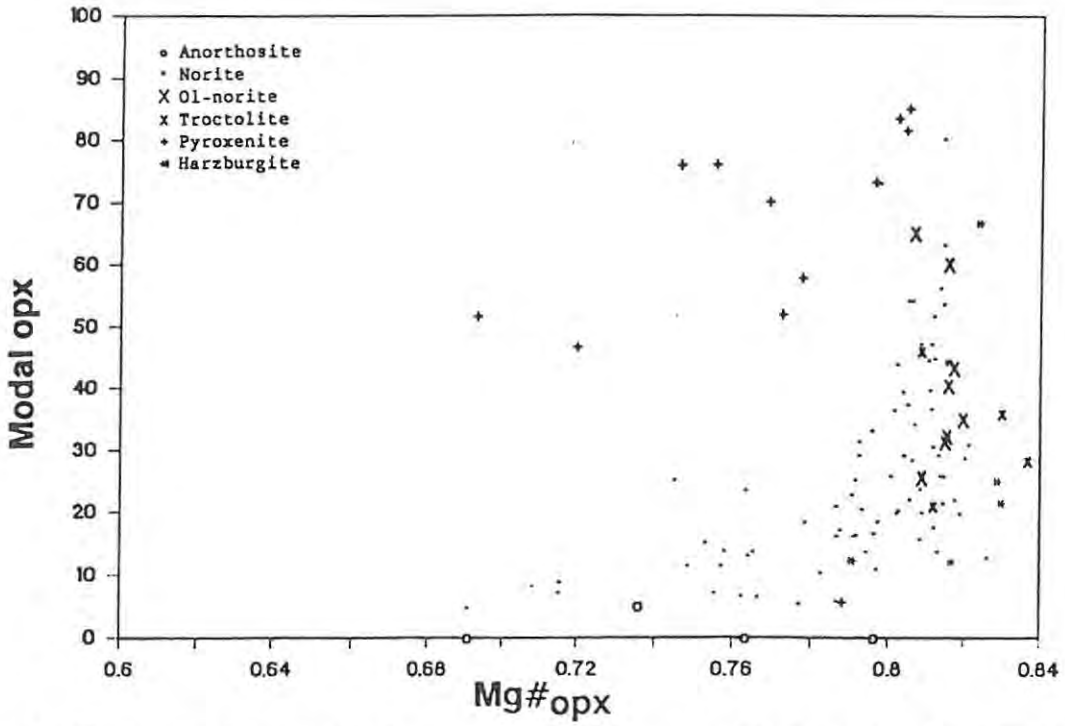

Fig. 3.6 Plot of modal percentage of orthopyroxene versus $Mg\#_{opx}$ shows two different compositional fields and trends: a noritic - olivine noritic - troctolitic field and a pyroxenitic field. Both correlations are positive in that rocks with high modal orthopyroxene tend to be high in $Mg\#_{opx}$.

Average modal compositions of the various rock types are presented in Table 3.1. Note that anorthosites, as defined in Chapter 1.5, contain no cumulus orthopyroxene. Table 3.2 presents a comparison of average modal compositions of norites, olivine norites and pyroxenites in the individual profiles. No systematic regional trend can be detected.

A more detailed discussion, involving a comparison of variations of modal compositions with stratigraphic height in the different cores will be presented in Chapter 7 (Fig. 7.5).

Table 3.1: Average modal compositions of the various rock types in the study interval (Pla = plagioclase, Opx = orthopyroxene, Ol = olivine, Chr = chromite, Cpx = clinopyroxene, cum = cumulus, ic = intercumulus, n = number of analyses)

Rock type	Pla(cum)	Opx(cum)	Ol	Chr	Pla(ic)	Opx(ic)	Cpx	Other	Total	n
Anorthosites	95.1	0.0	0.0	0.1	0.0	1.2	1.5	2.0	100.0	35
Leuconorites	78.4	17.6	0.0	0.1	0.0	0.7	2.3	0.9	100.0	85
Norites	47.7	45.8	1.4	0.2	0.1	0.1	2.8	2.0	100.0	22
Melanorites	25.1	73.0	0.0	0.0	1.8	0.0	0.0	0.2	100.0	2
Pyroxenites	0.1	74.1	0.0	1.2	13.0	0.5	4.5	6.6	100.0	19

Granular harzburgite	Pla(cum)	Opx(cum)	Ol	Chr	Pla(ic)	Opx(ic)	Cpx	Other	Total
EK22 299.1	0.0	42.3	32.7	0.3	12.4	8.6	0.9	2.8	100.0

Dunite	Pla(cum)	Opx(cum)	Ol	Chr	Pla(ic)	Opx(ic)	Cpx	Other	Total
EK22 295.7	0.0	0.0	91.7	0.3	7.0	0.0	0.0	1.0	100.0

Poikilitic harzburgites	Pla(cum)	Opx(cum)	Ol	Chr	Pla(ic)	Opx(ic)	Cpx	Other	Total
EK22 299.8	0.0	0.0	43.9	0.3	6.8	45.1	0.0	3.9	100.0
EK22 299.95	0.0	0.0	12.1	1.0	6.9	72.8	5.1	2.1	100.0
EK22 296.9	0.0	0.0	66.3	0.3	2.2	28.9	0.0	2.3	100.0
Mean	0.0	0.0	40.8	0.5	5.3	48.9	1.7	2.8	100.0

Troctolites	Pla(cum)	Opx(cum)	Ol	Chr	Pla(ic)	Opx(ic)	Cpx	Other	Total
IM 797.25	71.0	3.9	20.5	1.5	0.0	0.0	1.0	2.1	100.0
IM 798.00	67.0	6.5	21.4	1.5	0.0	0.0	1.6	2.0	100.0
IN 866.40	61.2	8.9	26.8	1.8	0.0	0.0	0.6	0.7	100.0
EK22 288.4b Top	35.5	0.0	31.7	3.1	0.0	26.6	0.0	3.1	100.0
EK22 288.90a	77.5	0.0	21.4	0.5	0.0	0.0	0.3	0.3	100.0
EK22 291.48	71.4	0.0	24.9	0.3	0.0	1.1	0.0	2.3	100.0
Mean	63.9	3.2	24.5	1.5	0.0	4.6	0.6	1.8	100.0

Table 3.2: Modal compositions of norites, olivine norites and pyroxenites in individual profiles (Pla = plagioclase, Opx = orthopyroxene, Ol = olivine, Chr = chromite, Cpx = clinopyroxene, cum = cumulus, ic = intercumulus, n = number of analyses)

Norites	Pla(cum)	Opx(cum)	Ol	Chr	Pla(ic)	Opx(ic)	Cpx	Other	Total	n
EK22	78.8	17.2	0.0	0.1	0.1	1.4	1.7	0.9	100.0	11
IN	67.4	30.3	0.0	0.2	0.0	0.3	1.6	0.2	100.0	11
IM	70.9	23.8	0.0	0.0	0.0	1.3	2.6	1.4	100.0	10
LK7	75.6	20.2	0.0	0.0	0.0	0.6	3.0	0.7	100.0	36
H3	66.1	28.7	0.7	0.3	0.2	0.2	2.3	1.6	100.0	41

Olivine norites	Pla(cum)	Opx(cum)	Ol	Chr	Pla(ic)	Opx(ic)	Cpx	Other	Total	n
IN	67.3	27.2	4.5	0.0	0.0	0.1	0.8	0.1	100.0	7
IM	64.2	26.8	6.4	0.1	0.0	0.0	1.2	1.5	100.0	7

Pyroxenites	Pla(cum)	Opx(cum)	Ol	Chr	Pla(ic)	Opx(ic)	Cpx	Other	Total	n
EK22	0.0	75.9	0.0	2.1	20.7	0.0	0.0	1.3	100.0	3
IN	0.0	84.1	0.2	0.6	7.4	0.0	7.2	0.5	100.0	5
IM	0.0	58.1	0.0	0.0	9.5	0.0	3.7	28.7	100.0	3
LK7	0.0	63.3	0.0	0.0	21.5	0.5	7.8	7.0	100.0	4
H3	0.3	78.8	0.0	2.6	11.4	2.3	1.6	3.0	100.0	4

3.11: Summary

The interval between the Merensky Reef and the UG2 chromitite is characterized by the abundance of a great variety of rock types. A number of features are worthy of note:

- Grain sizes of plagioclase are decoupled from the composition of plagioclase. This implies that they were subjected to significant modification after accumulation. This modification possibly included growth of large grains at the expense of smaller grains and led to adcumulates.

- The modal proportion of orthopyroxene and olivine is coupled with grain size variations of plagioclase, i.e., high proportions of orthopyroxene and olivine are correlated with smaller grain sizes of plagioclase. The modal proportion of the two ferromagnesian phases is coupled with their composition, i.e., a high proportion of

orthopyroxene and olivine corresponds with higher $Mg\#_{opx}$ within these rocks (note, however, that orthopyroxene in norites frequently displays higher Mg# and Cr content than orthopyroxene in pyroxenites).

- Anorthosites as defined in the study section (see Chapter 1.5), contain no cumulus orthopyroxene. Intercumulus orthopyroxene and clinopyroxene are usually concentrated in the form of clusters or so-called "mottles".

- Plagioclase in norites and olivine norites rarely declines below 50 vol%, thus limiting the frequency of melanorites. Both orthopyroxene and olivine within the two rock types usually host numerous small, well-rounded plagioclase inclusions.

- Four types of troctolites can be distinguished in the study section: (i) fine-grained and laminated (ii) coarser-grained, with anhedral olivine being elongated sub-parallel to the layering, (iii) coarse-grained, with extremely anhedral olivine occurring as clusters, strongly resembling "mottles" of anorthosites, and (iv) extremely fine-grained, only occurring in one sample within the Norite Marker of profile H3.

- Pyroxenites usually occur as meso- or orthocumulates; adcumulates are rare.

- Two types of harzburgite can be observed - a granular variety, which is very rare in the study section, and a poikilitic variety.

- Chromitites can be subdivided into three types within the studied interval: (i) massive chromitites (i.e. the UG2 chromitite), (ii) thin, isolated chromitite stringers (i.e. the Lone Chrome Seam), and (iii) thin chromitite stringers associated with ultramafic rocks (i.e. the Merensky Reef and the top and bottom chromitites of the P2-A and -B Markers).

CHAPTER 4: MINERAL CHEMISTRY

4.1: Introduction

The following chapter focuses on the chemistry of the most important mineral phases. Compositional variations of mineral and whole-rock data with stratigraphic height will be discussed in Chapter 6. A comparison (and correlation) along strike of mineral chemistry, whole-rock chemistry, and petrographical data in the individual intersections will be reserved for Chapter 7. Approximately 5500 microprobe analyses on ca. 270 samples have been executed for this study (orthopyroxene: 1600 analyses / 258 samples; cumulus and intercumulus plagioclase: 2500 / 240; plagioclase inclusions: 600 / 100; olivine: 200 / 40; chromite: 500 / 80; clinopyroxene: 60 / 20; plus representative analyses of amphibole and mica). Compositions adopted for individual samples represent average values of about 6 grains for orthopyroxene, 10 for plagioclase, 4 for plagioclase inclusions, 5 for olivine, 5 for chromite and 3 for clinopyroxene. Invariably, averages given are core compositions. Orthopyroxene, plagioclase, chromite and olivine were constantly checked for compositional zonation (see Chapter 4.9).

All analyses were executed at Rhodes University on a Jeol CXA-733 Superprobe. Throughout the 3 years of microprobe investigation, a beam diameter of 10 μm (orthopyroxene: 20 μm) was selected and check-calibrations of the instrument were performed on a weekly basis. A number of secondary in-house standards have been constantly monitored to measure possible instrumental drift on a daily basis. Focused 1 μm beam methods were used when minerals were analysed for zonation. Ranges of 2σ standard deviation on the average values (95% statistical confidence limit) are presented for one representative core in Fig. 7.1. Throughout this chapter the terms Fo and $Mg\#_{Ol}$ will be used synonymously for the cationic ratio of $Mg/(Mg+Fe^{2+})$ in olivine.

4.2: Plagioclase Feldspar

The feldspar minerals of the study section consist almost exclusively of members of the triclinic plagioclase binary system $NaAlSi_3O_8$ (albite) - $CaAl_2Si_2O_8$ (anorthite; Fig. 4.1). In rare cases, K_2O contents of up to 9 wt% have been measured in some orthopyroxene-hosted feldspar inclusions showing that K-feldspar does exist as a discrete phase here. The framework structure of feldspar may also host Rb, Sr, Pb, Ba, Fe^{2+}, Mg, Ti and P (Smith, 1975), while the tetrahedral site might accommodate minor amounts of B, Ga, Ge, and Fe^{3+}. Of these cations, only Fe^{2+} has been analysed in the present study.

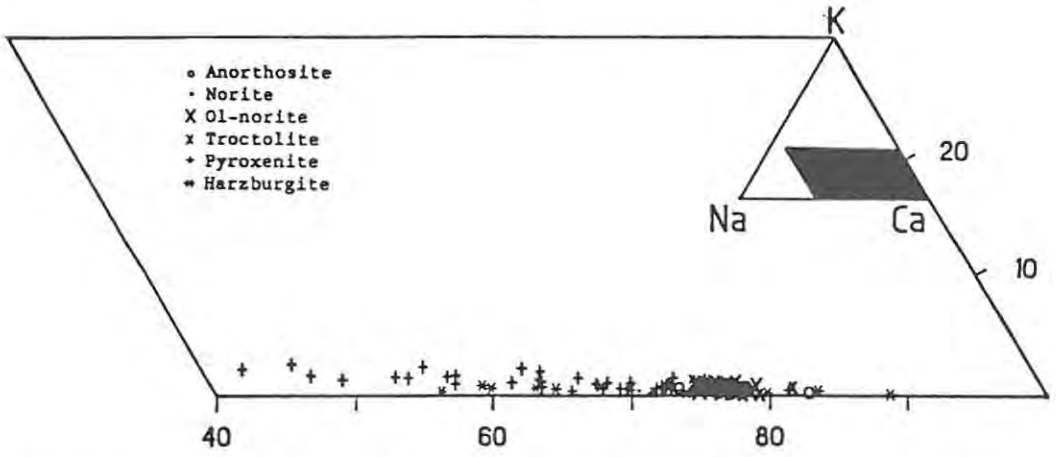

Fig. 4.1 Compositional range of plagioclase feldspar in the study section. Intercumulus plagioclase of pyroxenites shows the highest albite (and orthoclase) content.

Plagioclase feldspar shows apparently continuous solid solution between the albite (melting point at 1100°C in the pure anhydrous system) and the anorthite end-member (1550°C; Bowen, 1915). In reality, the situation is highly complex and imperfectly understood at the present time (Voll, 1971; Smith, 1975) with the existence of at least three solvi being known, but the present study does not address this aspect. As perfect equilibrium conditions are probably never attained and cation diffusion in plagioclase is very slow, zoned

crystals are superficially useful as a crude geothermometer, and consequently as an indicator of the history of the magma chamber. For various reasons, however, it is difficult to interpret compositional variations in plagioclase. The density differences between plagioclase and the host-magma are supposedly very small. Plagioclase is therefore likely to be carried in suspension for a long time and various types of zoning can occur in one grain.

Compositional reversals in successive zones may reflect supercooling due to a high cooling rate or reheating in response to a new magma influx. The cooling history of the chamber determines the amount of supercooling. Small, fast cooling chambers are likely to experience more supercooling than slowly cooling large bodies, which might have experienced frequent influxes of new magma. The degree of supercooling is critical as it is a major factor determining the plagioclase composition.

Changing volatile fugacities may also cause strong zonation. Boudreau (1988) noted that the addition of a volatile-rich fluid ($CaCl_2$) to a volatile-undersaturated melt will lower the liquidus and solidus temperatures of plagioclase and lead to preferential melting of the albite component (see also Johannes, 1978; and a summary of his data presented here in Fig. 4.2). In this way, calcic rims might be produced and additional silica set free.

$$2NaAlSi_3O_8 + CaCl_2 = CaAl_2Si_2O_8 + 2NaCl + 4SiO_2$$

It has been shown by numerous authors that effects arising out of composition and structure of the parent liquid may strongly influence plagioclase composition. The augite content of the liquid, which may increase rapidly in a closed intercumulus system, strongly affects An partitioning into plagioclase according to Morse & Nolan (1984).

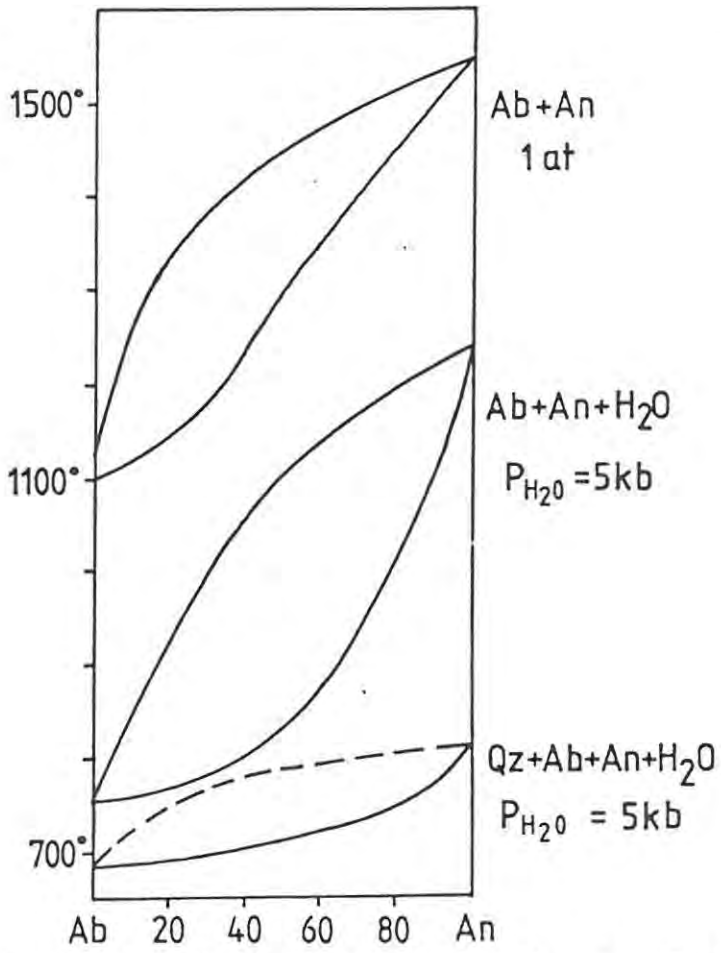

Fig. 4.2 Projections of solidus and liquidus relationships of the Ab + An + H_2O and Qz + Ab + An + H_2O systems at various experimental conditions, compiled from various authors (modified after Johannes, 1978).

Furthermore, the composition of the liquid and the appearance of other cumulus phases determine the amount of supersaturation in plagioclase component in the liquid. Plagioclase supersaturation is necessary to start nucleation (Wager, 1959), and crystallization of other phases increases supersaturation of plagioclase in the system. This also can be a feedback process as Si-rich, highly polymerized liquids have a low difference of free energy between plagioclase and the liquid, thus requiring higher supersaturation for nucleation (Morse, 1979a). Also, such liquids are unlikely to undergo rapid convection in the chamber. Convection creates relatively rapid pressure changes and therefore enhances nucleation (Morse, 1979a). The various types of zoning in plagioclase which reflect this sensitivity to different factors will be discussed in further detail in Chapter 4.9.1.

Longhi et al. (1976) suggested that Fe in plagioclase reflects the $Fe/(Fe^{2+}+Mg)$ ratio in the liquid. This would imply increase of Fe in plagioclase in the case of normal differentiation, and an inverse relationship with An content. This statement is not applicable to the total population of plagioclase in the study section as intercumulus plagioclase, which has the lowest An content, also shows the lowest Fe contents (Fig. 4.3a). If only cumulus plagioclase is plotted, no trend is detectable (Fig. 4.3b). The Fe content of plagioclase might, furthermore, be an indicator for the amount of supercooling. Longhi et al. (1976) pointed out that plagioclase excludes Fe and Mg more effectively if only small degrees of supercooling are maintained. The exchange coefficient $K_{pl/liq}^{Fe/Mg}$ also increases with increasing oxygen fugacity (Longhi et al. 1976).

Because of the strong and irregular zonation in plagioclase, factors like the "cut-effect" become very important in analysing plagioclase by microprobe methods. It is difficult to obtain representative average values unless one executes a large number of analyses, concentrates on the largest grains (with the exception of phenocrysts), and analyses only the cores of grains. Often, however, this core composition does not reflect the highest An value as plagioclase frequently displays reversed or skeletal (highly irregular oscillatory) zoning. This phenomenon has also been observed by Maaløe (1976) and Morse & Nolan (1984).

An values of cumulus plagioclase in the study section vary between 71% and 79%, with 3 samples showing values of 81.3, 82.6 and 88.8% (note that the latter two have not been plotted in Fig. 4.3(b)). It is of interest to note that some of the highest values obtained are those in some harzburgites (containing minor amounts of cumulus plagioclase) and troctolites (Fig.4.3a). The values for intercumulus plagioclase range from 41% to 83% with the highest values also being measured in olivine-bearing rocks. The An content of cumulus plagioclase is decoupled from $Mg\#_{opx}$ in samples where the two phases coexist (Fig. 4.3(c)).

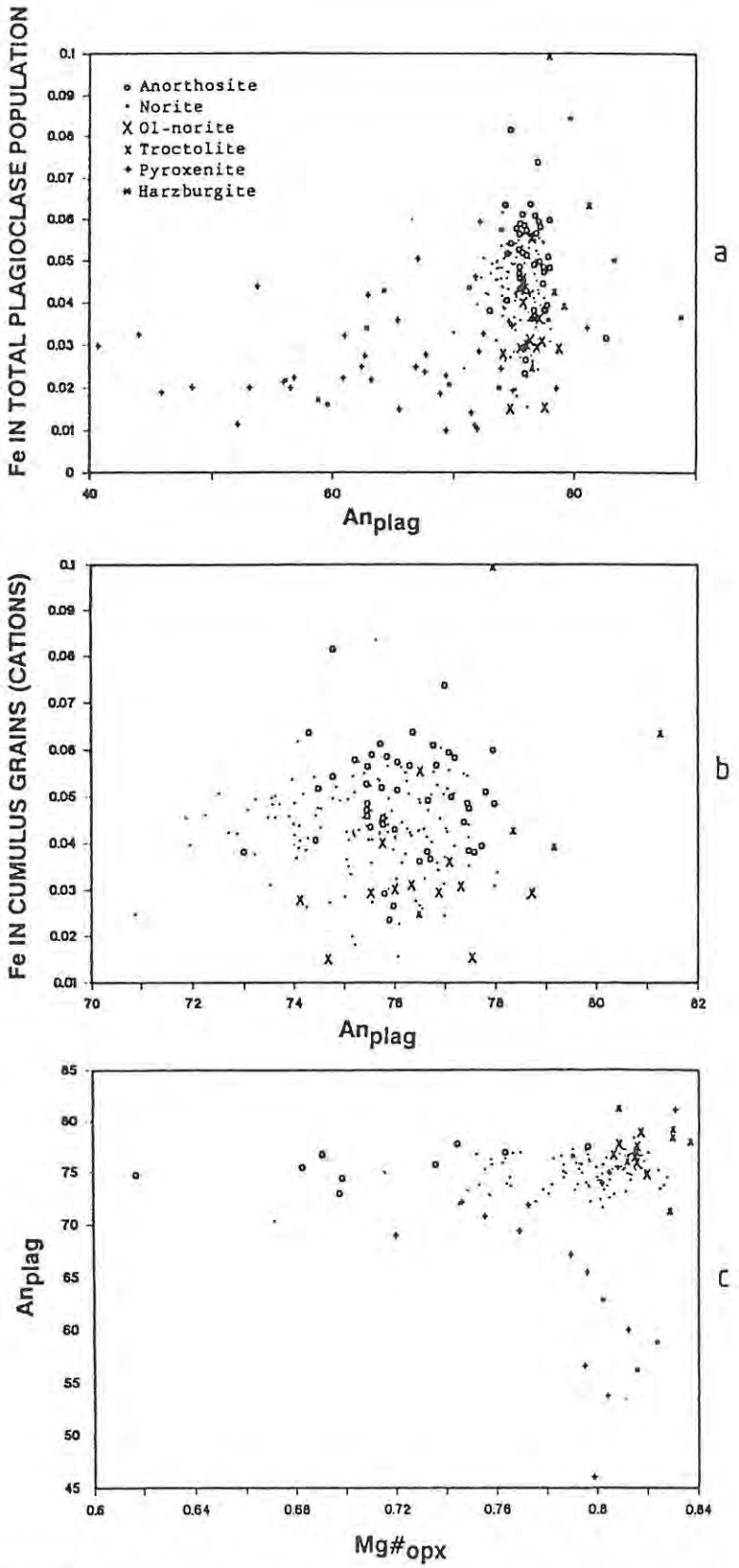

Fig. 4.3 (a) Plot of cationic Fe_{plag} versus An_{plag} indicating sympathetic Fe and An depletion in intercumulus (more sodic) plagioclase. (b) Plagioclase in anorthosites is enriched in Fe and An component relative to that in norites. (c) An content of plagioclase versus $Mg\#_{opx}$.

Atomic Fe ranges between 0.01 and 0.1 (0.1-0.65 wt% FeO), with the lowest values in intercumulus plagioclase. The An and Fe content of cumulus plagioclase are more or less independent of the rock type.

A common feature in norites and troctolites within the study section is the abundance of small, rounded plagioclase inclusions in orthopyroxene and olivine (see also Eales et al., 1986, 1990a, and 1991). They show on average slightly higher An values than associated cumulus grains (Table 4.1). This variation seems to be controlled by some regional pattern: inclusions at Amandelbult show mostly higher values than cumulus grains whereas inclusions at Crocodile River Mine are more sodic than coexisting cumulus grains (Table 4.1, see also Fig. 7.7). For this reason, Fig. 4.4(a), in which all analyses for the whole of the Western Bushveld are plotted, shows on average more or less similar values of An content for inclusions and normal cumulus grains. Eales et al. (1990a) and Reichhardt (1989) in studies of the UG1 Footwall Unit at Union Section and in the Eastern Bushveld, respectively, observed a somewhat different pattern where inclusions are more sodic than cumulus grains. Teigler (1990) in a study of pyroxenites of the UG1 Footwall Unit, and norites of the MG4 Footwall Unit, found inclusions to be compositionally similar to cumulus grains in the first case but more calcic in the second case.

Table 4.1: Average values for core compositions of cumulus feldspar grains, and inclusions, along 170 km of strike of the western limb. `n` refers to the number of separate samples investigated at each locality with 4-15 grains of each textural type being analysed in each sample.

	An (mol.%)			Fe (cations)			n
	cum.	incl.	diff.	cum.	incl.	diff.	
Amandelbult	75.8	77.2	1.37	0.041	0.044	0.003	10
Union	76.4	77.3	0.89	0.035	0.038	0.003	5
Impala North	77.1	77.7	0.59	0.037	0.044	0.007	8
Impala South	76.7	76.8	0.14	0.038	0.037	-0.001	14
Rustenburg	75.9	77.1	1.20	0.039	0.045	-0.006	7
Wolhuterskop West	73.8	74.1	0.33	0.047	0.052	0.005	22
Wolhuterskop East	75.3	75.2	-0.08	0.049	0.053	0.004	23
Crocodile River	75.2	74.5	-0.70	0.049	0.054	0.005	13
All Samples	75.4	75.7	0.30	0.045	0.048	0.003	102

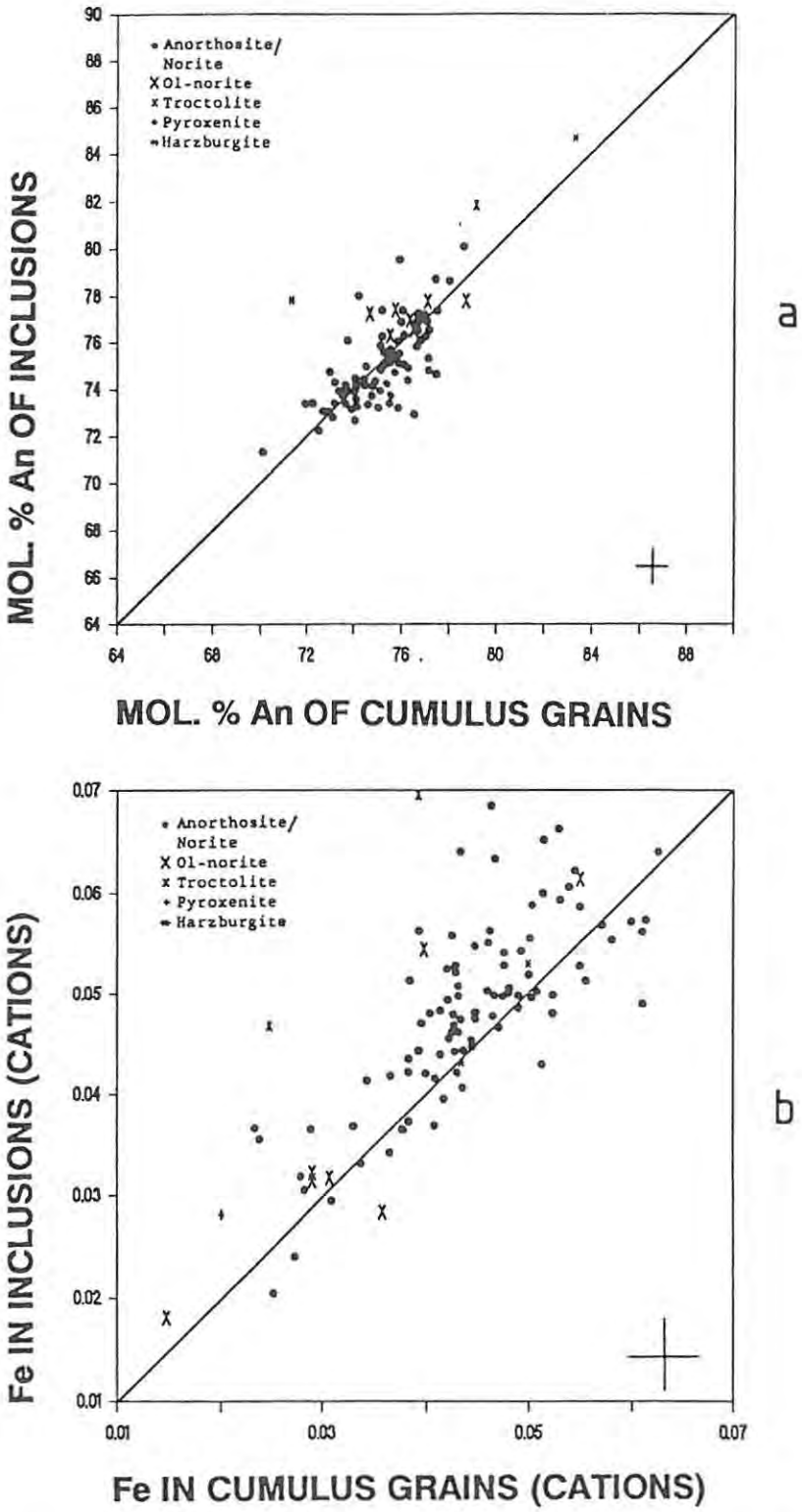

Fig. 4.4 (a) + (b) Composition of resorbed plagioclase inclusions within opx and olivine of norites, olivine norites, troctolites and harzburgites plotted against core compositions of associated cumulus plagioclase in some samples (note that some harzburgites and pyroxenites can contain cumulus plagioclase). Data are compiled from microprobe studies of 99 samples from the western limb of the complex. Average compositions for each sample are compiled from 4 - 15 microprobe analyses of each textural type of plagioclase. Crosses in bottom right corners indicate average 1 standard deviation for each plotted point.

Inclusions generally display higher Fe values than normal cumulus grains (Fig. 4.4(b), Table 4.1) and are mostly reverse zoned. It is not clear if this is due to postcumulus re-equilibration (an unlikely possibility considering the slow rate of diffusion of cations in plagioclase) or if it is further evidence for the formation of these inclusions in a residual melt before the intrusion of the influxes leading to the UG2 and Pseudoreef Units.

Inclusions in the study section are seen to be concentrated in the centre or towards the rim of orthopyroxene and olivine grains. Significant size differences exist but no systematical chemical variation seems to be attached to either their size or textural habit (i.e., degree of roundness).

4.3: Orthopyroxene

The composition of Ca-poor pyroxene in the interval under review is plotted within the conventional pyroxene triangle in Fig. 4.5. Only small amounts of Ca can be incorporated in the orthorhombic structure. As a result of its larger ionic size compared with Fe^{2+} and Mg, Ca levels decline further at low temperatures and exsolution of monoclinic diopside - hedenbergite ($Ca_2Si_2O_6$ - $CaFeSi_2O_6$) occurs in the form of fine (3-10 μm wide) lamellae // (100) (Deer et al., 1978). Exsolution also occurs in the form of blebs preferentially around plagioclase inclusions (Eales et al., 1990a), presumably in response to disorder in the orthopyroxene lattice. This phenomenon is attributed to heterogeneous nucleation at planar or linear defects, which is due to a high density of dislocations at grain boundaries (Champness & Lorimer, 1976). Typical bulk Ca contents of orthopyroxene in the study section are below 1.5 wt%. This was measured using an unfocused microprobe beam, so that the bulk composition of a grain rather than that of single lamellae or interlamellar spaces were determined.

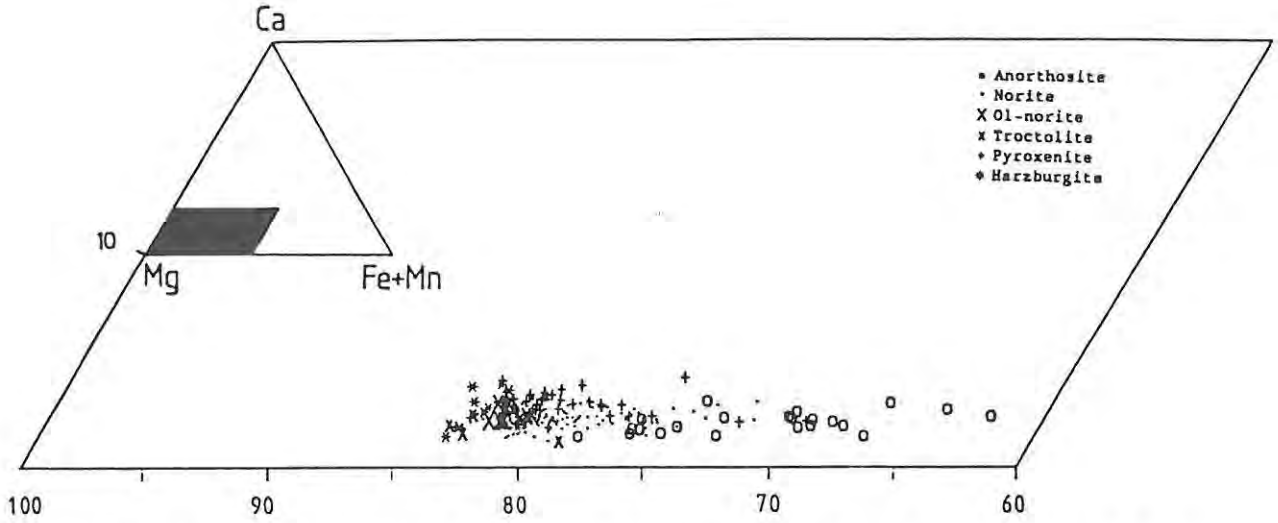

Fig. 4.5 Compositional range of orthopyroxene (cations) in the study section, plotted in the conventional pyroxene triangle. Note the high Fe + Mn content of anorthosite-hosted (mostly intercumulus) orthopyroxene and the gradation from norites into anorthosites.

Intercumulus orthopyroxene hosted by anorthosite yields the highest Fe (+Mn) values (Fig. 4.5) but the transition to cumulus orthopyroxene is clearly gradational. Orthopyroxene in olivine-bearing host-rocks tends to show the highest Mg# (Fig. 4.6(a)-(e)).

Enstatite ($Mg_2Si_2O_6$)and ferrosilite ($Fe_2Si_2O_6$) form a complete solid solution series. As a result of different melting temperatures of the two end-members the composition of the intermediate crystals could be used as a geothermometer as long as subsolidus equilibration with other phases could be excluded (see Lindsley, 1983). Even in the case of rapid fractionation of crystals and liquid, however, this is only partly possible. Accumulated crystals will equilibrate with each other, with other phases like chromite and olivine, and with intercumulus liquid. This is especially true over the long cooling history of a large complex. Additionally, Colson & Gust (1989) pointed out that equilibration of certain trace elements between melt and crystals smaller than 50 μm requires only about 1.5 hours. This fact alone renders recognition of crystals that have sunk over long distances problematic as one would anticipate hardly any compositional changes over a small- to medium-range stratigraphic interval if that were the case.

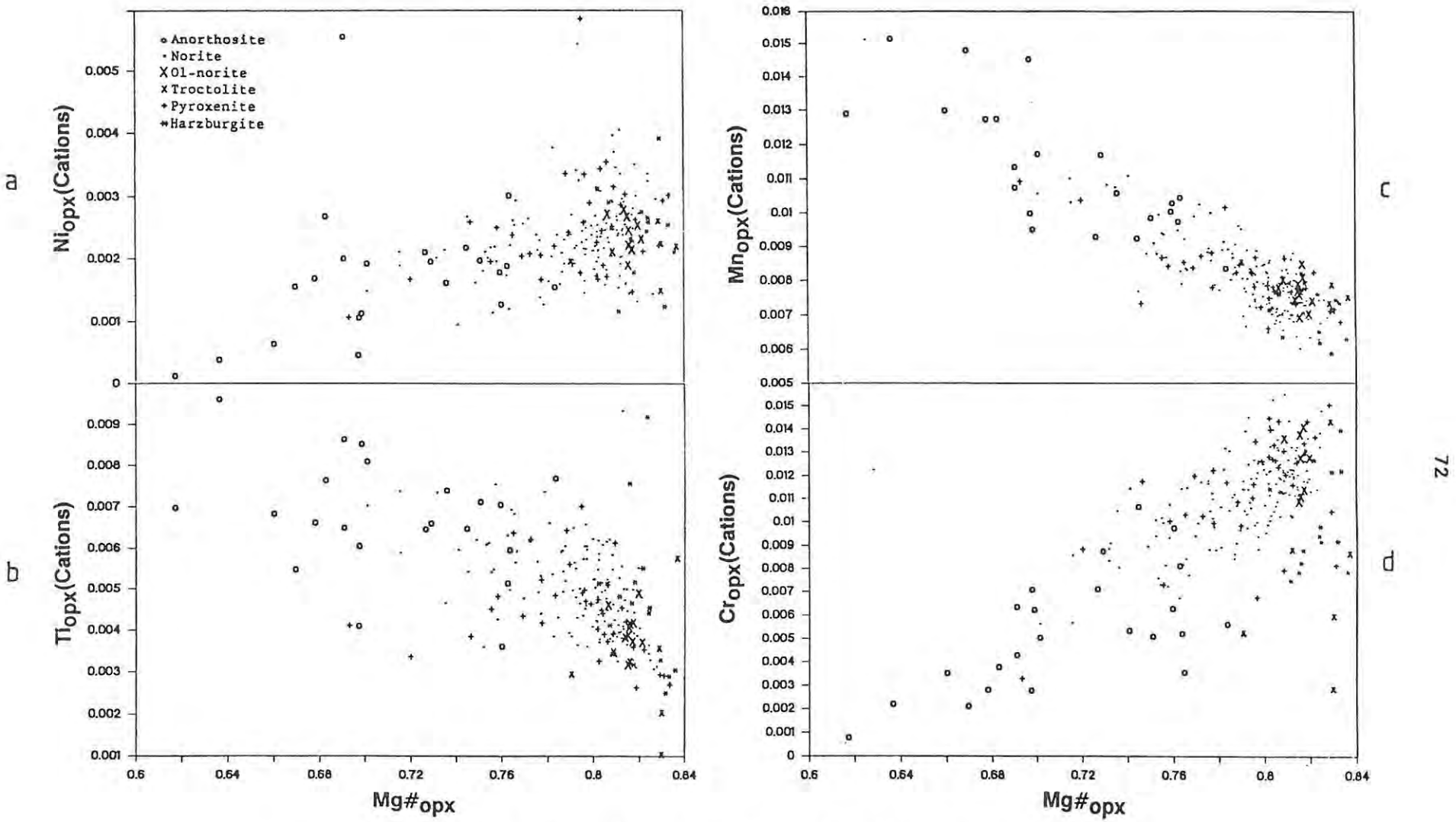

Fig. 4.6 Plot against $Mg\#_{opx}$ of (a) Ni, (b) Ti, (c) Mn, (d) Cr and (e) Al cations in orthopyroxene. Note the gradual enrichment of Mn and Ti and the depletion of Ni, Cr and Al in anorthosite-hosted orthopyroxene. Note also that pyroxenites do not show the maximum values of Mg#.

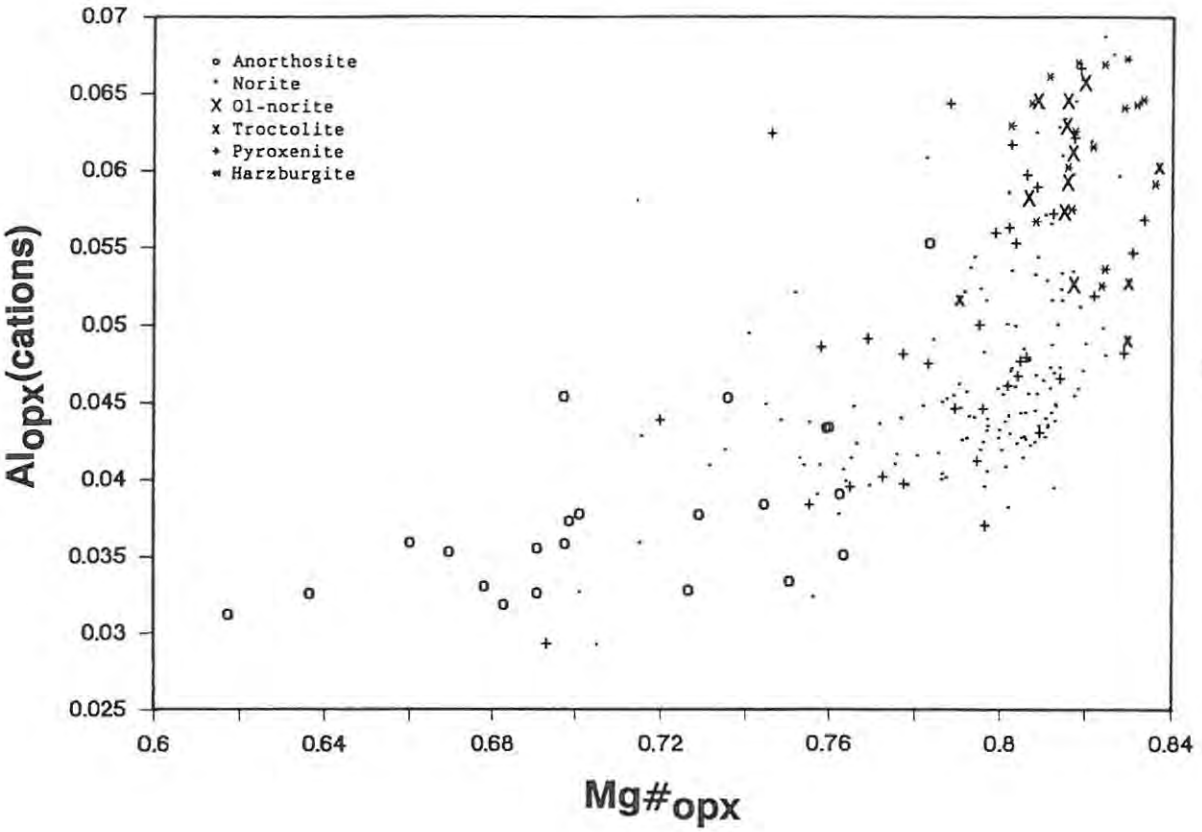

In immediate contact with chromite, Mg and Fe of orthopyroxene (and olivine) will be exchanged according to the following reaction (Roeder et al., 1979):

$$FeMgSi_2O_6 + Mg(CrAlFe^{3+})_2O_4 = Mg_2Si_2O_6 + Fe(CrAlFe^{3+})_2O_4$$

$$1/2\ Fe_2SiO_4 + Mg(CrAlFe^{3+})_2O_4 = 1/2\ Mg_2SiO_4 + Fe(CrAlFe^{3+})_2O_4$$

This leads to high Mg# of orthopyroxene (and olivine) in the vicinity of chromitite seams or dispersed chromite grains. In the latter case the effect is only detectable on a scale of ca. 100 - 200 µm within the affected grain and in the former case within 2 mm of the thin chromitite stringer in sample EK22 306.30 (Plate 1 and Fig. 4.7). Illustrations of this reaction are given, inter alia, by El Goresy et al. (1976) and Eales & Reynolds (1986).

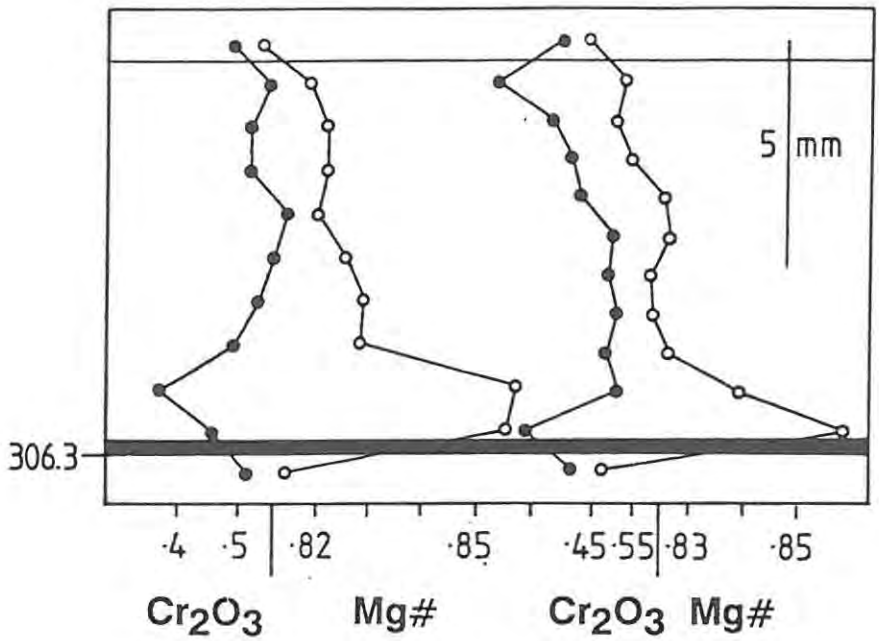

Fig. 4.7 Two detailed profiles (within one sample) across a thin pyroxenite layer with a thin basal chromitite stringer (sample EK22 306.3). The black band marks the chromitite, and the upper horizontal line indicates the top contact of the pyroxenite. Average compositions of 2 samples of the immediate leuconoritic foot and hangingwall below and above this interval are plotted for comparison.

Four types of orthopyroxene can be distinguished in the study section: (i) cumulus orthopyroxene, (ii) intercumulus orthopyroxene in anorthosites and norites, (iii) poikilitic orthopyroxene in harzburgites and (iv) orthopyroxene as reaction replacement of olivine in troctolites, olivine norites and harzburgites.

(i) Cumulus orthopyroxene displays a compositional range in Mg# between 0.70 and 0.84. In pyroxenites of the IM profile, values drop to 0.69, but the high proportions of amphibole and magnetite in these samples create serious doubt about whether these are primary values.

(ii) Intercumulus orthopyroxene covers a range of Mg# values from 0.62-0.77. This is significant insofar as a clear distinction between cumulus and intercumulus orthopyroxene apparently cannot be drawn on chemical grounds alone. Cumulus orthopyroxene has quite commonly continued to grow to form intercumulus overgrowths which, due to equilibration, display similar chemical characteristics as the core. It seems thus possible that some of the intercumulus orthopyroxene, which forms the poikilitic mottles in anorthosites, formed around cores of cumulus orthopyroxene (see Chapter 3.2) and the present composition represents an intermediate value between that of the early cumulus phase, and pyroxene crystallizing from the late interstitial liquid.

(iii) Poikilitic orthopyroxene reveals some of the highest Mg# obtained, its average value being 0.82. Ni and Cr values vary unsystematically. This is possibly due to the varying temperatures at which poikilitic crystallization occurs (which in turn is dependent on supercooling or the amount of volatiles). On the other hand, poikilitic orthopyroxene is not always clearly distinguishable from cumulus orthopyroxene, which might be the reason for the varying values.

(iv) Reaction-replacement orthopyroxene after olivine usually shows extremely low Ca, Cr, and Ti values, but perhaps surprisingly, Ni values in this variety are not elevated. Mg# of orthopyroxene in this environment is, as expected, in equilibrium with that of the olivine relict.

Ni trends are ill defined on the scale of the studied interval but usually decrease with ongoing differentiation. This leads to low Ni contents of orthopyroxene in some anorthosites (Fig. 4.6(a)). The reason for the poor correlation between Ni and Mg# in orthopyroxene of the interval under review might possibly be related to frequent mixing of depleted and fresh magma, which would disturb regular differentiation. Colson et al. (1988) point out that partitioning

coefficients between crystal and melt can vary more than 100% for individual trace elements, because of the combined effects of melt composition and temperature. Additionally, the concentration of Ni in orthopyroxene lies close to the detection limit of the electron microprobe (ca. 800 ppm).

Ti values in orthopyroxene increase with differentiation and thus behave much like Mn values (Fig. 4.6(b) and (c)) with the highest values usually in anorthosites (up to 0.31 wt%). Teigler (1990), however, found pyroxenitic sequences in the Lower Zone, where Ti is positively correlated with $Mg\#_{opx}$ and thus behaves in the opposite way. Some troctolites of the study section show extremely low values of Ti (down to 0.04 wt%) which is related to the low Ti content of replacement orthopyroxene. The regression equations of Ti_{opx} and Mn_{opx} versus $Mg\#_{opx}$, stated in the form y = xm + c, with R being the correlation coefficient and n the number of samples analysed (including all rock types), are listed below:

$Ti_{opx} = Mg\#_{opx} * -0.02 + 0.020$ R = 0.560 n = 278
$Mn_{opx} = Mg\#_{opx} * -0.03 + 0.035$ R = 0.867 n = 278

Similar to Ni, Cr is highly compatible into orthopyroxene. Cr_{opx} (cations) shows a fairly good correlation with $Mg\#_{opx}$ (Fig. 4.6(d)). The regression equations, including samples of core AE, analysed by Field (1987) are listed below:

$Cr_{opx} = Mg\#_{opx} * 0.058 - 0.035$ R = 0.799 (without harzburgites and troctolites, n = 249)
$Cr_{opx} = Mg\#_{opx} * 0.051 - 0.03$ R = 0.695 (n = 278, all rock types)

This correlation becomes weaker if one includes harzburgites and troctolites as orthopyroxene in these rocks is often of poikilitic nature (and as such shows lower Cr values).

Fig. 4.6(e) shows a comparatively good correlation between Al content and Mg# of orthopyroxene. According to Schearer et al. (1989) Al values in orthopyroxene drop sharply at the onset of plagioclase crystallization and will then resume a slightly decreasing trend with ongoing differentiation. The distribution of the values in the different rock types of the study section possibly confirms their findings: harzburgites show high Al contents which would reflect the fact that they formed before the onset of plagioclase crystallization. Pyroxenites cover a wider compositional field. Together with troctolites and olivine norites, harzburgites and pyroxenites define a curve which shows a slightly steeper slope than that of anorthosites and norites. This could possibly represent the sharp drop in Al values of orthopyroxene during the onset of plagioclase crystallization. During cotectic orthopyroxene and plagioclase crystallization (leading to the deposition of norites and anorthosites) Al values in orthopyroxene then show a gently decreasing trend on a low level.

In summary Ni contents generally lie between 0.05 - 0.1 wt% (0.001 - 0.004 cations), with some intercumulus orthopyroxene showing values down to 0.01 wt%. Ti shows a slight preference for intercumulus orthopyroxene. Generally values lie between 0.1 - 0.2 wt% (0.002 - 0.009 cations), with exceptional values above 0.3 wt% in some intercumulus orthopyroxene. Values in replacement orthopyroxene can drop to 0.04 wt% (0.001 cations). Mn values range from 0.20 wt% in harzburgites to 0.48 wt% in anorthosites (0.006 to 0.015 cations). Cr contents of cumulus and poikilitic orthopyroxene usually lie between 0.2 and 0.5 wt% (0.007 - 0.015 cations) , with intercumulus orthopyroxene showing lower values between 0.03 and 0.25 wt% (0.001 - 0.01 cations, Fig. 4.6(d)). Al levels lie between 0.75 wt% in anorthosites and 1.60 wt% in harzburgites (0.03 - 0.068 cations).

4.4: Olivine

Olivine is an orthosilicate within the solid solution series between forsterite (Mg_2SiO_4) and fayalite (Fe_2SiO_4), with melting points in the pure system of 1810°C and 1205°C, respectively. Fe and Mg are randomly substituted by Ni, Mn, Cr, and Ca (Deer et al., 1982) but the last two are present in the study section only at very low levels.

Olivine has been analysed in the UA, EK22, IN and IM cores in 41 samples of harzburgites, troctolites, olivine norites, pyroxenites, and one anorthosite. Additionally, 10 samples of core AE (Field, 1987) have been included into the data base. Olivine virtually disappears in the south-eastern part of the western limb of the complex and only one troctolitic sample was available for analysis of olivine at locality H3 (sample 1089.65).

Mg# of cumulus olivine ranges from 0.76 to 0.82. No correlation between rock type and MgO_{ol} exists and the same is true for Ni values, which range from 0.2 to 0.52 wt% (Fig. 4.8), with one exceptional value of 0.65 wt%. The highest Ni values have been found in olivine within the UG2 pyroxenite at locality EK22. There exists no correlation between grain size of olivine and $Mg\#_{ol}$ or Ni_{ol} (see also Botha, 1987).

The distribution of Fe and Mg between coexisting olivine, orthopyroxene, and clinopyroxene has been determined in the IM sequence and the regression equation may be compared with those of Murck (1985) and Barnes & Naldrett (1986).

		present writer	n	R	Murck (1985)	Barnes & Naldrett(1986)
$Fe^{2+}/Mg_{ol} = Fe^{2+}/Mg_{opx}$	*	1.18	8	0.932	1.09	1.14
$Fe^{2+}/Mg_{ol} = Fe^{2+}/Mg_{opx}$	*	1.14*	7	0.958		
$Fe^{2+}/Mg_{ol} = Fe^{2+}/Mg_{cpx}$	*	1.69	4	too small	1.43	1.32

* excluding sample IM 841.67 (anorthosite)

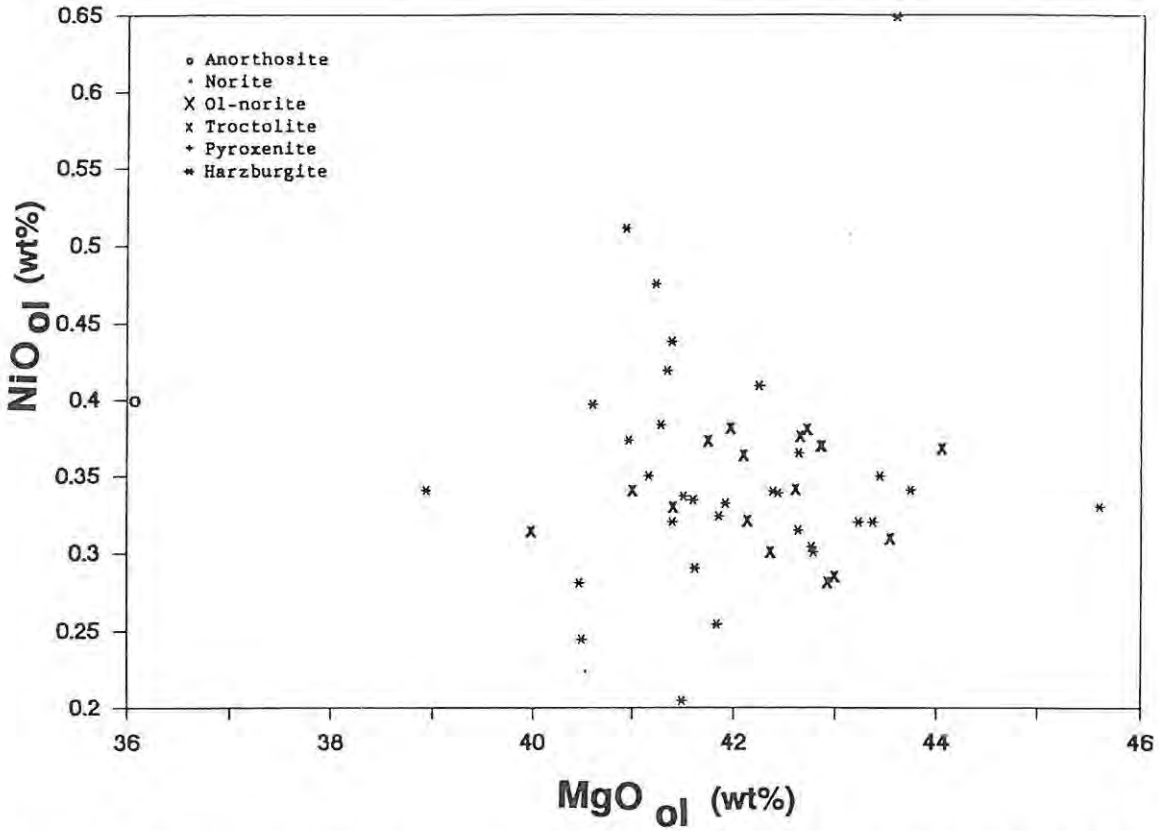

Fig. 4.8 NiO in olivine plotted against MgO in olivine. Note the low values of MgO in the anorthosite-hosted olivine (sample IM 841.67) on the extreme left side of the diagram.

The values obtained are similar to those of Murck (1985, Fig. 4.9(a) and (b)) and Barnes & Naldrett (1986). The difference between the two values quoted for $(Fe^{2+}/Mg)_{ol/opx}$ is due to the anhedral olivine in the mottled anorthosite (IM 841.67) plotting far off the regression line. The value for $Fe^{2+}/Mg_{ol/cpx}$ includes data for intercumulus clinopyroxene in the study section, which may account for the difference between this and other published values. Both regressions are calculated so as to pass through the origin and a slightly better correlation is given by expressions of the form y = mx + c.

$Fe^{2+}/Mg_{ol} = Fe^{2+}/Mg_{opx} * 1.653 - 0.115 \quad R = 0.974 \quad n = 8$

$Fe^{2+}/Mg_{ol} = Fe^{2+}/Mg_{cpx} * 0.589 + 0.178 \quad R = 0.744 \quad n = 4$

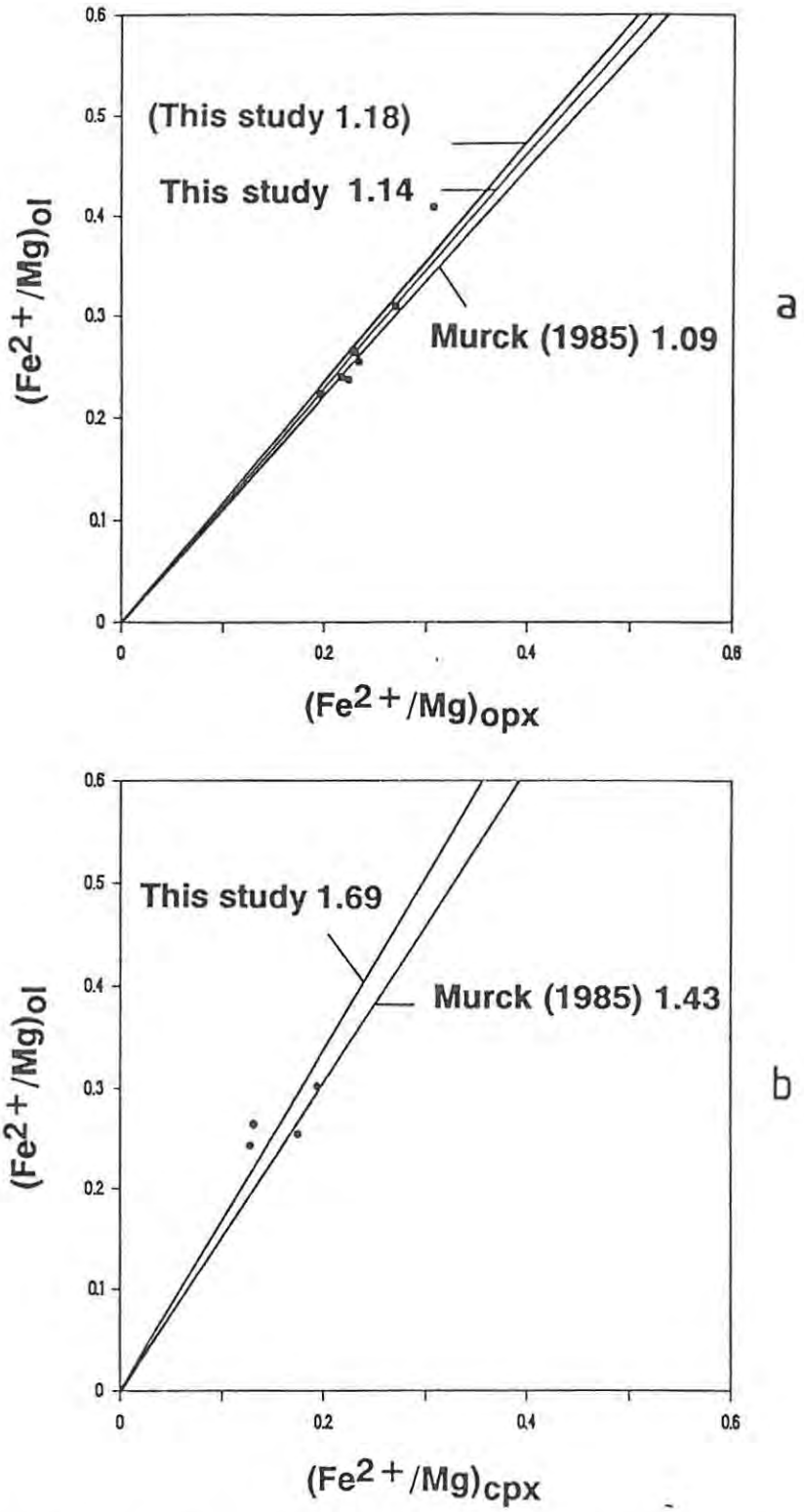

Fig. 4.9 (a) + (b) Atomic ratios of Fe^{2+}/Mg in olivine plotted against Fe^{2+}/Mg in coexisting orthopyroxene and clinopyroxene. Regression lines are computed so as to pass through the origin. Distribution coefficients according to Murck (1985) are shown for comparison.

Zonation of olivine is very uncommon in terms of all elements analysed and only detectable in close proximity to chromite, where elevated Mg values were observed within a restricted distance (100-200 μm) from the immediate contact with chromite.

In some anorthosites olivine occurs as anhedral, large crystals and is surrounded by a roughly circular rim-zone of intercumulus orthopyroxene, which poikilitically encloses plagioclase (Plate 10). The value of Fo_{71} is anomalously low for cumulus olivine in the Upper Critical Zone. Furthermore, olivine and orthopyroxene are here in disequilibrium, displaying the following relationship:

$$Fe^{2+}/Mg_{ol} = Fe^{2+}/Mg_{opx} * 1.21$$

Texturally, this assemblage resembles a "mottle". The evidence suggests that olivine in this case has not been formed cotectically. The same textures have been observed by Woussen et al. (1988) in the Lac-St.-Jean Anorthosite Complex and have been earlier interpreted in other anorthosite massifs as either features of late crystallization (De Waard & Romey, 1969; Maquil & Duchesne, 1984) or mafic mobilizates (Michot & Michot, 1969). It is of interest here that the anhedral olivine at Lac-St.Jean shows the same Fo values as in the study section. However, olivine and plagioclase in the study section do not occur in cotectic proportions as is the case at Lac-St.-Jean.

4.5: Chromite

Chromite compositions represent a complex solid solution within the spinel group. Their original composition is determined, inter alia, by variations in oxygen fugacity, temperature, and pressure (Ulmer, 1969; Hill & Roeder, 1974; Murck, 1985). Spinel becomes unstable in comparison with silicates with decreasing f_{O2} (Muan & Osborn, 1956; Roeder & Osborn, 1966). However, cation diffusivities in oxides are higher than in ferromagnesian silicates. Therefore, subsolidus

reaction with associated silicates and oxides such as magnetite, which is released by the deuteric oxidation of olivine, and re-equilibration amongst adjacent chromite grains tend to obscure the primary chemistry (McDonald, 1967; Cameron, 1975; Eales & Reynolds, 1986).

Fig. 4.10 shows the distribution of the trivalent cations Cr^{3+}, Al^{3+} and Fe^{3+} in the analysed chromites. The three cations and the (Fe/Ti) pair of ulvöspinel substitute for each other and the ratio of $100Fe^{3+} / (Fe^{3+}+Cr^{3+}+Al^{3+})$ is known to be positively correlated with oxygen fugacity (Ulmer, 1969; Hill & Roeder, 1974). Hence, seam chromitites of the Great Dyke, which are higher in $100Fe^{3+} / (Fe^{3+}+Cr^{3+}+Al^{3+})$ than chromitites from adjacent dunites, are thought to have been formed under elevated f_{O2} conditions (Wilson, 1982). However, Murck (1985) reported slightly depressed values of $100Fe^{3+} / (Fe^{3+}+Cr^{3+}+Al^{3+})$ in the G and H chromitite seams of the ultramafic zone of the Stillwater Complex compared to the foot- and hangingwall. This is characteristic also of the few analysed massive chromitites and their adjacent rocks in the study section. Three samples from the UG2 chromitite show distinctively lower values of $100Fe^{3+} / (Fe^{3+}+Cr^{3+}+Al^{3+})$ than chromite from the adjacent pyroxenitic or harzburgitic rocks (Fig. 4.10). The compositional field of massive chromitites is the closest to the Al-Cr tieline.

Another noteworthy feature of this diagram is the elongation of most compositional fields of the different host-rock types towards the Fe^{3+} corner. This might reflect oxygen control in the formation of chromite in general. Furthermore, the field of anorthosite-hosted chromite extends over a wide range of Fe^{3+}/Cr^{3+} ratios and stays roughly equidistant from the Al^{3+} corner. This possibly indicates coprecipitation of chromite and plagioclase, and the precipitation of chromite over a relatively long time-span. Additionally, this field shows lower Al^{3+} values than the other compositional fields (see also Botha, 1987): this is considered to be a result of the competition for Al^{3+} between plagioclase and late-crystallizing chromite.

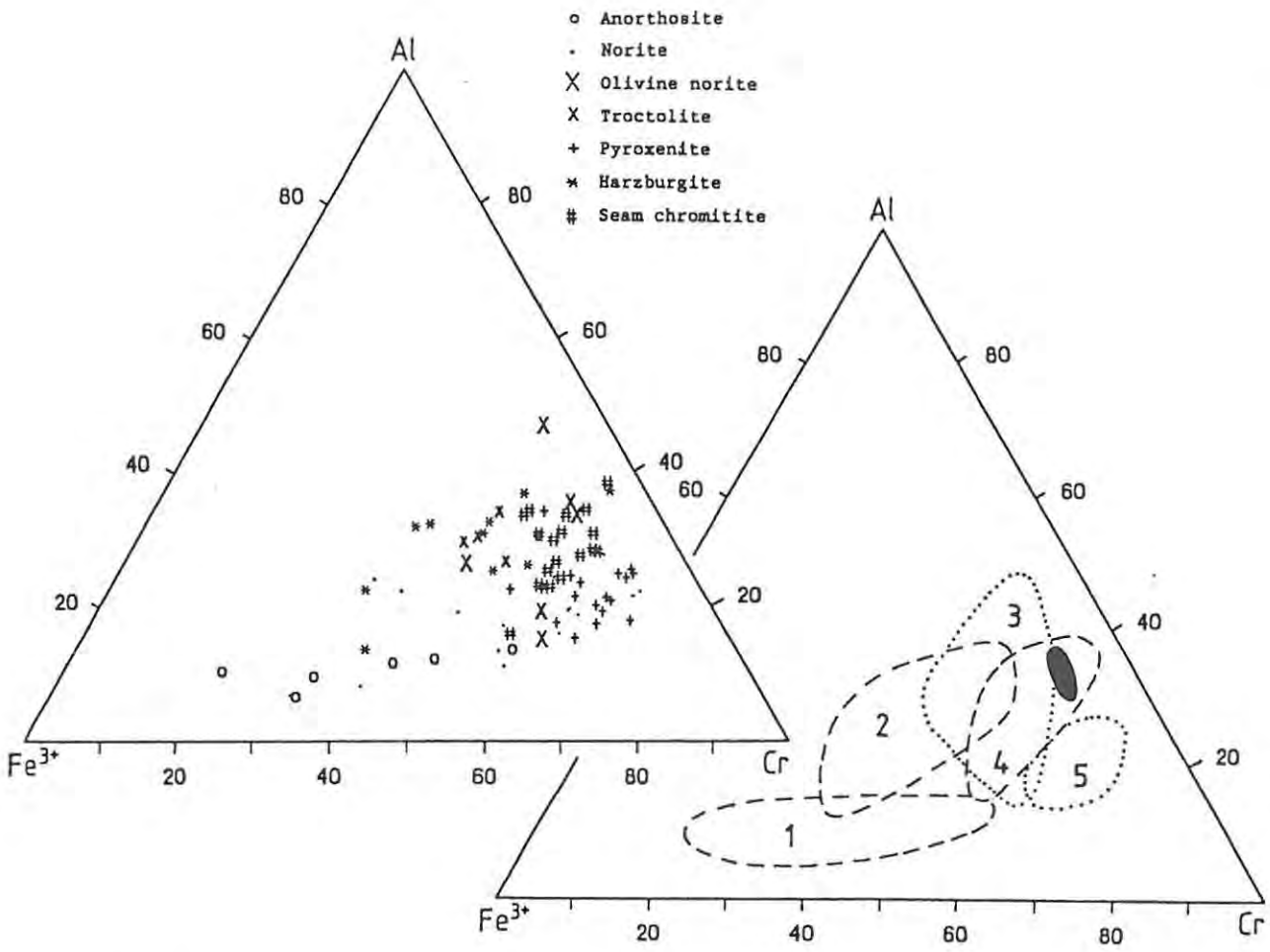

Fig. 4.10 Composition of chromites of the study section plotted in the triangular diagram of the dominant trivalent cations (in cation %). Hatch symbols indicate seam chromites. The black field represents the compositional field of 3 samples from the UG2 chromitite, within the field of seam chromites. 1 = anorthosite-hosted chromites; 2 = harzburgite-hosted chromites; 3 = olivine norite- and troctolite-hosted chromites; 4 = chromitite seams and stringers; 5 = pyroxenite hosted chromites. Chromites in norites more or less cover all compositional fields.

Olivine and orthopyroxene tend to exchange Fe^{2+} for Mg^{2+} cations of adjacent chromite. This exchange reaction, however, is very localized, not even affecting the whole silicate grain. Reaction between chromite and plagioclase seems to be insignificant.

Dispersed chromite in pyroxenites is preferentially hosted by intercumulus plagioclase and the grains tend to be larger there. This feature is explained by the assumption that chromite grains have more time to grow if they are not enclosed by the early cumulus phases.

It is well known that dispersed chromite of the Bushveld Upper Critical Zone shows higher chemical variation and lower Mg# than seam-chromite within the same sequence (Eales & Reynolds, 1986). Additionally, Botha (1987) observed that chromite in orthopyroxene of pyroxenites is depleted in Cr and Ti in comparison with chromite hosted by intercumulus plagioclase. This is possibly due to re-equilibration between orthopyroxene and chromite in orthopyroxene-hosted grains.

Cr/Fe ratio of chromite in the study section ranges from about 1.35 in the UG2 chromitite to around 1 in the UG2 pyroxenite. In norite-hosted chromite the ratio usually lies between 0.3 and 0.8, and in anorthosite-hosted grains it drops down to 0.1. Thin, isolated chromitite stringers have values of around 1. It thus seems that the Cr/Fe ratio is a fairly good indicator of fractionation processes. Furthermore, Fig. 6.9 shows that the composition of accessory chromite within intersection IM corresponds with that of coexisting orthopyroxene.

The chromite selvage around the lower hemisphere of spheroids of ultramafic rock ("boulders") in anorthosite constituting the Boulder Bed displays a relatively low Cr/Fe ratio of around 0.6, which tends to imply that one is dealing either with a secondary reaction chromite or with the result of subsolidus re-equilibration between chromite and secondary magnetite. Chromitite coating the upper hemisphere of the boulder, in the one analysed sample where it is exposed, shows a markedly higher Cr/Fe ratio than in the lower hemisphere (analyses 4-3, Table 4.2). This observation strengthens the postulate of a secondary origin for the lower chromitite.

Table 4.2: Representative chromite analyses from the study section.

	1	2	3	4	5	6	7
[wt%]							
TiO_2	1.42	0.99	2.82	0.94	3.31	15.88	0.78
Al_2O_3	14.35	10.94	17.67	9.11	4.14	1.37	11.77
Cr_2O_3	43.96	40.09	33.46	50.23	20.74	4.75	33.91
FeO	23.18	26.46	27.00	28.35	33.68	45.39	28.12
Fe_2O_3	8.35	15.33	12.40	6.98	37.64	32.57	6.44
MnO	0.29	0.37	0.39	0.42	0.45	0.90	0.31
NiO	0.11	0.10	0.17	0.05	0.25	0.00	0.04
MgO	7.65	4.72	6.38	3.46	0.69	0.07	3.80
Total	99.33	99.01	100.30	99.54	100.89	100.92	99.18
Cations (based on 32 oxygens)							
Ti	0.28	0.21	0.56	0.20	0.73	3.55	0.16
Al	4.50	3.58	5.48	3.01	1.43	0.48	3.84
Cr	9.25	8.80	6.96	11.13	4.81	1.12	10.49
Fe^{2+}	5.16	6.14	5.94	6.64	8.26	11.30	6.51
Fe^{3+}	1.68	3.20	2.45	1.47	8.30	7.30	1.34
Mn	0.07	0.09	0.09	0.10	0.11	0.23	0.07
Ni	0.02	0.02	0.04	0.01	0.06	0.00	0.01
Mg	3.04	1.95	2.50	1.45	0.30	0.03	1.57
Mg#	0.37	0.24	0.30	0.18	0.04	0.00	0.19
Cr/Fe	1.26	0.88	0.77	1.28	0.27	0.06	1.24
Cr/Al	2.06	2.46	1.27	3.70	3.36	2.33	2.73

Mg# = cationic $Mg/(Mg+Fe^{2+})$ ratio
Cr/Fe = weight ratio of the metals
Cr/Al = cationic Cr/Al ratio

1 UG2 Chromitite (LK7 1584.25B)
2 Lone Chrome (LK7 1424.28A)
3 "Boulder" lower contact chromite (BBBC Brakspruit)
4 "Boulder" upper contact chromite (BBTC Brakspruit)
5 Anorthosite (IM 843.6)
6 Anorthosite (IM 848.52)
7 Norite (IM 856)

Note: All analyses are recalculated to distribute Fe^{2+} and Fe^{3+} stoichiometrically.

One might envisage either the modification of original chromite by ascending volatile-rich liquids or, according to a mechanism suggested by Boudreau (1988), the resorption of orthopyroxene in response to increased volatile fugacity and the subsequent redistribution of the released Cr_2O_3 to form thin chromitite stringers usually accompanying pegmatoids or pegmatites in the Stillwater Complex.

Lee & Viljoen (1983) advocated that original chromite reacted with Al_2O_3 which was liberated by the reaction of calcic plagioclase with sodic intercumulus liquid. The Ca released by this reaction would yield Ca-enriched rims in coexisting plagioclase. Consequently, plagioclase with extremely Ca-enriched rims would coexist with reaction-chromite.

$$2(Mg,Fe)Cr_2O_4 + 2Al_2O_3 = 2(Mg,Fe)Al_2O_4 + 2Cr_2O_3$$

According to this model the excess Cr_2O_3 would be reprecipitated to anneal the reaction-chromite. The present writer, however, queries the paradox whereby reaction of plagioclase with a sodic residuum is capable of producing reversed zoning of plagioclase in this model.

4.6: Clinopyroxene

In the study section clinopyroxene is an intercumulus, accessory phase which rarely exceeds 2 vol%, although in exceptional cases up to 10 vol% may be observed in some mottled anorthosites and pyroxenites.

Three associations of clinopyroxene can be distinguished:

(i) clinopyroxene as an exsolution product within orthopyroxene, in the form of lamellae and irregular blebs
(ii) clinopyroxene as an intercumulus phase in norites and anorthosites, interstitial to other phases
(iii) clinopyroxene as large oikocrysts, enclosing orthopyroxene chadacrysts in pyroxenites and harzburgites

Types (ii) and (iii) also show exsolution lamellae of orthopyroxene.

Eighteen samples containing clinopyroxene have been analysed in the IM core. Most samples are diopsides (Subcommittee on Pyroxenes, 1989, Fig. 4.11 and 4.12). In 14 of the samples where both orthopyroxene and clinopyroxene were available for analysis, coexisting clinopyroxene-

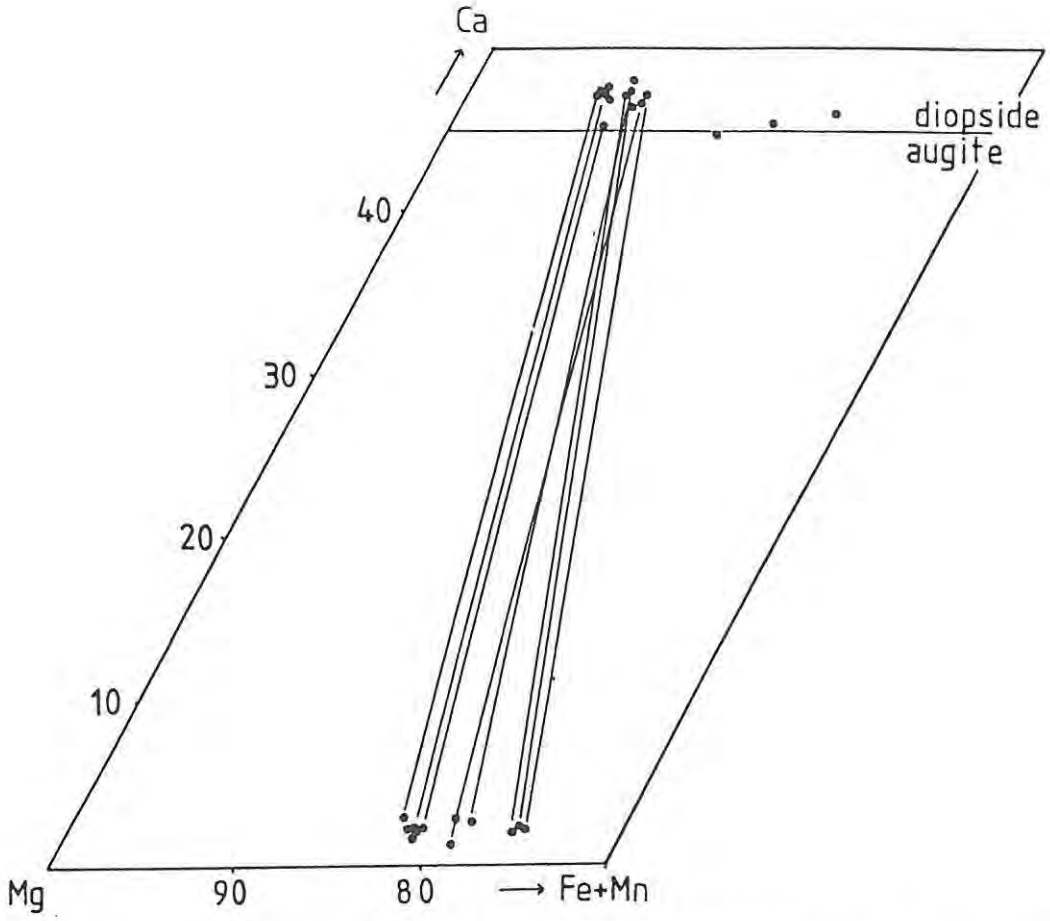

Fig. 4.11 Coexisting orthopyroxene-clinopyroxene pairs (cations) in profile IM, plotted into the pyroxene triangle.

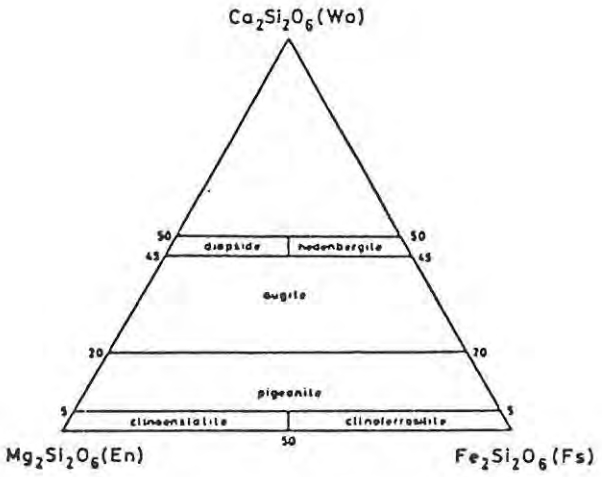

Fig. 4.12 Nomenclature of the Ca - Mg - Fe clinopyroxenes (from Subcommittee on Pyroxenes, 1989).

orthopyroxene pairs show a fractionation trend towards Fe-rich compositions (Fig. 4.11) and the extrapolated tielines intersect the Wo-En edge of the compositional triangle at about Wo_{77} - Wo_{80}.

Characteristically, 1σ standard deviation within each sample is small (below 1%) and a sympathetic variation between Mg# of coexisting clinopyroxene and orthopyroxene has been established (Fig. 4.13).

$$Mg\#_{cpx} = Mg\#_{opx} * 0.518 + 0.452 \quad R = 0.75 \quad n = 14$$

where n is the number of analysed clinopyroxene/orthopyroxene pairs. No correlation has been attempted with olivine as the data basis is to small.

$Mg\#_{cpx}$ ranges from 0.89 in olivine norites to 0.64 in anorthosites. The low Mg# encountered in anorthosites is worthy of note, and conforms with the iron-enrichment commonly encountered in the leucocratic rocks of most cycles in the Upper Critical Zone (Eales et al., 1990b; de Klerk, 1991). No significant compositional difference has been found between the three different types of clinopyroxene. This result varies from the findings of Botha (1987), who detected higher Mg# in exsolved clinopyroxene than in coexisting intercumulus clinopyroxene.

Average Cr contents of clinopyroxene in individual samples range from 0.77 wt% in olivine norites to 0.04 wt% in anorthosites. Individual analyses may reach up to 0.96 wt% Cr (Table 4.3). The range in composition as well as the maximum values are thus distinctly larger than in orthopyroxene.

Even if one considers the high partition coefficient of Cr into clinopyroxene (10, after Cox et al., 1979; and 40 after Campbell & Borley, 1974), the value of 0.77% in an intercumulus phase is surprisingly high.

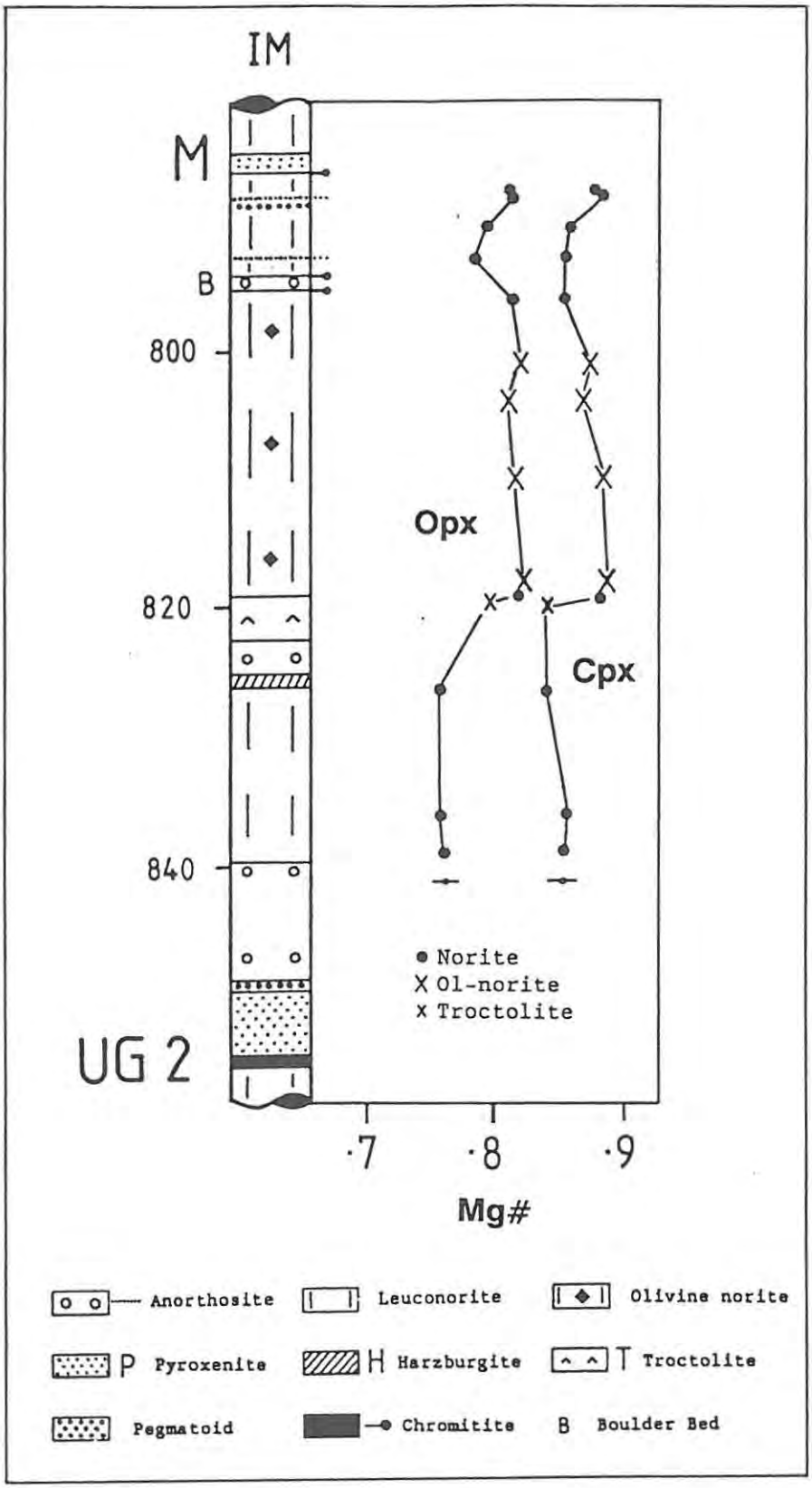

Fig. 4.13 Mg# of coexisting orthopyroxene and clinopyroxene at intersection IM. Error bars indicate 1 standard deviation.

Table 4.3: Typical clinopyroxene compositions in the study section and selected data from the Lower Critical Zone (Botha,1987; Teigler, 1990).

	1	2	3	4	5
[wt%]					
SiO_2	51.69	52.65	50.85	53.13	54.02
TiO_2	0.22	0.32	0.18	0.23	0.15
Al_2O_3	2.71	1.52	0.91	2.27	1.80
Cr_2O_3	0.96	0.82	0.04	1.10	0.79
FeO	4.14	3.74	12.27	4.14	3.25
MnO	0.12	0.10	0.31	0.14	0.05
NiO	0.03	0.06	0.00	na	0.04
MgO	16.38	16.88	11.80	17.40	17.08
CaO	23.38	23.90	22.51	21.24	22.73
Na_2O	0.39	0.32	0.21	0.38	0.45
Total	100.02	100.64	99.10	100.03	100.36
Cations (based on 6 oxygens)					
Si	1.90	1.93	1.95		1.96
Ti	0.01	0.01	0.01		0.00
Al	0.12	0.07	0.04		0.08
Cr	0.03	0.02	0.00		0.02
Fe	0.13	0.11	0.39		0.10
Mn	0.00	0.00	0.01		0.00
Ni	0.00	0.00	0.00		0.00
Mg	0.90	0.92	0.68		0.92
Ca	0.92	0.94	0.93		0.90
Na	0.01	0.01	0.00		0.03
Total	4.01	4.01	4.01		4.00
Mg#	0.88	0.89	0.63	0.88	0.90

1 Intercumulus clinopyroxene in olivine norite (sample IM 804.40)
2 Intercumulus clinopyroxene in norite (IM 787.90)
3 Intercumulus clinopyroxene in anorthosite (IM 848.52)
4 Oikocryst in pyroxenite, Lower Critical Zone (Botha, 1987, sample 208(1))
5 Exsolved lamella in orthopyroxene, base of Lower Critical Zone (Teigler, 1990, sample NG1 695.5)
na = not analysed

4.7: Amphibole

This inosilicate is a major phase only in some highly altered pyroxenites of the study section. It may occur as a deuteric alteration product of pyroxene as actinolite pseudomorphs (uralite) or as a late-stage phase, but, in general, amphibole is wholly absent from most Lower and Critical Zone rocks.

In the UG2 pyroxenite at locality IM, fibrous, pleochroic oxyhornblende in association with magnetite constitutes up to 20% of the rock. The irregular brown colour reveals a varying degree of oxidation throughout the mineral (Pichler & Schmitt-Riegraf, 1987). According to the nomenclature of the Subcommittee on Amphiboles (1978) the oxyhornblende at intersection IM would be classified as a magnesia-hornblende (Fig. 4.14). As the associated orthopyroxene shows an anomalously low Mg# (0.72 - 0.76), one might assume that late-stage liquids penetrated the rock to yield oxyhornblende and modify the composition of orthopyroxene. The associated magnetite probably resulted from destruction of the amphibole lattice, termed opacitization by Pichler & Schmitt-Riegraf (1987).

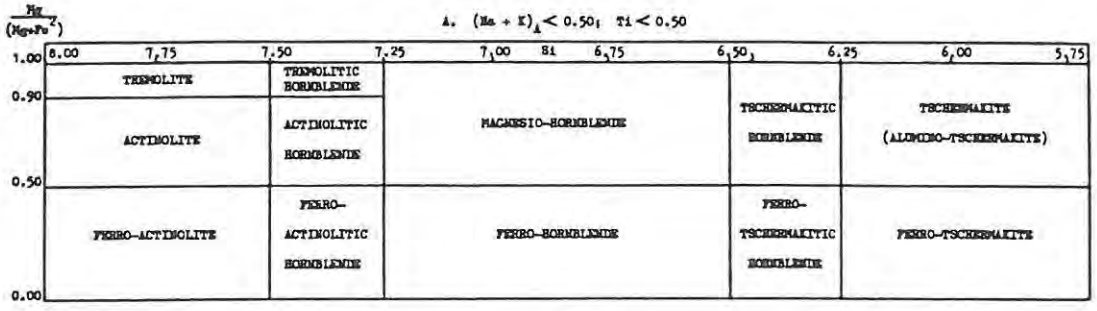

Fig. 4.14 Classification of calcic amphiboles in which $(Ca + Na)_B > 1.34$, $Na_B < 0.67$ (from Subcommittee on Amphiboles, 1978).

Table 4.4 shows that intercumulus amphibole from the Lower and Lower Critical Zones (data from Botha, 1987, and Teigler, 1990) displays significantly different chemism to that of the study section in that the former contains more Mg and less Al, total Fe, and Ti.

Table 4.4: Analyses of amphibole from the study section compared to intercumulus amphibole from the Lower Zone (Botha, 1987; Teigler, 1990). The first 5 analyses have been recalculated for Fe^{3+}, elsewhere Fe^{2+} has been assumed as total Fe.

	1	2	3	4	5	6	7	
[wt%]								
SiO_2	42.79	46.80	44.16	45.27	45.39	52.22	55.23	
TiO_2	2.81	1.80	2.81	2.20	2.32	0.35	0.04	
Al_2O_3	12.00	8.42	10.47	9.61	9.50	3.61	2.60	
Fe_2O_3	3.24	6.75	4.81	6.37	6.15	na	na	
FeO	4.80	3.21	5.37	3.94	3.41	3.54	4.11	
MnO	0.07	0.11	0.12	0.10	0.11	0.07	0.09	
MgO	15.38	15.61	14.12	14.93	15.33	22.08	22.62	
CaO	11.99	10.55	10.53	10.62	10.59	12.29	12.68	
Na_2O	1.21	1.39	1.75	1.51	1.54	0.77	0.40	
K_2O	1.33	0.48	0.57	0.61	0.61	0.36	na	
Cr_2O_3	na	na	na	na	na	0.93	0.11	
Total	95.64	95.11	94.72	95.15	94.95	96.27	97.91	
Cations (based on 23 oxygens)								
Si	6.29	6.82	6.53	6.64	6.65		7.63	Tetrahedral
Al	1.71	1.18	1.47	1.36	1.35		0.42	site
Al	0.37	0.27	0.36	0.30	0.29		na	c-site
Ti	0.31	0.20	0.31	0.24	0.26		0.00	
Fe^{3+}	0.36	0.74	0.54	0.70	0.68		na	
Fe^{2+}	0.59	0.39	0.67	0.48	0.42		0.47	
Mg	3.37	3.39	3.11	3.26	3.35		4.66	
Mn	0.01	0.01	0.02	0.01	0.01		0.01	
Ca	1.89	1.65	1.67	1.67	1.66		1.88	b-site
Na	0.11	0.35	0.33	0.33	0.34		0.11	
Na	0.23	0.04	0.17	0.10	0.10		na	a-site
K	0.25	0.09	0.11	0.11	0.11		na	
Mg#	0.85	0.90	0.82	0.87	0.89	0.92	0.91	

1) This study, sample IM 796.25, troctolite
2) " " IM 851.90, pyroxenite
3) " " " "
4) " " " "
5) " " " "
6) Botha 1987, sample 225(1), pyroxenite
7) Teigler 1990, sample NG1 690.9, pyroxenite
na = not analysed

4.8: Mica

In the interval between the UG2 chromitite and the Merensky Reef, mica occurs as a member of the phlogopite-annite solid solution series. In this series, phlogopite by definition has $X_{Mg} > 0.66$ and biotite $X_{Mg} < 0.66$, where X_{Mg} = atomic Mg/(Mg+Fe) (Fig. 4.15, Deer et al., 1962). The analyses (Table 4.5) show that the composition of mica in the study section lies in the phlogopite field. In comparison with the Lower Critical Zone (Teigler 1990), micas of the study section have significantly lower Mg#. This result is to be expected in view of the trends shown by the other ferromagnesian phases.

A representative analysis of a mica from the Merensky Unit (Kruger, 1982) plots in the range of values of the study interval, although the latter are not as enriched in Ti.

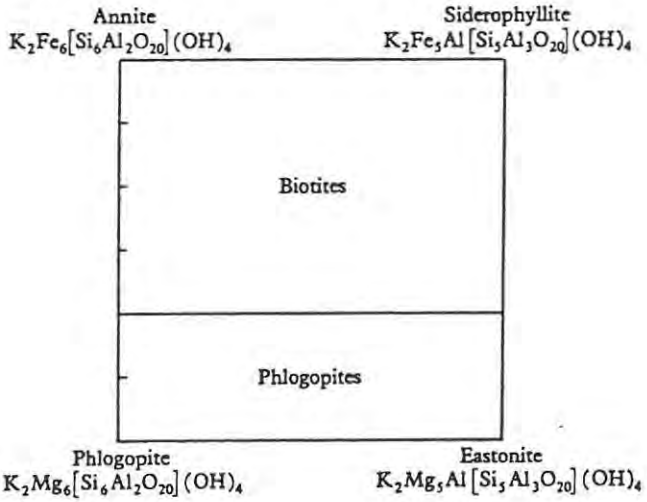

Fig. 4.15 Compositional fields of phlogopite and biotite. The division between them is arbitrarily chosen to be at Mg:Fe = 2:1 (from Deer et al., 1962).

Table 4.5: Mica analyses from the Critical and Lower Critical Zones.

	1	2	3	4	5
[wt%]					
SiO_2	39.09	38.57	38.19	40.24	39.43
TiO_2	1.35	1.78	3.51	2.81	5.58
Al_2O_3	14.84	14.62	15.31	13.98	13.62
Cr_2O_3	na	na	na	1.11	1.19
FeO	10.31	11.02	7.26	5.85	8.21
MnO	0.03	0.03	0.02	0.05	na
NiO	na	na	na	0.11	na
MgO	19.12	18.74	19.67	21.81	17.85
CaO	0.00	0.00	0.02	0.00	na
Na_2O	0.32	0.30	0.21	0.15	na
K_2O	8.81	8.29	9.29	na	9.23
Total	93.86	93.34	93.47	86.11	95.25
Cations (based on 23 oxygens)					
Si_{4+}	6.52	6.47	6.35	6.24	
Ti_{4+}	0.17	0.23	0.44	0.33	
Al_{3+}	2.92	2.89	3.00	2.55	
Cr_{3+}	0.00	0.00	0.00	0.14	
Fe_{2+}	1.44	1.55	1.01	0.76	
Mn_{2+}	0.00	0.00	0.00	0.01	
Ni_{2+}	0.00	0.00	0.00	0.01	
Mg_{2+}	4.75	4.68	4.87	5.04	
Ca_{2+}	0.00	0.00	0.00	0.00	
Na_+	0.03	0.02	0.02	0.05	
Total	15.83	15.84	15.70	15.12	
Mg#	0.77	0.75	0.83	0.87	

1+2 This study (UG2 pyroxenite, IM 851.9)
3 " (troctolite, IM 796.25)
4 Teigler (1990, pyroxenite 100 m below LG1, NG1 660.9)
5 Kruger (1982, Merensky Unit)
na = not analysed

4.9: Evaluation of Disequilibria: Zonation in Minerals

Disequilibrium conditions during crystallization (i.e. fractional crystallization) may not easily be detectable in zoning patterns of one or more ionic species within minerals as subsolidus processes often modify primary compositions. In other words, the absence of zoning does not necessarily indicate that equilibrium crystallization prevailed. Ionic species with high distribution coefficients and rates

of diffusion within one mineral commonly show subsolidus re-equilibration within that mineral.

The degree of primary disequilibrium mainly depends on the cooling rate of the magma (which controls the amount of supercooling) and the reaction rates of the different minerals. Thus, olivine with a high reaction rate for Mg and Fe will need more supercooling than plagioclase with its low reaction rate between mineral and melt to develop disequilibrium conditions between crystal and melt. The reaction rate in turn is dependent on the structure of the mineral, highly polymerized tectosilicates needing more time to equilibrate than ortho- or chainsilicates. Plagioclase equilibration is especially slow since it implies exchange of $(Ca^{2+}Al^{3+})$ for $(Na^{+}Si^{4+})$ pairs. For these reasons, plagioclase commonly is zoned in complex fashion, whereas orthopyroxene, olivine, and chromite are usually zoned only for one or two ionic species, if at all. In the following, zonation patterns of plagioclase and orthopyroxene will be discussed in greater detail.

4.9.1: Plagioclase Feldspar

The theoretically continuous solid solution series of plagioclase in the ideal case should yield crystals which change composition so as to remain constantly in equilibrium with the melt. However, plagioclase is virtually never unzoned, in spite of a small density difference between it and the melt, which most likely causes it to remain suspended in the liquid for a long time. This preservation of zonation is a result of its slow reaction rate. The abundance and variability of zoning in single crystals in a slowly cooling, large intrusion like the Bushveld Complex implies that the conditions in the chamber, or in different parts of the chamber, were subject to frequent change. Changing conditions in the chamber are inferred to be mainly related to frequent fresh magma influxes. To a degree, zonation may also reflect the nucleation of other phases competing for the same ionic species.

The different types of plagioclase zonation will briefly be presented in the following, for cumulus grains, resorbed cumulus inclusions in orthopyroxene and olivine, and intercumulus grains. Coefficients of variation which determine the reproducibility of the individual analysis are listed in Appendix IV. The coefficient for An content lies at 0.31%. Three basic types of zoning of An content can be distinguished in cumulus plagioclase: normal (i.e., zonation towards sodic rims), reversed and oscillatory zoning (Fig. 4.16).

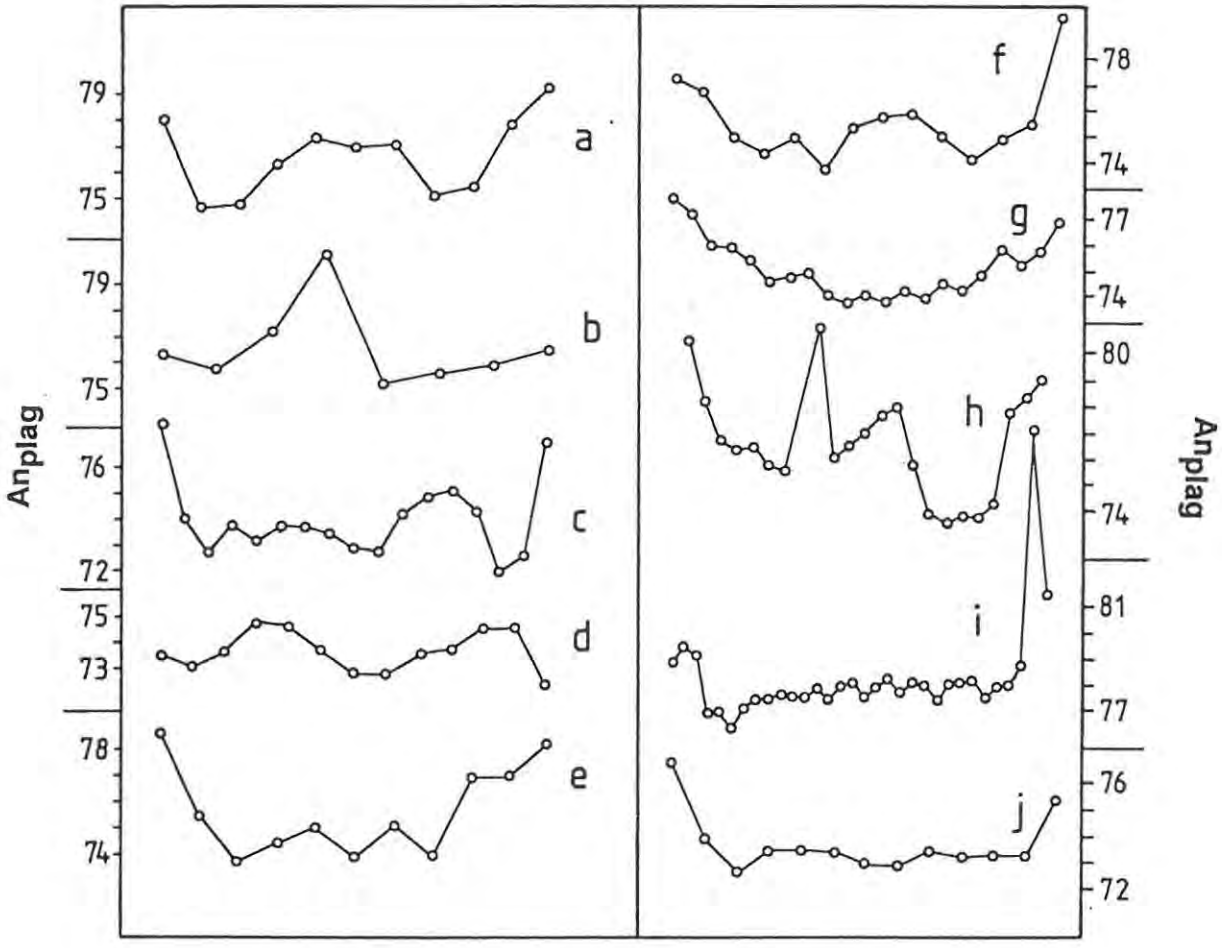

Fig. 4.16 Rim-to-rim zonation of cumulus plagioclase in norites and anorthosites. Limiting points are situated 5-10 μm from the grain boundary. (a) LK7 1562.25, width of grain is 130 μm. (b) LK7 1562.25, 130μm. (c) LK7 1577.45, 80μm. (d) LK7 1577.45, 120μm. (e) LK7 1577.45, 150μm. (f) LK7 1446.20, 80μm. (g) LK7 1446.20, 90μm. (h) LK71577.45, 100μm. (i) LK7 1577.45, 220μm. (j) H3 1206.95, 100μm. Each datum point represents one microprobe analysis.

Normal zoning is thought to occur in relatively fast cooling, simple fractionating magmas. Rarely do crystals exhibit normal zoning throughout the whole grain. Regular reversed zoning (Fig. 4.16(g)) may be caused by continuous addition of primitive magma, a temperature rise, pressure changes, or by accumulation of volatiles. Reversely zoned rims (Fig. 4.16(a), (b), (c), (e), (f), (g), (h), (i) and (j)) are possibly caused by rising temperature or oxygen fugacity (lowering the liquidus) which leads to preferential resorption of Ab component (Boudreau, 1988). Morse & Nolan (1984) suggested that increasing augite component within a closed intercumulus system can influence An partition with respect to plagioclase positively.

Multiple repetition of both reverse and normal zoning in one grain (Fig. 4.16(h)) is referred to as oscillatory zoning by Carr (1954) and Maaløe (1976). It has been explained by vigorous convection in a magma chamber (Carr, 1954), which would expose the suspended grain to continuously changing compositional, pressure and thermal environments. Bottinga et al. (1966) related oscillatory zoning to compositional fluctuations at more or less constant temperature. Maaløe (1976) pointed out that the zoning is probably a result of crystal growth, a) in a suspended state in the magma, and b) after deposition in an intercumulus environment. This caused the irregular outline of the zones.

Most cumulus plagioclase grains in the study section are reversely zoned to some degree as can be seen in the various types of zoning illustrated in Fig. 4.16. It is also evident that some grains are asymmetrically zoned. Apparently, such crystals were in contact with other grains at that stage, in which case larger grains may have grown at the expense of smaller ones (Maaløe). Alternatively, the availability of space resulting from primary porosity may have permitted more extended growth on one side of a crystal than on others. Ca enrichment may raise the An content by up to 8% in the outer zones of some crystals (Fig. 4.16(i)). Fe zonation in normal cumulus grains is negligible and has not been illustrated in Fig. 4.16.

Traverses through resorbed plagioclase inclusions, referred to in earlier parts of the text, are shown in Fig. 4.17. These often show irregular zonation which does not match the contour of the crystal. This means that remelting of plagioclase probably does not invariably follow compositional contours. Certain parts of the grain might be protected by other grains, or diffusion in the melt (which in turn is dependent on melt temperature and composition) might be statistically non-uniform. Nevertheless, one almost invariably finds An-rich rims which are possibly caused by the preferred remelting of Ab component (see above) or by chemical changes towards more primitive composition in the hybrid, presumably due to new magma influxes. Equilibration, i.e., diffusion of (Na^{+} Si^{4+}) molecules outwards and (Ca^{2+} Al^{3+}) molecules inwards will become less difficult the smaller the grain is. Therefore, zoning is fairly minor in the smaller plagioclase inclusions (Fig. 4.17 (a), (d), (e), (f), (g)).

Intercumulus plagioclase usually is normally zoned with respect to An component (Fig. 4.18). Possibly, the latent heat of crystallization in the immediate periphery of orthopyroxene cumulus grains caused plagioclase nucleation there to be deferred, and nucleation was therefore favoured in the intergranular spaces. However, as the nucleation rate must be regarded as low there, supersaturation was likely to exist and rapid poikilitic growth of late-stage phases becomes explainable. The possibility that small cumulus plagioclase grains form the cores of intercumulus plagioclase must be considered as well, as traverses on two grains from the UG2 pyroxenite at locality UA show (Fig. 4.18). Here, the central parts of the grains display a fairly constant level of An and only the outermost regions drop sharply in An content. Fig. 4.18(b) possibly shows two intergrown grains. It can also be seen that the sharp increase in Fe towards the rim of the grains is not necessarily coupled with a comparable decrease in An, which rules out the possibility of analyses being influenced by Fe radiation originating in the adjacent orthopyroxene grain.

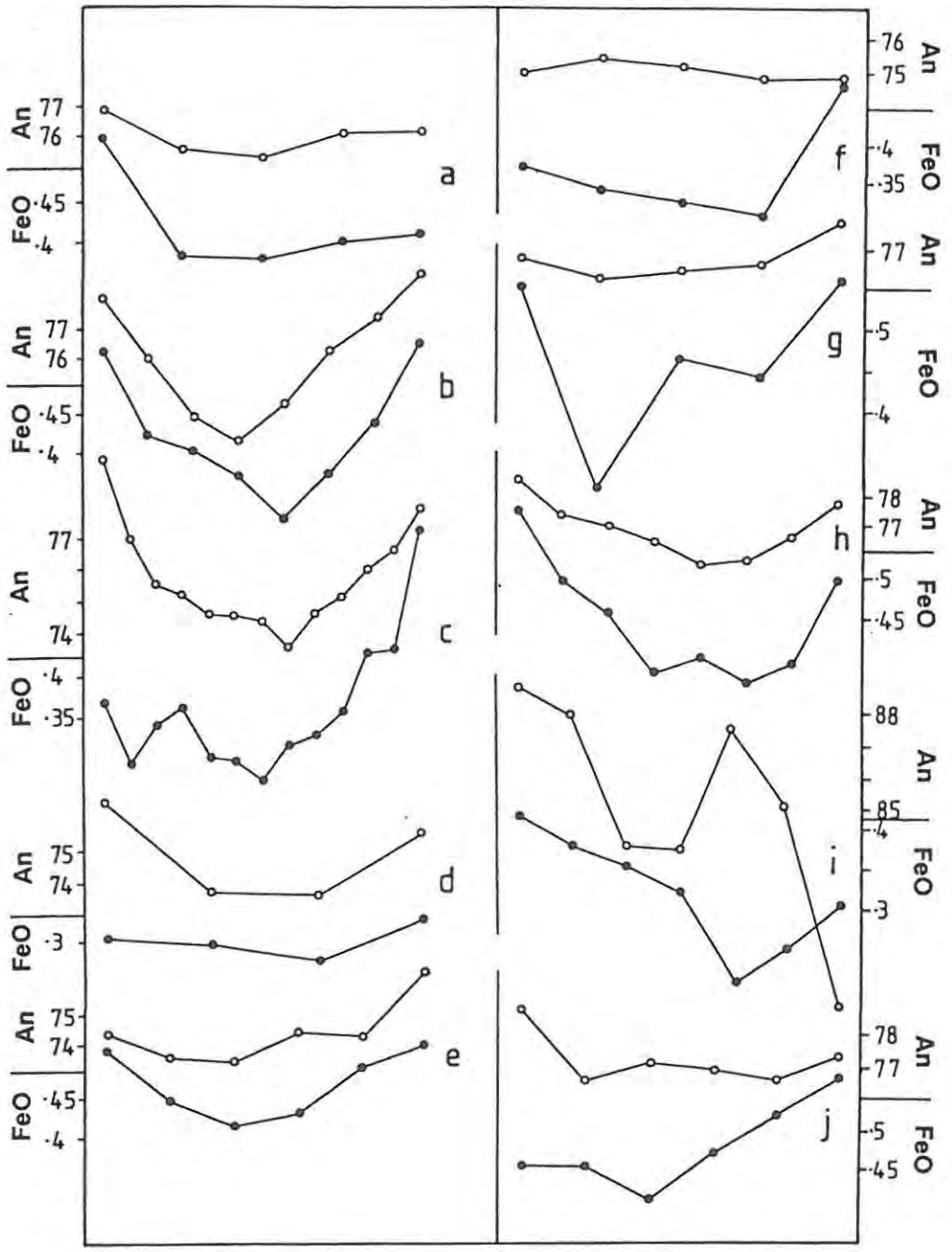

Fig. 4.17 Rim-to-rim zonation of resorbed plagioclase inclusions in cumulus orthopyroxene and olivine in norites and olivine norites. (a) LK7 1395.60, width of grain is 30μm. (b) H3 1250.35, 45μm. (c) H3 1250.35, 50μm. (d) LK7 1446.20, 20μm. (e) H3 1206.95, 35μm. (f) LK7 1446.20, 30μm. (g) LK7 1395.60, 30μm. (h) H3 1250.35, 45μm. (i) H3 1250.35, 40μm. (j) H3 1250.35, 40μm. FeO is expressed in wt%.

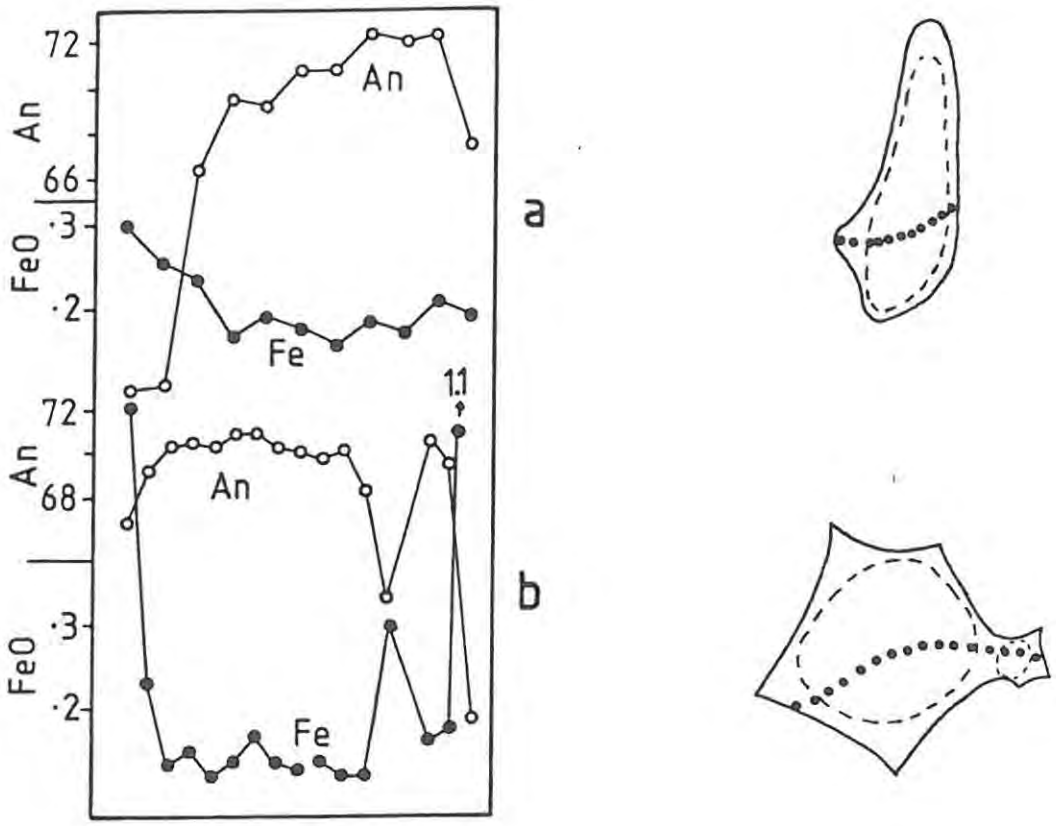

Fig. 4.18 Rim-to-rim zonation of intercumulus plagioclase (in pyroxenites). (a) UA 667.20, width of grain is 110μm. (b) UA 669.60, 220μm. Sketches on the right indicate position of the analyses within the grain. FeO is expressed in wt%.

Plagioclase inclusions and intercumulus grains usually display Fe enrichment towards their margins. Longhi et al. (1976) stated that Fe in plagioclase is a direct function of Fe/(Fe+Mg) in the melt, which would explain the observed zonation patterns. However, as can be seen in Appendix IV, the coefficient of variation for Fe in plagioclase lies at ca. 15%, thus rendering interpretation of Fe variations in plagioclase problematic.

4.9.2: Orthopyroxene

Orthopyroxene zonation is much weaker and more regularly developed than zonation of plagioclase (Fig. 4.19). The usual maximum variation in Mg# within a grain lies between 0.5% and 1%, the outer rims sometimes displaying a 2 % variation. This variation exceeds the coefficient of variation which lies at ca. 0.2% (see Appendix IV). Usually the grains are normally zoned with the rims showing lower Mg#, but oscillations of low amplitude (0.3%) are sporadically present. In some cases the outermost rim drops sharply in Mg# (Fig. 4.19(b) and (e)), but this depressed zone is not continuous around the crystal. Reversely zoned grains have not been encountered at all. Generally, orthopyroxene in pyroxenites (not shown in Fig. 4.19) is more irregularly zoned and shows lower maximum differences than orthopyroxene in norites.

Eighty per cent of all grains analysed, irrespective of their being in pyroxenites or norites, are zoned in such a way that they show Cr-rich cores and Cr-poor rims (Fig. 4.19(b), (d), (e), (f)). This zonation can reach 30% of the total value, which by far surpasses the coefficient of variation (ca. 2%, see Appendix IV). Analyses must be monitored constantly for Ca contents as the accidental analysis of clinopyroxene lamellae yields elevated Mg# and Cr contents in orthopyroxene.

Orthopyroxene usually is weakly zoned with respect to Al_2O_3, the cores being enriched and the rims depleted in Al_2O_3 (Fig. 4.19). This pattern has also been reported by Kruger (1982) and may be a result of simultaneous orthopyroxene and plagioclase crystallization, or a temperature effect. The solubility of Al in pyroxene is temperature dependent (Macgregor, 1974)

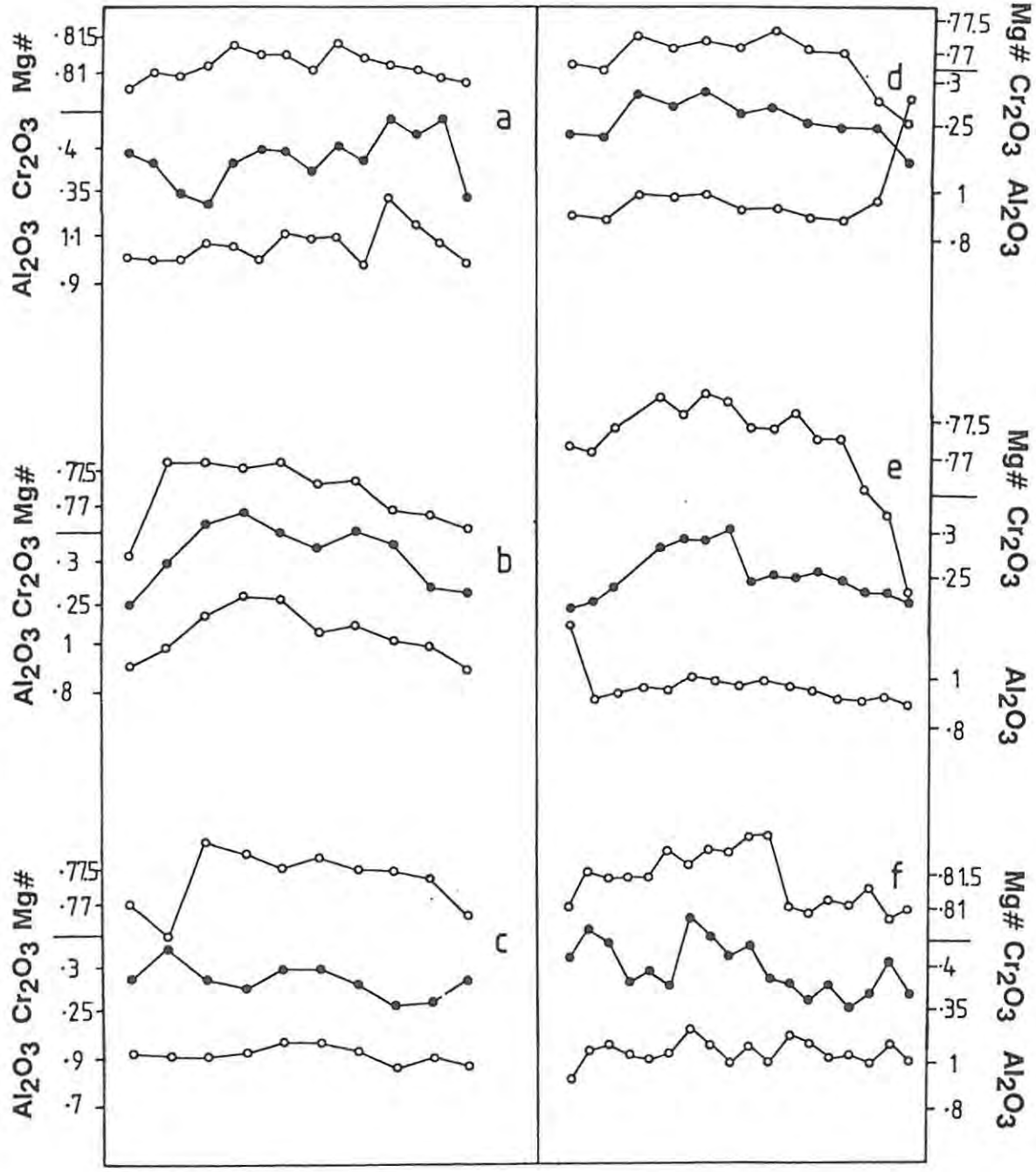

Fig. 4.19 Rim-to-rim zonation of orthopyroxene in norites. (a) LK7 1446.20, width of grain is 200μm. (b) LK7 1520.40, 180μm. (c) LK7 1520.40, 160μm. (d) LK7 1520.40, 150μm. (e) LK7 1520.40, 200μm. (f) LK7 1446.20, 210μm. Al_2O_3 and Cr_2O_3 are expressed in wt%.

If orthopyroxene (as well as olivine) is in contact with other ferromagnesian phases or chromite it shows distinct zonation in Mg# and Cr due to subsolidus exchange reaction of Mg^{2+} and Cr^{3+} cations from chromite against Fe^{2+} cations from the ferromagnesian phase. This reaction, however, is a very localized phenomenon and does not even affect the whole grain. For a detailed description of subsolidus processes in Bushveld chromite-orthopyroxene pairs see Eales & Reynolds (1986) and Botha (1987).

Unfortunately, zonation patterns from the study interval cannot be compared with other parts of the layered sequence, as very little precise information involving microprobe studies is available. However, Hoyle (1989) found orthopyroxene of pyroxenites in the Lower Zone to be normally zoned in Mg# and Cr.

4.10: Geothermometry

Equilibrium temperatures of orthopyroxene-clinopyroxene pairs have been applied to estimate temperatures in one representative core (IM) by means of the methods of Wood & Banno (1973) and Wells (1977). These methods essentially calibrate the temperature dependence of the following equilibration reaction:

$$Mg_2Si_2O_{6opx} = Mg_2Si_2O_{6cpx}$$

The temperatures obtained are listed in Table 4.6. Fig. 4.20 shows that the correlation with $Mg\#_{opx}$ is reasonably good with the exception of 3 samples (IM 804.40, 818.00 and 839.00).

Additionally, temperatures have been calculated for 18 samples from 5 cores (EK22, IN, IM, TF and LK7) according to the olivine-spinel geothermometer of Jackson (1969) and Roeder et al. (1979, Table 4.7). However, as Fe and Mg probably re-equilibrate down to temperatures far below the liquidus (Roeder et al., 1979), the obtained values are likely to represent the latest re-equilibration temperature of olivine and spinel.

Table 4.6: Equilibration temperatures for core IM (in °C), obtained by the orthopyroxene-clinopyroxene geothermometer of Wells (1977) and Wood & Banno (1973).

Sample	Wood & Banno °C	Wells °C	$Mg\#_{opx}$	Rock type
787.90	882	823	.811	Norite
788.32	875	824	.812	"
790.64	874	820	.792	"
793.22	892	834	.783	"
796.25	907	857	.812	"
801.00	911	865	.817	Olivine norite
804.00	994	956	.809	"
810.00	887	823	.815	"
818.00	953	885	.820	"
819.30	911	851	.815	Norite
819.85	884	843	.790	Troctolite
826.48	857	826	.752	Norite
836.00	796	747	.755	"
839.00	897	875	.758	"

Table 4.7: Equilibration temperatures between olivine and spinel, obtained by the thermometer of Jackson (1969) and Roeder et al. (1979).

	Sample	°C	Rock type
IM	788.80	402	Olivine norite
	796.25	526	Norite
	798.00	613	Troctolite
	810.10	664	Olivine norite
	818.00	727	"
	819.85	413	Troctolite
IN	863.12	313	Olivine norite
	866.40	620	Troctolite
EK22	288.40	453	Olivine norite
	288.95	390	Norite
	291.48	479	Troctolite
	299.95	297	Harzburgite
	306.50	563	"
	313.60	635	"
TF	866.50	662	"Boulder" harzburgite
LK7	1581.88	778	Harzburgite
	1585.85	639	"
UG2	Basal peg.	950	Pegmatoidal harzburgite

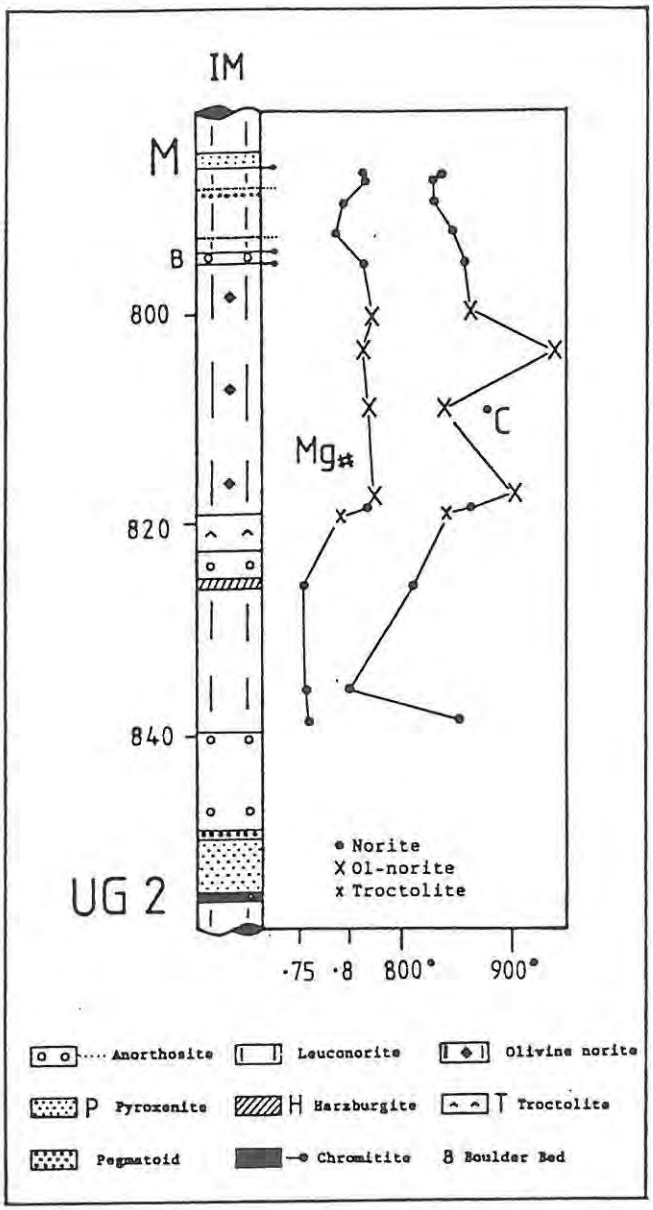

Fig. 4.20 $Mg\#_{opx}$ in the IM sequence in comparison with equilibration temperatures obtained by the orthopyroxene-clinopyroxene geothermometer of Wells (1977).

It is interesting to note that the basal pegmatoid of the UG2 chromitite shows by far the highest temperatures (Table 4.7). Furthermore, no match can be established between temperatures obtained from the two different geothermometers. This is contradictory to the results of Sinton (1977) and Medaris (1975).

4.11: Summary

- Cumulus plagioclase displays a fairly constant composition throughout the study interval. An values of intercumulus plagioclase scatter within a wider range but maximum values probably approach average values of cumulus grains. Plagioclase inclusions in orthopyroxene and olivine usually show elevated Fe and more or less similar An contents compared with cumulus grains.

- The distribution of Cr, Ni, Ti, Mn and Al in orthopyroxene exhibits a good correlation with Mg#, except for poikilitic and intercumulus orthopyroxene, which show a wider range of compositions.

- Values of Mg# of clinopyroxene and orthopyroxene appear to vary sympathetically.

- NiO and MgO contents of olivine are decoupled from each other.

- The composition of accessory chromite varies as a result of subsolidus reaction with coexisting orthopyroxene. Chromite within massive chromitite seams is compositionally more primitive (in terms of Mg# and Cr/Fe ratio) than accessory chromite because subsolidus reaction is inhibited by low orthopyroxene : chromite ratios.

- Mica within the study section falls in the compositional field of phlogopite. Mica is notably enriched in abundance in olivine-rich rocks.

- Amphibole as a discrete phase is very rare in the rocks of the study section and could only be identified in the UG2 pyroxenite at intersection IM, where it occurs as oxyhornblende.

- Zonation studies on cumulus plagioclase and plagioclase inclusions have revealed reversed zonation for Fe and An content. Intercumulus plagioclase is normally zoned for both parameters. Orthopyroxene is

usually weakly (and normally) zoned for Mg#, Cr and Al content. Olivine and chromite are unzoned.

- The results for the two-pyroxene and the olivine-spinel geothermometers exhibit no agreement between the two temperature ranges indicated.

CHAPTER 5: WHOLE-ROCK CHEMISTRY

5.1: Introduction

The whole-rock chemistry of the various rock types in the study section will be treated rather briefly here, as more specific comparisons of the different intersections along strike will follow in Chapter 7. Two hundred and twenty samples were prepared according to the method of Norrish & Hutton (1969) and analysed with a Phillips PW 1410 XRF spectrometer. Results are corrected for mass absorption and matrix effects. Ninety seven of the samples were analysed only for twelve trace elements (six of these by B. Walters in 1981). An additional twenty two samples from Union Section (core UA) and 33 samples from south-western Amandelbult (core AE) were analysed by W.J. de Klerk and M. Field, respectively, and incorporated into the database. All analyses were normalized to 100 wt% L.O.I.-free (including Cr_2O_3 and NiO) and a constant FeO/Fe_2O_3 ratio of 10 has been assumed. All analyses (plus values of L.O.I., H_2O^-, and original totals), including those by M. Field and W.J de Klerk, are listed in Appendix V.

5.2: Major Element Chemistry

Compositional variations of the major oxides are displayed in Fig. 5.1. SiO_2, FeO, TiO_2, and MnO usually increase in abundance with increasing MgO content in plagioclase-orthopyroxene cumulates, whereas Al_2O_3, Na_2O, and CaO decrease (Fig. 5.1). Harzburgites and chromitites, both being very poor in SiO_2 and rich in MgO and FeO, do not plot along these trends. K_2O shows more or less equal values for all rock types, with a slight enrichment in anorthosites and some pyroxenites. The latter phenomenon can be attributed to the high K_2O values of some intercumulus plagioclase.

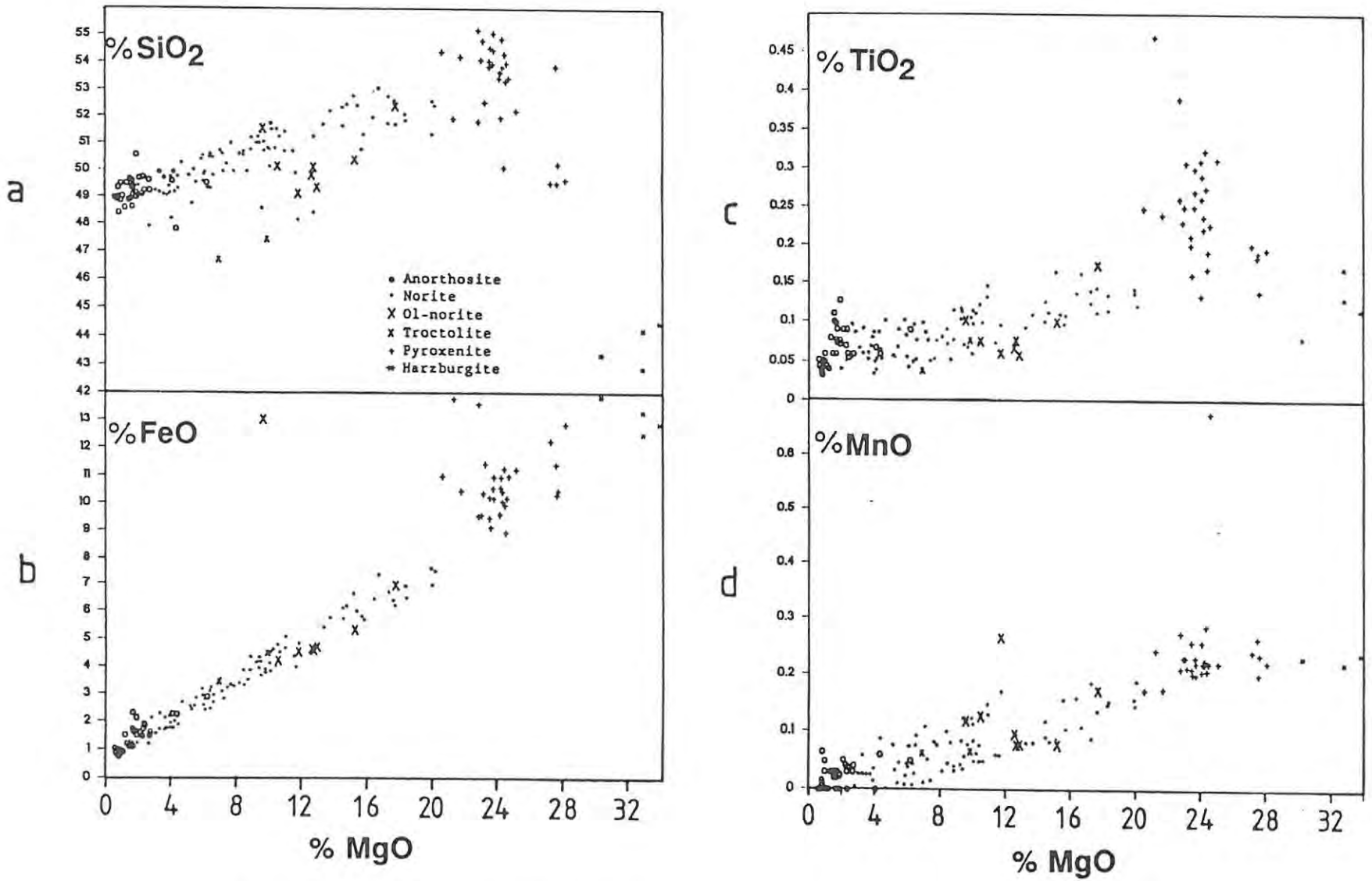

Fig. 5.1 (a)-(h) Variation diagrams of major elements, plotted against MgO (weight percentages). All data normalized to 100%, with H_2O and L.O.I. excluded.

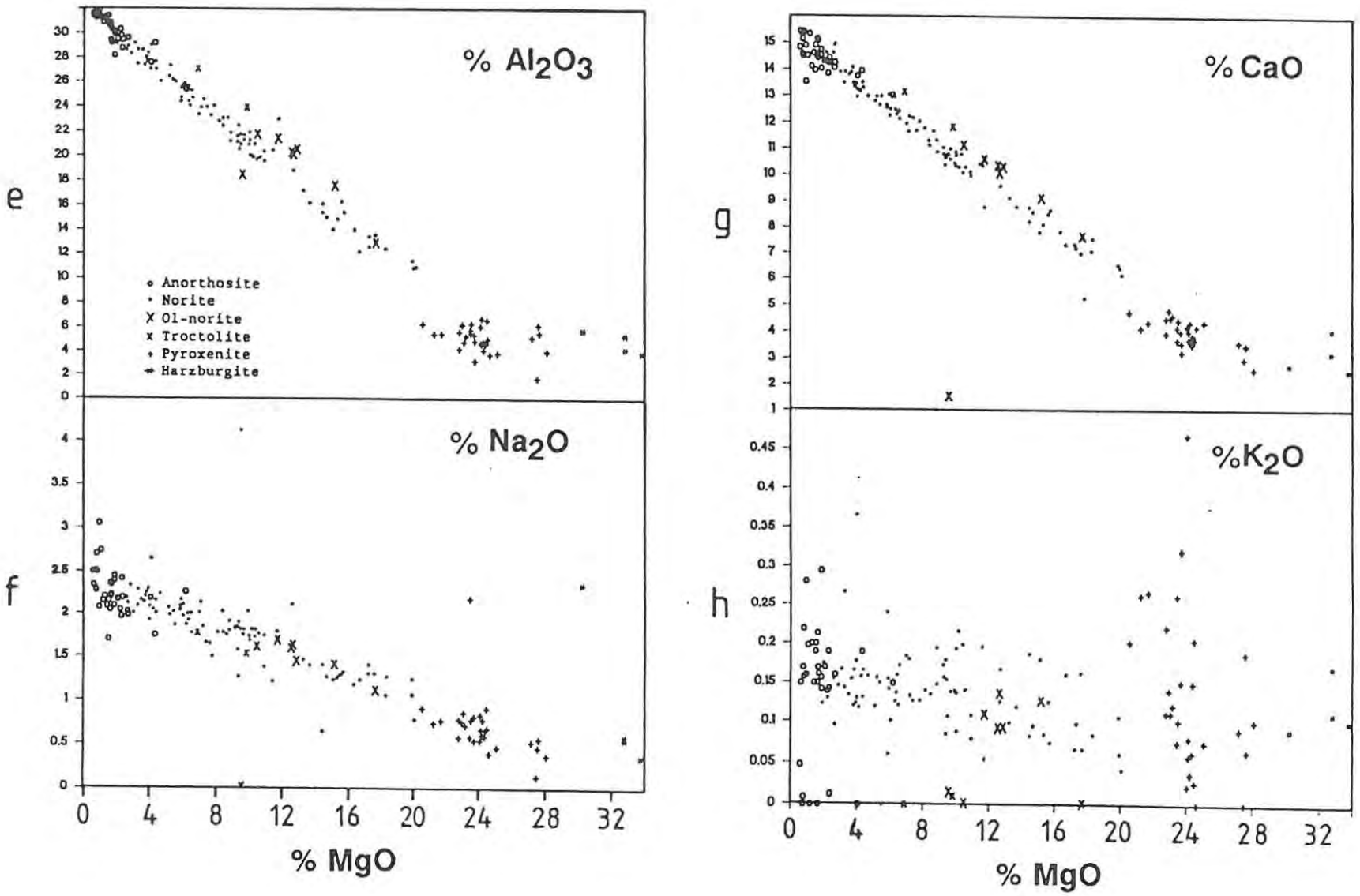
e
% Al_2O_3
Anorthosite
Norite
Ol-norite
Troctolite
Pyroxenite
Harzburgite
f
% Na_2O
0 4 8 12 16 20 24 28 32
% MgO
g
% CaO
h
% K_2O
0 4 8 12 16 20 24 28 32
% MgO

The compositional fields of olivine norites and troctolites diverge from the noritic field in the Al_2O_3, CaO, Na_2O, and SiO_2 plots. This is caused by the elevated MgO values of the former rocks at a constant amount of modal plagioclase, an effect related to the abundance of olivine. Olivine norites, troctolites, and norites show more or less similar levels of FeO, K_2O, MnO, Na_2O, and TiO_2. In most plots a notable gap or hiatus is developed between norites and pyroxenites. The average compositions and the compositional ranges of the different rock types are displayed in Table 5.1 and 5.2, respectively. Variations in the major element oxide Al_2O_3 have been used by Eales et al. (1988) in a classification scheme for pyroxene-plagioclase cumulates (Fig. 1.5). Table 5.2 shows that this scheme is mostly, but not entirely, applicable for the rocks of the study section although the present author uses different definitions for anorthosites and leuconorites than the authors cited above (see Chapter 1.5). Levels of MgO and Al_2O_3 are plotted against stratigraphic height in Figs. 5.5, 5.7, and 5.9 - 5.13.

Table 5.1: Average compositions of the various rock types in the study interval

Rock type	Anorthosites	Norites	Olivine norites	Pyroxenites	Troctolites	Harzburgites
SiO2	49.20	50.67	50.40	52.93	46.41	43.65
TiO2	0.06	0.09	0.08	0.25	0.36	0.15
Al2O3	30.63	22.24	19.64	4.78	22.02	4.08
Fe2O3	0.13	0.40	0.48	1.09	0.52	1.31
FeO	1.28	3.96	4.79	10.86	5.25	13.12
MnO	0.02	0.07	0.12	0.25	0.08	0.22
MgO	1.31	9.13	12.61	24.33	12.94	33.45
CaO	14.77	11.22	10.08	3.86	11.07	3.27
Na2O	2.43	1.85	1.48	0.61	1.34	0.38
K2O	0.14	0.13	0.05	0.13	0.04	0.13
P2O5	0.01	0.01	0.00	0.01	0.00	0.03

Table 5.2: Compositional range of the various rock types in the study interval

Rock type	Anorthosites		Norites		Olivine norites		Pyroxenites		Troctolites		Harzburgites	
	min	max	min	max	min	max	min	max	min	max	min	max
SiO2	48.42	50.59	48.00	53.19	49.11	52.38	49.67	54.88	45.68	47.48	42.87	44.49
TiO2	0.03	0.13	0.04	0.17	0.06	0.17	0.13	0.47	0.04	0.73	0.12	0.18
Al2O3	28.21	32.00	11.11	30.21	12.84	23.40	1.73	6.57	17.05	27.15	3.30	5.35
Fe2O3	0.08	0.21	0.13	0.76	0.36	0.69	0.89	1.38	0.34	0.71	1.25	1.36
FeO	0.77	2.13	1.28	7.60	3.61	6.92	8.93	13.79	3.44	7.15	12.48	13.58
MnO	0.00	0.07	0.00	0.19	0.07	0.26	0.17	0.67	0.06	0.12	0.16	0.24
MgO	0.58	2.36	1.94	20.11	8.63	17.70	20.54	28.05	6.88	19.21	32.76	34.53
CaO	13.56	15.45	6.27	15.02	7.61	11.81	2.55	4.73	8.85	13.16	3.15	4.04
Na2O	2.10	3.06	0.69	4.17	1.11	1.80	0.13	0.91	0.83	1.78	0.17	0.59
K2O	0.00	0.29	0.00	0.37	0.00	0.13	0.00	0.47	0.00	0.08	0.08	0.18
P2O5	0.00	0.06	0.00	0.06	0.00	0.01	0.00	0.13	0.00	0.01	0.00	0.06

5.3: Trace Element Chemistry

Trace element partitioning is influenced by a complex interplay between kinetic effects, temperature, pressure, melt composition, ionic radii, site sizes, and crystallization and accumulation rate (Jensen, 1973; Lindstrom, 1983; Möller, 1988; Ulmer, 1989; Hanson, 1989). The distribution of the different elements in the various rock types often reflects the ratio of cumulus to intercumulus phases. "Compatibility" might change drastically, even on a relatively small scale as within the study interval. For example, Ni, which is highly "compatible" in early olivine cumulates, might be "incompatible" in cycles dominated by plagioclase crystallization. Trace elements with high partition coefficients, like Cr in orthopyroxene-bearing systems, become depleted so fast that straight regression lines are unlikely in plots of one element against another. If one obtains linear relationships in these circumstances, some process other than simple fractionation in a closed system must be envisaged as well. Estimated partition coefficients of a number of trace elements are listed in Table 5.3 and the average concentration of the individual trace elements in the different rock types is presented in Table 5.4.

Table 5.3: A selection of information on distribution coefficients, taken from the literature

	olivine	orthopyroxene	clinopyroxene	plagioclase	spinel
Ni	10(2) 3.5-3.8(3) 3.4-4.8(6) 5-20(22)	1.1-3.1(1) 4(2) 3-5(3)	2(2) 2-4(3) 6.5(5)	0.01(2) 0.2(4)	5(2)
Cr	0.2(2) 2.7(9) 3.1-10(13) 0.25-25(22)	2(2)	10(2) 20(9) 40(12)	0.01(2) 0.1(11)	
V	0.04(1) 0.09(3) 0.05(9)	0.06-3.4(1) 0.3(3) 0.5-2.3(8)	1.5(3) 1.3(9) 0.94-4.1(12) 0.06.3.4(14)		38(1)
Co	1-7(1) 3.1(9) 4.8(17) 3-6(22)	1.2(7)	0.5-2(10) 1.7-4.9(5) 1.2(7) 1.2(9)	0.1(8) 0.026(7) 0.01-0.09(22)	3.4(7)
Sc	0.37(1) 0.33(7) 0.25(3) 0.15-0.2(22)	0.53-1.4(1) 3.3(7) 1.1(3)	3.1(3)	0.017-0.065(1) 0.008(7) 0.01(20) 0.01-0.08(22)	0.048(1)
Sr	0.003(1) 0.001(2) 0.1(18) 0.01-0.02(22)	0.018(1) 0.01(2)	0.07(2) 0.1(17)	2.2(2) 3.06(16) 1.75(21)	0.01(2)
Rb	0.001(2) 0.01(3)	0.004(1) 0.0006(15)	0.017(1) 0.001(2) 0.03(17)	0.94-3.3(18) 0.07(2)	
Zr	0.01(19) 0.015-0.1(22)	0.03(19)	0.12(1) 0.2-0.7(22)	0.01(19)	
Cu	0.47-0.27(1) 0.023(7)	0.071(7)	2.4-1.5(1)	0.004(7) 0.24(5)	
Zn	1.8(7)	0.49(2)		0.13(7)	

(1) Irving (1978), (2) Cox et al. (1979), (3) Frey et al. (1978)
(4) De Long (1974), (5) Ewart et al. (1973), (6) Leeman & Lindstrom (1978),
(7) Paster et al. (1974), (8) Jensen (1973), (9) Duke (1976),
(10) Lindstrom & Weill (1978), (11) Walker (1970), (12) Campbell & Borley (1974),
(13) Flower (1973), (14) Ringwood (1970), (15) Hanson (1977),
(16) Drake & Weill (1975), (17) Hart & Brooks (1974), (18) Phillpots & Schnetzler (1970)
(19) Pearce & Norry (1979), (20) Salpas et al. (1983), (21) Morse (1982),
(22) Lemarchand et al. (1987).

Table 5.4: Average concentration of the individual trace elements in the different rock types.

	Anorthosite	Norite	Pyroxenite	Harzburgite
Sr	400 - 500	100 - 400	30 - 90	≈ 70
Rb	0 - 10	0 - 10	0 - 20	0 - 8
Zr	0 - 15	0 - 15	0 - 55	0 - 10
Y	0 - 10	0 - 8	0 - 15	0 - 7
Nb	below 2	0	0	below 2
Zn	0 - 20	0 - 60	60 - 160	≈ 80
Cu	0 - 40	0 - 50	20 - 80	20 - 50
Ni	0 - 100	50 - 500	400 - 1200	≈ 1500
Co	0 - 20	10 - 100	80 - 200	≈ 160
Cr	0 - 100	100 - 2000	2000 - 4000	≈ 1000
V	0 - 30	10 - 100	90 - 150	≈ 50
Sc	0 - 7	3 - 30	20 - 50	≈ 10

Strontium, with an ionic radius of 1.18 Å, substitutes about equally for Ca (1.01 Å) and K (1.33 Å). The partitioning of Sr into plagioclase is therefore significantly higher than into the other cumulus phases and K_D lies somewhat above unity. The Sr content of the rock is mainly a function of the modal proportion of plagioclase, which is reflected in plots of Sr versus MgO (Fig. 5.2(a)) and V versus Sr (Fig. 5.3(a)). For reasons stated above, olivine norites, troctolites, and especially harzburgites, plot in different compositional fields than norites.

Korringa & Noble (1971) and Jensen (1973) show that D^{Sr}_{plag} increases with decreasing An content of the liquid. However, the total amount of Sr in the residual liquid decreases once plagioclase starts crystallizing, thus creating a counter-effect which largely offsets change in D^{Sr}_{plag} during crystallization (Fig. 5.2(a)).

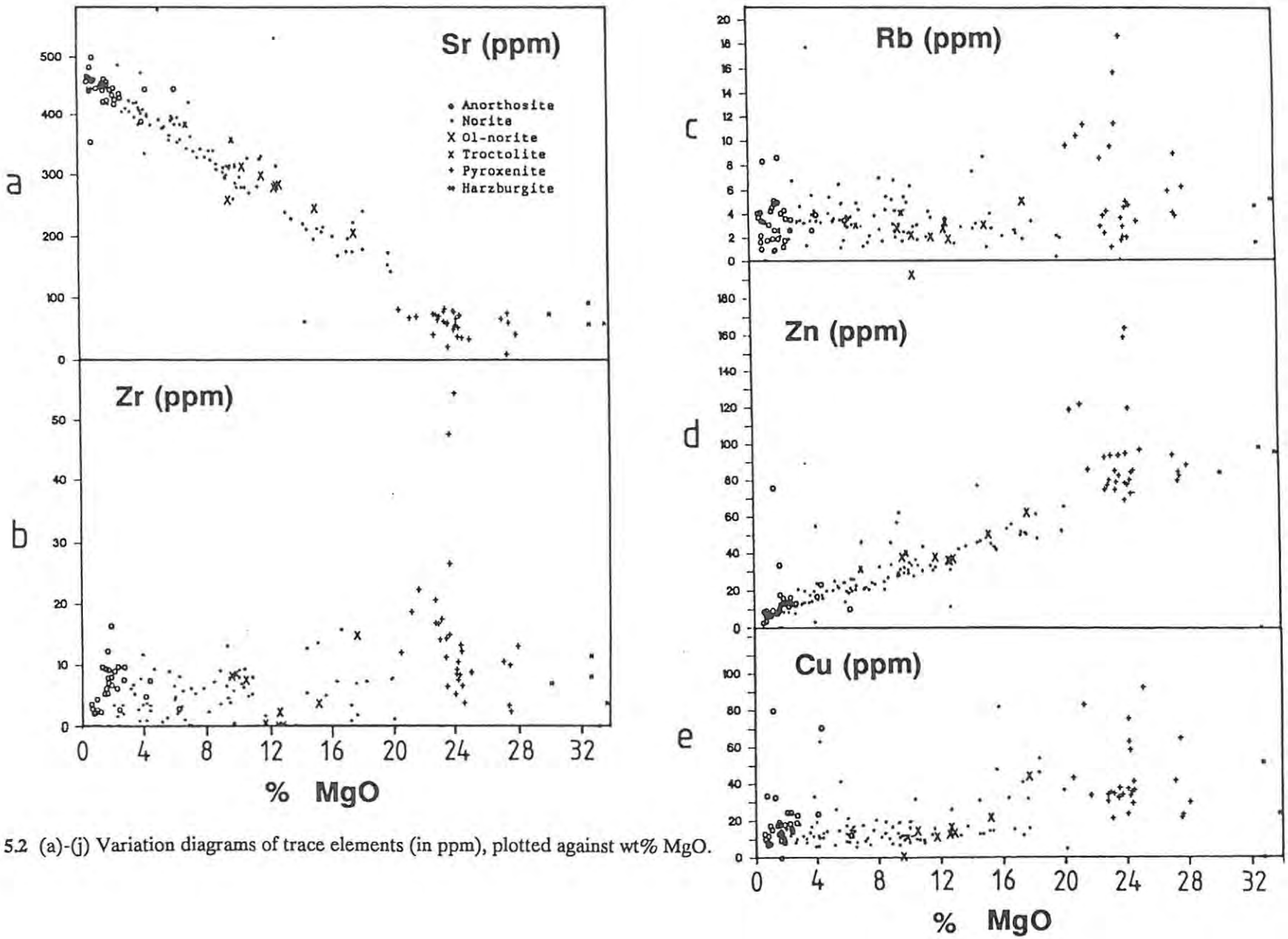

Fig. 5.2 (a)-(j) Variation diagrams of trace elements (in ppm), plotted against wt% MgO.

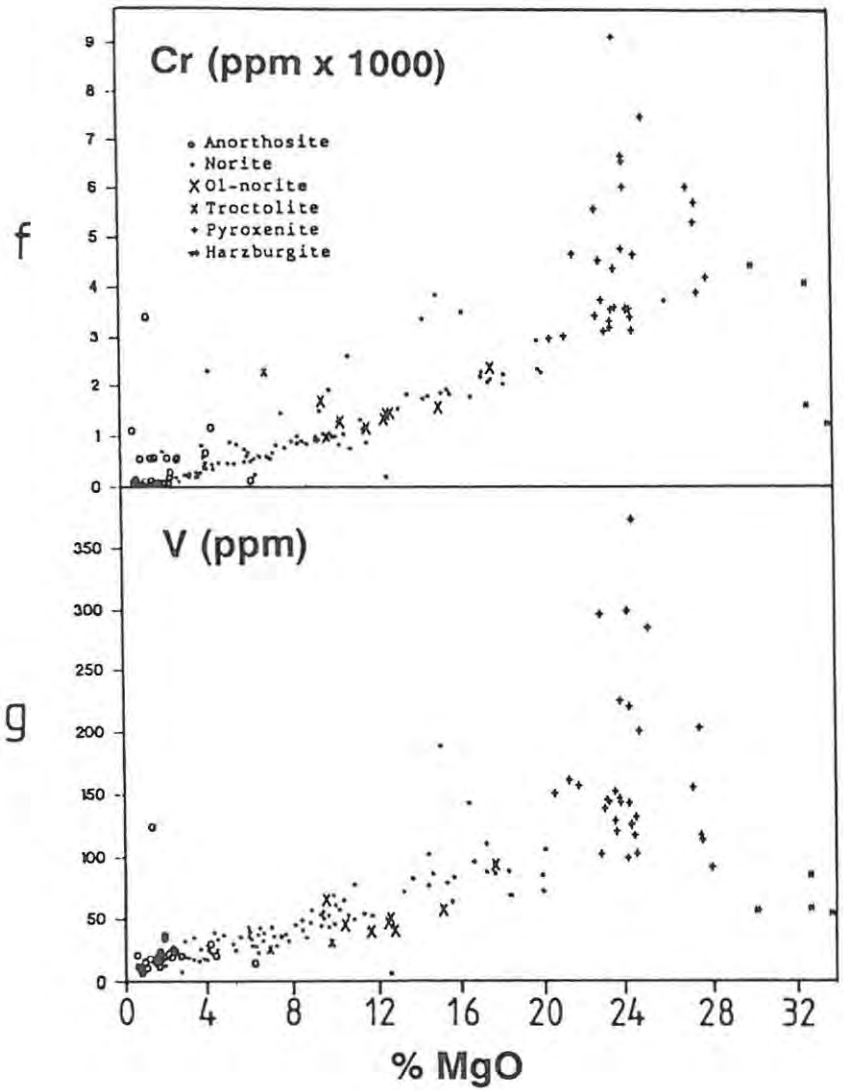
Cr (ppm x 1000)
Anorthosite
Norite
Ol-norite
Troctolite
Pyroxenite
Harzburgite
V (ppm)
% MgO

f

g

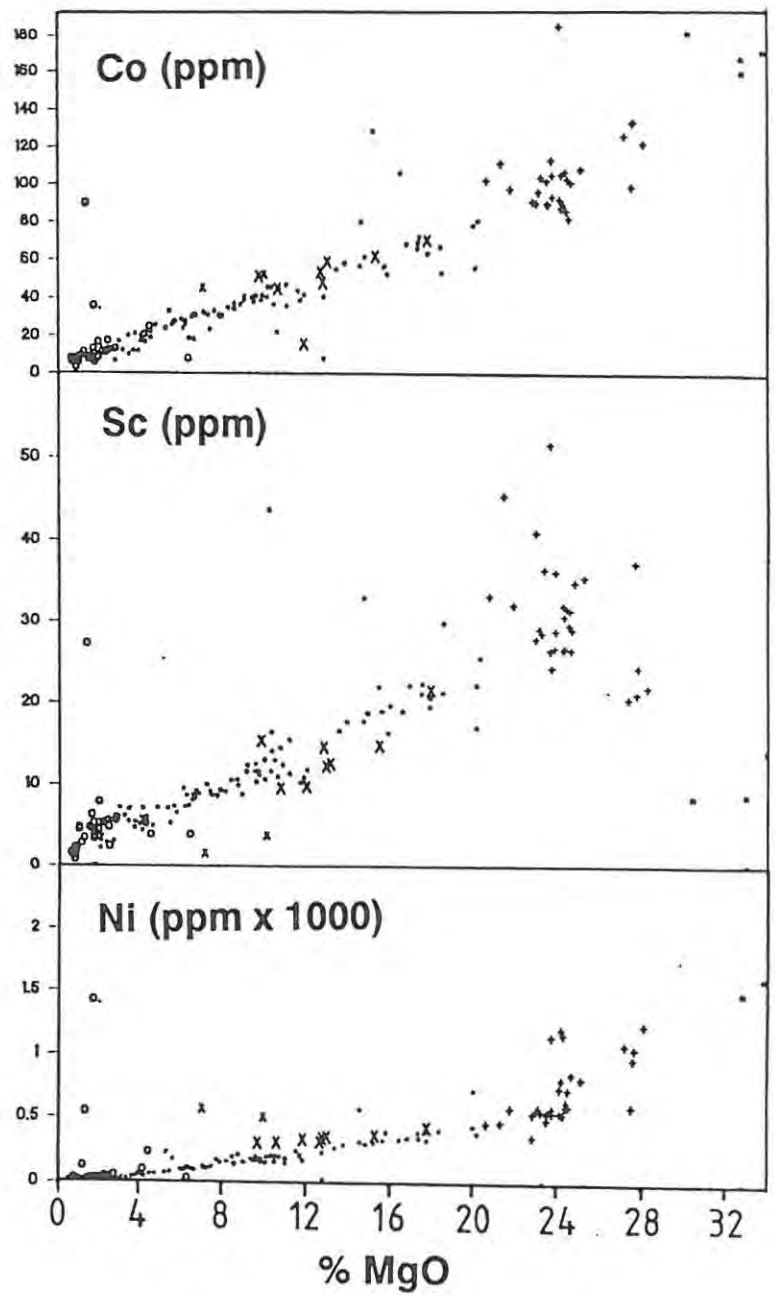
Co (ppm)
Sc (ppm)
Ni (ppm x 1000)
% MgO

h

i

j

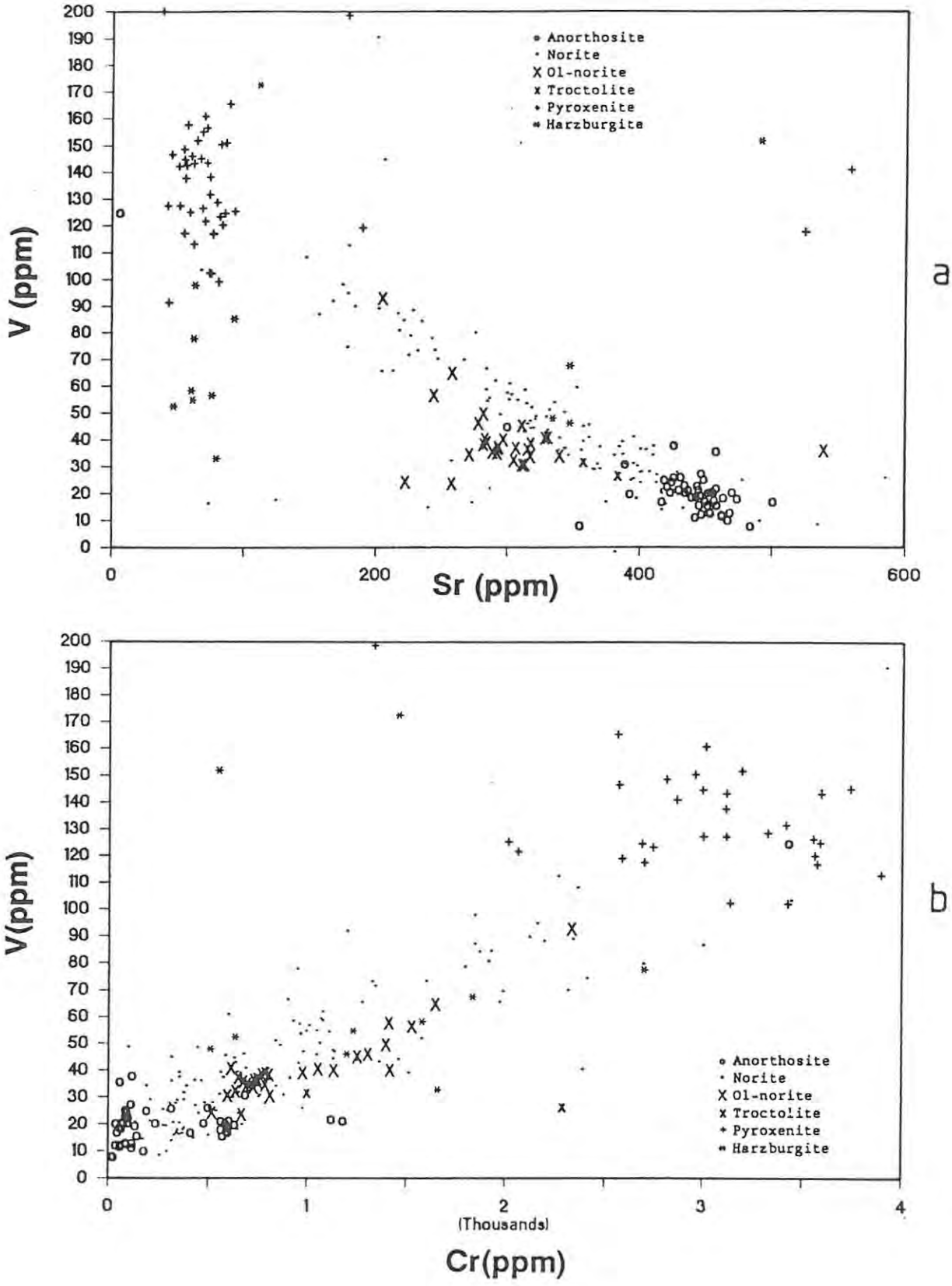

Fig. 5.3 Plot of whole-rock V against (a) Sr, and (b) Cr.

Some trace elements behave in a wholly incompatible manner at all stages, as, for all of the cumulus minerals in this study, they have partition coefficients much less than unity. Thus, their concentration in the rock depends in part on fractionation processes, but mainly on the proportion of intercumulus minerals representing trapped residual liquid. Those elements are Rb, Zr, Y, and Nb. Unfortunately, the levels of these elements in the study section are often close to the instrumental lower limit of detection (see Table 5.4 and Appendix V). Therefore, the values are considerably scattered. Ten different trace elements have been plotted against wt% MgO in Fig. 5.2 (Y and Nb have not been shown as most values are below the detection limit). Some samples of the UG2 pyroxenite, containing abundant modal chromite, have not been plotted. Levels of Sr are plotted against stratigraphic height in Figs. 5.5 - 5.13.

Rubidium, whose ionic radius (1.47 Å) is close to that of K (1.33 Å) partitions preferentially into K-feldspar and mica. Niobium and Zirconium are elements with high charge and small radius. Zr especially, with an ionic radius of 0.79 Å, does not enter significantly into any other cation site in common cumulus minerals. The usually positive correlation between Zr and Yttrium serves as further evidence that the two elements are almost invariably concentrated in the intercumulus liquid. Therefore, pyroxenites, which normally contain 10 - 20 vol% of intercumulus minerals, often show the highest levels of all four of these elements (Fig. 5.2(b) and (c) for Zr and Rb). It is of interest to note that the lowest levels of Zr, Y, and Rb in most cores can be found in the immediate footwall of the Merensky Reef. Unless recrystallization and remobilization modified original element concentration patterns this feature does not indicate crystallization of these rocks from the latest crystallizing liquids. Yttrium (with an ionic radius of 0.98 Å) substitutes in limited amounts for Ca (ionic radius: 1.01 Å), especially in orthopyroxene (see Lambert & Holland, (1973)). This might be a reason for the elevated Y values in pyroxenites. As anorthosites usually show the same Y values as norites, however, the author concludes that Y

becomes preferentially concentrated in the intercumulus melt. Levels of Zr are plotted against stratigraphic height in Figs. 5.5 - 5.13.

Zinc has distribution coefficients around unity for olivine, and slightly below unity for orthopyroxene (Table 5.3). It therefore shows slightly elevated values in pyroxenites (up to 30 ppm, Fig. 5.2(d)).

Copper partitions preferentially into sulphides and shows invariably low values for any rock type barren of sulphides (Fig. 5.2(e)). Only clinopyroxene shows partition coefficients above unity, but that does not directly concern this work.

Chromium has a high distribution coefficient with respect to chromite (ca. 500, Eales, pers.com.). The coefficient for orthopyroxene is about 2 and is likely to be below unity (see Table 5.3) with a preference for Mg-rich olivine (Deer et al., (1982). Flower (1973) found partition coefficients as high as 10 in ankaramites, and Duke (1976), who also found partition coefficients above unity in synthetic, quenched olivines, suggested that slowly cooled olivine exsolves chrome spinel and therefore yields lower partition coefficients. Chromium partitioning into olivine seems to be controlled in part by oxygen fugacity as olivine of lunar basalts shows unusually high Cr contents (Butler, 1972). Plagioclase rejects chromium almost completely. Pyroxenites show a wide range of Cr levels because they contain varying amounts of interstitial chromite in addition to Cr within orthopyroxene (Fig. 5.2(f)). The Cr-rich anorthosite in Fig. 5.2(f) is a sample from the footwall of the Merensky Reef and also shows elevated levels of V, Co, Sc, and Ni, attributable to the presence of both chromite and sulphides.

The use of Cr as a fractionation indicator is limited in cumulus rocks, as the crystallization of chromite can occur at different stages of differentiation, under the influence of temperature or oxygen fugacity. Because of its preferential partitioning into chromite and orthopyroxene, depletion of Cr in the crystallizing melt is rapid in a closed system.

Vanadium shows extremely high partitioning into spinel; lies around unity and partitioning into olivine is low (see Table 5.3). The high V values in some pyroxenites (Fig. 5.2(g)) are explained by the presence of dispersed chromite and poikilitic clinopyroxene (the partition coefficient of V into clinopyroxene lies slightly above unity). A plot of V versus Cr does not show a particularly good regression (Fig. 5.3(b)). However, the individual cores display better results than the total sample population even if there is no systematic regional pattern detectable (Table 5.5).

Table 5.5: Regression equations ($y = xm + c$) for individual cores along strike in the Western Bushveld Complex, for Cr_{wr}/V_{wr}. R = correlation coefficient; n = number of samples (including all rock types).

Core	y	x	m	c	R	n
UA	Cr_{wr}	V_{wr}	0.029	12.91	.984	23
7E[3]	Cr_{wr}	V_{wr}	0.042	13.85	.966	41
EK22	Cr_{wr}	V_{wr}	0.032	8.11	.961	20
60E[3]	Cr_{wr}	V_{wr}	0.053	3.08	.864	65
IN	Cr_{wr}	V_{wr}	0.032	9.83	.899	17
IM	Cr_{wr}	V_{wr}	0.044	-1.70	.961	19
LK7	Cr_{wr}	V_{wr}	0.042	20.68	.975	20
H3	Cr_{wr}	V_{wr}	0.038	14.76	.943	20
KR2	Cr_{wr}	V_{wr}	0.035	15.89	.942	20
All	Cr_{wr}	V_{wr}	0.038	12.52	.900	245

Olivine norites and norites again plot in fields that overlap only partially (Fig. 5.3(b)). Levels of V are plotted against stratigraphic height in Figs. 5.5 - 5.13.

Cobalt (Fig. 5.2(h)) partitions preferentially into spinel and olivine; values of K_D for orthopyroxene are around unity. Co preferentially substitutes for Mg, and Carr & Turekian (1961) report a good correlation with Mg contents in granitic rocks. Accordingly, the relationship between Co and Mg is linear in Fig. 5.2(h). Levels of Co are plotted against stratigraphic height in Figs. 5.5 - 5.13.

Scandium is completely rejected by plagioclase and spinel. D^{Sc}_{opx} lies around unity (Table 5.3) but D^{Sc}_{cpx} exceeds unity. Partitioning into olivine is minor. Sc values in the studied interval are therefore largely a function of the modal proportion of orthopyroxene and associated clinopyroxene and display a gradual increase from anorthosites into pyroxenites, with low values in harzburgites, where clinopyroxene is generally a minor phase.

Nickel is strongly compatible with respect to chromite, olivine, orthopyroxene, and sulphides. Thus it should in theory be a good fractionation indicator. The mineral chemistry, however, has shown that this is not necessarily the case in the study interval (Fig. 4.8) as Ni versus MgO_{opx} shows a poor correlation. One must therefore conclude that the system was not closed, and that new influxes of magma and subsequent mixing with residual liquid played an important role in the evolution of the studied rocks. Olivine norites, troctolites, and some olivine-bearing pyroxenites are enriched in Ni while the high-Ni anorthosite (Fig. 5.2(j)) is a sample from the immediate footwall of the Merensky Reef (sample $7E^3$ 398.05) which is enriched in sulphides.

If one compares the Sc versus Ni ratio for different rock types (Fig. 5.4(a)), it becomes clear that only norites show a consistent ratio whereas olivine norites and pyroxenites, as well as some anorthosites, show varying ratios and a generally poor regression relationship. Separation of data relating to individual cores, however (Fig. 5.4(b)), reveals that the quality of the correlation varies significantly for different parts of the Western Bushveld Complex. The three cores east of Rustenburg (LK7, H3, KR2), which are virtually olivine-free, show a good correlation, whereas the anorthosites and olivine-bearing norites of the $60E^3$ core have to be disregarded for correlations involving Ni. Levels of Ni are plotted against stratigraphic height in Figs. 5.5 - 5.13.

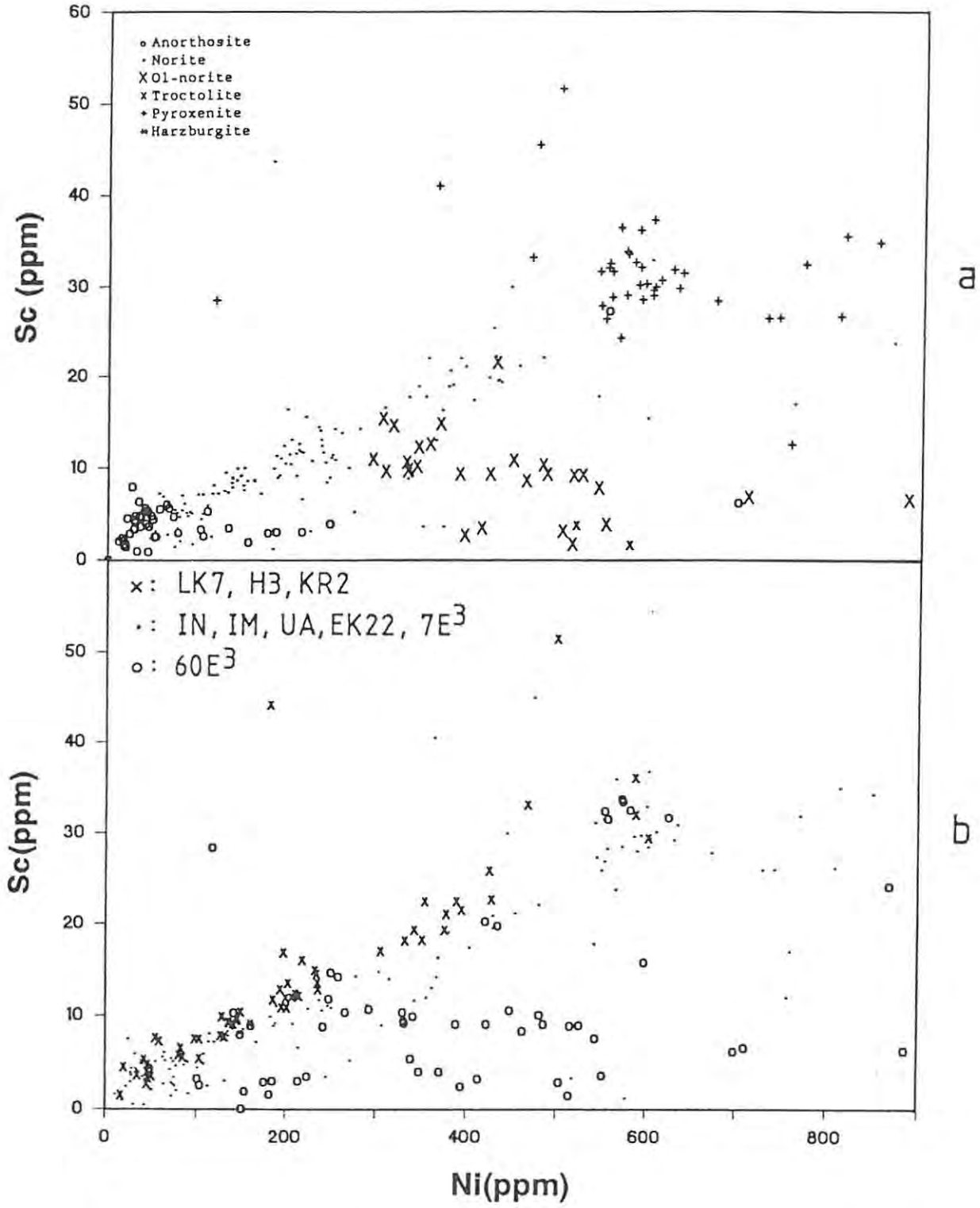

Fig. 5.4 (a) Plot of whole-rock Sc against Ni. Harzburgites are not plotted as they cluster around 2000 ppm Ni. (b) The same plot, distinguishing between different regions of the western limb (see text for further discussion).

Cr, V, Co, Ni, and Sc are compatible trace elements with respect to the ferromagnesian phases orthopyroxene and olivine and the fact that they all show linear correlations with MgO rather than exponential relationships favours a model of repeated replenishment (liquid mixing) in the chamber.

To establish chemical variations along strike, each core should be treated separately, as the regression lines for specific element ratios in different parts of the complex might have, or indeed should have, different slopes. This means that an incoherent regression for an element in the Western Lobe as a whole might show good regressions for the specific parts of the complex. Good regressions for individual cores, but with different slopes, would imply that primary chemical variations in the chamber exist along strike. In part, this type of behaviour has been established for Sc versus Ni (Fig. 5.4) and Cr versus V (Table 5.5)

The above method of investigation might be important as lithological variations, such as relative thicknesses of primitive and evolved cumulates, may result purely from regional variations in factors like changing heat flux, viscosity, and yield strength of the liquids. Even liquidus relationships might change for these reasons, as they are influenced by volatile fugacities.

As can be seen in Fig. 5.1 and 5.2, the plotting of levels of many elements in the total population of samples against MgO yields straight lines. This is a partial contradiction of the Sc versus Ni (Fig. 5.4(b)) and V versus Cr (Fig. 5.3(b)) trends (which revealed different slopes for different sections) because it implies that primary chemical variations in the chamber were indeed small during the deposition of the studied rocks and that the chamber was, compositionally, relatively homogeneous along strike.

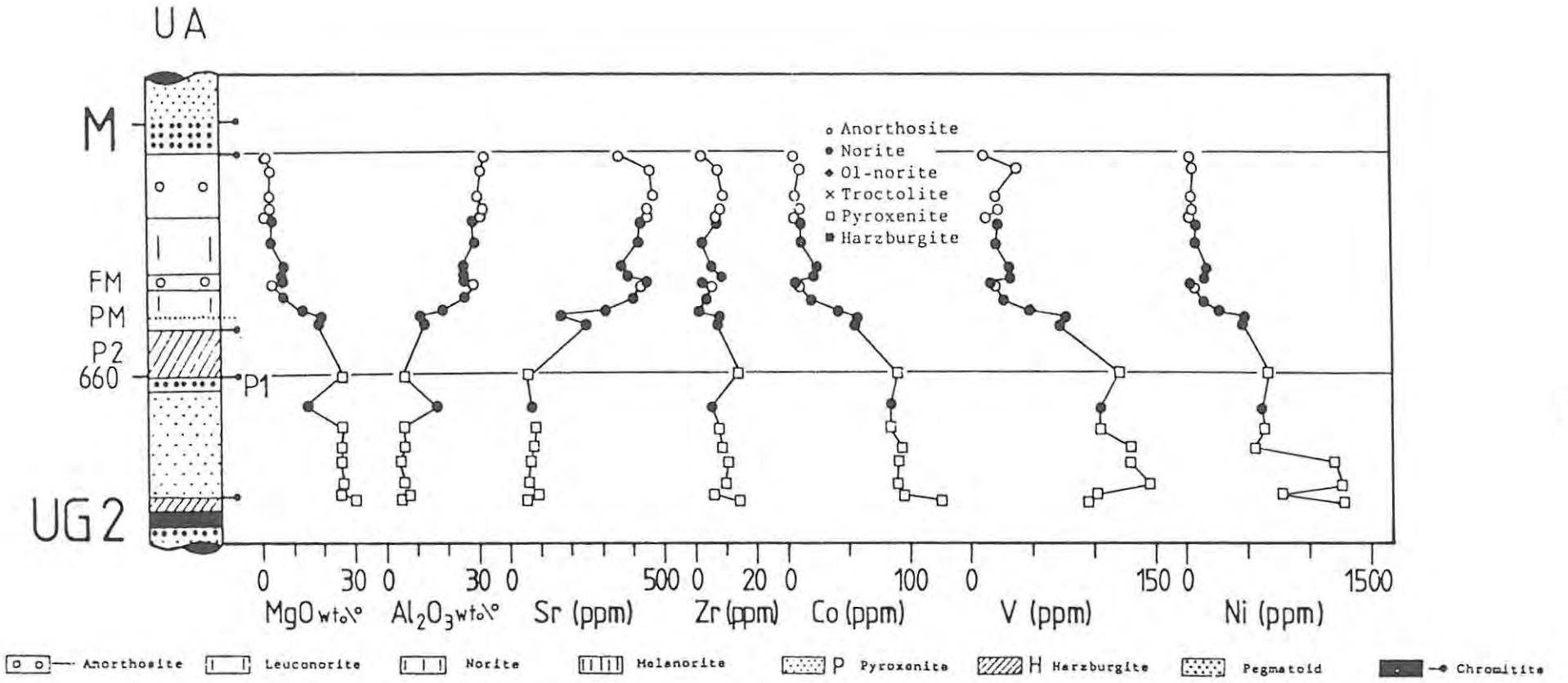

Fig. 5.5 Cryptic variations of whole rock chemical data displayed in core UA.

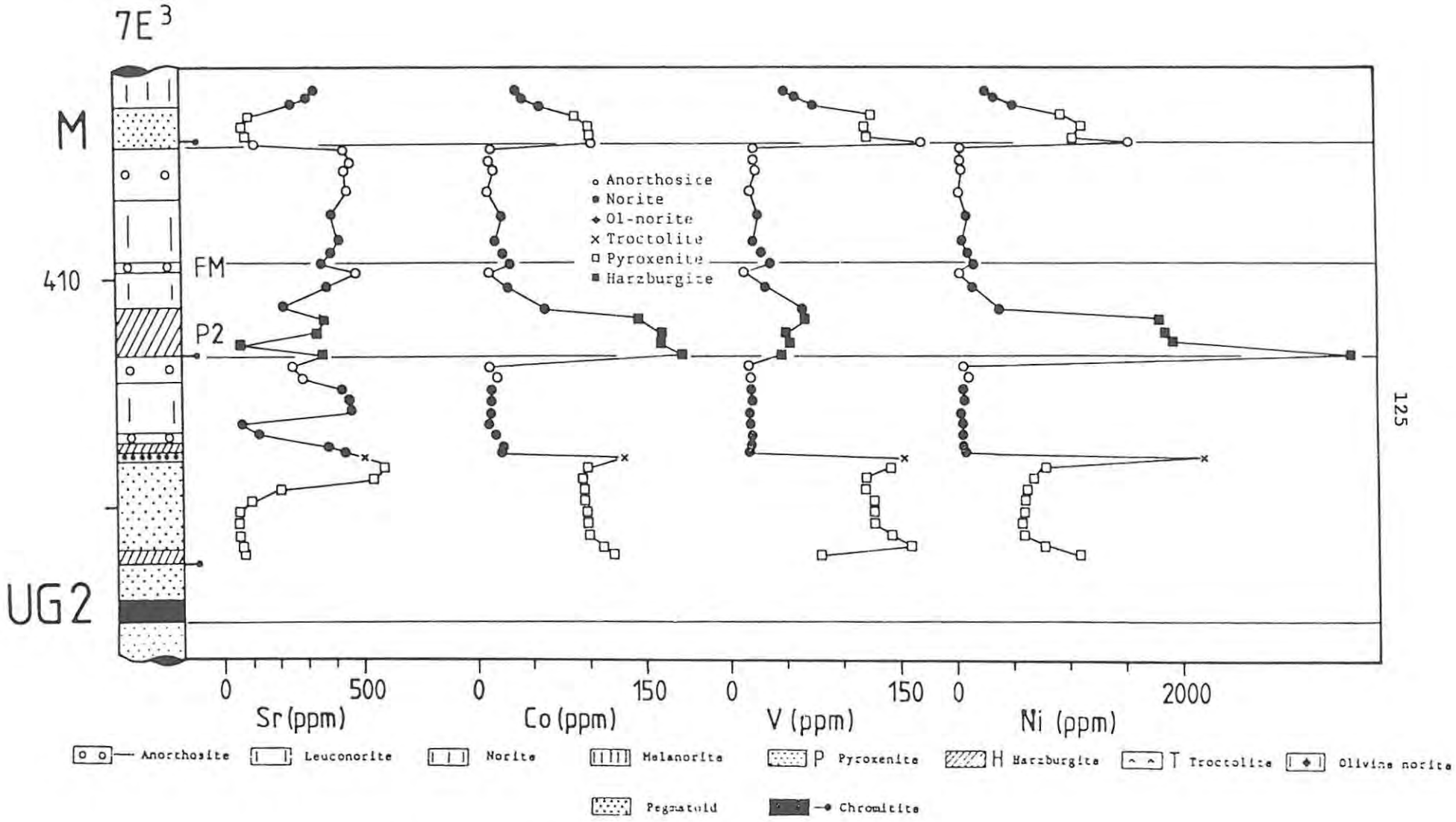

Fig. 5.6 Cryptic variations of whole rock chemical data displayed in core $7E^3$.

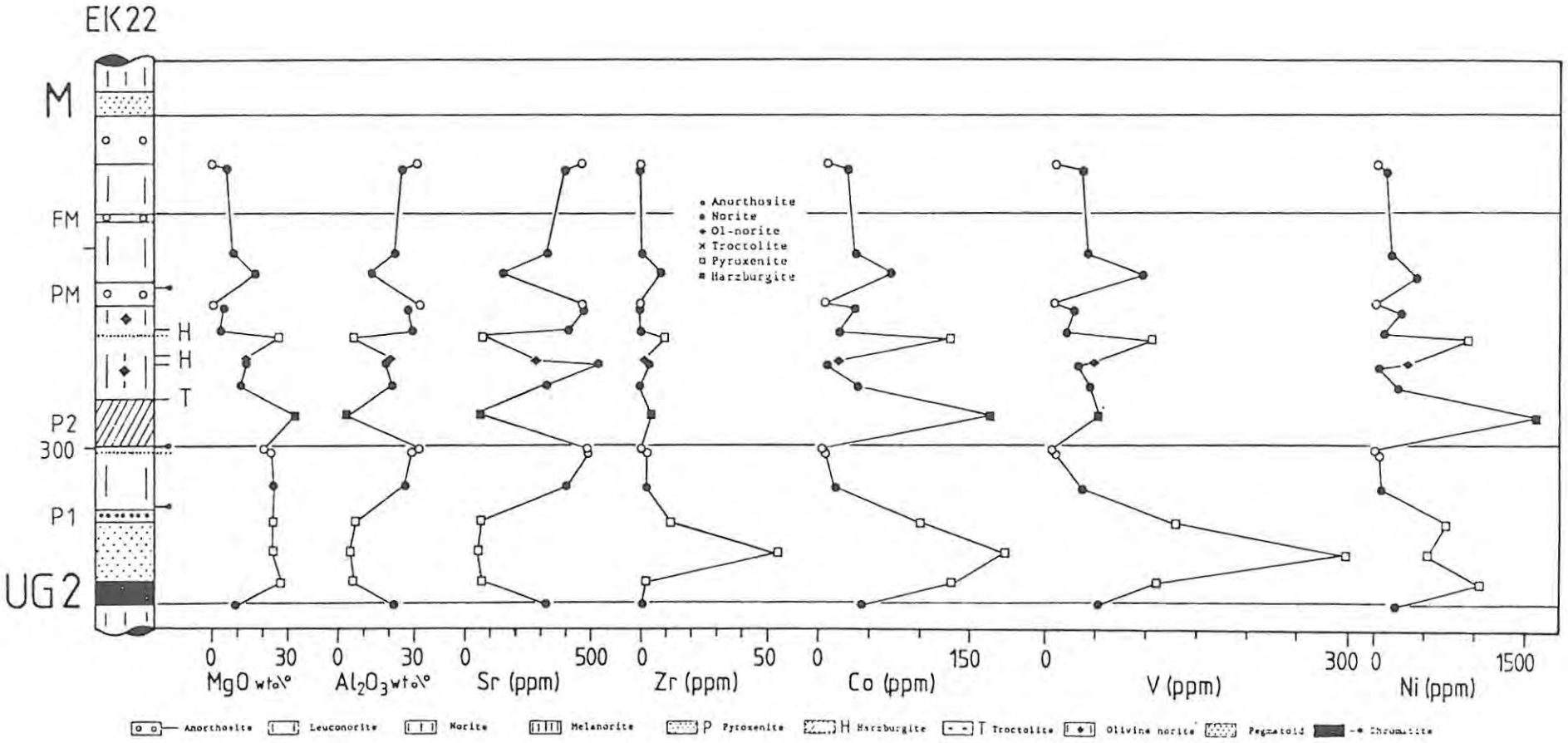

Fig. 5.7 Cryptic variations of whole rock chemical data displayed in core EK22.

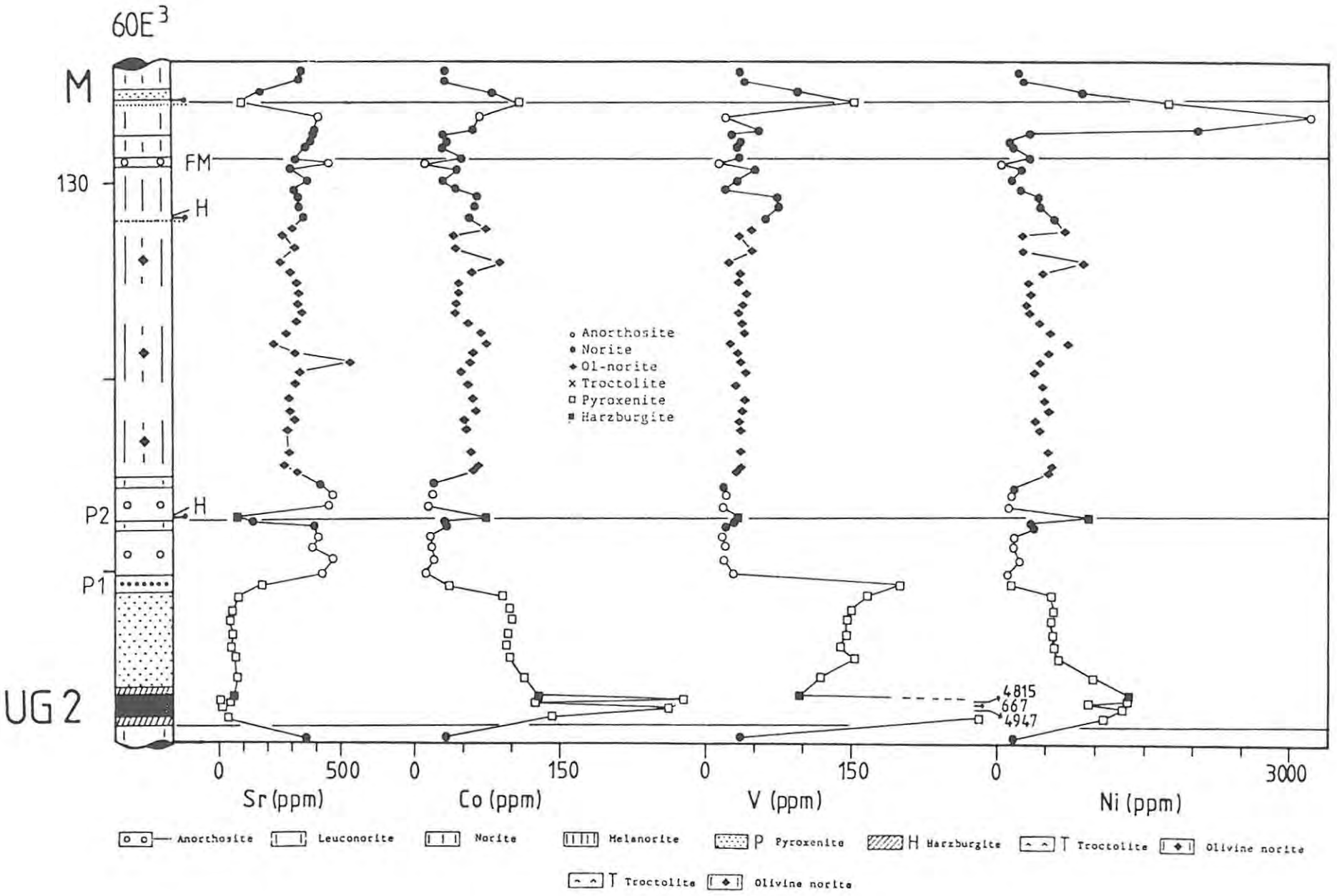

Fig. 5.8 Cryptic variations of whole rock chemical data displayed in core 60E^3.

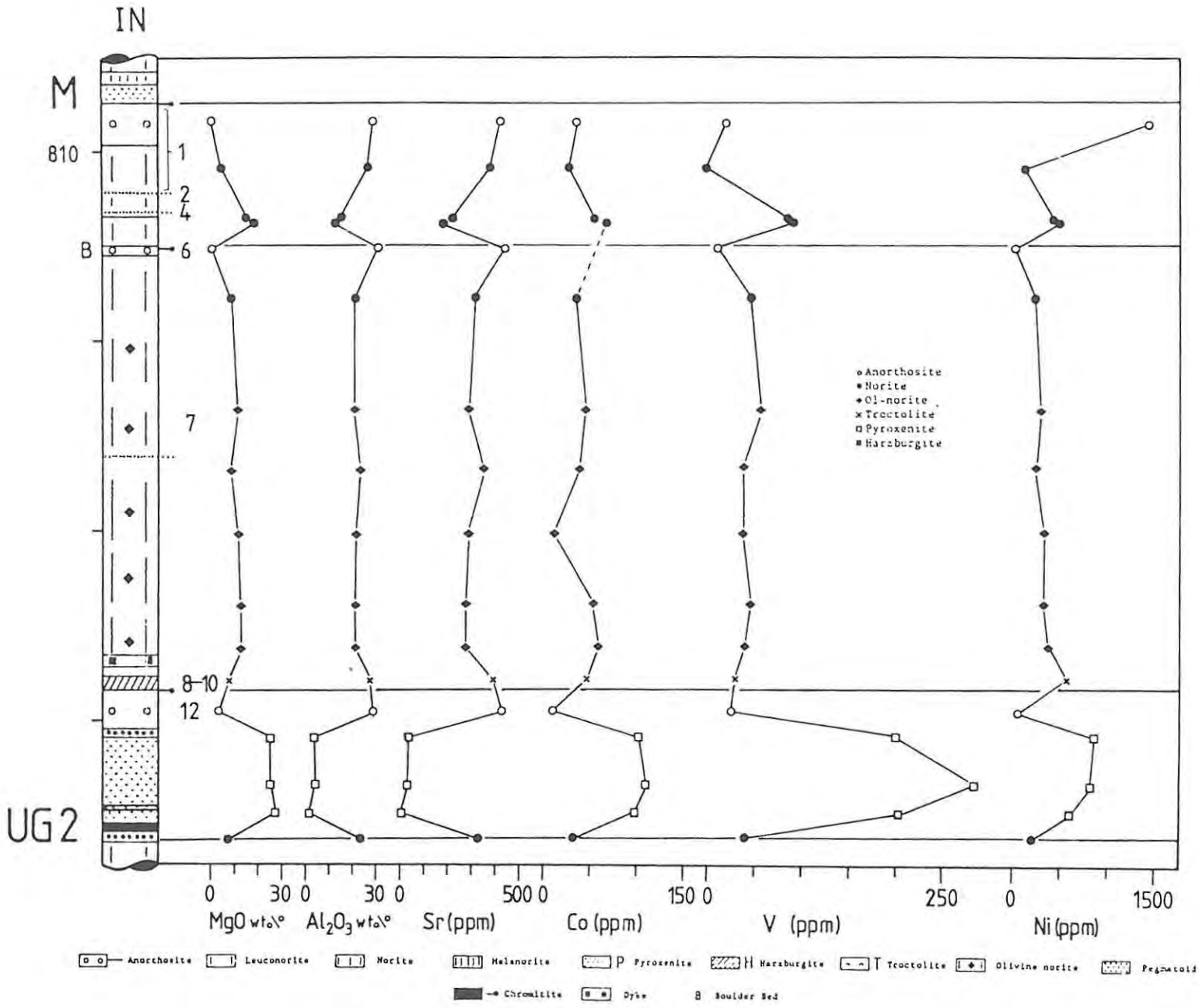

Fig. 5.9 Cryptic variations of whole rock chemical data displayed in core IN.

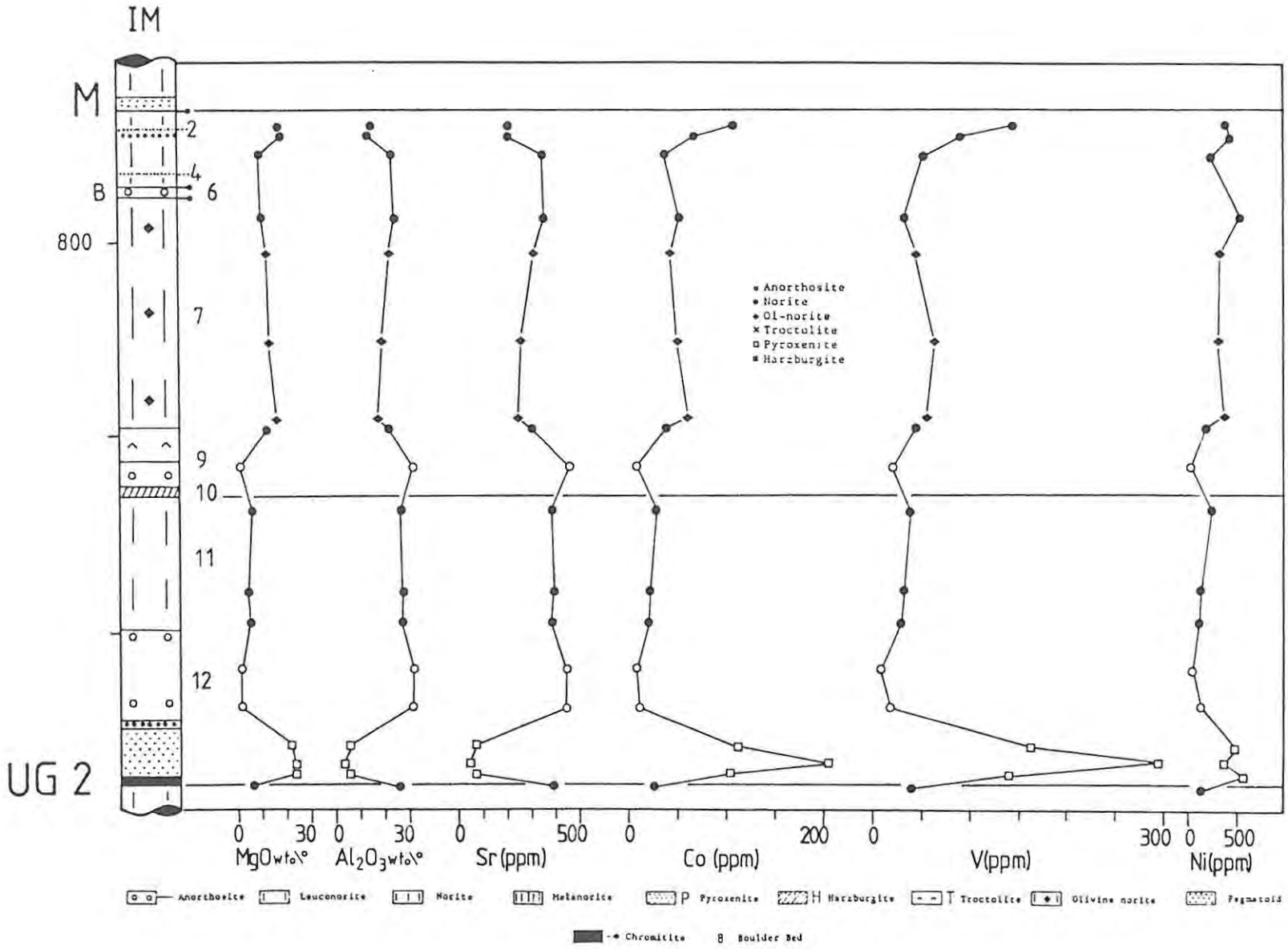

Fig. 5.10 Cryptic variations of whole rock chemical data displayed in core IM.

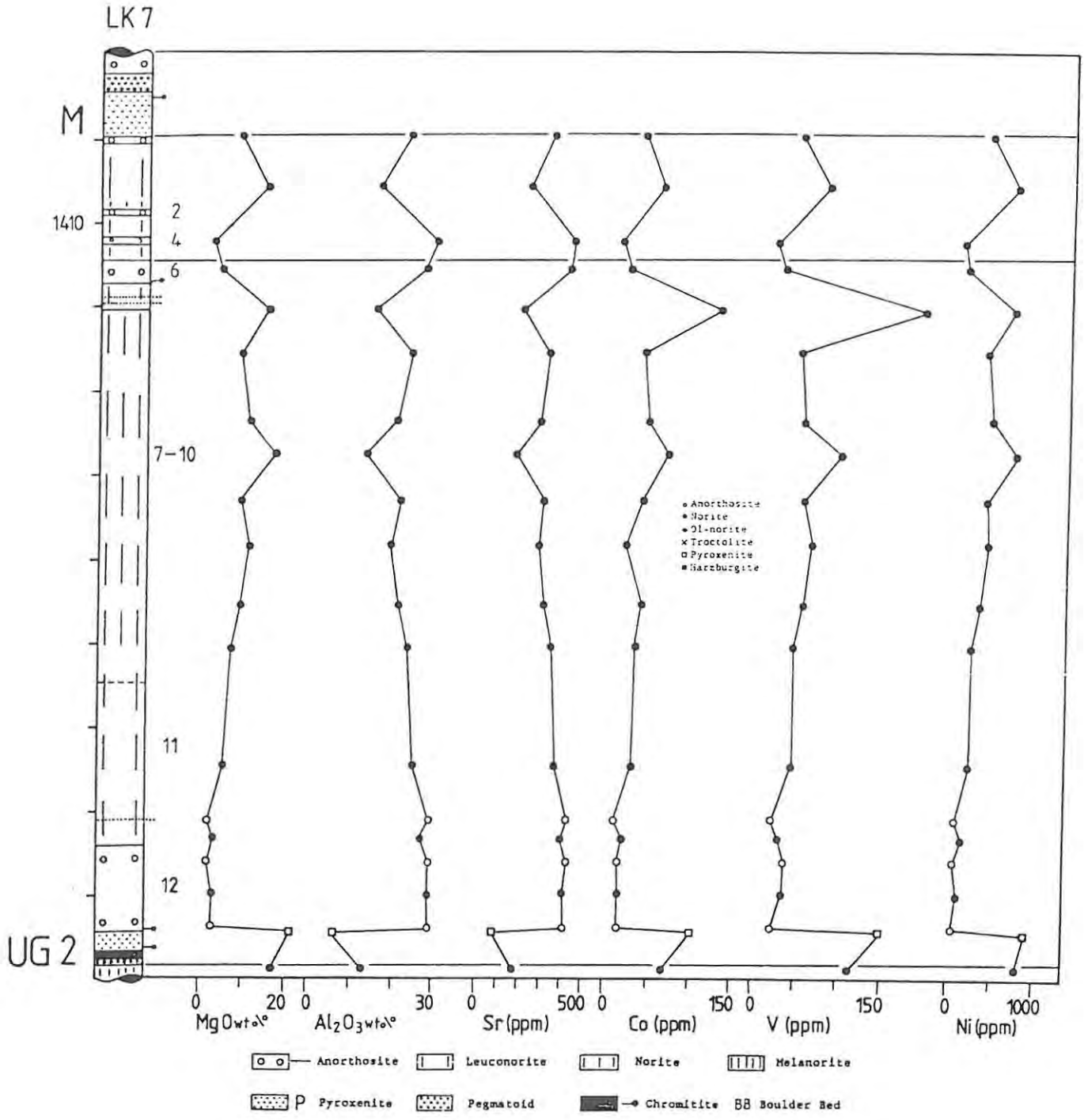

Fig. 5.11 Cryptic variations of whole rock chemical data displayed in core LK7.

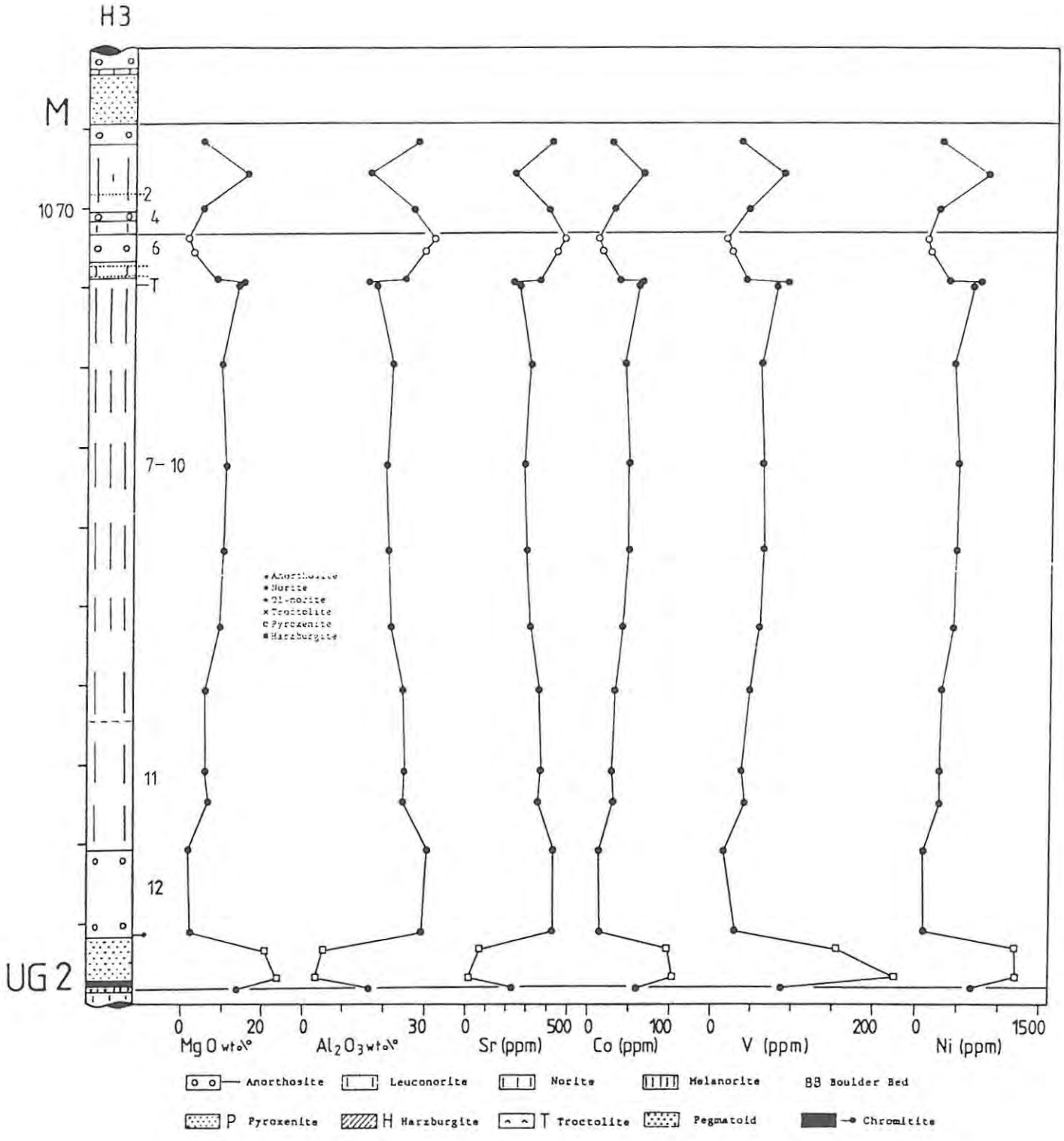

Fig. 5.12 Cryptic variations of whole rock chemical data displayed in core H3.

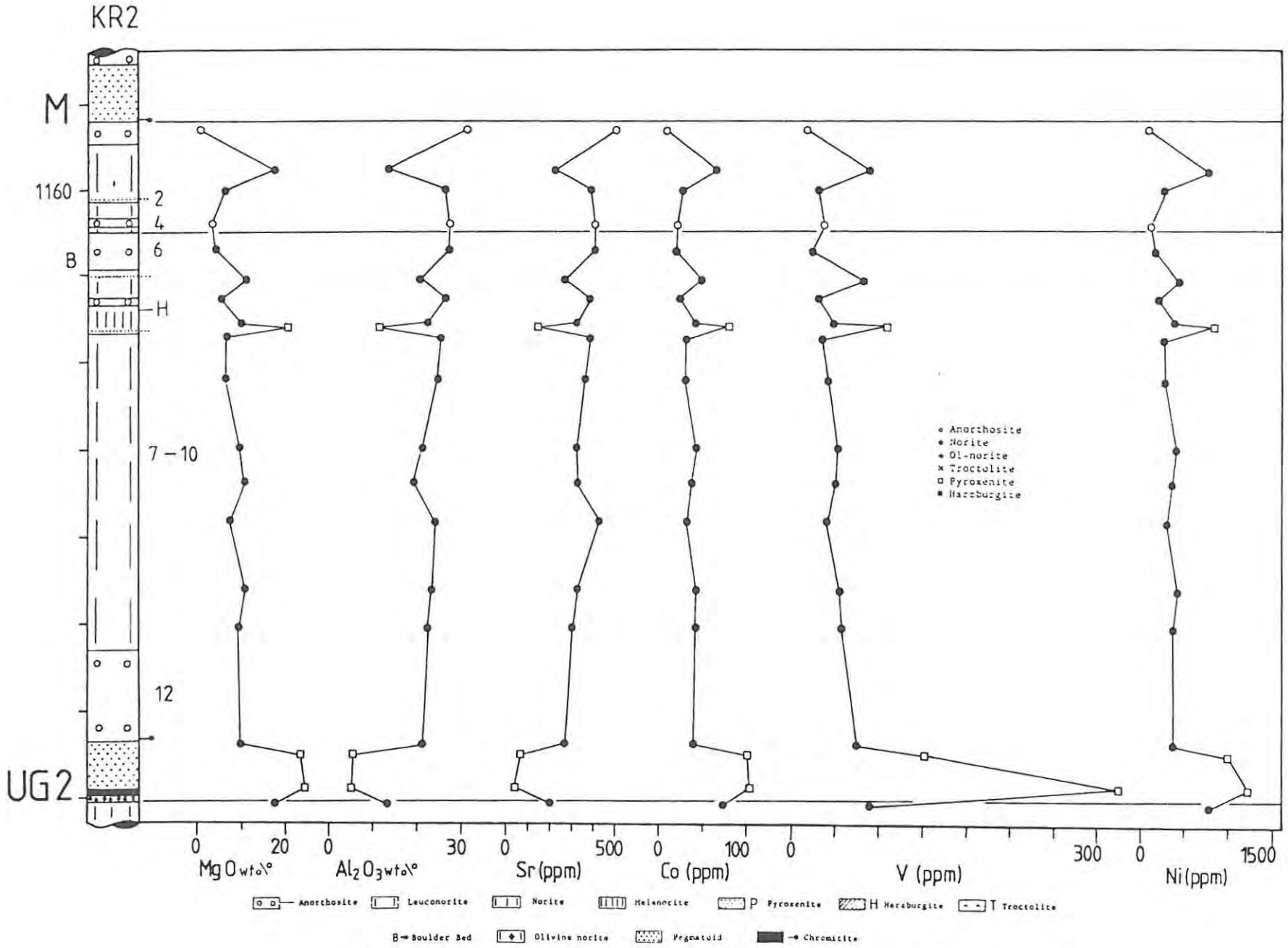

Fig. 5.13 Cryptic variations of whole rock chemical data displayed in core KR2.

5.4: The CIPW Norm

CIPW wt% norms of whole rock data (L.O.I.- and H_2O-free) were calculated on a program based on the method of Kelsey (1965). The results are tabulated together with the whole-rock data in Appendix V.

At Union and Amandelbult Sections normative olivine is common in most of the norites and anorthosites, even where modal olivine is not found. This pattern is less obvious in the southern sections. In intersection KR2 normative olivine increases again and appears not only below the FW 6 but at two further horizons below the Merensky Reef and in the central noritic part. It must be noted that the appearance of olivine in the norm may be caused by assumptions made during calculation (Eales, 1991, pers. com.). The norm is, in general, not an accurate analogue of the mode, for the following reasons:

(a) Fe^{2+}:Fe^{3+} ratios may be incorrect. Assigning more Fe as Fe^{3+}, expresses more iron as magnetite and thus less SiO_2 is consumed in forming orthopyroxene. If not enough Fe is expressed as Fe^{3+}, then olivine will appear in the norm.

(b) The failure of the norm to recognize the replacement of Si by Al in the tetrahedral sites of orthopyroxene, clinopyroxene, and mica. Thus, more Si is used to form pyroxene than is true in fact, and this leads to apparent Si deficiency, and hence the appearance of olivine.

In Fig. 5.5, normative compositions have been plotted in the triangular phase diagram Fo-An-Qz. Six groups of rocks can be distinguished: anorthosites (group 1) plot close to the An corner, norites (group 4) plot along the An-En tieline with highly variable proportions of An:En, and pyroxenites (group 5) on the same line just above En. A hiatus is developed between pyroxenites and norites, with few melanorites being recorded. Six harzburgite samples from the P2 Marker plot very close to the Fo-An tieline (group 6) and so do the troctolites (group 2). Olivine norites (group 3) plot in a separate field between troctolites and norites. Several points are worth noting:

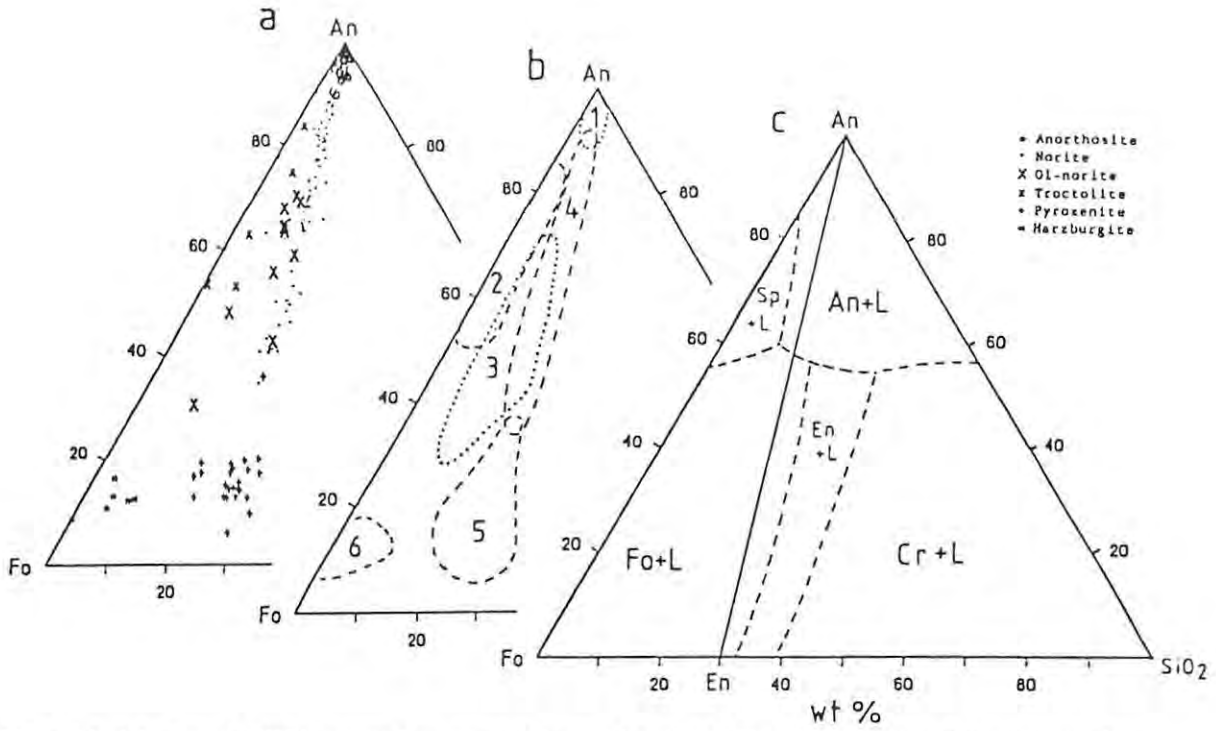

Fig. 5.14 (a) Plot of CIPW normative compositions of rocks of the study section (plus pyroxenites and harzburgites from Ellis, 1989), in ternary diagram of the system Fo - An - Silica. (b) Compositional fields of 1: anorthosites, 2: troctolites, 3: olivine norites, 4: norites, 5: pyroxenites, 6: harzburgites. (c) Phase boundaries in the simplified model system, after Andersen (1915) and Irvine (1975). En represents protoenstatite, the highly speculative tridymite-crystobalite boundary has been ommitted for simplicity.

- Anorthosites contain a varying amount of intercumulus orthopyroxene which shifts their composition towards En.

- The cotectic ratio of plagioclase : orthopyroxene in a norite is ca. 60:40. Norites in the study section, however, show a wide scatter of modal proportions which suggests that they have not been formed purely by bottom growth but that some kind of gravitational crystal sorting, or rhythmic nucleation, operated as well.

- Pyroxenites are composed of En plus a varying amount of intercumulus plagioclase. No sample crosses the Fo-En peritectic.

- Troctolites lie in a field parallel to the Fo-An join and very close to the Fo-An cotectic. Troctolites show a high amount of dispersed chromite which shifts their position close to the spinel field.

- The compositional field of olivine norites extends parallel to the troctolitic field but is slightly shifted towards the SiO_2 corner.

A plot of normative Mg# against normative An component (Fig. 5.6) reveals that pyroxenites and norites show constant Mg# with increasing An component, and anorthosites through norites show constant An component with increasing Mg# (see Fig. 4.3(c) for comparison). This observation has a significant implication: plagioclase of anorthosites and norites possibly formed at the same time and under similar magmatic conditions. It must be noted that the calculation procedure of the norms results in slightly unrealistic An contents, especially in orthopyroxene-rich rocks. Ca and Al of orthopyroxene is calculated as anorthite and this leads to spurious enrichment in normative An component in orthopyroxene-bearing rocks.

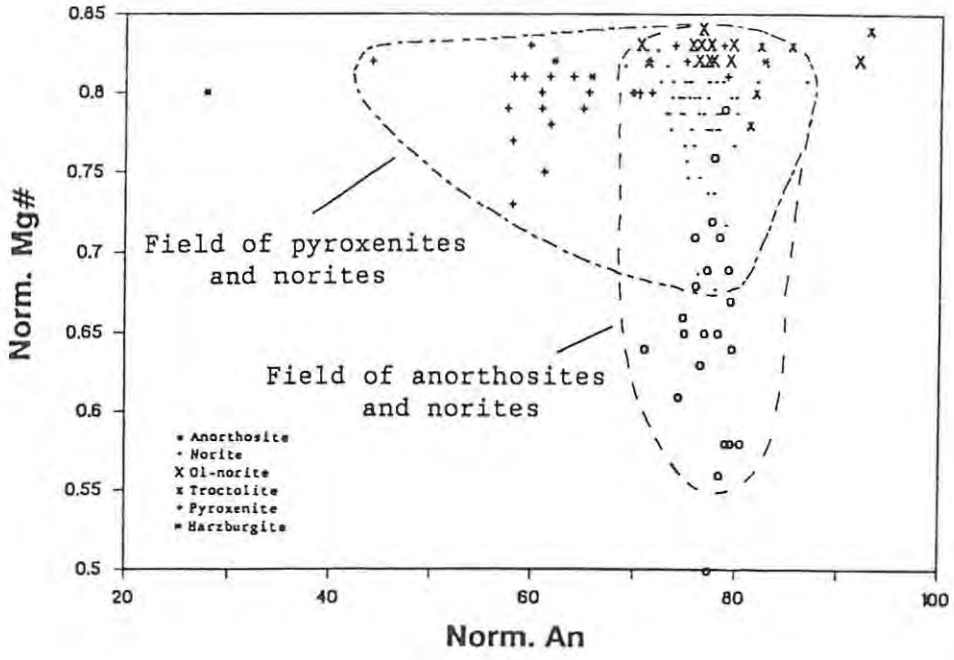

Fig. 5.15 Plot of normative Mg# versus normative An (An/An+Ab+Or). See text for further explanation.

5.5: Sr isotope data

6 samples from the IM core have been analysed for Sr isotope data by F.J. Kruger of the Bernard Price Institute (Table 5.6). This was done mainly to extend published data on the studied interval to other parts of the western limb. The limited number of analyses does not satisfy statistical requirements for far-reaching conclusions. Therefore, the results must be treated with caution. Calculations were made using the Geo Date programe compiled by the CSIR laboratory staff.

1.5 m below the Merensky Reef, the data show a significant inflection towards high values. This pattern is similar to that observed in the Merensky Unit at Atok Section (Lee & Butcher, 1989, Fig. 5.7) and could be interpreted as a result of mixing of two liquids (see Eales et al., 1986, 1990a).

Table 5.6: Sr isotope analyses of intersection IM

Sample	Rock type	Sr (ppm)	Rb (ppm)	$^{87}Rb/^{86}Sr$	$^{87}Sr/^{86}Sr$	Sr_i
	Merensky Reef	-	-	-	-	.7064 [1]
787.90	Norite	207	2.4	.0328	.7078±10	.7069±1
790.64	Norite	343	3.0	.0251	.7068±16	.7064±1
797.25	Troctolite	358	4.2	.0338	.7074±10	.7066±1
810.10	Olivine norite	259	2.6	.0290	.7070±10	.7064±1
825.25	Mott. anorthosite	459	4.2	.0265	.7068±10	.7064±1
847.50	Mott. anorthosite	446	1.8	.0119	.7066±10	.7064±1
	UG2 pyroxenite	-	-	-	-	.7063 [2]

1 recalculated value by Lee & Butcher (1989), Rustenburg Section
2 Eales et al., (1990a), Union Section
Notes: - $^{87}Sr/^{86}Sr_p$ = present day ratio, uncertainty is 2 standard error of the mean
- Sr_i = initial ratio calculated for an age of 2050 My, uncertainty is 1 standard error (68% certainty level)

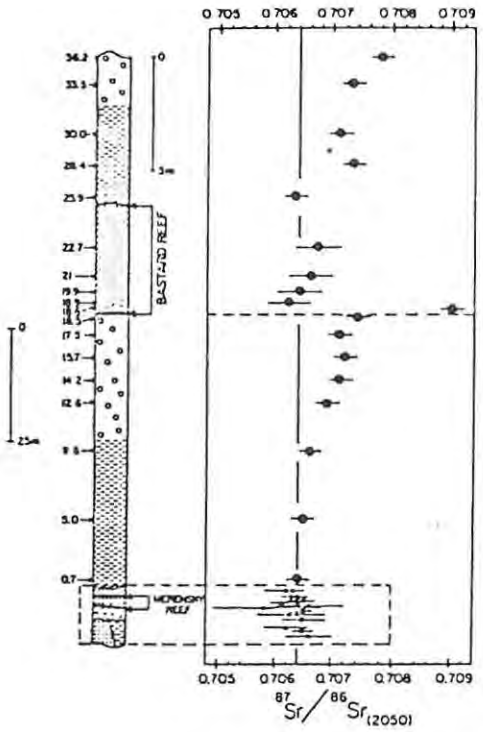

Fig. 5.16 Whole-rock Sr isotope data through a section from the Merensky Reef to the top of the Bastard Unit at Atok Section, Eastern Bushveld. Error bars represent 2σ standard deviations. (Fig. from Lee & Butcher, 1989).

5.6: Summary

- Most major and trace elements of the studied rocks exhibit a linear correlation against MgO, indicating the likelihood of frequent magma influxes during the deposition of the rocks.

- Trace elements Zr and Rb as well as major element K display a poor correlation with MgO content, reflecting their preferred association with intercumulus material.

- The normative proportions of the individual phases in pyroxenites and norites reveals a prominent gap between these two rock types (melanorite gap). This is considered to reflect the fact that the cotectic proportion between plagioclase and orthopyroxene lies at ca. 60 : 40 vol% and argues against long-range gravitational separation of orthopyroxene and plagioclase.

- The Sr isotope data show a similar pattern to that in the Merensky Unit at Atok Section.

CHAPTER 6: GEOCHEMICAL VARIATIONS WITHIN INDIVIDUAL SEQUENCES

6.1: Introduction

Cryptic variations of a number of selected geochemical parameters within the individual cores are displayed in Figs. 6.1 to 6.13. No mineral chemistry data could be generated for cores $7E^3$ and $60E^3$, and whole-rock analyses could not be performed for section TF. Modal and grain size analyses were not carried out in severely altered cores. Sample positions for mineral analyses and whole-rock compositions as well as modal and grain size measurements do not necessarily coincide, and some samples may not have been plotted in cases where the density of samples analysed is high and chemical or petrographic differences between individual samples are insignificant. Lines connecting data points within anorthosites are shown as broken lines, as mineral compositions may change over short intervals in anorthosites. In most other cases solid connecting lines have been drawn between sample points to facilitate the recognition of trends.

A range of 2σ standard deviation in mineral chemistry data in individual samples is presented for one arbitrarily selected core at the beginning of this chapter (Fig. 6.1). This displays low variation for $Mg\#_{opx}$, where 2σ usually is smaller than the size of the symbol drawn. Significant variations occur only in the UG2 pyroxenite. It is in that unit that one also finds the highest variation in An and Fe contents of plagioclase, and Cr in orthopyroxene. Standard deviations are so large here that, in some cases they cannot be represented within the confines of the diagram. All parameters show not only rather constant values but also relatively low standard deviations in the central noritic part of the sequence.

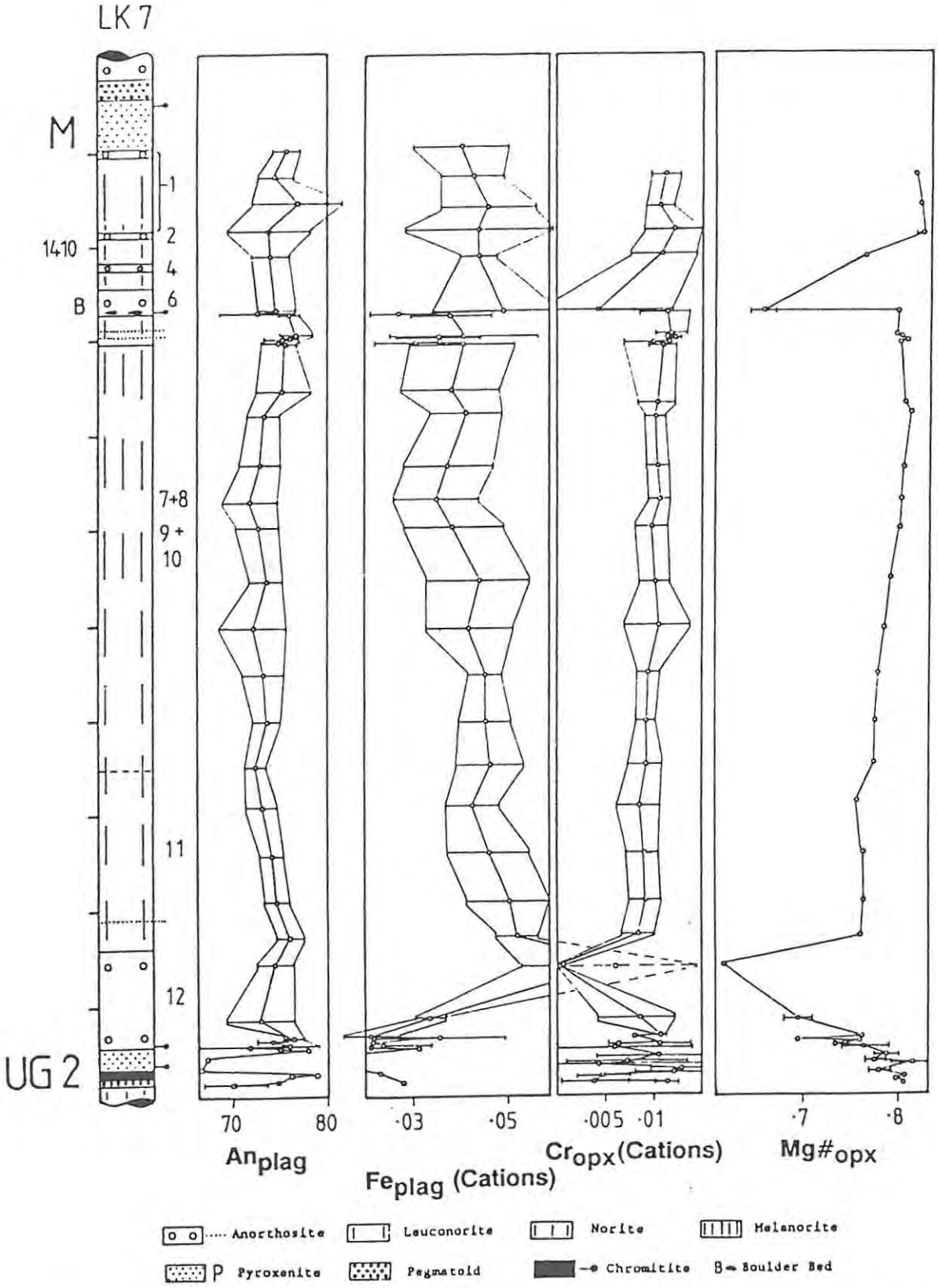

Fig. 6.1 Means and 2σ standard deviation of selected parameters in one representative core (LK7). Sample points represent average values of between 5 and 15 analyses for mineral chemistry data. Vertical scale is indicated by the marks on the left side of log. The distance between two marks in this and all succeeding logs in this chapter represents 20 m. Identification of the most important footwall layers is shown on the right side of profile.

6.2: The UA Sequence (RPM Union Section)

The whole-rock chemical data of the UA sequence has been generated by W.J. de Klerk (1991) in his study of the Upper Critical Zone, and made available to the author. Grain size analyses were not executed, as plagioclase grain shapes are very irregular here. Furthermore, parts of the core are altered.

As in most of the other cores, a good correlation can be observed between Mg# and Cr content of orthopyroxene for most samples (microprobe data; Fig. 6.2). However, no clear chemical cyclicity is detectable in the top part of the core in terms of $Mg\#_{opx}$ and Cr_{opx}. Both parameters show lower values above the Pothole Marker (PM) and Footwall Marker (FM) than below these anorthosites. Note that $Mg\#_{opx}$ and Cr_{opx} values of norites are frequently as high as or higher than those in pyroxenites and harzburgites. Note also that the Mg# in the P2 harzburgite seems to increase upwards (the P2 Marker cannot be subdivided here into discrete submembers). This weak trend, which is matched by olivine, will be seen to be more clearly defined in some of the other cores.

An values, as expected, are lower in intercumulus plagioclase of pyroxenites and harzburgites than in cumulus plagioclase of norites and anorthosites. The former values show wide scatter, an observation which will be confirmed in the other cores. An increase in An content towards the top of the interval, as noted by Kruger and Marsh (1985) near Rustenburg, cannot be detected. Note the comparatively high An content of intercumulus plagioclase in the pegmatoidal harzburgite of the Merensky Reef.

$Mg\#_{wr}$ matches the overall $Mg\#_{opx}$ trend. The Cr/V ratio is only meaningful in chromite-free rocks, in which case it follows the $Mg\#_{wr}$. Both parameters show a trend of decreasing values between the PM and the FM.

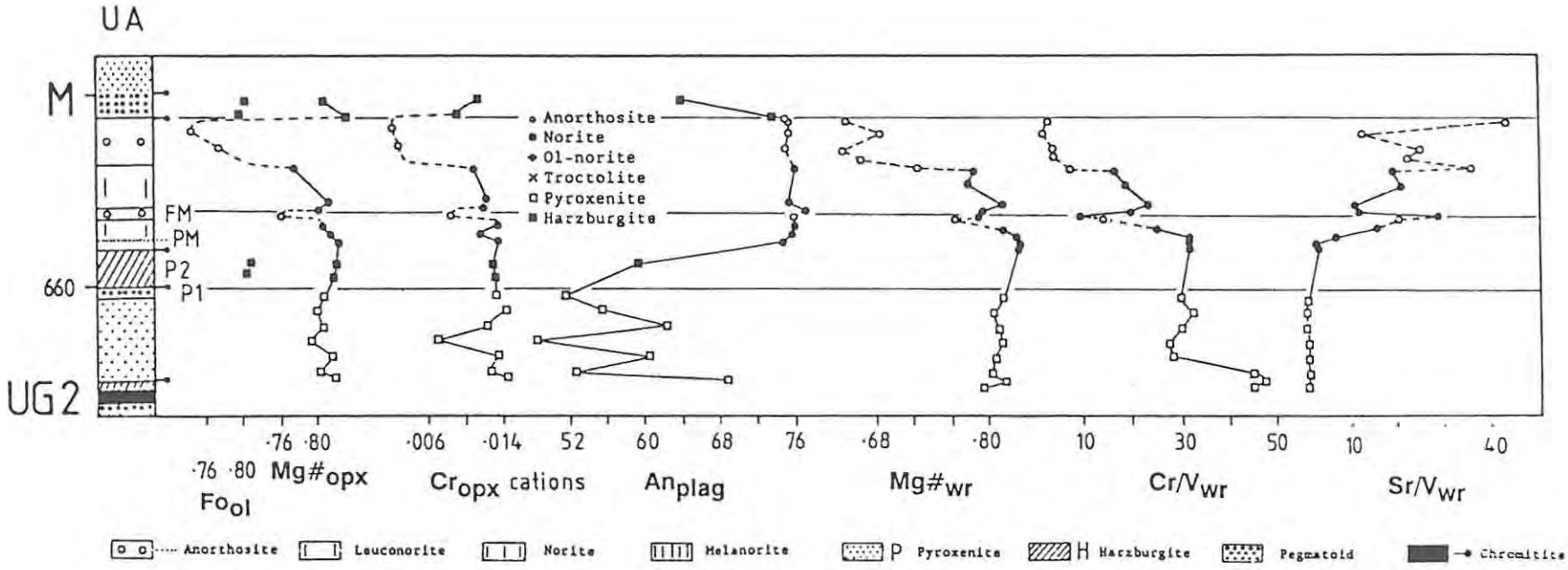

Fig. 6.2 Summary of the most important geochemical parameters displayed in core UA. Forsterite contents of olivine of 4 samples are plotted without connecting lines. FM = Footwall Marker, PM = Pothole Marker. Vertical scale as in Fig. 6.1

The Sr/V ratio reflects the modal proportions of plagioclase and orthopyroxene (in chromite-free rocks) and will therefore usually show the highest values in anorthosites and the lowest in pyroxenites.

6.3: The $7E^3$ Sequence (RPM Amandelbult Section)

Trace element data only are available for intersection $7E^3$. Sr/V and Cr/V ratios shown in Fig. 6.3 indicate the existence of two cycles (above the base of the P2-B/ -C Marker) in the upper part of the interval. The upper cycle, forming the immediate footwall of the Merensky Reef, is not clearly and regularly developed. The Footwall Marker is characterized by exceptionally high Sr values which is likely to reflect its monomineralic purity. The UG2 pyroxenite displays an upward-increasing Sr/V ratio which probably reflects an increasing proportion of intercumulus plagioclase seen in modal data (Chapter 3.5). Cr/V values are high in samples containing dispersed chromite and are notably depressed in the P1 Marker.

The troctolitic - leuconoritic - anorthositic package above the Upper Pseudoreef A shows two notable features. Sr/V values are higher in noritic than in anorthositic samples, and Cr/V values are lower in norites than in anorthosites. These two phenomena most likely can be related to the presence of dispersed chromite in the anorthosite. Furthermore, the transition from norite into anorthosite is geochemically gradational. Not surprisingly, the Ni/Sc ratio shows the highest values in the P2 harzburgites.

Y and Zr levels are both enhanced in the UG2 and Merensky pyroxenites, reflecting the concentration of the two elements in the interstitial phases. Zr generally shows higher values than Y and is marginally enriched in norites relative to anorthosites.

Zn and Cu usually behave similarly, with Cu being marginally higher. The Merensky pyroxenite, the P1 Marker, and parts of the P2 Marker show especially high values of Cu, reflecting their sulphide content.

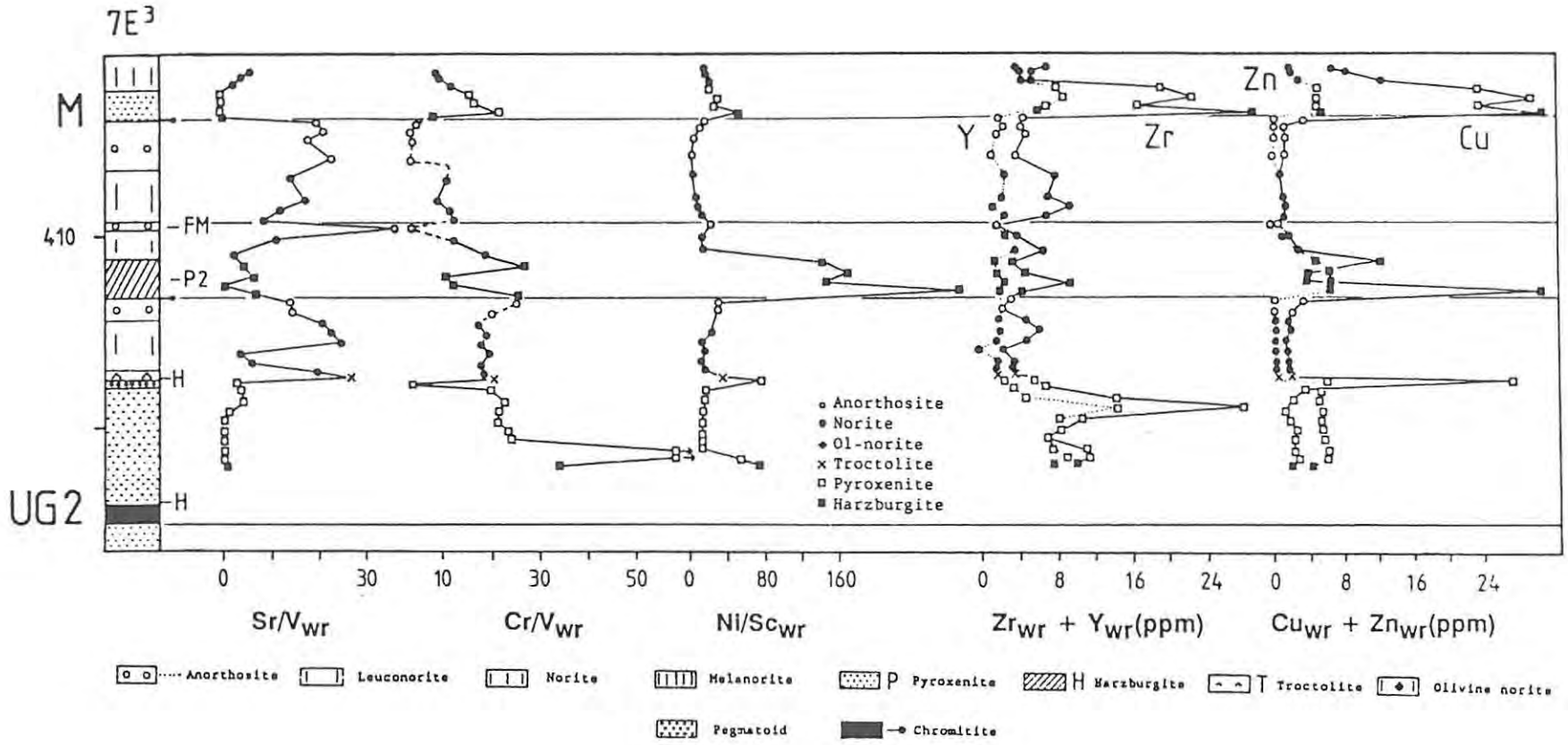

Fig. 6.3 Summary of the most important geochemical parameters displayed in core 7E^3. No mineral chemistry data were available for this core. FM = Footwall Marker. Vertical scale as in Fig. 6.1.

6.4: The EK22 Sequence (RPM Amandelbult Section)

The investigated succession at locality EK22 (Fig. 6.4) is more complex than those already discussed because the core is situated in an area where the harzburgite of the P2-C Marker apparently starts to split up.

In the uppermost part of the UG2 - Merensky Reef interval, two cycles of upwards-decreasing $Mg\#_{opx}$ can be observed. Cr contents of orthopyroxene behave less systematically where the modal percentage of orthopyroxene increases upwards in the leuconorite underlying the Merensky footwall anorthosite. If one ignores the harzburgites and pyroxenites with their high Mg#, a constant or gently upwards-increasing trend is detectable in $Mg\#_{opx}$, Cr_{opx}, and $Mg\#_{wr}$ in the interval between the P2-B harzburgite and the two uppermost cycles.

The P2-B harzburgite shows upwards-increasing values in Mg# of orthopyroxene and olivine, a trend which is more or less continued in the overlying thin harzburgites (P2-C Marker, see Table 7.4). Cr_{opx} scatters unsystematically in the P2 Marker, possibly because of the presence of dispersed chromite which undergoes subsolidus reaction with orthopyroxene (and olivine). No clear trend is recognizable in the UG2 pyroxenite in any one of the parameters presented.

An values for orthopyroxene-plagioclase cumulates are fairly constant, with an increase in the Ca member being detectable towards the top of the sequence. Note the very wide spread in values for the P2-B harzburgite and the UG2 pyroxenite, where plagioclase is intercumulus.

The modal analyses show that parts of the P2 Marker are in fact dunitic as no orthopyroxene is present here. A high proportion of these dunites, however, consist of highly altered, serpentinized and sericitized minerals, probably representing originally cumulus orthopyroxene and olivine.

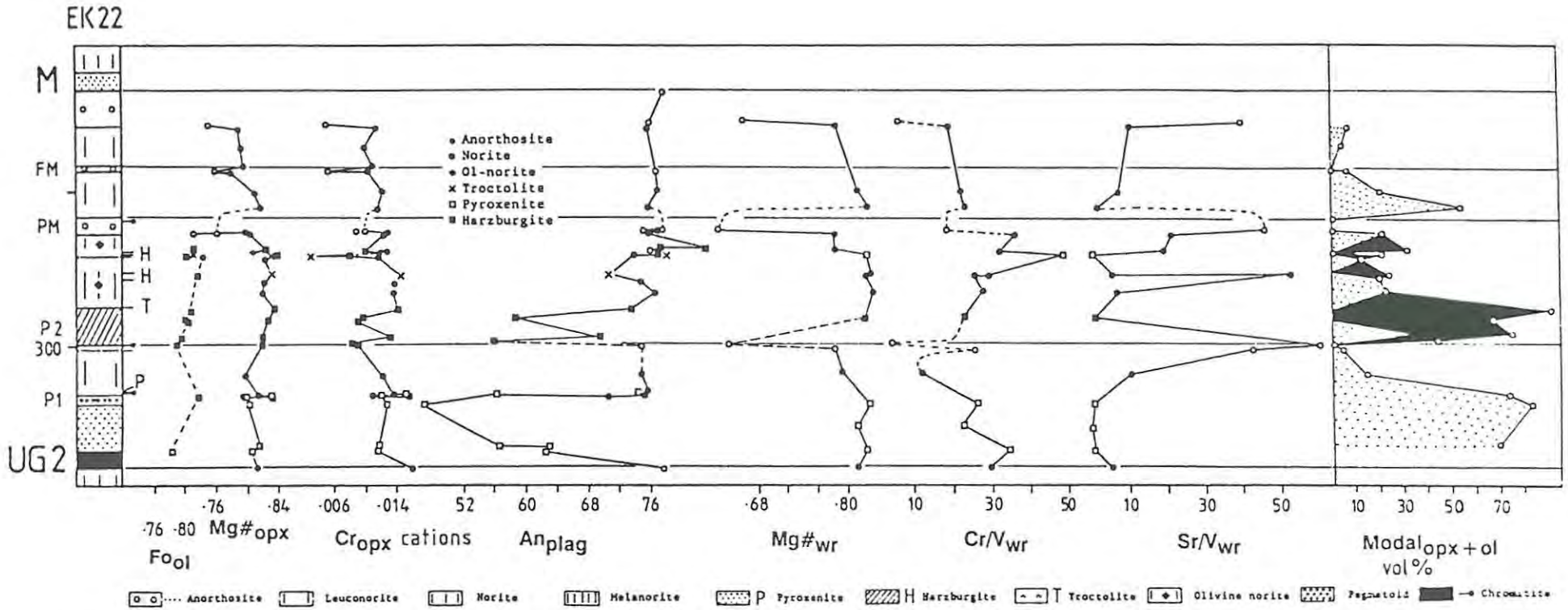

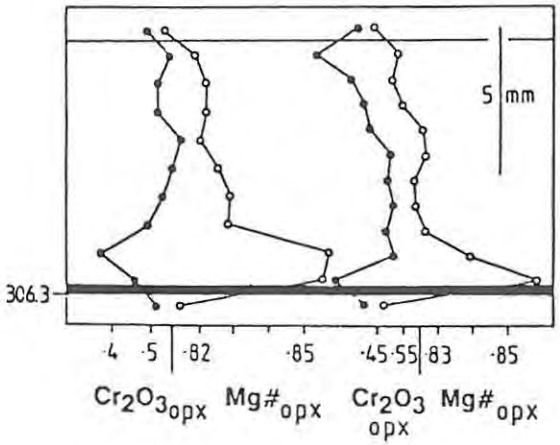

Fig. 6.4 (Top) Summary of the most important geochemical parameters displayed in core EK22. The black area represents olivine and the stippled area orthopyroxene, in the diagram illustrating modes. FM = Footwall Marker, PM = Pothole Marker. Vertical scale as in Fig. 6.1.

Fig. 6.5 (Left) Detailed profile across a thin pyroxenite layer with a thin basal chromitite stringer (sample EK22 306.3). The black band marks the chromitite, and the upper horizontal line indicates the top contact of the pyroxenite. Average compositions of 2 samples of the immediate leuconoritic foot- and hangingwall are plotted for comparison.

The pyroxenite, 1 cm thick, at 306.3 m with its underlying chromitite stringer (Plate 1) has been analysed in detail (Fig. 6.5). Orthopyroxene grains in close proximity to the chromitite stringer show elevated Mg# which is probably due to subsolidus equilibration with chromite. A constant decrease of $Mg\#_{opx}$ is detectable across the width of the pyroxenitic layer. The average values of the adjacent under- and overlying rocks are also plotted. Cr_{opx} exhibits comparatively depressed values just above the chromitite but remains at a fairly constant level across the rest of the layer. This is somewhat surprising, as it implies that chromite precipitation lead to only localized depletion of Cr in the host liquid.

6.5: The $60E^3$ Sequence (RPM Amandelbult Section)

Intersection $60E^3$ (Fig. 6.6) is situated in the far north-east of the Amandelbult lease area. As in the case of core $7E^3$, only whole-rock trace element data are available for this core.

The central noritic part of the study interval shows a relatively constant level of Sr/V and Cr/V ratios. In this respect the sequence here thus resembles the intersections in the south-western part of the Western Limb (i.e., profile IN), as will be shown later. Intermediate peaks in Ni/Sc ratio within this central part can be attributed to the presence of thin harzburgitic lenses or layers which fall within the section of core crushed. Cr/V values are elevated below the thin harzburgite in the lower part of the core (P2-B Marker), a feature which has also been observed in the footwall of the P2-B Marker at intersection $7E^3$ (Fig. 6.3). The Footwall Marker again yields the highest Sr/V ratio (see core $7E^3$).

As in core $7E^3$, Zr and Y yield similar trends, with Zr showing higher levels. Both are enriched in the UG2 pyroxenite and a constant level of concentration is maintained in the central part.

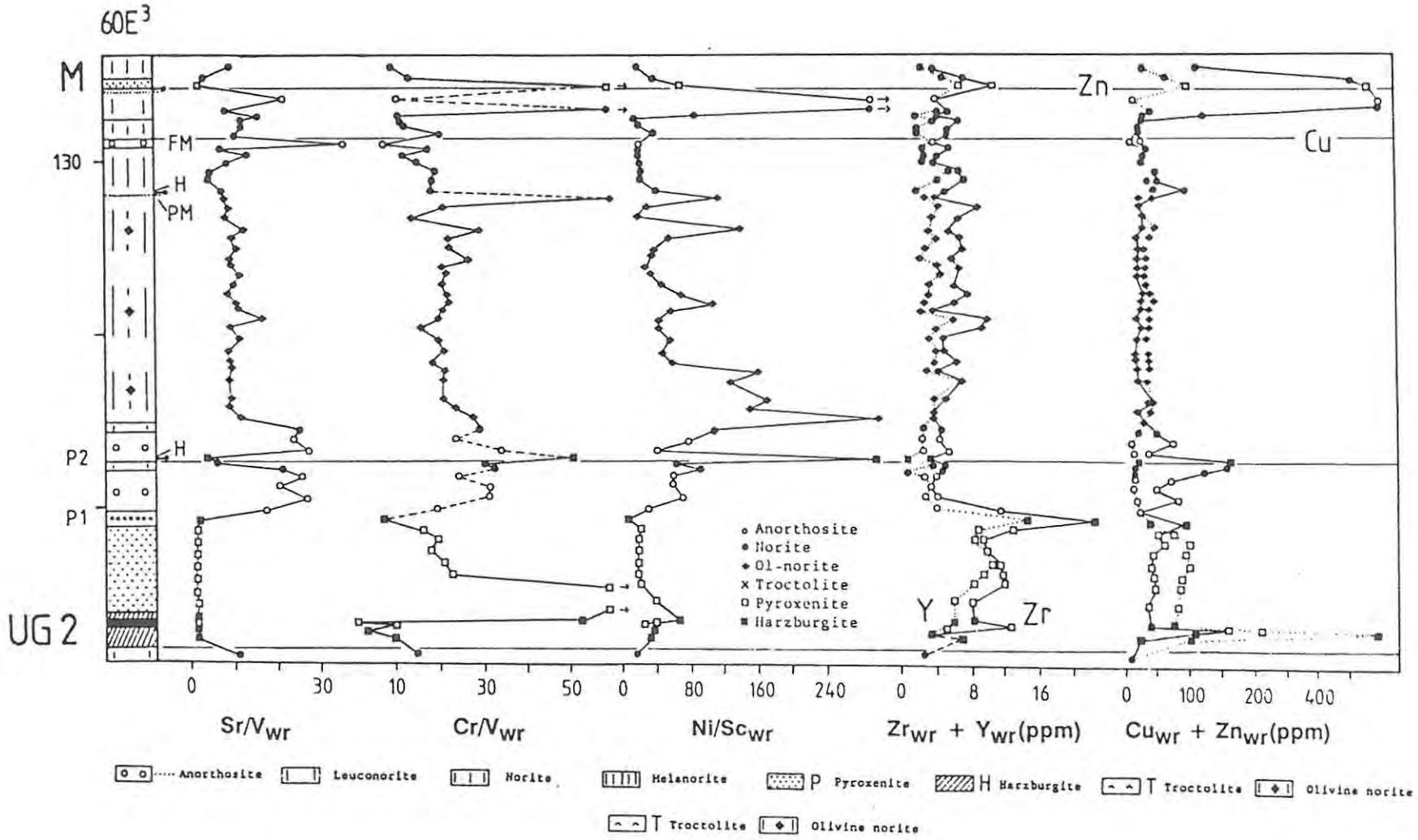

Fig. 6.6 Summary of the most important geochemical parameters displayed in core 60E^3. No mineral chemistry data were available for this core. FM = Footwall Marker, PM = Pothole Marker. Vertical scale as in Fig. 6.1.

Cu and Zn show the same geochemical behaviour as in core $7E^3$ with more or less similar values in the central part of the core and slightly higher Cu than Zn in the anorthositic-leuconoritic hangingwall of the UG2 pyroxenite. In the UG2 pyroxenite, Zn overtakes Cu in abundance.

6.6: The IN Sequence (Impala Platinum Mines, Bafokeng North Mine)

The two chemical parameters which can be compared with available data at localities IN (Fig. 6.7) and $60E^3$ (Fig. 6.6) in the north-east of Amandelbult (two intersections which are roughly 100 km apart from each other) show surprisingly strong similarities. Cr/V ratios peak roughly 20 m above the base of the UG2 pyroxenite and then drop slightly throughout the remaining part of the sequence (the anorthosites are ignored here for simplicity). The Sr/V ratio peaks at about the same position and then stays virtually constant. The other chemical ratios confirm the consistency of parameters in the central noritic part of the sequence, and even grain sizes of cumulus plagioclase show much less variation here than in the other parts of the sequence.

There is a sharp drop in Cr_{opx} in the pyroxenite and troctolite immediately overlying the thin chromitite stringer in the lower part of the sequence (P2-B Marker + Middling, marked by a square and an "x" in Fig. 6.7; see detailed log in Fig. 2.5). This implies that chromite precipitation has been catalyzed by some process to yield the chromitite stringer and a high amount of accessory chromite in the overlying pyroxenite and troctolite (see Cr/V_{wr} ratio). This process possibly has depleted the liquid in Cr to a comparatively low level. The orthopyroxene that then crystallized from this liquid reflects this depletion. Note also that the plagioclase in the thin pyroxenite shows an unusually high An content, especially so as it appears to be of intercumulus nature here.

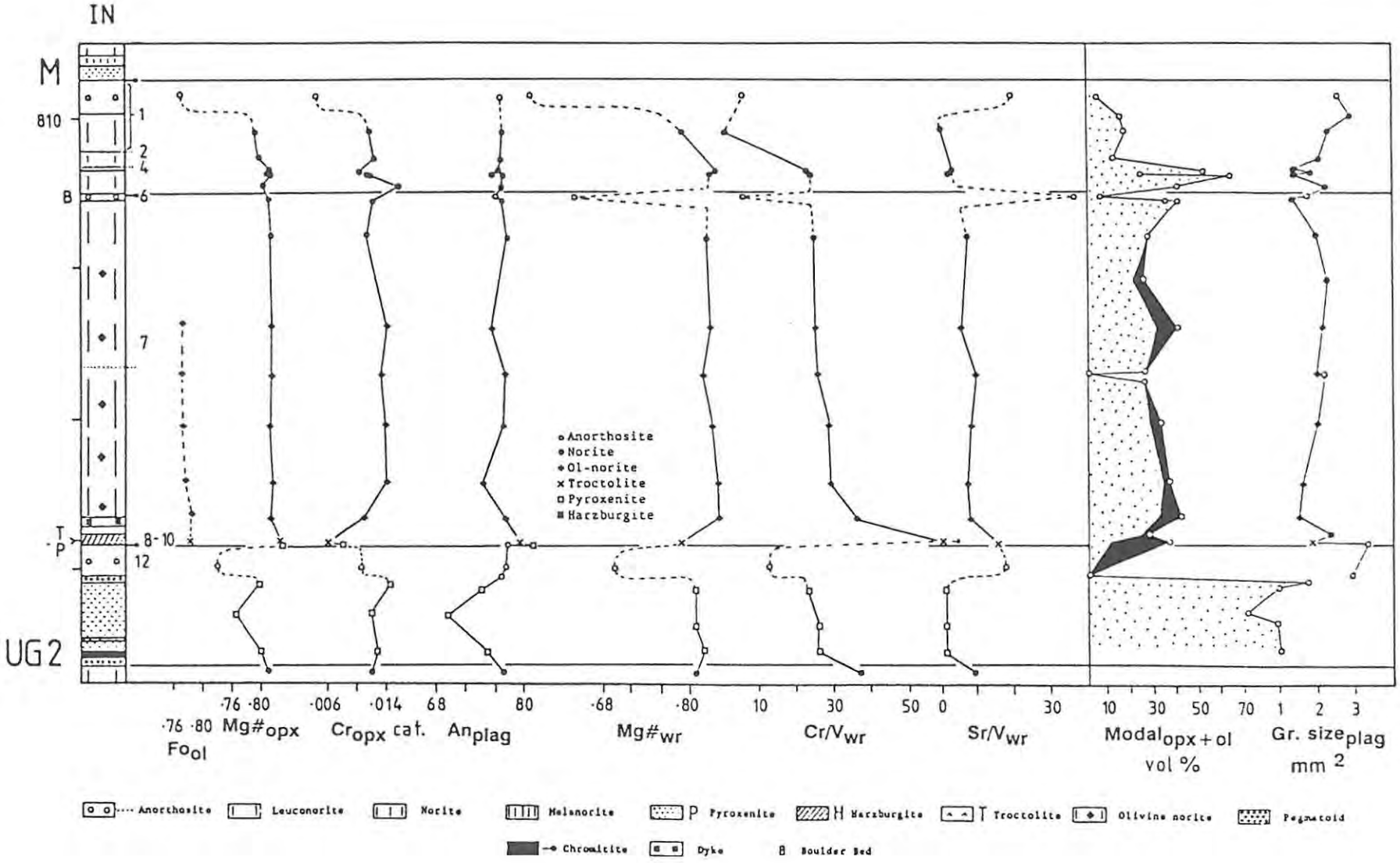

Fig. 6.7 Summary of the most important geochemical parameters displayed in core IN. Vertical scale as in Fig. 6.1.

The modal proportion of olivine stays fairly constant in the central olivine-noritic part of the sequence. The 40 m sequence of olivine norite displays consistent and more or less cotectic modal proportions (orthopyroxene+olivine / plagioclase = ca. 35:65).

6.7: The IM Sequence (Impala Platinum Mines, Wildebeestfontein North Mine)

Compared to intersection IN, the central olivine-noritic part (FW 7) of the IM core (Fig. 6.8) has become compressed and the FW 11+12 package has thickened. Nevertheless, the FW 7 still exhibits subdued variations in geochemical and petrographic parameters. Only the laminated troctolite, situated towards the top of FW 7, shows elevated values in $Mg\#_{opx}$. The low value of Cr_{opx} in this rock is typical for reaction replacement-type orthopyroxene which is the dominant type of orthopyroxene in this troctolite.

The central anorthosite (FW 9), which succeeds the very much thinned harzburgite of the P2-B Marker, shows a large amount of interstitial chromite which is reflected in its high Cr/V ratio. The harzburgite itself has not been analysed for whole-rock chemistry or modal proportions as it is affected by severe alteration.

The UG2 pyroxenite shows anomalously low values in Mg# of both orthopyroxene and whole-rock data, as well as Cr_{opx}. The rocks are highly altered and the presence of a substantial amount of hydrous phases such as oxyhornblende and mica, as well as magnetite, indicates that original compositions have been modified by secondary processes.

Towards the top of the FW 12 mottled anorthosite the "mottles" consist of intercumulus orthopyroxene with, in their centres, highly anhedral olivine of unusually low Fo content (Fo_{71}, Plate 12). This feature can also be observed in the footwall of the P2-B harzburgite at intersection $7E^3$.

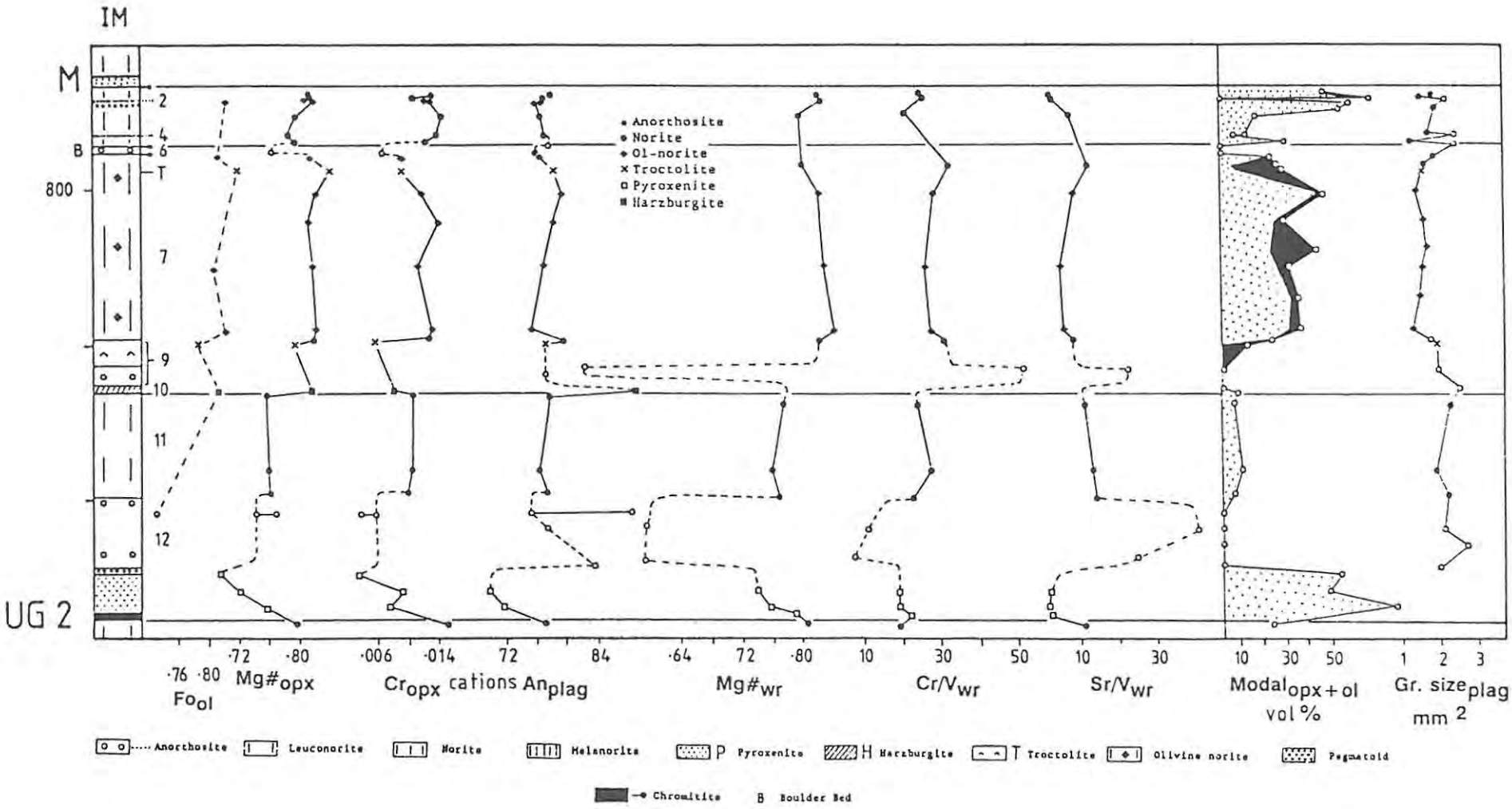

Fig. 6.8 Summary of the most important geochemical parameters displayed in core IM. Vertical scale as in Fig. 6.1.

The central part of the "mottle" shows markedly different geochemical properties relative to the rim-zone, as indicated in the tabulated data below:

Table 6.1: Chemistry of an orthopyroxene "mottle" with a core of olivine

		centre	n	rim	n
Mg#	(olivine)	0.710	3	-	
Mg#	(orthopyroxene)	0.764	7	0.740	2
Cr_2O_3	(orthopyroxene)	0.130	7	0.19	2
An	(cumulus plagioclase)	87.7	7	74.3	3

n = number of analyses

Three chemical ratios representative of chromite have been plotted against stratigraphic height in Fig. 6.9 and compared with $Mg\#_{opx}$ in coexisting samples. The most noteworthy feature is the fact that the central part of the profile can indeed be subdivided into two genetically different sections. Chromite in the upper part (FW 7) is geochemically more primitive than chromite in the lower part (FW 9-12). This pattern is matched by the trend of $Mg\#_{opx}$.

6.8: The TF Intersection (RPM Rustenburg Section, Turffontein shaft)

No whole-rock data are available for the TF sequence and the discussion will be confined to the essential mineral chemical ratios (Fig. 6.10). A constant trend in the FW 7+8 central norite seems to be indicated both in Mg# and Cr content of orthopyroxene. A "boulder" of the Boulder Bed shows comparatively low Cr values of orthopyroxene and high An content of plagioclase (up to An_{85}). Plagioclase in the "boulders" occurs as strongly and irregularly resorbed cumulus grains and as intercumulus grains. An contents of plagioclase within "boulders" are highly variable, as is to be expected, considering the different types of plagioclase.

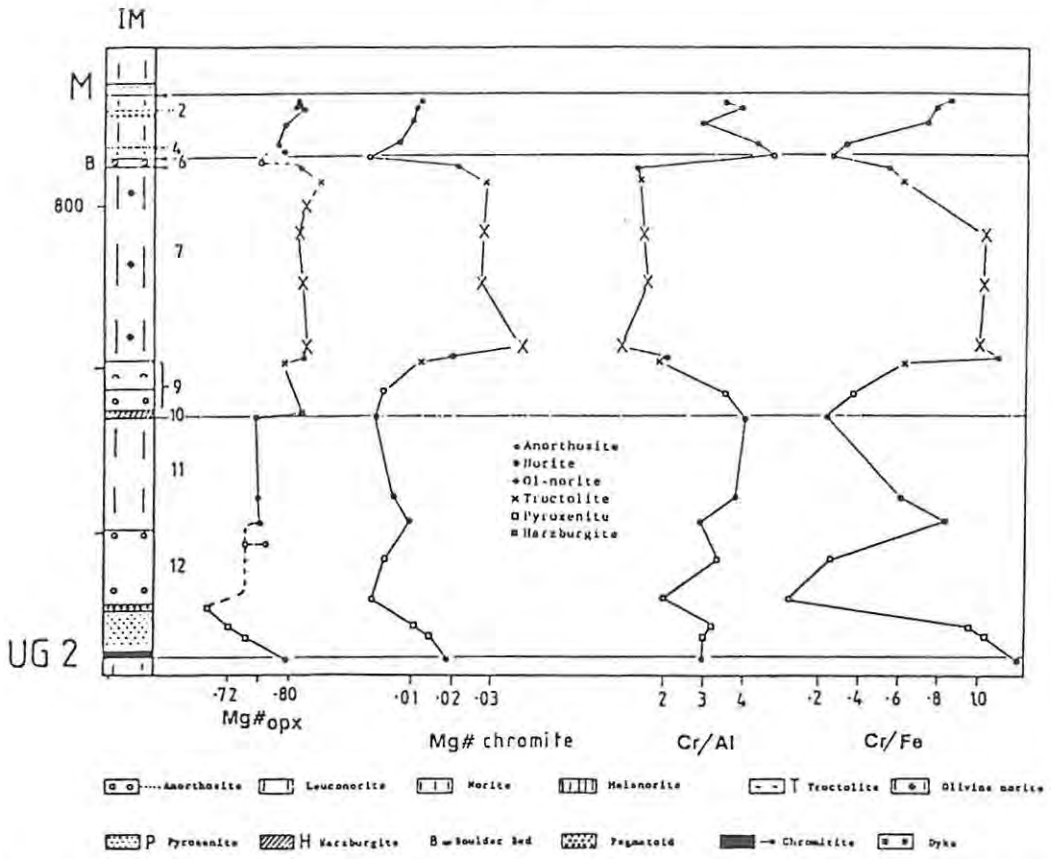

Fig. 6.9 Mg#, atomic Cr/Al ratio and Cr/Fe ratio (weight ratio of the metals) of dispersed cumulus chromite in core IM. Note the similar patterns traced by $Mg\#_{chromite}$ and $Mg\#_{opx}$, shown for comparison on left side of diagram. Vertical scale as in Fig. 6.1.

It is interesting to note that the anorthositic host of the "boulders" in the 5 analysed cases shows remarkably constant An values (Table 6.2).

Table 6.2: Average plagioclase composition in "boulders" and their adjacent footwall and hangingwall (Brakspruit shaft area is situated some 5 km south-east of Turffontein shaft area).

	An		Fe		n	
	boulder	matrix	boulder	matrix	boulder	matrix
TF (Turffontein)	83.3	77.2	0.32	0.38	3	5
Brakspruit	73.5	76.1	0.19	0.21	5	4
Rustenburg (Lee & Sharpe, 1980)	78.0	76.0	-	-	i.n.a.	
LK7	72.5	76.0	0.21	0.28	6	4
H3	71.8	76.1	0.30	0.30	8	6

i.n.a. = information not available

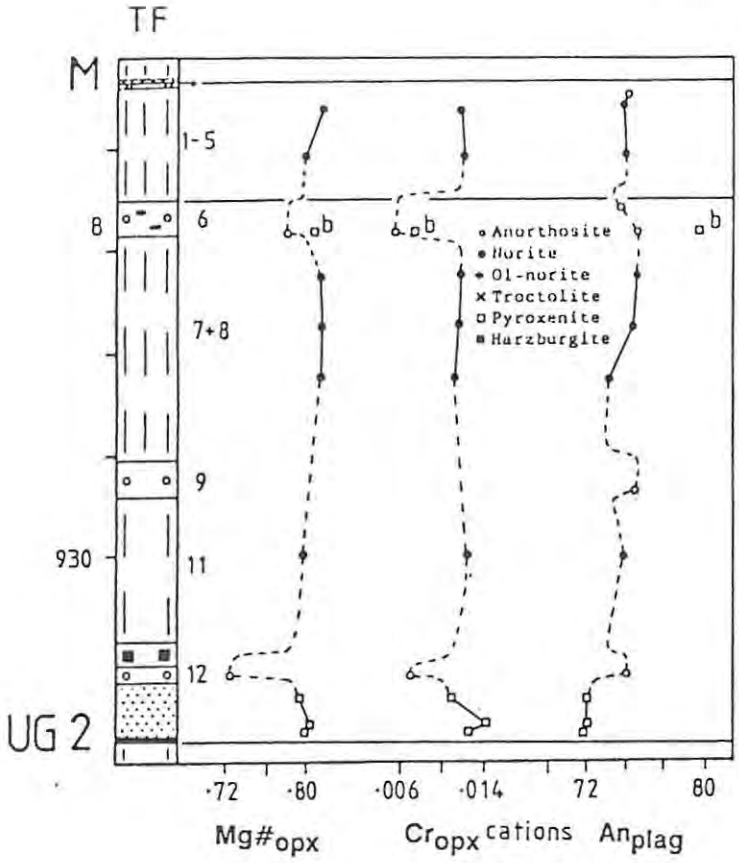

Fig. 6.10 Summary of the most important geochemical parameters displayed in intersection TF. No whole-rock data are available for this intersection. Vertical scale as in Fig. 6.1.

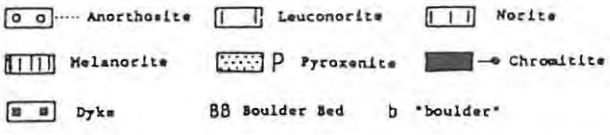

Chromite of both the upper and lower part of the chromite-rich selvage surrounding the "boulders" was analysed in two samples from RPM Brakspruit shaft area (samples BBBC and BBTC, Table 6.3). The basal chromite shows comparatively low values in Cr/Fe and Mg#. The values lie in the range of the accessory chromite of the immediate foot- and hangingwall, whereas chromite from the top contact zone displays significantly different values.

Table 6.3: Composition of chromite grains in the selvage surrounding a "boulder" at RPM Brakspruit shaft area (Samples BBBC (lower contact) and BBTC (upper contact))

	lower contact chromite	upper contact chromite
Cr/Fe	0.63	1.23
Mg#	0.29	0.26
Cr/Al	1.35	2.80

Cr/Fe = weight ratio of the metals
Cr/Al = cationic ratio of Cr/Al

The UG2 pyroxenite at intersection TF shows no systematic chemical trend within the limited thickness of the member.

6.9: The LK7 Sequence (Wolhuterskop)

The central noritic part of the study interval at locality LK7 (FW 7+8+9+10+11) shows a muted but consistent upward increase in $Mg\#_{opx}$, Cr_{opx}, and $Mg\#_{wr}$ (Fig. 6.11). This trend is so regular that the connecting lines in this case probably are statistically justified. An overall upward increase can also be detected in the modal proportion of orthopyroxene. As most parameters ($Mg\#_{opx}$, Cr_{opx}, modal proportion of orthopyroxene, An content and grain size of plagioclase) show a small inflection towards the base of this central noritic part (1520 m), it can possibly be subdivided into two subunits.

The An content of plagioclase remains relatively constant throughout the central part of the sequence compared with the overlying units, and grain sizes of plagioclase display a rather regular decrease from the FW 12 anorthosite upwards through the central noritic part; in the top part of the sequence grain sizes scatter considerably.

A "boulder" was intersected in the core at the base of the FW 6b anorthosite (see Fig. 2.3 for nomenclature). Its mineral chemistry does not differ significantly from that of the adjacent rocks. The UG2 pyroxenite shows a rough trend of decreasing $Mg\#_{opx}$ upwards, but minor reversals do occur as well.

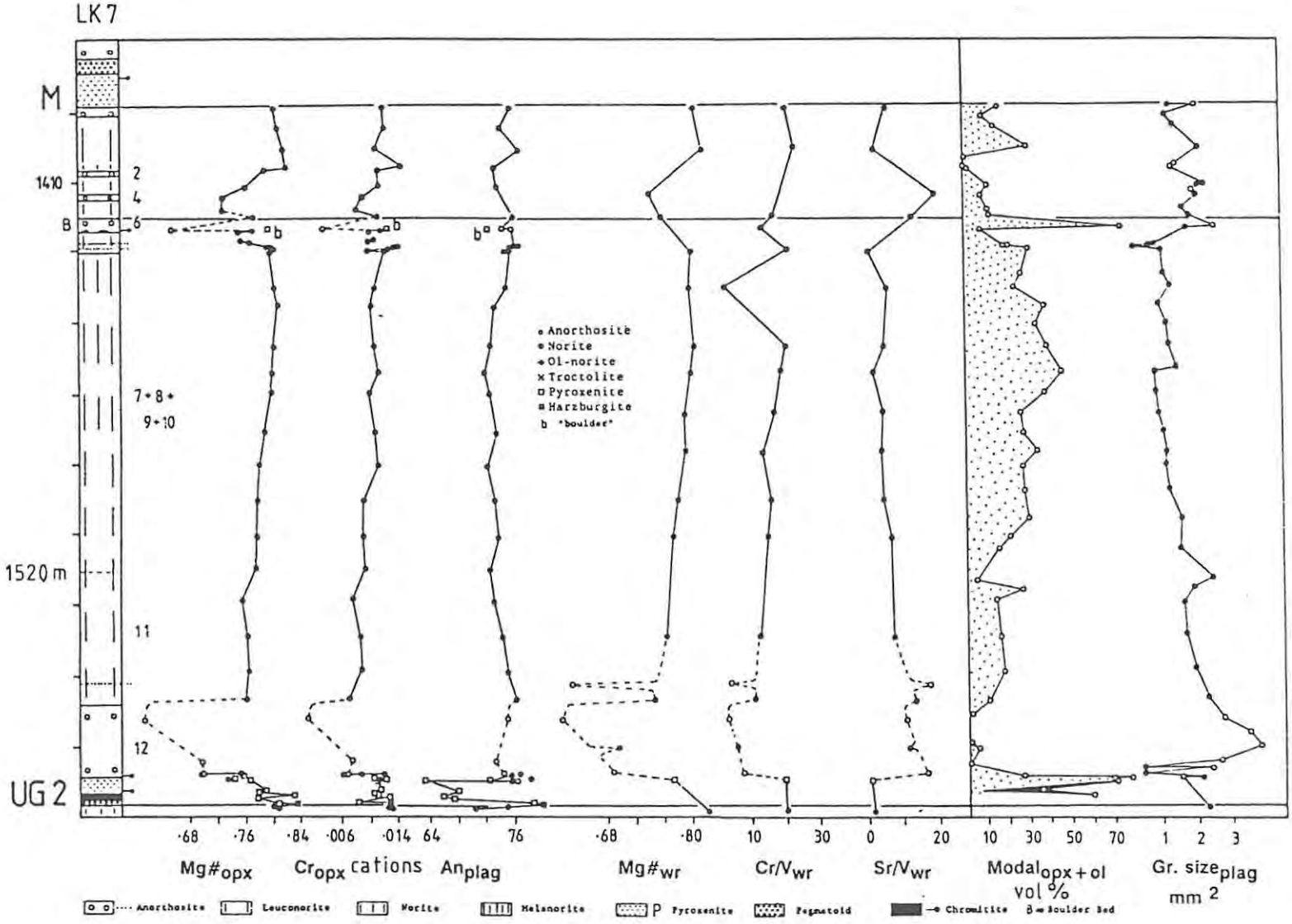

Fig. 6.11 Summary of the most important geochemical parameters displayed in core LK7. Vertical scale as in Fig. 6.1.

6.10: The H3 Sequence (Wolhuterskop)

Intersection H3 (Fig. 6.12) in many respects strongly resembles intersection LK7. The central noritic part, again, shows a gentle but consistent increase in $Mg\#_{opx}$, Cr_{opx}, $Mg\#_{wr}$, Cr/V_{wr}, and modal proportion of orthopyroxene with height, and a decrease in Sr/V_{wr} and grain size of plagioclase. Towards the base of the central noritic part, an inflection can be observed again in most parameters, as in profile LK7.

An values for plagioclase are very constant in the central noritic part, but scatter towards the top and base of the interval under review. A slight increase in An level is detectable towards the top of the central noritic part, and the interval as a whole. A thin, fine-grained troctolitic layer or lens towards the top of FW 7 shows anomalously high An values for plagioclase.

A "boulder" (or a thin pyroxenitic layer?) was intersected at a slightly higher level, relative to the base of the FW 6b anorthosite, than at locality LK7. It is of considerable interest that the $Mg\#_{opx}$ of the "boulders" seems to become less primitive along strike from localities Brakspruit and TF to localities LK7 and H3, i.e., from west to east, or as the distance from Union Section increases. This will be discussed in further detail in Chapter 7.

Standard deviations of grain sizes within individual samples show that the central noritic part appears to have formed under exceptionally constant physicochemical conditions in comparison with the rest of the interval.

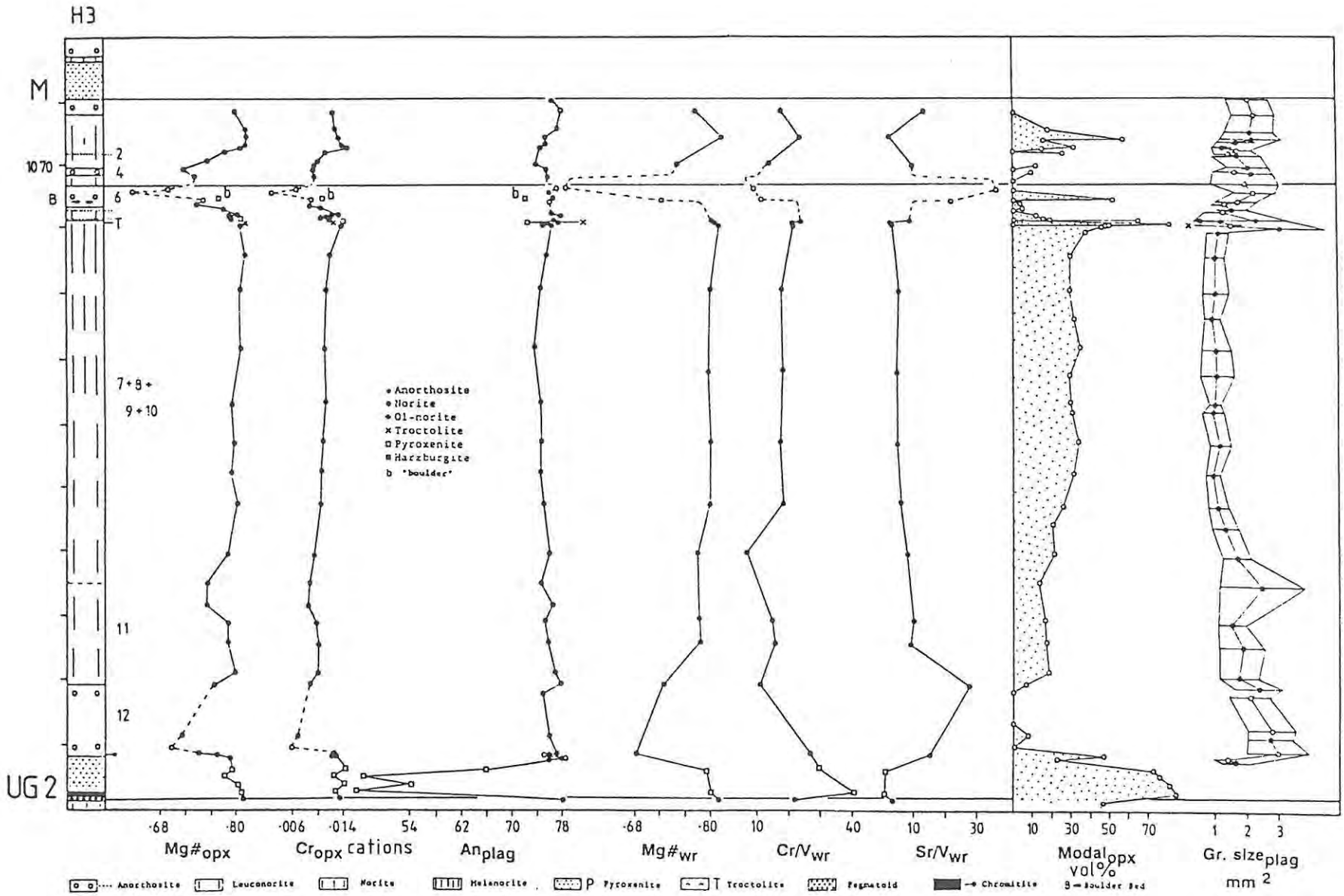

Fig. 6.12 Summary of the most important geochemical parameters displayed in core H3. 1σ standard deviations have been plotted for grain size measurements of cumulus plagioclase within each sample. Vertical scale as in Fig. 6.1.

6.11: The KR2 Sequence (Crocodile River Mine)

The KR2 sequence, situated in the Brits Graben, is in some respects chemically slightly different from the other intersections investigated (Fig. 6.13). The central noritic part (FW 7-11) still shows a consistent upward increase in $Mg\#_{opx}$ but both $Mg\#_{wr}$ and Cr/V_{wr} ratios decrease gently upwards and the Sr/V_{wr} ratio increases, indicating a decrease of the modal proportion of orthopyroxene. Thus, some of the geochemical parameters that shifted in sympathy in most other profiles, are decoupled in this part of the studied interval. Serpentinization of orthopyroxene, which is a common feature in the central noritic sequence at locality KR2, may explain the decoupling of the Mg# trends of orthopyroxene and whole-rock data. Direct point counting was considered to be relatively unrewarding due to severe alteration throughout the central part of the core and has not been executed, but grain sizes of plagioclase more or less reflect the trends of the other two cores in the south-eastern part of the western limb of the Bushveld Complex.

6.12: Summary

The geochemical data collected by the author shows that the different cores share a number of common chemical features:

(a) The central (noritic) part of the study interval in 7 of the 10 intersections ($60E^3$, IN, IM, TF, LK7, H3, and KR2) is characterized by uniformity with respect to lithology and chemistry: a 25 - 45 m package of olivine norite at intersections $60E^3$, IN, and IM displaying consistent chemical attributes, and a 45 - 115 m package of norites (usually grading downwards into leuconorites) at localities TF, LK7, H3, and KR2, displaying a muted but consistent upward increase in $Mg\#_{opx}$ and Cr_{opx}. In intersections UA, $7E^3$, and EK22 no comparable uniform central noritic sequence of any significant thickness is developed.

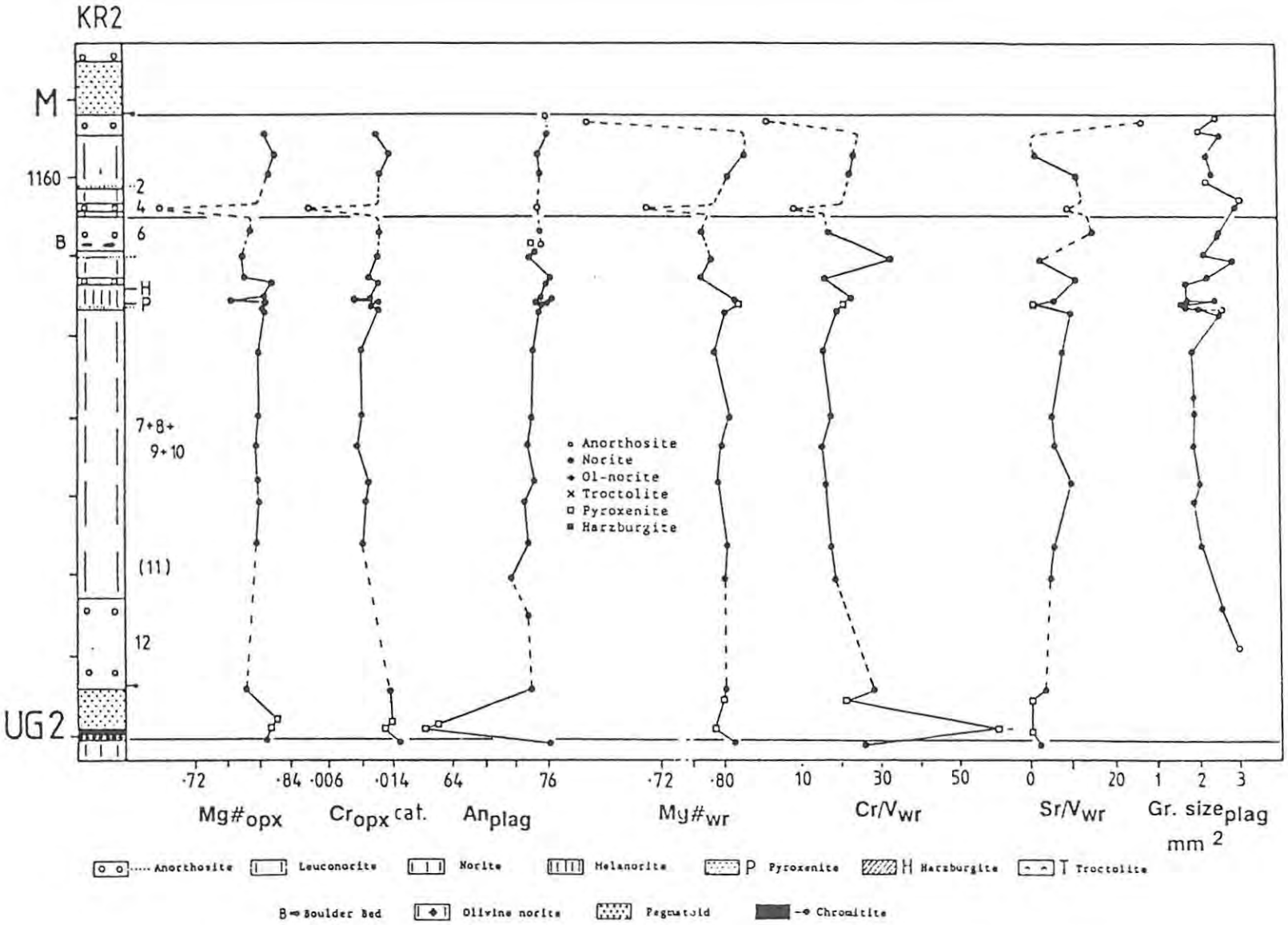

Fig. 6.13 Summary of the most important geochemical parameters displayed in core KR2. Vertical scale as in Fig. 6.1.

(b) Within the central noritic part, the three easternmost cores (LK7, H3, KR2) show a consistent decrease in grain size of cumulus plagioclase and an increase in the modal proportion of orthopyroxene with increasing stratigraphic height.

(c) The top and bottom parts of the interval under review (i.e., above and below the central noritic interval) are characterized by greater lithological and chemical variation.

(d) The An content of cumulus plagioclase is more or less uniform in anorthosites and norites, but a moderate increase towards the top of the studied interval can be detected in cores EK22, IM, LK7, H3, and KR2.

(e) Frequently, norites of the central noritic part, and in some cases in the immediate UG2 footwall, show higher $Mg\#_{opx}$ (but not Cr_{opx}) than samples of the underlying UG2 pyroxenite.

CHAPTER 7: CORRELATION ALONG STRIKE

7.1: Introduction

The lithostratigraphic, petrographic and geochemical data presented in the preceding chapters will now be used to attempt a lithological correlation of the different members of the studied interval. It is clear that certain layers in the Bushveld Complex are remarkably constant along strike, both lithologically and geochemically, e.g., the UG2 chromitite and pyroxenite. Other layers vary in chemical and lithological attributes along strike and the laws which govern these variations can only be determined if the stratigraphic correlation is correct. Variations along strike in the Merensky footwall succession have been studied earlier by Feringa (1959) at Union Section and Eales et al. (1988) in a limited study of the Western Bushveld.

A comparison of the section studied with the equivalent units in the Eastern Bushveld Complex is problematic insofar as the scale of the investigations published in the literature (Cameron, 1982; Gain, 1986; Mossom, 1986) is far bigger than that of the present study. Thus, individual anorthosite layers are generally not distinguished and classified. In general, the equivalent sequence in the Eastern Bushveld is much thicker (ca. 400 m) and an additional unit consisting of a chromitite layer (UG3) and an overlying pyroxenite can be distinguished ca. 40 m above the UG2 chromitite. The UG2 pyroxenite is generally overlain by a melanorite but the UG3 pyroxenite is succeeded by a 6 m anorthosite which in turn is overlain by a thick noritic sequence. Cameron (1982) established a trend of constant Mg# values of orthopyroxene within the latter sequence at Winterveld. Hence, basic similarities between western and eastern lobes seem to exist and an attempt to establish a more detailed correlation would be rewarding if more detailed logs were made available by the mining companies.

A correlation of anorthosites is especially difficult as zonation of plagioclase leads to highly variable analytical results in terms of

the mineral chemistry. Furthermore, cumulus plagioclase in the studied interval seems to have very consistent An levels (see Fig. 4.3(c) and 5.6). Work by Eales et al. (1990a) also indicates that anorthosites and norites in the footwall of the UG1 chromitite contain a mixed population of plagioclase. The density of plagioclase (2.65 for An_{70-90}, Campbell et al., 1978) is considered to be comparable to that of the evolved, presumably originally boninitic to tholeiitic host liquid (for a discussion on parental magmas see Chapter 8.2) and plagioclase could have remained suspended in the magma for a relatively long time. Different generations of plagioclase may therefore have mixed with each other and thus obscured any original whole-rock chemical differences between individual anorthosite layers. However, the formation of anorthosites does not follow wholly random processes, as the feasibility of correlating them clearly shows.

The discussion dealing with the correlation of the discrete units will start with the Union Section sequence because this intersection shows the most compressed sequence and is regarded by some authors as the most likely location of a major feeder zone in the Western Bushveld (Eales et al., 1988; Teigler, 1990).

7.2: The UG2 Chromitite and Pyroxenite

The UG2 chromitite and its overlying pyroxenite are the only layers in the interval under review which are unequivocally definable over the entire strike length in the western limb of the complex. At Union Section and, to a lesser degree, in parts of Amandelbult Section, a harzburgite may be developed between the chromitite and the pyroxenite (see Chapter 2.2, 2.3, 2.5). It is of interest to note in the context of this study that the footwall of the UG2 chromitite in all but two of the studied intersections (UA, $7E^3$) consists of a norite of remarkably consistent composition (Table 7.1). At Union Section the UG2 chromitite directly overlies the UG1 pyroxenite and at locality $7E^3$ it rests on a fault zone.

Table 7.1: Comparison of $Mg\#_{opx}$ and An content of plagioclase (core compositions) along strike in the noritic footwall of the UG2 chromitite. Intersection LF is situated at Crocodile River Mine (data for this core generated by Teigler, 1990).

Locality	EK22	IN	IM	TF	LK7	H3	KR2	LF
$Mg\#_{opx}$	.809	.813	.793	.803	.801	.811	.811	.815
n	7	5	5	4	7	6	6	4
An_{plag}	78.0	77.0	76.1	76.3	74.7	77.4	76.6	76.7
n	5	10	8	19	5	5	4	6

Samples of the UG2 chromitite could only be obtained for core LK7 because of existing mining company policies relating to the mineralized horizons. Additional data from the literature, however, make a comparison along strike possible (Table 7.2). No systematic cryptic variation can be detected along strike in either Cr/Fe ratio or Mg# of chromite; the values stay rather constant. In contrast to some of the overlying units, the total thickness of the UG2 chromitite layer (i.e., the main seam plus the leader seams) does not systematically change from Union Section to Brits (Crocodile River Mine). The thickness and number of the leader seams, however, is reduced at localities LK7, H3, and at Crocodile River Mine (profile KR2) compared with Union, Amandelbult, and Impala Sections. Furthermore, a pyroxenitic parting is introduced in the south-eastern extremities of the western limb (localities H3 and KR2). The pegmatoidal pyroxenite (or harzburgite), underlying the main chromitite, varies in thickness between 0 and 1m. This variation is laterally not systematic either.

The UG2 pyroxenite, like the underlying chromitite, does not display any systematic regional thickness variation (Table 7.3). Only in an area extending from the southern parts of Impala Section to locality LK7 near Wolhuterskop (representing a strike length of ca. 50 km) can a reduction in thickness amounting to a maximum of 50% be observed. Intersection $7E^3$ is located within a fault zone (see Chapter 2.3) which might account for the reduction in thickness observed here.

Table 7.2: The UG2 chromitite along strike in the Western Bushveld. Locations are listed in order of increasing distance from Union Section. Thickness includes leader seams.

	Cr/Fe	Mg#	Thickness (m)	n
Union	$1.38_{(3)}$	$.36_{(1)}$	$1.0_{(7)}$	-
Union	$1.40_{(2)}$	$.44_{(2)}$	$1.1_{(2)}$	135
Rooderand	-	-	$1.2_{(7)}$	-
Amandelbult	$1.30_{(1)}$	$.37_{(1)}$	$1.4_{(7)}$	-
Impala	$1.34_{(3)}$	-	$0.8_{(8)}$	-
Rustenburg	$1.38_{(1)}$	$.38_{(1)}$	$0.8_{(9)}$	-
Western Plats	$1.41_{(4)}$	-	$1.1_{(10)}$	49
Wolhuterskop	$1.29_{(5)}$	$.39_{(5)}$	$1.4_{(11)}$	3
Crocodile River	$1.37_{(6)}$	$.47_{(6)}$	$1.3_{(11)}$	6

1 Cousins & Feringa, 1964, whole-rock data of chromite concentrates
2 Eales & Reynolds, 1986, microprobe data
3 Vermaak, 1985, whole-rock data of chromite concentrates
4 Smits, 1988, microprobe data
5 This study, microprobe data
6 Teigler, 1990, microprobe data
7 J.C.I., in-house report (see Fig. 1.1(b) for location of core Rooderand)
8 Leeb-du Toit, 1986
9 Viljoen & Hieber, 1986
10 Farquhar, 1986
11 Rand Mines, in-house report; value represents average thickness of cores LK7 and H3

In contrast to the relative consistency in thickness of the pyroxenite along strike, variations along strike are evident in thickness of the harzburgite developed at Union and parts of Amandelbult Section immediately above the UG2 chromitite. At Union Section an average thickness of 2 m is recorded (Viljoen et al., 1986a). At Amandelbult thicknesses of 27 and 40 cm are recorded for profiles $7E^3$ and $60E^3$, respectively (RPM in-house logs). No harzburgite has been encountered at that position in profile EK22. Similarly, no harzburgite is recorded above the UG2 chromitite in the southern arm of the western limb. At Crocodile River Mine, however, minor olivine occurs at that stratigraphic level in some intersections.

Table 7.3: The UG2 pyroxenite in the Western Bushveld. Cores UB and UC are situated at Union Section (data made available by W.J. de Klerk)

	Mg# opx	Cr_2O_3 opx	Al_2O_3 opx	Mg# wr	MgO wr	Ni/Sc wr	Sr/Al_2O_3	Thickness (m)	n opx-wr
UA	.81	.44	1.36	.81	24.2	31	13.3	9.7	7-5
UB	-	-	-	-	25.6	-	-	-	-
UC	-	-	-	-	24.1	-	-	-	-
AE	.81	.27	1.33	.81	23.2	21	13.0	10.0	4-5
7E[3]	na	na	na	na	na	21	na	8.2	7
EK22	.79	.42	1.34	.83	24.2	29	11.0	7.0	3-2
60E[3]	na	na	na	na	na	18	na	10.5	6
IN	.80	.46	1.20	.80	25.7	21	8.9	10.0	3-3
IM*	.72	.22	0.86	.77	22.4	12	12.2	6.0	3-3
TF	.80	.45	1.07	na	na	na	na	8.0	3
WP	-	-	-	-	-	-	-	5-9	-
LK7	.78	.38	1.18	.77	20.5	14	13.2	5.1	5-1
H3	.80	.45	1.01	.79	22.9	17	10.8	11.0	4-2
KR2	.82	.46	1.17	.80	23.9	15	10.2	11.0	2-2

* highly altered succession
WP = Western Platinum Mine
na = not analysed

Some systematic variation along strike may be detected in grain size of orthopyroxene. In the south the layer generally seems to show a smaller average grain size of orthopyroxene, more pronounced foliation and better developed gradation from small grain sizes at the base into larger grain sizes towards the top of the pyroxenite. Pure adcumulates are generally rare and only characterize parts of the pyroxenite at localities IN and UA. This observation, however, cannot be quantified because of the low sample density. If true, the feature would be somewhat unexpected as one would anticipate the smallest grain sizes and a closer approach to adcumulus textures close to the supposed feeder zone in the north. It was argued in Chapter 3.9 that this behaviour may be explained by slow cooling due to a more persistent heat flux in the areas proximal to a feeder zone, leading to more complete equilibrium textures.

The chemical data presented in Table 7.3 have been generated by the author during the current study. It shows considerable spread in some parameters. Some of this data spread can probably be attributed to the fact that the UG2 pyroxenite is not a homogeneous layer but displays several compositional reversals through the member, as was shown in Chapter 6 for some of the cores (UA, IN, H3), and also by Eales (unpubl. data). Ni/Sc_{wr} ratios tend to show higher values in the northern sections. $Mg\#_{wr}$ and MgO_{wr} ratios possibly show similar trends whereas the Sr/Al_2O_{3wr} ratio seems to be more or less constant along strike. $Mg\#_{opx}$ and Cr_{opx} do not show any clear trend but Al_2O_{3opx} displays higher levels in the north. As a summary it would appear that chemical variations along strike seem to be minor and non-systematic in the UG2 chromitite but show detectable systematic variation in some parameters in the UG2 pyroxenite.

Fig. 7.1 presents a graphical display of changes in these geochemical parameters of the UG2 pyroxenite, along strike. Note that in all parameters, a reversal seems to occur towards Brits (core KR2).

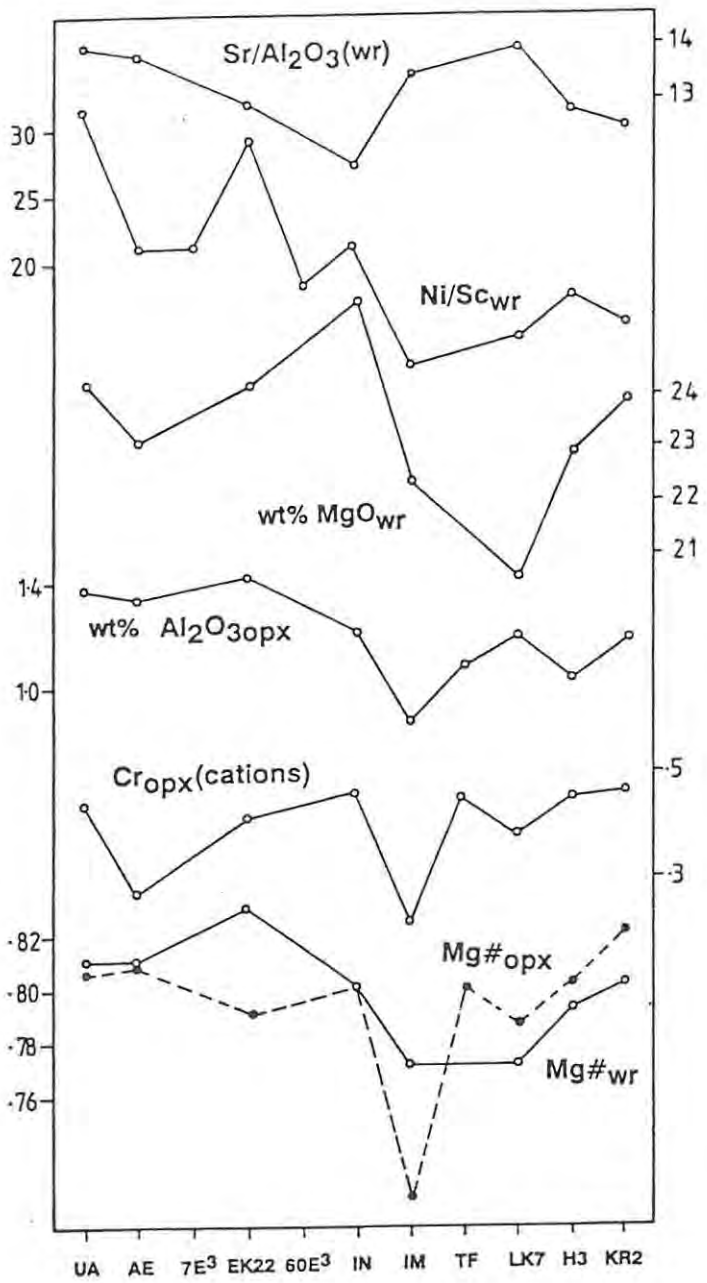

Fig. 7.1 Average composition of the UG2 pyroxenite along strike in the Western Bushveld (datum points represent average values of between 2 and 7 analyses, LK7 = 1 analysis). Note the reversal which usually occurs towards Brits (intersection KR2). Sequence from left to right represents increasing distance from Union Section.

7.3: The Lower Pseudoreef Unit (P1 Marker)

The P1 Marker, consisting typically of a pegmatoidal harzburgite at Union Section (Viljoen et al., 1986a) or pyroxenite at Amandelbult (Viljoen et al., 1986b) occurs as such mainly in the north-western part of the Western Bushveld. At Impala Section a pegmatoidal zone may be present at the top of the UG2 pyroxenite. Occasionally, a chromitite stringer may be developed at its top contact. The chromitite stringer, and sometimes a succeeding thin (1-5 cm) pyroxenite layer, possibly represent the Upper Pseudoreef A. It may also develop a thin top chromitite stringer and is separated from the UG2 pyroxenite in some cases by a thin (20-50 cm) leuconoritic parting. This introduction of a leucocratic parting is especially common in the south-eastern cores (LK7, H3, KR2, Plate 2). Furthermore, in these profiles, the pegmatoidal pyroxenite at the top of the UG2 pyroxenite has disappeared completely.

The pegmatoid forming the P1 Marker has been interpreted by some as a result of upward-moving fluids which become trapped within an orthocumulate layer (Barnes & Campbell, 1988). Generally, the P1 Marker is extremely difficult to correlate within the available core material along the complete strike length because of its highly variable appearance.

7.4: The Footwall Members 11 + 12 (FW 11 + 12)

These two members comprise the UG2 hangingwall anorthosite plus the overlying leuconorite which precede the upper portions of the P2 Marker (P2-B and -C) in most of the southern part of the western limb (localities IM, TF, LK7, H3, KR2). At Union Section this package is not developed (or preserved) and the massive harzburgites of the Upper Pseudoreef (A+B+C) directly overlie the P1 Marker. The sequence at Amandelbult Section, where FW 11 + 12 correspond with the interval between the Upper Pseudoreefs A and B, as defined by Eales et al.

(1988), constitutes a transitional facies (Fig. 7.2): the westernmost cores show a ca. 2 m anorthosite between the P2-A and the P2-B Markers (core EL17, inset in Fig. 7.2). Moving to the east towards intersection AE a leuconorite then underlies this anorthosite. Towards the middle part of the lease area, at 7E and 22E levels, a thin anorthosite begins to underlie this package (10E level reports a 1 m "spotted anorthosite" at this position). This anorthosite has disappeared again at 39E level. At 57E level the leuconorite has disappeared as well and the sequence shows a striking resemblance to intersection IN in the south-western part of the western limb. From 57E level eastwards the package consists mainly of anorthosite, with one or more thin intercalated leuconorites. At locality IN in the southern part of the western limb, the interval consists of 6 m of anorthosite. For these reasons a distinction between FW 12 and 11 is difficult to establish at Amandelbult and in the northern parts of Impala Section. At locality IM the FW 12 + 11 interval has thickened to roughly 22 m and shows gradation from an anorthosite at the base into leuconorite towards the top. This remains the typical sequence to the east. Between localities TF and LK7 the distinction between FW 11 and the overlying noritic package becomes difficult. An inflection is, however, detectable in $Mg\#_{opx}$, grain size of plagioclase, and modal proportion of orthopyroxene at about 30-40 m above the top of the FW 12 anorthosite in the LK7 and H3 cores (Fig. 7.3, 7.4, 7.5). The genesis of the FW 12 anorthosite, like the origin of anorthosites in general, is not yet clear. In some cases the transition from the UG2 pyroxenite into the FW 12 anorthosite is gradational.

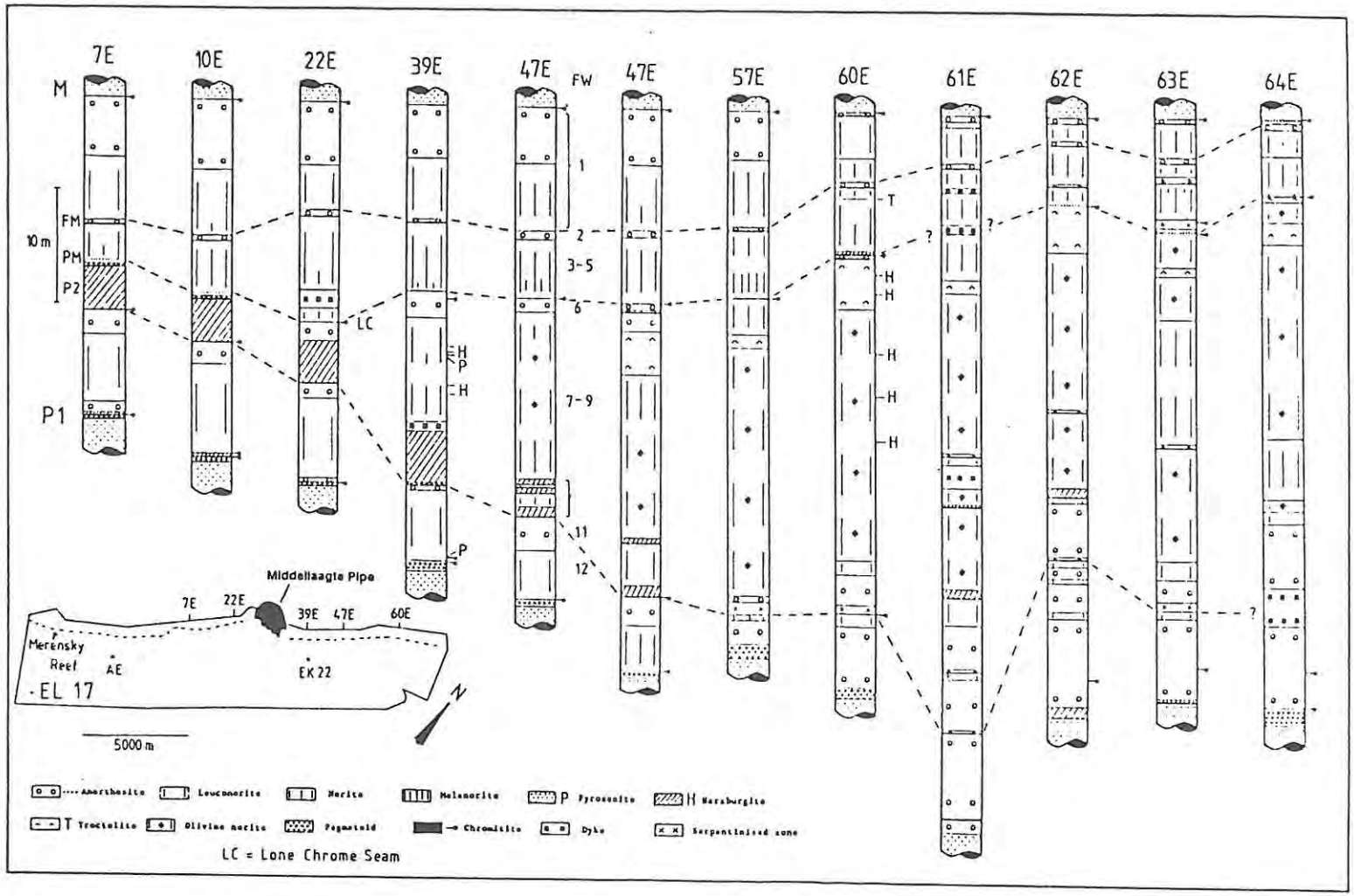

Fig. 7.2 The interval between the Merensky Reef and the P1 Marker along strike at Amandelbult Section. Core EK22 is situated on the 39E level. No detailed log is available for core AE. Stratigraphic data derived from author's logging and from RPM in-house logs. PM = Pothole Marker, FM = Footwall Marker, FW = Footwall Member.

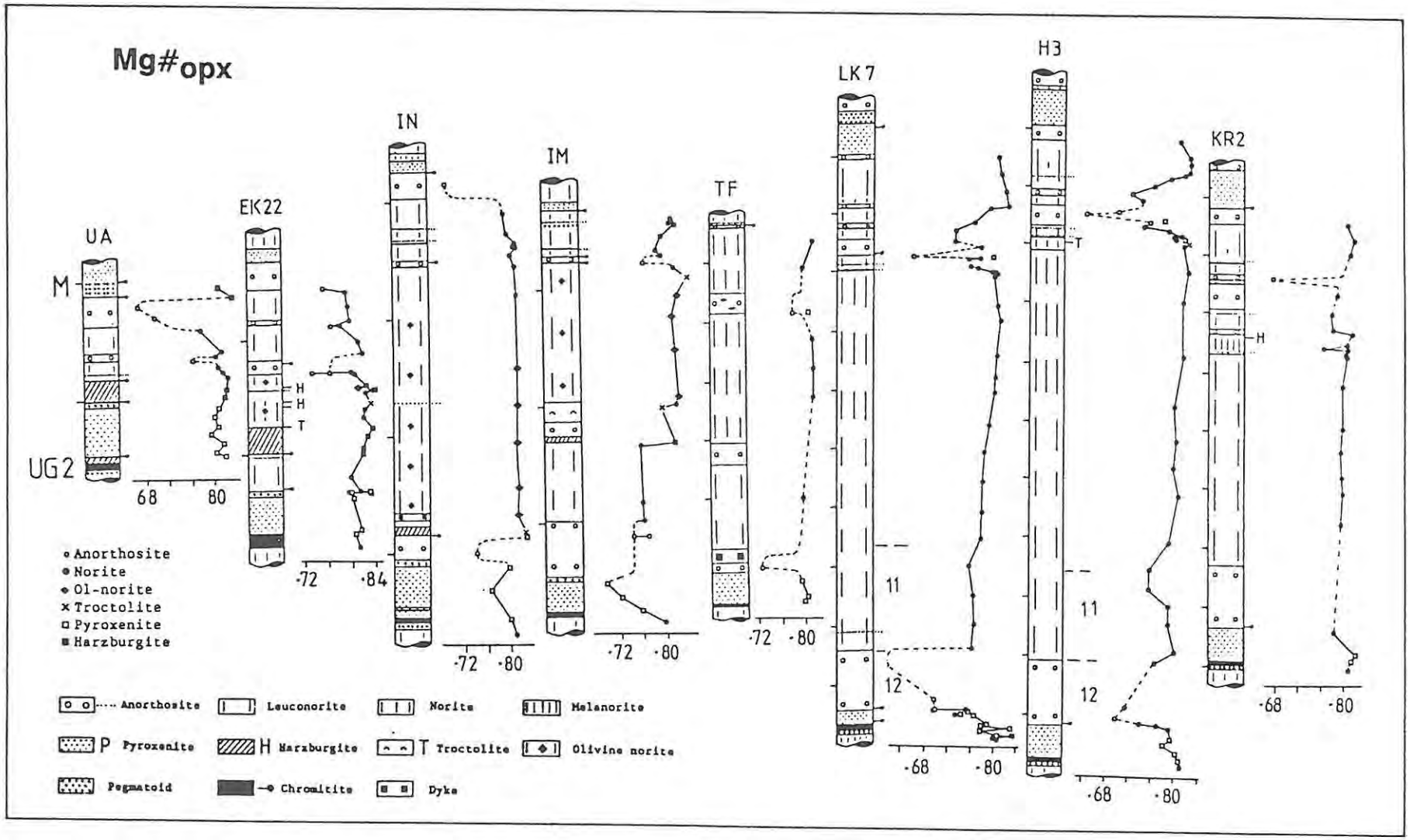

Fig. 7.3 $Mg\#_{opx}$ in the individual cores along strike in the Western Bushveld. Note change of scale between UA-EK22-IM-IN and TF-LK7-H3-KR2. In both cases, the distance between marks on the left side of columns represents 20 m.

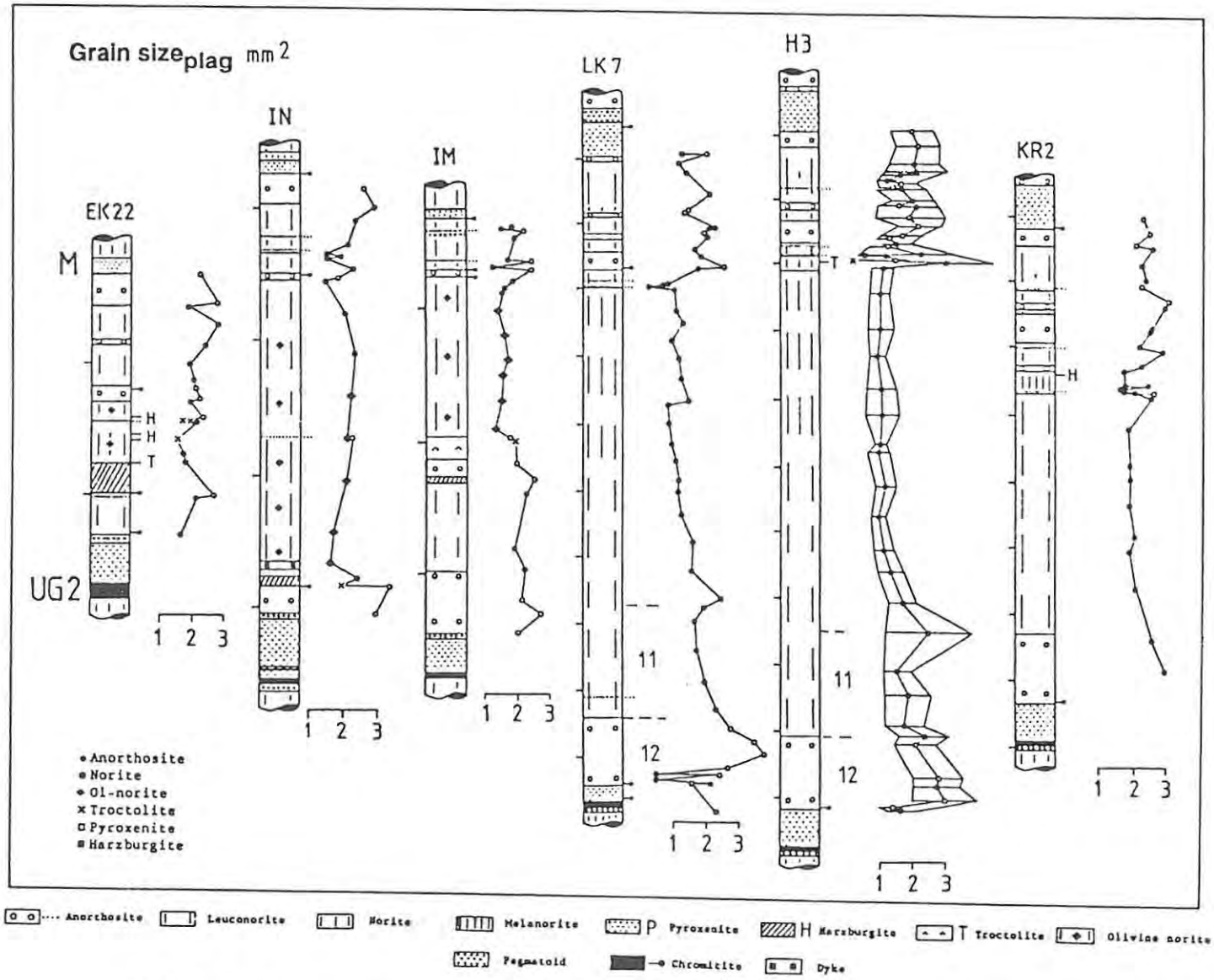

Fig. 7.4 Grain sizes of cumulus plagioclase (in mm^2) along strike in the Western Bushveld. Note change of scale. The 1 standard deviation of the 20 largest grains (see text for explanation) is displayed for one representative core. Vertical scale is 20 m between marks on left side of profiles.

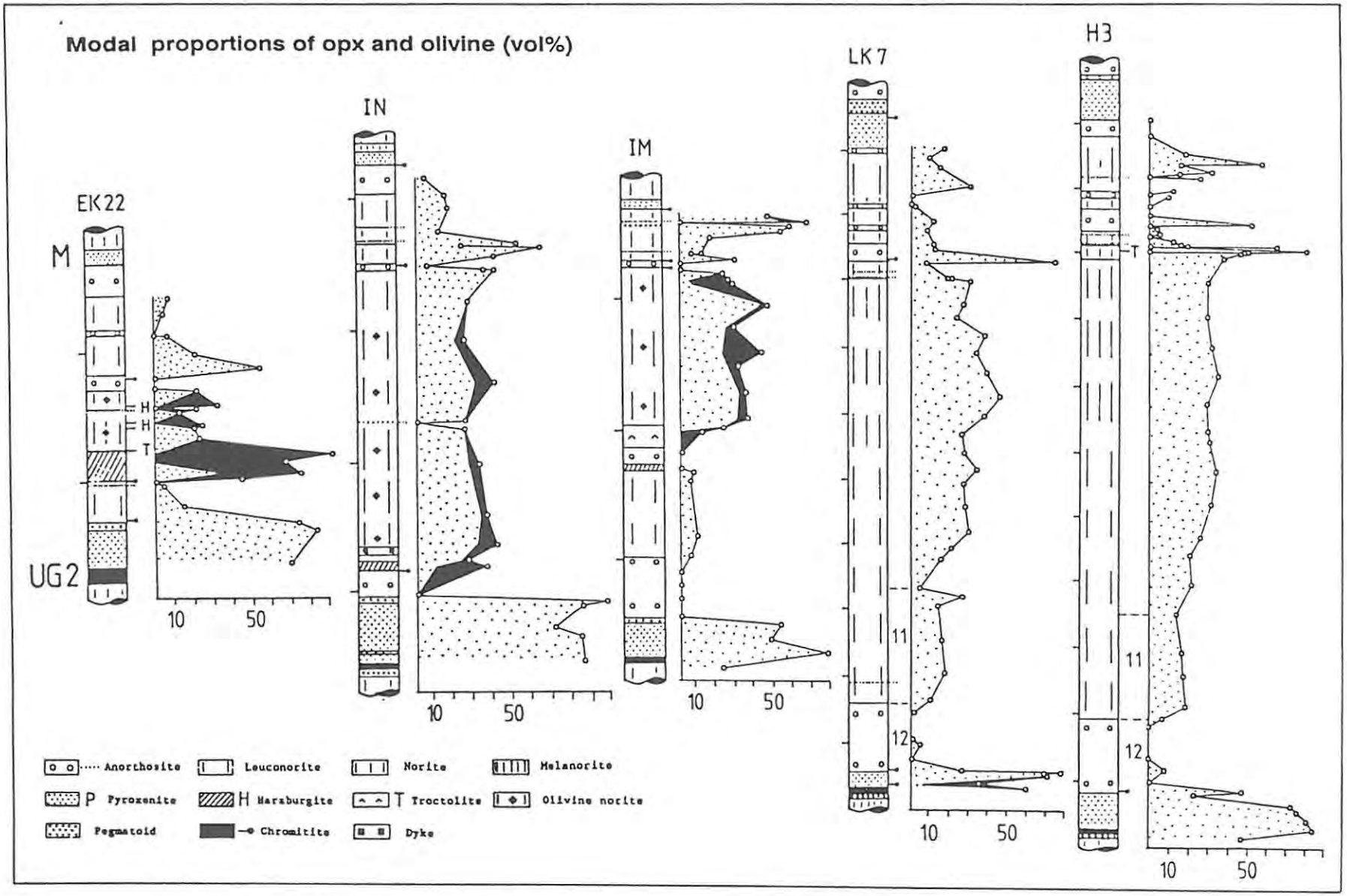

Fig. 7.5 Modal proportion (vol%) of orthopyroxene (stippled) and olivine (black) in five intersections along strike in the Western Bushveld. Vertical scale is 20 m between marks on left side of columns.

7.5: The Upper Pseudoreef Unit (P2 Marker) and the Footwall Members 10 to 7 (FW 10-7)

Harzburgitic development of the P2-A Marker can only be distinguished at Amandelbult Section and possibly at locality IN (i.e., in the northern part of Impala Section). At both localities the P2-A Marker may, however, consist only of a chromitite stringer developed at the top contact of the P1 pegmatoidal pyroxenite. Further towards the south-east (profiles IM, TF, LK7, H3, and KR2) this chromitite stringer and occasionally an associated thin pyroxenite are separated from the UG2 pyroxenite by an up to 50 cm leucocratic parting (Plate 2, see also Section 7.3). The thin pegmatoidal pyroxenite which overlies the FW 12 anorthosite at locality IN (Fig. 7.6, 7.7 and 7.8) is correlated by the present author with the P2-B Marker up to the Middling at Amandelbult. FW 9 is formed by troctolite at locality IN and an anorthosite at locality IM and is correlated by the present author with the P2 Middling at Amandelbult (Fig. 7.6). At south-western Amandelbult the contact between the troctolitic P2 Middling and the P2-C Marker is defined by a thin chromitite stringer. The Middling changes in appearance from troctolitic in the extreme south-west of Amandelbult towards anorthositic at intersection AE.

At locality IN the FW 9 is overlain by a harzburgitic interval of 20 cm (Fig. 7.7). This is not developed at intersection IM. The author assumes this to be the last occurrence of the P2-C Marker in the southern part of the western lobe and classifies it here as FW 8.

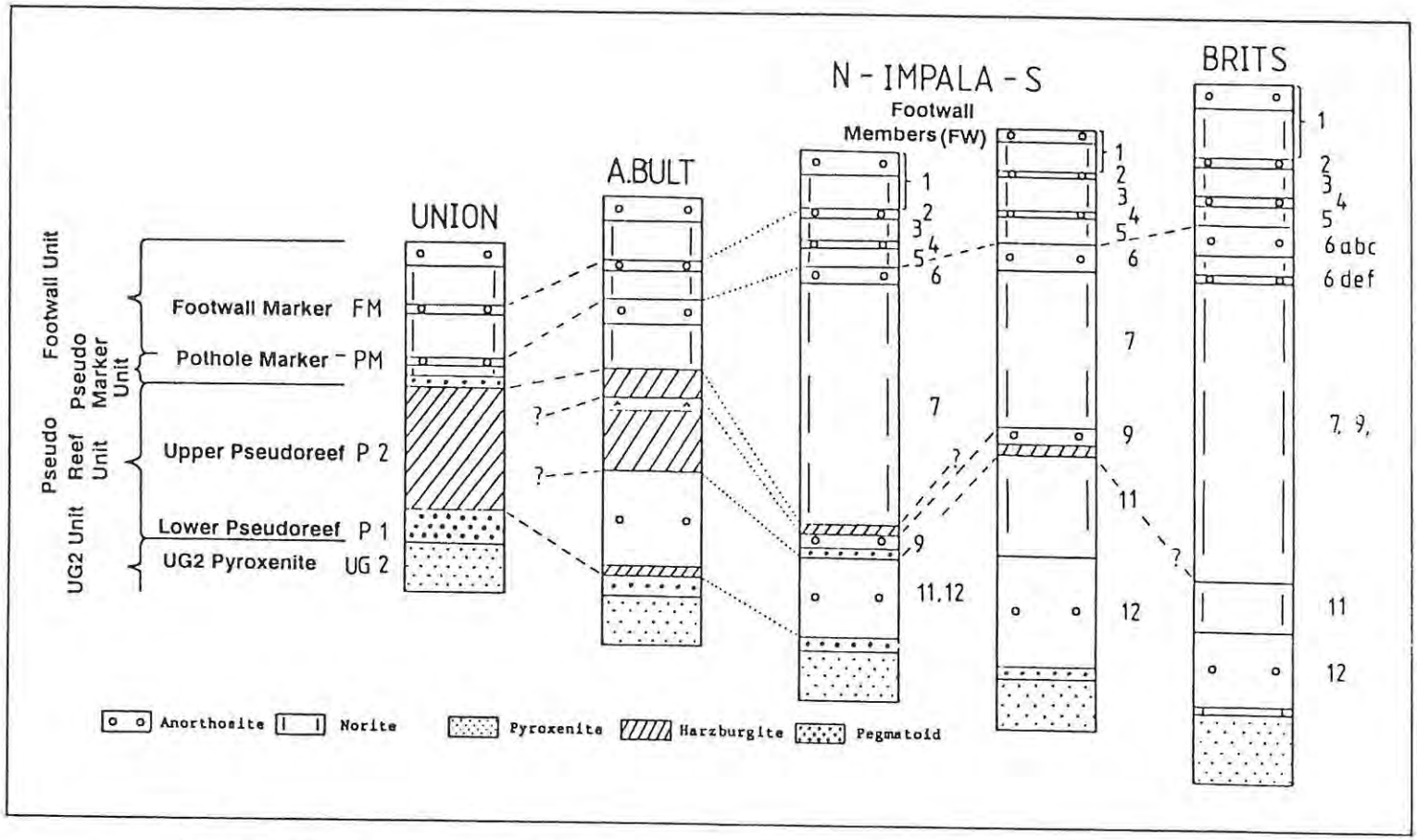

Fig. 7.6 Schematic presentation of the stratigraphy and nomenclature, used in this work, of the main distinguishable members in the interval between the UG2 pyroxenite and the Merensky Reef in the Western Bushveld Complex. Note the difference in nomenclature used at Union and Amandelbult Sections in the northern part of the western limb of the complex and that at Impala Section and the Brits area (Crocodile River Mine) in the southern part. (This diagram represents a re-presentation of Fig. 2.1, and is inserted here for the convenience of the reader. Columns are not drawn to a fixed scale).

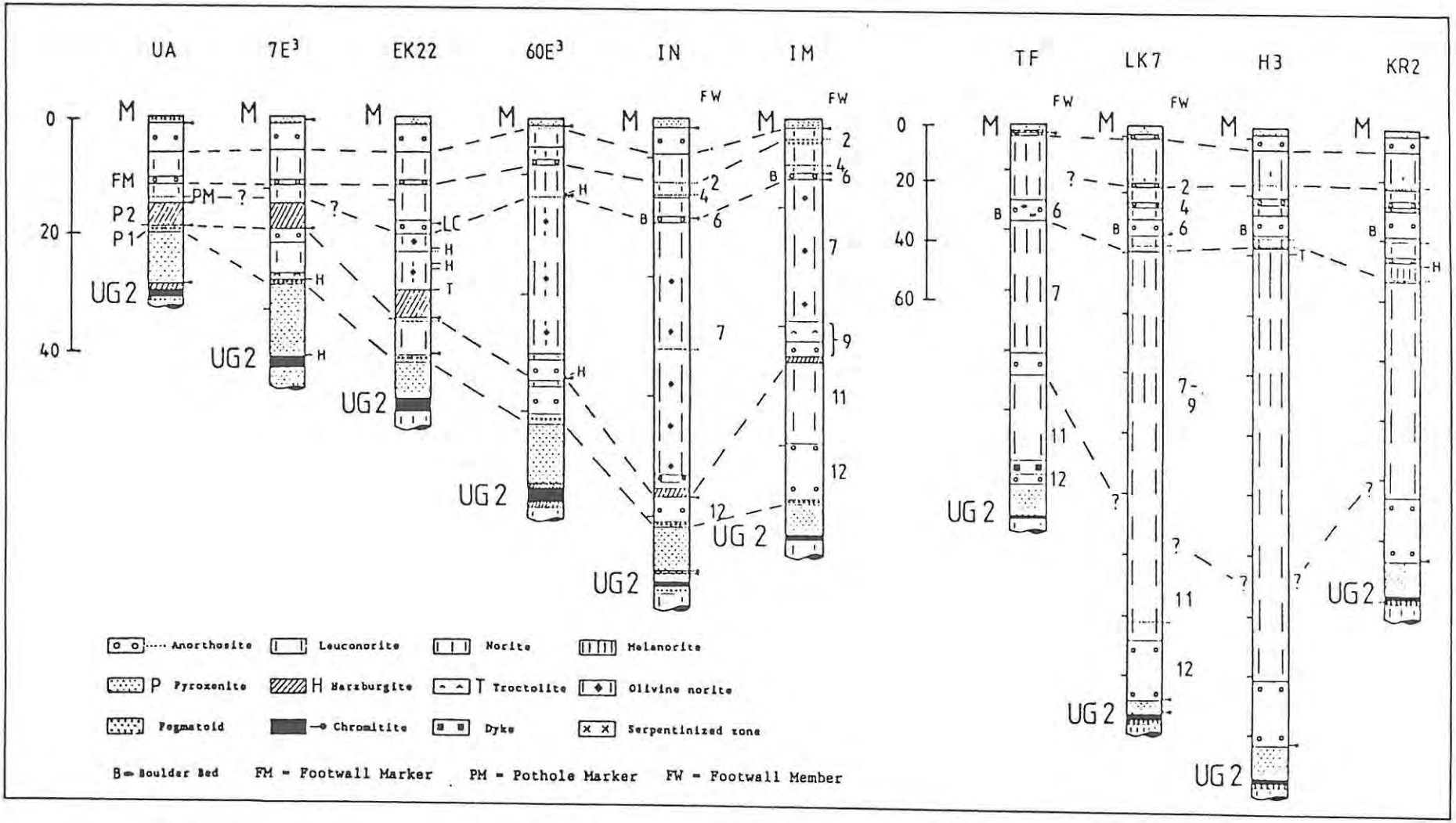

Fig. 7.7 Stratigraphy and provisional correlation of the interval under review in the investigated intersections. Note the change of scale between the 6 cores on the left-hand side and the 4 cores on the right-hand side of the diagram. The distance between marks (short lines on left side of profile) represents 20 m in each case. In some cases the thickness of thin layers is slightly exaggerated in order to show them more clearly. Question marks indicate that the correlation is tentative.

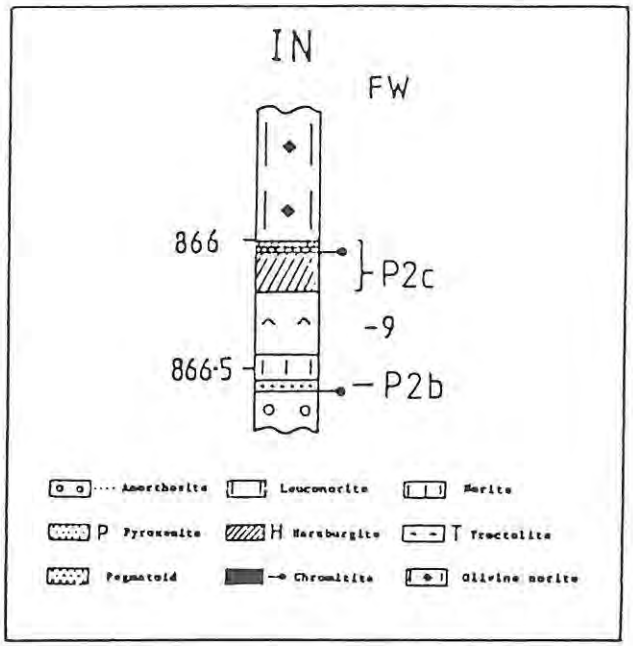

Fig. 7.8 Detailed profile of the sequence below and above FW 9 at locality IN (see text for explanation).

Towards the north-east of Amandelbult, at locality EK22, the P2-C Marker starts to split up into several thin harzburgite layers and at locality 60E[3] in the far north-east only a number of thin harzburgitic layers or schlieren are developed throughout the olivine-noritic central part of the intersection which is ca. 25 m thick (Fig. 7.2).

The hangingwall of the P2 Marker at Union Section consists of a 1 m succession (known as the Pseudo Marker Unit) grading from harzburgite into pyroxenite and melanorite before the first thin anorthosite (the Pothole Marker) appears (Fig. 7.6 and 7.7). The Pothole Marker is characterized by a remarkable consistency and can be traced across the entire strike length of the western limb if the correlation of the author is correct. It is not clear how the Pseudo Marker Unit should be grouped as the central olivine-noritic part at north-eastern Amandelbult (locality 60E[3]) and Impala Section (FW 7) probably represents a mixture between the upper part of the P2 influx, the Pseudo Marker influx and residual liquid.

Towards Brits in the extreme south-east the P2-B + -C harzburgites have disappeared, and between FW 11 and 7 the interval consists of a thick noritic package (Figs. 7.6 and 7.7). One can possibly locate the upper limit of FW 11 ca. 50 m above the UG2 pyroxenite where an inflection occurs in most geochemical parameters (Fig. 7.3, 7.4, 7.5). Above that horizon the norite becomes consistently more primitive with increasing stratigraphic height. This is reflected by an increasing proportion of modal orthopyroxene and increasing $Mg\#_{opx}$, $Mg\#_{wr}$, and Cr_{opx}. The entire package is thought to represent the equivalent of the P2-B + -C Marker + the Pseudo Marker Units at Union and Amandelbult Sections and to the FW member 7 at Impala (Fig. 7.6). It thus seems that the monomineralic olivine cumulates of the P2 Marker in the north gradually become diluted by orthopyroxene and plagioclase towards Rustenburg until olivine disappears totally between Rustenburg and Western Platinum Mine. A possible mechanism which could explain this gradual change along strike is proposed in Chapter 8.2.

This central noritic part (FW 7) is thus in many geochemical and petrographical attributes (grain $size_{plag}$, modal proportions and composition of orthopyroxene and plagioclase) very constant, in contrast with the adjacent units above and below it (see also Chapter 6.12).

The individual harzburgite layers which can be assigned to the P2-B and -C between central and north-eastern Amandelbult (Fig. 7.2), and which are separated from each other by leucocratic rocks, seem to be merged at Union and south-western Amandelbult, although separated at the latter locality by the leucocratic P2 Middling. This largely conceals the multicyclic character of this unit. Both the P2 harzburgite at intersections AE and EK22 and the norite, which replaces it in the south-eastern part of the western limb, show an increase in primitive character with height (see Table 7.4 and Fig. 7.3). At locality AE, where the P2-B and -C Markers are separated by the Middling anorthosite, this upward change can be observed in both

parts, with a reversion to lower Mg# (0.805) occurring at the base of the upper part (Table 7.4, sample 39.6) relative to the maximum $Mg\#_{ol}$ values (0.832) in the troctolitic Middling (sample 40.1). At locality EK22 the thin harzburgite layers which overlie the P2 main harzburgite also reflect higher values of $Mg\#_{ol}$ (Fig. 7.3, Table 7.4). Note, also, that a muted reversal occurs between samples 296.9 and 297.1 in intersection EK22, possibly representing the base of a new depositional cycle not defined by a lithological discontinuity.

Table 7.4: Mg# of olivine through the P2 at localities AE (data generated by Field, 19876) and EK22. Depths are indicated in metres.

AE				EK22			
Sample	Mg#	n		Sample	Mg#	n	
39.4	.853	7	Upper	288.40a	.809	6	thin harzburgite layer
39.5	.821	5	Pseudoreef C	288.90b	.803	7	(Upper Pseudoreef C)
39.6	.805	3		291.48	.817	7	"
40.1	.832	5	Middling	295.70	.808	5	Upper Pseudoreef B
40.2	.819	4	Upper	296.90	.800	6	"
42.0	.817	4	Pseudoreef B	297.10	.803	7	"
				299.10	.796	6	"
				299.80	.789	6	"
				299.95	.790	6	"

Several models may account for upward change in parameters indicating a shift towards more primitive traits, amongst them a constant or increased influx of more primitive liquid that mixed with resident liquid in the chamber (Eales et al., 1990a). This question will be addressed in Chapter 8.2. The P2-B + -C harzburgites can be geochemically compared along strike only at Amandelbult as they are serpentinized in core UA and could only be analysed in two samples available to the author. The sparse data seem to indicate no systematic change in Mg# of olivine along strike (Table 7.5) but the data from intersections $47E^3$ and $64E^3$ are so limited that conclusions should be drawn with caution.

Table 7.5: A comparison of the P2-B + -C harzburgite along strike from Union (core UA) and Amandelbult Sections

Core	UA	AE	$39E_3$	$44E^3$	$47E_3$	$64E_3$
$Mg\#_{ol}$	.806	.823	.802	na	.808	.809
Ni	.32	.32	.34	na	.31	.36
n	2	5	9	-	1	1
$Mg\#_{wr}$	na	.718	.724	.714	.718	na
n	-	2	1	1	1	-

na = not analysed

7.6: The Footwall Members 6 to 2 (FW 6 to 2)

One of the most variable sequences to be found in the Upper Critical Zone consists of a 5 - 35 m alternation of anorthosites, norites, and pyroxenites, together with the enigmatic Boulder Bed (Fig. 7.9), extending downwards from an horizon between 1 and 20 m below the Merensky Reef. Some of the layers can probably be correlated all around the western limb. Some show a great consistency in thickness along strike (FW 2), but others are developed only in parts of the western limb (FW 4 and the various sublayers of FW 6).

A detailed stratigraphic compilation of this part of the succession plus the overlying FW 1 is presented in Figs. 7.9 and 7.10. In addition to the stratigraphic relationships, use of the $Mg\#_{opx}$ of the norites has been investigated as an aid in correlation of the anorthosites. Fig 7.2 gives a detailed overview of the situation at Amandelbult.

The first anorthosite above the P2 (Upper Pseudoreef) Marker at Union Section is the so-called Pothole Marker (PM), a thin (2 cm) but very persistent (Viljoen et al., 1986a) layer which tops a well-graded sequence of harzburgite-norite known as the Pseudo Marker Unit (see Chapter 2.2). At south-western Amandelbult, this thin anorthosite usually directly overlies an equally thin pyroxenite, the two of them together being called the P2 Hangingwall Marker (note that both pyroxenite and anorthosite are not developed at locality $7E^3$).

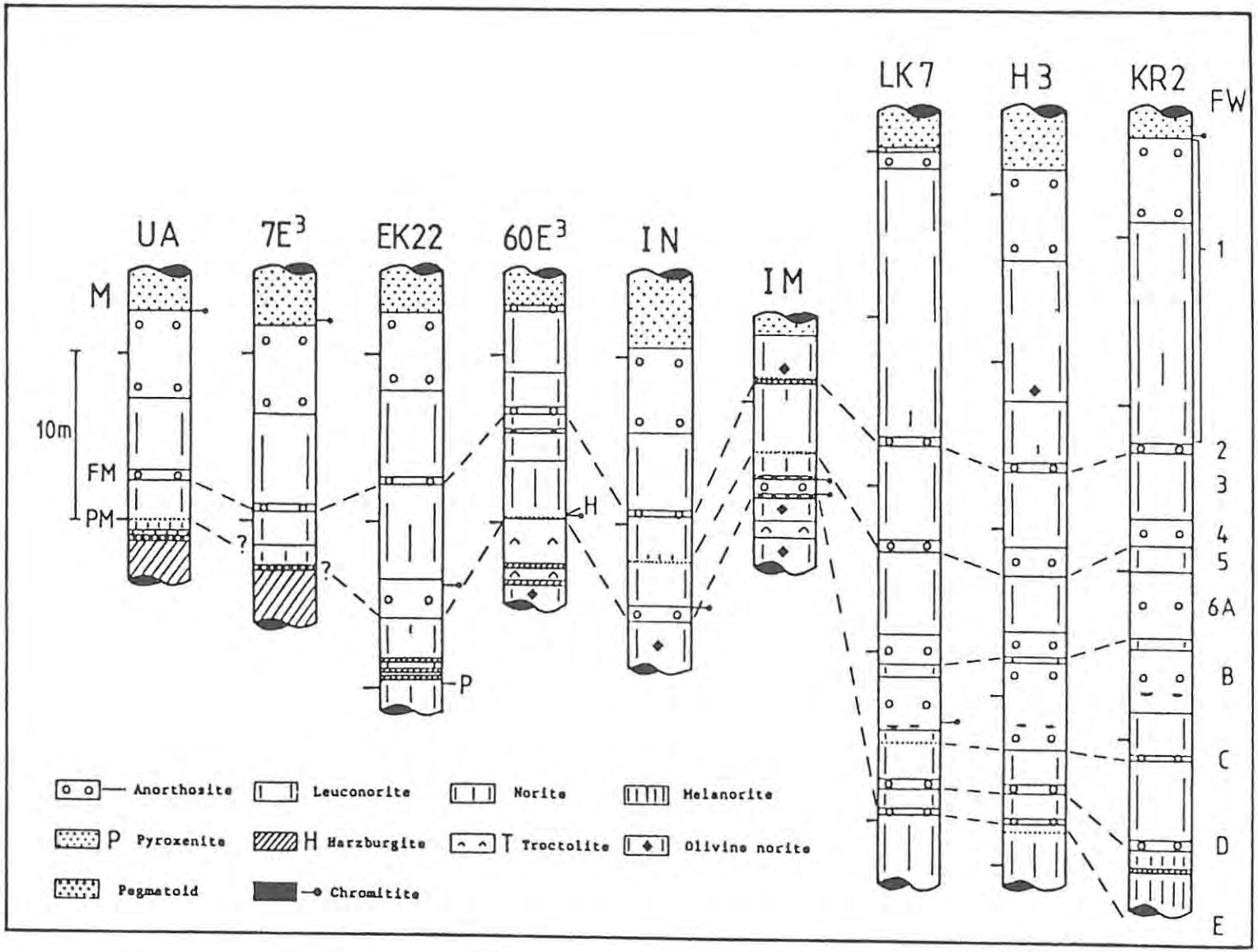

Fig. 7.9 Detailed stratigraphy and provisional correlation of the immediate footwall of the Merensky Reef. PM = Pothole Marker, FM = Footwall Marker, FW = Footwall Member.

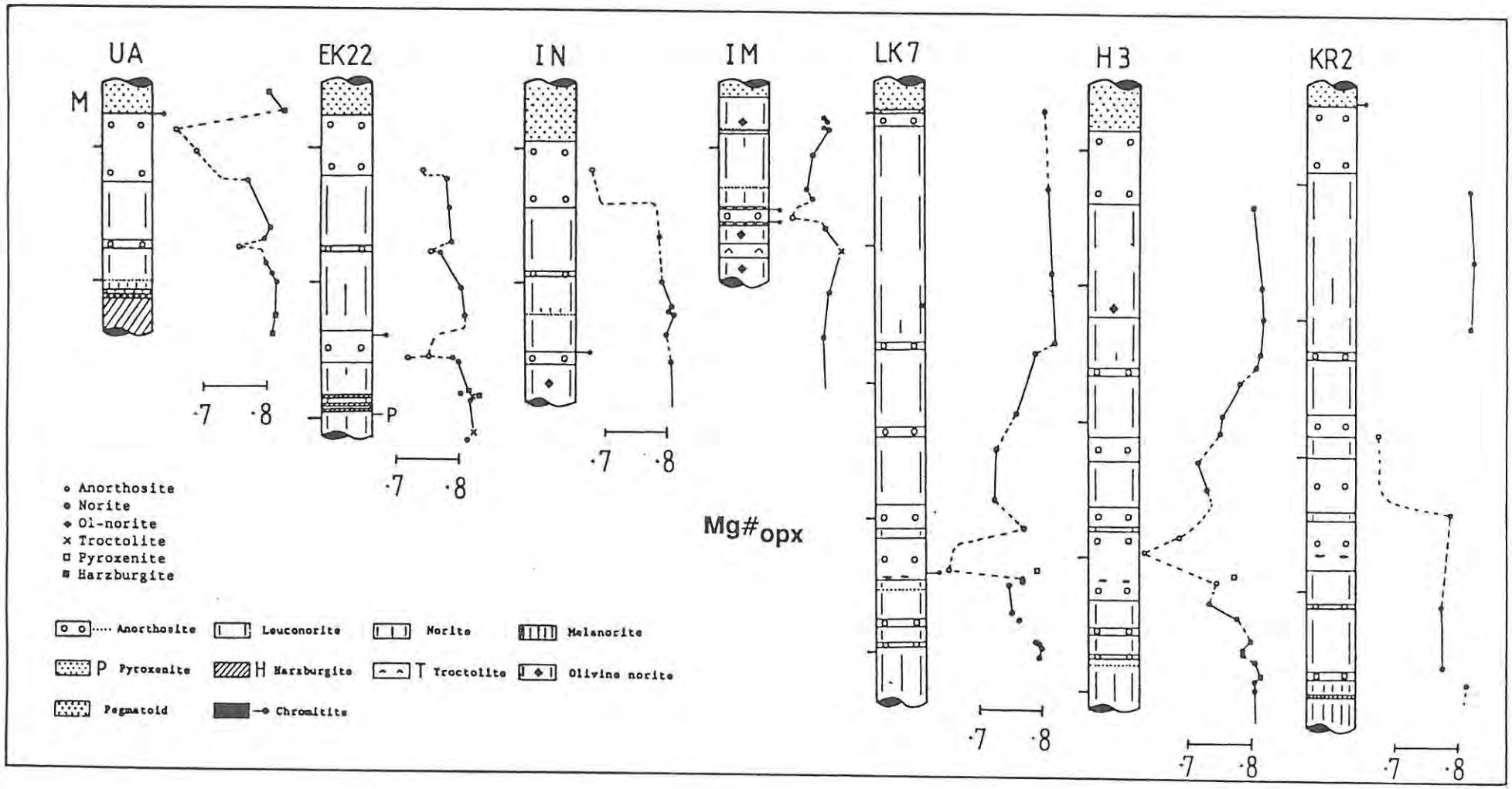

Fig. 7.10 $Mg\#_{opx}$ in the footwall succession of the Merensky Reef (FW 1 - 6) along strike in the Western Bushveld. All profiles are shown on same vertical scale, i.e., 10 m between marks on left side of columns (see Fig. 7.9 for nomenclature of footwall layers).

Towards the north-east of Amandelbult Section, this first anorthosite becomes thicker and a chromitite stringer, the so-called Lone Chrome Seam (LC), has developed towards its top (Fig. 7.2 and 7.9). Often, however, this chromitite may be found in the middle or even towards the base of this anorthosite. This, of course, is problematic under any interpretation. Orthopyroxene has been analysed in the norite above and below the anorthosite hosting the chromitite at No. 12 shaft in the northernmost part of Impala Section (Table 7.6, Sample INN), where the anorthosite is only 2 cm thick and the chromitite is located at its top contact.

A slightly higher level of $Mg\#_{opx}$ can be detected in the upper norite. It is difficult to equate results from the other intersections with this result as the thickness of the anorthosite can vary between 90 cm (locality IN) and 3 m (locality LK7). However, at most Impala intersections, the top norite displays lower Mg# than the underlying norite. This pattern can also be observed in the foot- and hangingwall of the Pothole Marker at Union Section (locality UA).

It thus seems possible that the anorthosite did not mark the end of a depositional cycle but merely a period of plagioclase deposition which was followed by continuing plagioclase-orthopyroxene accumulation, rather than a new primitive influx. This bears implications for the genesis of the LC as well. It is also noteworthy that the level of $Mg\#_{opx}$ values of both top and bottom norites more or less decrease from Union Section towards locality LK7 in the south-east. Systematic chemical variations along strike are thus more common in the upper part of the interval under review than in the underlying UG2 chromitite and pyroxenite.

Table 7.6: Microprobe data and $Mg\#_{opx}$ of the foot- and hangingwall norite of the FW 6 anorthosite (and the Pothole Marker at Union and Amandelbult Sections) along strike in the Western Bushveld. Sample INN represents locality 12 Shaft within the northernmost part of Impala Bafokeng North Mine

Locality:	UA	EK22	Bafokeng North 12 Shaft	IN	IM	LK7
Upper norite						
Sample	654.90	282.80a	INN	819.15	794.10	1421.10a
SiO_2	55.45	54.78	55.54	55.53	55.09	54.18
TiO_2	0.12	0.19	0.15	0.19	0.18	0.20
Al_2O_3	1.43	1.28	1.38	1.20	1.29	1.04
Cr_2O_3	0.41	0.41	0.51	0.54	0.42	0.40
FeO	12.00	12.03	11.43	12.44	13.44	14.17
MnO	0.20	0.27	0.27	0.24	0.26	0.33
NiO	0.05	0.08	0.11	0.11	0.05	0.08
MgO	29.82	29.62	29.67	28.58	28.46	27.65
CaO	1.15	1.47	1.25	1.25	1.26	1.57
Na_2O	0.00	0.03	0.02	0.02	0.02	0.02
Mg#	.816	.814	.822	.804	.791	.777
n	5	7	6	9	4	4

Lower norite						
Sample	655.50	286.05	INN	821.23b	796.25	1424.80
SiO_2	55.19	54.14	55.04	55.51	55.77	54.05
TiO_2	0.14	0.14	0.17	0.15	0.17	0.18
Al_2O_3	1.65	1.28	1.36	1.27	1.36	1.06
Cr_2O_3	0.48	0.44	0.50	0.43	0.31	0.42
FeO	11.22	12.63	11.56	12.01	12.04	14.53
MnO	0.21	0.25	0.28	0.26	0.24	0.31
NiO	0.12	0.08	0.10	0.08	0.10	0.11
MgO	29.49	28.80	29.17	28.90	29.16	28.08
CaO	1.54	1.20	1.39	1.20	0.87	1.58
Na_2O	0.03	0.01	0.01	0.03	0.01	0.03
Mg#	.824	.803	.818	.811	.812	.775
n	5	7	5	8	7	4

The Lone Chrome Seam can be correlated along strike from Amandelbult Section to Crocodile River Mine but the limited number of samples makes a systematic geochemical correlation tentative. However, the 5 samples analysed show a decrease in Cr/Fe ratio and Mg# of chromite, and an increase in Cr/Al ratio, along strike with increasing distance from Amandelbult (Table 7.7). This is what would be expected with increasing distance from a feeder zone and is in accord with the results of Table 7.6.

Table 7.7: Analyses of chromite constituting the Lone Chrome seam in the Western Bushveld (sample RS 38 originates from the southernmost parts of Impala Section)

	Amandelbult (EK22)	Impala (north)	Impala (south)	RPM Brakspruit Section	Wolhuterskop
Sample	284.25	INN	RS38	BBCR	LK7 1424.28a
TiO_2	0.68	0.88	1.74	1.70	2.12
Al_2O_3	17.28	17.81	10.99	16.54	10.51
Cr_2O_3	41.61	42.10	39.38	35.35	38.92
FeO(P)	29.33	28.70	38.47	37.13	40.93
FeO(C)	20.02	21.89	24.17	25.31	28.00
Fe_2O_3	10.34	7.57	15.89	13.14	14.37
MnO	0.31	0.29	0.33	0.30	0.35
NiO	0.09	0.14	0.14	0.19	0.09
MgO	9.70	8.48	6.73	6.47	4.29
Cr/Fe	1.25	1.29	.90	.84	.84
Mg#	.46	.40	.33	.31	.21
Cr/Al	1.63	1.59	2.30	2.50	2.49
n	30	4	62	5	6
An	76.38	76.80	77.06 (81.80)	79.05 (89.80)	74.77
n	4	22	6	5	7

An = An content of plagioclase in anorthositic footwall (values in brackets indicate An content of plagioclase within the chromitite stringer)

The occurrence of "boulders" towards the bottom of the FW 6 is mostly confined to the southern part of the western limb. However, "boulders" have been described at the base of the Merensky footwall anorthosite

and in the Footwall Marker at Union and Amandelbult Section (de Klerk, 1990, pers. com.), and in the FW 1 at Western Platinum Mine (Farquhar, 1986). Towards Brits, further anorthosites have developed beneath and above the FW 6 anorthosite. The anorthosite containing the "boulders" and the LC is therefore classified FW 6b and the over- and underlying anorthosites FW 6a, c, d, and e (see Fig. 7.6 and 7.9). Possibly, a slight decrease in $Mg\#_{opx}$ of "boulders" is detectable along strike from west to east (0.80-0.81 at locality TF (RPM Turffontein shaft, sample 866.50), 0.80-0.82 at Brakspruit Section (sample BBBC), 0.80 at locality LK7 (sample 1424.28B), and 0.78 at locality H3 (sample 1081.64)).

The next anorthosite higher up in the succession at Union Section (locality UA) is the Footwall Marker (FM) which may be absent in parts of the lease area. At Amandelbult this layer is well defined by its consistent thickness (Fig. 7.2) and its purity (see Fig. 6.3 and 6.6). In the north-eastern extremities of Amandelbult Section the distance between the FM and the Merensky Reef gradually decreases (Fig. 7.2). In the south the FM can be correlated with FW 2 (Fig. 7.6).

This correlation of the anorthosites cannot be proved beyond doubt. The orthopyroxene chemistry of the intercalated norites does not show conclusively that anorthosites, which may be similar in thickness, distance to fixed marker horizons like the Merensky Reef, and position relative to associated layers, are in fact equivalent. Hence, the sequence between the Pothole Marker and the Footwall Marker shows a trend of upward-decreasing $Mg\#_{opx}$ at Union and Amandelbult (Fig. 7.10). At locality IN, where the two layers are called FW 2 and 6, respectively, an intermediate anorthosite develops (FW 4), and the $Mg\#_{opx}$ increases upwards between FW 6 and 4 and then decreases between FW 4 and 2. At localities IM, LK7, and H3, $Mg\#_{opx}$ tends to increase between FW 4 and 2. Intersection IN therefore apparently represents a transitional sequence between the north-western cores (UA-EK22) and the south-eastern cores (IM, LK7, H3, KR2). In the vicinity of

Rustenburg, the footwall members 5 and 3 also seem to become more melanocratic upwards (Kruger, 1982). The plagioclase chemistry of the anorthosites themselves is not sufficiently distinctive to establish diagnostic differences.

An alternative way to correlate the upper part of the succession may be prompted by the exposures yielded by the development along strike at Amandelbult Section (Fig. 7.2). Here, it is apparent that the Footwall Marker in the north-east (57E - 64E) gradually approaches the Merensky Reef along strike until it more or less directly underlies the Reef. If one then considers that the succession at level 57E very much resembles that at locality IN, one might be persuaded to extend the trend, visible at Amandelbult (from level 57E to 64E) to the southern part of the western limb. It is then possible that at locality LK7, the FM or FW 2 has approached the Merensky Reef and at localities H3 and KR2, it directly underlies it. There is no definite answer to this problem at this stage but the latter concept would imply that with increasing distance from the supposed feeder zone at Union Section, the immediate footwall of the Merensky Reef becomes progressively eliminated, a fact which would be difficult to explain physically. Furthermore, a clearly defined footwall succession from FW 6 to FW 1 is described at Rustenburg (Kruger, 1982). The immediate footwall anorthosite of the Merensky Reef thins out towards Western Platinum Mine but seems to reappear at locality LK7.

7.7: The Footwall Member 1 (FW 1) and the Merensky Reef

The FW 1, consisting of a norite which grades upwards into anorthosite, forms the immediate footwall of the Merensky Reef. Apart from the north-eastern part of Amandelbult Section (Fig. 7.2) and the south-eastern part of Impala (locality IM, Fig. 7.9), it is relatively persistent along strike in thickness and geochemical signature. This assumes that the correlation of the author (Fig. 7.9) is correct. In some cases (cores EK22, IM, LK7, H3, KR2), a slight increase in An

content is detectable towards the top of the unit (see also Kruger & Marsh, 1985; Eales et al., 1988, Fig. 3), which has been interpreted as evidence for floating of plagioclase (Vermaak, 1976; Lee & Sharpe, 1980; Kruger & Marsh, 1985). A geochemical survey of the FW 1 norite along strike is compiled in Table 7.8. Somewhat surprisingly, the south-eastern cores (LK7, H3, KR2) show higher average $Mg\#_{opx}$, Cr_2O_{3opx}, and total MgO content and lower MnO content than the north-western cores (UA, EK22). It is not clear, at the present stage, how this feature can be explained.

Table 7.8: Orthopyroxene chemistry of the FW 1 norite along strike

Locality	$Mg\#_{opx}$	Cr_2O_{3opx}	MgO_{opx}	MnO_{opx}	n
UA	.797	.41	28.97	.28	3
EK22	.700	.38	28.75	.28	3
IN	.791	.41	28.38	.27	1
IM	.812	.41	28.86	.25	3
LK7	.819	.46	29.56	.22	3
H3	.808	.46	29.00	.26	4
KR2	.818	.46	29.33	.25	3

n = number of samples

The Merensky Reef shows considerable variability along strike in as much as its pegmatoidal character gradually disappears towards Brits. The average thickness of the Merensky pegmatoid at the various localities is as follows:

Union (UA): ca. 3 m (RPM in-house logs)
Amandelbult: 0 - 5 m (Viljoen et al., 1986b)
Impala: 0 - 40 cm (Leeb du-Toit, 1986)
Rustenburg: 25 cm (Viljoen & Hieber, 1986)
Western Platinum Mine: only in the vicinity of chromitite stringers
Wolhuterskop (LK7, H3): 0 - 85 cm (Rand Mines in-house logs)
Crocodile River Mine: 0 (Rand Mines in-house logs)

7.8: Lateral Variation in Standard Deviation of Mineral Chemistry Data

A comparison of the values of standard deviation from the mean of $Mg\#_{opx}$ or An_{plag} within individual samples might be of importance in evaluating how significant mixing processes were in the petrogenesis of the cumulate rocks. In the case of mixing of fresh, primitive magma with residual melt, which had borne orthopyroxene and plagioclase on the liquidus for some time, different values for Mg# and An might characterize newly formed orthopyroxene and plagioclase and the preexisting equivalents. If equilibration is incomplete (which is certainly the case with plagioclase), this difference in values will be represented by high values of standard deviation of all analyses performed on one sample. These values can be averaged for individual cores or special parts of the sequence and then compared with other parts of the same core, or the same interval in other cores along strike (Table 7.9).

Table 7.9: Average values and standard deviations of $Mg\#_{opx}$ and An content of cumulus plagioclase for the UG2 pyroxenite and the whole of the interval between the UG2 pyroxenite and the Merensky Reef. An values represent core compositions of cumulus plagioclase only.

	UA	EK22	IN	IM	TF	LK7	H3	KR2
$Mg\#_{total}$	.795	.81	.80	.78	.80	.78	.78	.80
$Mg\#_{UG2}$	.81	.79	.80	.72	.80	.78	.80	.82
Std_{total}	.0031	.0036	.0038	.0055	.0063	.0064	.0038	.0025
Std_{UG2}	.0034	.0048	.0030	.0011	.0021	.0073	.0029	.0026
n_{total}	20	35	20	26	12	53	48	23
n_{UG2}	7	3	3	3	3	5	4	2
$An\ (cum)_{total}$	76.0	76.2	76.7	77.3	76.1	74.7	75.7	75.2
Std_{total}	.88	1.15	1.12	1.79	1.58	1.10	1.04	0.97
n	11	18	20	25	11	37	48	27

$Mg\#_{total}$ = mean of all samples containing orthopyroxene
$Mg\#_{UG2}$ = mean of samples of UG2 pyroxenite
Std = standard deviation (1σ)
n = number of samples analysed

The standard deviation values for the UG2 pyroxenite show no systematic trend; they are all rather low with the exception of intersection LK7, where some of the samples were taken in close proximity to chromitites. This trend is in accordance with the geochemical and lithological consistency of this unit along strike (Chapter 7.2). If one averages the standard deviation values for Mg# of all samples for the individual cores a pattern emerges: a systematic increase in levels occurs from locality UA towards Rustenburg (locality TF), with a reversal occurring towards the Brits Graben (locality KR2, see also Fig. 7.1). One may interpret this trend to imply that near the presumed feeder zone (locality UA), the high heat flux caused orthopyroxene of different populations to re-equilibrate more effectively than in a distal (cooler) part of the chamber. Towards Brits, signs of a separate, minor feeder zone, or at least a zone of high heat flux, are detectable in many geochemical ratios (see the values of Mg# in Table 7.9 and Fig. 7.1) and in the fact that the sequence is more compressed in the Brits Graben (core KR2), thus disturbing the trend of thickness increase with increasing distance from Union Section.

Average standard deviations of An content of cumulus plagioclase (taking all analysed samples into account) show a similar pattern when compared with the trend of $Mg\#_{opx}$: increasing values from Union Section towards locality IM and a decrease from there to Brits. It is of interest to note here that the cores showing the highest average value of standard deviation also show the highest average value of An content. It is, however, not clear at the present stage why both peaks should be situated distally with respect to the feeder zones. It must be noted that processes other than fresh influxes of primitive magma can also create zonation, such as high accumulation rates or circulation of late-stage intercumulus fluids.

7.9: Inclusions in Plagioclase

Eales et al. (1990a) describe the existence of sub-rounded and partially resorbed inclusions of plagioclase in cumulus orthopyroxene and olivine in pyroxenites and norites of the UG1 Footwall Unit. This has led to a detailed analysis of plagioclase inclusions in the study section (Fig. 7.11, 7.12), parts of which study have been published with the present writer as co-author (Eales et al., 1991, in press).

7.9.1: The An Content of Plagioclase Inclusions

The majority of microprobe analyses show a higher An content in inclusions than in normal grains (Table 4.1, Fig. 7.11). This difference, however, is very small and usually in the range of 1 standard deviation (Fig. 7.11). Conclusions must therefore be drawn with the utmost caution. Note, also, that inclusions usually follow the compositional trend of the cumulus grains.

A systematic pattern seems to be indicated along strike in as much as, in the north, inclusions are enriched in Ca, whereas in the south-east the majority of inclusions are depleted in An content compared to cumulus grains (Table 4.1, Fig. 7.11). Furthermore, values rarely change significantly from one sample to the next. It appears, rather, that one or the other tendency persists in certain intervals of the sequence.

7.9.2: The Fe Content of Plagioclase Inclusions

Fig. 7.12 shows Fe contents of cumulus plagioclase, contrasted with plagioclase inclusions, along strike in selected cores (selected according to the number of samples analysed per core). The most important feature is that plagioclase inclusions show higher Fe contents than normal grains in most cases (70%, see also Table 7.10).

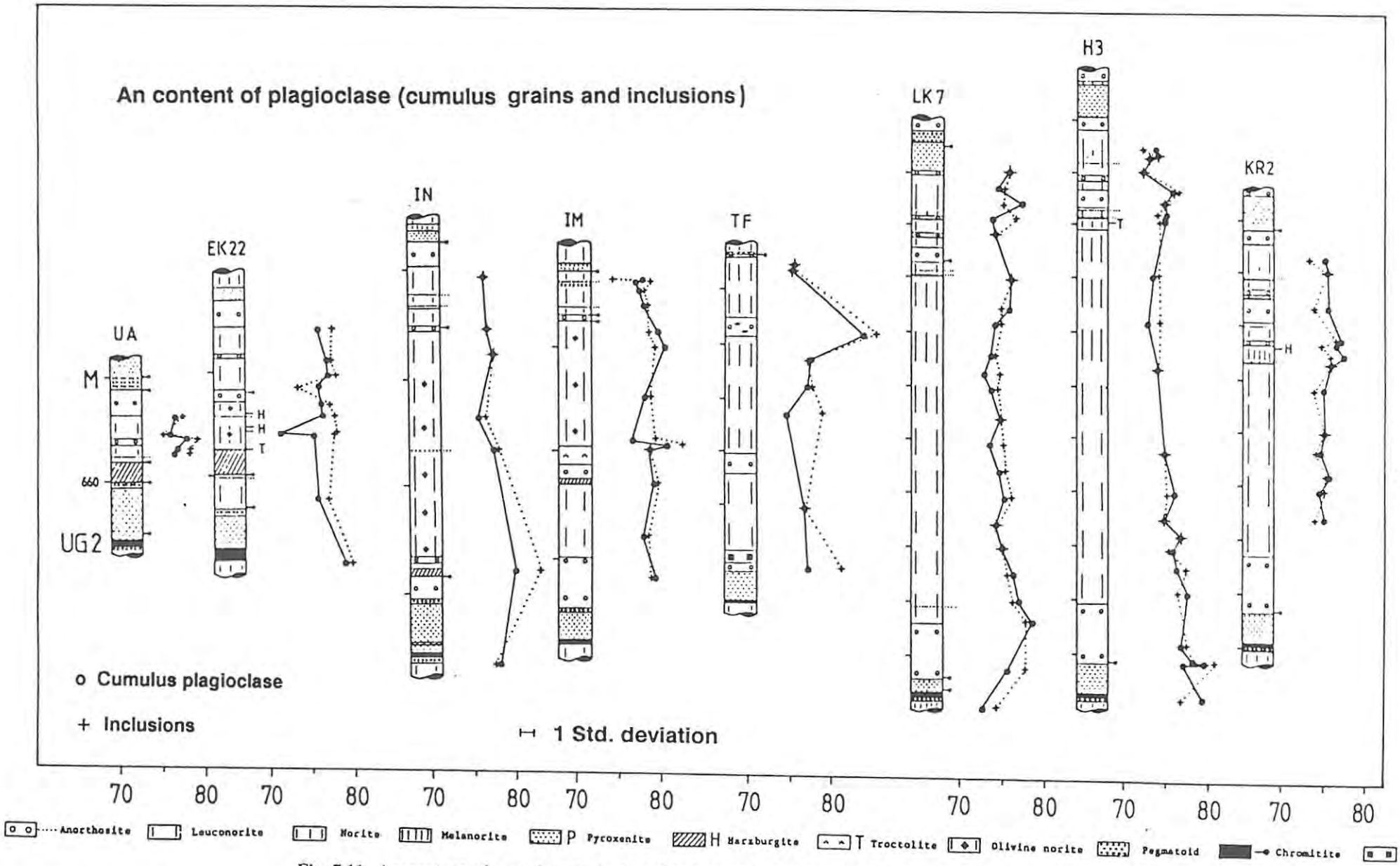

Fig. 7.11 An content of cumulus plagioclase (circles) and coexisting plagioclase inclusions (crosses) along strike in the Western Bushveld. Levels where inclusions are higher in An than cumulus grains are shown in yellow, levels where they are lower in blue. Note change of scale. Distance between marks on left side of columns represents 20 m in each case.

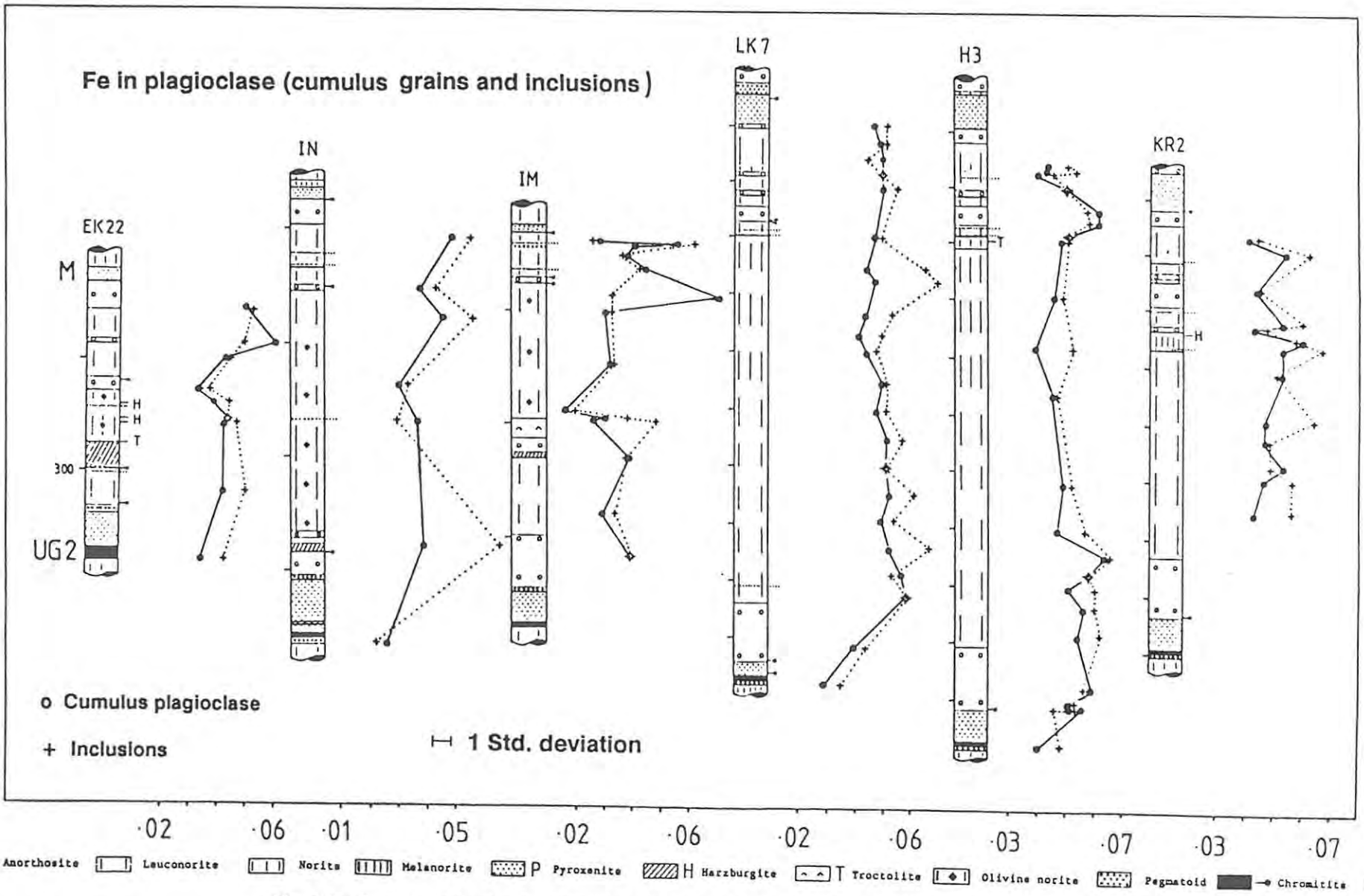

Fig. 7.12 Fe content (cations) of cumulus plagioclase (circles) and coexisting plagioclase inclusions (crosses). Levels where inclusions are higher in Fe than cumulus grains are shown in yellow, levels where they are lower in blue. Vertical scale is 20 m between marks on left side of columns.

Table 7.10: Plagioclase inclusions contrasted with cumulus plagioclase grains in individual cores. Numbers indicate the number of samples analysed in each core.

	An			Fe		
Inclusions are:	higher	similar	lower	higher	similar	lower
UA	4	-	1	2	1	2
EK22	8	1	1	7	1	2
IN	5	1	1	5	-	2
IM	8	2	4	8	1	5
TF	4	1	2	6	-	1
LK7	12	4	6	17	3	2
H3	6	10	7	16	4	3
KR2	3	-	10	10	-	3
Total	50	19	32	71	10	20
Percentage	49	19	32	70	10	20

This trend is most pronounced in the three south-eastern cores. This is the opposite of the trend defined by An contents, where the three south-eastern cores (and the Union Section core) show the smallest differences between cumulus plagioclase and plagioclase inclusions (Fig. 7.11). This result, if it is representative, would be expected as An and Fe contents in plagioclase are supposedly correlated in a negative way (high An and low Fe content in early crystallizing plagioclase). Hence, An-enriched inclusions in the north correlate with more or less similar Fe values in inclusions and cumulus grains (Tables 4.1 and 7.10), whereas An-depleted inclusions correlate with Fe enrichment in the south-east.

It might thus be concluded that, at the time of resorption of suspended plagioclase, the liquid was more evolved at Brits than in the north and the suspended plagioclase accordingly became enriched in Ab and Fe content (see Table 4.1). These resorbed plagioclase grains were then incorporated within cumulus orthopyroxene and olivine and the subsequently formed cumulus plagioclase (resulting from the hybridization of residual and fresh magma) shows more primitive compositions than inclusions at Brits, with higher An values and lower Fe contents. In the north, the second generation plagioclase did not reach the primitive values of the inclusions. A possible explanation

would be that inclusions here were more severely resorbed due to the proximity of the feeder zone, but this problem certainly warrants more research.

The number of inclusions with higher, lower or similar An and Fe contents compared with cumulus grains is shown for each core in Table 7.10.

The Fe content of cumulus grains shows patterns similar to those followed by other chemical ratios (Fig. 7.13); the central noritic part is an interval of rather constant values (see profiles IN, LK7, H3, and KR2) in comparison with the enclosing intervals. Intercumulus plagioclase (UG2 pyroxenite, P2 harzburgite) shows distinctly lower Fe contents than cumulus plagioclase (Fig. 7.13).

7.10: Grain Size Measurements

Fig. 7.4 compiles the results of the grain size analyses of cumulus plagioclase in 6 cores around the western limb. Standard deviations (1σ) within each sample are presented for one representative core (H3). The most interesting features are summarized below.

- The bottom and top parts of all sections spanning the interval between the UG2 and Merensky pyroxenites show the largest grain sizes.

- The central noritic part of the sequence shows small variation in grain size.

- The central part in cores LK7, H3, and KR2 displays a trend of upward-diminishing grain size.

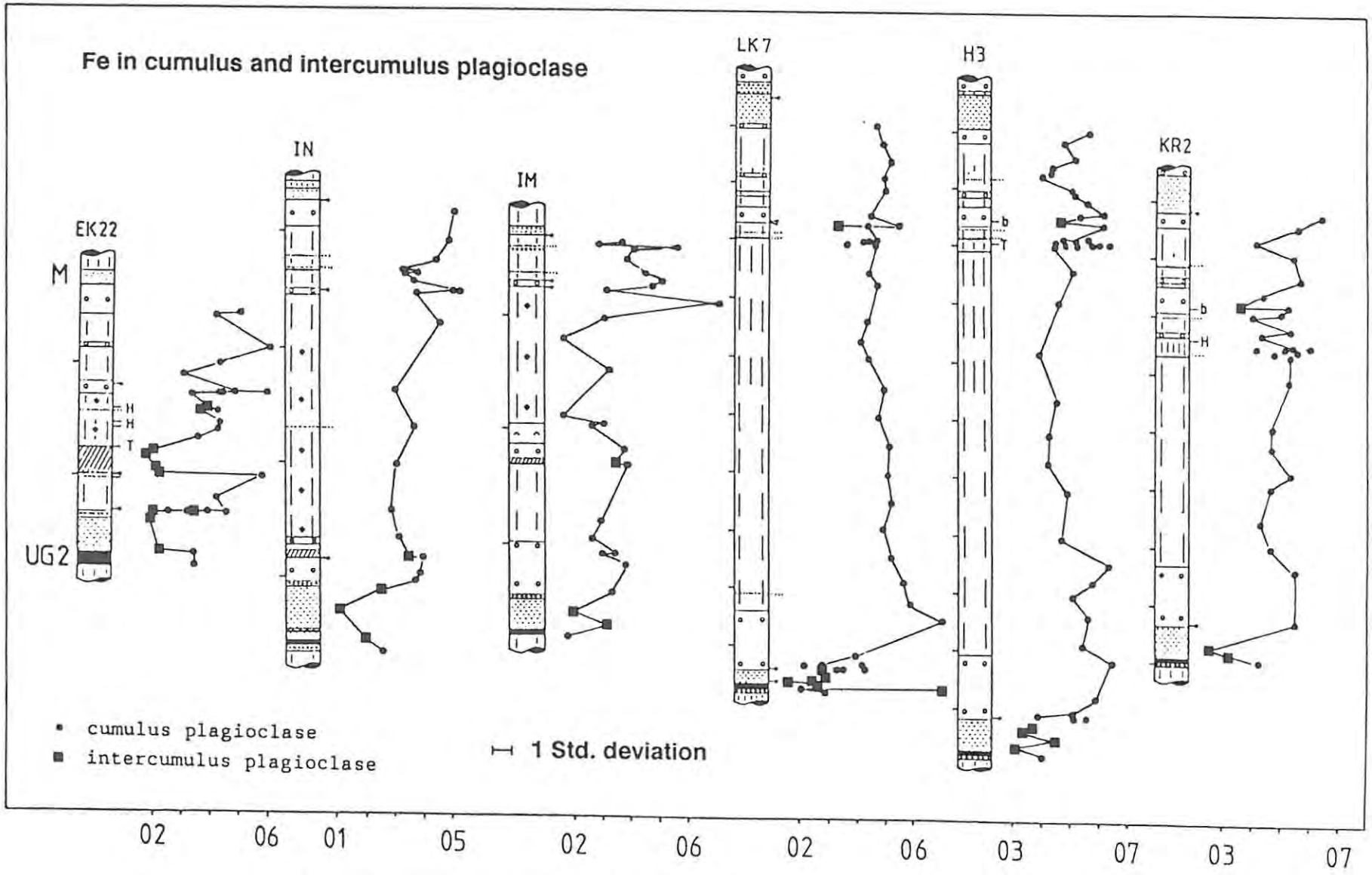

Fig. 7.13 Fe content (cations) of cumulus and intercumulus plagioclase along strike in the Western Bushveld Complex. Vertical scale is 20 m between marks on left side of columns.

- The inflection which is developed in the lower central part of cores LK7 and H3, and somewhat more weakly in core KR2, can possibly be correlated with the base of the P2-B Marker at localities IN and IM.

7.11: Rock Modes

Fig. 7.5 shows a comparison along strike of modal proportions of orthopyroxene and olivine in 5 cores. The most notable features include:

- Modal olivine in the interval under review is confined to cores EK22, IN, and IM (apart from that encountered in cores UA, AE, in a harzburgitic lens above the UG2 chromitite in core LK7, and in a thin troctolite lens within the Norite Marker in core H3).

- At locality EK22 two cycles of upward-decreasing proportions of orthopyroxene can be distinguished: the first one extends from the top of the UG2 pyroxenite to the base of the P2-B harzburgite. The second is developed between the top of the Pothole Marker anorthosite (FW 6, 283.63 m) and the top of the Footwall Marker (277.40 m). The extremely high values of modal olivine belong to the P2 harzburgites.

- The sequence above the central troctolite at locality IM can possibly be correlated with the central part at locality IN even although the latter is twice as thick. The grain size data (Fig. 7.4) and the values of $Mg\#_{opx}$ (Fig. 7.3) point to a similar correlation.

- Cores H3 and LK7 show an increasing modal amount of orthopyroxene with height in the central part of the sequence. If one adds up all samples from all cores (except KR2, which, due to alteration, can only be indirectly analysed for modal proportions by means of the

Sr/V_{wr} ratio) a weakly positive correlation between modal proportion of orthopyroxene and $Mg\#_{opx}$ can be observed (Fig. 3.6). The inflection which occurs about 55 m above the top of the UG2 pyroxenite in profiles LK7 and H3 (Fig. 7.5) can possibly be correlated with the base of the P2-B Marker at localities IN and IM.

Average modal compositions (vol %), derived from point counting, have been calculated for the interval under review at the different localities and are presented in Table 7.11. A method of calculation has been chosen, whereby the average modal percentage of a phase within a layer has been multiplied with the relative thickness of the layer, thus yielding a weighted average. All rock types have been included in the calculations. It becomes clear that the modal proportion of plagioclase increases as one moves away from Union Section whereas the proportions of orthopyroxene and olivine decrease.

Table 7.11: Average modal composition of the studied interval in various intersections along strike (Pla = cumulus plagioclase, Opx = cumulus orthopyroxene, Ol = olivine, ic = intercumulus, Chr = chromite, Cpx = clinopyroxene, Oth = others).

	UA	7E[3]	EK22	60E[3]	IN	IM	LK7	H3
Pla	39.1	52.2	51.5	54.9	62.9	63.9	71.3	77.3
Opx	31.3	26.4	29.3	30.7	27.7	26.6	23.7	17.9
Ol	7.8	5.7	4.7	4.4	3.4	3.6	-	-
Pla(ic)	5.4	3.8	3.1	2.6	1.6	1.3	0.4	0.6
Opx(ic)	9.8	6.4	5.8	2.8	0.7	0.9	0.6	0.7
Chr	0.5	0.5	0.4	0.3	0.2	0.1	0.1	0.1
Cpx	2.7	2.4	2.6	2.1	1.7	1.9	2.4	2.5
Oth	3.4	2.7	2.6	2.2	1.8	1.9	1.5	0.8
Total	100.0	100.0	100.0	100.0	100.0	100.0	100.0	100.0

CHAPTER 8: DISCUSSION AND CONCLUSIONS

The fundamental analytical data have been presented on preceding pages with little attempt to interpret the data. This format has been adhered to so as not to allow bias or slant to appear. The following section now summarizes and attempts to interpret these data.

8.1: A Selection of Petrological Models (Based on Considerations of Densities of Liquids) for the Formation of Layered Complexes and the Bushveld Layered Complex in Particular.

In 1968, Wager & Brown applied the cumulus or crystal settling theory (von Buch, 1825; Darwin, 1844; Wager & Deer, 1939; Hess, 1960; Wager et al., 1960) to the Bushveld Complex. They demanded that the total magma volume of the complex be intruded in several stages, thus leading to mixing of early residues with fresh primitive magma. A further replenishment is held to have occurred at the level of the Merensky Reef. This led to the formation of an immiscible sulphide liquid and the deposition of the platiniferous reef (Wager & Brown, loc. cit., p. 405). The accompanying turbulence of this mixing event led to the prominent erosive structures like potholes. Crystals nucleated and grew within the magma at unspecified localities. Once they were big enough and gravitational forces exceeded the yield strength of the magma, which they regarded to be small, crystals would have started to sink to the floor, aided by convection and density currents. According to different densities, shapes and sizes, they were sorted to form modally distinct layers.

Vermaak (1976) implied that plagioclase (An_{70-90}) would float in a basaltic magma because of its relatively low density (2.65 g/cm^3, Campbell et al., 1978). An anorthositic mat of early-formed plagioclase with elevated An values would thus have been formed in zones of compositional, density, or temperature inversion at a level higher than the floor of the chamber. This mat would act as a trap for

volatiles, thus leading to rapid growth of ferromagnesian phases to form "boulder"-like aggregations. These "boulders" then sank through the magma to the floor and formed the Pseudoreef, Boulder Bed and Merensky Reef horizons.

McBirney & Noyes (1979), in their work on the Skaergaard Complex argued that crystal settling was difficult to achieve at any stage other than the first stage of the cooling history of a magma chamber. The viscosity and yield strength of magma are known to increase significantly with crystallization (Bottinga & Weill, 1970; Campbell et al., 1978). The authors therefore deduced that crystallization took place in a boundary layer, which advanced with solidification away from the floor, roof and walls, a concept which is probably more applicable to the Skaergaard Complex than to the Bushveld Complex. Crystals nucleated and grew in these zones, which advanced more rapidly than crystals could sink or float, thus preventing them from being gravitationally removed. Bottom crystallization as a concept in layered intrusions was first proposed by Jackson (1961, 1970), but McBirney & Noyes were the first to combine this with the mechanism of double-diffusive convection (Turner & Chen, 1974).

Morse (1979a) tried to evade the problem of settling and floating of crystals in the Kiglapait Intrusion by suggesting a process of combined sinking of feldspar and mafic minerals in convective currents. This was coupled with oscillatory nucleation of the different phases. Both processes had earlier been described independently by Coats (1936) and Wager (1959), respectively. If one takes cooling through the roof and convection for granted, oscillatory nucleation would have occurred when the cooled liquid moved down near the walls of the complex, and the pressure increased rapidly. Crystallization would have proceeded near the floor where feedback cyclic supersaturation of the different phases led to the pronounced layering. The release of additional latent heat of crystallization is supposed to have caused a warming-up and subsequent rise of the melt, and re-initiation of the process.

Rice (1981) noted that cooling would occur mainly through the roof in a constantly heated chamber. He cited numerous examples from the engineering literature in which nucleation and crystallization proceeded from the roof downwards. In that case reverse fractionation trends would result. If supercooling can be achieved at the floor, crystallization can occur from the floor upwards as well. After about 65% crystallization, convection in the magma chamber would cease and the central part of the chamber would crystallize in situ.

The model by Irvine et al. (1983) proposed that both the Stillwater and the Bushveld Complex crystallized from two different magmas, an ultramafic ("U") and an anorthositic ("A") type. They used parental magma compositions, calculated from sill phases in the Eastern Bushveld (Sharpe, 1978; 1981) to model a liquid path of descent for their U liquid with the crystallization order olivine - orthopyroxene - plagioclase - clinopyroxene. The necessity of an "A"-type liquid of different lineage (with the crystallization order plagioclase - olivine - clinopyroxene - orthopyroxene) arose, because it seems impossible to leave the plagioclase-orthopyroxene cotectic in a slowly cooling chamber to create up to 500 m of anorthosite in the Stillwater Complex. Also, the formation of chromitites probably requires mixing of two contrasting magma types (Irvine, 1977; et al. 1983; and Sharpe, 1986; Fig. 8.1, 8.2).

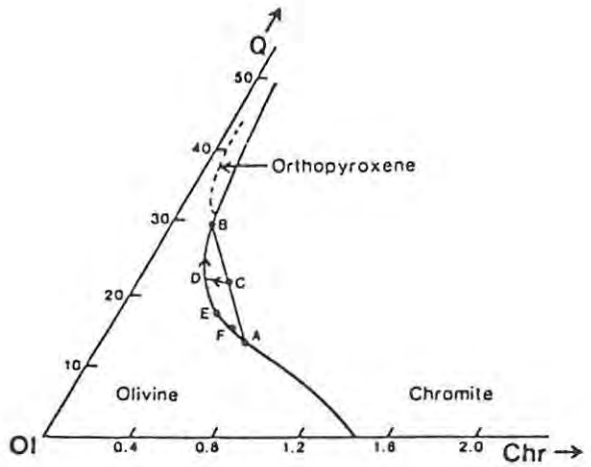

Fig. 8.1 Calculated and inferred phase boundaries of parental magma of the Muskox Intrusion, drawn in the system olivine - chromite - quartz. Point A is thought to represent composition of the parental magma (figure from Campbell & Turner, 1986 after Irvine, 1977).

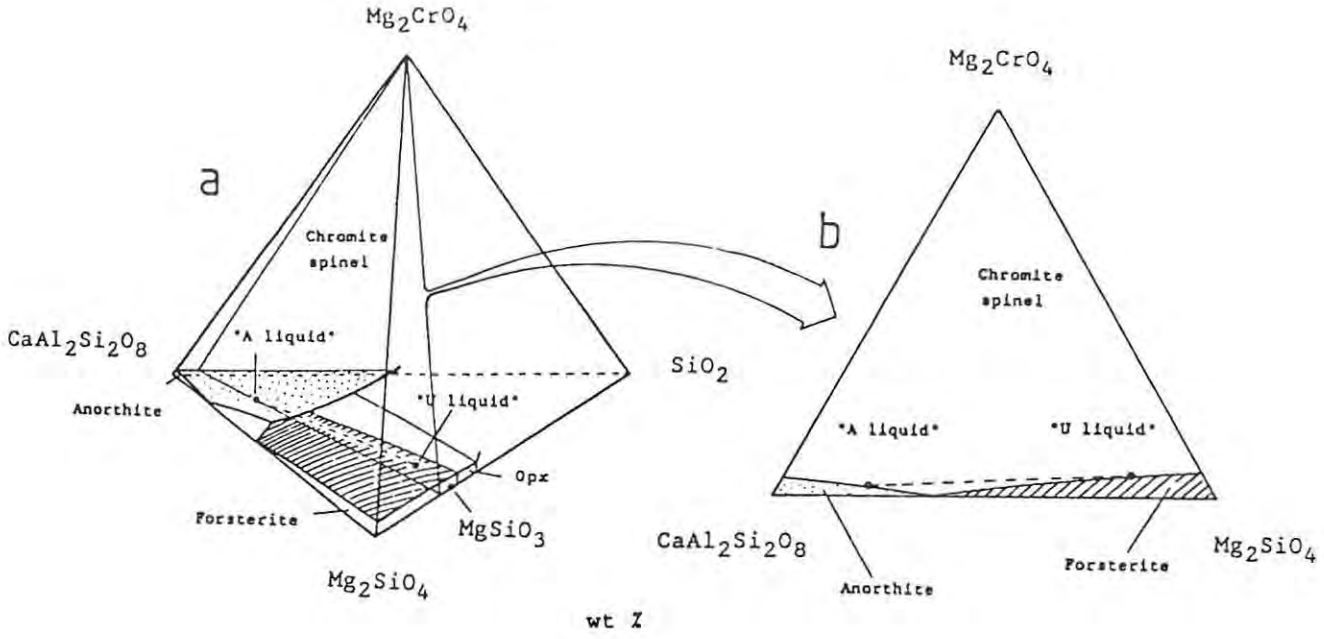

Fig. 8.2 (a) Liquidus diagram of the system Mg_2SiO_4 - $CaAl_2Si_2O_8$ - SiO_2 - $MgCr_2O_4$. Mixing of Cr_2O_3-bearing, but chromite-undersaturated melts of different composition ("A" and "U") can yield hybrids with only chromite on the liquidus (Fig. modified after Irvine & Sharpe, 1986). (b) plane within the tetrahedron of (a), showing mixing line between "A" and "U" liquid. See text for further explanation.

These authors hypothesized that a dense, relatively cool and SiO_2 depleted "A"-type liquid intruded into the chamber and spread out on the floor below the "U"-type liquid derivatives. This process would disturb the stratification of the chamber because the "A"-type liquid is denser mainly because it is cooler and because of its low SiO_2 content. Double diffusive convection (Turner, 1973; Turner & Chen, 1974; Turner & Gustafson, 1978) would thus result in finger-mixing between the two liquid layers. This process depends on whether the component with the larger diffusivity (heat rather than a chemical gradient in this case) is predominant in the upper or lower layer. In the case discussed above the temperature is higher in the upper layer. The density differences between the layers would decrease when the

upper part of the lower layer became heated and the lower part of the upper layer cooled. Mixing would gradually occur in the form of fingers protruding into the adjoining layers. In the opposite case, a warmer and denser liquid may underlie a cooler and less dense liquid. This case is the normal one, which would become established sooner or later in every magma chamber. Mixing then would occur only on a small scale as the density differences between the layers would increase with cooling. In that case, the only interaction between the doubly diffusive convecting layers would result when light liquid residue escaped into the overlying layer. The lowermost layer would thus be eliminated after a certain time and crystallization would proceed on a sloping floor in the down-dip direction.

It is of interest to note that, according to Irvine et al. (1983), successive influxes of "A"-type liquid would raise the liquid column and lead to repetitive deposition of the resulting layers. This would have economic implications, as it suggests that the platiniferous reefs are discontinuous downdip and that reserves of PGE are much smaller than estimated. No information is currently available from deep drilling further downdip of the current mining operations to indicate that this interpretation is correct.

Campbell et al. (1983) argued that as soon as a magma starts crystallizing plagioclase, the density of the residual liquid would increase because of the enrichment of elements such as Mg, Fe, P, etc. (Fig. 8.3). Thus, under certain circumstances, a fresh influx of primitive magma could be lighter than the fractionated magma. It would then rise as a plume and spread out at some particular level according to its density. The high cooling rate would cause vigorous convection and mixing to create a hybrid liquid during the rise and spreading out of the plume. At the contact with the underlying liquid layer, finger mixing would occur and ferromagnesian phases crystallize in the fingers to form discrete "boulders", or coalesce on the floor to create, in the Bushveld case, the Merensky Reef and Pseudoreefs.

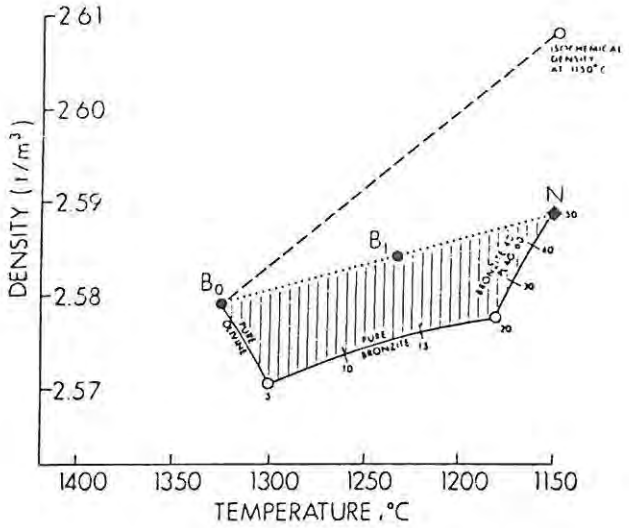

Fig. 8.3 Density variation of a liquid, successively crystallizing fractionating minerals. Based on a presumably representative sample of a primitive influx, calculated from data of Bottinga et al., 1982 (figure from Naldrett et al., 1986, after Barnes & Naldrett, 1985).

Naldrett et al. (1986) refined and modified this model. The fresh influx, spreading out as a plume according to its density, and convecting vigorously, would crystallize ferromagnesian phases which would eventually slow down convection. Crystal-laden suspensions would concentrate at the bottom of the floating layer. At some stage, downspouts of this suspension would sink to and spread out on the floor in the form of density currents, to create the Pseudoreefs, Boulder Bed and Merensky Reef. Potholes would form as a result of mechanical erosion, when the downspouts reached the floor.

Hatton (1988) proposed a model whereby the cumulates of the Lower and Critical Zones of the Bushveld Complex can be related to three different parental magma types, B1, B2 and B3. According to this model which is based on work on the marginal rocks of the eastern compartment of the complex (Sharpe, 1981) B1 shows the chemical characteristics of a boninite (i.e., has olivine on the liquidus). B1 would be the equivalent of the "U-type" liquid of Irvine et al., (1983) and is considered to be the parental magma of the ultramafic cumulates of the Lower Zone. B2 and B3 are of tholeiitic lineage, have

plagioclase on the liquidus and resemble Irvine's "A-type" liquid. They are inferred to have been emplaced during the deposition of the cumulates of the Critical Zone. By means of density calculations the author demanded that B1 was less dense than B2 or B3. Therefore, it would have been elevated during the intrusion of B2 or B3. Cooling of B1 by the underlying B2/B3 magmas would have led to the crystallization of orthopyroxene within B1, which increased the bulk density of the latter liquid. This, presumably, would have caused the B1 crystal-liquid suspension to sink to the floor of the chamber, and the mixing of B1 with B2/B3 led to chromite precipitation.

Eales et al. (1986, 1988, 1990 a,b) saw the formation of cyclic units of the lower and critical zones as a result of numerous new influxes of primitive magma, a concept which has been postulated first by Cooper (1936) and subsequently by Brown (1956) and Irvine & Smith (1967). Eales et al. (loc.cit.) believe that mafic cumulates at the base of cyclic units represent cumulates that separated from primitive influxes, whereas overlying norites and anorthosites represent cumulates derived from liquids progressively hybridized with residua in the chamber. This argument they based mainly on Sr-isotopic evidence. The development of the preceding unit might be interrupted at any stage by a new influx, thus leading to incomplete (beheaded) units. A complete unit would consist of chromitite - harzburgite - pyroxenite - norite - anorthosite. Geochemical and lithological variations along strike in the Western Bushveld Complex led the authors to suggest the existence of a major feeder zone in the vicinity of Union Section. Intruding magma would thus have spread out on the floor and thermally-mechanically eroded the footwall rocks (see also Feringa, 1959) or inhibited the deposition of lower- temperature cumulates. With increasing distance from the feeder zone, this effect would diminish, thus leading to increased thickness of the footwall rocks and a chemically less primitive character of the overlying mafic cumulates (Fig. 8.4). Thus, the UG2, Merensky and Bastard Units are inferred to have been formed by the same process. The last two cycles, however, succeeded (in their model) the emplacement of the Main Zone liquid pulse. This is implied by a constant increase in Sr_i ratio from

the base of the Merensky Unit up to the Main Zone, with a reversal occurring at the level of the Bastard Reef. Such a reversal was subsequently documented by Lee & Butcher, (1990).

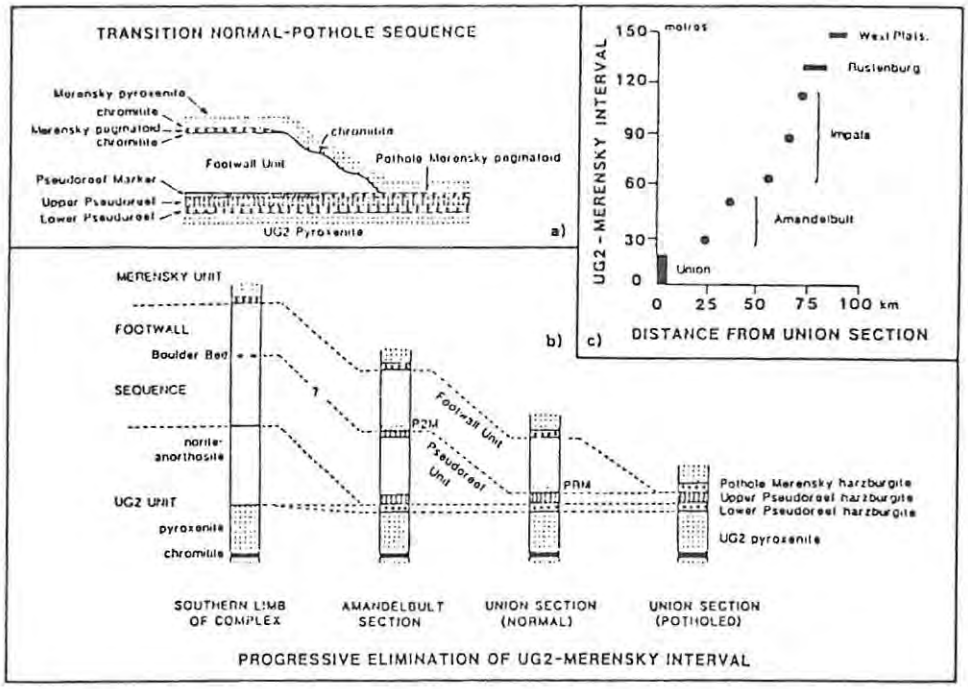

Fig. 8.4 (a) Generalized section, showing elimination of Merensky footwall at Union Section through potholing. Scale distorted. (b) Generalized section to illustrate increasing elimination of Merensky footwall cumulates in the Western Bushveld by thermo-mechanical erosion and/or other processes. Scale distorted. (c) Thickness of interval between UG2 pyroxenite and Merensky Reef plotted against distance from Union Section, regarded as being close to an irruptive centre (figure from Eales et al., 1988).

Each of these models would appear to explain some features but neglect others. This is simply, because up to now, no one model has been able to cover every aspect of the cumulus rocks in the Bushveld or other layered complexes. Wager & Brown (1968) did not consider the possibility of plagioclase flotation or the aspect that, due to yield strength properties of the magma, crystals might not be able to sink or float at all. This also applies to Vermaak's model (1976). McBirney & Noyes (1979) and Morse (1979a) offered no explanation for layers of pure plagioclase rocks of considerable thickness. Rice's model of roof crystallization (1981) cannot explain the Sr-isotopic data and the overall fractionation trend of the Bushveld layered sequence. Irvine

et al. (1983) could only assume the presence of a discrete anorthositic liquid, as no equivalent sill phases have ever been found. Also, these authors have generalized the stratigraphy in the Western Bushveld in so far as the reefs are frequently not underlain by anorthosites, and the main anorthosite in the interval under review (FW 12) does not precede an ultramafic layer but rather grades up into a leuconorite. Furthermore, Hattingh (1986) claimed that parts of the Main Zone crystallized horizontally and not in a down-dip direction.

The mechanisms of Campbell et al. (1983) and Naldrett et al. (1986) are based on fluid-dynamic modelling by Turner & Gustafson (1978). Therefore they are largely dependent on the validity of density estimates of the relevant liquids. These estimates, however, seem to neglect possible changes in magma densities, resulting from retention of suspended crystals within the liquids.

Hatton (1988) assumed cooling to occur mainly through the floor. This would seem unlikely due to the latent heat of crystallization, released during adcumulus growth within the underlying, semi-consolidated cumulate pile (Morse, 1988).

The geochemical trends which Eales et al. (1986; 1988; 1990a,b) observed along strike at Union and Amandelbult Sections do not necessarily continue in the south (see Fig. 7.1). Furthermore, the concept of massive footwall erosion cannot explain the exceptional lateral compositional uniformity of layers like the UG2 chromitite or to a lesser degree the UG2 pyroxenite. One would anticipate that the erosion would have been more effective in parts of the chamber proximal to a feeder zone than more distally to this feeder, thus affecting the overlying primitive liquid through hybridization in a variable way. Furthermore, work by Huppert & Sparks (1980), Huppert et al. (1984) and Sparks & Huppert (1984) indicated that magma chambers may develop a stratification of horizontal liquid layers. This stratification will be restored after replenishment of the chamber by undifferentiated influxes rather than being disturbed by large-scale mixing processes.

8.2: A Model for the Formation of the Interval Under Review

The purpose of this research project was to investigate whether, and if so, how the sequence between the UG2 chromitite and the Merensky Reef changes laterally along strike. The results are equivocal for different parts of the sequence. The UG2 chromitite and, to a lesser degree, the UG2 pyroxenite show limited and unsystematic variation along strike, both lithologically and geochemically (Table 7.2 and 7.3). Most of the other individually correlatable members, however, display considerable lateral variation (see Chapter 7).

UG2 Unit

The development of a model will be started with a review of the UG2 Unit (i.e., the UG2 chromitite and pyroxenite). It shows both limited and unsystematic variation of average composition along a strike length of 170 km in the western lobe but rather variable composition with height within the layer, and in each of 26 separate profiles examined by Eales (pers. comm. 1991) along the full strike length of the western limb, significant inter-sample variations of Mg# are seen, with prominent reversals near the base, middle or top of the layer. Mg# shifts are as much as >0.82 to ca. 0.75. Basic premises that could account for this relative uniformity along strike, are:

(a) the formation of the package was not affected by lateral variation in magmatic conditions, or
(b) magmatic conditions during deposition were more or less uniform along strike, or
(c) the composition of the parent liquid was rejuvenated by repeated influxes of primitive liquid from time to time.

An important question must follow: why is the overlying sequence of plagioclase cumulates less homogeneous along strike? It would appear that:

(d) the formation of the latter sequence was more affected by the laterally variable conditions than was the UG2 Unit, or
(e) the laterally uniform magmatic conditions changed after the deposition of the UG2 Unit.

In reducing the possible answers to these questions, the author assumes that a relatively uniform layer has not been formed by two or more different processes. Is it then possible that the formation of a package which consists predominantly of chromite and orthopyroxene should hardly have been affected by lateral variation in magmatic conditions, while the directly overlying sequence has been affected so thoroughly (point (a) above) ? This appears improbable and could only be visualized if the primitive magma, which was parental to the UG2 Unit, contained suspended crystals at the time of intrusion into the chamber.

It must be asked whether the magmatic conditions could have remained unchanged along strike during the deposition of the UG2 Unit (point (b) above). A major chamber like the western lobe must have been fed by at least one, or possibly more feeder zones. This will at the very least have caused patterns of different heat flux in different parts of the chamber ("heat flux" being defined here as the motion of heat released by the feeder zone and the liquids issuing from it).

Consequently, melt viscosities, gas fugacities, convection velocities, re-dissolution of already-formed cumulates, assimilation and a number of other variables could not have been uniform throughout the chamber either. All these factors together with the probability of repeated rejuvenation of the parent liquid, should have imposed variability during the formation of the UG2 Unit along strike.

If one assumes, however, that the UG2 influx was one of the major influxes in the history of the Upper Critical Zone, whose derivatives in the form of primitive cumulate rocks show little change along strike, one could conclude that magmatic conditions were influenced or

modified to roughly the same extent in most parts of the chamber. The composition of the magma in the chamber would only have developed a strong lateral gradient when the influx rate (i.e., rate of intrusion) decreased again. The upper parts of the interval under review might then show a more pronounced chemical variation along strike (see Figs. 7.3, 7.4, 7.5; Table 7.6, 7.7).

If it is accepted that the UG2 Unit has not been formed by two or more different processes, any model which suggests footwall erosion in response to a basal flow to be an important process on a regional scale, encounters serious problems. The amount of thermo-mechanical footwall erosion would clearly be higher close to an eruptive centre. This is valid even in the above-mentioned case of a large influx (which would ultimately tend to cause roughly uniform magmatic conditions along strike), simply because superheated conditions, which would have facilitated erosion would have prevailed for a longer time span here. Hence, the laterally variable amount of erosion would presumably have affected the formation of the UG2 Unit.

Furthermore, the amount of chromite concentrated in the UG2 chromitite seems to require mixing of large amounts of primitive and evolved liquid, a process to be discussed later in this Section. This mixing is difficult to envisage in any process involving basal flows, as Huppert & Sparks (1980), Huppert et al. (1984), and Sparks & Huppert (1984) state that mixing would be minor in such a case.

Some kind of gravitative sinking of crystals or semi-crystallized liquid (Campbell et al. (1983), Naldrett et al. (1986)) thus seems to be more compatible with the lithological and geochemical features of the UG2 Unit than the spreading out of a fresh influx along the floor. This implies that the liquid forming the UG2 influx was less dense than the lowest portions of the, presumably, density stratified residual liquid at this stage. Density calculations by Campbell & Turner (1986, Fig. 8.5) and Barnes & Naldrett (1986, Fig. 8.3) seem to confirm this model.

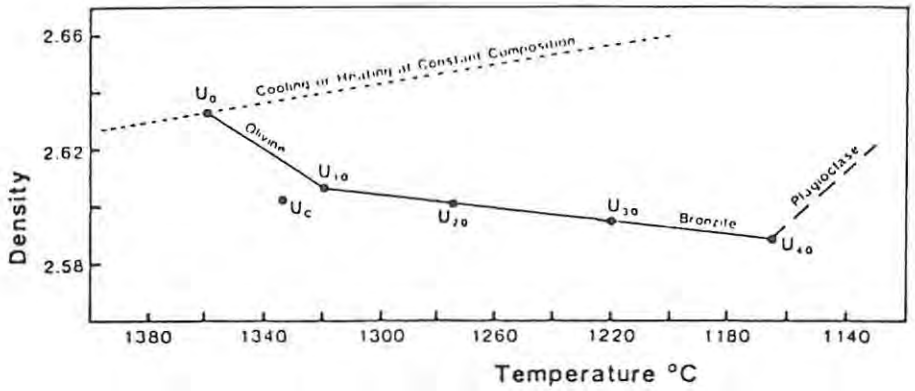

Fig. 8.5 Density variation of "U" magma and its fractionation products. See text for further explanation (figure modified after Campbell & Turner, 1986).

These authors suggest that the density of magmatic liquid increases sharply during plagioclase crystallization, thus surpassing the density of the original primitive liquid at one stage. This seems especially possible if the residual liquid contained suspended plagioclase (density 2.65 g/cm^3, Campbell et al., 1978) and orthopyroxene (3.3 g/cm^3 , Deer et al., 1978).

As mentioned in Chapter 7.2 the UG2 pyroxenite is not perfectly uniform as olivine occurs at its base at Union Section and, to a lesser degree, Amandelbult Section. Furthermore, MgO and Al_2O_3 contents of orthopyroxene seem to be slightly higher in the northern part of the western limb than in the southern arm (Table 7.3). The present author explains this with the inference that the residual liquid underlying the UG2 plume at Union Section probably was less evolved than in the Brits area. Mixing of primitive with evolved magma, situated within the anorthite stability field due to resorption of suspended plagioclase, would thus have resulted in a hybrid having the crystallization order chromite - olivine - orthopyroxene - plagioclase + orthopyroxene in areas proximal to the feeder, and chromite - orthopyroxene - plagioclase + orthopyroxene distally to the feeder (Fig. 8.2 & 8.6).

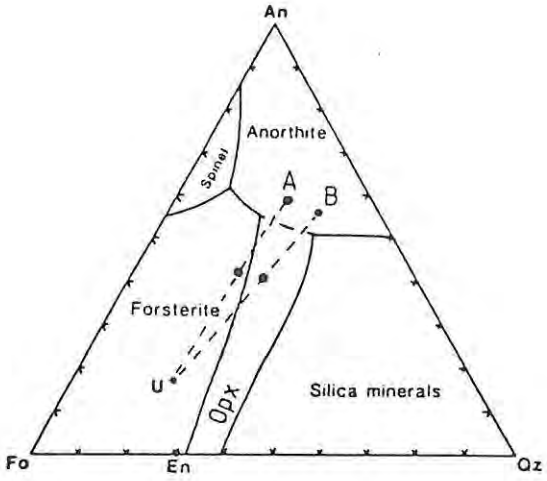

Fig. 8.6 Schematic diagram, illustrating mixing between primitive magma (UG2 influx: U) with evolved residual magma at Union Section (A), and in the south-eastern sector of the western limb (B), shown within the system forsterite - anorthite - silica - chromite (as in Fig. 8.2, after Irvine & Sharpe, 1986).

A slight reversal in geochemical trends can be observed to occur at Crocodile River Mine (locality KR2, Table 7.3). This is coupled with the reappearance of minor olivine at the base of the pyroxenite and a thickness decrease of the latter in this intersection, which possibly indicate the existence of a minor feeder zone there. The mixing process between primitive and evolved magma is considered to have provided heated conditions and the combination of thermal and mechanical effects probably caused local development of potholes. Due to the lack of exposure and a paucity of literature on the UG1 Unit, these are currently documented, in the case of the UG2 footwall, mainly at Crocodile River Mine.

In the waning stages of the UG2 influx, or series of influxes, the heat flux from the feeder would have decreased and a lateral temperature gradient would ultimately have developed. It will then have taken a different time span for liquids in different parts of the

complex to begin plagioclase crystallization (i.e., for the crystallizing UG2 liquid to reach the plagioclase - orthopyroxene cotectic). Close to the feeder zone, more time will have been required than further away because of the more elevated temperatures. This, however, should not have significantly affected the total thickness of the UG2 pyroxenite unless a further influx occurred before this cotectic was reached at all localities along strike. A further influx (in our case the Pseudoreef influxes), once it occurred, would have been deposited on a footwall of varying thickness. Close to the feeder, the plagioclase-orthopyroxene cotectic might not yet have been reached and the rocks of the first Pseudoreef pulse (P1) deposited directly on top of the UG2 pyroxenite (Union Section). The P1 influx must be considered as having been comparatively small as its derivatives can mainly be observed in the northern part of the western limb. The same applies to the first P2 pulse, the P2-A influx. The P2-B and -C influxes were more significant. At Union Section their derivatives cannot be distinguished from the P2-A rocks, and they were presumably deposited directly on top of them. Further away, at Amandelbult Section, a thin succession of leucocratic rocks was deposited prior to the P2-B influx, and at the distal end of the chamber (Crocodile River Mine) a thick package of anorthosites and norites would have had time enough to accumulate before the effects of the P2-B and -C influxes resulted in a gradational reversal towards more primitive cumulates.

A problem yet unsolved is the large amount of chromite accumulated in the UG2 chromitite. Mass balance calculations (Reynolds, 1987) which assume that the primitive magma contains approximately 0.15 wt% Cr_2O_3 (=1000 ppm Cr) indicate that 1 m of chromitite, containing around 50 wt% of Cr_2O_3, requires a magma layer of 667 m (assuming 50% Cr depletion during chromite precipitation) to yield the necessary mass of chromite. Even at double this amount of Cr in the parent magma layer, at least 330 m of magma is required. That does not include the amount of Cr_2O_3 which is incorporated in orthopyroxene (0.4 wt%). The Cr content of parental magmas of the Lower Zone has, however, been

calculated to be not higher than 0.20 wt% (Harmer & Sharpe 1985). It remains unclear if the efficiency of extraction of chromium from the magma can be increased, as no experimental setting can realistically simulate geological timespans. The shape of the complex and the extension of the chromitite layers have also been the subject of speculation to overcome the mass balance problems. The possibility that the intruding fresh magma already contained suspended chromite is difficult to assess. One certainly would expect to find occasional compositionally discrete grains in the usually homogeneous population of chromites within massive chromitites (see Eales & Reynolds, 1986). This was not observed in the study section. Furthermore, a chromite-charged liquid would seem unlikely to be capable of intruding the chamber as a plume.

Even if the mass balance problem is ignored in the present discussion, the formation of chromitite layers is still a matter of dispute. Sampson (1932) and McDonald (1965) suggested that immiscible chromium-rich liquids where the source of chromitite layers. The dependence of chromite precipitation on oxygen fugacity and pressure has been regarded as critical in chromite formation by Ulmer (1969) and Cameron (1978), respectively. The mixing of two contrasting liquids with the resulting hybrid being shifted into the chromite stability field has been modelled in different ways:

- Irvine (1977) proposed mixing of evolved liquid residua with fresh, primitive influxes of magma of the same lineage (Fig. 8.1).
- Irvine et al. (1983) and Irvine & Sharpe (1986) suggested a process of mixing between primitive "U"-type and anorthositic "A"-type liquid (Fig. 8.2).
- Campbell et al., (1983) and Naldrett et al., (1986), envisaged a model in which crystal-liquid suspensions of primitive liquid, having been intruded into the chamber as a plume, sank under gravity into, and mixed with underlying evolved residual liquid.
- Scoon and Teigler (1990) claimed thermo-chemical-mechanical erosion of semi-consolidated leucocratic footwall to be responsible for the mixing.

However, in respect of the latter model it must be noted that none of the chromitites of the Lower Critical Zone apart from those described by Teigler (1990) in the Brits area are associated with leucocratic rocks. Furthermore, as mentioned before, the chromitite would be expected to show lateral variation in Scoon & Teigler's model as the amount of footwall erosion would have been larger close to the feeder than more distally from it.

The work of Hiemstra at Western Platinum Mine (1985, 1986; Fig. 8.7) showed that the main UG2 chromitite layer is not a homogeneous layer but that it can be subdivided into a number of subcycles showing different geochemical trends. Furthermore, the existence of leader seams and the introduction of a pyroxenitic parting at Crocodile River Mine implies that the formation of the layer can possibly be related to several discrete, smaller mixing events.

Most models imply a temperature decrease in the event of mixing of fresh and residual liquids, which, according to Murck and Campbell (1986) triggers chromite precipitation as a result of decreasing Cr solubility with declining temperatures.

In summary, therefore, the author accepts a plume model for the emplacement of the UG2 Unit for the following reasons:

(a) the relative uniformity of the UG2 pyroxenite and chromitite over great strike distances,
(b) the requirement that large volumes of liquid are needed to supply the Cr_2O_3 necessary for deposition of the chromitite layer, and
(c) the requirement that thorough mixing and hybridization within the phase volume of chromite occurred.

It is important to note, in this context, that both the UG2 chromitite and pyroxenite could not have crystallized from a single large-volume mass of liquid but a series of smaller pulses. This is indicated by comparatively rapid compositional shifts within both layers.

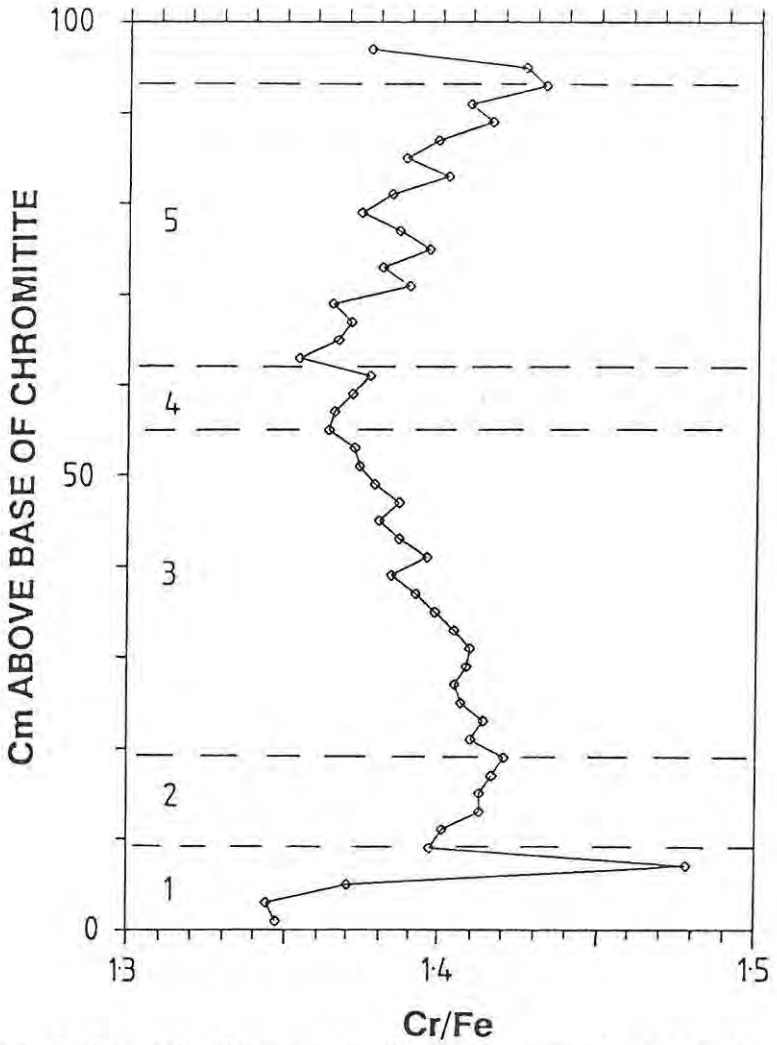

Fig. 8.7 Cr/Fe ratio (weight ratio of the metals) of chromite across the width of the UG2 chromitite (compiled from data from Hiemstra, 1986). Sample spacing is 2 cm. The layer can possibly be sub-divided into 5 depositional cycles.

One may argue that fractionation between proximal and distal facies would seem possible not only in the case of a basal flow or liquid but also in a plume model. This is because cooling is likely to be more efficient in a plume than in a bottom flow where the fresh liquid is in contact with the hot, crystalline floor. However, the present author tends to believe that the high heat flux during the initial stages of an influx, in the case of a plume model, outweighed any cooling of the intruding liquid from below. At the present time no method is developed to quantitatively compare cooling effects in plume models with those in basal flow models.

The P1 Marker (Lower Pseudoreef)

The succeeding ultramafic rocks in the sequence under review belong to the P1 Marker, an ultramafic pegmatoid. It was mentioned in Chapter 7.3 that the layer is laterally highly impersistent: with the exception of some parts of Impala Section it is usually not developed in the southern arm of the western limb. In this respect it resembles the Merensky pegmatoid which also shows poor development in the south-eastern extremities of the western limb (see Chapter 7.7). Barnes & Campbell (1988) suggested that the pegmatoidal character of the Merensky Reef is related to recrystallization of an orthocumulate layer in response to interaction with late magmatic fluids. The present author believes that this model may also provide an explanation for the formation of the P1 Marker, especially so as it offers an interpretation for the laterally variable attributes of the P1 Marker: a more persistent heat flux proximally located with respect to the feeder conceivably enhanced the circulation of late magmatic fluids within the crystal pile.

The P2 Markers (Upper Pseudoreefs)

Like the P1 Marker, the various P2 Marker harzburgites (P2-A, -B, and -C; Fig. 8.8) are laterally much less consistent than the UG2 chromitite or pyroxenite and one concludes that the P2 influxes were much smaller than the UG2 influx. The P2 influxes are anomalous in that their fractionated derivatives (pyroxenites) are missing. Only at Union Section is a transition from the P2 main harzburgite (P2-B and -C) into pegmatoidal harzburgite, pyroxenite, melanorite and anorthosite observed. This transitional unit is called the Pseudo Marker Unit (Viljoen et al., 1986b) and, because it features a thin chromitite stringer at the contact between the P2 main harzburgite and pegmatoidal harzburgite, it is considered to be a separate cyclic unit.

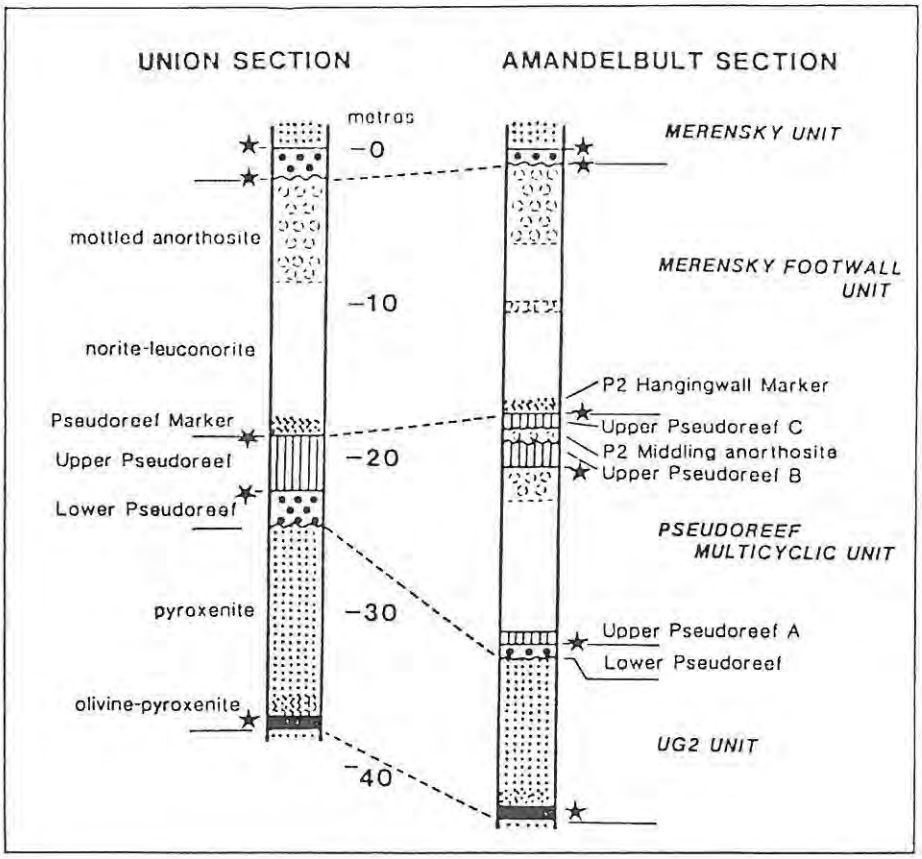

Fig. 8.8 Correlation of Upper and Lower Pseudoreefs at Union and Amandelbult Sections. Asterisks denote chromitite layers (figure from Eales et al., 1988).

The stratigraphic relationship between the P2 Marker and its hangingwall led Campbell et al. (1983) and Naldrett et al. (1986) to propose their model of gravitative accumulation of olivine-laden suspensions at the floor of the chamber (see Section 8.1).

If one compares the UG2 and the P2 ultramafic units it becomes clear that some fundamental differences exist. The P2 unit does not contain any massive chromitite or pyroxenite. The UG2 influx did not deposit harzburgite although at Union Section and in some intersections at Amandelbult the UG2 chromitite may be overlain by up to 2 m of harzburgite.

To discuss this problem it is necessary to reflect on the crystallization order of the hypothetical "U"-type magma, which is considered to be the parental magma of the Lower and Lower Critical Zones (Campbell & Turner, 1986; Hatton & von Gruenewaldt, 1987). According to Irvine et al. (1983), the crystallization order of such a liquid would be olivine - orthopyroxene - orthopyroxene + plagioclase - clinopyroxene + plagioclase. Massive chromite precipitation is likely to occur only in the case of mixing between this "U"-type magma and an evolved liquid of either the same or a different lineage ("A"-type liquid of Irvine et al., 1983, see Fig. 8.2). Consequent upon the mixing, and depending on the relative volumetric proportions of the mixing partners, the resulting hybrid is likely to have either left the olivine stability field or, at the least, to have approached the boundaries of this field (i.e., the olivine-orthopyroxene peritectic or the olivine-plagioclase cotectic, depending on the composition of the evolved mixing partner). It must be noted that there is no evidence in the study interval which justifies the postulation that the A-liquid involved at this level is of a different magmatic lineage to the parental liquid. Sr isotope ratios are similar for the pyroxenites, norites, troctolites and anorthosites (see Table 5.6, and Teigler, 1990).

It must therefore be concluded that the P2 influx, which precipitated only minor chromite, was either not subjected to major mixing processes or was of limited volume. The former postulate is in accordance with slightly higher values of $Mg\#_{opx}$ in the P2 Marker compared with the UG2 pyroxenite at localities UA, EK22 and IN (Figs. 6.2, 6.4, 6.7). It is thus conceivable that the P2 influx intruded as a basal flow. As the author assumes that UG2 and P2 parental liquids both had more or less the same composition and density, the question arises why the UG2 should have intruded as a plume and the P2 as a basal flow. The residual liquid in the chamber into which the two influxes intruded may have changed its density, i.e., become lighter by the time the P2 pulse was emplaced. The present author suggests that the ultimate mixing between the UG2 influx and the underlying

evolved and denser liquid layers (having crystallized plagioclase for some time), which is coupled with a temperature decrease, triggered chromite precipitation (Fig. 8.2). According to Figs. 8.3 and 8.4 this hybrid would have had a lower density than the original residual liquid, but still a higher one than the primitive UG2 and P2 influxes. After chromite and orthopyroxene precipitated from this hybrid to deposit the UG2 chromitite and pyroxenite, it seems possible that the hybrid was lighter than the next pulse of primitive liquid, intruding as the P2 influx. However, the information on density variations in fractionating magmas is somewhat controversial: Campbell & Turner (1986) argue that the density of a magma decreases during crystallization of orthopyroxene whereas Barnes & Naldrett (1986) postulate a density increase (presumably in response to cooling, which they estimate to be the dominant density controlling factor (Fig. 8.3)).

It has been argued that, because of the laterally variable heat flux pattern, any new influx would probably have led to deposition on a footwall of varying thickness. This can indeed be observed in the studied interval in the case of the P2-B and -C (Fig. 7.7) as is shown schematically in Fig. 8.9. Even the P2-A Marker seems to become separated from the underlying P1 Marker (or UG2 pyroxenite) by the introduction of a leucocratic parting in the southern arm of the western limb. Eales et al. 1988 observed that , as the P2-B + -C harzburgites become thinner along strike, the footwall under it thickens (Fig. 7.7). This they suggested could be due to thermal erosion by a mechanism like "complete" potholing. Either footwall erosion or non-deposition, at the present stage of research, seem to be able to explain the observed features in this unit.

The next question focuses on the gradation of the P2 harzburgite into olivine norite at Amandelbult and Impala Sections. This brings one back to considerations of lateral heat flux gradients. In the case of the relatively small P2 influx this gradient would have been much steeper than during the emplacement of the UG2 Unit because the total

amount of P2 magma would have been insufficient to modify magmatic conditions (i.e. temperatures) in all parts of the chamber. In other words, temperatures in the proximal areas were higher than in parts of the chamber distally located with respect to the feeder zone. Thus, the further one moves away from the feeder, the more viscous, cool and dense the residual melt will have been, especially since plagioclase crystallization was more advanced in these parts of the chamber. The P2 melt, intruding along the floor, would gradually have begun to mix more intensely with the overlying residual melt along strike because of the changing density contrasts between primitive and residual liquid (the density of the residual liquid would gradually have increased along strike due to the effect of cooling, plagioclase crystallization and increasing content of suspended crystals, and at one stage surpassed the density of the P2 liquid). Pure olivine cumulates at the bottom would have become thinner and finally disappeared. Suspended olivine within the P2 melt would have been preserved by partial reaction replacement and mantling with orthopyroxene. This progressive disappearance of the different P2 pulses can be observed at Amandelbult Section between 22E and 57E areas (Fig. 7.2).

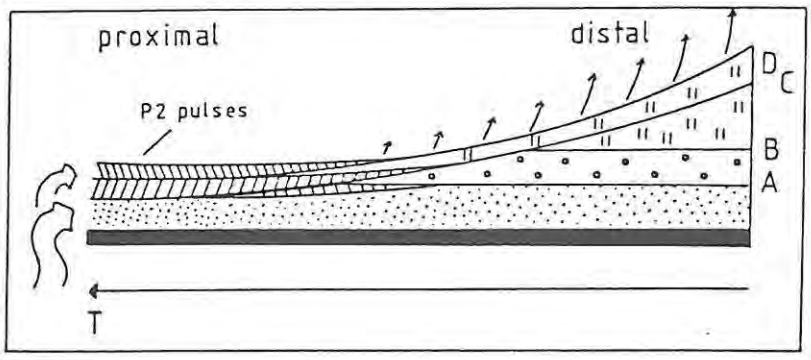

Fig. 8.9 Schematic picture of the successive deposition of cumulates, beginning with the UG2 chromitite (black layer) and ending with the influx of the P2 along strike. (A) marks the end of deposition of UG2 pyroxenite. (B) indicates boundary between FW 12 and 11 in the south-east of the western limb. (C) marks the contact between FW 11 and the FW 7 noritic package. Stage (B) and (C) have not been reached close to the feeder at the time of the first pulse of P2 influx (P1 influx has been omitted for simplification). The second pulse of the P2 influx is separated from the first pulse in the more distal areas. T indicates heatflux from the feeder. Arrows indicate increasing mixing. See text for further explanation.

Chromite precipitation in response to minor mixing with the overlying liquid column and reaction with partly consolidated leucocratic footwall rocks could result in the frequently observed top and bottom chromitite stringers of the P2 (and P1), respectively (Plate 16).

The last phase in the development of the P2 multicyclic unit along strike is the disappearance of olivine east of Rustenburg. The most likely explanation is that the hybrid of P2 and the overlying melt became more and more evolved along strike, and its composition was gradually moving towards the orthopyroxene-plagioclase cotectic. The mixing of the P2 influx probably occurred initially with supernatant cotectic orthopyroxene-plagioclase liquid, thus leading to a hybrid with a composition close to the olivine-orthopyroxene peritectic. Crystallization of minor olivine and then orthopyroxene resulted, with protection of some of this olivine from reaction replacement by mantling with orthopyroxene. Ongoing resorption of suspended plagioclase in the residual liquid due to the P2 heat flux then shifted the resulting mixture towards the orthopyroxene-plagioclase cotectic.

The Central Noritic Part of the Sequence

It remains to be considered how the upward increase in Mg# of orthopyroxene and olivine, as well as whole-rock data throughout the P2 harzburgite (cores AE, UA and EK22) and further towards Brits in the central noritic sequence, could have been achieved (see Figs. 6.2, 6.4, 7.3). Data by Eales et al. (1990a) and Teigler (1990) show upward-increasing $Mg\#_{opx}$ to be a common feature in some units of the Lower and Lower Critical Zone. The model of Eales et al. (1990a) proposes a progressive magma influx of primitive liquid to be responsible for the increasing values. Irvine (1980) suggested that a process of infiltration metasomatism by which intercumulus liquid moved upwards through the semi-consolidated crystal pile may be responsible for compositional shifts in mineral chemistry towards more

evolved values. This, he claimed, is due to reequilibration of primitive phases with the more evolved intercumulus liquids. However, this possibility seems unlikely in the case of the present study as one would expect high concentrations of incompatible trace elements like Zr, Rb, etc. to correlate with low Mg#. This could not be established by the author, the levels of Zr and Rb within the central noritic part of the sequence at intersections LK7, H3 and KR2 being mostly close to the detection limit and higher values showing no correlation with low Mg#. Furthermore, upward-increasing values of Mg# are shown by both pyroxene and whole rock data and thus cannot be due to partitioning of Fe into plagioclase or some other phase.

Rough estimates (Tables 8.1 and 8.2) show that a progressive influx, which gradually diminishes the relative proportion of evolved liquid, can indeed achieve an overall increase in $Mg\#_{wr}$ in the resulting hybrid.

Table 8.1: A: Average composition of 5 quench-textured micropyroxenites, thought to represent parental liquids of the Lower Zone (data from Hatton & Sharpe, 1988). B: Estimated composition of residual liquid, derived by 50 % fractionation of parental liquid of Cawthorn & Davis, (1983). Data from Barnes & Naldrett, (1986). A constant ratio of 10 has been assumed for the ratio of FeO/Fe_2O_3.

	A	B
SiO_2	56.24	57.08
TiO_2	0.32	0.59
Al_2O_3	11.48	14.83
Fe_2O_3	0.84	0.95
FeO	8.42	9.54
MgO	12.98	5.01
CaO	6.40	7.80
Na_2O	1.73	2.37
K_2O	0.87	1.70
MgO:FeO	3:2	1:2
Mg#	.73	.47

Table 8.2: Mass relationships of Fe and Mg in continuously replenished mixtures of primitive (composition A in Table 8.2) and residual (composition B in Table 8.1) magma. Original mixing proportions between residual and primitive liquid are assumed to be 10 : 1, respectively.

	Residual magma			New influx			Hybrid	
	FeO: MgO	$Mg\#_{wr}$		FeO: MgO	$Mg\#_{wr}$		FeO: MgO	$Mg\#_{wr}$
(1)	20 : 10	.47	+	2 : 3	.73	=	22 : 13	.513
(2)	22 : 13	.51	+	2 : 3	.73	=	24 : 16	.543
(3)	24 : 16	.54	+	2 : 3	.73	=	26 : 19	.566
(4)	26 : 19	.57	+	2 : 3	.73	=	28 : 22	.583

By means of the equilibrium equations of Roeder & Emslie (1970) values of Mg# of olivine can be calculated if one knows the composition of the liquid:

$$K_D = \frac{x^{Ol}_{FeO}}{x^{Liq}_{FeO}} * \frac{x^{Liq}_{MgO}}{x^{Ol}_{MgO}} = 0.3$$

$Mg\#_{opx}$ can then be deduced by means of the following regression equation, derived from the data of the study section and stated in the form $y = mx + c$:

$$Mg\#_{opx} = Mg\#_{ol} * 0.634 + 0.31 \qquad R = 0.894 \qquad n = 31$$

The derived values of $Mg\#_{opx}$ are listed below. Also listed are values of $Mg\#_{opx}$ representing ca. 40 m steps up stratigraphic height within the central leuconoritic/noritic sequence observed in intersection H3.

$Mg\#_{wr}$ (from Table 8.2)	$Mg\#_{ol}$ (calculated)	$Mg\#_{opx}$ (calculated)	$Mg\#_{opx}$ (H3) (observed)
0.513	0.773	0.800	0.767
0.543	0.793	0.813	0.786
0.566	0.807	0.822	0.796
0.583	0.819	0.829	0.813

The absence of reversely zoned orthopyroxene in the study section, however, (Chapter 4.9.3), creates some problems for this model, as one would anticipate that at least sporadic reversed zoning should have been preserved. It is of interest that reversed zoning in orthopyroxene has been observed in the UG1 Footwall Unit (Eales, pers. com.) where reversals in term of whole-rock data, with increasing stratigraphic height, are well established (Eales et al., 1990a).

The relative consistency of parameters such as An and Fe content of plagioclase, grain size of plagioclase, Mg# and Cr content of orthopyroxene in the central noritic sequence implies that this replenishment occurred in a more or less consistent way rather than in the form of distinct pulses. However, fluid dynamic processes in magma chambers are very poorly understood and it is likely that other physical processes could also be responsible for the upward increase in Mg#.

Footwalls 6 to 1

As was shown in Chapter 7, a correlation of the upper part (FW 6 to 1) of the interval under review is complicated, as geochemical trends vary considerably along strike. However, certain layers are fairly distinctive and lithologically consistent, like the Merensky footwall anorthosite, the Footwall Marker, and the Footwall Member 6 with its associated Lone Chrome Seam and Boulder Bed.

The origin of the "boulders" remains controversial. The present author is not equipped to contribute to the debate because of the limited number of samples analysed. Lee & Sharpe (1980) suggested a model of in situ formation of "boulders" through aggregation in response to silicate liquid immiscibility. Their main argument is that the immediate foot- and hangingwall of single "boulders" is virtually undisturbed. These authors suggested further that the varying chemical composition of individual "boulders" argues against break-up of a

pyroxenitic layer, as suggested by Jones (1976). It remains unclear, however, how in situ formation of individual "boulders" could create such petrographic differentiation, while the in situ formation of an uninterrupted layer does not. Furthermore, if "boulders" are situated below potholes, activation of late-stage, volatile-rich liquids might be expected to have led to modification of their chemistry and caused variable chemistry between individual "boulders". Additionally, how and why should these aggregations have been formed at that particular position? Lee & Sharpe (1980) suggested an increase in volatile fugacity of the melt as the result of a floating mat of plagioclase which acted as a trap for upward migrating volatiles. Under those conditions, the liquidus relationships would change for most cumulus phases, leading possibly to rapid aggregation of orthopyroxene clusters. These authors claim to have detected supporting evidence for this in elevated An values of plagioclase towards the top of the Merensky footwall cyclic unit.

The Lone Chrome seam can possibly be related to a minor influx during a period of anorthosite accumulation. It is interesting to note in this context that the LC is missing at Union and Impala and at Amandelbult it is situated towards the top of a thin anorthosite, whereas at Rustenburg and towards Brits the layer is situated closer to the base of a much thicker anorthosite.

Generally, it can be said that the upper part of the studied interval consists of an alternation of leuconorites and anorthosites. The number of anorthosites increases from 3 at Union Section to 8 at Crocodile River Mine. Thus, a roughly linear change along strike does occur in this part of the succession. If one assumes that the sequence is complete near Brits one must ask if parts of the succession have been eroded by primitive influxes at Union, or for some reason not been deposited. The first possibility is unlikely as certain layers like the FW 1 anorthosite underlying the primitive Merensky Reef and pyroxenite can be correlated along the entire strike length and show relatively consistent thickness (exceptions are north-eastern

Amandelbult and the area between central Impala Section and locality LK7). Thus, non-deposition of felsic cumulates due to a temporarily higher heat flux from the feeder zone is assumed here to be the reason for the reduced thickness of the column in the north-west. It must be noted, however, that footwall erosion must certainly be considered to be an important process on a local scale, as the correlation between thinning of the sequence and extensive potholing at Union Section suggests (Eales et al., 1988).

Anorthosites

One of the main problems which has yet to be solved in the interpretation of layered complexes is the formation of pure plagioclase cumulates. Supercooling is an unlikely process in a large complex and supersaturation, in part dependent on viscosity, yield strength and convection velocities, is unlikely to reach such levels as to create anorthosites up to 20 m thick, like the FW 12. At Stillwater, anorthosites reach up to 500 m in thickness (Irvine et al., 1983).

Eales et al. (1990a) suggested that an influx of a primitive liquid pulse which spread out along the floor would cause heating of the overlying residual liquid, from which orthopyroxene and plagioclase were crystallizing on the cotectic. If preferential settling of orthopyroxene from the residual liquid occurred, the latter would become enriched in suspended plagioclase phenocrysts. Resorption of this plagioclase during heating would then bring the residual liquid into the primary phase volume of plagioclase. This could result, when this liquid cooled once more, in the formation of anorthosites, succeeded by leuconorites.

Chemical data from the foot- and hangingwall of the FW 6 anorthosite (Table 7.6) along strike showed that the anorthosites are not necessarily to be interpreted as the final stage in a cyclic unit in

the study interval, but that they might also be the result of mineral sorting effects (see Chapter 7.6). Sorting processes have long been suggested to explain monomineralic cumulates (Wager & Brown, 1968; Goode, 1976). The main sorting process is thought to be related to the different densities of the various minerals. The relatively dense orthopyroxene would thus preferentially sink to the floor and light plagioclase might have floated to the roof. Yield strength considerations oppose these ideas and alternative models involve separate anorthositic liquids of silica-undersaturated high-alumina basaltic composition which are thought to have been formed by deep-seated fractionation of mantle-derived liquids (Irvine & Sharpe, 1982; Irvine et al, 1983; Harmer & Sharpe, 1985; Czamanske & Bohlen, 1990). The latter authors described features like the absence of any mafic cumulate minerals, limited variation in An or Sr content with stratigraphic height, and larger grain sizes in anorthosites, and argued in favour of the intrusion of crystal-laden anorthositic suspensions, and against in situ formation. In the study section, however, small, supposedly cumulus orthopyroxene cores can sometimes be observed in "mottles" and plagioclase grain sizes are not significantly different in anorthosites and norites (Fig. 3.1(d)). The other two features mentioned, (lack of variation in An and Sr content with height) could equally be explained by the fact that the densities of plagioclase and the crystallizing liquid are thought to be roughly similar and plagioclase is likely to remain suspended in the magma for a relatively long time. This may lead to mixing of plagioclase of different generations.

The possibility of mineral sorting based on particle shape has not yet been seriously considered to account for monomineralic rocks. The process certainly requires significant convection (strictly speaking, however, centripetal forces are time-dependent and should operate even at very low velocities, if enough time is available). The process could work on the basis that plagioclase and orthopyroxene, as long as they are suspended, crystallize as columnar grains and as more tabular crystals, respectively. It is a well known fact in dynamic

sedimentology that the shape of particles is an important factor affecting the settling velocity of minerals (Briggs et al. 1962; Krumbein, 1942). Lane (1938) and Baba & Komar (1981) showed that the settling velocity of sand grains increases with grain diameter and above 0.1 - 0.5 mm, settling velocities of spherical grains are higher than those of grains of irregular shape (Fig. 8.10). The ratio of surface area / mass, (called "s-m ratio") and thus friction, is higher for irregularly shaped grains. The latter are therefore transported faster in a current. Relatively small grains are also transported faster because of a higher "s-m ratio". Newly crystallized plagioclase should thus concentrate in areas of high velocity within the convection current relative to suspended orthopyroxene. Additionally, the density difference between magma and crystal is much smaller in the case of plagioclase, which further increases the efficiency of transport. It is interesting to note in this context that, quite frequently, the contact between a pyroxenite or a norite and an overlying anorthosite is sharp (onset of plagioclase crystallization and preferred concentration of small plagioclase grains in convection current?) whereas that between an anorthosite and an overlying leuconorite is transitional. It may be envisaged that the gradual increase in grain size of plagioclase with ongoing crystallization decreased the efficiency of the sorting process and led to co-deposition of suspended plagioclase and orthopyroxene.

Thus, in the case of significant current velocities, one might expect sorting to occur at the onset of crystallization of any mineral. This could well be a contributary factor to the formation of plagioclase cumulates as modelled on page 217, p2. A sorting process by itself, as modelled above, seems to be unable to create adcumulates as the initial porosity in a plagioclase-bearing crystal mush presumably was relatively high and considerable amounts of orthopyroxene should be present in the resulting rock. Further work is indicated to resolve this problem.

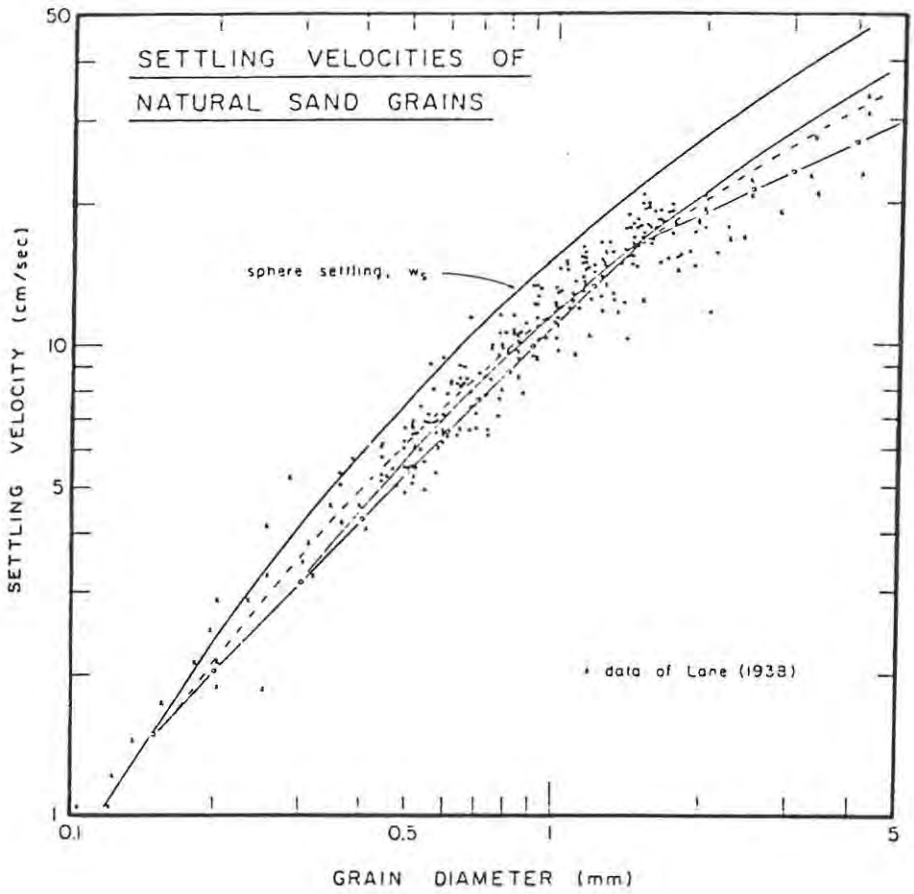

Fig. 8.10 Settling velocity of sand grains versus grain diameter. The upper curve applies for settling of spheres, the lower curves for subspherical grains (figure modified after Baba & Komar, 1981).

8.3: Conclusion

The author proposes a major influx which did not spread out on the floor to be responsible for the UG2 chromitite and pyroxenite. It is argued that the modification of the composition of the magma because of the footwall erosion would otherwise have been significant along strike. It is believed that this influx rose in the supernatant liquid to a level determined by relative densities, spread out laterally, mixed with the underlying magma by means of finger mixing, and started crystallizing chromite and later orthopyroxene. The deposition of the chromitite may have occurred in several pulses, as data by Hiemstra

(1986) and lithological evidence like the development of a pyroxenitic parting and chromitiferous leader seams indicate. The mixing process is assumed to have led to heated conditions and the combination of thermal, chemical and mechanical effects was likely to be sufficient for the formation of potholes, encountered in the footwall of the UG2 chromitite.

The various P2 influxes probably intruded along the floor of the chamber. This inhibited mixing with evolved liquid and precipitation of chromite. After the deposition of a variable amount of olivine, convective overturn with the supernatant liquid brought the hybrid close to the orthopyroxene-plagioclase cotectic, so as to deposit orthopyroxene-plagioclase cumulates. The sequence between the base of the P2 and the anorthositic-leuconoritic top part of the interval displays substantial thickening as one moves away from Union Section. Simultaneously, the interval between P1 and P2-B + C becomes thicker as the latter unit becomes thinner along strike. This led to the concept of a proximal and distal facies, first proposed by Eales et al. (1988).

Anorthosites possibly have formed by a combination of different processes. The residual liquid, having fractionated mainly orthopyroxene, and containing suspended plagioclase, is believed to have been warmed up (possibly by the P2 influxes which spread out as basal flows). As a result, suspended plagioclase was partly resorbed (as indicated by inclusions in orthopyroxene and olivine of the FW 11 - 7 leuconorites and norites) and the composition of the melt shifted into the primary phase volume of plagioclase. With cooling, anorthosites, and then leuconorites were deposited. Sorting effects might have been significant as well. However, research is not advanced enough to permit a definite statement.

The top part of the sequence investigated consists of a number of well correlatable anorthosites and leuconorites (norites). The fact that a correlation seems to be possible persuades this writer that

significant footwall erosion on a regional scale did not occur in response to the Merensky influx. It is conceded that the number of units, and their thickness, decreases between the putative distal and proximal facies, but this author attributes this to control exerted on the crystallization processes by the thermal regime.

CHAPTER 9: SUMMARY

This thesis has presented results of a lithological, petrographical and geochemical investigation of the interval between the UG2 chromitite and the Merensky Reef in the Western Bushveld, as exposed by numerous borehole cores and underground exposures. The main aim of the study was to document the lateral variability of the distinguishable units and layers by means of a lithological and geochemical correlation. The existence of lateral lithological variability was described previously by numerous authors but Eales et al. (1988) were the first to recognize a linear relationship between the thickness of the described interval and the distance of the respective intersections from a proposed feeder zone at Union Section. Possible mechanisms responsible for these lateral changes have been evaluated, and a genetic model proposed in the present work.

The various areas of study include:

(a) RPM Amandelbult Section, from which 15 cores have been investigated.
(b) RPM Union Section (1 core).
(c) Impala Platinum Mines (2 cores and a number of underground samples).
(d) RPM Rustenburg Section (underground samples).
(e) An area near Wolhuterskop (2 cores).
(f) Crocodile River Mine (1 core).

The various methods of investigation have included:

1. Logging of boreholes $7E^3$, EK22, $60E^3$, In, IM, LK7, H3 and KR2.
2. Petrographic studies, including determinations of mineral modes by point counting, and grain size measurements of ca. 200 samples.
3. Whole-rock geochemical analyses of ca. 250 samples.
4. Electron microprobe analyses of ca. 270 samples.
5. Sr isotope analysis of 6 samples.

Lithology:

Lithologically, a number of layers are correlatable along strike in the western lobe. These include the UG2 chromitite and pyroxenite, the Footwall Marker, the Lone Chrome Seam and the Merensky Footwall anorthosite. Other layers and units are more or less correlatable in certain parts of the western limb, like the Pseudoreef Markers in the northern part and the Boulder Bed in the southern part of the western limb.

Petrography:

Modal compositions and grain size analyses were mainly used to establish the correlation of the central noritic part, which shows a relatively constant proportion of orthopyroxene and a comparatively low and constant grain size of cumulus plagioclase. Grain sizes and mineral modes in the upper part of the sequence are highly irregular and difficult to correlate.

Whole-rock chemistry:

The whole-rock chemistry shows a good correlation with the microprobe data, with the exception of core KR2, where an upward decrease in $Mg\#_{wr}$ and an increase in modal proportion of plagioclase (as revealed by increasing Sr/V ratios) in the central noritic part is coupled with an upward increase in $Mg\#_{opx}$. The bulk composition of the UG2 pyroxenite has been compared along strike (Table 7.3); the results reveal systematic variations along strike in some parameters (Ni/Sc_{wr}, Al_2O_{3opx}) but most parameters show no systematic variation. The small number of samples analysed for Sr isotopes in one intersection (IM) limits the possibilities of correlation by this technique, but a trend similar to that in the study section can be detected in the Merensky Unit at Atok Section (Lee & Butcher, 1989).

Mineralogy:

Detailed microprobe analyses focussed on several areas:

- The establishment of a correlation of geochemical trends along strike, notably the consistency or mute upward increase of $Mg\#_{opx}$ in the central noritic part around the western lobe.
- The study of geochemical variation of certain minerals in individual layers along strike (Lone Chrome Seam, UG2 chromitite and UG2 pyroxenite, Boulder Bed).
- The small-scale cryptic variation in certain minerals within a clearly defined layer or unit, like olivine and orthopyroxene within the Upper Pseudoreef.
- The petrological implications of resorbed plagioclase inclusions in orthopyroxene and olivine.
- Zonation studies on plagioclase, orthopyroxene, olivine and chromite. As mentioned by numerous other workers, plagioclase shows significant and highly variable zonation in this part of the Upper Critical Zone. Orthopyroxene shows very little zonation with respect to Mg# but, usually, normal zonation in Cr_2O_3. Neither olivine nor chromite show any zonation of individual grains with respect to the analysed elements. The three latter phases, however, show zonation on a small scale when they are in contact with each other, which may be attributed to sub-solidus equilibration.

Based on the compilation of the generated data, and taking into account published work of numerous other workers, a model has been proposed which explains the reduced thickness of certain layers in some parts of the complex with non-deposition of cumulates. A relationship is believed to exist between non-deposition and proximity to a postulated feeder zone.

REFERENCES

Andersen, O. (1915). The system anorthite - forsterite - silica. *Am. J. Sci.*, **39**, 407 - 454.

Baba, J. and Komar, P.D. (1981). Measurements and analysis of settling velocities of natural quartz sand grains. *J. Sed. Petrol.*, **51**, 631 - 640.

Ballhaus, C.G. (1988). Potholes of the Merensky Reef at Brakspruit Shaft, Rustenburg Platinum Mines: Primary Disturbances in the Magmatic Stratigraphy. *Econ. Geol.*, **83**, 1140 - 1158.

Ballhaus, C.G. and Stumpfl, E.F. (1985a). Occurrence and petrological significance of graphite in the Upper Critical Zone, Western Bushveld Complex, South Africa. *E. Plan. Sci. Lett.*, **74**, 58 - 68.

---------- ---------- (1985c). Graphite, platinum and the C-O-H-S system, (abstr.). *Can. Min.*, **23**, 293 - 294.

---------- ---------- (1985b). Fluid inclusions in Merensky and Bastard Reefs, Western Bushveld Complex, (abstr.). *Can. Min.*, **23**, 294.

Barnes, S.J. and Campbell, I.H. (1988). Role of late magmatic fluids in Merensky - type platinum deposits: a discussion. *Geology*, **16**, 488 - 491.

Barnes, S.J. and Naldrett, A.J. (1985). Geochemistry of the J-M (Howland) Reef of the Stillwater Complex, Minneapolis Adit Area I. Sulfide Chemistry and Sulfide-Olivine Equilibrium. *Econ. Geol.*, **80**, 627 - 645.

---------- ---------- (1986). Geochemistry of the J-M Reef of the Stillwater Complex, Minneapolis Adit Area II: Silicate Mineral Chemistry and Petrogenesis. *J. Petrol.*, **27**, 791 - 825.

Barry, J.A. (1964). Pothole and koppie investigation at Rustenburg Platinum Mines. *Int. Rep., (unpubl.), J.C.I*, 5pp.

Botha, M.J. (1987). *Petrology and geochemistry of the lower group chromitites and host rocks on the farm Zandspruit 168 JP, Western Bushveld Complex.* M.Sc. thesis, (unpubl.), Rhodes University, 216 pp.

Bottinga, Y., Kudo, A. and Weill, D.F. (1966). Some observations of oscillatory zoning and crystallization of magmatic plagioclase. *Am. Mineralogist*, **51**, 792.

Bottinga, Y. and Weill, D.F. (1970). Densities of liquid silicate systems calculated from partial molar volumes of oxide components. *Am. J. Sci.*, **269**, 169 - 182.

Bottinga, Y., Weill, D.F. and Richet, P. (1982). Density calculations for silicate liquids I: Revised method for aluminosilicate compositions. *Geochim. Cosmochim. Acta*, **46**, 909 - 919.

Boudreau, A.E. (1988). Investigations of the Stillwater Complex IV: The role of volatiles in the petrogenesis of the J-M Reef, Minneapolis Adit Section. *Can. Min.*, **26**, 193 - 208.

Bowen, N.L. (1915). Crystallization differentiation in silicate liquids. *Am. J. Sci.*, **39**, 175 - 191.

Brandeis, G. and Marsh, B.D. (1989). Superheat absence as indicator of convective liquidus in magma, 193, (Abstr.). *28th int. Geol. Congr., Washington, D.C.*, **Vol 1.**

Briggs, L.I., McCulloch, D.S. and Moser, F. (1962). The hydraulic shape of sand particles. *J. Sed. Petrol.*, **32**, 645 - 646.

Brown, G.M. (1956). The layered ultrabasic rocks of Rhum, Inner Hebrides. *Philos. Trans. Roy. Soc. London*, **B 240**, 1 - 53.

Buntin, T.J., Grandstaff, D.E., Ulmer, G.C. and Gold, D.P. (1985). A pilot study of geochemical and redox relationships between potholes and adjacent normal Merensky Reef of the Bushveld Complex. *Econ. Geol.*, **80**, 975 - 987.

Burger, A.J. and Coertze, F.J. (1973). Radiometric age measurements on rocks from Southern Africa to the end of 1971. *Geol. Surv. S. Afr.*, **Bull. 58**, 46 pp.

Butler, P. (1972). Compositional characteristics of olivines from Apollo 12 samples. *Geochim. Cosmochim.Acta*, **36**, 773 - 785.

Cameron, E.N. (1969). Postcumulus changes in the Eastern Bushveld Complex. *Am. Mineralogist*, **54**, 754 -779.

---------- (1975). Postcumulus and subsolidus equilibration of chromite and coexisting silicates in the Eastern Bushveld Complex. *Geochim. Cosmochim. Acta*, **39**, 1021 - 1033.

---------- (1978). The Lower Zone of the Eastern Bushveld Complex in the Olifants River Trough. *J. Petrol.*, **19**, 437 - 462.

---------- (1980). Evolution of the Lower Critical Zone, Central Sector, and Its Chromite Deposits. *Econ. Geol.*, **75**, 845 - 871.

---------- (1982). The Upper Critical Zone of the Eastern Bushveld Complex - Precursor of the Merensky Reef. *Econ. Geol.* **77**, 1307 - 1327.

Campbell, I.H. (1986). A Fluid Dynamic Model for the Potholes of the Merensky Reef. *Econ. Geol.*, **81**, 1118 - 1125.

Campbell, I.H. and Borley, G.D. (1974). The Geochemistry of Pyroxenes from the Lower Layered Series of the Jimberlana Intrusion, Western Australia. *Contr. Min. Petrol.*, **47**, 281 - 297.

Campbell, I.H., Naldrett, A.J. and Barnes, S.J. (1983). A Model for the Origin of the Platinum-Rich Sulfide Horizons in the Bushveld and Stillwater Complexes, *J. Petrol.*, **24**, 133 - 165.

Campbell, I.H., Roeder, P.L. and Dixon, J.M. (1978). Plagioclase Buoyancy in Basaltic Liquids as Determined with a Centrifuge Furnace. *Contr. Min. Petrol.*, **67**, 369 - 377.

Campbell, I.H. and Turner, J.S. (1986). The role of convection in the formation of platinum and chromitite deposits in layered intrusions, 236 - 278. In Scarfe, C. M., Ed., *Silicate melts: their properties and structure applied to problems in geochemistry, petrology, economic geology and planetary geology.* Short course handb., Min. Ass. Can., Edmonton, 319 pp.

Carr, J.M. (1954). Zoned plagioclases in layered gabbros of the Skaergaard intrusion, east Greenland. *Mineralog. Mag.*, **30**, 367 - 375.

Carr, M.H. and Turekian, K.K. (1961). The geochemistry of Cobalt. *Geochim. Cosmochim. Acta*, **23**, 9.

Champness, P.E. and Lorimer, G.W. (1976). Exsolution in silicates, 174 - 204. In Wenk, H.-R., Ed., *Electron microscopy in mineralogy.* Springer Verlag, Berlin - Heidelberg - New York, 564 pp.

Coats, R.R. (1936). Primary banding in basic plutonic rocks. *J. Geol.*, **44**, 407 - 419.

Coertze, F.J., Burger, A.J., Walraven, F., Marlow, A.G. and McCaskie, D.R. (1978). Field relations and age determinations in the Bushveld Complex. *Trans. Geol. Soc. S. Afr.*, **81**, 1 - 11.

Colson, R.O. and Gust, D. (1989). Effects of pressure on partitioning of trace elements between low-Ca pyroxene and melt. *Am. Mineralogist.*, **74**, 31 - 36.

Colson, R.O., McKay, G.A. and Taylor, L.A. (1988). Temperature and composition dependencies of trace element partitioning: olivine / melt and low-Ca pyroxene / melt. *Geochim. Cosmochim. Acta*, **52**, 539 - 553.

Cooper, J.R. (1936). Geology of the southern half of the Bay of Islands Igneous Complex. *Newfoundland Dept. of Nat. Resources Geol. Sect.*, **Bull. 4**, 1 - 62.

Cousins, C.A. (1959). The structure of the mafic portion of the Bushveld Igneous Complex. *Trans. Geol. Soc. S. Afr.*, **62**, 179 - 189.

---------- (1964). The platinum deposits of the Merensky Reef, 225-237. In Haughton, S.H., Ed., *The geology of some ore deposits in Southern Africa, Vol. 2*, Geol. Soc. S. Afr. 739 pp.

---------- (1969). The Merensky Reef of the Bushveld Igneous Complex, 239-251. In Wilson, H.D.B., Ed., Magmatic Ore Deposits. *Econ. Geol.*, **Monogr. 4**, 366 pp.

---------- and Feringa, G. (1964). The chromite deposits of the western belt of the Bushveld Complex, 183 - 202. In Haughton, S.H., Ed., *The geology of some ore deposits in Southern Africa, Vol. 2*, Geol. Soc. S. Afr. 730 pp.

Cox, K.G., Bell, J.D. and Pankhurst, R.J. (1979). *The interpretation of igneous rocks.* George Allen and Unwin, London, 450 pp.

Czamanske, G.K. and Bohlen, S.R. (1990). The Stillwater Complex and its anorthosites: an accident of magmatic underplating? *Am. Mineralogist.*, **75**, 37 - 45.

Darwin, C. (1844). *Geological observation on the volcanic islands, visited during the voyage of H.M.S. Beagle, together with some brief notices on the geology of Australia and the Cape of Good Hope. Being the second part of the geology of the voyage of the Beagle, under the command of Capt. Fitzroy, R.N., during the years 1832-1836.* Smith & Elder, London, 175 pp.

Deer, W.A., Howie, P.A. and Zussman, J. (1962). *Rock forming minerals, Vol. 3, Sheet silicates*, Longman Group Ltd., London - New York, 270 pp.

---------- ---------- ---------- (1978). *Rock forming minerals, Vol. 2a, Single chain silicates*, Longman Group Ltd.,London - New York, 668 pp.

---------- ---------- ---------- (1982). *Rock forming minerals, Vol. 1a, Orthosilicates*, Longman Group Ltd., London - New York, 919 pp.

De Klerk, W.J. (1991). *Petrogenesis of the Upper Critical Zone in the Western Bushveld Complex with emphasis on the UG1 Footwall and Bastard Units.* Ph.D. thesis (unpubl.), Rhodes University.

DeLong, S.E. (1974). Distribution of Rb, Sr and Ni in igneous rocks, central and western Aleutian Islands, Alaska. *Geochim. Cosmochim. Acta*, **38**, 245 - 266.

De Waard, D. and Romey, W.D. (1969). Petrogenetic relationships in the anorthosite - charnockite series of Snowy Mountain Dome, south central Adirondacks. In Isachsen, Y.W., Ed., Origin of anorthosites and related rocks. *N.Y. State Mus. Sci. Serv.*, **Mem. 18**, 307 - 315.

Drake, M.J. and Weill, D.F (1971). Petrology of Apollo 11 sample 10071. A differentiated mini - igneous complex. *Earth. Plan. Sci. Lett.*, **13**, 61 - 70.

---------- ---------- (1975). Partition of Sr, Ba, Ca, Y, Eu^{2+}, Eu^{3+} and other REE between plagioclase feldspar and magmatic liquid: an experimental study. *Geochim. Cosmochim. Acta*, **39**, 689 - 712.

Duke, J.M. (1976). Distribution of the Period Four Transition Elements among Olivine, Calcic Clinopyroxene and Mafic Silicate Liquid: Experimental Results. *J. Petrol.*, **17**, 499 - 521.

Eales, H.V., De Klerk, W.J., Butcher, A.R. and Kruger, F.J. (1990a). The cyclic unit beneath the UG1 chromitite (UG1FW unit) at RPM Union Section Platinum Mine - Rosetta stone of the Bushveld Upper Critical Zone? *Mineralog. Mag.*, **54**, 23 - 43.

Eales, H.V., De Klerk, W.J. and Teigler, B. (1990b). Evidence for magma mixing processes within the Critical and Lower Zones of the northwestern Bushveld Complex, South Africa. *Chem. Geol.*, **88**, 261 - 278.

Eales, H.V., Field, M., De Klerk, W.J. and Scoon, R.N. (1988). Regional trends of chemical variation and thermal erosion in the Upper Critical Zone, Western Bushveld Complex. *Mineralog. Mag.*, **52**, 63 - 79.

Eales, H.V., Maier, W.D. and Teigler, B. (1991). The significance of corroded feldspar inclusions in pyroxenites and norites of the Lower and Critical Zones, Western Bushveld Complex (in press.). *Mineralog. Mag.*

Eales, H.V., Marsh, J.S., Mitchell, A.A., De Klerk, W.J., Kruger, F.J. and Field, M. (1986). Some geochemical constraints upon models for the crystallization of the Upper Critical Zone - Main Zone interval, northwestern Bushveld Complex. *Mineralog. Mag.*, **50**, 567 - 582.

Eales, H.V. and Reynolds, I.M. (1986). Cryptic Variations within Chromitites of the Upper Critical Zone, Northwestern Bushveld Complex. *Econ. Geol.*, **81**, 1056 - 1066.

El Goresy, A., Prinz, M. and Ramdohr, P. (1976). Zoning in spinels as an indicator of the crystallization histories of mare basalts. *Proc. 7th Lunar Sci. Conf.*, 1261 - 1279.

Ellis, M. (1989). *A petrographical, mineralogical and geochemical study of the Pseudoreef and Merensky Footwall cyclic units along strike at Amandelbult Section, RPM.* B.Sc. Hons. thesis, (unpubl.), Rhodes University, 78 pp.

Engelbrecht, J.P. (1985). The Chromites of the Bushveld Complex in the Nietverdient Area. *Econ. Geol.*, **80**, 896 - 910.

Ewart, A., Bryan, W.B. and Gill, J.B. (1973). Mineralogy and Geochemistry of the Younger Volcanic Islands of Tonga, S.W. Pacific. *J. Petrol.*, **14**, 429 - 465.

Farquhar, J. (1986). The Western Platinum Mine, 1135 - 1142. In Anhaeusser, C.R. and Maske, S., Eds., *Mineral deposits of Southern Africa, Vol.2*, 2335 pp.

Ferguson, J. and Botha, E. (1963). Some aspects of igneous layering in the basic zones of the Bushveld Complex. *Trans. Geol. Soc. S. Afr.*, **66**, 259 - 278.

Feringa, G. (1959). The geological succession in a portion of the north-western Bushveld (Union Section) and its interpretation. *Trans. Geol. Soc. S. Afr.*, **61**, 219 - 232.

Field, M. (1986). *The petrology and geochemistry of the Upper Critical Zone of the Bushveld Complex at the Amandelbult Section of Rustenburg Platinum Mines Ltd., northwestern Transvaal, South Africa.* M.Sc. thesis, (unpubl.), Rhodes University, 129 pp.

Flower, M.F.J. (1973). Trace-element distribution in lava flows from Anjouan and Grande Comore, western Indian Ocean. *Chem. Geol.*, **12**, 81 - 98.

Frey, F.A., Green, D.H. and Roy, S.D. (1978). Integrated Models for Basalt Petrogenesis: A Study of Quartz Tholeiites to Olivine Melilitites from South Eastern Australia, Utilizing Geochemical and Experimental Petrological Data. *J. Petrol.*, **19**, 463 - 513.

Gain, S.B. (1986). The Upper Group Chromitite Layers at Maandagshoek, Eastern Bushveld Complex, 1197-1208. In Anhaeusser, C.R. and Maske, S., Eds., *Mineral Deposits of Southern Africa*, Vol.2, Geol. Soc. S. Afr., 2335 pp.

Goode, A.D.T. (1976). Small Scale Primary Cumulus Igneous Layering in the Kalka Layered Intrusion, Giles Complex, Central Australia. *J. Petrol.*, **17**, 379 - 397.

Hall, A.L. (1932). The Bushveld Igneous Complex in the central Transvaal. *Geol. Surv. S. Afr.*, **Mem. 28**, 544 pp.

Hamilton, P.J. (1977). Sr-isotope and trace element studies of the Great Dyke and Bushveld mafic phase and their relation to early proterozoic magma genesis in South Africa. *J. Petrol.*, **18**, 24 - 52.

Hanson, G.N. (1977). Geochemical evaluation of the suboceanic mantle. *J. Geol. Soc. Lond.*, **134**, 235 - 253.

---------- (1989). An approach to trace element modeling using a simple igneous system as an example, 79 - 97. In Ribbe, P.H., *Geochemistry and mineralogy or rare earth elements*. Min. Soc. Am., Reviews in mineralogy 21, Min. Soc. Am., 348 pp.

Harmer, R.E. and Sharpe, M.R. (1985). Field Relations and Strontium Isotope Systematics of the Eastern Bushveld Complex. *Econ. Geol.*, **80**, 813 - 837.

Hart, S.R. and Brooks, C. (1974). Clinopyroxene - matrix partitioning of K, Rb, Cs, Sr and Ba. *Geochim. Cosmochim. Acta*, **38**, 1799 - 1806.

Hattingh, P.J. (1986). The palaeomagnetism of the Main Zone of the Eastern Bushveld Complex. *Tectonophysics*, **124**, 271 - 295.

Hatton, C.J. (1988). Densities and liquidus temperatures of Bushveld parental magmas as constraints on the formation of the Merensky Reef. In Prendergast, M.D., Ed., *Proc. Fifth Magmatic Sulphide Conference*, Institution of Mining and Metallurgy.

Hess, H.H. (1960). Stillwater Igneous Complex, Montana: a quantitative mineralogical study. *Geol. Soc. Am.*, **Mem. 80**, 230 pp.

Hiemstra, S.A. (1985). The Distribution of Some Platinum-Group Elements in the UG-2 Chromitite Layer of the Bushveld Complex. *Econ. Geol.*, **80**, 944 - 957.

---------- (1986). The Distribution of Chalcophile and Platinum - Group Elements in the UG-2 Chromitite Layer of the Bushveld Complex. *Econ. Geol.*, **81**, 1080 - 1086.

Hill, R. and Roeder, P. (1974). The crystallization of spinel from basaltic liquid as a function of oxygen fugacity. *J. Geol.*, **82**, 709 - 729.

Hoyle, P. (1989). *A study of the petrography and mineral chemistry of centimetre-scale layering from the Lower Zone, Bushveld Complex.* B.Sc. Hons. thesis, (unpubl.), Rhodes University, 44 pp.

Hulbert, L.J. and Von Gruenewaldt, G. (1986). The structure and petrology of the upper and lower chromitite layers on the farms Grasvally and Zoetveld, south of Potgietersrus, 1237 - 1249. In Anhaeusser, C.R. and Maske, S., Eds., *Mineral deposits of Southern Africa, Vol. 2*, Geol. Soc. S. Afr., 2335 pp.

Hunter, D.R. (1976). Some Enigmas on the Bushveld Complex. *Econ. Geol.*, **71**, 229 - 248.

Hunter, R.H. (1987). Textural equilibrium in layered igneous rocks, 473 - 503. In Parsons, I., Ed., *Origins of Igneous Layering*, D. Reidel Publishing Company, Dordrecht - Boston - Lancaster - Tokyo, 666 pp.

Huppert, H.E. and Sparks, R.S.J. (1980).The Fluid Dynamics of a Basaltic Magma Chamber Replenished by Influx of Hot, Dense Ultrabasic Magma. *Contr. Min. Petrol.*, **75**, 279 - 289.

Huppert, H.E., Sparks, R.S.J. and Turner, J.S. (1984). Some effects of viscosity in the dynamics of magma chambers. *J. Geophys. Res.*, **89**, 6857 - 6877.

Irvine, T.N. (1974). Petrology of the Duke Island Ultramafic Complex, Southeastern Alaska. *Geol. Soc. Am.*, **Mem. 138**, 240 pp.

---------- (1977). Origin of chromitite layers in the Muskox intrusion and other stratiform intrusions: A new interpretation. *Geology*, **5**, 273 - 277.

---------- (1980). Magmatic infiltration metasomatism, double diffusive fractional crystallization and adcumulus growth in the Muskox Intrusion and other layered intrusions, 325 - 383. In Hargraves, R.B., Ed., *Physics of magmatic processes*. Princeton Univ. Press, 385pp.

---------- (1982). Terminology for layered intrusions. *J. Petrol.*, **23**, 127 - 162.

Irvine, T.N., Keith, D.W. and Todd, S.G. (1983). The J-M Platinum-Palladium Reef of the Stillwater Complex, Montana, II: Origin by Double-Diffusive Convective Magma Mixing and Implications for the Bushveld Complex. *Econ. Geol.*, **78**, 1287 - 1334.

Irvine, T.N. and Sharpe, M.R. (1982). Source - rock compositions and depths of origin of Bushveld and Stillwater magmas. *Carnegie Inst., Washington*, **Yearb. 81**, 294 - 303.

---------- ---------- (1986). Magma mixing and the origin of stratiform oxide ore zones in the Bushveld and Stillwater Complexes. In Gallagher, M.J., Ixer, R.A., Neary, C.R. and Prichard, H.M., Eds., *Metallogeny of basic and ultrabasic rocks*, Proc. of conf., 183 - 198.

Irvine, T.N. and Smith, C.H. (1967). The ultramafic rocks of the Muskox Intrusion, Northwest Territories, Canada, 38 - 49. In Wyllie, P.J., Ed., *Ultramafic and Related Rocks*, Wiley, New York, 464 pp.

Irving, A.J. (1978). A review of experimental studies of crystal / liquid trace element partitioning. *Geochim. Cosmochim. Acta*, **42**, 743 - 770.

Jackson, E.D. (1961). Primary textures and mineral associations in the ultramafic zone of the Stillwater Complex, Montana. *Geol. Surv.*, **Prof. Pap. 358**, 106 pp.

---------- (1969). Chemical variation in coexisting chromite and olivine in the chromitite zones of the Stillwater Complex. *Econ. Geol.*, **Monogr. 4**, 41 - 71.

---------- (1970). The cyclic unit in layered intrusions - a comparison of repetitive stratigraphy in the ultramafic parts of the Stillwater, Muskox, Great Dyke and Bushveld Complexes, 391 - 424. *Geol. Soc. S. Afr.*, **Spec. Publ. 1**, 763 pp.

Jensen, B.B. (1973). Patterns of trace element partitioning. *Geochim. Cosmochim. Acta*, **37**, 2227 - 2242.

Johannes, W. (1978). Melting of Plagioclase in the System Ab-An-H_2O and Qz-Ab-An-H_2O at P_{H2O} = 5 kbars, an Equilibrium Problem. *Contr. Min. Petrol.*, **66**, 295 - 303.

Jones, J.P. (1976). Pegmatoidal nodules in the layered rocks of the Bafokeng leasehold area. *Trans. Geol. Soc. S. Afr.*, **79**, 312 - 320.

Kelsey, C.H. (1965). Calculation of the C.I.P.W. Norm. *Mineralog. Mag.*, **34**, 276 - 282.

Kinloch, E.D. (1982). Regional Trends in the Platinum-Group Mineralogy of the Critical Zone of the Bushveld Complex, South Africa. *Econ. Geol.*, **77**, 1328 - 1347.

---------- and Peyerl, W. (1990). Platinum-group minerals in various rock-types of the Merensky Reef: genetic implications. *Econ. Geol.*, **85**, 537 - 555.

Korringa, M.K. and Noble, D.C. (1971). Distribution of Sr and Ba between natural feldspar and igneous melt. *Earth. Plan. Sci. Lett.*, **11**, 147 - 151.

Kruger, F.J. (1982). *The petrology of the Merensky cyclic unit and associated rocks and their significance in the evolution of the Western Bushveld Complex*. Ph.D. thesis (unpubl.), Rhodes University, 123 pp.

Kruger, F.J. and Marsh, J.S. (1985). The Mineralogy, Petrology, and Origin of the Merensky Cyclic Unit in the Western Bushveld Complex. *Econ. Geol.*, **80**, 958 - 974.

Krumbein, W.C. (1942b). Settling velocity and flume behaviour of nonspherical particles. *Trans. Am. Geoph. Union*, **23**, 621 - 633.

Lambert, R.S. and Holland, J.G. (1974). Yttrium geochemistry applied to petrogenesis utilizing calcium - yttrium relationships in minerals and rocks. *Geochim. Cosmochim. Acta*, **38**, 1393 - 1414.

Lane, E.W. (1938). Notes on the formation of sand. *Trans. Am. Geoph. Union*, **18**, 505 - 508.

Lee, C.A. and Butcher, A.R. (1989). Cyclicity in the Sr-isotopic stratigraphy through the Merensky and Bastard Reef units, Atok section, eastern Bushveld Complex, (Abstr.). *Conference on the origin of Mineralization in southern African Layered Intrusions.* Univ. of the Witwatersrand, Johannesburg.

---------- ---------- (1990). Cyclicity in the Sr-Isotope Stratigraphy through the Merensky and Bastard Reef Units, Atok Section, Eastern Bushveld Complex. *Econ. Geol.*, **85**, 877 - 883.

Lee, C.A. and Sharpe, M.R. (1980). Further examples of silicate liquid immiscibility and spherical aggregation in the Bushveld Complex. *Earth. Plan. Sci. Lett.*, **48**, 131 - 147.

---------- ---------- (1986). The structural setting of the Bushveld Complex, 1031 - 1038. In Anhaeusser, C.R. and Maske, S., Eds., *Mineral Deposits of Southern Africa*, Vol. 2, Geol. Soc. S. Afr., 2335 pp.

Lee, C.A., Sharpe, M.R. and Viljoen, E.A. (1983). The chemistry of minor chromite layers in the Bushveld Complex, with special reference to chromite-plagioclase reaction, (Abstr.). *Symposium on the Bushveld Complex*, Institute for Geological Research on the Bushveld Complex, Pretoria, 103 pp.

Leeb-du Toit, A. (1986). The Impala Platinum Mines, 1091 - 1106. In Anhaeusser, C.R. and Maske, S., Eds., *Mineral deposits of Southern Africa, Vol.2*, Geol. Soc. S. Afr., 2335 pp.

Leeman, W.P. and Lindstrom, D.J. (1978). Partitioning of Ni^{2+} between basaltic and synthetic melts and olivines - an experimental study. *Geochim. Cosmochim. Acta*, **42**, 801 - 816.

Lemarchand, F., Villemant, B. and Calas, G. (1987). Trace element distribution coefficients in alkaline series. *Geochim. Cosmochim. Acta*, **51**, 1071 - 1081.

Lindsley, D.H. (1983). Pyroxene thermometry. *Am. Mineralogist*, **68**, 477 - 493.

Lindstrom, D.J. (1983). Kinetic effects on trace element partitioning. *Geochim. Cosmochim. Acta*, **47**, 617 - 622.

---------- and Weill, D.F. (1978). Partitioning of transition metals between diopside and coexisting silicate liquids: I. Nickel, cobalt, and manganese. *Geochim. Cosmochim. Acta*, **42**, 817 - 831.

Lofgren, G. (1980). Experimental studies on the dynamic crystallization of silicate melts, 487 - 551. In Hargraves, R.B., Ed., *Physics of magmatic processes*, Princeton Univ. Press, 585 pp.

Longhi, J., Walker, D. and Hays, J.F. (1976). Fe and Mg in plagioclase. *Proc. 7th Lunar Sci. Conf.*, 1281 - 1300.

Macgregor, I.D. (1974). The system $MgO-Al_2O_3-SiO_2$: Solubility of Al_2O_3 in Enstatite for Spinel and Garnet Peridotite Compositions. *Am. Mineralogist*, **59**, 110 - 119.

Maaloe, S. (1976). The Zoned Plagioclase of the Skaergaard Intrusion, East Greenland. *J. Petrol.*, **17**, 398 - 419.

Maquil, R. and Duchesne, J.-C. (1984). Géothermométrie par les pyroxènes et mise en place du masif anorthositique d'Egersund - Ogna (Rogaland, Norvège méridionale). *Ann. Soc. Géol. Belg.*, **107**, 27 - 49.

Marsh, J.S. (1979). *A manual for X-ray fluorescence determination of major and trace elements in natural silicate rock minerals*. Manual, (unpubl.), Rhodes University, 41 pp.

Maun, A. and Osborn, E.F. (1956). Phase equilibria at liquidus temperatures in the system MgO - FeO - Fe_2O_3 - SiO_2. *J. Am. Cer. Soc.*, **39**, 791 - 802.

McBirney, A.R. and Noyes, R.M. (1979). Crystallization and Layering of the Skaergaard Intrusion. *J. Petrol.*, **20**, 487 - 554.

McCallum, I.S., Raedeke, L.D. and Mathez, E.A. (1980). Investigations of the Stillwater Complex: Part I. Stratigraphy and structure of the Banded Zone. *Am. J. Sci.*, **280 A**, 59 - 87.

McDonald, J.A. (1965). Liquid Immiscibility as one Factor in Chromitite Seam Formation in the Bushveld Complex. *Econ. Geol.*, **60**, 1674 - 1685.

---------- (1967). Evolution of Part of the Lower Critical Zone, Farm Ruighoek, Western Bushveld. *J. Petrol.*, **8**, 165 - 209.

Medaris, L.G. (1975). Coexisting spinel and silicates in alpine peridotites of the granulite facies. *Geochim. Cosmochim. Acta*, **39**, 947 - 958.

Meyer, R. and De Beer, J.H. (1987). Structure of the Bushveld Complex from resistivity measurements. *Nature*, **325**, 610 - 612.

Michot, J. and Michot, P. (1969). The problem of anorthosite: the South Rogaland igneous complex, southwestern Norway. In Isachsen, Y.M., Ed., Origin of Anorthosite and Related Rocks. *N.Y. State Mus. Sci. Serv.*, **Mem. 18**, 399 - 423.

Morse, S.A. (1979a). Kiglapait geochemistry I: Systematics, Sampling, and Density. *J. Petrol.*, **20**, 555 - 590.

---------- (1979b). Reaction constants for En - Fo - Si - equilibria: an adjustment and some applications. *Am. J. Sci.*, **279**, 1060 - 1069.

---------- (1980). *Basalts and Phase Diagrams*. Springer Verlag, New York - Heidelberg - Berlin, 493 pp.

---------- (1982). Kiglapait geochemistry, V: Strontium. *Geochim. Cosmochim. Acta*, **46**, 223 - 234.

---------- (1986). Convection in aid of adcumulus growth. *J. Petrol.* **27**, 1183 - 1214.

---------- (1988). Motion of crystals, solute, and heat in layered intrusions. *Can. Min.*, **26**, 209 - 224.

Morse, S.A. and Nolan, K.M. (1984). Origin of strongly reversed rims on plagioclase in cumulates. *Earth. Plan. Sci. Lett.*, **68**, 485 - 498.

Möller, P. (1988).The dependence of partition coefficients on differences of ionic volumes in crystal-melt systems. *Contr. Min. Petrol.*, **99**, 62 - 69.

Mossom, R.J. (1986). The Atok Platinum Mine (1143-1154). In Anhaeusser, C.R. and Maske, S., Eds., *Mineral Deposits of Southern Africa*, Vol. 2, Geol. Soc. S. Afr., 2335 pp.

Murck, B.W. (1985). *Factors Influencing the Formation of Chromite Seams*. Ph.D. thesis, (unpubl.), University of Toronto, 141 pp.

Naldrett, A.J., Gasparini, E.C., Barnes, S.J., Von Gruenewaldt, G. and Sharpe, M.R. (1986). The Upper Critical Zone of the Bushveld Complex and the Origin of Merensky-type Ores. *Econ. Geol.*, **81**, 1105 - 1117.

Naldrett, A.J. and Wilson, A.H. (1990). Horizontal and vertical variations in noble-metal distribution in the Great Dyke of Zimbabwe: A model for the origin of the PGE mineralization by fractional segregation of sulphide. *Chem. Geol.*, **88**, 279 - 300.

Norrish, K. and Hutton, J.T. (1969). An accurate X-ray spectrographic method for analysis of a wide range of geological samples. *Geochim. Cosmochim. Acta*, **33**, 431 - 453.

Paster, T.P., Schauwecker, D.S. and Haskin, L.A. (1974). The behaviour of some trace elements during solidification of the Skaergaard layered series. *Geochim. Cosmochim. Acta*, **38**, 1549 - 1577.

Pearce, J.A. and Norry, M.J. (1979). Petrogenetic Implications of Ti, Zr, Y and Nb Variations in Volcanic Rocks. *Contr. Min. Petrol.*, **69**, 33 - 47.

Philpotts, J.A. and Schnetzler, C.C. (1970). Phenocryst - matrix partition coefficients for K, Rb, Sr and Ba, with applications to anorthosite and basalt genesis. *Geochim. Cosmochim. Acta*, **34**, 307 - 322.

Pichler, H. and Schmitt-Riegraf, C. (1987). *Gesteinsbildende Minerale im Dünnschliff*, Enke Verlag, Stuttgart, 230 pp.

Poldervaart, A. and Hess, H.H. (1951). Pyroxenes in the crystallization of basaltic magmas. *J. Geol.*, **59**, 472 - 489.

Poulton, K. (1986). *A petrographic and geochemical study of FW3 below pothole and normal Merensky Reef at Impala Platinum Mines: implications for the genesis of potholes.* B.Sc. Hons. project (unpubl.), University of the Witwatersrand, 80 pp.

Reichhardt, F.J. (1989). *A petrological investigation of the transition from the lower to the upper critical zone in the central sector of the eastern Bushveld.* Ph.D. thesis (unpubl.), University of Pretoria.

Reynolds, I.M. (1979). Grain boundary relationships in some Bushveld titaniferous magnetite cumulates. *Geol. Soc. S. Afr. 18th Congr. Proc.*, (ext. abstr.), 297 - 299.

---------- (1987). *Ore deposits associated with mafic and ultramafic rocks.* Manual, (unpubl.), Rhodes University.

Rice, A. (1981). Convective Fractionation: A Mechanism to Provide Cryptic Zoning (Macrosegregation), Layering, Crescumulates, Banded Tuffs and Explosive Volcanism in Igneous Processes. *J. Geophys. Res.*, **86**, 405 - 417.

Ringwood, A.E. (1970). Petrogenesis of Apollo 11 basalts and implications for lunar origin. *J. Geophys. Res.*, **75**, 6453 - 6479.

Rhodes, R.C. (1975). New evidence for impact origin of the Bushveld Complex, South Africa. *Geology*, **3**, 549 - 554.

Roeder, P.L., Campbell, I.H. and Jamieson, H.E. (1979). A re-evaluation of the olivine - spinel geothermometer. *Contr. Min. Petrol.*, **68**, 325 - 334.

Roeder, P.L. and Osborn, E.F. (1966). Experimental data for the system MgO - FeO - Fe_2O_3 - $CaAl_2Si_2O_8$ - SiO_2 and their petrologic implication. *Am. J. Sci.*, **264**, 428 - 480.

Salpas, P.A., Haskin, L.A. and McCallum, I.S. (1983). Stillwater anorthosites: a lunar analogue? *J. Geophys. Res.*, **88**, b27 - b39.

Sampson, E. (1932). Magmatic chromite deposits in Southern Africa. *Econ. Geol.*, **27**, 113 - 144.

Schearer, C.K., Papike, J.J., Simon, S.B. and Shimizu, N. (1989). An ion microprobe study of the intra-crystalline behaviour of REE and selected trace elements in pyroxene from mare basalts with different cooling and crystallization histories. *Geochim. Cosmochim. Acta*, **53**, 1041 - 1054.

Schiffries, C.M. (1984). The Bushveld hydrothermal system. *27th Int. Geol. Congr. (abstr.)*, **2**, 385 - 386.

Schmidt, E.R. (1952). The structure and composition of the Merensky Reef and associated rocks in the Rustenburg Platinum Mine. *Trans. Geol. Soc. S. Afr.*, **55**, 234 - 279.

Scoon, R.N. (1985). *Discordant bodies of postcumulus, ultramafic rock in the Upper Critical Zone of the Bushveld Complex: iron-rich ultramafic pegmatite bodies at Amandelbult and the Driekop platiniferous ultramafic pipe*. Ph.D. thesis, (unpubl.), Rhodes University, 265 pp.

Scoon, R.N. and Teigler, B. (1990). Platinum-group element mineralization in the Critical Zone of the Bushveld Complex: Classification and origin. *23rd Earth Science Congr. of the Geological Society of South Africa (abstr.)*, 501 - 504.

Sharpe, M.R. (1978). "Cone - type" diabases from the eastern Transvaal - representatives of a quenched magma. *Trans. Geol. Soc. S. Afr.*, **81**, 373 - 378.

---------- (1981). The chronology of magma influxes to the eastern compartment of the Bushveld Complex as exemplified by its marginal border group. *J. Geol. Soc. London* , **138**, 307 - 326.

Sharpe, M.R., Bahat, D. and von Gruenewaldt, G. (1981). The concentric elliptical structure of feeder sites to the Bushveld Complex and possible economic implications. *Trans. Geol. S. Afr.*, **84**, 239 - 244.

Sharpe, M.R. and Snyman, J.A. (1980). A model for the emplacement of the eastern compartment of the Bushveld Complex. *Tectonophysics*, **65**, 85 - 110.

Sinton, J.M. (1977). Equilibration History of the Basal Alpine - Type Peridotite, Red Mountain, New Zealand. *J. Petrol.*, **18**, 216 - 246.

Smith, J.V. (1975). Some chemical properties of feldspars, SM 18 - 29. In Ribbe, P.H., Ed., *Feldspar mineralogy. Vol. 2.*

Smits, G. (1988). The distribution of cobalt in mineral constituents of the Merensky Reef and UG2 chromitite layer of the Bushveld Complex. *Mintek (Mineralogy Div.) Report*, **M356**, 7 pp.

South African Committee for Stratigraphy (SACS), (1980). *Stratigraphy of Southern Africa. Part 1. Lithostratigraphy of South Africa, South West Africa/Namibia, and the Republics of Bophuthatswana, Transkei and Venda.* Hbk. Geol. Surv. S. Afr. 8, 690 pp.

Sparks, R.S.J. and Huppert, H.E. (1984). Density changes during the fractional crystallization of basaltic magmas: fluid dynamic implications. *Contr. Min. Petrol.*, **85**, 300 - 309.

Streckeisen, A. (1974). Classification and nomenclature of plutonic rocks. *Geol. Rundschau*, **63(2)**, 773 - 786.

Subcommittee on amphiboles (1978). Nomenclature of amphiboles. *Can. Min.*, **16**, 501 - 520.

Subcommittee on pyroxenes (1989). Nomenclature of pyroxenes. *Can. Min.*, **27**, 143 - 156.

Tankard, A.J., Jackson, M.P.A., Eriksson, K.A., Hobday, D.K., Hunter, D.R. and Minter, W.E.L. (1982). *Crustal Evolution of Southern Africa*, Springer Verlag, Berlin-Heidelberg-New York, 523 pp.

Teigler, B. (1990). *Mineralogy, petrology and geochemistry of the Lower and Lower Critical Zones, northwestern Bushveld Complex.* Ph.D. thesis (unpubl.), Rhodes University, 247 pp.

Truter, F.C. (1955). Modern concepts of the Bushveld Igneous Complex. *C.C.T.A., South Reg. Comm. Geol.*, **1**, 77 - 92.

Turner, A.R., Wolfgram, D. and Barnes, S.J. (1985). Geology of the Stillwater County Sector of the J-M Reef, including the Minneapolis Adit. In Czamanske, G.K., and Zientek, M.L., Eds., The Stillwater Complex, Montana: Geology and Guide. *Montana Bur. Mines Geol.*, **Spec. Publ. 92**, 210 - 231.

Turner, J.S. (1973). *Buoyancy effects in fluids.* Cambridge Univ. Press, 367 pp.

Turner, J.S. and Chen, C.F. (1974). Two-dimensional effects of double-diffusive convection. *J. Fluid Mech.*, **63**, 577 - 593.

Turner, J.S. and Gustafson, L.B. (1978). The Flow of Hot Saline Solutions from Vents in the Sea Floor: Some Implications for Exhalative Sulfide and Other Ore Deposits. *Econ. Geol.*, **73**, 1082 - 1100.

Ulmer, G.L. (1969). Experimental investigations of chromite spinels. *Econ. Geol.*, **Monogr. 4**, 114 - 131.

Ulmer, P. (1989). The dependence of the Fe^{2+} - Mg cation - partitioning between olivine and basaltic liquid on pressure, temperature and composition. An experimental study to 30 kbars. *Contr. Min. Petrol.*, **101**, 261 - 273.

Van Biljon, W.J. (1979). Goud is nie waar dit gevind word nie! *Trans. Geol. Soc. S. Afr.*, **79**, 155 - 167.

Vermaak, C.F. (1976). The Merensky Reef - Thoughts on its Environment and Genesis. *Econ. Geol.*, **71**, 1270 - 1298.

---------- (1985). The UG2 layer - South Africa's slumbering chromite giant. *Chromium Rev.*, **5**.

Viljoen, M.J., De Klerk, W.J., Coetzer, P.M., Hatch, N.P., Kinloch, E. and Peyerl, W. (1986). The Union Section of Rustenburg Platinum Mines Limited, with reference to the Merensky Reef, 1061 - 1090. In Anhaeusser, C.R. and Maske, S., Eds., *Mineral deposits of Southern Africa, Vol. 2*, Geol. Soc. S. Afr., 2335 pp.

Viljoen, M.J. and Feuchtwanger, T. (1977). The northern gap area of the Bushveld Igneous Complex: results of a thermal scanner survey and a summary of available information. *J.C.I. Fundamental Res. Rep. (unpubl.)*, **65**, 14 pp.

Viljoen, M.J. and Hieber, R. (1986). The Rustenburg Section of Rustenburg Platinum Mines Limited, with reference to the Merensky Reef, 1107 - 1134. In Anhaeusser, C.R. and Maske, S., Eds., *Mineral deposits of Southern Africa, Vol. 2*, Geol. Soc. S. Afr., 2335 pp.

Viljoen, M.J. and Scoon, R.N. (1985). The Distribution and Main Geologic Features of Discordant Bodies of Iron-Rich Ultramafic Pegmatite in the Bushveld Complex. *Econ. Geol.*, **80**, 1109 - 1128.

Viljoen, M.J., Theron, J., Underwood, B., Walters, B.M., Weaver, J. and Peyerl, W. (1986). The Amandelbult Section of Rustenburg Platinum Mines Limited, with reference to the Merensky Reef, 1041 - 1060. In Anhaeusser, C.R. and Maske, S., Eds., *Mineral deposits of Southern Africa, Vol. 2*, Geol. Soc. S. Afr., 2335 pp.

Voll, G. (1971). Entmischung von Plagioklasen mit An_{50-55} zu An_{18} + An_{93}. *Fortschr. Mineral.*, **49**, 61 - 63.

Von Buch, L. (1825). *Physikalische Beschreibung der Kanarischen Inseln*, Berlin.

Von Gruenewaldt, G. (1979). A review of some recent concepts of the Bushveld Complex, with particular reference to sulfide mineralization. *Can. Min.*, **17**, 233 - 256.

Von Gruenewaldt, G., Sharpe, M.R. and Hatton, C.J. (1985). The Bushveld Complex: Introduction and Review. *Econ. Geol.*, **80**, 803 - 812.

Wager, L.R. (1959). Differing powers of crystal nucleation as a factor producing diversity in layered igneous intrusions. *Geol. Mag.*, **96**, 75 - 80.

Wager, L.R. and Brown, G.M. (1968). *Layered Igneous Rocks*. Oliver and Boyd, Edinburgh and London, 588 pp.

Wager, L.R., Brown, G.M. and Wadsworth, W.J. (1960). Types of Igneous Cumulates. *J. Petrol.*, **1**, 73 - 85.

Wager, L.R. and Deer, W.A. (1939). Geological investigation in Eastern Greenland, Pt. 3: The petrology of the Skaergaard Intrusion, Kongerdlugssuaq, East Greenland. *Medd. om Groenland*, **105**, 1 - 352.

Walker, K.R. (1970). The Palisade Sill, New Jersey. A reinvestigation. *Geol. Soc. Am.*, **Spec. Pap. III**, 178.

Walraven, F., Armstrong, R.A. and Kruger, F.J. (1990). A chronostratigraphic framework for the north - central Kaapvaal craton, the Bushveld Complex and the Vredefort structure. *Tectonophysics*, **171**, 23 - 48.

Wells, R.A. (1977). Pyroxene Thermometry in Simple and Complex Systems. *Contr. Min. Petrol.*, **62**, 129 - 139.

Willemse, J. (1969). The Geology of the Bushveld Igneous Complex, the Largest Repository of Magmatic Ore Deposits in the World, 1 -22. *Econ. Geol.*, **Monogr. 4**, 366 pp.

Wilson, A.H. (1982) The Geology of the Great 'Dyke', Zimbabwe: The Ultramafic Rocks. *J. Petrol.* **23**, 240 - 292.

Wood, B.J. and Banno, S. (1973). Garnet - Orthopyroxene and Orthopyroxene - Clinopyroxene Relationships in Simple and Complex Systems. *Contr. Min. Petrol.*, **42**, 109 - 124.

Woussen, G., Martignole, J. and Nantel, S. (1988). The Lac - St - Jean Anorthosite in the St - Henri - de - Taillon area (Greenville Province): a relic of a layered complex. *Can. Min.*, **26**, 1013 - 1025.

APPENDIX I

Borehole log of core UA (Sampled and logged by W.J. de Klerk)

Depth in metres	
622.10 - 639.50	Feldspathic pyroxenite
639.50 - 642.50	Pegmatoidal feldspathic pyroxenite (Merensky Reef), with chromitite stringer developed at top and bottom contact
642.50 - 647.82	Mottled anorthosite
647.82 - 652.20	Leuconorite
652.20 - 652.70	Mottled anorthosite
652.70 - 655.50	Leuconorite, with a 2cm anorthosite layer at 655.20
655.50 - 656.20	Melanorite, grading into pyroxenite with a 20 cm poikilitic harzburgite at the base
656.20 - 660.00	Poikilitic harzburgite, coarse-grained, with a 1 cm top and bottom chromitite stringer
660.00 - 661.10	Pegmatoidal feldspathic harzburgite
661.10 - 669.80	Feldspathic pyroxenite
669.80 - 670.80	Poikilitic harzburgite
670.80 - 671.90	Chromitite (UG2)
671.90 - 672.20	Pegmatoidal pyroxenite
672.20 - 673.60	Pyroxenite

Borehole log of core $7E^3$ (Sampled by B. Walters, 1981; logged by W.D. Maier, 1990)

Depth in metres	
395.14 - 397.74	Feldspathic pyroxenite
397.74 - 398.35	Pegmatoidal feldspathic pyroxenite (Merensky Reef), with a 1 cm chromitite stringer at top and bottom contact
398.35 - 403.60	Mottled anorthosite
403.60 - 409.03	Leuconorite
409.03 - 409.46	Mottled anorthosite
409.46 - 411.51	Leuconorite, grading into norite
411.51 - 412.81	Norite
412.81 - 413.10	Pegmatoidal harzburgite
413.10 - 416.80	Poikilitic harzburgite, coarse-grained and occasionally feldspathic, with a 3 mm basal chromitite
416.80 - 418.90	Mottled anorthosite, olivine-bearing, grading into leuconorite
418.90 - 424.38	Leuconorite, grading into mottled anorthosite
424.38 - 425.32	Troctolite, coarse-grained
425.32 - 425.41	Poikilitic feldspathic harzburgite, with a 3mm basal chromitite and 1 cm disseminated chromite zone at the top
425.41 - 425.80	Pegmatoidal pyroxenite
425.80 - 434.00	Feldspathic pyroxenite

434.00 - 434.27	Poikilitic harzburgite
434.27 - 434.42	Chromitite (UG2)
434.42 - 435.51	Serpentinized fault zone, ± 14 m displacement
435.51 - 438.67	Feldspathic pyroxenite

Borehole log of core EK22 (Logged and sampled by W.D. Maier, 1989)

Depth in metres

265.42 - 266.55	Feldspathic pyroxenite (Merensky pyroxenite)
266.55 - 267.59	Feldspathic pegmatite
267.59 - 272.15	Mottled anorthosite
272.15 - 277.40	Norite
277.40 - 277.82	Mottled anorthosite
277.82 - 283.63	Leuconorite, grading into norite
283.63 - 285.90	Mottled anorthosite, with a 1cm chromitite stringer (Lone Chrome seam) at 284.22
285.90 - 288.20	Norite, grading into leuconorite
288.20 - 288.32	Poikilitic harzburgite
288.32 - 288.60	Leuconorite, 3cm of anorthosite at the top
288.65 - 288.90	Five cm of poikilitic harzburgite, underlain by 15 cm of troctolite, grading into poikilitic harzburgite
288.90 - 288.95	Leuconorite
288.95 - 289.02	Feldspathic pyroxenite
289.02 - 291.43	Norite
291.43 - 291.53	Olivine norite grading into troctolite and poikilitic harzburgite
291.53 - 292.10	Leuconorite
292.10 - 292.25	Melanocratic dyke
292.25 - 292.30	Poikilitic feldspathic harzburgite
292.30 - 294.27	Norite
294.27 - 295.00	Leucocratic dyke
295.00 - 295.37	Leuconorite, olivine-bearing at base
295.37 - 299.85	Feldspathic harzburgite
299.85 - 300.02	Poikilitic harzburgite, with 1 mm basal chromitite
300.02 - 300.40	Anorthosite
300.40 - 306.45	Leuconorite, with a 1 cm pyroxenite with basal chromitite stringer at 306.30
306.45 - 307.30	Pegmatoidal pyroxenite, chromitite stringer plus overlying 5 mm troctolite at top
307.30 - 314.15	Feldspathic pyroxenite, with lens of feldspathic harzburgite at 313.60
314.15 - 314.30	Chromitite (UG2 "leader")
314.30 - 314.40	Pyroxenite
314.40 - 314.50	Chromitite (UG2 "leader")
314.50 - 314.60	Pyroxenite
314.60 - 315.50	Chromitite (UG2)
315.50 - 315.61	Pegmatoidal harzburgite
315.61 - 322.15	Norite

Borehole log of core 60E[3] (Sampled by B. Walters, 1981; logged by W.D. Maier, 1990)

Depth in metres

121.67 - 122.09	Feldspathic pyroxenite (Merensky Reef), with a 1 cm chromitite stringer at top and bottom contact
122.09 - 122.38	Anorthosite
122.38 - 125.91	Leuconorite
125.91 - 128.08	Norite, olivine-bearing at base
128.08 - 128.43	Anorthosite, grading into norite
128.43 - 129.35	Norite
129.35 - 129.45	Troctolite
129.45 - 131.19	Leuconorite, grading into norite
131.19 - 134.42	Norite
134.42 - 134.47	Pegmatoidal harzburgite, with a 1 cm basal chromitite
134.47 - 134.50	Anorthosite
134.50 - 134.96	Olivine norite, fine-grained and laminated ("streaky"), 2cm of anorthosite at base
134.96 - 135.11	Norite
135.11 - 136.11	Olivine norite
136.11 - 136.26	Troctolite
136.26 - 137.58	Olivine norite, fine-grained and laminated
137.58 - 137.78	Poikilitic harzburgite
137.78 - 160.04	Olivine norite
139.30 - 139.60	Poikilitic feldspathic harzburgite
141.10 - 141.15	" " "
144.90 - 145.00	" " "
145.55 - 145.70	" " "
144.70 - 144.73	Melanorite
147.20 - 147.60	Poikilitic feldspathic harzburgite
152.00 - 152.30	" " "
160.04 - 160.34	Troctolite
160.34 - 161.50	Leuconorite, grading into anorthosite
161.50 - 165.13	Mottled anorthosite
164.35 - 164.85	Altered zone, with basal 1 cm chromitite
165.13 - 165.92	Leuconorite, grading into anorthosite
165.92 - 171.04	Mottled anorthosite
171.04 - 172.10	Pegmatoidal harzburgite, with disseminated chromite zone at top
172.10 - 182.64	Feldspathic pyroxenite
182.64 - 183.08	Poikilitic harzburgite
183.08 - 183.18	Pyroxenite
183.18 - 183.34	Chromitite (UG2)
183.34 - 183.48	Pyroxenite
183.48 - 183.68	Chromitite (UG2)
183.68 - 185.44	Pegmatoidal harzburgite, grading into pegmatoidal pyroxenite
185.44 - 188.10	Leuconorite

Borehole log of core IN (Sampled by R.H. Smithies and B. Teigler, 1987, logged by W.D. Maier, 1990)

Depth in metres

802.74 - 804.52	Feldspathic pyroxenite (Merensky pyroxenite), with a 2.5cm thick chromitite stringer at the base
804.52 - 809.50	Mottled anorthosite
809.50 - 814.20	Leuconorite
814.20 - 814.55	Anorthosite
809.50 - 817.14	Leuconorite
817.14 - 817.20	Melanorite
817.20 - 817.30	Anorthosite
817.30 - 817.50	Leuconorite
817.50 - 820.02	Norite, with 0.5 cm thick chromitite stringer at base
820.02 - 820.95	Mottled anorthosite
820.95 - 833.30	Olivine norite
833.30 - 835.50	Olivine norite, fine-grained and laminated
835.50 - 866.02	Olivine norite
863.60 - 864.13	Pegmatite
866.02 - 866.05	Harzburgite (1cm), underlain by pyroxenite (1cm) plus basal 0.2cm thick chromitite
866.05 - 866.20	Harzburgite
866.20 - 866.45	Troctolite
866.45 - 866.55	Norite
866.55 - 866.58	Pegmatoidal pyroxenite, with a 2mm thick basal chromitite
866.58 - 871.34	Mottled anorthosite
871.34 - 871.80	Harzburgite, coarse-grained, with 15 cm of pegmatoidal pyroxenite at the base
871.80 - 881.21	Pyroxenite
878.93 - 879.03	Chromitite
879.10 - 879.22	Chromitite
879.43 - 879.46	Chromitite
880.12 - 880.17	Chromitite
881.21 - 881.73	Chromitite (UG2)
881.73 - 882.60	Pegmatoidal pyroxenite, with basal 0.3cm thick chromitite
882.60 - 890.67	Leuconorite

Borehole log of core IM (Sampled by R.H. Smithies and B. Teigler, 1987; logged by W.D. Maier, 1990)

Depth in metres

785.00 - 786.39	Feldspathic pyroxenite (Merensky pyroxenite), with a 1.5 cm basal chromitite stringer
786.39 - 788.54	Leuconorite, grading into norite and olivine norite
788.54 - 788.60	Anorthosite, with sporadic pegmatoidal harzburgite at top
788.60 - 788.66	Pegmatoidal harzburgite
788.66 - 793.18	Norite, grading into leuconorite

793.18 - 794.48	Norite, with two 5 cm anorthosite layers at 793.22-793.35, the upper one being sulphide bearing
794.48 - 795.59	Mottled anorthosite, with 1 cm basal chromitite and a 1 cm disseminated chromite zone towards top
795.59 - 795.79	Altered zone
795.79 - 797.20	Olivine norite
797.20 - 798.10	Olivine norite, fine-grained and laminated
798.10 - 819.50	Olivine norite
819.50 - 823.80	Troctolite, grading into mottled anorthosite
823.80 - 825.83	Mottled anorthosite, olivine-bearing towards top
825.83 - 826.00	Leuconorite
826.00 - 826.15	Poikilitic feldspathic harzburgite
826.15 - 838.50	Norite, grading into leuconorite and mottled anorthosite
838.50 - 848.91	Mottled anorthosite, olivine-bearing at top
848.91 - 849.50	Pegmatite
849.50 - 855.04	Pyroxenite, coarse-grained at top
855.04 - 855.24	Chromitite (UG2), with sporadic pegmatoid at base
855.24 - 855.49	Anorthosite

Underground log of intersection TF (Sampled by C.A. Lee, 1989)

Depth in metres

836.10 - 837.05	Feldspathic pyroxenite
837.05 - 837.30	Pegmatoidal pyroxenite (Merensky Reef), with 1cm top and bottom chromitite stringer
837.30 - 837.70	Mottled anorthosite
837.70 - 860.05	Norite
860.05 - 867.00	Mottled anorthosite, with pyroxenitic/harzburgitic "boulders" towards the base
867.00 - 911.00	Norite, olivine-bearing towards the top
911.00 - 918.20	Mottled anorthosite
918.20 - 946.30	Norite
946.30 - 951.80	Dyke
951.80 - 954.70	Mottled anorthosite
954.70 - 965.20	Feldspathic pyroxenite
965.20 - 966.00	Chromitite (UG2)
966.00 - 966.40	Feldspathic pyroxenite
966.40 - 968.30	Norite

Borehole log of core LK7 (Sampled and logged by W.D. Maier, 1988)

Depth in metres

1378.91 - 1389.70	Feldspathic pyroxenite (Merensky pyroxenite), with chromitite stringer at base
1389.70 - 1389.85	Leuconorite
1389.85 - 1391.00	Mottled anorthosite
1391.00 - 1407.05	Leuconorite, grading into norite
1407.05 - 1407.65	Mottled anorthosite
1407.65 - 1413.25	Leuconorite
1413.25 - 1414.00	Mottled anorthosite

1414.00 - 1418.95	Leuconorite
1418.95 - 1420.05	Mottled anorthosite
1420.05 - 1421.55	Leuconorite
1421.55 - 1424.65	Mottled anorthosite, with a 5 mm chromitite at 1424.20 (Lone Chrome seam) and a pyroxenitic "boulder" at 1424.30
1424.65 - 1425.20	Leuconorite
1425.20 - 1425.40	Mottled anorthosite
1425.40 - 1427.60	Leuconorite
1427.60 - 1428.10	Anorthosite
1428.10 - 1429.23	Leuconorite
1429.23 - 1429.54	Anorthosite
1429.54 - 1430.95	Norite, interlayered with leuconorite and anorthosite lenses and schlieren ("Norite Marker")
1430.95 - 1558.20	Norite, grading into leuconorite
1558.20 - 1578.55	Mottled anorthosite, with a leuconoritic layer at 1569.8
1575.85 - 1575.88	Norite, fine-grained
1577.45 - 1577.50	Norite, fine-grained
1578.55 - 1578.63	Pyroxenite, with 2 mm chromitite at top and bottom contact
1578.63 - 1578.70	Mottled anorthosite
1578.70 - 1583.68	Feldspathic pyroxenite, with a 17 cm thick UG2 "leader" chromitite at 1582.52 - 1582.69
1583.68 - 1585.19	Chromitite (UG2)
1585.19 - 1586.70	Pegmatoidal harzburgite
1586.70 -	Norite

Borehole log of core H3 (Sampled and logged by W.D. Maier, 1988)

Depth in metres

1036.26 - 1048.62	Feldspathic pyroxenite (Merensky pyroxenite)
1048.62 - 1054.00	Mottled anorthosite
1054.00 - 1062.15	Leuconorite, grading into norite and olivine norite
1062.15 - 1066.05	Leuconorite, grading into norite, "Corona structures" throughout both of them
1066.05 - 1066.60	Mottled anorthosite, grading into leuconorite
1066.60 - 1071.10	Leuconorite
1071.10 - 1072.90	Mottled anorthosite
1072.90 - 1076.25	Leuconorite
1076.25 - 1077.70	Mottled anorthosite
1077.70 - 1078.05	Leuconorite
1078.05 - 1083.20	Mottled anorthosite, pyroxenitic "boulder" intersected at 1081.79
1083.20 - 1085.30	Leuconorite
1085.30 - 1085.80	Mottled anorthosite
1085.80 - 1087.35	Leuconorite
1087.35 - 1087.60	Mottled anorthosite
1087.60 - 1088.00	Norite, with 5 cm anorthosite at base

1088.00 - 1092.00	Leuconorite, interlayered with anorthosites ("Norite Marker"). One cm of pyroxenite at 1089.25 and 2 cm of fine-grained troctolite at 1089.65
1092.00 - 1232.00	Norite, grading into leuconorite
1232.00 - 1252.00	Mottled anorthosite, with leuconoritic zone at 1246.65
1252.00 - 1252.60	Leuconorite, interlayered with anorthosite
1252.60 - 1253.30	Mottled anorthosite
1253.30 - 1253.45	Leuconorite, with a 3 mm chromitite stringer at top
1253.45 - 1264.10	Pyroxenite
1264.10 - 1265.30	Chromitite (UG2), with a 2 cm pyroxenite at 1265.18
1265.30 - 1265.95	Pegmatoidal pyroxenite
1265.95 - 1270.79	Norite

Borehole log of core KR2 (Sampled and logged by W.D. Maier, 1988)

Depth in metres

1130.79 - 1144.06	Feldspathic pyroxenite (Merensky pyroxenite), with a 3 mm chromitite at the base
1144.06 - 1149.10	Mottled anorthosite
1149.10 - 1155.00	Leuconorite
1155.00 - 1160.00	Norite
1160.00 - 1162.25	Leuconorite
1162.25 - 1162.83	Mottled anorthosite
1162.83 - 1166.87	Leuconorite
1166.87 - 1168.50	Mottled anorthosite
1168.50 - 1170.05	Leuconorite
1170.05 - 1178.46	Mottled anorthosite, 2 pyroxenitic "boulders" intersected at 1177.00 and 1177.70
1174.10 - 1174.70	Leuconorite
1178.46 - 1181.00	Leuconorite
1181.00 - 1181.20	Mottled anorthosite
1181.20 - 1185.90	Norite, grading into leuconorite
1185.90 - 1186.73	Mottled anorthosite, with 20cm of leuconorite at the base
1186.73 - 1187.65	Melanorite
1187.65 - 1187.75	Poikilitic harzburgite
1187.75 - 1191.58	Melanorite
1191.58 - 1193.75	Melanorite, interlayered with anorthosite ("Norite Marker")
1193.75 - 1276.10	Norite, grading into leuconorite
1276.10 - 1287.04	Mottled anorthosite
1287.04 - 1287.38	Leuconorite, with irregular chromitite stringers at base
1287.38 - 1298.14	Pyroxenite
1298.14 - 1299.67	Chromitite (UG2)
1299.67 - 1300.40	Pegmatoidal pyroxenite
1300.40 - 1305.79	Norite

APPENDIX II

Rock Modes

Modal compositions (in vol %) of 193 samples from 6 cores have been determined by the author for 8 components (cumulus and intercumulus orthopyroxene, cumulus and intercumulus plagioclase, olivine, chromite, cpx, others (mica, amphibole, magnetite, sulphides, alteration phases)) by the point-counting technique. In section UA, only the modal composition of the UG2 pyroxenite has been determined.

The following abbreviations have been used in the tables:

pla = plagioclase
opx = orthopyroxene
cpx = clinopyroxene
chr = chromite
ol = olivine
oth = others
ic = intercumulus
cum = cumulus

Modal compositions in the EK22 sequence

Sample	Pla	Opx	Ol	Chr	Pla(ic)	Opx(ic)	Cpx	Other	Total
272.25	83.4	6.7	0.0	0.0	0.0	4.8	3.5	1.6	100.0
274.78	92.9	4.3	0.0	0.0	0.0	1.7	0.8	0.3	100.0
277.90 a	96.0	0.0	0.0	0.0	0.0	3.1	0.9	0.0	100.0
277.90 b	89.1	6.2	0.0	0.0	0.0	1.7	2.5	0.5	100.0
280.65	76.4	20.8	0.0	0.0	0.0	2.2	0.6	0.0	100.0
282.80 a	42.3	54.4	0.0	0.0	0.0	0.0	2.5	0.8	100.0
284.25	96.0	0.0	0.0	0.0	0.0	0.0	4.0	0.0	100.0
285.80 a	97.1	0.0	0.0	0.9	0.0	2.0	0.0	0.0	100.0
286.05	74.5	21.1	0.0	0.0	0.0	1.6	2.8	0.0	100.0
288.40 b top	35.5	0.0	31.7	3.1	0.0	26.6	0.0	3.1	100.0
288.40 b base	99.0	0.0	0.0	0.0	0.0	0.0	1.0	0.0	100.0
288.90 a	77.5	0.0	21.4	0.5	0.0	0.0	0.3	0.3	100.0
288.95	81.2	13.6	0.0	0.0	0.0	0.0	3.9	1.3	100.0
291.48	71.4	0.0	24.9	0.3	0.0	1.1	0.0	2.3	100.0
292.05	73.9	20.6	0.0	0.3	0.0	2.7	0.0	2.5	100.0
293.60 a	75.5	22.8	0.0	0.3	0.0	0.2	0.9	0.3	100.0
295.70	0.0	0.0	91.7	0.3	7.0	0.0	0.0	1.0	100.0
296.90	0.0	0.0	66.3	0.3	2.2	28.9	0.0	2.3	100.0
299.10	0.0	42.3	32.7	0.3	12.4	8.6	0.9	2.8	100.0
299.80	0.0	0.0	43.9	0.3	6.8	45.1	0.0	3.9	100.0
299.95	0.0	0.0	12.1	1.0	6.9	72.8	5.1	2.1	100.0
300.27	97.4	0.0	0.0	0.3	0.3	0.0	1.0	1.0	100.0
300.60 a	94.4	4.0	0.0	0.3	0.3	0.0	1.0	0.0	100.0
303.90	82.7	14.3	0.0	0.3	0.3	0.0	0.0	2.4	100.0
306.50 b	0.0	74.1	0.0	2.0	21.9	0.0	0.0	2.0	100.0
307.66	0.0	83.5	0.0	0.5	15.0	0.0	0.0	1.0	100.0
313.00	0.0	70.0	0.0	3.8	25.2	0.0	0.0	1.0	100.0

Modal compositions in the IN sequence

Sample	Pla	Opx	Ol	Chr	Pla(ic)	Opx(ic)	Cpx	Other	Total
806.92	89.3	5.5	0.0	2.7	0.0	0.0	2.5	0.0	100.0
809.77	81.1	15.5	0.0	0.0	0.0	0.9	2.4	0.1	100.0
811.78	79.9	17.1	0.0	0.0	0.0	2.3	0.7	0.0	100.0
815.38	86.5	11.7	0.0	0.0	0.0	0.0	1.8	0.0	100.0
817.10	45.0	52.5	0.0	0.0	0.0	0.0	0.5	2.0	100.0
817.50	72.0	24.5	0.0	0.0	0.0	0.0	3.5	0.0	100.0
817.68	34.5	64.0	0.0	0.0	0.0	0.0	1.4	0.1	100.0
819.15	57.4	40.2	0.0	0.0	0.0	0.0	2.4	0.0	100.0
820.55	93.8	0.9	0.0	0.0	0.0	4.4	0.9	0.0	100.0
821.23 a	64.4	35.0	0.0	0.0	0.0	0.0	0.6	0.0	100.0
821.23 b	59.0	40.5	0.0	0.0	0.0	0.0	0.4	0.1	100.0
826.00	72.1	26.6	0.0	0.0	0.0	0.0	0.9	0.4	100.0
831.72	74.7	20.5	3.4	0.0	0.0	0.0	1.2	0.2	100.0
837.86	57.5	31.0	9.7	0.0	0.0	0.5	1.0	0.3	100.0
844.00 top+base	72.4	25.7	1.0	0.0	0.0	0.0	0.9	0.0	100.0
844.00 mid	99.0	0.0	0.0	0.0	0.0	0.0	0.0	1.0	100.0
850.73	67.8	26.9	5.0	0.0	0.0	0.0	0.3	0.0	100.0
858.55	65.5	33.0	1.2	0.0	0.0	0.0	0.3	0.0	100.0
863.12	59.0	30.6	9.5	0.0	0.0	0.0	0.6	0.3	100.0
865.52	74.1	22.9	1.4	0.0	0.0	0.0	1.4	0.2	100.0
866.40	61.2	8.9	26.8	1.8	0.0	0.0	0.6	0.7	100.0
870.92	97.8	0.0	0.0	0.0	0.0	1.1	1.1	0.0	100.0
871.93	0.0	97.5	0.0	1.0	0.0	0.0	1.4	0.1	100.0
872.50	0.0	84.6	0.0	0.3	14.3	0.0	0.8	0.0	100.0
875.75	0.0	70.0	0.0	0.0	8.0	0.0	20.6	1.4	100.0
877.28	0.0	83.5	0.8	1.0	1.0	0.0	12.6	1.1	100.0
880.50	0.0	85.0	0.0	0.5	13.6	0.0	0.8	0.1	100.0

Modal compositions in the IM sequence

Sample	Pla	Opx	Ol	Chr	Pla(ic)	Opx(ic)	Cpx	Other	Total
787.90	48.7	45.4	0.0	0.0	0.0	0.0	0.8	5.1	100.0
788.32	51.3	45.6	0.0	0.0	0.0	0.0	0.6	2.5	100.0
788.60 a	29.2	58.2	6.6	0.0	0.0	0.0	1.5	4.5	100.0
788.60 b top	99.0	0.0	0.0	0.0	0.0	0.0	0.0	1.0	100.0
788.80	39.0	48.7	11.0	0.0	0.0	0.0	0.3	1.0	100.0
789.75	44.9	52.1	0.0	0.0	0.0	0.0	2.6	0.4	100.0
790.64	81.9	15.2	0.0	0.0	0.0	0.0	2.0	0.9	100.0
793.22 b	79.9	11.1	0.0	0.0	0.0	0.0	8.8	0.3	100.0
793.22 c	93.0	5.4	0.0	0.0	0.0	1.0	0.5	0.1	100.0
794.10	67.0	28.2	0.0	0.0	0.0	0.0	2.9	1.9	100.0
794.53	97.3	0.0	0.0	0.0	0.0	0.0	2.3	0.4	100.0
795.50	91.0	0.0	0.0	0.0	0.0	0.0	0.0	9.0	100.0
796.25	75.2	16.6	4.4	0.5	0.0	0.0	0.3	3.0	100.0
797.25	71.0	3.9	20.5	1.5	0.0	0.0	1.0	2.1	100.0
798.00	67.0	6.5	21.4	1.5	0.0	0.0	1.6	2.0	100.0
801.00	54.3	41.0	2.0	0.0	0.0	0.0	2.0	0.8	100.0
804.40	71.0	23.3	2.0	0.0	0.0	0.0	1.0	2.7	100.0
808.00	54.7	21.5	21.7	0.0	0.0	0.0	0.6	1.5	100.0
810.10	65.9	24.6	6.4	0.0	0.0	0.0	1.6	1.5	100.0
814.00 a	63.5	30.3	3.6	0.0	0.0	0.0	2.3	0.3	100.0
818.00	64.6	30.2	4.4	0.0	0.0	0.0	0.4	0.4	100.0
819.30	75.6	22.2	0.0	0.3	0.0	0.0	1.0	1.0	100.0
819.85	85.6	0.0	11.7	0.0	0.0	1.3	0.0	1.4	100.0
823.05	99.0	0.0	0.0	0.6	0.0	0.0	0.3	0.1	100.0
825.55	95.4	0.0	0.0	0.0	0.0	0.0	4.5	0.1	100.0
826.10 b	40.0	5.8	6.1	1.9	0.0	0.0	3.0	43.2	100.0
827.65	91.7	4.9	0.0	0.0	0.0	0.0	1.0	2.4	100.0
836.00	88.0	8.0	0.0	0.0	0.0	0.0	3.1	0.9	100.0
839.00	79.1	4.6	0.0	0.0	0.0	12.0	3.4	0.9	100.0
841.67	81.0	0.0	10.0	0.0	0.0	3.5	4.0	1.5	100.0
843.61	94.6	0.0	0.0	0.8	0.0	0.0	2.0	2.6	100.0
845.80	95.0	0.0	0.0	0.0	0.0	0.0	0.0	5.0	100.0
848.52	88.4	0.0	0.0	0.6	0.0	7.5	0.0	3.5	100.0
849.50	0.0	51.6	0.0	0.0	1.8	0.0	1.8	44.8	100.0
851.90	0.0	46.6	0.0	0.0	21.0	0.0	7.0	25.4	100.0
853.95	0.0	76.0	0.0	0.0	5.6	0.0	2.4	16.0	100.0
856.00	77.2	21.3	0.0	0.0	0.0	0.0	0.8	0.7	100.0
859.22	83.4	14.3	0.0	0.0	0.0	0.0	1.4	0.9	100.0

Modal compositions in the LK7 sequence

Sample	Pla	Opx	Ol	Chr	Pla(ic)	Opx(ic)	Cpx	Other	Total
1389.70	75.4	16.5	0.0	0.0	0.0	7.4	0.0	0.7	100.0
1392.50 a	87.2	8.6	0.0	0.0	0.0	2.8	1.1	0.3	100.0
1395.60	85.0	14.5	0.0	0.0	0.0	0.0	0.5	0.0	100.0
1401.95	70.2	29.3	0.0	0.0	0.0	0.0	0.5	0.0	100.0
1407.05	94.0	0.0	0.0	0.0	0.0	3.1	2.0	0.9	100.0
1407.85	93.1	2.0	0.0	0.0	0.0	1.0	1.9	2.0	100.0
1412.35 a	79.7	10.6	0.0	0.0	0.0	1.8	1.4	6.5	100.0
1415.05	86.0	8.2	0.0	0.0	0.0	1.9	3.0	0.9	100.0
1418.90 a	83.6	10.7	0.0	0.0	0.0	0.0	5.7	0.0	100.0
1421.10 a	86.1	10.9	0.0	0.0	0.0	1.0	1.0	1.0	100.0
1424.28 b top	0.0	73.9	0.0	0.0	17.4	0.4	1.2	7.1	100.0
1424.80	91.8	7.2	0.0	0.0	0.0	0.0	1.0	0.0	100.0
1429.54	76.0	17.5	0.0	0.0	0.0	0.0	6.5	0.0	100.0
1429.73 base	76.5	20.7	0.0	0.0	0.0	0.0	1.3	1.5	100.0
1430.10 mid	66.4	29.2	0.0	0.0	0.0	0.0	4.4	0.0	100.0
1437.25 b	70.7	26.4	0.0	0.0	0.0	0.0	0.7	2.2	100.0
1441.25 a	74.4	22.9	0.0	0.0	0.0	0.0	2.5	0.2	100.0
1446.20	59.2	37.4	0.0	0.0	0.0	0.0	3.4	0.0	100.0
1451.60	64.6	33.1	0.0	0.0	0.0	0.0	2.3	0.0	100.0
1457.35	59.6	38.2	0.0	0.0	0.0	0.4	1.8	0.0	100.0
1464.56	38.9	44.7	0.0	0.0	0.0	0.0	16.0	0.4	100.0
1470.00 a	54.9	37.3	0.0	0.0	0.0	0.2	7.6	0.0	100.0
1476.10	69.9	25.1	0.0	0.0	0.0	0.0	5.0	0.0	100.0
1481.26	72.7	26.0	0.0	0.0	0.0	0.0	0.5	0.8	100.0
1487.00 a	64.8	32.2	0.0	0.0	0.0	0.0	2.1	0.9	100.0
1491.10	72.4	26.0	0.0	0.0	0.0	0.0	1.4	0.2	100.0
1498.00	71.6	26.4	0.0	0.0	0.0	0.0	1.8	0.2	100.0
1506.00	70.5	28.3	0.0	0.0	0.0	0.0	1.0	0.2	100.0
1511.10 b	79.8	19.2	0.0	0.0	0.0	0.0	1.0	0.0	100.0
1515.00	81.0	13.2	0.0	0.0	0.0	0.3	5.5	0.0	100.0
1523.10	93.8	3.5	0.0	0.0	0.0	1.5	0.6	0.6	100.0
1525.80	70.5	24.2	0.0	0.0	0.0	0.0	4.0	1.3	100.0
1528.90 a	77.2	12.3	0.0	0.0	0.0	0.0	5.3	5.2	100.0
1539.10	84.1	13.8	0.0	0.0	0.0	1.4	0.7	0.0	100.0
1548.85 b	81.3	14.5	0.0	0.0	0.0	0.0	4.0	0.2	100.0
1556.56	90.6	7.5	0.0	0.0	0.0	0.4	0.9	0.6	100.0
1562.25 b	97.0	0.0	0.0	0.0	0.0	1.0	2.0	0.0	100.0
1566.00 a	93.8	0.0	0.0	0.0	0.0	2.0	4.2	0.0	100.0
1569.80	87.1	2.9	0.0	0.0	0.0	1.0	9.0	0.0	100.0
1573.75 a	92.1	0.0	0.0	0.0	0.0	5.9	2.0	0.0	100.0
1575.95 b base	97.0	0.0	0.0	0.0	0.0	3.0	0.0	0.0	100.0
1577.45 top	73.8	24.4	0.0	0.0	0.0	0.0	1.8	0.0	100.0
1578.43 b base	0.0	67.3	0.0	0.0	23.3	0.0	7.9	1.5	100.0
1578.43 c top	0.0	75.9	0.0	2.3	8.6	0.0	7.5	5.7	100.0
1578.43 c base	98.9	0.0	0.0	0.0	0.0	0.0	1.1	0.0	100.0
1578.70	0.0	68.8	0.0	0.0	19.7	0.0	9.0	2.5	100.0
1581.88 b	0.0	5.5	18.9	1.7	21.6	40.3	10.6	1.4	100.0
1582.70 a	0.0	57.7	0.0	0.0	23.3	1.0	6.5	11.5	100.0

Modal compositions in the H3 sequence

Sample	Pla	Opx	Ol	Chr	Pla(ic)	Opx(ic)	Cpx	Other	Total
1049.80	95.2	0.0	0.0	0.0	0.0	0.0	0.0	4.8	100.0
1054.10	98.0	0.0	0.0	0.0	0.0	0.0	2.0	0.0	100.0
1060.05	79.7	18.5	0.0	0.0	0.0	0.0	1.8	0.0	100.0
1062.50	40.1	56.9	0.0	0.0	0.0	0.0	2.5	0.5	100.0
1063.25	82.5	16.0	0.0	0.0	0.0	0.0	1.5	0.0	100.0
1065.05	67.6	31.4	0.0	0.0	0.0	0.0	1.0	0.0	100.0
1066.00	57.1	15.4	0.0	0.0	0.0	0.0	13.5	14.0	100.0
1066.80	93.0	0.0	0.0	0.0	0.0	0.0	0.0	7.0	100.0
1067.15	71.0	26.5	0.0	0.0	0.0	0.0	1.0	1.5	100.0
1071.05	80.5	12.3	0.0	0.0	0.0	0.0	7.0	0.2	100.0
1072.70	95.0	0.0	0.0	0.0	0.0	0.0	0.0	5.0	100.0
1073.00	84.8	9.6	0.0	0.0	0.0	1.6	1.0	3.0	100.0
1076.25	93.6	0.0	0.0	0.0	0.0	0.0	4.8	1.6	100.0
1078.80	94.7	0.0	0.0	0.0	0.0	0.0	5.3	0.0	100.0
1081.64 c	25.1	51.7	0.0	0.6	0.0	0.0	0.6	22.0	100.0
1082.10	95.3	0.0	0.0	0.0	0.0	2.7	2.0	0.0	100.0
1083.15	92.2	3.8	0.0	0.0	0.0	1.0	3.0	0.0	100.0
1084.85	92.0	5.7	0.0	0.0	0.0	0.0	2.1	0.2	100.0
1085.60	95.2	0.0	0.0	0.0	0.0	0.0	0.0	4.8	100.0
1086.50	84.3	12.2	0.0	0.0	0.0	0.0	0.9	2.6	100.0
1087.65	81.0	15.8	0.0	0.0	0.0	2.6	0.3	0.3	100.0
1088.10 a top	33.0	65.1	0.0	0.0	1.9	0.0	0.0	0.0	100.0
1088.10 a base	94.6	0.0	0.0	1.6	0.0	1.8	1.2	0.8	100.0
1088.10 b	79.6	19.6	0.0	0.0	0.0	0.0	0.0	0.8	100.0
1089.25 top	17.1	80.9	0.0	0.0	1.6	0.0	0.0	0.4	100.0
1089.40 b top+bas	47.3	49.7	0.0	0.0	2.0	0.0	1.0	0.0	100.0
1089.40 b mid	99.1	0.0	0.0	0.0	0.0	0.0	0.9	0.0	100.0
1089.65	14.3	46.0	29.7	0.8	1.0	0.0	0.0	8.2	100.0
1090.20 a	44.7	46.0	0.0	0.0	0.0	0.0	9.0	0.3	100.0
1090.20 b	50.5	48.0	0.0	0.0	0.0	0.3	0.6	0.6	100.0
1091.80	60.0	38.2	0.0	0.3	0.0	0.6	0.9	0.0	100.0
1099.35	68.3	30.0	0.0	0.0	0.0	0.0	1.3	0.4	100.0
1110.05	67.4	30.0	0.0	0.3	0.0	0.0	2.0	0.3	100.0
1118.50	62.7	32.0	0.0	0.0	0.0	0.3	4.0	1.0	100.0
1127.50	62.7	35.0	0.0	0.0	0.0	0.6	1.3	0.4	100.0
1135.35	69.7	29.6	0.0	0.0	0.0	0.0	0.7	0.0	100.0
1144.10	69.0	30.0	0.0	0.0	0.0	0.0	0.7	0.3	100.0
1146.90	66.2	30.7	0.0	0.0	0.0	0.7	1.1	1.3	100.0
1156.46	64.2	34.0	0.0	0.0	0.0	0.3	1.1	0.4	100.0
1166.10	66.0	32.2	0.0	0.0	0.0	0.0	0.6	1.2	100.0
1175.80	68.5	26.7	0.0	0.0	0.0	0.0	3.6	1.2	100.0
1182.20	77.3	21.0	0.0	0.0	0.0	0.0	0.8	0.9	100.0
1191.50	76.0	21.8	0.0	0.0	0.0	0.0	1.9	0.3	100.0
1200.30	81.7	14.1	0.0	0.0	0.0	0.0	3.9	0.3	100.0
1211.85	80.1	17.1	0.0	0.0	0.0	0.0	2.3	0.5	100.0
1219.05	78.0	18.0	0.0	0.0	0.0	0.0	3.5	0.5	100.0
1228.25	74.4	19.3	0.0	0.0	0.0	0.0	5.7	0.6	100.0
1231.35	90.3	6.8	0.0	0.0	0.0	0.0	2.3	0.6	100.0
1233.90	92.2	0.0	0.0	0.0	0.0	0.0	0.0	7.8	100.0
1244.05	88.6	0.0	0.0	0.0	0.0	0.0	0.0	11.4	100.0
1246.65	89.2	7.7	0.0	0.0	0.0	0.0	2.8	0.3	100.0
1250.35	91.7	0.0	0.0	0.0	0.0	3.1	5.2	0.0	100.0
1252.50	45.2	47.9	0.0	2.0	0.0	0.0	4.9	0.0	100.0
1253.30 a	68.0	23.6	0.0	6.3	0.0	1.3	0.3	0.5	100.0
1256.75	1.0	73.2	0.0	0.0	16.3	6.5	0.7	2.3	100.0
1258.45	0.0	75.8	0.0	2.2	10.8	2.6	4.2	4.4	100.0
1261.15 a	0.0	81.5	0.0	6.7	10.5	0.0	0.0	1.3	100.0
1263.60	0.0	84.8	0.0	1.6	8.0	0.0	1.5	4.1	100.0
1266.28	51.0	48.0	0.0	0.0	0.3	0.0	0.0	0.7	100.0

APPENDIX III

Grain Size Analyses

211 samples of 6 cores (EK22, IN, IM, LK7, H3, KR2) have been analysed for grain sizes of cumulus plagioclase. A technique has been chosen whereby long and short axes of the 20 biggest grains of each sample have been used to calculate a size representative of each slide. Grains which are more than 30 % larger than the average grain size were excluded from this process.

11 samples of the UG2 pyroxenite in 2 cores (UA, H3) have been analysed for grain sizes of orthopyroxene. The same technique as described above has been used.

Grain size analyses (plagioclase):

Core	Rock type	Sample	Grain size [mm2]
UA	o	642.80	1.58
UA	o	644.00	1.68
UA	o	645.70	1.77
UA	.	647.90	1.63
UA	.	649.40	1.80
UA	.	651.30	1.58
UA	.	652.30	2.15
UA	o	652.60	2.43
UA	.	652.90	1.81
UA	.	654.10	1.52
UA	.	654.90	1.44
UA	.	655.50	1.92
EK22	o	267.70	2.26
EK22	o	271.75	2.80
EK22	.	272.25	1.86
EK22	.	274.78	2.76
EK22	.	277.90	2.41
EK22	.	280.65	1.89
EK22	.	282.80	2.01
EK22	o	284.25	2.10
EK22	o	285.80	2.24
EK22	.	286.05	1.92
EK22	o	288.40 b	2.30
EK22	x	288.90 a	1.93
EK22	x	288.90 b base	1.71
EK22	.	288.95 a	2.12
EK22	x	291.48	1.54
EK22	.	292.05	1.54
EK22	.	293.60 a	1.71
EK22	.	295.00	1.79
EK22	o	300.27	2.67
EK22	.	300.60	2.09
EK22	.	306.30 base	1.64
IN	o	806.92	2.53
IN	.	809.77	2.82
IN	.	811.78	2.26
IN	.	815.78	2.01
IN	.	817.10	1.34
IN	.	817.50 top	1.81
IN	.	817.68	1.35
IN	.	819.15	2.15
IN	o	820.55	1.70
IN	.	821.23	1.30
IN	X	826.00	1.91
IN	X	831.70	2.18
IN	X	837.80	2.06
IN	X	844.00	1.91
IN	o	844.00 mid	2.08
IN	X	850.73	1.90
IN	X	858.55	1.50
IN	X	863.12	1.36
IN	X	865.52	2.21
IN	x	866.40	1.72
IN	o	866.67 base	3.17

Grain size analyses (plagioclase):

Core	Rock type	Sample	Grain size [mm2]
IN	o	870.92	2.78
IM	.	787.90	1.74
IM	.	788.32	1.43
IM	X	788.60	1.94
IM	o	788.60	2.12
IM	.	789.75	1.83
IM	.	793.22	1.64
IM	o	793.22	2.35
IM	.	794.10	1.21
IM	o	794.53	2.34
IM	X	796.25	1.80
IM	X	797.25	1.55
IM	X	798.00	1.46
IM	X	801.00	1.34
IM	X	804.40	1.51
IM	X	808.00	1.63
IM	X	810.10	1.49
IM	X	814.00	1.42
IM	X	818.00	1.25
IM	.	819.30	1.69
IM	x	819.85	1.86
IM	o	823.05	1.88
IM	o	825.55	2.44
IM	.	827.65	2.16
IM	.	836.00	1.81
IM	.	839.00	2.08
IM	o	843.61	2.02
IM	o	845.80	2.57
IM	o	848.52	1.90
LK7	.	1389.70	1.34
LK7	o	1389.90	2.08
LK7	.	1392.50	1.23
LK7	.	1395.60	1.43
LK7	.	1401.95	2.14
LK7	o	1407.05	1.49
LK7	o	1407.85	1.40
LK7	.	1412.35	2.26
LK7	.	1412.35	2.11
LK7	o	1413.90	1.99
LK7	.	1415.05	2.06
LK7	.	1418.90	1.65
LK7	.	1421.10	1.84
LK7	o	1424.28	2.56
LK7	.	1424.80	1.75
LK7	.	1429.54	0.65
LK7	.	1429.73	0.84
LK7	.	1430.10	0.25
LK7	.	1430.90	1.03
LK7	.	1437.25	1.06
LK7	.	1441.25	1.28
LK7	.	1446.20	0.94
LK7	.	1451.60	1.16
LK7	.	1457.35	1.19
LK7	.	1463.95	1.43

Grain size analyses (plagioclase):

Core	Rock type	Sample	Grain size [mm2]
LK7	.	1464.56	0.79
LK7	.	1470.00	0.82
LK7	.	1476.10	0.88
LK7	.	1481.26	1.01
LK7	.	1487.00	1.11
LK7	.	1491.10	1.07
LK7	.	1498.00	1.18
LK7	.	1506.00	1.51
LK7	.	1515.00	1.44
LK7	.	1523.10	2.31
LK7	.	1525.80	1.85
LK7	.	1528.90	1.53
LK7	.	1539.10	1.61
LK7	.	1548.25	1.83
LK7	.	1556.56	2.16
LK7	o	1562.25	2.61
LK7	o	1566.00	3.36
LK7	o	1569.80	3.68
LK7	o	1573.75	2.54
LK7	.	1575.95	0.35
LK7	o	1575.95	2.24
LK7	.	1577.45	0.37
LK7	.	1578.43	2.02
LK7	o	1578.43	1.48
LK7	o	1587.00	2.18
H3	o	1049.80	2.04
H3	o	1054.10	2.21
H3	.	1060.05	2.07
H3	.	1062.50	2.14
H3	.	1063.25	1.68
H3	.	1065.05	1.22
H3	o	1066.00	1.69
H3	o	1066.80	1.41
H3	.	1067.15	1.65
H3	.	1071.05	2.02
H3	o	1072.70	1.61
H3	.	1073.00	2.15
H3	o	1076.25	1.93
H3	o	1078.80	2.16
H3	o	1082.10	1.70
H3	o	1083.15	1.32
H3	.	1084.85	1.48
H3	o	1085.60	1.24
H3	.	1087.65	2.28
H3	.	1088.10 a top	0.56
H3	.	1088.10 b	1.17
H3	o	1089.40 central	1.47
H3	x	1089.65	0.19
H3	.	1090.20 a	3.00
H3	.	1090.20 b	1.14
H3	.	1091.80	1.07
H3	.	1099.35	0.97
H3	.	1110.05	0.96
H3	.	1118.50	0.89

Grain size analyses (plagioclase):

Core	Rock type	Sample	Grain size [mm2]
H3	.	1127.50	1.02
H3	.	1135.35	1.03
H3	.	1144.10	0.99
H3	.	1146.90	0.92
H3	.	1156.45	1.08
H3	.	1166.10	0.93
H3	.	1175.80	1.04
H3	.	1182.20	1.27
H3	.	1191.50	1.67
H3	.	1200.30	2.39
H3	.	1211.85	1.43
H3	.	1219.05	1.79
H3	.	1228.25	1.65
H3	.	1231.35	2.31
H3	o	1233.90	2.08
H3	o	1244.05	2.72
H3	.	1246.65	2.65
H3	o	1250.35	2.87
H3	o	1252.50	1.34
H3	.	1253.30 a base	1.56
KR2	o	1141.12	1.54
KR2	o	1146.00	1.71
KR2	o	1149.25	1.33
KR2	.	1150.15	1.79
KR2	.	1155.45	1.46
KR2	.	1160.40	1.56
KR2	o	1162.20 b	1.44
KR2	o	1166.35	2.31
KR2	.	1168.55	2.16
KR2	.	1174.10	1.74
KR2	.	1175.50	1.69
KR2	.	1179.95	1.39
KR2	.	1181.20	2.08
KR2	.	1185.90	1.45
KR2	.	1187.30 b	0.91
KR2	.	1191.20	0.91
KR2	.	1191.58	1.64
KR2	.	1192.10 top	0.80
KR2	.	1193.45 a top	1.24
KR2	o	1193.45 b top	1.82
KR2	.	1193.45 b base	0.91
KR2	.	1194.20	1.77
KR2	.	1203.75	1.07
KR2	.	1214.95	1.10
KR2	.	1219.75	1.10
KR2	.	1227.15	1.10
KR2	.	1236.40	1.26
KR2	.	1241.30	1.09
KR2	.	1251.90	1.27
KR2	.	1267.35	1.77
KR2	o	1276.55	2.18

Grain size analyses (orthopyroxene):

Core	Rock type	Sample	Grain size [mm2]
H3	+	1256.57	10.01
H3	+	1258.45	6.45
H3	+	1261.15	3.52
H3	+	1263.60	1.96
UA	+	661.30	13.85
UA	+	662.70	10.79
UA	+	664.30	10.97
UA	+	667.20	8.61
UA	+	668.90	9.24
UA	+	669.60	6.55
UA	+	670.20	4.99

APPENDIX IV

Electron Microprobe Operating Conditions

All electron microprobe analyses were executed on a Jeol CXA-733 Superprobe at Rhodes University. Samples of intersection AE were analysed by Field in 1986. Five samples of section EK22 are from Ellis (1989) and no standard deviation of $Mg\#_{opx}$, $Mg\#_{ol}$ or An_{plag} could be obtained. All other analyses were executed by the author.

The microprobe was operated at 15 kV and a beam current of 25 nA, using four wave length dispersive crystal spectrometers (with LIF 200, PET and TAP being used as diffracting crystals). A number of international and in-house standards were used for calibration: Orapa (0-12) ilmenite; A236 ilmenite; Rhodes jadeite; Rhodes Ni-magnetite; St. John's Island olivine; 8256 fayalite; JVPL orthoclase; PSU-1A orthoclase; PSU-PX1 pyroxene; Rhodes rhodonite; UK rhodonite; U.C.T. spinel; M114 willemite. The counting times were 30 sec at the peak position and 10 sec at the background position. Most analyses were performed with a defocused 10 μm beam; chromite analyses were executed with a focused beam.

The approximate number of microprobe analyses completed by the author is listed below:

Phase	Samples	Analyses
orthopyroxene	250	1600
plagioclase (cumulus+intercumulus)	240	2500
plagioclase (inclusions)	100	600
olivine	41	205
chromite	80	500
cpx	18	54
amphibole	2	5
mica	2	3
Total	260	5470

The following abbreviations and symbols are used in the tables:

An	= cationic ratio of 100 * Ca/(Ca+Na+K)
Ab	= cationic ratio of 100 * Na/(Ca+Na+K)
Or	= cationic ratio of 100 * K/(Ca+Na+K)
Mg#	= cationic ratio of Mg/(Mg+Fe)
Cr/Fe	= weight ratio of the metals Cr/Fe
Cr/Al	= cationic ratio of Cr/Al
(P)	= value from microprobe analysis
(C)	= recalculated value assuming stoichiometry
n	= number of analyses per sample used to calculate average composition and standard deviation
std	= standard deviation (1σ)
o	= anorthosite
.	= norite
X	= olivine norite
x	= troctolite
+	= pyroxenite
*	= harzburgite
#	= chromitite

The analytical precision (reproducibility) was tested by 10 closely spaced analyses in the central domain of various phases. The coefficients of variation, calculated as (100 * 1 standard deviation) / mean concentration have been determined for the 4 main minerals in this study, namely plagioclase, orthopyroxene, chromite and olivine. They are presented at the beginning of this section. The coefficients are highest for phases of low concentration (beneath or around 0.2 wt %) such as FeO and K_2O in plagioclase (15.4 and 8.13 % respectively), NiO and MnO in orthopyroxene (9.74 and 7.93 % respectively), MnO in olivine (6.85 %) and NiO in chromite (15.62 %). The high variation of CaO in orthopyroxene is related to partial analysis of cpx exsolution lamellae. The following abbreviations were used:

sd = 1 Standard deviation
c.v.% = coefficient of variation (in %)

Determination of coefficients of variation: plagioclase

Sample EK 284.25

	1	2	3	4	5	6	7	8	9	10	mean	st	c.v.%
[wt%]													
SiO2	49.75	49.93	49.85	50.09	49.66	49.64	49.79	49.82	49.70	49.53	49.78	0.151	0.30
Al2O3	32.46	32.55	32.55	32.46	32.46	32.73	32.54	32.42	31.95	32.32	32.44	0.194	0.60
FeO	0.13	0.20	0.16	0.15	0.17	0.20	0.18	0.19	0.22	0.22	0.18	0.028	15.40
CaO	15.62	15.84	15.71	15.68	15.65	15.72	15.77	15.61	15.80	15.51	15.69	0.092	0.58
Na2O	2.63	2.67	2.58	2.63	2.57	2.60	2.65	2.56	2.56	2.58	2.60	0.037	1.43
K2O	0.13	0.13	0.11	0.11	0.11	0.13	0.11	0.10	0.12	0.11	0.12	0.009	8.13
Total	100.72	101.31	100.97	101.13	100.63	101.02	101.03	100.71	100.35	100.28	100.82		
Cations (based on 32 oxygens)													
Si	9.026	9.016	9.024	9.050	9.020	8.988	9.012	9.038	9.060	9.027	9.026	0.019	0.21
Al	6.942	6.928	6.944	6.912	6.948	6.983	6.942	6.932	6.863	6.943	6.934	0.029	0.42
Fe	0.020	0.030	0.024	0.023	0.026	0.030	0.028	0.029	0.033	0.034	0.028	0.004	15.57
Ca	3.037	3.064	3.046	3.035	3.046	3.049	3.058	3.034	3.085	3.029	3.048	0.016	0.53
Na	0.925	0.935	0.906	0.922	0.905	0.913	0.930	0.900	0.905	0.912	0.915	0.011	1.23
K	0.029	0.029	0.026	0.026	0.025	0.031	0.025	0.024	0.029	0.025	0.027	0.002	8.09
Total	19.980	20.002	19.970	19.968	19.971	19.993	19.994	19.958	19.975	19.970	19.978		
An	76.09	76.06	76.57	76.20	76.60	76.36	76.20	76.65	76.76	76.36	76.39	0.2346	0.31

Determination of coefficients of variation: orthopyroxene

Sample INN

	1	2	3	4	5	6	7	8	9	10	mean	st	c.v.%
[wt%]													
SiO2	55.54	55.53	55.54	55.37	55.48	55.19	55.24	55.08	55.21	55.22	55.34	0.165	0.30
TiO2	0.16	0.16	0.15	0.15	0.17	0.15	0.13	0.16	0.16	0.15	0.15	0.010	6.57
Al2O3	1.43	1.42	1.41	1.41	1.44	1.44	1.43	1.43	1.44	1.44	1.43	0.011	0.76
Cr2O3	0.52	0.51	0.51	0.52	0.52	0.52	0.52	0.53	0.55	0.52	0.52	0.010	1.83
FeO	11.49	11.43	11.24	11.27	11.43	11.34	11.31	11.32	11.47	11.52	11.38	0.095	0.84
MnO	0.22	0.23	0.26	0.28	0.26	0.23	0.23	0.22	0.25	0.23	0.24	0.019	7.93
NiO	0.08	0.10	0.11	0.12	0.09	0.11	0.10	0.10	0.10	0.11	0.10	0.010	9.74
MgO	29.76	29.71	29.79	29.69	29.59	29.52	29.61	28.89	29.75	29.54	29.58	0.249	0.84
CaO	0.81	0.73	0.87	0.79	0.99	0.98	0.79	1.52	0.73	0.77	0.90	0.225	25.01
Na2O	0.00	0.00	0.00	0.00	0.00	0.00	0.00	0.01	0.00	0.00	0.00	0.003	233.16
Total	100.03	99.83	99.87	99.62	99.96	99.48	99.36	99.25	99.66	99.50	99.66		
Cations (based on 6 oxygens)													
Si	1.965	1.968	1.967	1.966	1.965	1.964	1.967	1.967	1.962	1.965	1.966	0.002	0.09
Ti	0.004	0.004	0.004	0.004	0.004	0.004	0.003	0.004	0.004	0.004	0.004	0.000	6.48
Al	0.060	0.059	0.059	0.059	0.060	0.060	0.060	0.060	0.060	0.060	0.060	0.001	0.87
Cr	0.015	0.014	0.014	0.015	0.015	0.015	0.015	0.015	0.015	0.015	0.015	0.000	1.94
Fe	0.340	0.339	0.333	0.335	0.339	0.337	0.337	0.338	0.341	0.343	0.338	0.003	0.84
Mn	0.007	0.007	0.008	0.009	0.008	0.007	0.007	0.007	0.007	0.007	0.007	0.001	7.83
Ni	0.002	0.003	0.003	0.003	0.002	0.003	0.003	0.003	0.003	0.003	0.003	0.000	9.84
Mg	1.570	1.569	1.572	1.572	1.562	1.566	1.571	1.538	1.576	1.567	1.566	0.010	0.64
Ca	0.031	0.028	0.033	0.030	0.037	0.037	0.030	0.058	0.028	0.029	0.034	0.009	25.27
Na	0.000	0.000	0.000	0.000	0.000	0.000	0.000	0.000	0.000	0.000	0.000	0.000	233.30
Total	3.993	3.991	3.993	3.993	3.993	3.994	3.992	3.991	3.996	3.993	3.993		
Mg#	0.822	0.822	0.825	0.824	0.822	0.823	0.824	0.820	0.822	0.820	0.822	0.0016	0.19

Determination of coefficients of variation: olivine

Sample IN 866.4

	1	2	3	4	5	6	7	8	9	10	mean	st	c.v.%
[wt%]													
SiO2	39.46	39.29	39.27	39.43	39.54	39.16	39.38	39.29	39.38	39.18	39.34	0.116	0.30
FeO	17.42	17.85	17.88	18.14	17.88	18.23	17.93	17.70	17.90	17.95	17.89	0.211	1.18
MnO	0.23	0.21	0.21	0.22	0.19	0.20	0.19	0.21	0.19	0.22	0.21	0.014	6.85
NiO	0.41	0.39	0.41	0.37	0.43	0.38	0.38	0.39	0.40	0.41	0.40	0.017	4.30
MgO	41.78	41.82	41.93	41.87	41.92	41.95	42.32	41.97	41.97	41.83	41.94	0.143	0.34
CaO	0.01	0.00	0.01	0.00	0.00	0.00	0.02	0.01	0.01	0.01	0.01	0.005	75.86
Total	99.32	99.56	99.71	100.02	99.96	99.93	100.22	99.57	99.86	99.59	99.77		
Cations (based on 4 oxygens)													
Si	1.010	1.005	1.004	1.005	1.007	1.000	1.001	1.005	1.005	1.003	1.005	0.003	0.26
Fe	0.373	0.382	0.382	0.387	0.381	0.390	0.381	0.379	0.382	0.384	0.382	0.004	1.12
Mn	0.005	0.004	0.005	0.005	0.004	0.004	0.004	0.005	0.004	0.005	0.004	0.000	6.99
Ni	0.009	0.008	0.008	0.008	0.009	0.008	0.008	0.008	0.008	0.008	0.008	0.000	4.36
Mg	1.594	1.595	1.597	1.591	1.592	1.597	1.604	1.600	1.596	1.596	1.596	0.004	0.23
Ca	0.000	0.000	0.000	0.000	0.000	0.000	0.000	0.000	0.000	0.000	0.000	0.000	75.67
Total	2.990	2.995	2.996	2.995	2.993	3.000	2.999	2.995	2.995	2.997	2.995		
Mg#	0.810	0.807	0.807	0.804	0.807	0.804	0.808	0.809	0.807	0.806	0.807	0.0018	0.22

Determination of coefficients of variation: chromite

Sample INN

	1	2	3	4	5	6	7	8	9	10	mean	st	c.v.%
[wt%]													
TiO2	0.88	0.88	0.90	0.87	0.89	0.90	0.90	0.89	0.92	0.90	0.89	0.014	1.57
Al2O3	18.13	18.14	18.23	18.42	17.99	18.07	18.09	18.17	17.89	17.97	18.11	0.141	0.78
Cr2O3	41.94	41.70	41.96	41.63	41.44	41.68	42.18	42.21	41.41	41.97	41.81	0.269	0.64
FeO(P)	28.96	28.89	28.77	28.55	28.52	28.72	29.14	29.05	28.05	28.51	28.72	0.307	1.07
FeO(C)	21.97	22.00	22.01	22.09	21.80	21.90	22.20	22.05	21.61	21.92	21.96	0.154	0.70
Fe2O3	7.77	7.65	7.51	7.18	7.46	7.58	7.71	7.78	7.15	7.33	7.51	0.219	2.92
MnO	0.29	0.30	0.29	0.31	0.27	0.30	0.30	0.33	0.29	0.32	0.30	0.016	5.17
NiO	0.14	0.09	0.13	0.14	0.10	0.11	0.13	0.13	0.13	0.15	0.13	0.020	15.62
MgO	8.58	8.49	8.55	8.37	8.44	8.50	8.50	8.61	8.43	8.43	8.49	0.070	0.82
Total(P)	98.93	98.48	98.83	98.29	97.66	98.28	99.24	99.39	97.12	98.25	98.45		
Total(C)	99.70	99.24	99.58	99.01	98.41	99.04	100.02	100.17	97.84	98.99	99.20		
Cations (based on 32 oxygens)													
Ti	0.172	0.173	0.175	0.170	0.176	0.176	0.176	0.173	0.183	0.176	0.175	0.003	1.93
Al	5.540	5.568	5.575	5.663	5.569	5.559	5.518	5.527	5.567	5.535	5.562	0.039	0.69
Cr	8.599	8.587	8.609	8.587	8.604	8.600	8.630	8.615	8.646	8.671	8.615	0.026	0.30
Fe2	4.764	4.793	4.777	4.818	4.789	4.780	4.805	4.760	4.773	4.790	4.785	0.017	0.36
Fe3	1.517	1.499	1.466	1.410	1.474	1.489	1.501	1.512	1.421	1.441	1.473	0.036	2.44
Mn	0.065	0.067	0.065	0.068	0.061	0.067	0.065	0.073	0.065	0.071	0.067	0.003	4.88
Ni	0.028	0.018	0.028	0.029	0.020	0.024	0.028	0.028	0.028	0.033	0.026	0.004	15.54
Mg	3.315	3.294	3.305	3.255	3.306	3.306	3.278	3.312	3.317	3.283	3.297	0.019	0.57
Mg#	0.410	0.407	0.409	0.403	0.408	0.409	0.406	0.410	0.410	0.407	0.408	0.002	0.54
Cr/Fe	1.275	1.271	1.284	1.284	1.279	1.277	1.274	1.279	1.300	1.296	1.282	0.009	0.69
Cr/Al	1.552	1.542	1.544	1.516	1.545	1.547	1.564	1.559	1.553	1.567	1.549	0.013	0.87

Plagioclase analyses: UA-sequence

Sample	641.00	642.50 Top	642.50 Base	642.80	644.00	645.70	647.90	651.30	652.30	652.90	654.10	654.90	655.50	658.00	661.30	662.70	664.30	665.70	667.20	668.90	669.60
Rock type	*	*	o	o	o	o	.	.	.	o	.	.	.	*	+	+	+	+	+	+	+
[wt%]																					
SiO2	51.44	49.97	49.31	48.36	49.28	48.44	48.44	48.38	48.86	48.85	48.79	49.13	49.10	52.61	55.00	54.03	52.34	55.32	51.77	54.04	50.47
Al2O3	29.92	31.50	32.03	31.82	31.78	31.59	31.99	31.81	32.21	31.23	32.03	32.23	31.90	29.03	28.21	28.79	29.37	27.27	29.35	28.09	31.13
FeO	0.28	0.38	0.31	0.38	0.30	0.31	0.27	0.26	0.27	0.37	0.18	0.15	0.12	0.11	0.08	0.14	0.18	0.13	0.14	0.13	0.15
CaO	13.39	15.64	15.96	15.85	16.13	16.04	15.85	15.89	16.19	16.07	16.25	16.14	15.70	12.78	11.02	11.72	12.80	10.29	12.83	11.14	14.60
Na2O	4.05	2.96	2.79	2.73	2.77	2.79	2.64	2.72	2.53	2.68	2.69	2.72	2.79	4.71	5.42	4.92	4.07	5.93	4.44	5.28	3.51
K2O	0.10	0.12	0.13	0.10	0.13	0.14	0.12	0.13	0.11	0.12	0.12	0.12	0.11	0.11	0.26	0.27	0.21	0.22	0.19	0.25	0.09
Total	99.17	100.57	100.53	99.24	100.38	99.32	99.32	99.20	100.17	99.32	100.07	100.50	99.72	99.34	99.98	99.87	98.97	99.15	98.72	98.93	99.95
Cations (based on 32 oxygens)																					
Si	9.44	9.10	9.00	8.95	9.01	8.96	8.95	8.95	8.95	9.03	8.95	8.96	9.02	9.62	9.93	9.79	9.60	10.07	9.54	9.88	9.22
Al	6.47	6.76	6.89	6.94	6.85	6.89	6.96	6.94	6.95	6.80	6.92	6.93	6.90	6.26	6.01	6.15	6.35	5.85	6.37	6.05	6.70
Fe	0.04	0.06	0.05	0.06	0.05	0.05	0.04	0.04	0.04	0.06	0.03	0.02	0.02	0.02	0.01	0.02	0.03	0.02	0.02	0.02	0.02
Ca	2.63	3.05	3.12	3.14	3.16	3.18	3.14	3.15	3.18	3.18	3.19	3.16	3.09	2.50	2.13	2.28	2.51	2.01	2.53	2.18	2.86
Na	1.44	1.05	0.99	0.98	0.98	1.00	0.95	0.98	0.90	0.96	0.96	0.96	0.99	1.67	1.90	1.73	1.44	2.09	1.58	1.87	1.24
K	0.02	0.03	0.03	0.02	0.03	0.03	0.03	0.03	0.02	0.03	0.03	0.03	0.03	0.02	0.06	0.06	0.05	0.05	0.04	0.06	0.02
Total	20.05	20.05	20.07	20.09	20.07	20.11	20.06	20.09	20.04	20.06	20.08	20.07	20.04	20.10	20.04	20.03	19.98	20.08	20.09	20.06	20.06
An	64.25	73.96	75.44	75.84	75.75	75.45	76.32	75.75	77.45	76.30	76.41	76.09	75.21	59.62	52.13	55.97	62.67	48.41	60.88	53.11	69.36
Ab	35.19	25.35	23.84	23.61	23.53	23.75	22.99	23.49	21.94	23.04	22.92	23.21	24.16	39.78	46.37	42.52	36.03	50.37	38.04	45.50	30.12
Or	0.56	0.68	0.73	0.55	0.72	0.80	0.69	0.76	0.61	0.66	0.67	0.70	0.63	0.60	1.49	1.52	1.24	1.24	1.05	1.41	0.51
1 Standard deviation [wt%]																					
SiO2	0.33	0.75	0.22	0.33	0.14	0.23	0.23	0.29	0.25	0.25	0.20	0.12	0.56	0.91	0.80	0.54	1.59	1.04	1.82	1.81	0.49
Al2O3	0.12	0.36	0.19	0.15	0.25	0.12	0.14	0.12	0.11	0.21	0.22	0.18	0.38	0.74	0.51	0.36	1.05	0.62	1.05	1.11	0.32
FeO	0.02	0.04	0.05	0.02	0.02	0.05	0.04	0.06	0.02	0.03	0.02	0.02	0.02	0.05	0.03	0.03	0.06	0.01	0.02	0.03	0.02
CaO	0.20	0.49	0.13	0.20	0.18	0.12	0.15	0.24	0.14	0.20	0.28	0.14	0.50	0.97	0.64	0.39	1.37	0.78	1.42	1.32	0.41
Na2O	0.09	0.23	0.10	0.12	0.07	0.05	0.11	0.06	0.08	0.07	0.10	0.08	0.25	0.53	0.35	0.23	0.64	0.55	0.78	0.81	0.22
K2O	0.01	0.04	0.01	0.01	0.01	0.02	0.02	0.01	0.02	0.01	0.01	0.01	0.02	0.02	0.08	0.05	0.05	0.08	0.05	0.05	0.01
An	0.77	2.10	0.80	0.99	0.60	0.43	0.88	0.71	0.71	0.67	0.97	0.69	2.26	4.45	2.90	2.00	6.20	4.00	6.80	6.80	1.90
n	5	4	6	8	8	7	5	6	5	8	5	5	8	3	6	6	7	4	8	5	6

Plagioclase analyses: AE sequence (Field, 1987)

Sample	27	27	29	32	33	35	36	38	39.4	39.5	39.6	40.1	42	43	45	46	47	48	49	51	55	57
Rock type	+	+	o	.	.	o	.	.	*	*	*	*	+	o	.	.	.	*	+	+	+	+
[wt%]																						
SiO2	49.95	49.55	48.48	49.19	47.12	49.42	49.30	48.69	49.26	49.07	49.15	53.20	48.90	49.00	48.98	48.57	49.04	50.22	53.59	53.84	52.80	54.07
Al2O3	31.58	31.67	32.50	31.75	33.27	31.65	32.05	32.49	31.97	31.74	32.11	30.10	31.97	32.29	32.06	31.88	31.69	31.37	29.32	29.11	29.79	29.07
FeO	0.23	0.25	0.30	0.26	0.26	0.27	0.22	0.27	0.19	0.14	0.28	0.15	0.30	0.32	0.27	0.25	0.23	0.15	0.11	0.10	0.14	0.09
CaO	15.14	15.35	16.75	15.65	17.54	15.72	15.99	16.44	15.76	15.57	15.80	12.97	15.64	16.39	16.09	16.21	15.96	14.74	12.58	12.51	12.57	12.32
Na2O	2.86	2.60	2.03	2.45	1.68	2.57	2.49	2.23	2.39	2.65	2.42	3.95	2.42	2.09	2.33	2.35	2.35	2.96	4.33	4.37	4.02	4.52
K2O	0.08	0.12	0.13	0.12	0.05	0.10	0.14	0.17	0.14	0.04	0.14	0.20	0.10	0.14	0.16	0.12	0.21	0.07	0.23	0.29	0.16	0.25
Total	99.83	99.53	100.20	99.41	99.91	99.85	100.19	100.29	99.70	99.21	99.90	100.57	99.33	100.22	99.18	99.39	99.46	99.03	100.16	100.22	99.49	100.32
Cations (based on 32 oxygens)																						
Si	9.14	9.10	8.88	9.05	8.68	9.07	9.01	8.91	9.03	9.04	9.00	9.59	9.01	8.96	8.98	8.96	9.03	9.20	9.69	9.73	9.61	9.76
Al	6.81	6.85	7.02	6.88	7.22	6.84	6.90	7.00	6.91	6.89	6.93	6.39	6.94	6.96	6.93	6.93	6.88	6.77	6.25	6.20	6.39	6.18
Fe	0.04	0.04	0.05	0.04	0.04	0.04	0.03	0.04	0.03	0.02	0.04	0.02	0.05	0.05	0.04	0.04	0.04	0.02	0.02	0.02	0.02	0.01
Ca	2.97	3.02	3.29	3.08	3.46	3.09	3.13	3.22	3.10	3.07	3.10	2.50	3.09	3.21	3.16	3.21	3.15	2.89	2.44	2.42	2.45	2.38
Na	1.01	0.92	0.72	0.87	0.60	0.91	0.88	0.79	0.85	0.95	0.86	1.38	0.86	0.74	0.83	0.84	0.84	1.05	1.52	1.53	1.42	1.58
K	0.02	0.03	0.03	0.03	0.01	0.02	0.03	0.04	0.03	0.01	0.03	0.05	0.02	0.03	0.04	0.03	0.05	0.02	0.05	0.07	0.04	0.06
Total	19.98	19.95	19.99	19.96	20.01	19.98	20.00	20.01	19.95	19.99	19.97	19.93	19.97	19.95	19.98	20.01	19.98	19.95	19.97	19.97	19.92	19.97
An	74.20	76.03	81.38	77.38	85.02	76.73	77.35	79.49	77.85	76.33	77.67	63.75	77.66	80.60	78.51	78.68	78.02	73.05	60.80	60.24	62.76	59.25
Ab	25.33	23.25	17.85	21.89	14.71	22.69	21.83	19.52	21.35	23.47	21.49	35.08	21.74	18.60	20.57	20.60	20.78	26.54	37.87	38.12	36.27	39.29
Or	0.47	0.72	0.77	0.72	0.27	0.58	0.82	1.00	0.80	0.20	0.84	1.17	0.60	0.80	0.91	0.71	1.21	0.41	1.32	1.65	0.97	1.45

Plagioclase analyses: EK22 sequence

Sample	267.70	271.75	272.25	277.90 b	280.65	282.80 a	284.25	285.70 Net	285.70	285.80 b-Top	285.80 b-Base	286.05	288.40 a	288.40 b	288.40 b-Base	288.90 a	288.90 b	288.95	291.48	292.05	293.60 a	295.70	296.90	299.10	299.80	300.27
Rock type	o	o	.	.	.	.	o	o	o	o	.	.	*	*	o	x	*	.	*	.	.	*	*	*	*	o
[wt%]																										
SiO2	48.25	48.99	48.81	48.92	48.50	48.75	49.81	47.87	48.06	48.87	49.47	48.93	45.71	48.76	49.11	49.09	49.00	49.21	49.49	49.26	48.77	49.38	53.21	50.73	54.10	49.57
Al2O3	32.00	31.71	31.67	31.45	31.51	32.02	32.45	31.48	31.25	31.49	32.07	32.15	33.97	32.45	32.22	32.11	32.37	31.61	30.78	31.92	31.69	31.60	29.14	31.16	28.59	31.71
FeO	0.39	0.33	0.27	0.40	0.28	0.20	0.26	0.31	0.38	0.28	0.29	0.22	0.24	0.25	0.25	0.28	0.23	0.24	0.28	0.28	0.23	0.13	0.11	0.14	0.14	0.38
CaO	16.19	16.27	15.84	15.93	16.56	15.71	15.67	16.71	16.64	15.95	16.13	15.81	18.66	16.08	16.22	16.29	16.14	15.52	15.40	15.45	15.98	15.76	12.52	14.90	11.55	15.52
Na2O	2.46	2.72	2.69	2.56	2.64	2.68	2.60	2.53	2.65	2.78	2.51	2.68	1.30	2.51	2.73	2.45	2.50	2.94	3.39	2.74	2.59	3.08	4.75	3.54	4.94	2.73
K2O	0.12	0.11	0.12	0.13	0.14	0.12	0.13	0.11	0.13	0.12	0.14	0.12	0.01	0.12	0.11	0.07	0.07	0.10	0.05	0.12	0.11	0.04	0.15	0.08	0.05	0.15
Total	99.40	100.14	99.39	99.38	99.63	99.48	100.92	99.01	99.11	99.49	100.62	99.91	99.88	100.16	100.64	100.29	100.30	99.30	99.40	99.77	99.37	99.99	99.88	100.54	99.37	100.05
Cations (based on 32 oxygens)																										
Si	8.92	8.99	9.00	9.03	8.95	8.98	9.03	8.90	8.93	9.01	9.01	8.97	8.46	8.93	8.96	8.97	8.95	9.05	9.13	9.03	9.00	9.05	9.67	9.22	9.83	9.07
Al	6.97	6.86	6.88	6.84	6.86	6.95	6.93	6.90	6.85	6.85	6.88	6.95	7.41	7.00	6.92	6.92	6.97	6.85	6.69	6.90	6.89	6.82	6.24	6.67	6.12	6.84
Fe	0.06	0.05	0.04	0.06	0.04	0.03	0.04	0.05	0.06	0.04	0.04	0.03	0.04	0.04	0.04	0.04	0.04	0.04	0.04	0.04	0.03	0.02	0.02	0.02	0.02	0.06
Ca	3.20	3.20	3.13	3.15	3.28	3.10	3.04	3.33	3.31	3.15	3.15	3.11	3.70	3.15	3.17	3.19	3.16	3.06	3.05	3.04	3.16	3.09	2.44	2.90	2.25	3.04
Na	0.88	0.97	0.96	0.92	0.94	0.96	0.91	0.91	0.96	0.99	0.89	0.95	0.47	0.89	0.96	0.87	0.88	1.05	1.21	0.97	0.93	1.09	1.67	1.25	1.74	0.97
K	0.03	0.03	0.03	0.03	0.03	0.03	0.03	0.03	0.03	0.03	0.03	0.03	0.00	0.03	0.03	0.02	0.02	0.02	0.01	0.03	0.03	0.01	0.03	0.02	0.01	0.03
Total	20.05	20.08	20.05	20.02	20.11	20.04	19.98	20.12	20.14	20.08	20.01	20.04	20.07	20.03	20.08	20.01	20.02	20.06	20.14	20.02	20.03	20.09	20.07	20.08	19.98	20.01
An	77.94	76.29	76.00	76.91	77.03	75.87	76.38	77.96	77.07	75.51	77.37	76.03	88.75	77.46	76.21	78.34	77.81	74.05	71.32	75.19	76.86	73.74	58.84	69.62	56.18	75.21
Ab	21.39	23.07	23.33	22.37	22.18	23.43	22.89	21.40	22.23	23.83	21.82	23.27	11.19	21.85	23.18	21.28	21.79	25.36	28.39	24.14	22.53	26.05	40.32	29.95	43.51	23.96
Or	0.67	0.64	0.67	0.72	0.79	0.70	0.73	0.64	0.70	0.66	0.81	0.70	0.06	0.69	0.61	0.38	0.40	0.59	0.29	0.67	0.62	0.21	0.84	0.42	0.31	0.84
1 Standard deviation [wt%]																										
SiO2	0.43	0.26	0.46	0.37	0.23	0.31	0.35	0.10	0.23	0.30	0.20	0.24	1.43	0.33	0.63	1.31	0.76	1.02	0.91	0.78	0.17	0.31	1.57	0.54	0.49	0.47
Al2O3	0.31	0.17	0.24	0.16	0.20	0.15	0.10	0.17	0.08	0.21	0.25	0.21	1.16	0.27	0.29	0.99	0.63	0.64	0.55	0.48	0.13	0.26	1.01	0.36	0.30	0.29
FeO	0.02	0.02	0.01	0.03	0.03	0.04	0.05	0.01	0.01	0.04	0.05	0.02	0.03	0.03	0.04	0.07	0.03	0.02	0.04	0.04	0.04	0.02	0.06	0.03	0.02	0.02
CaO	0.30	0.12	0.26	0.18	0.21	0.28	0.18	0.15	0.11	0.21	0.09	0.13	1.25	0.25	0.40	1.00	0.69	0.24	0.82	0.42	0.19	0.21	1.33	0.47	0.48	0.34
Na2O	0.17	0.10	0.17	0.11	0.06	0.15	0.11	0.06	0.04	0.11	0.06	0.10	0.73	0.11	0.20	0.55	0.38	0.42	0.47	0.29	0.09	0.13	0.78	0.24	0.51	0.16
K2O	0.02	0.01	0.02	0.01	0.01	0.01	0.01	0.01	0.01	0.02	0.02	0.01	0.01	0.02	0.02	0.05	0.03	0.03	0.02	0.06	0.02	0.01	0.04	0.02	0.02	0.02
An	1.44	0.89	1.41	0.6	0.46	1.23	1.15	0.53	0.35	0.91		0.85	6.31		0.99			2.86	3.97	2.53	0.86	1.03	6.4	2.07	3.51	1.46
n	7	13	6	7	12	5	4	4	5	7	8	8	6	8	7	4	9	6	6	7	7	5	6	5	4	8

Sample	303.90	306.30 Top	306.30 Mid	306.30 Base	306.50 a	306.50 b-Top	306.50 b-Base	307.66	313.00 Top	313.00 Base	313.60 b	315.90
Rock type	.	.	+	.	.	.	+	+	+	+	*	.
[wt%]												
SiO2	48.40	49.17	49.44	49.17	48.81	50.47	53.91	56.94	54.14	52.27	51.64	47.93
Al2O3	31.34	31.40	31.33	31.51	31.85	31.48	29.27	26.83	28.57	29.75	29.55	32.14
FeO	0.27	0.30	0.22	0.26	0.21	0.17	0.13	0.13	0.15	0.14	0.22	0.22
CaO	15.97	15.99	15.86	16.14	16.40	14.97	12.08	9.78	12.11	13.44	13.29	16.53
Na2O	2.81	2.75	2.85	2.74	2.78	3.33	4.94	6.19	4.97	4.24	4.28	2.50
K2O	0.16	0.14	0.15	0.13	0.12	0.12	0.29	0.29	0.17	0.12	0.11	0.11
Total	98.95	99.73	99.86	99.94	100.17	100.54	100.63	100.16	100.10	99.97	99.10	99.43
Cations (based on 32 oxygens)												
Si	8.99	9.04	9.08	9.03	8.95	9.17	9.71	10.23	9.80	9.51	9.49	8.86
Al	6.86	6.81	6.78	6.82	6.89	6.75	6.22	5.69	6.09	6.38	6.40	7.00
Fe	0.04	0.05	0.03	0.04	0.03	0.03	0.02	0.02	0.02	0.02	0.03	0.03
Ca	3.18	3.15	3.12	3.17	3.22	2.92	2.33	1.89	2.35	2.62	2.62	3.27
Na	1.01	0.98	1.01	0.97	0.99	1.17	1.73	2.15	1.74	1.50	1.52	0.90
K	0.04	0.03	0.03	0.03	0.03	0.03	0.07	0.07	0.04	0.03	0.03	0.03
Total	20.11	20.06	20.06	20.06	20.11	20.06	20.07	20.04	20.04	20.06	20.09	20.10
An	75.20	75.68	74.85	75.96	76.04	70.88	56.55	45.95	56.85	63.21	62.84	78.02
Ab	23.92	23.52	24.31	23.29	23.29	28.44	41.85	52.45	42.23	36.11	36.54	21.35
Or	0.88	0.80	0.84	0.74	0.67	0.68	1.60	1.60	0.92	0.68	0.62	0.62
1 Standard deviation [wt%]												
SiO2	0.29	0.22	0.30	0.29	0.37	1.96	0.23	2.64	0.32	0.69	1.31	0.20
Al2O3	0.21	0.22	0.32	0.24	0.24	0.97	0.18	1.56	0.26	0.56	0.68	0.04
FeO	0.01	0.03	0.03	0.01	0.02	0.05	0.02	0.01	0.03	0.01	0.04	0.03
CaO	0.16	0.12	0.32	0.18	0.24	1.55	0.26	1.81	0.24	0.73	0.98	0.16
Na2O	0.09	0.07	0.11	0.14	0.14	0.89	0.18	0.87	0.09	0.39	0.52	0.08
K2O	0.01	0.01	0.01	0.01	0.02	0.00	0.01	0.09	0.04	0.02	0.02	0.02
An	0.8	0.48	1.1	1.11	1.18	7.55	1.43	8.22	0.99	3.42	4.53	0.68
n	7	6	3	6	8	3	3	7	3	7	5	5

Plagioclase analyses: IN sequence

Sample	806.92	811.78	815.38	817.10	817.50	817.68	819.15	820.55	821.23 b	826.00	837.86	844.00	850.73	858.55	863.12	866.40	866.67 Top	866.67 Base	869.60	870.92	872.50	875.75	880.50	883.14
Rock type	o	.	.	.	.	.	.	o	.	.	.	.	.	.	.	x	+	o	o	o	+	+	+	.
[wt%]																								
SiO2	49.19	48.50	48.51	48.25	48.44	48.57	49.34	48.08	48.89	48.97	48.58	49.05	48.31	48.84	48.82	48.00	47.66	48.39	48.40	48.93	49.82	50.89	49.26	48.66
Al2O3	32.07	31.80	31.87	31.68	31.70	32.16	32.33	32.52	32.47	32.32	32.71	32.53	32.30	31.45	32.54	32.57	32.56	31.84	32.44	32.83	32.24	31.00	32.17	33.03
FeO	0.32	0.31	0.28	0.20	0.24	0.21	0.23	0.33	0.24	0.29	0.19	0.23	0.19	0.18	0.20	0.25	0.22	0.26	0.25	0.24	0.16	0.06	0.13	0.16
CaO	16.23	16.06	16.20	16.18	15.86	16.25	16.02	15.78	16.26	16.18	15.69	16.00	16.23	15.69	16.29	16.67	16.96	16.31	16.33	15.92	15.27	14.65	15.18	15.78
Na2O	2.66	2.62	2.66	2.70	2.75	2.62	2.61	2.66	2.63	2.52	2.72	2.54	2.63	2.94	2.62	2.41	2.14	2.52	2.57	2.59	2.85	3.46	2.71	2.53
K2O	0.11	0.12	0.14	0.11	0.14	0.10	0.13	0.14	0.13	0.12	0.13	0.14	0.11	0.14	0.04	0.03	0.07	0.09	0.07	0.12	0.20	0.18	0.16	0.11
Total	100.58	99.41	99.66	99.13	99.13	99.91	100.67	99.51	100.63	100.41	100.02	100.49	99.77	99.23	100.51	99.93	99.61	99.41	100.06	100.64	100.54	100.24	99.60	100.28
Cations (based on 32 oxygens)																								
Si	8.98	8.96	8.94	8.94	8.97	8.92	8.98	8.87	8.92	8.94	8.90	8.94	8.89	9.02	8.91	8.83	8.80	8.94	8.88	8.91	9.06	9.26	9.03	8.88
Al	6.90	6.92	6.92	6.92	6.92	6.96	6.93	7.07	6.98	6.96	7.06	6.99	7.01	6.85	7.00	7.06	7.08	6.93	7.02	7.05	6.91	6.65	6.95	7.11
Fe	0.05	0.05	0.04	0.03	0.04	0.03	0.04	0.05	0.04	0.04	0.03	0.04	0.03	0.03	0.03	0.04	0.03	0.04	0.04	0.04	0.02	0.01	0.02	0.03
Ca	3.17	3.18	3.20	3.21	3.15	3.20	3.12	3.12	3.18	3.17	3.08	3.13	3.20	3.11	3.18	3.28	3.36	3.23	3.21	3.11	2.97	2.86	2.98	3.09
Na	0.94	0.94	0.95	0.97	0.99	0.93	0.92	0.95	0.93	0.89	0.97	0.90	0.94	1.05	0.93	0.86	0.77	0.90	0.91	0.92	1.00	1.22	0.96	0.90
K	0.03	0.03	0.03	0.03	0.03	0.02	0.03	0.03	0.03	0.03	0.03	0.03	0.02	0.03	0.01	0.01	0.02	0.02	0.02	0.03	0.05	0.04	0.04	0.03
Total	20.06	20.07	20.09	20.10	20.08	20.07	20.03	20.09	20.07	20.04	20.07	20.03	20.09	20.09	20.06	20.08	20.05	20.06	20.08	20.04	20.01	20.04	19.99	20.02
An	76.65	76.66	76.48	76.36	75.53	76.96	76.65	76.05	76.83	77.47	75.52	77.08	76.87	74.12	77.31	79.15	81.09	77.71	77.57	76.70	73.91	69.36	74.90	76.98
Ab	22.72	22.64	22.76	23.03	23.68	22.45	22.59	23.17	22.45	21.83	23.72	22.13	22.54	25.11	22.46	20.69	18.51	21.76	22.04	22.61	24.96	29.64	24.15	22.35
Or	0.63	0.70	0.76	0.61	0.80	0.58	0.77	0.79	0.72	0.70	0.77	0.79	0.59	0.78	0.23	0.16	0.40	0.53	0.39	0.69	1.13	1.00	0.95	0.67
1 Standard deviation [wt%]																								
SiO2	0.45	0.22	0.18	0.42	0.22	0.26	0.39	0.23	0.30	0.15	0.36	0.40	0.34	0.87	0.54	0.67	0.10	1.39	0.31	0.43	0.37	1.11	0.18	0.21
Al2O3	0.20	0.32	0.21	0.30	0.14	0.15	0.26	0.10	0.15	0.18	0.22	0.22	0.14	0.58	0.38	0.47	0.11	0.66	0.25	0.28	0.21	0.79	0.17	0.22
FeO	0.05	0.05	0.03	0.02	0.02	0.03	0.03	0.03	0.06	0.09	0.05	0.04	0.02	0.04	0.03	0.23	0.03	0.02	0.04	0.02	0.05	0.01	0.02	0.02
CaO	0.26	0.15	0.08	0.12	0.16	0.15	0.32	0.08	0.17	0.10	0.36	0.47	0.08	0.83	0.36	0.47	0.09	0.88	0.42	0.20	0.31	0.98	0.28	0.18
Na2O	0.16	0.06	0.04	0.12	0.09	0.04	0.18	0.07	0.03	0.09	0.20	0.17	0.09	0.39	0.20	0.32	0.04	0.52	0.13	0.15	0.14	0.48	0.08	0.08
K2O	0.01	0.03	0.02	0.01	0.01	0.01	0.02	0.01	0.02	0.01	0.02	0.02	0.01	0.04	0.01	0.02	0.02	0.03	0.03	0.02	0.02	0.05	0.02	0.01
An	1.25	0.63	0.28	0.87	0.77	0.2	0.63	0.54	0.4	0.63	1.76	1.72	0.7	3.66	1.73	2.65	1.4	0.4	1.3	1.21	1.36	4.3	1.64	0.64
n	5	7	6	5	4	6	4	5	10	8	11	9	5	5	8	10	4	5	10	5	6	4	4	10

Plagioclase analyses: IH sequence

Sample	776.40	787.90	788.32	788.60 a	788.80	790.64	793.22 b	794.53	795.50	796.25	798.00	801.00	804.40	810.10	818.00	819.30	819.85	823.50	826.48	826.70	836.00 b	839.00	841.67 In	841.67 Out	843.61	848.52
Rock type	o	.	.	.	.	.	.	o	.	.	x	.	.	.	.	.	x	o	.	*	.	.	o	o	o	o
[wt%]																										
SiO2	48.67	49.00	49.11	49.59	48.95	48.62	48.98	48.65	49.29	48.29	48.46	48.09	48.53	48.31	48.82	47.96	49.16	49.40	48.97	45.37	49.05	48.98	45.54	48.77	48.25	47.45
Al2O3	32.22	32.44	32.37	32.61	32.31	32.02	32.24	32.18	31.92	32.45	33.05	32.95	32.09	32.95	31.86	32.81	32.25	32.31	32.34	34.47	32.40	32.27	33.90	31.71	32.12	33.60
FeO	0.32	0.23	0.18	0.36	0.26	0.24	0.29	0.33	0.30	0.19	0.65	0.19	0.10	0.20	0.10	0.19	0.16	0.24	0.25	0.21	0.19	0.16	0.21	0.18	0.25	0.21
CaO	16.16	16.07	15.81	15.77	15.72	15.92	16.00	16.09	16.01	15.84	15.93	16.13	16.46	15.85	15.77	16.32	15.78	15.85	15.91	18.36	15.80	15.94	18.20	15.54	15.93	17.08
Na2O	2.55	2.49	2.60	2.60	2.70	2.66	2.61	2.55	2.79	2.71	2.47	2.35	2.60	2.69	2.92	2.40	2.64	2.62	2.59	1.31	2.77	2.65	1.40	2.62	2.62	1.94
K2O	0.07	0.14	0.14	0.11	0.12	0.15	0.15	0.13	0.14	0.09	0.03	0.09	0.06	0.04	0.05	0.08	0.07	0.11	0.06	0.01	0.09	0.09	0.01	0.53	0.09	0.06
Total	99.99	100.37	100.20	101.05	100.07	99.60	100.26	99.94	100.45	99.58	100.42	99.81	99.83	100.03	99.51	99.76	100.06	100.53	100.11	99.74	100.30	100.09	99.26	99.37	99.27	100.34
Cations (based on 32 oxygens)																										
Si	8.93	8.95	8.97	8.98	8.96	8.95	8.96	8.93	9.00	8.89	8.84	8.83	8.92	8.85	8.99	8.82	8.99	9.00	8.96	8.40	8.96	8.96	8.47	9.01	8.92	8.69
Al	6.97	6.98	6.97	6.96	6.97	6.95	6.95	6.96	6.87	7.04	7.11	7.13	6.95	7.11	6.91	7.11	6.95	6.93	6.97	7.52	6.97	6.96	7.43	6.90	7.00	7.25
Fe	0.05	0.04	0.03	0.06	0.04	0.04	0.04	0.05	0.05	0.03	0.10	0.03	0.02	0.03	0.01	0.03	0.02	0.04	0.04	0.03	0.03	0.03	0.03	0.03	0.04	0.03
Ca	3.18	3.14	3.09	3.06	3.08	3.14	3.14	3.17	3.13	3.13	3.11	3.17	3.24	3.11	3.11	3.22	3.09	3.09	3.12	3.64	3.09	3.13	3.63	3.08	3.15	3.35
Na	0.91	0.88	0.92	0.91	0.96	0.95	0.92	0.91	0.99	0.97	0.87	0.84	0.93	0.95	1.04	0.86	0.94	0.92	0.92	0.47	0.98	0.94	0.51	0.94	0.94	0.69
K	0.02	0.03	0.03	0.03	0.03	0.04	0.03	0.03	0.03	0.02	0.01	0.02	0.01	0.01	0.01	0.02	0.02	0.03	0.01	0.00	0.02	0.02	0.00	0.12	0.02	0.01
Total	20.05	20.02	20.02	20.00	20.04	20.06	20.05	20.05	20.07	20.08	20.04	20.03	20.07	20.07	20.08	20.06	20.01	20.01	20.02	20.07	20.06	20.04	20.07	20.07	20.07	20.03
An	77.44	77.47	76.48	76.90	75.75	76.14	76.57	77.12	75.45	76.00	77.95	78.71	77.53	76.33	74.67	78.62	76.47	76.49	76.98	88.51	75.55	76.47	87.72	74.33	76.64	82.64
Ab	22.15	21.75	22.73	22.84	23.54	22.99	22.58	22.11	23.78	23.49	21.88	20.74	22.14	23.42	25.02	20.95	23.12	22.87	22.65	11.45	23.91	23.02	12.21	22.67	22.83	17.00
Or	0.42	0.78	0.78	0.65	0.71	0.87	0.85	0.77	0.78	0.51	0.17	0.55	0.33	0.25	0.31	0.43	0.41	0.65	0.37	0.05	0.54	0.51	0.07	3.01	0.53	0.36
1 Standard deviation [wt%]																										
SiO2	0.24	0.39	0.57	0.82	0.26	0.25	0.23	0.34	0.46	0.20	0.70	0.79	0.27	0.56	0.40	1.11	0.91	0.18	0.24	0.24	0.36	0.32	1.38	1.07	0.25	0.41
Al2O3	0.20	0.36	0.38	0.40	0.27	0.16	0.14	0.27	0.24	0.20	0.23	0.32	0.17	0.42	0.25	0.93	0.40	0.13	0.22	0.23	0.18	0.19	1.00	0.60	0.24	0.45
FeO	0.02	0.19	0.02	0.12	0.06	0.02	0.03	0.03	0.06	0.03	0.66	0.04	0.03	0.06	0.03	0.07	0.01	0.03	0.06	0.03	0.04	0.03	0.06	0.02	0.03	0.02
CaO	0.16	0.38	0.46	0.54	0.29	0.19	0.15	0.20	0.27	0.19	0.25	0.54	0.18	0.47	0.21	0.98	0.45	0.15	0.24	0.23	0.20	0.22	1.04	0.74	0.31	0.43
Na2O	0.10	0.16	0.21	0.28	0.23	0.13	0.09	0.11	0.18	0.10	0.20	0.29	0.13	0.21	0.12	0.56	0.34	0.08	0.14	0.13	0.11	0.12	0.61	0.05	0.11	0.21
K2O	0.01	0.02	0.02	0.03	0.02	0.02	0.02	0.02	0.02	0.02	0.02	0.03	0.00	0.02	0.01	0.03	0.03	0.01	0.01	0.02	0.02	0.02	0.00	0.67	0.02	0.02
An	0.74	1.49	1.93	2.59	1.91	1.08	0.78	1.02	1.46	0.94	1.58	2.68	1.03	1.96	1.03	4.98	1.65	0.92	1.08	1.24	0.98	1.03	5.29	4.01	0.79	1.87
n	6	10	9	4	8	9	16	7	5	8	6	13	6	6	4	9	5	7	12	4	19	21	7	3	15	8

Plagioclase analyses: TF sequence

Sample	851.90	853.95	856.00	866.20 Top	866.20 Base
Rock type	+	+	.	o	o
[wt%]					
SiO2	50.57	50.02	49.67	49.96	49.50
Al2O3	30.99	31.08	32.27	31.98	31.95
FeO	0.12	0.20	0.11	0.21	0.19
CaO	14.53	14.77	15.87	15.25	15.58
Na2O	3.59	3.32	2.69	2.95	2.81
K2O	0.09	0.10	0.10	0.12	0.09
Total	99.88	99.49	100.71	100.47	100.12
Cations (based on 32 oxygens)					
Si	9.24	9.18	9.02	9.09	9.05
Al	6.68	6.73	6.91	6.86	6.88
Fe	0.02	0.03	0.02	0.03	0.03
Ca	2.85	2.91	3.09	2.97	3.05
Na	1.27	1.18	0.95	1.04	1.00
K	0.02	0.02	0.02	0.03	0.02
Total	20.07	20.06	20.01	20.02	20.02
An	68.88	70.71	76.07	73.52	75.00
Ab	30.61	28.71	23.34	25.78	24.51
Or	0.50	0.58	0.59	0.70	0.49
1 Standard deviation [wt%]					
SiO2	3.25	2.20	0.20	0.12	0.38
Al2O3	2.10	1.33	0.16	0.33	0.31
FeO	0.02	0.05	0.02	0.01	0.01
CaO	2.55	1.65	0.14	0.26	0.35
Na2O	1.51	0.97	0.10	0.15	0.17
K2O	0.05	0.05	0.02	0.05	0.01
An	6.57	8.35	1.54	2.32	2.32
n	10	8	8	5	10

Sample	840.00	842.00	851.00	862.00	866.50	866.50	875.00	885.00	895.00	917.10	930.00	953.00	957.00	962.00	964.00
Rock type	.	.	.	o	*	o	.	.	.	o	.	o	+	+	+
[wt%]															
SiO2	48.63	49.06	48.02	48.45	46.49	48.17	48.62	48.53	49.18	48.20	49.09	48.98	49.95	49.89	49.93
Al2O3	31.38	31.63	31.18	31.49	32.57	31.34	31.41	31.62	31.41	31.45	31.47	31.77	31.36	30.94	31.12
FeO	0.28	0.28	0.29	0.38	0.32	0.38	0.26	0.27	0.26	0.48	0.29	0.15	0.07	0.07	0.09
CaO	16.47	16.37	16.45	16.22	17.99	16.74	16.67	16.51	16.03	16.52	16.35	16.46	15.57	15.57	15.43
Na2O	2.82	2.81	2.80	2.83	1.96	2.66	2.63	2.67	2.99	2.65	2.80	2.78	3.25	3.30	3.34
K2O	0.12	0.15	0.14	0.12	0.06	0.11	0.14	0.14	0.14	0.11	0.16	0.18	0.16	0.13	0.10
Total	99.70	100.30	98.87	99.48	99.38	99.39	99.73	99.74	100.01	99.41	100.16	100.32	100.35	99.91	100.02
Cations (based on 32 oxygens)															
Si	8.97	8.99	8.94	8.96	8.64	8.93	8.97	8.95	9.03	8.93	9.01	8.97	9.12	9.15	9.14
Al	6.82	6.83	6.84	6.86	7.14	6.85	6.83	6.87	6.80	6.87	6.81	6.86	6.75	6.69	6.72
Fe	0.04	0.04	0.04	0.06	0.05	0.06	0.04	0.04	0.04	0.07	0.05	0.02	0.01	0.01	0.01
Ca	3.26	3.21	3.28	3.21	3.59	3.32	3.29	3.26	3.15	3.28	3.21	3.23	3.04	3.06	3.03
Na	1.01	1.00	1.01	1.01	0.70	0.96	0.94	0.96	1.06	0.95	1.00	0.99	1.15	1.17	1.19
K	0.03	0.04	0.03	0.03	0.01	0.03	0.03	0.03	0.03	0.03	0.04	0.04	0.04	0.03	0.02
Total	20.13	20.11	20.16	20.13	20.14	20.14	20.10	20.11	20.12	20.13	20.11	20.11	20.10	20.11	20.11
An	75.85	75.68	75.86	75.54	83.30	77.19	77.18	76.72	74.22	76.99	75.69	75.88	71.95	71.76	71.46
Ab	23.50	23.48	23.37	23.81	16.37	22.21	22.06	22.49	25.00	22.37	23.43	23.15	27.17	27.50	28.00
Or	0.65	0.84	0.76	0.65	0.33	0.60	0.75	0.79	0.78	0.64	0.89	0.97	0.88	0.74	0.54
1 Standard deviation [wt%]															
SiO2	0.25	0.30	0.16	0.32	2.42	0.36	0.41	0.27	1.41	0.28	0.22	0.84	0.82	0.60	0.85
Al2O3	0.17	0.22	0.11	0.16	1.52	0.24	0.31	0.19	0.94	0.05	0.24	0.46	0.51	0.37	0.31
FeO	0.02	0.04	0.03	0.03	0.05	0.02	0.01	0.01	0.02	0.03	0.02	0.02	0.03	0.03	0.03
CaO	0.14	0.24	0.13	0.27	1.71	0.25	0.32	0.16	1.13	0.12	0.15	0.57	0.73	0.51	0.42
Na2O	0.08	0.13	0.05	0.11	0.93	0.11	0.19	0.09	0.67	0.07	0.12	0.37	0.38	0.21	0.22
K2O	0.02	0.04	0.01	0.02	0.03	0.01	0.01	0.01	0.04	0.01	0.02	0.14	0.06	0.02	0.03
An	0.65	1.11	0.47	1.98	8.00	0.95	1.55	0.72	5.60	0.57	0.95	2.84	3.34	1.00	1.94
n	7	5	6	7	3	5	6	8	7	6	7	6	7	5	7

Plagioclase analyses: LK7 sequence

Sample	1389.70	1395.60	1401.95	1407.05	1412.35 b	1421.10 a	1424.28 a	1424.28 b-Top	1424.28 b-Base	1429.54	1429.73 Top	1429.73 Base	1430.10	1430.90 Top	1430.90 Base	1441.25 a	1446.20	1457.35	1464.56	1470.00 a	1481.26	1491.10	1500.95 b	1511.10 b	1520.40	1528.90 a
Rock type	.	.	.	.	.	.	o	+	o	.	.	.	.	.	-	.	.	.	.	.	.	.	.	.	.	.
[wt%]																										
SiO2	49.56	49.02	48.60	49.31	49.47	49.24	48.93	50.14	49.73	49.36	49.27	49.43	49.18	49.22	49.31	49.49	49.62	49.59	50.24	49.79	50.11	50.44	49.56	49.57	49.34	49.83
Al2O3	32.05	32.27	31.64	31.46	32.45	31.74	32.47	31.34	31.99	31.99	32.14	32.07	32.28	31.89	31.97	31.97	32.33	32.03	31.40	32.21	31.70	31.45	31.21	32.24	31.81	32.19
FeO	0.30	0.31	0.33	0.32	0.32	0.29	0.35	0.21	0.28	0.30	0.28	0.27	0.27	0.23	0.30	0.28	0.30	0.28	0.27	0.28	0.32	0.31	0.33	0.33	0.34	0.31
CaO	15.87	15.42	16.24	15.49	15.38	16.05	15.25	15.21	15.89	16.08	15.93	15.84	15.69	15.82	15.86	15.68	15.07	15.13	15.22	14.91	15.31	15.11	15.18	15.30	15.08	14.93
Na2O	2.71	2.83	2.57	2.95	2.89	2.67	2.75	3.12	2.67	2.54	2.63	2.67	2.67	2.82	2.72	2.75	2.90	2.99	3.17	2.99	2.92	3.09	2.96	2.90	3.04	2.92
K2O	0.12	0.12	0.13	0.16	0.15	0.14	0.15	0.11	0.16	0.20	0.13	0.14	0.21	0.12	0.15	0.18	0.16	0.19	0.17	0.17	0.18	0.18	0.17	0.19	0.18	0.18
Total	100.62	99.98	99.51	99.69	100.66	100.13	99.90	100.14	100.73	100.47	100.39	100.44	100.30	100.11	100.30	100.34	100.38	100.20	100.46	100.35	100.54	100.57	99.40	100.53	99.80	100.38
Cations (based on 32 oxygens)																										
Si	9.02	8.98	8.97	9.06	9.00	9.02	8.97	9.16	9.04	9.01	8.99	9.02	8.98	9.01	9.01	9.03	9.04	9.05	9.15	9.07	9.12	9.17	9.12	9.03	9.05	9.07
Al	6.88	6.97	6.88	6.82	6.96	6.85	7.01	6.74	6.86	6.88	6.91	6.89	6.95	6.88	6.89	6.88	6.94	6.89	6.74	6.91	6.80	6.74	6.77	6.92	6.88	6.91
Fe	0.05	0.05	0.05	0.05	0.05	0.04	0.05	0.03	0.04	0.05	0.04	0.04	0.04	0.04	0.05	0.04	0.05	0.04	0.04	0.04	0.05	0.05	0.05	0.05	0.05	0.05
Ca	3.10	3.03	3.21	3.05	3.00	3.15	2.99	2.98	3.10	3.14	3.12	3.10	3.07	3.10	3.11	3.07	2.94	2.96	2.97	2.91	2.98	2.94	2.99	2.98	2.96	2.91
Na	0.96	1.01	0.92	1.05	1.02	0.95	0.97	1.10	0.94	0.90	0.93	0.94	0.95	1.00	0.96	0.97	1.02	1.06	1.12	1.05	1.03	1.09	1.06	1.03	1.08	1.03
K	0.03	0.03	0.03	0.04	0.04	0.03	0.04	0.03	0.04	0.05	0.03	0.03	0.05	0.03	0.03	0.04	0.04	0.04	0.04	0.04	0.04	0.04	0.04	0.04	0.04	0.04
Total	20.03	20.05	20.06	20.07	20.05	20.05	20.03	20.04	20.02	20.02	20.03	20.03	20.04	20.06	20.04	20.03	20.02	20.05	20.06	20.02	20.02	20.03	20.04	20.05	20.07	20.01
An	75.84	74.53	77.17	73.71	74.00	76.24	74.77	72.49	75.99	76.89	76.46	76.00	75.54	75.08	75.71	75.16	73.48	72.86	71.94	72.69	73.58	72.24	73.22	73.63	72.50	73.08
Ab	23.47	24.78	22.06	25.36	25.13	22.97	24.35	26.86	23.11	21.99	22.80	23.19	23.27	24.21	23.46	23.83	25.60	26.06	27.11	26.35	25.39	26.70	25.80	25.29	26.48	25.86
Or	0.69	0.69	0.76	0.93	0.87	0.79	0.88	0.65	0.90	1.12	0.75	0.82	1.19	0.71	0.83	1.00	0.93	1.07	0.95	0.96	1.03	1.05	0.98	1.08	1.03	1.06
1 Standard deviation [wt%]																										
SiO2	0.33	0.13	0.71	0.58	0.35	0.19	0.43	0.53	0.30	1.42	0.15	0.44	0.49	0.33	0.12	0.55	0.29	0.33	0.47	0.33	0.36	0.48	0.30	0.30	0.19	0.36
Al2O3	0.20	0.20	0.31	0.46	0.22	0.11	0.21	0.25	0.07	1.00	0.12	0.16	0.33	0.45	0.07	0.28	0.22	0.20	0.25	0.26	0.16	0.36	0.24	0.15	0.24	0.22
FeO	0.04	0.02	0.04	0.05	0.01	0.02	0.06	0.02	0.03	0.05	0.03	0.03	0.03	0.04	0.02	0.04	0.02	0.03	0.03	0.03	0.04	0.03	0.01	0.02	0.02	0.02
CaO	0.26	0.21	0.50	0.45	0.26	0.16	0.25	0.40	0.13	0.61	0.08	0.24	0.26	0.37	0.11	0.22	0.18	0.24	0.27	0.29	0.33	0.35	0.25	0.28	0.14	0.10
Na2O	0.09	0.15	0.25	0.26	0.13	0.10	0.14	0.24	0.06	0.11	0.04	0.12	0.12	0.13	0.06	0.19	0.10	0.14	0.18	0.14	0.11	0.19	0.13	0.18	0.06	0.11
K2O	0.03	0.02	0.06	0.02	0.02	0.02	0.04	0.05	0.01	0.02	0.02	0.03	0.02	0.06	0.02	0.01	0.02	0.03	0.02	0.04	0.07	0.03	0.02	0.05	0.01	0.02
An	0.76	1.06	2.48	2.27	1.17	0.69	1.13	1.93	0.59	0.82	0.28	1.00	1.10	1.50	0.53	1.52	0.84	1.20	1.50	1.26	1.00	1.73	1.10	0.80	0.49	0.85
n	6	6	3	4	5	7	7	6	4	8	3	5	15	4	6	5	5	6	7	15	7	6	6	10	7	6

Sample	1539.10	1548.85 b	1556.56	1562.25 b	1573.75 a	1577.45 Top	1577.45 Mid	1577.45 Mid	1577.45 Base	1578.43 c-Top	1578.43 c-Base	1578.68 Top	1578.68 Base	1579.20	1581.88 b	1582.70 a	1583.25 a	1584.23 b	1585.38	1585.85	1586.65	1587.00
Rock type	.	.	.	o	o	o	.	.	o	+	o	.	.	+	+	+	+	+	+	*	.	.
[wt%]																						
SiO2	49.68	49.09	49.37	49.34	49.81	49.32	48.93	48.99	49.75	50.69	49.20	48.85	48.07	52.08	50.76	50.55	50.89	51.00	47.35	47.26	48.35	50.95
Al2O3	31.95	32.39	32.31	31.69	32.29	31.32	31.64	32.04	31.60	31.27	32.22	32.61	32.99	30.40	31.27	31.44	31.08	31.34	33.12	33.15	32.20	31.33
FeO	0.34	0.36	0.37	0.53	0.25	0.18	0.13	0.17	0.27	0.19	0.17	0.22	0.21	0.27	0.18	0.16	0.10	0.16	0.13	0.55	0.18	0.22
CaO	15.45	15.45	15.82	15.72	15.10	15.82	15.97	15.75	15.38	14.84	15.75	16.11	16.81	13.45	14.66	14.55	14.15	14.48	16.90	17.23	16.11	14.55
Na2O	2.86	2.76	2.63	2.82	3.00	2.95	2.83	2.59	2.78	3.06	2.65	2.87	2.55	4.25	3.74	3.79	4.08	3.84	2.53	2.40	2.94	3.33
K2O	0.18	0.18	0.16	0.17	0.13	0.13	0.13	0.11	0.21	0.18	0.15	0.12	0.11	0.20	0.19	0.09	0.06	0.17	0.06	0.04	0.12	0.17
Total	100.50	100.25	100.68	100.27	100.58	99.71	99.64	99.66	100.00	100.21	100.15	100.79	100.73	100.64	100.81	100.57	100.36	101.00	100.08	100.63	99.89	100.55
Si	9.05	8.97	8.99	9.03	9.05	9.07	9.01	9.00	9.10	9.23	8.99	8.90	8.78	9.43	9.21	9.18	9.25	9.23	8.71	8.67	8.89	9.24
Al	6.86	6.98	6.93	6.84	6.92	6.79	6.86	6.94	6.81	6.71	6.94	7.00	7.10	6.49	6.68	6.73	6.66	6.68	7.18	7.17	6.98	6.70
Fe	0.05	0.06	0.06	0.08	0.04	0.03	0.02	0.03	0.04	0.03	0.03	0.03	0.03	0.04	0.03	0.02	0.01	0.02	0.02	0.08	0.03	0.03
Ca	3.03	3.03	3.09	3.08	2.94	3.12	3.15	3.10	3.02	2.89	3.08	3.14	3.29	2.61	2.85	2.83	2.76	2.81	3.33	3.39	3.18	2.83
Na	1.01	0.98	0.93	1.00	1.06	1.05	1.01	0.92	0.99	1.08	0.94	1.01	0.90	1.49	1.32	1.33	1.44	1.35	0.90	0.85	1.05	1.17
K	0.04	0.04	0.04	0.04	0.03	0.03	0.03	0.03	0.05	0.04	0.04	0.03	0.03	0.05	0.04	0.02	0.01	0.04	0.01	0.01	0.03	0.04
Total	20.04	20.05	20.03	20.07	20.03	20.08	20.08	20.01	20.01	19.98	20.02	20.12	20.13	20.10	20.13	20.13	20.14	20.13	20.16	20.17	20.15	20.01
An	74.17	74.77	76.13	74.78	72.99	74.24	75.16	76.54	74.43	72.11	75.97	75.12	77.97	62.97	67.71	67.64	65.52	66.91	78.47	79.70	74.71	70.00
Ab	24.79	24.17	22.94	24.27	26.27	25.00	24.11	22.80	24.34	26.87	23.16	24.21	21.39	35.94	31.25	31.84	34.15	32.14	21.21	20.09	24.64	29.03
Or	1.03	1.06	0.94	0.95	0.74	0.75	0.73	0.66	1.23	1.02	0.87	0.67	0.63	1.09	1.04	0.51	0.33	0.95	0.32	0.21	0.65	0.98
SiO2	0.14	0.24	0.29	0.28	0.47	0.41	0.20	0.13	0.17	0.40	0.84	0.49	0.66	1.56	1.10	1.60	0.34	0.60	0.78	0.37	0.56	0.49
Al2O3	0.10	0.15	0.15	0.17	0.36	0.29	0.15	0.09	0.20	0.27	0.56	0.26	0.40	1.12	0.95	1.11	0.19	0.33	0.47	0.64	0.33	0.19
FeO	0.03	0.03	0.02	0.15	0.01	0.03	0.03	0.02	0.05	0.01	0.03	0.09	0.04	0.43	0.05	0.13	0.03	0.02	0.02	0.67	0.03	0.12
CaO	0.15	0.13	0.32	0.29	0.37	0.28	0.16	0.06	0.17	0.36	0.62	0.27	0.48	1.30	1.13	1.37	0.21	0.41	0.57	0.65	0.44	0.37
Na2O	0.07	0.10	0.07	0.10	0.23	0.15	0.06	0.06	0.10	0.19	0.32	0.16	0.25	0.71	0.66	0.73	0.12	0.23	0.31	0.25	0.23	0.20
K2O	0.02	0.04	0.02	0.07	0.02	0.03	0.02	0.01	0.12	0.01	0.01	0.02	0.03	0.04	0.04	0.04	0.02	0.03	0.03	0.01	0.02	0.01
An	0.62	0.71	0.76	1.03	1.98	1.28	0.49	0.21	0.53	2.90	1.76	1.36	2.26	6.11	5.39	6.32	0.96	1.89	2.65	2.33	2.00	1.43
n	6	5	5	8	5	5	5	6	4	4	4	7	7	7	5	7	6	6	5	6	5	5

Plagioclase analyses: H3 sequence

Sample	1050.80	1054.10 a	1060.05	1062.50	1065.05	1066.10	1071.05 a	1073.00	1075.15	1078.80	1080.00	1081.64 c-Top	1081.64 c-Base	1083.75	1086.50	1087.30	1087.65	1088.10 a	1089.25 Top	1089.25 Mid	1089.25 Base	1089.40 b-Top	1089.40 b-Mid	1089.40 b-Base	1089.65 Top	1089.65 Base
Rock type	.	o	.	.	.	.	.	.	.	o	.	+	.	o	.	.	.	.	.	+	.	.	o	.	x	.
[wt%]																										
SiO2	48.86	48.10	48.97	49.51	49.68	49.32	49.69	49.15	49.18	48.89	48.73	49.96	49.47	48.97	49.25	49.20	48.42	49.62	49.33	49.83	48.74	49.91	49.47	49.37	48.03	49.47
Al2O3	31.83	31.81	32.12	31.97	32.05	31.40	31.70	31.72	31.67	32.01	31.34	31.76	32.18	32.39	31.73	31.79	31.47	32.03	31.95	31.17	31.85	31.98	31.83	32.08	33.04	32.16
FeO	0.36	0.31	0.33	0.28	0.28	0.26	0.33	0.34	0.36	0.40	0.34	0.30	0.30	0.40	0.33	0.36	0.31	0.31	0.32	0.39	0.34	0.29	0.38	0.29	0.42	0.34
CaO	16.07	16.21	16.37	15.66	15.55	15.87	15.42	15.90	16.10	16.24	15.90	14.95	15.94	15.65	15.98	16.31	16.25	15.76	15.85	14.95	15.99	15.61	15.75	15.99	16.72	15.78
Na2O	2.71	2.51	2.61	2.77	2.73	2.87	2.96	2.81	2.81	2.65	2.77	3.18	2.65	2.68	2.71	2.55	2.74	2.67	2.58	3.02	2.53	2.73	2.63	2.53	2.05	2.61
K2O	0.10	0.14	0.15	0.17	0.17	0.26	0.15	0.13	0.15	0.10	0.15	0.10	0.16	0.15	0.15	0.13	0.16	0.17	0.17	0.24	0.16	0.16	0.17	0.17	0.13	0.16
Total	99.93	99.08	100.56	100.36	100.45	99.98	100.25	100.06	100.28	100.30	99.23	100.24	100.70	100.23	100.15	100.36	99.35	100.57	100.19	99.60	99.61	100.68	100.23	100.43	100.38	100.51
Cations (based on 32 oxygens)																										
Si	8.98	8.92	8.95	9.03	9.05	9.05	9.08	9.01	9.01	8.95	9.02	9.11	9.00	8.96	9.02	9.00	8.96	9.04	9.02	9.15	8.98	9.07	9.04	9.01	8.79	9.01
Al	6.89	6.95	6.92	6.88	6.88	6.79	6.82	6.86	6.84	6.91	6.83	6.83	6.90	6.98	6.85	6.85	6.87	6.88	6.89	6.75	6.91	6.85	6.86	6.90	7.13	6.91
Fe	0.06	0.05	0.05	0.04	0.04	0.04	0.05	0.05	0.06	0.06	0.05	0.05	0.05	0.06	0.05	0.06	0.05	0.05	0.05	0.06	0.05	0.04	0.06	0.04	0.06	0.05
Ca	3.16	3.22	3.20	3.06	3.04	3.12	3.02	3.12	3.16	3.19	3.15	2.92	3.11	3.07	3.14	3.20	3.22	3.08	3.10	2.94	3.16	3.04	3.08	3.13	3.28	3.08
Na	0.96	0.90	0.92	0.98	0.96	1.02	1.05	1.00	1.00	0.94	0.99	1.12	0.94	0.95	0.96	0.90	0.98	0.94	0.91	1.08	0.90	0.96	0.93	0.89	0.73	0.92
K	0.02	0.03	0.03	0.04	0.04	0.06	0.04	0.03	0.04	0.02	0.03	0.02	0.04	0.03	0.03	0.03	0.04	0.04	0.04	0.06	0.04	0.04	0.04	0.04	0.03	0.04
Total	20.07	20.07	20.08	20.04	20.01	20.09	20.05	20.07	20.09	20.07	20.08	20.05	20.03	20.05	20.05	20.04	20.12	20.02	20.01	20.04	20.04	20.00	20.01	20.01	20.02	20.01
An	76.21	77.47	76.96	75.03	75.17	74.24	73.55	75.20	75.39	76.76	75.43	71.81	76.14	75.71	75.87	77.37	75.94	75.80	76.50	72.19	77.05	75.28	76.05	77.01	81.26	76.28
Ab	23.22	21.74	22.22	24.01	23.88	24.30	25.58	24.05	23.76	22.66	23.74	27.65	22.93	23.46	23.28	21.90	23.18	23.25	22.53	26.40	22.03	23.80	22.97	22.00	18.01	22.81
Or	0.57	0.79	0.82	0.96	0.95	1.45	0.86	0.75	0.86	0.58	0.83	0.55	0.92	0.84	0.85	0.73	0.88	0.95	0.97	1.40	0.92	0.92	0.98	0.99	0.74	0.91
1 Standard deviation [wt%]																										
SiO2	0.14	0.13	0.26	0.55	0.21	0.54	0.32	0.43	0.31	0.24	0.38	0.27	0.20	0.38	0.28	0.34	0.31	0.29	0.62	0.43	0.35	0.24	0.56	0.31	0.91	0.44
Al2O3	0.14	0.08	0.15	0.39	0.12	0.43	0.39	0.36	0.24	0.19	0.21	0.18	0.13	0.32	0.22	0.22	0.16	0.19	0.24	0.23	0.17	0.17	0.14	0.07	0.85	0.44
FeO	0.04	0.04	0.03	0.03	0.04	0.02	0.02	0.03	0.02	0.05	0.04	0.30	0.03	0.04	0.02	0.02	0.03	0.05	0.02	0.11	0.07	0.04	0.05	0.02	0.11	0.04
CaO	0.19	0.08	0.14	0.48	0.17	0.48	0.20	0.35	0.28	0.19	0.27	0.15	0.09	0.16	0.27	0.21	0.22	0.23	0.34	0.43	0.19	0.14	0.17	0.04	0.84	0.32
Na2O	0.04	0.06	0.10	0.25	0.06	0.21	0.14	0.18	0.15	0.11	0.19	0.10	0.09	0.10	0.11	0.11	0.11	0.14	0.12	0.22	0.12	0.03	0.08	0.09	0.48	0.15
K2O	0.01	0.03	0.01	0.02	0.01	0.14	0.02	0.03	0.02	0.01	0.03	0.01	0.01	0.02	0.01	0.01	0.01	0.03	0.02	0.01	0.02	0.02	0.00	0.01	0.04	0.03
An	0.46	0.41	0.76	2.22	0.65	0.82	1.00	1.65	0.13	0.89	1.55	0.86	0.66	0.86	1.02	0.95	0.94	0.87	1.24	2.00	1.06	0.45	0.72	0.71	2.89	1.34
n	4	4	13	16	6	5	7	11	7	11	8	8	6	25	7	8	5	13	3	4	4	3	5	3	7	8

Sample	1090.20 a	1090.20 b	1099.35	1110.05	1127.50	1144.10	1156.46	1166.10	1175.80	1191.50	1200.30	1206.95	1211.85	1219.05	1228.25	1231.35	1233.90	1246.65	1252.08	1252.50 Top	1252.50 Base	1253.30 a-Top	1253.30 a-Mid	1253.30 a-Base	1256.75	1258.45	1261.15 a	1263.60	1266.28
Rock type	.	.	.	.	.	.	.	.	.	.	.	.	.	.	.	.	.	.	.	o	.	.	o	.	+	+	+	+	.
[wt%]																													
SiO2	49.94	49.41	48.77	49.74	50.29	49.39	49.30	49.70	49.70	49.12	49.60	49.35	49.76	49.16	48.97	48.28	49.54	49.35	48.85	49.07	48.84	48.73	48.43	48.90	51.23	56.77	55.07	58.09	49.22
Al2O3	31.99	31.87	31.44	31.63	31.93	31.59	31.71	31.79	32.05	31.81	31.72	31.48	32.13	31.68	31.91	32.05	31.07	32.04	31.51	31.50	31.49	32.34	32.19	31.87	30.54	26.69	28.16	26.07	32.49
FeO	0.29	0.28	0.32	0.29	0.25	0.29	0.27	0.27	0.32	0.30	0.41	0.37	0.33	0.36	0.35	0.36	0.42	0.38	0.32	0.34	0.24	0.36	0.33	0.29	0.23	0.21	0.29	0.20	0.26
CaO	15.40	15.88	16.00	15.39	15.12	15.52	15.33	15.71	15.69	15.55	15.45	15.59	15.38	15.68	15.92	16.21	15.84	15.83	15.96	15.98	16.02	16.37	16.31	15.75	13.72	9.41	11.05	8.69	15.97
Na2O	2.79	2.71	2.84	2.88	2.95	2.85	2.84	2.92	2.87	2.72	2.88	2.66	2.78	2.77	2.64	2.58	2.95	2.77	2.61	2.95	2.87	2.53	2.47	2.75	3.85	6.30	5.29	6.73	2.45
K2O	0.19	0.16	0.15	0.17	0.16	0.16	0.15	0.17	0.16	0.13	0.17	0.14	0.13	0.14	0.15	0.13	0.13	0.15	0.16	0.12	0.12	0.16	0.15	0.14	0.25	0.45	0.41	0.38	0.19
Total	100.60	100.32	99.53	100.10	100.70	99.81	99.60	100.56	100.78	99.64	100.24	99.59	100.51	99.79	99.94	99.61	99.94	100.51	99.41	99.95	99.58	100.49	99.89	99.69	99.83	99.83	100.27	100.17	100.58
Cations (based on 32 oxygens)																													
Si	9.08	9.03	9.00	9.09	9.12	9.06	9.06	9.06	9.04	9.03	9.07	9.07	9.05	9.03	8.99	8.91	9.10	9.00	9.01	9.02	9.00	8.91	8.91	8.99	9.35	10.24	9.93	10.41	8.96
Al	6.85	6.86	6.84	6.82	6.83	6.83	6.87	6.83	6.87	6.89	6.83	6.82	6.89	6.86	6.90	6.97	6.72	6.89	6.85	6.82	6.84	6.97	6.98	6.91	6.57	5.67	5.99	5.51	6.97
Fe	0.04	0.04	0.05	0.04	0.04	0.04	0.04	0.04	0.05	0.05	0.06	0.06	0.05	0.05	0.05	0.06	0.06	0.06	0.05	0.05	0.04	0.06	0.05	0.04	0.04	0.03	0.04	0.03	0.04
Ca	3.00	3.11	3.16	3.01	2.94	3.05	3.02	3.07	3.06	3.06	3.03	3.07	3.00	3.09	3.13	3.20	3.12	3.09	3.16	3.15	3.16	3.21	3.21	3.10	2.69	1.82	2.14	1.67	3.12
Na	0.98	0.96	1.01	1.02	1.04	1.02	1.01	1.03	1.01	0.97	1.02	0.95	0.98	0.99	0.94	0.92	1.05	0.98	0.93	1.05	1.03	0.90	0.88	0.98	1.36	2.20	1.85	2.34	0.86
K	0.04	0.04	0.04	0.04	0.04	0.04	0.04	0.04	0.04	0.03	0.04	0.03	0.03	0.03	0.04	0.03	0.03	0.03	0.04	0.03	0.03	0.04	0.04	0.03	0.06	0.10	0.09	0.09	0.04
Total	20.01	20.04	20.10	20.03	20.00	20.05	20.03	20.06	20.06	20.03	20.05	20.01	20.01	20.05	20.05	20.09	20.08	20.06	20.04	20.11	20.10	20.07	20.06	20.06	20.07	20.07	20.04	20.05	20.00
An	74.52	75.70	75.07	73.99	73.21	74.10	74.27	74.11	74.47	75.36	74.08	75.85	74.77	75.17	76.24	77.08	74.30	75.29	76.48	74.48	75.03	77.44	77.80	75.42	65.41	44.11	53.75	40.77	77.44
Ab	24.39	23.38	24.08	25.06	25.85	24.74	24.86	24.96	24.65	23.88	24.96	23.36	24.47	24.02	22.89	22.16	24.99	23.88	22.60	24.87	24.31	21.64	21.34	23.80	33.17	53.37	45.32	57.10	21.46
Or	1.09	0.92	0.85	0.95	0.94	0.91	0.87	0.93	0.88	0.76	0.96	0.82	0.76	0.81	0.88	0.76	0.70	0.83	0.93	0.65	0.66	0.92	0.87	0.77	1.42	2.53	2.32	2.14	1.10
1 Standard deviation [wt%]																													
SiO2	0.46	0.39	0.19	0.36	0.15	0.43	0.17	0.18	0.20	0.12	0.22	1.07	0.35	0.23	0.46	0.18	0.49	0.45	0.36	0.21	0.22	0.27	0.33	0.35	1.78	0.66	1.04	1.22	0.38
Al2O3	0.17	0.29	0.18	0.29	0.25	0.28	0.15	0.08	0.15	0.17	0.23	0.40	0.21	0.23	0.10	0.14	0.67	0.25	0.26	0.19	0.15	0.14	0.30	0.27	1.25	0.43	0.77	0.70	0.10
FeO	0.03	0.02	0.02	0.03	0.05	0.04	0.03	0.03	0.04	0.04	0.04	0.03	0.02	0.03	0.05	0.01	0.04	0.03	0.03	0.03	0.03	0.03	0.03	0.02	0.09	0.05	0.32	0.05	0.01
CaO	0.21	0.27	0.20	0.17	0.10	0.29	0.31	0.20	0.14	0.07	0.33	0.66	0.12	0.21	0.21	0.02	0.49	0.23	0.30	0.07	0.14	0.15	0.27	0.31	1.34	0.41	0.78	0.70	0.27
Na2O	0.14	0.14	0.08	0.15	0.04	0.19	0.06	0.09	0.07	0.09	0.15	0.25	0.09	0.13	0.11	0.08	0.21	0.14	0.16	0.10	0.10	0.12	0.14	0.17	0.82	0.35	0.49	0.46	0.12
K2O	0.04	0.03	0.02	0.03	0.01	0.03	0.01	0.01	0.03	0.02	0.03	0.03	0.03	0.02	0.01	0.01	0.03	0.02	0.02	0.03	0.02	0.01	0.01	0.02	0.07	0.10	0.06	0.04	0.01
An	1.08	1.16	0.73	1.25	0.38	1.51	0.47	2.20	0.45	0.63	1.37	1.50	0.79	1.03	0.95	0.34	1.95	1.07	1.48	0.66	0.63	1.53	1.24	1.44	7.02	2.18	3.88	3.00	1.17
n	8	13	4	4	3	15	7	6	12	4	6	6	6	7	6	5	8	18	4	6	6	9	10	12	6	5	12	5	5

Plagioclase analyses: KR2 sequence

Sample	1146.00	1150.15	1155.45	1160.40	1168.55	1174.10	1177.70 Top	1177.70 Base	1179.95	1181.20	1185.90	1187.30 b	1191.20	1191.58 a	1192.10 Top	1192.10 Base	1193.45 Top	1193.45 Base	1194.20	1203.75	1219.75	1227.15	1236.20	1241.30	1251.90	1260.30
Rock type	o	.	.	.	o	.	+	o	.	.	.	.	.	.	.	.	.	.	.	.	.	.	.	.	.	.
[wt%]																										
SiO2	49.44	48.93	49.32	49.16	49.51	49.47	48.97	48.48	49.08	49.30	48.60	49.05	49.40	49.09	49.62	48.94	48.72	48.42	48.76	49.54	49.85	49.25	49.24	50.18	49.07	50.22
Al2O3	32.46	32.47	32.30	32.06	32.44	32.51	31.90	31.84	32.27	31.71	32.14	32.44	32.14	32.54	32.49	32.50	32.08	32.13	31.94	31.79	32.12	31.71	32.21	31.56	31.65	31.61
FeO	0.42	0.37	0.27	0.36	0.37	0.29	0.23	0.34	0.33	0.26	0.34	0.28	0.35	0.39	0.27	0.33	0.31	0.36	0.34	0.34	0.31	0.30	0.34	0.30	0.28	0.30
CaO	15.70	15.87	15.42	15.64	15.53	15.61	15.35	15.56	15.42	15.20	15.88	15.75	15.54	15.96	15.58	15.85	15.61	15.86	15.59	15.57	15.32	15.28	15.48	15.17	15.35	14.78
Na2O	2.60	2.57	2.66	2.69	2.70	2.70	2.75	2.65	2.77	2.84	2.56	2.61	2.68	2.52	2.74	2.55	2.71	2.62	2.71	2.83	2.81	2.88	2.77	2.89	2.90	3.11
K2O	0.13	0.14	0.18	0.14	0.14	0.15	0.22	0.16	0.14	0.16	0.13	0.14	0.12	0.14	0.17	0.17	0.12	0.12	0.13	0.16	0.15	0.15	0.16	0.17	0.12	0.14
Total	100.75	100.34	100.15	100.04	100.68	100.72	99.42	99.02	100.00	99.46	99.66	100.28	100.22	100.65	100.87	100.34	99.57	99.50	99.49	100.24	100.56	99.59	100.19	100.28	99.36	100.16
Cations (based on 32 oxygens)																										
Si	8.99	8.94	9.01	9.00	9.00	8.99	9.02	8.97	8.99	9.07	8.94	8.96	9.02	8.94	9.00	8.94	8.97	8.93	8.98	9.05	9.06	9.05	9.00	9.15	9.04	9.16
Al	6.95	6.99	6.95	6.92	6.95	6.96	6.92	6.95	6.96	6.87	6.97	6.98	6.92	6.99	6.95	7.00	6.96	6.98	6.94	6.85	6.88	6.87	6.94	6.78	6.87	6.79
Fe	0.06	0.06	0.04	0.05	0.06	0.04	0.04	0.05	0.05	0.04	0.05	0.04	0.05	0.06	0.04	0.05	0.05	0.06	0.05	0.05	0.05	0.05	0.05	0.05	0.04	0.05
Ca	3.06	3.11	3.02	3.07	3.02	3.04	3.03	3.09	3.03	3.00	3.13	3.08	3.04	3.12	3.03	3.10	3.08	3.13	3.08	3.05	2.98	3.01	3.03	2.96	3.03	2.89
Na	0.92	0.91	0.94	0.96	0.95	0.95	0.98	0.95	0.98	1.01	0.91	0.92	0.95	0.89	0.96	0.90	0.97	0.94	0.97	1.00	0.99	1.03	0.98	1.02	1.04	1.10
K	0.03	0.03	0.04	0.03	0.03	0.04	0.05	0.04	0.03	0.04	0.03	0.03	0.03	0.03	0.04	0.04	0.03	0.03	0.03	0.04	0.04	0.04	0.04	0.04	0.03	0.03
Total	20.01	20.03	20.00	20.03	20.02	20.02	20.04	20.05	20.04	20.02	20.04	20.03	20.01	20.03	20.03	20.03	20.05	20.06	20.05	20.04	20.01	20.04	20.04	19.99	20.05	20.01
An	76.36	76.77	75.47	75.66	75.46	75.53	74.59	75.73	74.92	74.09	76.84	76.30	75.69	77.13	75.09	76.72	75.53	76.46	75.51	74.55	74.42	73.90	74.83	73.63	74.01	71.86
Ab	22.91	22.45	23.50	23.56	23.73	23.59	24.15	23.35	24.29	24.99	22.40	22.89	23.59	22.05	23.92	22.32	23.76	22.83	23.75	24.54	24.68	25.21	24.27	25.41	25.31	27.33
Or	0.74	0.79	1.03	0.78	0.81	0.88	1.26	0.92	0.79	0.91	0.77	0.81	0.71	0.82	1.00	0.96	0.70	0.71	0.74	0.91	0.89	0.89	0.90	0.97	0.68	0.81
1 Standard deviation [wt%]																										
SiO2	0.28	0.36	0.42	0.24	0.35	0.41	0.23	0.29	0.37	0.40	0.42	0.28	0.19	0.21	0.14	0.27	0.42	0.30	0.25	0.24	0.17	0.38	0.20	0.16	0.17	0.28
Al2O3	0.16	0.17	0.24	0.24	0.30	0.08	0.09	0.37	0.14	0.20	0.21	0.07	0.14	0.14	0.16	0.14	0.25	0.10	0.23	0.34	0.19	0.18	0.18	0.20	0.17	0.23
FeO	0.01	0.04	0.03	0.03	0.02	0.02	0.02	0.02	0.03	0.02	0.03	0.03	0.02	0.02	0.01	0.02	0.03	0.02	0.02	0.03	0.03	0.04	0.03	0.02	0.02	0.03
CaO	0.15	0.14	0.30	0.15	0.22	0.13	0.12	0.18	0.18	0.10	0.12	0.16	0.07	0.06	0.10	0.07	0.11	0.14	0.05	0.14	0.11	0.09	0.15	0.13	0.07	0.05	0.13
Na2O	0.11	0.10	0.17	0.12	0.14	0.05	0.06	0.11	0.10	0.12	0.16	0.07	0.06	0.10	0.07	0.11	0.14	0.05	0.14	0.11	0.09	0.15	0.13	0.07	0.05	0.13
K2O	0.01	0.01	0.02	0.01	0.02	0.02	0.05	0.01	0.02	0.03	0.02	0.00	0.01	0.02	0.01	0.02	0.02	0.01	0.01	0.01	0.02	0.02	0.02	0.02	0.01	0.02
An	0.87	0.75	1.47	0.95	1.20	0.38	0.40	1.01	0.90	0.90	1.50	0.58	0.60	0.84	0.68	0.98	0.44	1.31	1.18	1.05	0.71	1.27	1.11	0.68	0.41	1.12
n	5	6	9	8	7	4	3	4	6	5	8	5	7	6	4	5	6	5	8	6	6	8	5	6	5	6

Plagioclase analyses: Additional samples

Sample	1269.35	1287.25 b	1295.85	1297.40	1300.90
Rock type	.	.	+	+	.
[wt%]					
SiO2	49.10	49.42	52.73	52.90	48.56
Al2O3	31.79	31.98	30.30	29.68	32.03
FeO	0.35	0.36	0.16	0.21	0.27
CaO	15.27	15.32	12.69	12.42	15.51
Na2O	2.88	2.81	4.00	4.14	2.51
K2O	0.14	0.16	0.34	0.38	0.16
Total	99.53	100.04	100.23	99.72	99.04
Cations (based on 32 oxygens)					
Si	9.03	9.04	9.54	9.62	8.98
Al	6.89	6.90	6.46	6.36	6.98
Fe	0.05	0.05	0.02	0.03	0.04
Ca	3.01	3.00	2.46	2.42	3.07
Na	1.03	1.00	1.40	1.46	0.90
K	0.03	0.04	0.08	0.09	0.04
Total	20.05	20.03	19.97	19.98	20.00
An	73.97	74.41	62.40	61.01	76.63
Ab	25.22	24.69	35.62	36.77	22.41
Or	0.81	0.91	1.98	2.21	0.96
1 Standard deviation [wt%]					
SiO2	0.28	0.62	0.39	0.33	0.44
Al2O3	0.34	0.43	0.31	0.18	0.32
FeO	0.02	0.04	0.03	0.01	0.01
CaO	0.25	0.51	0.28	0.25	0.29
Na2O	0.08	0.27	0.10	0.09	0.21
K2O	0.01	0.03	0.04	0.03	0.03
An	0.79	2.42	1.05	0.96	1.85
n	6	6	7	6	4

	Lone Chrome Seam						Boulder Bed			Merensky Reef				LK5	LK5	
Sample	RS3B base	RS3B top	RS3B Seam	BBCR Base	BBCR Seam	BBCR Top	BBBC Outside	BBBC Inside	BBBC Rim	BSIM Top	BSIM Base	BSIMTC Top	BSIMTC Seam	1488.26 Inside	1488.26 Outside	BM 277.3 Top
Rock type	o	o	#	o	#	o	o	*	*	*	*	o	+	*	.	o
[wt%]																
SiO2	48.41	47.97	48.15	47.53	44.95	48.18	48.44	49.02	47.67	48.83	48.75	51.10	48.38	47.04	48.27	48.13
Al2O3	32.55	32.14	33.25	32.74	34.66	32.33	32.34	32.03	32.52	32.64	32.71	31.26	33.39	32.93	32.11	32.47
FeO	0.33	0.29	0.24	0.24	0.20	0.25	0.20	0.19	0.20	0.10	0.13	0.14	0.13	0.31	0.30	0.28
CaO	16.48	16.26	17.27	16.56	18.56	16.07	16.00	15.45	16.47	16.10	16.14	14.50	16.82	16.77	15.97	16.48
Na2O	2.62	2.52	2.07	2.39	1.16	2.63	2.68	2.99	2.42	2.70	2.59	3.67	2.35	2.40	2.78	2.60
K2O	0.14	0.13	0.08	0.06	0.01	0.12	0.13	0.14	0.09	0.11	0.15	0.21	0.07	0.04	0.10	0.13
Total	100.52	99.31	101.06	99.53	99.55	99.59	99.79	99.80	99.36	100.50	100.47	100.87	101.15	99.49	99.54	100.09
Cations (based on 32 oxygens)																
Si	8.86	8.88	8.76	8.78	8.35	8.88	8.91	9.00	8.82	8.91	8.90	9.25	8.78	8.71	8.91	8.84
Al	7.02	7.01	7.13	7.13	7.58	7.03	7.01	6.93	7.09	7.02	7.04	6.67	7.15	7.18	6.98	7.03
Fe	0.05	0.05	0.04	0.04	0.03	0.04	0.03	0.03	0.03	0.02	0.02	0.02	0.02	0.05	0.05	0.04
Ca	3.23	3.22	3.37	3.28	3.69	3.17	3.15	3.04	3.26	3.15	3.16	2.81	3.27	3.33	3.16	3.25
Na	0.93	0.90	0.73	0.85	0.42	0.94	0.96	1.06	0.87	0.96	0.92	1.29	0.83	0.86	1.00	0.93
K	0.03	0.03	0.02	0.01	0.00	0.03	0.03	0.03	0.02	0.03	0.03	0.05	0.02	0.01	0.02	0.03
Total	20.12	20.09	20.05	20.09	20.07	20.09	20.08	20.09	20.08	20.07	20.06	20.08	20.07	20.14	20.11	20.12
An	77.06	77.56	81.82	79.05	89.80	76.61	76.16	73.52	78.62	76.20	76.84	67.83	79.47	79.29	75.59	77.23
Ab	22.16	21.74	17.73	20.61	10.14	22.69	23.11	25.72	20.88	23.16	22.32	31.02	20.09	20.47	23.82	22.02
Or	0.78	0.72	0.46	0.35	0.09	0.71	0.73	0.77	0.49	0.63	0.83	1.14	0.42	0.24	0.59	0.74
1 Standard deviation [wt%]																
SiO2	0.19	0.55	0.02	1.28	1.13	0.22	0.29	0.82	0.51	0.58	0.59	0.02	1.50	1.02	0.76	0.41
Al2O3	0.27	0.19	0.10	0.88	0.94	0.09	0.33	0.50	0.06	0.49	0.27	0.05	1.02	0.73	0.14	0.26
FeO	0.02	0.03	0.01	0.04	0.01	0.03	0.03	0.09	0.03	0.03	0.01	0.00	0.01	0.13	0.02	0.02
CaO	0.14	0.26	0.09	0.98	0.99	0.16	0.34	0.59	0.39	0.60	0.29	0.10	1.21	0.83	0.28	0.24
Na2O	0.05	0.22	0.06	0.57	0.60	0.10	0.11	0.38	0.15	0.24	0.13	0.02	0.65	0.47	0.22	0.14
K2O	0.01	0.04	0.01	0.03	0.01	0.01	0.03	0.05	0.01	0.04	0.01	0.01	0.02	0.03	0.02	0.01
An	0.81	0.98	0.70	5.04	5.19	0.86	1.10	3.17	1.50	2.38	1.15	0.09	5.70	4.06	1.72	1.10
n	6	4	2	4	2	4	7	16	2	5	3	2	2	7	3	6

Plagioclase analyses (inclusions): UA-sequence

Sample	647.90	651.30	652.30	654.10	654.90	668.90
Rock-type	.	.	.	.	.	+
[wt%]						
SiO2	48.54	48.68	48.45	48.37	48.71	55.40
Al2O3	32.05	31.89	32.42	32.30	32.58	27.36
FeO	0.30	0.24	0.26	0.20	0.24	0.18
CaO	15.92	15.77	16.39	16.54	16.49	10.21
Na2O	2.53	2.83	2.39	2.53	2.54	5.57
K2O	0.10	0.14	0.09	0.11	0.10	0.42
Total	99.45	99.55	100.00	100.05	100.65	99.15
Cations (based on 32 oxygens)						
Si	8.95	8.97	8.89	8.88	8.89	10.08
Al	6.96	6.93	7.01	6.99	7.00	5.87
Fe	0.05	0.04	0.04	0.03	0.04	0.03
Ca	3.14	3.11	3.22	3.25	3.22	1.99
Na	0.90	1.01	0.85	0.90	0.90	1.96
K	0.02	0.03	0.02	0.03	0.02	0.10
Total	20.03	20.09	20.04	20.09	20.07	20.02
An	77.19	74.92	78.71	77.84	77.81	49.14
Ab	22.21	24.32	20.78	21.55	21.63	48.45
Or	0.60	0.76	0.52	0.61	0.55	2.42
1 Standard deviation [wt%]						
SiO2	0.19	0.26	0.20	0.18	0.58	0.01
Al2O3	0.13	0.23	0.04	0.11	0.24	0.00
FeO	0.03	0.04	0.05	0.01	0.05	0.03
CaO	0.10	0.29	0.12	0.20	0.38	0.05
Na2O	0.05	0.16	0.10	0.12	0.23	0.14
K2O	0.01	0.02	0.01	0.01	0.02	0.02
An	0.46	1.28	0.74	0.97	2.00	0.77
n	3	4	3	4	3	2

Plagioclase analyses (inclusions): EK22 sequence

Sample	272.25	277.90	280.65	282.80	286.05	288.40 b-Base	291.48	292.05	303.90	315.90
Rock-type	.	.	.	.	.	o	*	.	.	.
[wt%]										
SiO2	48.60	48.46	48.36	49.38	48.68	48.89	47.88	48.47	48.41	47.82
Al2O3	31.92	31.43	31.81	31.74	32.35	32.66	31.90	32.52	31.54	32.11
FeO	0.34	0.32	0.29	0.19	0.24	0.29	0.28	0.30	0.32	0.27
CaO	16.25	16.11	16.72	15.28	16.05	16.11	16.54	16.07	16.26	16.64
Na2O	2.49	2.54	2.55	2.98	2.56	2.49	2.58	2.53	2.66	2.39
K2O	0.17	0.10	0.13	0.12	0.12	0.14	0.04	0.07	0.16	0.11
Total	99.77	98.96	99.85	99.69	99.99	100.58	99.22	99.96	99.36	99.34
Cations (based on 32 oxygens)										
Si	8.95	8.99	8.91	9.06	8.93	8.91	8.87	8.89	8.96	8.85
Al	6.93	6.87	6.91	6.87	6.99	7.02	6.97	7.03	6.88	7.01
Fe	0.05	0.05	0.04	0.03	0.04	0.04	0.04	0.05	0.05	0.04
Ca	3.20	3.20	3.30	3.01	3.15	3.15	3.28	3.16	3.22	3.30
Na	0.89	0.91	0.91	1.06	0.91	0.88	0.93	0.90	0.95	0.86
K	0.04	0.02	0.03	0.03	0.03	0.03	0.01	0.02	0.04	0.03
Total	20.05	20.05	20.11	20.05	20.05	20.03	20.11	20.05	20.10	20.09
An	77.58	77.36	77.81	73.46	77.07	77.55	77.81	77.55	76.46	78.88
Ab	21.48	22.08	21.50	25.88	22.25	21.66	21.99	22.05	22.65	20.49
Or	0.94	0.56	0.69	0.66	0.67	0.79	0.20	0.40	0.89	0.63
1 Standard deviation [wt%]										
SiO2	0.30	0.15	0.06	0.62	0.13	0.58	0.47	0.49	0.32	0.21
Al2O3	0.08	0.09	0.07	0.24	0.09	0.46	0.40	0.18	0.23	0.13
FeO	0.07	0.03	0.01	0.03	0.04	0.09	0.04	0.03	0.04	0.02
CaO	0.32	0.04	0.11	0.43	0.11	0.49	0.44	0.24	0.15	0.11
Na2O	0.10	0.08	0.06	0.25	0.05	0.28	0.22	0.09	0.04	0.04
K2O	0.11	0.01	0.02	0.04	0.01	0.04	0.01	0.02	0.06	0.01
An	1.29	0.60	0.52	2.10	0.39	2.59	1.89	0.82	0.43	0.43
n	6	4	4	4	5	4	6	5	5	4

Plagioclase analyses (inclusions): IN sequence

Sample	811.78	821.23 b	826.00	837.86	844.00	866.40	883.14
Rock-type	.	.	.	.	.	x	.
[wt%]							
SiO2	48.69	48.57	48.91	48.45	48.85	47.30	49.08
Al2O3	31.80	32.58	32.31	32.82	32.92	32.92	32.87
FeO	0.35	0.28	0.36	0.21	0.18	0.45	0.14
CaO	16.03	16.40	16.17	15.82	15.84	17.10	15.75
Na2O	2.60	2.61	2.50	2.64	2.43	2.09	2.62
K2O	0.14	0.11	0.12	0.12	0.12	0.01	0.09
Total	99.61	100.55	100.38	100.07	100.34	99.88	100.54
Cations (based on 32 oxygens)							
Si	8.97	8.87	8.94	8.88	8.91	8.72	8.93
Al	6.90	7.02	6.96	7.09	7.08	7.16	7.05
Fe	0.05	0.04	0.06	0.03	0.03	0.07	0.02
Ca	3.16	3.21	3.17	3.10	3.09	3.38	3.07
Na	0.93	0.92	0.89	0.94	0.86	0.75	0.92
K	0.03	0.03	0.03	0.03	0.03	0.00	0.02
Total	20.06	20.09	20.04	20.06	20.00	20.07	20.02
An	76.71	77.15	77.61	76.26	77.72	81.88	76.46
Ab	22.52	22.22	21.71	23.03	21.60	18.06	23.00
Or	0.77	0.63	0.68	0.70	0.68	0.06	0.55
1 Standard deviation [wt%]							
SiO2	0.17	0.13	0.15	0.13	0.22	0.78	
Al2O3	0.12	0.05	0.12	0.13	0.15	0.55	
FeO	0.03	0.02	0.10	0.06	0.03	0.34	
CaO	0.14	0.07	0.08	0.20	0.37	0.55	
Na2O	0.07	0.02	0.10	0.05	0.09	0.33	
K2O	0.04	0.01	0.02	0.03	0.01	0.01	
An	0.78	0.12	0.75	0.50	0.99	2.73	
n	3	4	3	6	4	3	1

Plagioclase analyses (inclusions): IM sequence

Sample	788.32	788.60	788.80	790.64	793.22	798.00	801.00	810.10	818.00	819.30	819.85	826.48	836.00	843.61
Rock-type	.	.	.	.	.	x	.	.	.	.	x	.	.	o
[wt%]														
SiO2	50.35	49.63	48.74	48.53	48.91	48.90	48.39	48.16	48.19	47.77	49.50	49.02	48.97	48.27
Al2O3	31.53	32.60	32.37	32.11	32.30	33.13	32.89	33.05	32.14	33.19	32.42	32.29	32.49	32.41
FeO	0.16	0.40	0.35	0.23	0.27	0.21	0.20	0.21	0.12	0.24	0.31	0.24	0.21	0.24
CaO	15.02	15.79	15.95	15.97	16.10	15.95	15.97	15.97	16.26	16.67	15.94	15.87	15.86	15.52
Na2O	2.93	2.61	2.50	2.62	2.58	2.62	2.47	2.62	2.64	2.21	2.65	2.55	2.74	2.62
K2O	0.18	0.11	0.12	0.14	0.14	0.04	0.09	0.04	0.03	0.07	0.06	0.06	0.08	0.11
Total	100.17	101.15	100.03	99.60	100.30	100.68	100.01	100.05	99.37	100.15	100.88	100.02	100.35	99.18
Cations (based on 32 oxygens)														
Si	9.17	8.98	8.93	8.94	8.94	8.88	8.87	8.83	8.90	8.76	8.99	8.97	8.94	8.91
Al	6.77	6.96	6.99	6.97	6.96	7.09	7.10	7.14	6.99	7.17	6.94	6.96	6.99	7.05
Fe	0.02	0.06	0.05	0.03	0.04	0.03	0.03	0.03	0.02	0.04	0.05	0.04	0.03	0.04
Ca	2.93	3.06	3.13	3.15	3.16	3.10	3.13	3.14	3.22	3.28	3.10	3.11	3.10	3.07
Na	1.03	0.92	0.89	0.93	0.91	0.92	0.88	0.93	0.94	0.78	0.93	0.90	0.97	0.94
K	0.04	0.03	0.03	0.03	0.03	0.01	0.02	0.01	0.01	0.02	0.01	0.01	0.02	0.03
Total	19.98	20.01	20.03	20.06	20.05	20.04	20.03	20.07	20.08	20.05	20.02	20.00	20.06	20.04
An	73.14	76.49	77.37	76.53	76.91	76.92	77.74	76.92	77.19	80.37	76.62	77.24	75.86	76.10
Ab	25.81	22.86	21.94	22.67	22.30	22.86	21.72	22.84	22.65	19.21	23.05	22.44	23.67	23.25
Or	1.04	0.65	0.70	0.81	0.79	0.22	0.55	0.24	0.16	0.41	0.33	0.33	0.47	0.65
1 Standard deviation [wt%]														
SiO2		0.94	0.06	0.21	0.07	0.23	0.17	0.49	0.38	1.43	0.25	0.18	0.26	0.25
Al2O3		0.46	0.10	0.03	0.07	0.22	0.17	0.39	0.33	1.10	0.26	0.03	0.13	0.02
FeO		0.12	0.04	0.02	0.04	0.05	0.04	0.07	0.03	0.06	0.13	0.04	0.05	0.00
CaO		0.62	0.08	0.12	0.02	0.26	0.21	0.41	0.31	1.20	0.25	0.22	0.12	0.14
Na2O		0.32	0.01	0.13	0.04	0.10	0.08	0.16	0.22	0.68	0.08	0.10	0.07	0.08
K2O		0.03	0.02	0.01	0.01	0.02	0.02	0.02	0.02	0.04	0.03	0.01	0.02	0.01
An		2.99	0.10	1.00	0.28	0.98	0.69	1.57	1.87	6.13	0.79	0.92	0.57	0.31
n	1	3	2	3	3	6	4	5	4	5	4	3	6	2

Plagioclase analyses (inclusions): TF sequence

Sample	840.00	842.00	866.50	875.00	885.00	895.00	930.00	953.00
Rocktype	.	.	*	.	.	.	.	o
[wt%]								
SiO2	48.63	49.12	45.92	48.82	48.42	48.33	48.96	48.01
Al2O3	31.53	31.72	32.89	31.48	31.84	32.09	31.86	32.43
FeO	0.28	0.32	0.34	0.28	0.27	0.37	0.32	0.24
CaO	16.62	16.31	18.42	16.57	16.75	16.94	16.48	17.39
Na2O	2.79	2.77	1.80	2.68	2.65	2.54	2.81	2.43
K2O	0.12	0.16	0.06	0.13	0.13	0.11	0.16	0.03
Total	99.96	100.39	99.44	99.96	100.06	100.37	100.57	100.52
Cations (based on 32 oxygens)								
Si	8.95	8.99	8.55	8.98	8.91	8.87	8.95	8.80
Al	6.84	6.84	7.22	6.83	6.90	6.94	6.87	7.01
Fe	0.04	0.05	0.05	0.04	0.04	0.06	0.05	0.04
Ca	3.28	3.20	3.68	3.27	3.30	3.33	3.23	3.41
Na	0.99	0.98	0.65	0.96	0.94	0.90	1.00	0.86
K	0.03	0.04	0.01	0.03	0.03	0.03	0.04	0.01
Total	20.14	20.10	20.17	20.10	20.13	20.13	20.13	20.13
An	76.23	75.82	84.67	76.77	77.19	78.21	75.77	79.70
Ab	23.11	23.32	14.99	22.49	22.08	21.20	23.36	20.13
Or	0.66	0.86	0.34	0.73	0.73	0.59	0.87	0.17
1 Standard deviation [wt%]								
SiO2	0.18	0.14	1.06	0.08	0.15	0.38	0.37	0.34
Al2O3	0.03	0.14	0.85	0.29	0.13	0.15	0.13	0.24
FeO	0.03	0.03	0.05	0.03	0.01	0.08	0.03	0.07
CaO	0.08	0.09	0.83	0.16	0.09	0.20	0.16	0.22
Na2O	0.09	0.04	0.47	0.06	0.05	0.12	0.11	0.12
K2O	0.01	0.02	0.03	0.01	0.01	0.01	0.04	0.01
An	0.67	0.34	4.06	0.54	0.46	0.97	0.97	1.00
n	5	5	7	5	3	4	5	4

Plagioclase analyses (inclusions): LK7 sequence

Sample	1389.70	1395.60	1401.95	1407.05	1412.35 b	1430.10	1441.25 a	1446.20	1457.35	1464.56	1470.00 a	1481.26	1491.10
Rock-type	.	.	.	.	-	.	.	.	.	.	.	.	.
[wt%]													
SiO2	49.54	48.88	49.08	48.32	49.26	49.30	49.91	49.28	49.30	49.77	49.70	49.97	50.28
Al2O3	32.13	32.40	31.11	32.01	32.36	32.43	31.75	32.17	32.17	31.58	32.25	32.01	31.66
FeO	0.33	0.33	0.28	0.32	0.36	0.32	0.42	0.45	0.34	0.32	0.31	0.33	0.33
CaO	15.71	15.61	15.75	16.04	15.35	15.71	15.39	15.04	15.16	15.47	15.04	15.29	15.28
Na2O	2.71	2.76	2.78	2.66	2.85	2.67	2.87	2.76	2.91	2.96	2.90	2.91	2.91
K2O	0.12	0.12	0.20	0.13	0.16	0.20	0.14	0.23	0.23	0.14	0.19	0.17	0.17
Total	100.54	100.11	99.19	99.48	100.35	100.63	100.48	99.92	100.12	100.24	100.38	100.67	100.63
Cations (based on 32 oxygens)													
Si	9.02	8.95	9.07	8.92	8.99	8.98	9.09	9.02	9.02	9.09	9.05	9.08	9.14
Al	6.90	6.99	6.78	6.96	6.96	6.96	6.82	6.94	6.93	6.80	6.92	6.85	6.78
Fe	0.05	0.05	0.04	0.05	0.05	0.05	0.06	0.07	0.05	0.05	0.05	0.05	0.05
Ca	3.07	3.06	3.12	3.17	3.00	3.07	3.00	2.95	2.97	3.03	2.93	2.98	2.97
Na	0.96	0.98	1.00	0.95	1.01	0.94	1.01	0.98	1.03	1.05	1.02	1.02	1.02
K	0.03	0.03	0.05	0.03	0.04	0.05	0.03	0.05	0.05	0.03	0.05	0.04	0.04
Total	20.02	20.06	20.06	20.09	20.05	20.04	20.02	20.02	20.06	20.05	20.02	20.02	20.00
An	75.67	75.22	74.97	76.34	74.16	75.59	74.18	74.11	73.23	73.66	73.31	73.66	73.67
Ab	23.62	24.10	23.92	22.92	24.93	23.28	25.01	24.56	25.47	25.52	25.56	25.37	25.35
Or	0.71	0.68	1.11	0.74	0.92	1.13	0.81	1.33	1.30	0.82	1.13	0.97	0.98
1 Standard deviation [wt%]													
SiO2	0.09	0.22	0.36	0.30	0.16	0.21	0.67	0.46	0.17	0.04	0.24	0.25	0.36
Al2O3	0.11	0.30	0.26	0.15	0.20	0.22	0.34	0.24	0.09	0.09	0.22	0.29	0.12
FeO	0.03	0.06	0.01	0.03	0.04	0.05	0.09	0.18	0.06	0.07	0.03	0.04	0.03
CaO	0.10	0.32	0.17	0.09	0.18	0.30	0.31	0.20	0.08	0.12	0.12	0.17	0.11
Na2O	0.04	0.16	0.10	0.06	0.11	0.12	0.32	0.07	0.03	0.05	0.05	0.11	0.03
K2O	0.01	0.02	0.03	0.01	0.02	0.01	0.01	0.04	0.12	0.02	0.09	0.01	0.02
An	0.25	1.46	0.93	0.47	0.98	1.12	2.37	0.17	0.46	0.50	0.52	0.92	0.23
n	3	6	4	6	5	8	3	3	5	4	13	3	4

Sample	1500.95	1511.10	1520.40	1528.90	1539.10	1548.85	1556.56	1573.75	1587.00
	b	b		a		b		a	
Rock-type	.	.	.	.	.	.	.	o	.
[wt%]									
SiO2	49.51	49.43	49.13	49.58	49.93	48.99	49.68	49.30	50.63
Al2O3	31.35	32.31	32.01	32.17	31.79	32.08	32.16	32.63	31.50
FeO	0.36	0.33	0.39	0.35	0.43	0.34	0.38	0.28	0.22
CaO	15.29	15.45	15.08	15.03	15.32	15.34	15.63	15.49	14.89
Na2O	2.92	2.80	3.06	2.97	2.96	2.89	2.75	2.79	3.17
K2O	0.16	0.21	0.16	0.15	0.15	0.16	0.15	0.11	0.16
Total	99.59	100.54	99.83	100.24	100.58	99.80	100.75	100.60	100.57
Cations (									
Si	9.10	9.00	9.01	9.05	9.09	8.99	9.03	8.97	9.19
Al	6.79	6.94	6.92	6.92	6.82	6.94	6.89	7.00	6.74
Fe	0.06	0.05	0.06	0.05	0.07	0.05	0.06	0.04	0.03
Ca	3.01	3.02	2.96	2.94	2.99	3.02	3.04	3.02	2.90
Na	1.04	0.99	1.09	1.05	1.04	1.03	0.97	0.98	1.12
K	0.04	0.05	0.04	0.03	0.04	0.04	0.03	0.02	0.04
Total	20.04	20.05	20.09	20.04	20.04	20.07	20.03	20.04	20.02
An	73.65	74.37	72.49	73.06	73.48	73.92	75.24	74.97	71.52
Ab	25.43	24.41	26.59	26.09	25.65	25.15	23.91	24.42	27.55
Or	0.92	1.23	0.91	0.85	0.87	0.93	0.86	0.61	0.93
1 Standar									
SiO2	0.24	0.49	0.21	0.17	0.49	0.39	0.43	0.21	0.14
Al2O3	0.05	0.49	0.06	0.21	0.29	0.38	0.26	0.17	0.34
FeO	0.03	0.01	0.02	0.03	0.08	0.02	0.03	0.01	0.01
CaO	0.16	0.26	0.17	0.17	0.31	0.39	0.28	0.18	0.28
Na2O	0.05	0.10	0.06	0.08	0.23	0.23	0.15	0.06	0.18
K2O	0.01	0.14	0.01	0.01	0.02	0.03	0.02	0.02	0.03
An	0.52	1.03	3.12	0.63	1.86	2.09	1.37	0.68	1.59
n	4	5	5	4	3	5	5	5	2

Plagioclase analyses (inclusions): H3 sequence

Sample	1062.50	1065.05	1066.00	1071.05	1078.80	1083.75	1087.65	1088.10	1089.40	1090.20	1110.05	1127.50	1144.10
				a				a	b	b			
Rock-type	.	.	.	.	o	o	.	.	.	.	.	.	.
[wt%]													
SiO2	49.92	49.73	49.29	49.66	48.78	49.08	48.59	49.66	49.93	49.62	49.68	50.10	49.35
Al2O3	31.72	32.04	31.45	31.94	32.28	32.57	31.59	32.00	31.91	31.67	31.89	31.71	31.76
FeO	0.33	0.35	0.29	0.33	0.37	0.38	0.33	0.31	0.31	0.33	0.31	0.34	0.30
CaO	15.42	15.45	15.93	15.32	16.39	15.62	15.96	15.67	15.63	15.67	15.39	15.41	15.42
Na2O	2.97	2.73	2.93	2.90	2.58	2.71	2.88	2.74	2.71	2.77	2.79	2.82	2.83
K2O	0.16	0.16	0.18	0.14	0.09	0.14	0.14	0.14	0.20	0.19	0.15	0.15	0.16
Total	100.53	100.45	100.06	100.29	100.49	100.49	99.49	100.52	100.70	100.25	100.21	100.52	99.82
Cations (based on 32 oxygens)													
Si	9.09	9.06	9.04	9.06	8.92	8.95	8.97	9.05	9.08	9.07	9.07	9.12	9.05
Al	6.81	6.88	6.80	6.87	6.96	7.00	6.88	6.87	6.84	6.82	6.86	6.80	6.87
Fe	0.05	0.05	0.04	0.05	0.06	0.06	0.05	0.05	0.05	0.05	0.05	0.05	0.05
Ca	3.01	3.01	3.13	3.00	3.21	3.05	3.16	3.06	3.04	3.07	3.01	3.00	3.03
Na	1.05	0.96	1.04	1.03	0.91	0.96	1.03	0.97	0.96	0.98	0.99	0.99	1.00
K	0.04	0.04	0.04	0.03	0.02	0.03	0.03	0.03	0.05	0.04	0.03	0.03	0.04
Total	20.05	20.00	20.10	20.03	20.07	20.05	20.12	20.02	20.01	20.03	20.01	20.00	20.04
An	73.46	75.08	74.29	73.88	77.44	75.53	74.83	75.35	75.26	74.97	74.68	74.51	74.41
Ab	25.61	24.00	24.73	25.29	22.07	23.67	24.39	23.84	23.62	23.97	24.48	24.64	24.66
Or	0.93	0.92	0.98	0.83	0.49	0.80	0.78	0.81	1.12	1.06	0.84	0.85	0.93
1 Standard deviation [wt%]													
SiO2	0.31	0.16	0.18	0.45	0.12	0.33	0.46	0.06	0.61	0.52	0.13	0.12	0.07
Al2O3	0.19	0.19	0.12	0.18	0.03	0.24	0.16	0.06	0.27	0.24	0.06	0.09	0.13
FeO	0.02	0.04	0.04	0.02	0.05	0.03	0.02	0.01	0.03	0.04	0.02	0.02	0.01
CaO	0.37	0.17	0.22	0.22	0.01	0.21	0.11	0.07	0.43	0.27	0.08	0.07	0.12
Na2O	0.17	0.10	0.09	0.16	0.04	0.11	0.09	0.08	0.24	0.29	0.05	0.02	0.02
K2O	0.01	0.02	0.01	0.01	0.01	0.02	0.02	0.01	0.02	0.05	0.01	0.00	0.01
An	1.60	0.84	0.85	1.25	0.30	1.02	0.64	0.56	2.14	2.12	0.38	0.19	0.12
n	3	4	3	3	2	12	3	2	3	3	4	3	3

Sample	1175.80	1191.50	1200.30	1206.95	1211.85	1219.05	1228.25	1246.65	1252.08	1253.30 a-Mid	1253.30 a-Base	1266.28
Rock-type	.	.	.	.	.	.	.	.	.	o	.	.
[wt%]												
SiO2	49.60	49.33	49.59	48.77	49.63	48.99	49.05	49.35	48.75	48.65	48.27	49.85
Al2O3	32.08	31.71	31.76	31.80	31.98	31.89	31.88	32.19	31.62	32.06	32.62	32.07
FeO	0.34	0.36	0.42	0.37	0.39	0.38	0.40	0.37	0.34	0.29	0.35	0.31
CaO	15.75	15.36	15.37	15.97	15.06	15.98	15.72	15.93	16.01	15.97	16.51	15.42
Na2O	2.90	2.83	2.90	2.76	2.79	2.64	2.81	2.71	2.61	2.59	2.34	2.72
K2O	0.14	0.14	0.17	0.13	0.13	0.22	0.10	0.16	0.11	0.13	0.15	0.23
Total	100.81	99.74	100.21	99.80	99.97	100.10	99.96	100.71	99.43	99.70	100.23	100.60
Cations (based on 32 oxygens)												
Si	9.02	9.06	9.06	8.97	9.07	8.98	9.00	8.99	8.99	8.95	8.85	9.07
Al	6.87	6.86	6.84	6.90	6.89	6.89	6.89	6.91	6.88	6.95	7.05	6.87
Fe	0.05	0.06	0.06	0.06	0.06	0.06	0.06	0.06	0.05	0.05	0.05	0.05
Ca	3.07	3.02	3.01	3.15	2.95	3.14	3.09	3.11	3.16	3.15	3.24	3.00
Na	1.02	1.01	1.03	0.99	0.99	0.94	1.00	0.96	0.93	0.92	0.83	0.96
K	0.03	0.03	0.04	0.03	0.03	0.05	0.02	0.04	0.03	0.03	0.04	0.05
Total	20.07	20.03	20.05	20.09	19.99	20.06	20.07	20.05	20.05	20.05	20.06	20.00
An	74.44	74.39	73.81	75.62	74.35	76.09	75.14	75.79	76.75	76.73	78.94	74.84
Ab	24.78	24.83	25.22	23.67	24.88	22.69	24.26	23.31	22.60	22.53	20.20	23.84
Or	0.78	0.79	0.97	0.71	0.77	1.22	0.60	0.90	0.65	0.74	0.86	1.32
1 Standard deviation [wt%]												
SiO2	0.16	0.31	0.19	0.35	0.34	0.81	0.17	0.23	0.19	0.29	0.43	0.16
Al2O3	0.13	0.06	0.21	0.06	0.10	0.43	0.11	0.09	0.22	0.20	0.39	0.17
FeO	0.04	0.04	0.03	0.06	0.07	0.02	0.12	0.03	0.04	0.04	0.02	0.04
CaO	0.12	0.09	0.18	0.13	0.08	0.51	0.09	0.02	0.08	0.22	0.32	0.21
Na2O	0.06	0.08	0.16	0.08	0.04	0.29	0.05	0.04	0.10	0.13	0.17	0.17
K2O	0.02	0.02	0.01	0.01	0.02	0.12	0.03	0.01	0.03	0.02	0.01	0.02
An	0.50	0.68	1.24	0.59	0.17	2.79	0.53	0.24	0.68	1.14	1.48	1.38
n	8	4	3	6	4	3	6	2	3	6	4	5

Plagioclase analyses (inclusions): KR2 sequence

Sample	1155.45	1160.40	1174.10	1185.90	1187.30 b	1191.58 a	1194.20	1203.75	1219.75	1227.15	1236.20	1241.30	1251.90
Rock-type	.	.	.	.	.	.	.	.	.	.	.	.	.
[wt%]													
SiO2	49.81	49.01	50.01	48.64	49.61	49.12	49.09	49.41	50.05	49.31	49.42	49.57	49.55
Al2O3	32.04	32.18	32.14	32.21	32.06	32.40	31.86	31.79	32.26	31.76	32.09	32.09	31.66
FeO	0.29	0.41	0.30	0.39	0.31	0.38	0.43	0.33	0.42	0.31	0.32	0.37	0.37
CaO	15.10	15.44	15.24	15.83	15.38	15.58	15.57	15.31	15.37	15.15	15.32	15.33	15.15
Na2O	2.87	2.63	2.86	2.61	2.80	2.66	2.74	2.95	2.81	2.93	2.80	2.85	3.05
K2O	0.18	0.14	0.16	0.14	0.13	0.19	0.12	0.13	0.12	0.17	0.16	0.15	0.10
Total	100.29	99.81	100.72	99.82	100.29	100.32	99.82	99.93	101.02	99.64	100.10	100.35	99.88
Cations (based on 32 oxygens)													
Si	9.08	8.99	9.08	8.94	9.05	8.97	9.01	9.05	9.06	9.06	9.03	9.04	9.08
Al	6.88	6.96	6.88	6.98	6.89	6.97	6.90	6.87	6.88	6.88	6.91	6.90	6.84
Fe	0.04	0.06	0.04	0.06	0.05	0.06	0.07	0.05	0.06	0.05	0.05	0.06	0.06
Ca	2.95	3.04	2.96	3.12	3.01	3.05	3.06	3.01	2.98	2.98	3.00	3.00	2.98
Na	1.01	0.93	1.01	0.93	0.99	0.94	0.97	1.05	0.99	1.04	0.99	1.01	1.08
K	0.04	0.03	0.04	0.03	0.03	0.04	0.03	0.03	0.03	0.04	0.04	0.03	0.02
Total	20.01	20.01	20.01	20.06	20.02	20.04	20.04	20.05	20.00	20.05	20.02	20.03	20.06
An	73.65	75.82	73.98	76.37	74.63	75.57	75.34	73.59	74.64	73.37	74.49	74.22	72.89
Ab	25.30	23.35	25.11	22.80	24.60	23.32	23.97	25.67	24.69	25.63	24.59	24.93	26.56
Or	1.05	0.83	0.92	0.83	0.77	1.11	0.68	0.74	0.68	0.99	0.92	0.86	0.55
1 Standard deviation [wt%]													
SiO2	0.61		1.48	0.22	0.34	0.41	0.36	0.26		0.09	0.31	0.15	0.30
Al2O3	0.48		0.97	0.20	0.32	0.12	0.40	0.07		0.06	0.12	0.18	0.21
FeO	0.04		0.06	0.04	0.03	0.02	0.06	0.07		0.06	0.08	0.04	0.02
CaO	0.52		1.11	0.19	0.31	0.41	0.26	0.35		0.10	0.12	0.16	0.25
Na2O	0.30		0.57	0.08	0.11	0.08	0.15	0.15		0.03	0.03	0.06	0.16
K2O	0.04		0.08	0.02	0.01	0.04	0.01	0.01		0.01	0.01	0.02	0.01
An	2.58		5.48	0.76	1.05	1.02	1.36	1.40		0.24	0.27	0.54	1.34
n	8	1	5	9	5	3	3	4	1	5	5	4	4

Orthopyroxene analyses: UA sequence

Sample	641.00	642.50	644.00	645.70	647.90	651.30	652.30	652.90	654.10	654.90	655.50	658.00	659.30	661.30	662.70	664.30	665.70	667.20	668.90	669.60
Rock type	*	*	o	o	.	.	.	o	.	.	.	*	*	+	+	+	+	+	+	+
[wt%]																				
SiO2	55.04	55.96	53.24	53.28	54.84	55.41	55.23	53.80	55.00	55.45	55.19	54.96	55.64	55.09	55.10	54.78	54.53	54.83	54.69	55.56
TiO2	0.15	0.09	0.20	0.15	0.19	0.16	0.16	0.19	0.18	0.12	0.14	0.21	0.12	0.15	0.12	0.14	0.17	0.13	0.17	0.10
Al2O3	1.54	1.55	0.80	1.04	1.00	1.13	1.21	0.92	1.17	1.43	1.65	1.48	1.51	1.39	1.48	1.41	0.87	1.48	1.31	1.60
Cr2O3	0.40	0.33	0.07	0.10	0.37	0.43	0.42	0.28	0.47	0.41	0.48	0.45	0.46	0.46	0.50	0.43	0.24	0.47	0.45	0.51
FeO	12.32	10.83	20.32	18.86	14.39	12.12	12.98	15.41	12.74	12.00	11.22	11.63	11.71	11.91	12.81	12.17	13.05	11.66	12.68	11.42
MnO	0.25	0.25	0.47	0.46	0.30	0.26	0.28	0.32	0.24	0.20	0.21	0.25	0.24	0.27	0.25	0.25	0.28	0.26	0.24	0.26
NiO	0.10	0.04	0.05	0.02	0.08	0.11	0.11	0.06	0.10	0.05	0.12	0.10	0.08	0.09	0.06	0.12	0.11	0.05	0.12	0.09
MgO	28.92	30.03	23.10	24.37	27.95	29.52	29.44	27.78	29.62	29.82	29.49	30.04	29.41	28.21	29.20	28.38	28.68	29.27	29.11	28.93
CaO	1.62	0.91	0.72	0.93	1.23	1.08	0.86	0.94	1.30	1.15	1.54	2.00	1.81	1.65	1.60	1.21	0.90	1.41	1.34	1.72
Na2O	0.02	0.01	0.00	0.01	0.02	0.00	0.02	0.01	0.03	0.00	0.03	0.06	0.03	0.04	0.03	0.02	0.01	0.02	0.02	0.03
Total	100.35	100.00	98.98	99.22	100.36	100.22	100.70	99.71	100.85	100.63	100.08	101.17	101.00	99.24	101.15	98.90	98.86	99.58	100.13	100.21
Cations (based on 6 oxygens)																				
Si	1.95	1.97	1.99	1.97	1.96	1.97	1.96	1.95	1.95	1.96	1.96	1.94	1.96	1.97	1.95	1.97	1.97	1.96	1.95	1.97
Ti	0.00	0.00	0.01	0.00	0.00	0.00	0.00	0.01	0.00	0.00	0.00	0.01	0.00	0.00	0.00	0.00	0.00	0.00	0.00	0.00
Al	0.06	0.06	0.04	0.05	0.04	0.05	0.05	0.04	0.05	0.06	0.07	0.06	0.06	0.06	0.06	0.06	0.04	0.06	0.06	0.07
Cr	0.01	0.01	0.00	0.00	0.01	0.01	0.01	0.01	0.01	0.01	0.01	0.01	0.01	0.01	0.01	0.01	0.01	0.01	0.01	0.01
Fe	0.37	0.32	0.63	0.58	0.43	0.36	0.38	0.47	0.38	0.35	0.33	0.34	0.34	0.36	0.38	0.37	0.39	0.35	0.38	0.34
Mn	0.01	0.01	0.01	0.01	0.01	0.01	0.01	0.01	0.01	0.01	0.01	0.01	0.01	0.01	0.01	0.01	0.01	0.01	0.01	0.01
Ni	0.00	0.00	0.00	0.00	0.00	0.00	0.00	0.00	0.00	0.00	0.00	0.00	0.00	0.00	0.00	0.00	0.00	0.00	0.00	0.00
Mg	1.53	1.58	1.28	1.34	1.49	1.56	1.56	1.50	1.56	1.57	1.56	1.58	1.54	1.51	1.54	1.52	1.54	1.56	1.55	1.53
Ca	0.06	0.03	0.03	0.04	0.05	0.04	0.03	0.04	0.05	0.04	0.06	0.08	0.07	0.06	0.06	0.05	0.04	0.05	0.05	0.07
Na	0.00	0.00	0.00	0.00	0.00	0.00	0.00	0.00	0.00	0.00	0.00	0.00	0.00	0.00	0.00	0.00	0.00	0.00	0.00	0.00
Total	4.00	3.99	3.99	4.00	4.00	4.00	4.01	4.02	4.02	4.00	4.00	4.02	4.00	3.99	4.01	3.99	4.00	4.00	4.01	3.99
Mg#	0.807	0.832	0.670	0.697	0.776	0.813	0.802	0.763	0.806	0.816	0.824	0.822	0.817	0.809	0.802	0.806	0.797	0.817	0.804	0.819
1 Standard deviation [wt%]																				
SiO2	0.25	0.20	0.22	0.39	0.28	0.23	0.27	0.04	0.11	0.21	0.16	0.12	0.09	0.22	0.17	0.18	0.29	0.20	0.22	0.12
TiO2	0.02	0.01	0.03	0.05	0.06	0.03	0.03	0.02	0.04	0.01	0.03	0.05	0.02	0.03	0.03	0.03	0.06	0.03	0.04	0.01
Al2O3	0.01	0.09	0.04	0.32	0.03	0.19	0.09	0.13	0.08	0.10	0.11	0.02	0.10	0.15	0.11	0.18	0.19	0.14	0.15	0.10
Cr2O3	0.05	0.07	0.01	0.03	0.02	0.06	0.04	0.08	0.02	0.01	0.04	0.03	0.09	0.04	0.03	0.09	0.09	0.07	0.06	0.03
FeO	0.27	0.11	0.29	0.28	0.40	0.24	0.15	0.63	0.11	0.17	0.07	0.21	0.17	0.25	0.25	0.49	0.15	0.16	0.32	0.18
MnO	0.02	0.01	0.04	0.02	0.03	0.03	0.03	0.00	0.02	0.01	0.01	0.02	0.03	0.02	0.03	0.03	0.02	0.01	0.01	0.03
NiO	0.01	0.01	0.01	0.01	0.01	0.02	0.01	0.00	0.03	0.03	0.03	0.01	0.01	0.01	0.02	0.02	0.02	0.02	0.03	0.02
MgO	0.46	0.61	0.31	0.23	0.27	0.22	0.19	0.30	0.07	0.20	0.14	0.16	0.37	0.11	0.07	0.47	0.31	0.37	0.29	0.23
CaO	0.46	0.53	0.06	0.21	0.39	0.44	0.23	0.17	0.18	0.24	0.16	0.21	0.61	0.27	0.17	0.58	0.38	0.41	0.34	0.32
Na2O	0.01	0.01	0.00	0.01	0.00	0.01	0.00	0.00	0.01	0.00	0.01	0.01	0.02	0.01	0.01	0.02	0.01	0.01	0.01	0.00
Mg#	0.002	0.004	0.006	0.003	0.004	0.002	0.002	0.009	0.001	0.002	0.001	0.003	0.000	0.003	0.003	0.007	0.003	0.002	0.004	0.002
n	4	4	5	3	4	6	5	2	5	5	5	4	4	5	6	5	7	7	6	5

Orthopyroxene analyses: AE sequence (Field, 1987)

Sample	27	29	32	33	36	38	39.4	39.5	40.1	40.2	42	43	45	46	47	48	49	51	55	57
Rock type	+	o	.	.	.	.	*	*	*	*	+	0	.	.	.	*	+	+	+	+
[wt%]																				
SiO2	54.38	54.98	55.15	55.30	55.61	55.99	55.47	55.25	55.24	55.99	55.33	54.80	55.17	54.91	55.34	55.49	55.67	55.77	55.27	55.78
TiO2	0.28	0.24	0.33	0.26	0.22	0.16	0.17	0.17	0.25	0.16	0.10	0.30	0.27	0.36	0.23	0.14	0.22	0.24	0.17	0.18
Al2O3	1.66	1.20	1.11	1.01	1.30	1.61	1.62	1.65	1.54	1.61	1.70	0.98	1.02	1.12	1.24	1.48	1.22	1.26	1.50	1.26
Cr2O3	0.23	0.26	0.28	0.19	0.30	0.28	0.32	0.26	0.32	0.28	0.32	0.23	0.24	0.26	0.30	0.27	0.23	0.30	0.28	0.32
FeO	11.83	14.65	14.60	13.84	11.78	11.08	9.53	10.19	10.96	11.08	10.68	16.46	14.55	13.16	13.27	10.59	12.39	12.53	11.77	11.64
MnO	0.28	0.32	0.31	0.29	0.25	0.24	0.27	0.24	0.25	0.24	0.23	0.35	0.32	0.28	0.24	0.26	0.25	0.27	0.24	0.28
NiO	0.74	0.39	0.49	0.16	0.13	0.98	0.36	0.01	0.80	0.98	0.65	0.45	0.65	0.85	0.16	0.01	0.00	0.94	0.51	0.97
MgO	28.74	27.39	27.49	28.16	29.13	29.98	30.36	30.01	29.80	29.98	29.65	26.45	27.65	27.85	28.16	30.01	29.00	28.94	28.51	28.97
CaO	1.52	1.40	1.43	1.09	1.54	1.25	1.67	1.58	1.59	1.25	1.49	0.93	1.14	1.52	1.31	1.51	1.17	1.50	2.10	1.82
Na2O	0.03	0.02	0.02	0.01	0.02	0.02	0.03	0.04	0.03	0.02	0.03	0.01	0.01	0.02	0.02	0.01	0.02	0.04	0.05	0.03
Total	99.02	100.54	100.77	100.23	100.25	100.67	99.56	99.45	100.07	100.67	99.60	100.54	100.43	99.53	100.17	99.83	100.25	100.92	99.99	100.35
Cations (based on 6 oxygens)																				
Si	1.95	1.97	1.97	1.98	1.97	1.97	1.96	1.96	1.96	1.96	1.96	1.97	1.97	1.97	1.97	1.96	1.97	1.97	1.97	1.97
Ti	0.01	0.01	0.01	0.01	0.01	0.00	0.01	0.01	0.01	0.00	0.00	0.01	0.01	0.01	0.01	0.00	0.01	0.01	0.01	0.01
Al	0.07	0.05	0.05	0.04	0.05	0.07	0.07	0.07	0.06	0.07	0.07	0.04	0.04	0.05	0.05	0.06	0.05	0.05	0.06	0.05
Cr	0.01	0.01	0.01	0.01	0.01	0.01	0.01	0.01	0.01	0.01	0.01	0.01	0.01	0.01	0.01	0.01	0.01	0.01	0.01	0.01
Fe	0.36	0.44	0.44	0.44	0.35	0.33	0.28	0.30	0.32	0.35	0.32	0.50	0.45	0.40	0.40	0.31	0.37	0.37	0.35	0.34
Mn	0.01	0.01	0.01	0.01	0.01	0.01	0.01	0.01	0.01	0.01	0.01	0.01	0.01	0.01	0.01	0.01	0.01	0.01	0.01	0.01
Ni	0.00	0.00	0.00	0.00	0.00	0.00	0.00	0.00	0.00	0.00	0.00	0.00	0.00	0.00	0.00	0.00	0.00	0.00	0.00	0.00
Mg	1.54	1.42	1.46	1.46	1.54	1.54	1.60	1.59	1.57	1.56	1.57	1.42	1.47	1.50	1.50	1.58	1.53	1.52	1.51	1.53
Ca	0.06	0.05	0.05	0.06	0.06	0.06	0.06	0.06	0.06	0.05	0.06	0.04	0.04	0.05	0.05	0.06	0.05	0.06	0.80	0.07
Na	0.00	0.00	0.00	0.00	0.00	0.00	0.00	0.00	0.00	0.00	0.00	0.00	0.00	0.00	0.00	0.00	0.00	0.00	0.00	0.00
Total	4.00	3.95	4.00	4.00	4.00	3.98	4.00	4.00	4.01	4.00	4.00	4.00	4.01	3.99	3.99	4.00	4.00	4.00	4.72	3.99
Mg#	0.813	0.763	0.770	0.770	0.815	0.826	0.850	0.840	0.829	0.819	0.832	0.741	0.765	0.791	0.791	0.835	0.807	0.805	0.812	0.816
n	4	5	10	3	5	6	2	4	2	6	3	4	8	5	5	6	5	12	4	8

Orthopyroxene analyses: EK22-sequence

Sample	271.75	272.25	274.70	277.32	277.90 a	277.90 b	280.65	282.80 a	285.70 Net	285.80 b-Top	285.80 b-Base	286.05	288.40 a	288.40 b	288.40 b-Base	288.90 a	288.90 b	288.95	291.48	292.05	293.60 a	295.70	296.90	297.10	299.10	299.80
Rock type	o	.	.	.	o	.	.	.	o	o	.	.	*	X	.	x	*	.	x	.	.	*	*	*	*	*
[wt%]																										
SiO2	54.96	54.77	54.59	54.83	54.40	54.30	55.06	54.78	53.38	53.90	54.69	54.94	55.09	55.23	55.41	55.54	55.51	54.47	54.89	54.94	55.20	55.35	55.29	55.38	55.43	55.12
TiO2	0.26	0.19	0.16	0.21	0.22	0.17	0.15	0.19	0.13	0.24	0.16	0.14	0.17	0.14	0.14	0.04	0.12	0.12	0.13	0.15	0.15	0.11	0.35	0.17	0.20	0.28
Al2O3	0.79	1.08	1.03	1.15	0.82	1.04	1.09	1.28	1.01	0.88	1.24	1.28	1.60	1.49	1.51	1.18	1.42	1.62	1.54	1.57	1.55	1.57	1.26	1.29	1.62	1.44
Cr2O3	0.18	0.40	0.35	0.39	0.18	0.36	0.43	0.41	0.34	0.30	0.45	0.44	0.35	0.46	0.44	0.10	0.28	0.41	0.51	0.49	0.48	0.50	0.34	0.33	0.47	0.29
FeO	16.23	13.84	13.57	13.48	15.12	14.25	12.37	12.03	15.55	17.47	13.07	12.63	11.27	11.59	12.43	11.33	10.90	11.41	11.29	11.42	11.58	10.95	11.45	11.42	11.78	11.86
MnO	0.33	0.27	0.30	0.26	0.34	0.28	0.26	0.27	0.33	0.38	0.25	0.25	0.22	0.25	0.27	0.26	0.21	0.25	0.25	0.27	0.27	0.25	0.25	0.21	0.27	0.24
NiO	0.07	0.06	0.08	0.09	0.10	0.05	0.10	0.08	0.04	0.07	0.08	0.08	0.09	0.08	0.11	0.05	0.07	0.05	0.09	0.11	0.10	0.09	0.09	0.09	0.06	0.08
MgO	27.40	28.63	28.59	29.05	27.37	27.84	29.36	29.62	27.60	26.36	28.50	28.80	29.62	29.87	29.43	30.97	31.13	29.75	30.62	28.96	29.12	30.65	30.02	30.08	29.69	29.46
CaO	0.83	1.25	1.08	1.12	0.81	1.13	0.93	1.47	1.16	0.77	0.75	1.20	1.28	1.04	1.41	0.54	0.73	1.68	1.27	1.41	1.55	1.95	1.41	1.30	1.61	1.30
Na2O	0.01	0.00	0.02	0.01	0.01	0.01	0.01	0.03	0.01	0.02	0.01	0.01	0.02	0.00	0.02	0.01	0.01	0.01	0.01	0.01	0.02	0.05	0.02	0.04	0.03	0.03
Total	101.05	100.50	99.76	100.59	99.37	99.44	99.76	100.17	99.57	100.40	99.21	99.75	99.70	100.32	101.16	100.03	100.39	99.78	100.59	99.32	100.03	101.46	100.47	100.30	101.15	100.10
Cations (based on 6 oxygens)																										
Si	1.97	1.96	1.96	1.95	1.97	1.96	1.96	1.95	1.94	1.96	1.97	1.96	1.96	1.96	1.95	1.96	1.95	1.94	1.94	1.96	1.96	1.94	1.95	1.96	1.95	1.96
Ti	0.01	0.01	0.00	0.01	0.01	0.00	0.00	0.01	0.00	0.01	0.00	0.00	0.00	0.00	0.00	0.00	0.00	0.00	0.00	0.00	0.00	0.00	0.01	0.00	0.01	0.01
Al	0.03	0.05	0.04	0.05	0.04	0.04	0.05	0.05	0.04	0.04	0.05	0.05	0.07	0.06	0.06	0.05	0.06	0.07	0.06	0.07	0.06	0.06	0.05	0.05	0.07	0.06
Cr	0.01	0.01	0.01	0.01	0.01	0.01	0.01	0.01	0.01	0.01	0.01	0.01	0.01	0.01	0.01	0.00	0.01	0.01	0.01	0.01	0.01	0.01	0.01	0.01	0.01	0.01
Fe	0.49	0.41	0.41	0.40	0.46	0.43	0.37	0.36	0.47	0.53	0.39	0.38	0.33	0.34	0.37	0.33	0.32	0.34	0.33	0.34	0.34	0.32	0.34	0.34	0.35	0.35
Mn	0.01	0.01	0.01	0.01	0.01	0.01	0.01	0.01	0.01	0.01	0.01	0.01	0.01	0.01	0.01	0.01	0.01	0.01	0.01	0.01	0.01	0.01	0.01	0.01	0.01	0.01
Ni	0.00	0.00	0.00	0.00	0.00	0.00	0.00	0.00	0.00	0.00	0.00	0.00	0.00	0.00	0.00	0.00	0.00	0.00	0.00	0.00	0.00	0.00	0.00	0.00	0.00	0.00
Mg	1.46	1.52	1.53	1.54	1.48	1.50	1.56	1.57	1.50	1.43	1.53	1.53	1.57	1.58	1.55	1.63	1.63	1.58	1.61	1.54	1.54	1.60	1.58	1.58	1.56	1.56
Ca	0.03	0.05	0.04	0.04	0.03	0.04	0.04	0.06	0.05	0.03	0.03	0.05	0.05	0.04	0.05	0.02	0.03	0.06	0.05	0.05	0.06	0.07	0.05	0.05	0.06	0.05
Na	0.00	0.00	0.00	0.00	0.00	0.00	0.00	0.00	0.00	0.00	0.00	0.00	0.00	0.00	0.00	0.00	0.00	0.00	0.00	0.00	0.00	0.00	0.00	0.00	0.00	0.00
Total	4.01	4.01	4.01	4.01	4.00	4.01	4.00	4.01	4.03	4.01	4.00	4.00	4.00	4.00	4.01	4.01	4.01	4.02	4.02	3.99	4.00	4.02	4.01	4.01	4.01	4.00
Mg#	0.751	0.787	0.790	0.793	0.763	0.777	0.809	0.814	0.760	0.729	0.795	0.803	0.824	0.821	0.808	0.830	0.836	0.823	0.829	0.819	0.818	0.833	0.824	0.824	0.818	0.816
1 Standard deviation [wt%]																										
SiO2	0.13	0.25	0.35	0.31	0.07	0.30	0.15	0.14	0.14	0.08	0.23	0.21	0.13	0.18	0.07	0.44	0.22	0.15	0.15	0.13	0.18	0.12	0.17	0.38	0.27	0.12
TiO2	0.05	0.04	0.02	0.12	0.01	0.05	0.02	0.04	0.03	0.02	0.04	0.03	0.03	0.03	0.02	0.04	0.04	0.02	0.01	0.03	0.01	0.02	0.09	0.06	0.06	0.21
Al2O3	0.06	0.14	0.06	0.11	0.02	0.17	0.12	0.15	0.09	0.05	0.19	0.09	0.07	0.42	0.13	0.26	0.10	0.06	0.05	0.08	0.06	0.07	0.10	0.14	0.13	0.25
Cr2O3	0.02	0.04	0.04	0.05	0.00	0.07	0.04	0.04	0.10	0.01	0.09	0.03	0.11	0.11	0.06	0.09	0.10	0.03	0.05	0.05	0.01	0.03	0.07	0.09	0.06	0.10
FeO	0.19	0.18	0.53	0.18	0.27	0.30	0.11	0.28	0.43	0.38	0.14	0.25	0.14	0.18	0.44	0.25	0.16	0.18	0.31	0.18	0.26	0.19	0.05	0.20	0.24	0.15
MnO	0.03	0.01	0.02	0.01	0.01	0.03	0.03	0.02	0.01	0.03	0.01	0.03	0.02	0.03	0.01	0.03	0.03	0.04	0.03	0.02	0.02	0.01	0.02	0.03	0.03	0.00
NiO	0.00	0.02	0.02	0.01	0.04	0.03	0.02	0.02	0.01	0.01	0.01	0.02	0.02	0.02	0.01	0.02	0.02	0.01	0.02	0.01	0.01	0.01	0.01	0.02	0.02	0.02
MgO	0.22	0.17	0.21	0.47	0.11	0.23	0.43	0.37	0.12	0.27	0.21	0.33	0.38	0.28	0.13	0.28	0.10	0.29	0.28	0.36	0.32	0.21	0.32	0.15	0.15	0.31
CaO	0.16	0.29	0.06	0.49	0.02	0.45	0.54	0.50	0.30	0.05	0.17	0.43	0.42	0.42	0.35	0.13	0.10	0.44	0.49	0.30	0.52	0.29	0.38	0.30	0.45	0.45
Na2O	0.01	0.01	0.01	0.00	0.00	0.01	0.01	0.02	0.00	0.01	0.01	0.01	0.01	0.01	0.01	0.01	0.01	0.01	0.01	0.01	0.01	0.02	0.01	0.02	0.02	0.02
Mg#	0.003	0.002	0.003	0.001	0.004	0.003	0.002	0.002	0.006	0.006	0.002	0.003	0.003	0.003	0.005			0.010	0.003	0.004	0.002	0.002	0.001		0.003	0.002
n	4	6	4	4	3	7	7	7	3	3	5	7	6	6	5	4	4	4	7	6	7	3	5	7	4	6

Sample	299.95	303.90	306.30 Top+Base	306.30 Mid	306.50 a Top	306.50 a Base	306.50 b	307.66	313.00	313.60 b	315.90
Rock type	*	.	.	+	.	*	+	+	+	*	.
[wt%]											
SiO2	55.25	54.48	55.06	54.96	54.41	54.98	54.83	54.68	55.05	54.83	54.56
TiO2	0.17	0.18	0.13	0.12	0.19	0.12	0.18	0.17	0.17	0.19	0.15
Al2O3	1.37	1.06	1.53	1.44	1.30	1.62	1.18	1.33	1.36	1.50	1.31
Cr2O3	0.31	0.42	0.48	0.52	0.38	0.43	0.41	0.45	0.41	0.40	0.56
FeO	11.85	13.53	12.07	11.17	13.43	11.15	12.88	12.92	12.09	12.54	12.48
MnO	0.27	0.28	0.24	0.25	0.24	0.20	0.27	0.24	0.26	0.24	0.26
NiO	0.08	0.11	0.13	0.11	0.19	0.14	0.20	0.10	0.10	0.11	0.14
MgO	29.62	29.28	28.78	30.10	29.04	30.41	28.06	28.78	29.38	28.57	29.61
CaO	1.13	1.16	1.36	1.39	1.24	1.56	1.54	1.70	1.39	1.63	1.46
Na2O	0.00	0.03	0.01	0.00	0.00	0.01	0.03	0.05	0.01	0.03	0.01
Total	100.07	100.52	99.80	100.05	100.43	100.62	99.58	100.43	100.21	100.03	100.54
Cations (based on 6 oxygens)											
Si	1.96	1.94	1.96	1.95	1.94	1.94	1.97	1.95	1.96	1.96	1.94
Ti	0.00	0.00	0.00	0.00	0.01	0.00	0.00	0.00	0.00	0.01	0.00
Al	0.06	0.04	0.06	0.06	0.05	0.07	0.05	0.06	0.06	0.06	0.05
Cr	0.01	0.01	0.01	0.02	0.01	0.01	0.01	0.01	0.01	0.01	0.02
Fe	0.35	0.40	0.36	0.33	0.40	0.33	0.39	0.39	0.36	0.37	0.37
Mn	0.01	0.01	0.01	0.01	0.01	0.01	0.01	0.01	0.01	0.01	0.01
Ni	0.00	0.00	0.00	0.00	0.01	0.00	0.01	0.00	0.00	0.00	0.00
Mg	1.57	1.56	1.53	1.59	1.55	1.60	1.50	1.53	1.55	1.52	1.57
Ca	0.04	0.04	0.05	0.05	0.05	0.06	0.06	0.06	0.05	0.06	0.06
Na	0.00	0.00	0.00	0.00	0.00	0.00	0.00	0.00	0.00	0.00	0.00
Total	4.00	4.02	4.00	4.01	4.02	4.02	4.00	4.01	4.01	4.00	4.02
Mg#	0.817	0.794	0.809	0.828	0.794	0.829	0.795	0.799	0.812	0.802	0.809
1 Standard deviation [wt%]											
SiO2	0.30	0.17	0.14	0.34	0.19	0.26	0.38	0.24	0.33	0.13	0.16
TiO2	0.04	0.04	0.03	0.02	0.03	0.01	0.04	0.03	0.05	0.06	0.01
Al2O3	0.21	0.10	0.15	0.07	0.36	0.11	0.28	0.12	0.16	0.08	0.13
Cr2O3	0.11	0.05	0.03	0.06	0.15	0.11	0.10	0.03	0.07	0.02	0.05
FeO	0.18	0.32	0.53	0.84	0.73	0.17	0.31	0.18	0.40	0.42	0.17
MnO	0.02	0.03	0.02	0.03	0.04	0.02	0.02	0.02	0.03	0.03	0.02
NiO	0.02	0.01	0.02	0.03	0.03	0.02	0.01	0.02	0.01	0.01	0.02
MgO	0.47	0.17	0.49	0.75	0.41	0.51	0.46	0.11	0.41	0.35	0.26
CaO	0.45	0.34	0.46	0.18	0.34	0.51	0.46	0.23	0.25	0.53	0.25
Na2O	0.01	0.01	0.01	0.01	0.00	0.01	0.01	0.01	0.01	0.01	0.00
Mg#	0.002	0.003	0.003	0.008	0.010	0.003	0.005	0.002	0.007	0.004	0.003
n	6	6	10	10	4	4	5	6	7	5	7

Orthopyroxene analyses: IN sequence

Sample	806.92	811.78	815.38	817.10	817.50	817.68	819.15	821.23 b	826.00	837.86	844.00	850.73	858.55	863.12	866.40	866.67	869.60	872.50	875.75	880.50	883.14	893.70
Rock type	o	.	.	.	.	.	.	.	.	.	.	X	X	X	x	+	o	+	+	+	.	+
[wt%]																						
SiO2	53.78	55.08	54.88	54.98	54.82	55.53	55.26	55.51	55.33	54.58	54.58	54.88	53.99	55.35	55.34	55.28	54.31	54.84	54.05	55.20	55.53	55.52
TiO2	0.24	0.19	0.17	0.15	0.15	0.15	0.19	0.15	0.17	0.14	0.14	0.15	0.14	0.12	0.08	0.11	0.24	0.18	0.16	0.14	0.35	0.20
Al2O3	0.75	1.07	1.23	1.14	1.27	1.26	1.20	1.27	1.24	1.52	1.50	1.50	1.44	1.41	1.26	1.30	0.90	1.33	1.15	1.13	0.95	1.00
Cr2O3	0.15	0.41	0.43	0.37	0.40	0.42	0.54	0.43	0.40	0.50	0.47	0.49	0.49	0.39	0.21	0.29	0.37	0.51	0.42	0.45	0.43	0.33
FeO	19.28	13.38	13.12	12.21	12.34	12.02	12.44	12.01	11.80	11.88	11.96	11.83	11.80	11.68	10.97	10.86	16.19	12.49	14.80	12.33	12.06	13.35
MnO	0.35	0.27	0.24	0.27	0.28	0.22	0.24	0.26	0.23	0.26	0.24	0.26	0.28	0.25	0.24	0.24	0.30	0.22	0.27	0.25	0.24	0.28
NiO	0.19	0.10	0.07	0.14	0.08	0.06	0.11	0.08	0.10	0.09	0.10	0.07	0.07	0.09	0.08	0.10	0.07	0.08	0.07	0.07	0.09	0.08
MgO	24.18	28.38	28.87	29.58	29.19	29.57	28.58	28.90	29.09	29.38	29.30	29.31	29.55	28.99	30.03	29.94	26.48	28.37	27.65	28.49	29.37	27.97
CaO	0.97	1.31	1.19	1.40	1.27	1.15	1.25	1.20	1.17	1.59	1.23	1.43	1.41	1.04	0.79	0.87	0.96	1.72	1.45	1.27	0.84	1.35
Na2O	0.01	0.02	0.03	0.01	0.03	0.01	0.02	0.03	0.01	0.03	0.02	0.01	0.02	0.01	0.02	0.02	0.01	0.03	0.03	0.02	0.01	0.02
Total	99.88	100.20	100.25	100.26	99.82	100.37	99.82	99.84	99.53	99.97	99.55	99.91	99.19	99.33	99.01	99.00	99.83	99.76	100.05	99.34	99.67	100.10
Cations (based on 6 oxygens)																						
Si	1.98	1.97	1.96	1.95	1.96	1.96	1.97	1.97	1.97	1.94	1.95	1.95	1.94	1.97	1.97	1.97	1.97	1.96	1.95	1.98	1.97	1.98
Ti	0.01	0.01	0.00	0.00	0.00	0.00	0.00	0.00	0.00	0.00	0.00	0.00	0.00	0.00	0.00	0.00	0.01	0.00	0.00	0.00	0.01	0.01
Al	0.03	0.04	0.05	0.05	0.05	0.05	0.05	0.05	0.05	0.06	0.06	0.06	0.06	0.06	0.05	0.05	0.04	0.06	0.05	0.05	0.04	0.04
Cr	0.00	0.01	0.01	0.01	0.01	0.01	0.02	0.01	0.01	0.01	0.01	0.01	0.01	0.01	0.01	0.01	0.01	0.01	0.01	0.01	0.01	0.01
Fe	0.59	0.40	0.39	0.36	0.37	0.36	0.37	0.36	0.35	0.35	0.36	0.35	0.35	0.35	0.33	0.32	0.49	0.37	0.45	0.37	0.36	0.40
Mn	0.01	0.01	0.01	0.01	0.01	0.01	0.01	0.01	0.01	0.01	0.01	0.01	0.01	0.01	0.01	0.01	0.01	0.01	0.01	0.01	0.01	0.01
Ni	0.01	0.00	0.00	0.00	0.00	0.00	0.00	0.00	0.00	0.00	0.00	0.00	0.00	0.00	0.00	0.00	0.00	0.00	0.00	0.00	0.00	0.00
Mg	1.33	1.51	1.53	1.57	1.55	1.56	1.52	1.53	1.55	1.56	1.56	1.55	1.58	1.54	1.60	1.59	1.43	1.51	1.49	1.52	1.56	1.49
Ca	0.04	0.05	0.05	0.05	0.05	0.04	0.05	0.05	0.04	0.06	0.05	0.05	0.05	0.04	0.03	0.03	0.04	0.07	0.06	0.05	0.03	0.06
Na	0.00	0.00	0.00	0.00	0.00	0.00	0.00	0.00	0.00	0.00	0.00	0.00	0.00	0.00	0.00	0.00	0.00	0.00	0.00	0.00	0.00	0.00
Total	4.00	4.00	4.01	4.01	4.01	4.00	3.99	3.99	3.99	4.01	4.01	4.00	4.02	3.99	4.00	3.99	4.00	4.00	4.01	3.99	3.99	3.99
Mg#	0.691	0.791	0.797	0.812	0.808	0.814	0.804	0.811	0.815	0.815	0.814	0.815	0.817	0.816	0.830	0.831	0.745	0.802	0.769	0.805	0.813	0.789
1 Standard deviation [wt%]																						
SiO2	0.12	0.09	0.13	0.27	0.28	0.24	0.51	0.16	0.06	0.16	0.26	0.11	0.14	0.25	0.15	0.19	0.28	0.21	0.19	0.27	0.19	0.26
TiO2	0.02	0.02	0.04	0.02	0.04	0.02	0.04	0.03	0.01	0.02	0.02	0.03	0.00	0.01	0.04	0.02	0.04	0.03	0.04	0.01	0.38	0.04
Al2O3	0.07	0.09	0.18	0.22	0.21	0.19	0.15	0.13	0.07	0.06	0.01	0.07	0.04	0.07	0.14	0.18	0.10	0.14	0.24	0.17	0.13	0.29
Cr2O3	0.03	0.06	0.06	0.07	0.08	0.08	0.22	0.04	0.03	0.05	0.04	0.03	0.02	0.05	0.09	0.04	0.07	0.03	0.10	0.05	0.09	0.08
FeO	0.65	0.20	0.16	0.33	0.36	0.26	0.20	0.20	0.15	0.07	0.25	0.28	0.22	0.23	0.14	0.34	0.66	0.26	0.45	0.21	0.19	0.34
MnO	0.01	0.02	0.02	0.02	0.02	0.01	0.02	0.01	0.02	0.01	0.03	0.03	0.00	0.03	0.03	0.01	0.03	0.02	0.02	0.02	0.02	0.02
NiO	0.02	0.02	0.02	0.02	0.03	0.02	0.01	0.02	0.02	0.02	0.02	0.02	0.02	0.02	0.02	0.03	0.01	0.04	0.02	0.01	0.02	0.03
MgO	0.51	0.35	0.20	0.43	0.39	0.29	0.35	0.26	0.30	0.09	0.34	0.09	0.15	0.23	0.23	0.39	0.51	0.21	0.23	0.36	0.26	0.45
CaO	0.08	0.39	0.24	0.55	0.31	0.41	0.42	0.30	0.52	0.27	0.38	0.28	0.26	0.27	0.38	0.46	0.29	0.16	0.39	0.45	0.15	0.53
Na2O	0.00	0.01	0.01	0.01	0.01	0.01	0.01	0.01	0.01	0.00	0.01	0.01	0.00	0.01	0.01	0.01	0.00	0.01	0.01	0.01	0.00	0.02
Mg#	0.012	0.002	0.002	0.004	0.006	0.003	0.003	0.003	0.001	0.001	0.003	0.003	0.002	0.003	0.002	0.005	0.011	0.001	0.006	0.002	0.003	0.004
n	4	5	5	5	10	6	9	8	8	6	6	5	3	9	5	6	5	6	5	6	5	8

Orthopyroxene analyses: IM sequence

Sample	776.40	787.90	788.32	788.60 a	788.80	790.64	793.22 b	794.10	795.50	796.25	798.00	801.00	804.40	810.10	818.00	819.30	819.85	826.48	826.70	836.00 b	839.00	841.67 in	841.67 out	849.51 b	851.90	853.95	856.00
Rock type	o	.	.	X	X	.	.	.	o	.	x	X	X	X	X	.	x	.	*	.	.	o	o	+	+	+	.
[wt%]																											
SiO2	53.49	55.21	56.05	55.59	55.51	55.18	53.94	55.09	54.65	55.77	55.47	56.04	54.62	55.43	54.36	55.34	55.78	54.90	54.72	54.77	55.12	54.68	54.09	53.54	53.80	54.96	55.45
TiO2	0.24	0.12	0.21	0.17	0.16	0.21	0.15	0.18	0.26	0.17	0.22	0.16	0.13	0.12	0.18	0.14	0.11	0.14	0.31	0.20	0.16	0.12	0.17	0.15	0.12	0.17	0.14
Al2O3	0.76	1.36	1.24	1.39	1.54	1.25	1.44	1.29	1.03	1.36	1.45	1.26	1.53	1.37	1.56	1.47	1.23	1.23	1.59	1.03	0.97	1.59	1.32	0.67	1.01	0.90	1.28
Cr2O3	0.10	0.45	0.37	0.43	0.45	0.50	0.47	0.42	0.22	0.31	0.31	0.40	0.48	0.39	0.45	0.43	0.19	0.36	0.28	0.35	0.33	0.13	0.19	0.11	0.30	0.26	0.52
FeO	20.02	12.06	11.87	12.23	11.65	13.25	13.88	13.44	15.56	12.04	10.78	11.56	12.25	11.88	11.63	11.95	13.41	15.53	11.98	15.26	15.27	14.86	16.13	19.34	17.53	15.47	12.88
MnO	0.41	0.26	0.24	0.26	0.23	0.26	0.30	0.26	0.33	0.24	0.25	0.27	0.26	0.25	0.23	0.23	0.28	0.30	0.23	0.31	0.28	0.27	0.29	0.35	0.33	0.28	0.27
NiO	0.06	0.09	0.07	0.09	0.08	0.07	0.13	0.05	0.06	0.10	0.08	0.07	0.07	0.09	0.09	0.06	0.07	0.06	0.11	0.08	0.07	0.11	0.09	0.04	0.06	0.07	0.08
MgO	23.65	28.95	28.77	28.62	28.90	28.25	28.03	28.46	27.56	29.16	31.00	29.01	29.06	29.35	29.67	29.43	28.38	26.43	29.55	26.43	26.82	27.04	25.81	24.49	25.29	26.79	27.69
CaO	0.97	0.90	1.04	1.14	1.27	1.40	1.32	1.26	0.92	0.87	1.03	1.03	1.08	1.04	1.46	1.09	0.60	1.05	1.17	1.14	0.97	0.47	0.65	1.05	1.02	1.17	1.42
Na2O	0.00	0.01	0.01	0.03	0.01	0.03	0.03	0.02	0.02	0.01	0.01	0.01	0.01	0.02	0.02	0.02	0.01	0.01	0.02	0.02	0.03	0.01	0.01	0.01	0.03	0.02	0.02
Total	99.69	99.42	99.87	99.94	99.79	100.39	99.67	100.46	100.61	100.03	100.61	99.81	99.49	99.93	99.63	100.16	100.07	100.01	99.95	99.58	100.04	99.27	98.75	99.76	99.50	100.09	99.74
Cations (based on 6 oxygens)																											
Si	1.98	1.97	1.99	1.98	1.97	1.97	1.95	1.96	1.96	1.98	1.95	1.99	1.95	1.97	1.94	1.96	1.99	1.98	1.95	1.98	1.98	1.98	1.98	1.97	1.97	1.98	1.98
Ti	0.01	0.00	0.01	0.00	0.00	0.01	0.00	0.00	0.01	0.00	0.01	0.00	0.00	0.00	0.00	0.00	0.00	0.00	0.01	0.01	0.00	0.00	0.00	0.00	0.00	0.00	0.00
Al	0.03	0.06	0.05	0.06	0.06	0.05	0.06	0.05	0.04	0.06	0.06	0.05	0.06	0.06	0.07	0.06	0.05	0.05	0.07	0.04	0.04	0.07	0.06	0.03	0.04	0.04	0.05
Cr	0.00	0.01	0.01	0.01	0.01	0.01	0.01	0.01	0.01	0.01	0.01	0.01	0.01	0.01	0.01	0.01	0.01	0.01	0.01	0.01	0.01	0.00	0.01	0.00	0.01	0.01	0.01
Fe	0.62	0.36	0.35	0.36	0.35	0.39	0.42	0.40	0.47	0.36	0.32	0.34	0.37	0.35	0.35	0.35	0.40	0.47	0.36	0.46	0.46	0.45	0.49	0.60	0.54	0.47	0.39
Mn	0.01	0.01	0.01	0.01	0.01	0.01	0.01	0.01	0.01	0.01	0.01	0.01	0.01	0.01	0.01	0.01	0.01	0.01	0.01	0.01	0.01	0.01	0.01	0.01	0.01	0.01	0.01
Ni	0.00	0.00	0.00	0.00	0.00	0.00	0.00	0.00	0.00	0.00	0.00	0.00	0.00	0.00	0.00	0.00	0.00	0.00	0.00	0.00	0.00	0.00	0.00	0.00	0.00	0.00	0.00
Mg	1.30	1.54	1.52	1.52	1.53	1.50	1.51	1.51	1.47	1.54	1.62	1.53	1.55	1.55	1.58	1.55	1.51	1.42	1.57	1.43	1.44	1.46	1.41	1.35	1.38	1.44	1.48
Ca	0.04	0.03	0.04	0.04	0.05	0.05	0.05	0.05	0.04	0.03	0.04	0.04	0.04	0.04	0.06	0.04	0.02	0.04	0.04	0.04	0.04	0.02	0.03	0.04	0.04	0.05	0.05
Na	0.00	0.00	0.00	0.00	0.00	0.00	0.00	0.00	0.00	0.00	0.00	0.00	0.00	0.00	0.00	0.00	0.00	0.00	0.00	0.00	0.00	0.00	0.00	0.00	0.00	0.00	0.00
Total	4.00	3.99	3.98	3.99	3.99	4.00	4.01	4.00	4.01	3.99	4.01	3.98	4.00	4.00	4.02	4.00	3.98	3.99	4.01	3.99	3.99	3.99	3.98	4.01	4.00	3.99	3.98
Mg#	0.678	0.811	0.812	0.807	0.816	0.792	0.703	0.791	0.759	0.812	0.837	0.817	0.809	0.815	0.820	0.815	0.790	0.752	0.815	0.755	0.758	0.764	0.740	0.693	0.720	0.755	0.793
1 Standard deviation [wt%]																											
SiO2	0.13	0.18	0.25	0.22	0.12	0.62	0.21	0.04	0.40	0.36	0.16	0.42	0.11	0.39	0.28	0.19	0.35	0.24	0.48	0.19	0.19	0.26	0.05	0.21	0.23	0.15	0.14
TiO2	0.03	0.02	0.05	0.05	0.05	0.07	0.03	0.05	0.02	0.05	0.04	0.03	0.03	0.04	0.03	0.04	0.03	0.03	0.04	0.04	0.04	0.05	0.02	0.06	0.04	0.03	0.02
Al2O3	0.03	0.05	0.18	0.28	0.14	0.09	0.18	0.19	0.14	0.19	0.06	0.19	0.15	0.24	0.08	0.18	0.19	0.07	0.21	0.18	0.16	0.09	0.21	0.10	0.28	0.08	0.13
Cr2O3	0.00	0.02	0.05	0.08	0.05	0.27	0.06	0.12	0.02	0.09	0.03	0.08	0.06	0.09	0.03	0.06	0.07	0.05	0.07	0.07	0.07	0.08	0.02	0.02	0.13	0.06	0.05
FeO	0.26	0.06	0.20	0.31	0.17	0.36	0.28	0.23	0.27	0.31	0.37	0.20	0.23	0.09	0.34	0.22	0.35	0.21	1.41	0.67	0.57	0.44	0.56	0.63	1.07	0.44	0.28
MnO	0.03	0.01	0.01	0.02	0.02	0.03	0.02	0.01	0.01	0.02	0.02	0.02	0.01	0.03	0.01	0.02	0.03	0.03	0.03	0.02	0.03	0.02	0.03	0.03	0.03	0.02	0.01
NiO	0.02	0.02	0.02	0.02	0.02	0.02	0.02	0.03	0.00	0.03	0.01	0.02	0.02	0.02	0.02	0.02	0.01	0.02	0.02	0.03	0.02	0.01	0.01	0.02	0.01	0.01	0.02
MgO	0.06	0.30	0.59	0.26	0.24	0.41	0.24	0.24	0.24	0.23	0.39	0.40	0.29	0.20	0.20	0.33	0.23	0.30	0.94	0.32	0.37	0.38	0.51	0.48	0.50	0.46	0.38
CaO	0.14	0.31	0.27	0.27	0.40	0.31	0.27	0.37	0.14	0.21	0.51	0.29	0.31	0.30	0.39	0.30	0.09	0.54	0.33	0.52	0.52	0.09	0.01	0.41	0.31	0.57	0.60
Na2O	0.00	0.01	0.01	0.01	0.01	0.01	0.00	0.01	0.01	0.01	0.01	0.01	0.01	0.01	0.01	0.01	0.01	0.00	0.01	0.01	0.01	0.00	0.00	0.01	0.01	0.02	0.01
Mg#	0.003	0.002	0.003	0.003	0.003	0.007	0.003	0.002	0.003	0.004	0.004	0.003	0.002	0.001	0.004	0.004	0.005	0.023	0.001	0.009	0.006	0.007	0.010	0.010	0.016	0.005	0.002
n	3	5	13	6	5	6	4	4	4	7	4	8	3	7	7	6	6	8	5	7	9	7	2	6	6	10	5

Orthopyroxene analyses: TF sequence

Sample	842.00	851.00	866.50	866.50	875.00	885.00	895.00	930.00	953.00	957.00	962.00	964.00
Rock type	.	.	*	o	.	.	.	.	o	+	+	+
[wt%]												
SiO2	54.94	54.26	54.87	54.64	54.87	54.98	54.37	54.55	53.95	54.77	55.15	54.75
TiO2	0.21	0.18	0.18	0.29	0.19	0.18	0.13	0.23	0.24	0.26	0.19	0.15
Al2O3	1.14	1.40	1.57	1.31	1.28	1.23	1.43	1.05	0.77	0.98	1.14	1.10
Cr2O3	0.43	0.44	0.26	0.20	0.42	0.42	0.40	0.45	0.25	0.39	0.51	0.45
FeO	11.91	12.94	12.21	13.99	11.82	11.85	11.97	13.20	17.45	13.35	12.61	12.90
MnO	0.23	0.22	0.26	0.28	0.26	0.25	0.25	0.28	0.30	0.27	0.25	0.26
NiO	0.05	0.07	0.04	0.05	0.10	0.09	0.08	0.09	0.07	0.06	0.06	0.06
MgO	30.35	29.39	29.44	28.39	29.62	30.03	29.99	29.12	26.05	28.98	29.44	29.28
CaO	1.34	1.40	1.03	0.75	1.56	1.26	1.16	1.36	1.18	1.38	1.06	1.35
Na2O	0.01	0.03	0.01	0.00	0.02	0.02	0.01	0.03	0.00	0.01	0.01	0.02
Total	100.61	100.33	99.89	99.89	100.13	100.32	99.79	100.35	100.26	100.45	100.42	100.31
Cations (based on 6 oxygens)												
Si	1.94	1.94	1.95	1.96	1.95	1.95	1.94	1.95	1.96	1.95	1.96	1.95
Ti	0.01	0.00	0.00	0.01	0.01	0.00	0.00	0.01	0.01	0.01	0.01	0.00
Al	0.05	0.06	0.07	0.06	0.05	0.05	0.06	0.04	0.03	0.04	0.05	0.05
Cr	0.01	0.01	0.01	0.01	0.01	0.01	0.01	0.01	0.01	0.01	0.01	0.01
Fe	0.35	0.39	0.36	0.42	0.35	0.35	0.36	0.39	0.53	0.40	0.37	0.38
Mn	0.01	0.01	0.01	0.01	0.01	0.01	0.01	0.01	0.01	0.01	0.01	0.01
Ni	0.00	0.00	0.00	0.00	0.00	0.00	0.00	0.00	0.00	0.00	0.00	0.00
Mg	1.60	1.56	1.56	1.52	1.57	1.59	1.59	1.55	1.41	1.54	1.56	1.56
Ca	0.05	0.05	0.04	0.03	0.06	0.05	0.04	0.05	0.05	0.05	0.04	0.05
Na	0.00	0.00	0.00	0.00	0.00	0.00	0.00	0.00	0.00	0.00	0.00	0.00
Total	4.02	4.02	4.01	4.00	4.01	4.01	4.02	4.02	4.01	4.01	4.01	4.02
Mg#	0.820	0.802	0.811	0.783	0.817	0.819	0.817	0.797	0.727	0.795	0.806	0.802
1 Standard deviation [wt%]												
SiO2	0.21	0.21	0.07	0.18	0.24	0.21	0.22	0.13	0.49	0.24	0.24	0.26
TiO2	0.04	0.03	0.02	0.02	0.02	0.03	0.01	0.03	0.06	0.07	0.02	0.02
Al2O3	0.10	0.13	0.10	0.24	0.08	0.14	0.09	0.03	0.20	0.13	0.04	0.13
Cr2O3	0.03	0.03	0.14	0.05	0.03	0.03	0.09	0.02	0.09	0.06	0.02	0.06
FeO	0.06	0.26	0.23	0.95	0.26	0.20	0.13	0.26	1.95	0.24	0.16	0.20
MnO	0.02	0.02	0.02	0.03	0.02	0.02	0.03	0.03	0.02	0.02	0.02	0.02
NiO	0.01	0.02	0.03	0.01	0.02	0.01	0.02	0.03	0.01	0.01	0.02	0.02
MgO	0.07	0.23	0.49	0.48	0.35	0.21	0.17	0.20	1.39	0.14	0.23	0.23
CaO	0.11	0.33	0.68	0.07	0.54	0.28	0.25	0.21	0.37	0.30	0.19	0.29
Na2O	0.00	0.01	0.01	0.00	0.01	0.01	0.01	0.01	0.01	0.01	0.01	0.01
Mg#	0.001	0.003	0.017	0.030	0.002	0.002	0.002	0.003	0.033	0.002	0.002	0.002
n	7	7	4	3	7	8	7	6	7	7	7	7

Orthopyroxene analyses: LK7 sequence

Sample	1389.70	1395.60	1401.95	1407.05	1407.85	1412.35 b	1415.05	1418.90	1421.10 a	1424.28 a	1424.28 b	1424.80	1425.20 a
Rock type	.	.	.	.	.	.	.	.	.	o	+	.	.
[wt%]													
SiO2	55.53	55.18	55.43	55.49	54.57	54.65	53.35	53.88	54.18	52.90	54.97	54.05	53.90
TiO2	0.22	0.19	0.15	0.13	0.18	0.21	0.24	0.24	0.20	0.24	0.14	0.18	0.19
Al2O3	1.03	1.08	1.17	1.16	1.01	1.06	1.00	0.91	1.04	0.82	1.04	1.06	1.11
Cr2O3	0.44	0.45	0.41	0.53	0.41	0.41	0.32	0.29	0.40	0.12	0.45	0.42	0.41
FeO	12.37	12.09	11.43	11.34	13.37	14.68	17.07	17.13	14.17	20.73	13.16	14.53	14.68
MnO	0.24	0.23	0.21	0.23	0.31	0.28	0.39	0.36	0.33	0.41	0.27	0.31	0.31
NiO	0.09	0.09	0.10	0.09	0.07	0.09	0.06	0.02	0.08	0.02	0.08	0.11	0.09
MgO	29.24	29.51	29.24	29.93	28.71	26.94	26.21	26.18	27.65	22.60	29.03	28.08	28.38
CaO	1.27	1.44	1.72	1.28	1.46	1.39	1.14	1.13	1.57	1.48	1.27	1.58	1.22
Na2O	0.02	0.01	0.02	0.01	0.02	0.01	0.03	0.03	0.02	0.01	0.01	0.03	0.03
Total	100.43	100.26	99.89	100.20	100.11	99.72	99.79	100.18	99.63	99.34	100.42	100.35	100.32
Cations (based on 6 oxygens)													
Si	1.97	1.96	1.97	1.96	1.95	1.97	1.95	1.96	1.96	1.97	1.96	1.94	1.94
Ti	0.01	0.01	0.00	0.00	0.00	0.01	0.01	0.01	0.01	0.01	0.00	0.00	0.01
Al	0.04	0.05	0.05	0.05	0.04	0.05	0.04	0.04	0.04	0.04	0.04	0.05	0.05
Cr	0.01	0.01	0.01	0.01	0.01	0.01	0.01	0.01	0.01	0.00	0.01	0.01	0.01
Fe	0.37	0.36	0.34	0.34	0.40	0.44	0.52	0.52	0.43	0.65	0.39	0.44	0.44
Mn	0.01	0.01	0.01	0.01	0.01	0.01	0.01	0.01	0.01	0.01	0.01	0.01	0.01
Ni	0.00	0.00	0.00	0.00	0.00	0.00	0.00	0.00	0.00	0.00	0.00	0.00	0.00
Mg	1.54	1.56	1.55	1.58	1.53	1.45	1.43	1.42	1.49	1.26	1.54	1.51	1.52
Ca	0.05	0.05	0.07	0.05	0.06	0.05	0.04	0.04	0.06	0.06	0.05	0.06	0.05
Na	0.00	0.00	0.00	0.00	0.00	0.00	0.00	0.00	0.00	0.00	0.00	0.00	0.00
Total	4.00	4.01	4.00	4.00	4.01	3.99	4.02	4.01	4.01	4.00	4.01	4.02	4.03
Mg#	0.808	0.813	0.820	0.825	0.793	0.766	0.732	0.731	0.777	0.660	0.797	0.775	0.775
1 Standard deviation [wt%]													
SiO2	0.20	0.14	0.29	0.28	0.13	0.09	0.10	0.04	0.12	0.18	0.07	0.06	0.08
TiO2	0.03	0.03	0.02	0.02	0.02	0.06	0.06	0.05	0.04	0.02	0.03	0.05	0.00
Al2O3	0.07	0.07	0.06	0.08	0.10	0.10	0.12	0.10	0.17	0.25	0.07	0.16	0.01
Cr2O3	0.04	0.02	0.03	0.07	0.04	0.07	0.07	0.07	0.06	0.15	0.03	0.04	0.02
FeO	0.16	0.22	0.14	0.59	0.24	0.38	0.37	0.17	0.17	0.47	0.14	0.33	0.13
MnO	0.02	0.04	0.03	0.02	0.04	0.03	0.04	0.01	0.01	0.02	0.02	0.01	0.04
NiO	0.01	0.02	0.01	0.02	0.02	0.02	0.02	0.01	0.02	0.01	0.01	0.02	0.01
MgO	0.18	0.32	0.16	0.34	0.22	0.25	0.24	0.24	0.24	0.36	0.26	0.15	0.32
CaO	0.16	0.36	0.21	0.34	0.33	0.39	0.17	0.26	0.42	0.35	0.36	0.14	0.03
Na2O	0.00	0.01	0.01	0.01	0.01	0.01	0.01	0.00	0.01	0.01	0.01	0.01	0.01
Mg#	0.002	0.002	0.002	0.009	0.002	0.004	0.006	0.002	0.001	0.014	0.007	0.002	0.004
n	6	6	5	7	4	6	4	3	4	3	5	4	4

Sample	1425.20	1427.50	1428.10	1429.54	1429.73	1429.73	1430.10	1430.10	1430.90	1430.90	1441.25	1446.20	1457.35	1464.56	1470.00	1481.26	1491.10	1500.95	1511.10	1520.40	1528.90	1539.10	1548.85	1556.56	1562.25	1573.75
	b				Top	Base	Top	Base	b-Top	b-Base	a				a			b	b		a		b		b	a
Rock type	.	.	.	.	.	.	.	.	.	.	.	.	.	.	.	.	.	.	.	.	.	.	.	.	o	o
[wt%]																										
SiO2	53.97	54.44	54.34	55.00	54.58	54.57	55.53	55.41	55.15	54.86	54.98	55.81	55.57	55.62	54.82	54.61	55.18	54.96	55.18	54.57	54.75	54.17	55.04	54.99	53.09	54.21
TiO2	0.21	0.17	0.21	0.23	0.22	0.23	0.17	0.23	0.21	0.23	0.19	0.18	0.16	0.17	0.18	0.24	0.20	0.25	0.28	0.21	0.28	0.26	0.26	0.24	0.25	0.22
Al2O3	0.95	0.99	0.96	1.01	1.12	1.05	1.07	1.03	0.92	1.02	0.99	1.05	1.07	1.06	0.97	1.02	1.02	0.99	0.95	0.97	0.93	0.94	0.99	0.90	0.71	0.83
Cr2O3	0.36	0.38	0.35	0.48	0.47	0.50	0.47	0.49	0.36	0.44	0.39	0.37	0.38	0.40	0.35	0.37	0.38	0.32	0.32	0.31	0.26	0.29	0.30	0.24	0.03	0.25
FeO	15.70	15.78	14.70	12.87	12.46	12.63	12.39	12.57	12.82	12.88	12.45	12.12	12.50	12.67	12.72	13.49	13.81	13.92	14.10	14.26	15.44	14.96	14.82	15.08	23.25	18.78
MnO	0.34	0.37	0.32	0.25	0.28	0.27	0.23	0.24	0.27	0.25	0.23	0.23	0.23	0.26	0.24	0.23	0.24	0.26	0.26	0.29	0.29	0.26	0.31	0.31	0.41	0.32
NiO	0.07	0.07	0.08	0.08	0.08	0.06	0.09	0.09	0.09	0.08	0.06	0.06	0.09	0.08	0.09	0.07	0.09	0.06	0.05	0.08	0.08	0.08	0.09	0.06	0.00	0.04
MgO	27.08	27.74	27.70	28.21	28.40	28.72	28.89	29.26	29.12	28.85	28.93	29.22	28.95	28.81	28.80	28.67	28.17	27.80	27.78	27.62	27.01	27.16	27.11	27.12	21.03	24.31
CaO	1.05	0.97	1.43	1.26	1.82	1.44	1.62	0.96	1.35	1.41	1.34	1.39	1.45	1.26	1.13	1.06	0.97	1.05	1.33	1.54	1.06	1.49	1.37	1.42	1.16	1.29
Na2O	0.01	0.02	0.02	0.01	0.02	0.01	0.01	0.00	0.02	0.02	0.02	0.02	0.01	0.01	0.00	0.01	0.01	0.01	0.01	0.01	0.01	0.02	0.02	0.01	0.02	0.02
Total	99.74	100.93	100.12	99.40	99.45	99.49	100.49	100.28	100.30	100.05	99.58	100.45	100.40	100.35	99.31	99.77	100.30	99.60	100.25	99.86	100.09	99.62	100.31	100.37	99.94	100.27
Cations (based on 6 oxygens)																										
Si	1.96	1.95	1.96	1.97	1.96	1.96	1.97	1.97	1.96	1.96	1.97	1.97	1.97	1.97	1.97	1.96	1.97	1.98	1.97	1.97	1.97	1.96	1.98	1.97	1.99	1.98
Ti	0.01	0.00	0.01	0.01	0.01	0.01	0.00	0.01	0.01	0.01	0.01	0.00	0.00	0.00	0.00	0.01	0.01	0.01	0.01	0.01	0.01	0.01	0.01	0.01	0.01	0.01
Al	0.04	0.04	0.04	0.04	0.05	0.04	0.04	0.04	0.04	0.04	0.04	0.04	0.04	0.04	0.04	0.04	0.04	0.04	0.04	0.04	0.04	0.04	0.04	0.04	0.03	0.04
Cr	0.01	0.01	0.01	0.01	0.01	0.01	0.01	0.01	0.01	0.01	0.01	0.01	0.01	0.01	0.01	0.01	0.01	0.01	0.01	0.01	0.01	0.01	0.01	0.01	0.00	0.01
Fe	0.48	0.47	0.44	0.39	0.37	0.38	0.37	0.37	0.38	0.38	0.37	0.36	0.37	0.38	0.38	0.40	0.41	0.42	0.42	0.43	0.47	0.45	0.44	0.45	0.73	0.57
Mn	0.01	0.01	0.01	0.01	0.01	0.01	0.01	0.01	0.01	0.01	0.01	0.01	0.01	0.01	0.01	0.01	0.01	0.01	0.01	0.01	0.01	0.01	0.01	0.01	0.01	0.01
Ni	0.00	0.00	0.00	0.00	0.00	0.00	0.00	0.00	0.00	0.00	0.00	0.00	0.00	0.00	0.00	0.00	0.00	0.00	0.00	0.00	0.00	0.00	0.00	0.00	0.00	0.00
Mg	1.46	1.48	1.49	1.51	1.52	1.54	1.53	1.55	1.54	1.54	1.54	1.54	1.53	1.52	1.54	1.53	1.50	1.49	1.48	1.48	1.45	1.47	1.45	1.45	1.17	1.32
Ca	0.04	0.04	0.06	0.05	0.07	0.06	0.06	0.04	0.05	0.05	0.05	0.05	0.05	0.05	0.04	0.04	0.04	0.04	0.05	0.06	0.04	0.06	0.05	0.05	0.05	0.05
Na	0.00	0.00	0.00	0.00	0.00	0.00	0.00	0.00	0.00	0.00	0.00	0.00	0.00	0.00	0.00	0.00	0.00	0.00	0.00	0.00	0.00	0.00	0.00	0.00	0.00	0.00
Total	4.01	4.02	4.01	3.99	4.00	4.01	4.00	4.00	4.01	4.01	4.00	3.99	4.00	3.99	4.00	4.01	3.99	3.99	3.99	4.00	4.00	4.01	3.99	4.00	3.99	3.99
Mg#	0.755	0.758	0.771	0.796	0.802	0.802	0.806	0.806	0.802	0.800	0.806	0.811	0.805	0.802	0.801	0.791	0.784	0.781	0.778	0.775	0.757	0.764	0.765	0.762	0.617	0.698
1 Standard deviation [wt%]																										
SiO2	0.32	0.36	0.25	0.21	0.04	0.06	0.11	0.06	0.08	0.13	0.15	0.11	0.11	0.14	0.23	0.15	0.22	0.20	0.21	0.08	0.31	0.16	0.20	0.17	0.04	0.12
TiO2	0.03	0.04	0.01	0.05	0.02	0.03	0.02	0.03	0.04	0.02	0.05	0.03	0.03	0.03	0.02	0.02	0.04	0.04	0.07	0.04	0.02	0.08	0.05	0.04	0.02	0.06
Al2O3	0.13	0.11	0.09	0.13	0.01	0.05	0.03	0.08	0.05	0.09	0.05	0.13	0.03	0.07	0.06	0.04	0.03	0.04	0.10	0.07	0.06	0.07	0.07	0.07	0.04	0.20
Cr2O3	0.09	0.08	0.04	0.03	0.01	0.02	0.02	0.06	0.03	0.03	0.02	0.04	0.02	0.01	0.03	0.03	0.02	0.02	0.02	0.03	0.03	0.03	0.03	0.02	0.01	0.09
FeO	0.16	0.32	0.09	0.23	0.05	0.11	0.20	0.06	0.11	0.30	0.21	0.30	0.20	0.16	0.19	0.19	0.29	0.17	0.12	0.34	0.22	0.33	0.24	0.27	0.41	0.95
MnO	0.03	0.00	0.02	0.01	0.02	0.01	0.01	0.01	0.02	0.02	0.02	0.01	0.03	0.01	0.04	0.02	0.02	0.02	0.02	0.01	0.02	0.02	0.02	0.01	0.05	0.03
NiO	0.02	0.03	0.04	0.01	0.01	0.02	0.03	0.02	0.01	0.03	0.01	0.03	0.02	0.01	0.02	0.01	0.02	0.01	0.02	0.01	0.02	0.02	0.02	0.01	0.01	0.02
MgO	0.24	0.23	0.27	0.21	0.14	0.17	0.07	0.19	0.08	0.29	0.30	1.13	0.22	0.10	0.23	0.13	9.98	0.13	0.23	0.16	0.22	0.26	0.16	0.28	0.28	0.66
CaO	0.25	0.32	0.32	0.31	0.23	0.26	0.02	0.34	0.26	0.38	0.37	0.86	0.38	0.24	0.32	0.16	0.52	0.17	0.41	0.33	0.26	0.41	0.25	0.44	0.03	0.39
Na2O	0.01	0.01	0.01	0.00	0.01	0.01	0.00	0.01	0.01	0.01	0.01	0.01	0.01	0.01	0.00	0.01	0.01	0.01	0.01	0.01	0.01	0.01	0.01	0.01	0.00	0.01
Mg#	0.003	0.001	0.004	0.002	0.002	0.001	0.001	0.003	0.001	0.001	0.003	0.002	0.002	0.002	0.003	0.002	0.133	0.003	0.001	0.004	0.004	0.003	0.002	0.003	0.007	0.015
n	3	4	4	6	3	3	5	5	4	3	6	6	6	6	6	6	6	5	5	6	6	6	4	6	3	6

Sample	1577.45 Top	1577.45 Mid	1577.45 Mid	1577.45 Base	1578.43 c-Top	1578.43 c-Base	1578.68 b	1579.20	1581.88 b	1582.70 a	1583.25 a	1584.23 b	1585.35	1585.85	1586.65	1587.00
Rock type	.	.	.	o	+	+	.	+	+	+	+	+	+	*	.	.
[wt%]																
SiO2	53.40	54.30	54.72	54.04	54.66	54.07	54.84	55.47	55.23	55.72	55.67	55.23	55.63	55.92	54.94	55.50
TiO2	0.26	0.20	0.19	0.31	0.18	0.14	0.17	0.24	0.24	0.15	0.11	0.19	0.13	0.10	0.19	0.23
Al2O3	0.76	0.77	0.96	0.86	1.14	1.45	0.99	0.94	1.52	0.94	1.15	1.13	1.36	1.37	1.09	1.15
Cr2O3	0.20	0.29	0.40	0.21	0.35	0.41	0.37	0.36	0.38	0.35	0.37	0.43	0.28	0.44	0.43	0.45
FeO	18.77	15.80	14.90	18.53	15.27	15.52	16.25	14.92	12.96	13.73	11.00	13.83	12.48	10.75	12.64	12.34
MnO	0.34	0.31	0.27	0.31	0.28	0.24	0.35	0.28	0.27	0.26	0.24	0.29	0.21	0.23	0.26	0.24
NiO	0.05	0.04	0.04	0.04	0.09	0.09	0.07	0.08	0.12	0.06	0.08	0.07	0.09	0.11	0.07	0.09
MgO	24.71	27.49	26.98	24.10	26.85	25.60	25.31	27.21	27.05	26.90	29.91	27.09	29.51	30.18	28.51	28.92
CaO	1.22	0.88	0.91	1.12	1.02	2.03	1.24	1.15	1.84	1.40	1.14	1.36	0.92	0.93	1.50	1.05
Na2O	0.03	0.03	0.01	0.01	0.01	0.01	0.03	0.01	0.07	0.01	0.02	0.03	0.03	0.00	0.02	0.01
Total	99.75	100.11	99.41	99.54	99.84	99.56	99.62	100.67	99.69	99.52	99.69	99.65	100.64	100.01	99.64	99.97
Cations (based on 6 oxygens)																
Si	1.97	1.96	1.98	1.99	1.97	1.97	1.99	1.98	1.98	2.00	1.97	1.98	1.96	1.97	1.97	1.97
Ti	0.01	0.01	0.01	0.01	0.00	0.00	0.00	0.01	0.01	0.00	0.00	0.01	0.00	0.00	0.01	0.01
Al	0.03	0.03	0.04	0.04	0.05	0.06	0.04	0.04	0.06	0.04	0.05	0.05	0.06	0.06	0.05	0.05
Cr	0.01	0.01	0.01	0.01	0.01	0.01	0.01	0.01	0.01	0.01	0.01	0.01	0.01	0.01	0.01	0.01
Fe	0.58	0.48	0.45	0.57	0.46	0.47	0.49	0.45	0.39	0.41	0.33	0.42	0.37	0.32	0.38	0.37
Mn	0.01	0.01	0.01	0.01	0.01	0.01	0.01	0.01	0.01	0.01	0.01	0.01	0.01	0.01	0.01	0.01
Ni	0.00	0.00	0.00	0.00	0.00	0.00	0.00	0.00	0.00	0.00	0.00	0.00	0.00	0.00	0.00	0.00
Mg	1.36	1.48	1.46	1.32	1.44	1.39	1.37	1.45	1.44	1.44	1.58	1.45	1.55	1.59	1.52	1.53
Ca	0.05	0.03	0.04	0.04	0.04	0.08	0.05	0.04	0.07	0.05	0.04	0.05	0.03	0.04	0.06	0.04
Na	0.00	0.00	0.00	0.00	0.00	0.00	0.00	0.00	0.00	0.00	0.00	0.00	0.00	0.00	0.00	0.00
Total	4.01	4.01	3.99	3.98	3.99	3.99	3.98	3.99	3.98	3.97	3.99	3.98	4.00	3.99	4.00	3.99
Mg#	0.701	0.756	0.763	0.699	0.758	0.746	0.735	0.765	0.788	0.777	0.829	0.777	0.808	0.833	0.801	0.807
1 Standard deviation [wt%]																
SiO2	0.20	0.24	0.19	0.23	0.07	0.16	0.29	0.19	0.49	0.19	0.38	0.22	0.16	0.35	0.28	0.16
TiO2	0.04	0.03	0.00	0.01	0.02	0.01	0.03	0.03	0.10	0.05	0.01	0.04	0.04	0.01	0.01	0.03
Al2O3	0.12	0.05	0.06	0.03	0.18	0.13	0.20	0.08	0.38	0.20	0.11	0.04	0.12	0.13	0.09	0.05
Cr2O3	0.05	0.03	0.01	0.01	0.06	0.01	0.07	0.03	0.11	0.10	0.07	0.02	0.06	0.06	0.03	0.02
FeO	0.81	0.56	0.59	0.05	0.29	0.19	0.46	0.28	0.72	0.67	0.34	0.35	0.09	0.20	0.49	0.14
MnO	0.01	0.03	0.01	0.02	0.01	0.02	0.02	0.03	0.02	0.03	0.02	0.03	0.03	0.02	0.02	0.02
NiO	0.02	0.02	0.01	0.00	0.01	0.01	0.03	0.03	0.02	0.01	0.01	0.02	0.01	0.00	0.02	0.02
MgO	0.59	0.44	0.17	0.11	0.18	0.16	0.14	0.18	1.06	0.39	0.25	0.15	0.28	0.52	0.61	0.21
CaO	0.37	0.13	0.06	0.01	0.16	0.23	0.29	0.25	0.84	0.50	0.27	0.21	0.30	0.24	0.91	0.26
Na2O	0.01	0.00	0.01	0.01	0.00	0.01	0.01	0.01	0.14	0.01	0.00	0.01	0.03	0.00	0.02	0.01
Mg#	0.013	0.009	0.008	0.001	0.005	0.001	0.006	0.003	0.012	0.009	0.005	0.010	0.005	0.001	0.003	0.001
n	4	6	3	3	3	3	7	6	8	7	6	5	4	3	7	6

Orthopyroxene analyses: H3 sequence

Sample	1054.10 b	1060.05	1062.50	1065.05	1066.00	1067.15	1069.60	1071.05 a	1073.00	1075.15	1078.80	1080.10	1081.64	1082.10	1083.75	1084.85	1086.50	1087.30	1087.65	1088.10 a	1089.25 Mid	1089.40 b	1089.65	1090.20 a	1090.20 b	1099.35
Rock type	.	.	.	.	.	.	.	.	.	.	o	o	+	o	.	.	.	.	.	.	+	.	.	.	.	.
[wt%]																										
SiO2	54.63	55.29	55.19	54.70	54.90	54.72	53.76	54.56	53.43	53.40	53.17	52.51	54.62	53.41	53.79	54.40	55.32	55.24	54.90	55.59	55.72	54.72	55.59	55.31	54.88	55.20
TiO2	0.17	0.15	0.18	0.18	0.20	0.24	0.22	0.23	0.22	0.27	0.31	0.34	0.23	0.25	0.27	0.23	0.16	0.20	0.15	0.14	0.15	0.20	0.18	0.19	0.21	0.16
Al2O3	1.15	1.17	1.19	1.10	1.11	1.03	1.02	1.04	0.99	0.96	0.81	0.74	0.95	0.94	1.06	0.95	1.11	1.09	1.08	1.01	1.14	1.02	1.13	1.03	1.07	1.08
Cr2O3	0.42	0.43	0.45	0.47	0.50	0.38	0.33	0.32	0.30	0.31	0.22	0.07	0.36	0.29	0.28	0.35	0.45	0.38	0.34	0.42	0.48	0.40	0.42	0.42	0.46	0.40
FeO	12.92	12.04	11.61	12.20	12.85	14.04	15.45	15.87	17.52	16.87	19.13	22.48	14.60	15.93	16.58	14.10	13.04	13.62	13.37	12.18	11.94	12.48	12.27	12.66	12.31	11.96
MnO	0.25	0.29	0.24	0.25	0.25	0.26	0.34	0.29	0.33	0.35	0.36	0.48	0.29	0.31	0.34	0.32	0.28	0.30	0.32	0.23	0.25	0.24	0.22	0.26	0.24	0.27
NiO	0.05	0.07	0.10	0.06	0.08	0.06	0.06	0.06	0.07	0.07	0.07	0.01	0.07	0.09	0.06	0.08	0.09	0.08	0.08	0.08	0.09	0.06	0.11	0.08	0.07	0.08
MgO	28.36	29.19	28.43	29.54	29.51	28.03	26.30	26.51	24.72	25.80	23.98	22.09	27.84	26.16	25.90	27.69	29.16	28.33	28.10	28.60	29.36	29.11	29.08	29.32	29.15	29.23
CaO	1.31	1.46	1.58	1.50	1.33	1.27	0.95	1.51	1.65	1.58	1.10	1.35	1.18	1.22	1.57	1.42	1.35	1.65	1.31	1.48	1.31	1.29	1.25	1.23	1.59	1.41
Na2O	0.02	0.03	0.02	0.02	0.01	0.02	0.01	0.01	0.02	0.02	0.01	0.03	0.00	0.02	0.03	0.01	0.01	0.01	0.03	0.01	0.01	0.01	0.02	0.02	0.02	0.03
Total	99.27	100.12	98.99	100.02	100.74	100.05	98.44	100.40	99.23	99.63	99.15	100.11	100.14	98.60	99.86	99.54	100.97	100.91	99.68	99.74	100.45	99.53	100.27	100.49	99.99	99.81
Cations (based on 6 oxygens)																										
Si	1.97	1.96	1.98	1.95	1.95	1.96	1.97	1.97	1.97	1.95	1.97	1.96	1.96	1.96	1.96	1.96	1.96	1.96	1.97	1.98	1.97	1.96	1.97	1.96	1.96	1.97
Ti	0.00	0.00	0.00	0.00	0.01	0.01	0.01	0.01	0.01	0.01	0.01	0.01	0.01	0.01	0.01	0.01	0.00	0.01	0.00	0.00	0.00	0.01	0.00	0.01	0.01	0.00
Al	0.05	0.05	0.05	0.05	0.05	0.04	0.04	0.04	0.04	0.04	0.04	0.03	0.04	0.04	0.05	0.04	0.05	0.05	0.05	0.04	0.05	0.04	0.05	0.04	0.04	0.05
Cr	0.01	0.01	0.01	0.01	0.01	0.01	0.01	0.01	0.01	0.01	0.01	0.00	0.01	0.01	0.01	0.01	0.01	0.01	0.01	0.01	0.01	0.01	0.01	0.01	0.01	0.01
Fe	0.39	0.36	0.35	0.36	0.38	0.42	0.47	0.48	0.54	0.52	0.59	0.70	0.44	0.49	0.51	0.43	0.39	0.40	0.40	0.36	0.35	0.37	0.36	0.38	0.37	0.36
Mn	0.01	0.01	0.01	0.01	0.01	0.01	0.01	0.01	0.01	0.01	0.01	0.02	0.01	0.01	0.01	0.01	0.01	0.01	0.01	0.01	0.01	0.01	0.01	0.01	0.01	0.01
Ni	0.00	0.00	0.00	0.00	0.00	0.00	0.00	0.00	0.00	0.00	0.00	0.00	0.00	0.00	0.00	0.00	0.00	0.00	0.00	0.00	0.00	0.00	0.00	0.00	0.00	0.00
Mg	1.52	1.55	1.52	1.57	1.56	1.50	1.44	1.42	1.36	1.41	1.33	1.23	1.49	1.43	1.41	1.49	1.54	1.50	1.50	1.52	1.55	1.55	1.54	1.55	1.55	1.55
Ca	0.05	0.06	0.06	0.06	0.05	0.05	0.04	0.06	0.06	0.06	0.04	0.05	0.05	0.05	0.06	0.05	0.05	0.06	0.05	0.06	0.05	0.05	0.05	0.05	0.06	0.05
Na	0.00	0.00	0.00	0.00	0.00	0.00	0.00	0.00	0.00	0.00	0.00	0.00	0.00	0.00	0.00	0.00	0.00	0.00	0.00	0.00	0.00	0.00	0.00	0.00	0.00	0.00
Total	4.00	4.00	3.98	4.01	4.02	4.00	3.99	4.00	4.00	4.01	4.00	4.01	4.01	4.00	4.01	4.00	4.01	4.00	4.00	3.99	4.00	4.01	3.99	4.00	4.01	4.00
Mg#	0.796	0.812	0.814	0.812	0.804	0.781	0.752	0.749	0.715	0.732	0.691	0.636	0.772	0.745	0.736	0.778	0.799	0.788	0.789	0.807	0.814	0.806	0.809	0.805	0.808	0.813
1 Standard deviation [wt%]																										
SiO2	0.16	0.15	0.13	0.14	0.11	0.15	0.13	0.25	0.22	0.26	0.07	0.22	0.38	0.05	0.71	0.14	0.20	0.17	0.20	0.27	0.28	0.12	0.08	0.31	0.29	0.48
TiO2	0.03	0.02	0.02	0.03	0.03	0.02	0.02	0.03	0.05	0.03	0.02	0.03	0.06	0.03	0.13	0.03	0.02	0.04	0.02	0.02	0.02	0.03	0.03	0.04	0.03	0.03
Al2O3	0.08	0.08	0.05	0.10	0.07	0.04	0.05	0.15	0.13	0.05	0.03	0.02	0.07	0.06	0.19	0.07	0.13	0.07	0.06	0.07	0.13	0.09	0.15	0.08	0.10	0.07
Cr2O3	0.02	0.02	0.01	0.03	0.02	0.04	0.03	0.03	0.07	0.02	0.02	0.02	0.08	0.04	0.09	0.02	0.03	0.05	0.01	0.06	0.02	0.02	0.03	0.03	0.08	0.01
FeO	0.10	0.19	0.38	0.25	0.19	0.24	0.17	0.32	0.22	0.25	0.19	0.51	1.13	0.26	0.41	0.08	0.07	0.29	0.12	0.25	0.25	0.19	0.24	0.23	0.32	0.34
MnO	0.01	0.01	0.02	0.02	0.02	0.01	0.02	0.03	0.03	0.02	0.02	0.04	0.02	0.03	0.02	0.01	0.02	0.02	0.01	0.01	0.03	0.01	0.01	0.03	0.01	0.03
NiO	0.03	0.02	0.02	0.03	0.02	0.01	0.02	0.01	0.01	0.01	0.02	0.01	0.02	0.03	0.02	0.02	0.02	0.02	0.02	0.01	0.03	0.01	0.01	0.02	0.02	0.02
MgO	0.19	0.17	0.26	0.30	0.19	0.15	0.20	0.17	0.12	0.11	0.22	0.39	0.99	0.08	0.17	0.11	0.02	0.16	0.20	0.30	0.17	0.39	0.31	0.15	0.34	0.26
CaO	0.38	0.30	0.27	0.49	0.33	0.21	0.12	0.31	0.22	0.12	0.07	0.02	0.28	0.24	0.26	0.11	0.00	0.18	0.18	0.61	0.22	0.28	0.25	0.16	0.57	0.32
Na2O	0.00	0.01	0.01	0.01	0.01	0.00	0.01	0.01	0.01	0.01	0.00	0.00	0.01	0.00	0.02	0.01	0.00	0.01	0.00	0.01	0.01	0.00	0.01	0.01	0.01	0.02
Mg#	0.001	0.002	0.005	0.003	0.003	0.003	0.003	0.004	0.003	0.003	0.004	0.009	0.020	0.003	0.005	0.004	0.001	0.003	0.002	0.003	0.003	0.004	0.004	0.003	0.005	0.002
n	4	9	7	4	5	3	4	9	5	4	4	3	12	3	7	3	3	5	4	5	9	8	6	7	8	7

Sample	1110.05	1127.50	1144.10	1156.46	1166.10	1175.80	1191.50	1200.30	1206.95	1211.85	1219.05	1228.25	1231.35	1246.65	1250.35	1252.08	1252.50	1253.30 a	1256.75	1258.45	1261.15	1263.60	1266.28
Rock type	.	.	.	.	.	.	.	.	.	.	.	.	.	.	o	.	.	.	+	+	+	+	.
[wt%]																							
SiO2	55.39	55.31	54.86	54.77	54.74	55.29	54.92	55.01	54.56	55.16	55.04	54.99	53.68	53.39	53.77	54.11	53.76	54.54	55.14	54.49	54.93	55.01	54.81
TiO2	0.23	0.20	0.18	0.22	0.21	0.20	0.22	0.23	0.23	0.20	0.23	0.23	0.22	0.27	0.29	0.22	0.23	0.15	0.18	0.18	0.16	0.23	0.20
Al2O3	1.02	1.09	1.09	1.01	1.02	1.01	0.95	0.99	0.97	0.97	0.97	0.98	1.00	0.84	0.87	1.17	1.04	1.10	1.06	1.13	1.11	1.02	1.04
Cr2O3	0.38	0.37	0.37	0.36	0.35	0.34	0.30	0.27	0.26	0.31	0.33	0.32	0.27	0.20	0.17	0.40	0.41	0.41	0.47	0.41	0.47	0.43	0.44
FeO	12.55	12.25	13.21	13.45	13.22	13.09	13.52	15.77	15.73	13.68	13.81	13.29	14.97	18.28	18.57	16.30	14.87	13.52	12.78	14.03	12.47	12.22	12.07
MnO	0.24	0.27	0.22	0.27	0.26	0.29	0.29	0.29	0.33	0.29	0.28	0.27	0.27	0.36	0.38	0.36	0.34	0.32	0.26	0.33	0.26	0.29	0.25
NiO	0.09	0.08	0.07	0.09	0.08	0.08	0.07	0.07	0.07	0.07	0.07	0.08	0.10	0.07	0.07	0.03	0.09	0.08	0.09	0.08	0.08	0.11	0.09
MgO	28.88	28.67	28.27	29.38	28.27	29.48	27.93	26.99	27.08	28.29	28.70	29.30	27.57	25.76	24.43	26.15	28.24	28.63	27.98	28.42	28.73	29.12	29.09
CaO	1.75	1.41	1.43	1.25	1.26	1.20	1.28	1.18	1.26	1.10	1.21	1.14	1.27	1.26	1.18	1.42	1.18	1.15	1.78	1.53	1.44	1.54	1.63
Na2O	0.04	0.02	0.02	0.02	0.02	0.01	0.02	0.02	0.01	0.02	0.02	0.00	0.01	0.01	0.01	0.01	0.02	0.01	0.03	0.04	0.02	0.03	0.02
Total	100.56	99.66	99.71	100.79	99.40	101.00	99.51	100.84	100.51	100.18	100.64	100.58	99.36	100.44	99.73	100.18	100.18	99.90	99.77	100.64	99.68	99.99	99.63
Cations (based on 6 oxygens)																							
Si	1.97	1.97	1.97	1.95	1.97	1.96	1.97	1.97	1.96	1.97	1.96	1.96	1.95	1.95	1.98	1.96	1.94	1.96	1.97	1.95	1.96	1.96	1.96
Ti	0.01	0.01	0.00	0.01	0.01	0.01	0.01	0.01	0.01	0.01	0.01	0.01	0.01	0.01	0.01	0.01	0.01	0.00	0.00	0.00	0.00	0.01	0.01
Al	0.04	0.05	0.05	0.04	0.04	0.04	0.04	0.04	0.04	0.04	0.04	0.04	0.04	0.04	0.04	0.05	0.04	0.05	0.04	0.05	0.05	0.04	0.04
Cr	0.01	0.01	0.01	0.01	0.01	0.01	0.01	0.01	0.01	0.01	0.01	0.01	0.01	0.01	0.01	0.01	0.01	0.01	0.01	0.01	0.01	0.01	0.01
Fe	0.37	0.37	0.40	0.40	0.40	0.39	0.41	0.47	0.47	0.41	0.41	0.40	0.45	0.56	0.57	0.49	0.45	0.41	0.38	0.42	0.37	0.36	0.36
Mn	0.01	0.01	0.01	0.01	0.01	0.01	0.01	0.01	0.01	0.01	0.01	0.01	0.01	0.01	0.01	0.01	0.01	0.01	0.01	0.01	0.01	0.01	0.01
Ni	0.00	0.00	0.00	0.00	0.00	0.00	0.00	0.00	0.00	0.00	0.00	0.00	0.00	0.00	0.00	0.00	0.00	0.00	0.00	0.00	0.00	0.00	0.00
Mg	1.53	1.53	1.51	1.56	1.52	1.55	1.50	1.44	1.45	1.51	1.52	1.55	1.49	1.40	1.34	1.41	1.52	1.53	1.49	1.51	1.53	1.55	1.55
Ca	0.07	0.05	0.05	0.05	0.05	0.05	0.05	0.05	0.05	0.04	0.05	0.04	0.05	0.05	0.05	0.06	0.05	0.04	0.07	0.06	0.06	0.06	0.06
Na	0.00	0.00	0.00	0.00	0.00	0.00	0.00	0.00	0.00	0.00	0.00	0.00	0.00	0.00	0.00	0.00	0.00	0.00	0.00	0.00	0.00	0.00	0.00
	4.00	3.99	4.00	4.02	4.00	4.01	3.99	4.00	4.01	4.00	4.01	4.01	4.02	4.02	3.99	4.00	4.03	4.01	3.99	4.02	4.00	4.00	4.01
Mg#	0.804	0.807	0.792	0.796	0.792	0.801	0.786	0.753	0.754	0.787	0.787	0.797	0.767	0.715	0.701	0.741	0.772	0.790	0.796	0.783	0.804	0.809	0.811
1 Standard deviation [wt%]																							
SiO2	0.18	0.11	0.25	0.15	0.16	0.36	0.21	0.15	0.18	0.38	0.38	0.29	0.14	0.29	0.16	0.24	0.68	0.63	0.15	0.16	0.22	0.33	0.23
TiO2	0.04	0.03	0.04	0.04	0.05	0.02	0.02	0.04	0.02	0.05	0.04	0.04	0.04	0.06	0.07	0.06	0.01	0.04	0.03	0.06	0.03	0.04	0.01
Al2O3	0.02	0.09	0.08	0.05	0.05	0.04	0.07	0.04	0.02	0.13	0.04	0.03	0.06	0.10	0.04	0.09	0.12	0.16	0.09	0.16	0.17	0.07	0.03
Cr2O3	0.01	0.02	0.03	0.01	0.02	0.01	0.03	0.02	0.00	0.05	0.01	0.02	0.03	0.08	0.02	0.02	0.04	0.05	0.06	0.03	0.05	0.02	0.04
FeO	0.14	0.26	0.19	0.29	0.27	0.16	0.29	0.13	0.07	0.24	0.32	0.21	0.19	0.57	0.12	0.31	0.21	1.23	0.17	0.35	0.21	0.24	0.22
MnO	0.01	0.03	0.01	0.02	0.02	0.02	0.02	0.01	0.03	0.01	0.01	0.01	0.02	0.03	0.03	0.03	0.01	0.04	0.01	0.02	0.02	0.01	0.04
NiO	0.01	0.02	0.02	0.01	0.02	0.02	0.03	0.01	0.02	0.02	0.02	0.02	0.02	0.02	0.01	0.01	0.01	0.04	0.03	0.01	0.02	0.02	0.03
MgO	0.20	0.26	0.29	0.36	0.20	0.14	0.20	0.17	0.13	0.31	0.14	0.10	0.10	0.37	0.21	0.35	0.16	0.49	0.16	0.18	0.28	0.26	0.25
CaO	0.20	0.41	0.36	0.20	0.28	0.19	0.44	0.35	0.31	0.31	0.15	0.14	0.08	0.22	0.23	0.19	0.20	0.39	0.27	0.53	0.43	0.41	0.50
Na2O	0.01	0.01	0.01	0.01	0.01	0.01	0.01	0.01	0.01	0.01	0.01	0.00	0.01	0.01	0.00	0.01	0.01	0.01	0.02	0.01	0.01	0.01	0.02
Mg#	0.001	0.004	0.004	0.005	0.002	0.002	0.003	0.001	0.001	0.004	0.004	0.003	0.003	0.009	0.003	0.006	0.002	0.018	0.002	0.003	0.005	0.002	0.002
n	4	7	10	5	8	9	7	3	5	8	6	4	3	6	3	4	5	8	5	4	11	5	6

Orthopyroxene analyses: KR2 sequence

Sample	1150.15	1155.45	1160.40	1168.55	1174.10	1181.20	1185.90	1187.30 b	1191.20	1191.58 a	1192.10	1193.45	1194.20	1203.75	1219.75	1227.15	1236.20	1241.30	1251.90	1287.85	1295.83	1297.40	1300.90
Rock type	.	.	.	o	.	.	.	-	.	.	.	.	.	.	.	.	.	.	.	.	+	+	.
[wt%]																							
SiO2	55.64	55.16	55.33	53.32	55.59	55.03	54.32	54.58	54.69	54.71	54.95	55.65	55.25	55.31	55.12	54.85	54.71	55.57	54.96	54.08	55.29	54.86	55.31
TiO2	0.17	0.13	0.17	0.27	0.16	0.20	0.22	0.12	0.16	0.18	0.15	0.16	0.15	0.16	0.22	0.22	0.20	0.14	0.25	0.16	0.13	0.16	0.17
Al2O3	1.07	1.20	1.10	0.73	1.06	1.07	0.99	1.09	1.05	0.94	1.05	1.05	1.11	1.06	1.03	1.03	1.03	1.13	0.94	1.16	1.24	1.10	1.03
Cr2O3	0.44	0.50	0.45	0.13	0.45	0.44	0.39	0.43	0.40	0.33	0.44	0.41	0.43	0.36	0.36	0.33	0.38	0.37	0.36	0.46	0.48	0.44	0.51
FeO	11.89	11.28	11.74	19.54	13.15	13.74	13.69	11.68	12.17	14.49	11.99	12.27	12.01	12.76	12.65	12.97	12.74	12.58	12.99	13.56	11.26	11.77	12.16
MnO	0.26	0.25	0.25	0.41	0.30	0.30	0.27	0.24	0.27	0.33	0.29	0.29	0.28	0.28	0.25	0.29	0.26	0.29	0.27	0.29	0.27	0.24	0.24
NiO	0.12	0.12	0.09	0.09	0.12	0.07	0.06	0.12	0.09	0.09	0.07	0.09	0.12	0.08	0.09	0.09	0.08	0.07	0.06	0.08	0.07	0.10	0.09
MgO	28.84	29.64	29.51	23.60	28.22	27.65	28.14	29.57	29.27	27.16	29.25	29.17	28.77	28.87	28.79	28.57	28.57	28.74	28.52	27.68	29.18	28.94	29.22
CaO	1.30	1.57	1.61	1.06	1.59	1.53	1.35	1.34	1.30	1.39	1.57	1.14	1.48	1.75	1.34	1.07	1.28	1.17	1.03	1.72	2.01	1.58	1.22
Na2O	0.01	0.03	0.02	0.02	0.01	0.03	0.02	0.02	0.02	0.01	0.03	0.02	0.01	0.02	0.01	0.01	0.01	0.01	0.01	0.04	0.03	0.03	0.03
Total	99.74	99.87	100.26	99.17	100.64	100.04	99.43	99.21	99.42	99.64	99.79	100.25	99.61	100.64	99.85	99.44	99.26	100.08	99.38	99.23	99.97	99.21	99.99
Cations (based on 6 oxygens)																							
Si	1.98	1.96	1.96	1.98	1.97	1.97	1.96	1.96	1.96	1.98	1.96	1.97	1.97	1.96	1.97	1.97	1.97	1.98	1.97	1.96	1.96	1.97	1.97
Ti	0.00	0.00	0.00	0.01	0.00	0.01	0.01	0.00	0.00	0.00	0.00	0.00	0.00	0.00	0.01	0.01	0.01	0.00	0.01	0.00	0.00	0.00	0.00
Al	0.04	0.05	0.05	0.03	0.04	0.05	0.04	0.05	0.04	0.04	0.04	0.04	0.05	0.04	0.04	0.04	0.04	0.05	0.04	0.05	0.05	0.05	0.04
Cr	0.01	0.01	0.01	0.00	0.01	0.01	0.01	0.01	0.01	0.01	0.01	0.01	0.01	0.01	0.01	0.01	0.01	0.01	0.01	0.01	0.01	0.01	0.01
Fe	0.35	0.34	0.35	0.61	0.39	0.41	0.41	0.35	0.36	0.44	0.36	0.36	0.36	0.38	0.38	0.39	0.38	0.37	0.39	0.41	0.33	0.35	0.36
Mn	0.01	0.01	0.01	0.01	0.01	0.01	0.01	0.01	0.01	0.01	0.01	0.01	0.01	0.01	0.01	0.01	0.01	0.01	0.01	0.01	0.01	0.01	0.01
Ni	0.00	0.00	0.00	0.00	0.00	0.00	0.00	0.00	0.00	0.00	0.00	0.00	0.00	0.00	0.00	0.00	0.00	0.00	0.00	0.00	0.00	0.00	0.00
Mg	1.53	1.57	1.56	1.31	1.49	1.48	1.51	1.58	1.56	1.46	1.56	1.54	1.53	1.53	1.53	1.53	1.53	1.52	1.53	1.49	1.54	1.55	1.55
Ca	0.05	0.06	0.06	0.04	0.06	0.06	0.05	0.05	0.05	0.05	0.06	0.04	0.06	0.07	0.05	0.04	0.05	0.04	0.04	0.07	0.08	0.06	0.05
Na	0.00	0.00	0.00	0.00	0.00	0.00	0.00	0.00	0.00	0.00	0.00	0.00	0.00	0.00	0.00	0.00	0.00	0.00	0.00	0.00	0.00	0.00	0.00
Total	3.99	4.00	4.00	3.99	3.99	3.99	4.01	4.01	4.01	4.00	4.01	3.99	3.99	4.01	4.00	4.00	4.00	3.99	4.00	4.01	4.00	4.00	4.00
Mg#	0.812	0.824	0.818	0.683	0.793	0.782	0.786	0.819	0.811	0.770	0.813	0.809	0.810	0.801	0.802	0.797	0.800	0.803	0.796	0.784	0.822	0.814	0.811
1 Standard deviation [wt%]																							
SiO2	0.63	0.11	0.33	0.13	0.23	0.17	0.24	0.20	0.25	0.08	0.14	0.10	0.13	0.27	0.36	0.14	0.11	0.47	0.07	0.15	0.18	0.15	0.08
TiO2	0.02	0.02	0.01	0.04	0.03	0.05	0.04	0.02	0.01	0.02	0.02	0.01	0.02	0.03	0.02	0.04	0.02	0.05	0.03	0.03	0.02	0.02	0.02
Al2O3	0.03	0.04	0.05	0.05	0.02	0.13	0.06	0.07	0.05	0.05	0.07	0.03	0.06	0.09	0.05	0.02	0.04	0.08	0.04	0.08	0.06	0.12	0.06
Cr2O3	0.02	0.02	0.04	0.04	0.04	0.06	0.03	0.02	0.01	0.03	0.02	0.03	0.02	0.03	0.01	0.01	0.01	0.02	0.02	0.02	0.02	0.04	0.01
FeO	0.50	0.15	0.20	0.43	0.25	0.39	0.24	0.17	0.17	0.33	0.14	0.20	0.33	0.39	0.20	0.19	0.09	0.34	0.09	0.13	0.20	0.18	0.22
MnO	0.02	0.02	0.03	0.03	0.04	0.04	0.02	0.02	0.01	0.01	0.01	0.01	0.02	0.04	0.01	0.01	0.02	0.02	0.02	0.03	0.02	0.02	0.02
NiO	0.01	0.02	0.02	0.02	0.00	0.01	0.02	0.02	0.01	0.01	0.01	0.01	0.02	0.01	0.01	0.02	0.01	0.02	0.02	0.01	0.02	0.03	0.02
MgO	0.54	0.24	0.30	0.29	0.36	0.54	0.16	0.20	0.13	0.20	0.23	0.18	0.29	0.31	0.18	0.08	0.28	0.47	0.25	0.15	0.31	0.22	0.15
CaO	0.38	0.27	0.45	0.04	0.36	0.86	0.32	0.39	0.23	0.35	0.33	0.15	0.43	0.66	0.27	0.12	0.31	0.34	0.10	0.18	0.19	0.28	0.33
Na2O	0.01	0.01	0.01	0.01	0.01	0.03	0.01	0.01	0.01	0.01	0.01	0.01	0.00	0.01	0.01	0.01	0.01	0.01	0.00	0.01	0.01	0.01	0.01
Mg#	0.004	0.002	0.002	0.007	0.002	0.002	0.002	0.002	0.002	0.003	0.001	0.003	0.004	0.003	0.002	0.002	0.001	0.002	0.002	0.002	0.003	0.002	0.003
n	5	7	5	4	4	7	6	6	6	4	7	7	6	5	5	6	4	4	5	4	7	6	6

Orthopyroxene analyses: P1 marker at LK5 sequence							Orthopyroxene analyses: Boulder Bed (Brakspruit)				Orthopyroxene analyses: Merensky Reef (Brakspruit)		
Sample	1488.26 A-Top	1488.26 A-Above	1488.26 A-Below	1488.26 B-Above	1488.26 B-Below	1488.26 B-Base	BBBC Rim	BBBC Base	BBC Mid	BBTC Top	BSIM	BSIMTC Below	BSIMTC Above
Rock-type	.	+	+	+	+	.	.	*	+	+	*	+	+
[wt%]													
SiO2	53.64	54.86	54.70	55.25	55.15	55.00	54.41	54.99	54.60	54.86	54.77	54.85	54.82
TiO2	0.15	0.14	0.14	0.11	0.14	0.15	0.28	0.16	0.19	0.24	0.19	0.25	0.13
Al2O3	0.96	1.13	1.36	1.11	0.98	0.99	1.34	1.43	1.19	1.39	1.30	1.34	1.31
Cr2O3	0.35	0.48	0.45	0.39	0.35	0.28	0.27	0.30	0.47	0.50	0.41	0.43	0.40
FeO	14.19	13.30	13.24	12.91	14.20	15.18	12.75	11.66	12.65	12.79	12.17	12.73	11.96
MnO	0.28	0.28	0.27	0.29	0.32	0.35	0.27	0.26	0.26	0.29	0.25	0.28	0.28
NiO	0.08	0.07	0.06	0.07	0.06	0.06	0.07	0.05	0.11	0.07	0.04	0.11	0.11
MgO	27.42	29.30	29.03	28.66	27.82	26.80	28.78	29.63	28.71	29.01	29.29	28.63	29.64
CaO	1.15	0.96	0.94	0.95	0.86	1.14	0.74	0.83	1.01	1.25	1.57	1.10	1.00
Na2O	0.00	0.02	0.01	0.01	0.01	0.01	0.02	0.02	0.02	0.06	0.01	0.02	0.02
Total	98.23	100.54	100.19	99.74	99.88	99.97	98.93	99.33	99.21	100.43	100.00	99.74	99.67
Cations (based on 6 oxygens)													
Si	1.96	1.95	1.95	1.97	1.98	1.98	1.96	1.96	1.96	1.95	1.95	1.96	1.96
Ti	0.00	0.00	0.00	0.00	0.00	0.00	0.01	0.00	0.01	0.01	0.01	0.01	0.00
Al	0.04	0.05	0.06	0.05	0.04	0.04	0.06	0.06	0.05	0.06	0.05	0.06	0.05
Cr	0.01	0.01	0.01	0.01	0.01	0.01	0.01	0.01	0.01	0.01	0.01	0.01	0.01
Fe	0.43	0.40	0.39	0.39	0.43	0.46	0.38	0.35	0.38	0.38	0.36	0.38	0.36
Mn	0.01	0.01	0.01	0.01	0.01	0.01	0.01	0.01	0.01	0.01	0.01	0.01	0.01
Ni	0.00	0.00	0.00	0.00	0.00	0.00	0.00	0.00	0.00	0.00	0.00	0.00	0.00
Mg	1.50	1.55	1.54	1.53	1.49	1.44	1.54	1.58	1.54	1.54	1.56	1.53	1.58
Ca	0.05	0.04	0.04	0.04	0.03	0.04	0.03	0.03	0.04	0.05	0.06	0.04	0.04
Na	0.00	0.00	0.00	0.00	0.00	0.00	0.00	0.00	0.00	0.00	0.00	0.00	0.00
Total	4.01	4.01	4.01	3.99	3.99	3.99	4.00	4.00	4.00	4.01	4.01	4.00	4.01
Mg#	0.775	0.797	0.796	0.798	0.777	0.759	0.801	0.819	0.802	0.802	0.811	0.800	0.815
1 Standard deviation [wt%]													
SiO2		0.19	0.21	0.43	0.02		0.39	0.42	0.13	0.56	0.24	0.05	0.44
TiO2		0.01	0.01	0.00	0.01		0.02	0.06	0.03	0.09	0.01	0.02	0.02
Al2O3		0.01	0.17	0.21	0.05		0.10	0.29	0.16	0.30	0.15	0.01	0.31
Cr2O3		0.01	0.05	0.05	0.03		0.01	0.07	0.04	0.07	0.06	0.02	0.12
FeO		0.21	0.19	0.39	0.28		0.56	0.12	0.31	0.64	0.23	0.26	0.29
MnO		0.01	0.03	0.04	0.01		0.03	0.03	0.02	0.01	0.00	0.00	0.04
NiO		0.03	0.02	0.03	0.01		0.01	0.02	0.02	0.01	0.02	0.02	0.02
MgO		0.31	0.33	0.37	0.14		0.40	0.32	0.16	0.44	0.33	0.10	0.29
CaO		0.12	0.13	0.21	0.05		0.02	0.11	0.20	0.36	0.38	0.28	0.30
Na2O		0.00	0.01	0.01	0.01		0.01	0.01	0.01	0.02	0.01	0.00	0.01
Mg#		0.008	0.006	0.007	0.004		0.009	0.003	0.004	0.010	0.004	0.004	0.004
n	1	3	6	2	3	1	2	4	6	5	4	2	4

Olivine analyses: AE sequence

Sample	27	39.4	39.5	39.6	40.1	40.2	42	48	55
Rock type	*	*	*	*	x	*	*	*	*
wt%									
SiO2	39.55	40.75	39.85	39.90	40.01	40.15	40.13	40.11	39.90
FeO	18.52	14.06	16.91	17.92	15.68	16.95	16.87	16.57	18.69
MnO	0.22	0.19	0.22	0.26	0.20	0.21	0.22	0.19	0.23
NiO	0.32	0.33	0.32	0.29	0.31	0.32	0.34	0.35	0.35
MgO	41.40	45.60	43.37	41.62	43.54	43.23	42.38	43.44	41.16
CaO	0.02	0.02	0.01	0.02	0.01	0.02	0.02	0.01	0.02
Total	100.06	101.03	100.69	100.00	99.96	100.88	99.97	100.68	100.38
Cations (based on 4 oxygens)									
Si	1.01	1.01	1.00	1.01	1.01	1.01	1.02	1.01	1.01
Fe	0.40	0.29	0.36	0.38	0.33	0.36	0.36	0.35	0.40
Mn	0.00	0.00	0.00	0.01	0.00	0.00	0.00	0.00	0.00
Ni	0.01	0.01	0.01	0.01	0.01	0.01	0.01	0.01	0.01
Mg	1.57	1.68	1.63	1.58	1.64	1.62	1.60	1.63	1.56
Ca	0.00	0.00	0.00	0.00	0.00	0.00	0.00	0.00	0.00
Total	2.99	2.99	3.00	2.99	2.99	2.99	2.98	2.99	2.99
Mg#	0.799	0.853	0.821	0.805	0.832	0.820	0.817	0.824	0.797

Olivine analyses: UA sequence

Sample	641.00	642.50	658.00	659.30	288.40 a	288.40 b	288.90 a	288.90 b	288.95
Rock type	*	*	*	*	*	x	x	*	x
wt%									
SiO2	38.72	39.32	38.51	38.82	39.13	38.81	39.16	39.14	39.25
FeO	18.68	18.22	18.47	17.92	17.76	18.07	18.03	18.50	16.75
MnO	0.21	0.21	0.22	0.23	0.22	0.21	0.23	0.21	0.21
NiO	0.44	0.32	0.31	0.33	0.41	0.38	0.28	0.34	0.37
MgO	41.39	41.86	42.63	41.92	42.25	42.65	42.92	42.44	44.05
CaO	0.01	0.01	0.00	0.00	0.01	0.02	0.01	0.01	0.02
Total	99.46	99.94	100.15	99.23	99.77	100.14	100.63	100.63	100.65
Cations (based on 4 oxygens)									
Si	1.00	1.00	0.98	1.00	1.00	0.99	0.99	0.99	0.99
Fe	0.40	0.39	0.39	0.39	0.38	0.39	0.38	0.39	0.35
Mn	0.00	0.00	0.00	0.00	0.00	0.00	0.00	0.00	0.00
Ni	0.01	0.01	0.01	0.01	0.01	0.01	0.01	0.01	0.01
Mg	1.59	1.59	1.62	1.61	1.61	1.62	1.62	1.61	1.65
Ca	0.00	0.00	0.00	0.00	0.00	0.00	0.00	0.00	0.00
Total	3.00	3.00	3.02	3.00	3.00	3.01	3.01	3.01	3.01
Mg#	0.798	0.804	0.804	0.807	0.809	0.808	0.809	0.803	0.824
1 Standard deviation [wt%]									
SiO2	0.13	0.08	0.16	0.29	0.16	0.35	0.15	0.37	0.37
FeO	0.43	0.43	0.17	0.16	0.40	0.34	0.23	0.15	1.85
MnO	0.02	0.01	0.01	0.00	0.02	0,01	0.01	0.02	0.04
NiO	0.04	0.01	0.01	0.03	0.02	0.01	0.02	0.03	0.05
MgO	0.19	0.58	0.17	0.37	0.29	0.12	0.25	0.35	1.60
CaO	0.01	0.00	0.00	0.00	0.00	0.01	0.01	0.01	0.01
Mg#	0.004	0.005	0.002	0.001	0.003	0.004			0.021
n	4	4	4	4	6	6	8	7	3

Olivine analyses: EK22 sequence

Sample	291.48	295.70	296.90	297.10	299.10	299.80	299.95	306.50 a	313.60
Rock type	*	*	*	*	*	*	*	*	*
wt%									
SiO2	38.98	38.63	38.49	37.96	38.58	38.07	38.90	38.82	38.63
FeO	17.45	18.14	18.96	18.75	19.05	19.65	19.64	17.44	20.09
MnO	0.19	0.24	0.23	0.23	0.22	0.22	0.22	0.19	0.22
NiO	0.34	0.30	0.36	0.30	0.33	0.38	0.42	0.65	0.51
MgO	43.74	42.78	42.63	42.77	41.60	41.28	41.35	43.58	40.93
CaO	0.01	0.00	0.03	0.03	0.00	0.01	0.01	0.03	0.01
Total	100.71	100.09	100.72	100.04	99.78	99.62	100.53	100.70	100.39
Cations (based on 4 oxygens)									
Si	0.99	0.99	0.98	0.97	0.99	0.98	0.99	0.98	0.99
Fe	0.37	0.39	0.40	0.40	0.41	0.43	0.42	0.37	0.43
Mn	0.00	0.01	0.01	0.01	0.00	0.00	0.00	0.00	0.00
Ni	0.01	0.01	0.01	0.01	0.01	0.01	0.01	0.01	0.01
Mg	1.65	1.63	1.62	1.64	1.59	1.59	1.58	1.65	1.57
Ca	0.00	0.00	0.00	0.00	0.00	0.00	0.00	0.00	0.00
Total	3.01	3.01	3.02	3.03	3.01	3.02	3.01	3.02	3.01
Mg#	0.824	0.817	0.808	0.800	0.803	0.796	0.789	0.790	0.817	0.784
1 Standard deviation [wt%]									
SiO2	0.25	0.29	0.11	0.18	0.07	0.27	0.16	0.19	0.19
FeO	0.59	0.20	0.12	0.13	0.11	0.21	0.16	0.14	0.41
MnO	0.02	0.01	0.01	0.02	0.01	0.01	0.01	0.01	0.01
NiO	0.02	0.02	0.02	0.03	0.02	0.03	0.02	0.03	0.06
MgO	0.31	0.08	0.09	0.12	0.26	0.12	0.20	0.09	0.35
CaO	0.01	0.00	0.00	0.01	0.00	0.01	0.01	0.00	0.01
Mg#	0.006	0.002	0.001		0.001	0.002	0.002	0.001	0.005
n	7	5	6	7	6	6	6	5	6

Olivine analyses: IM sequence									Olivine analyses: IN sequence						Olivine analyses: Additional samples								
Sample	788.80	796.25	798.00	810.00	818.00	819.85	826.00	841.67	837.86	844.10	850.73	858.55	863.12	866.40	Bou2 boulder	BBBC boulder	Bou boulder	BSIM Mer.Reef	UG2-Peg	TF 895	LK7 1581.88 b	LK7 1585.38	H3 1089.65
Rock type	x	x	x	x	x	x	*	o	x	x	x	x	x	x	*	*	*	*	*	*	*	*	x
wt%																							
SiO2	38.62	38.64	39.32	38.36	39.00	37.92	39.47	37.72	38.86	38.12	39.23	38.46	38.57	38.51	38.94	39.73	38.65	38.14	38.82	38.96	38.85	38.71	39.26
FeO	18.48	19.15	17.18	19.72	18.57	21.80	19.27	26.31	19.01	18.99	18.91	19.02	18.05	18.33	18.70	19.78	19.35	21.42	18.90	18.83	21.40	20.75	17.99
MnO	0.19	0.22	0.20	0.21	0.20	0.23	0.23	0.24	0.20	0.21	0.19	0.22	0.20	0.22	0.23	0.25	0.23	0.25	0.21	0.15	0.22	0.17	0.20
NiO	0.34	0.33	0.29	0.34	0.30	0.31	0.37	0.40	0.32	0.37	0.38	0.37	0.38	0.36	0.20	0.24	0.25	0.28	0.47	0.34	0.34	0.40	0.37
MgO	42.61	41.41	42.99	41.00	42.36	39.99	40.96	36.07	42.13	41.75	41.97	42.85	42.72	42.10	41.49	40.49	41.84	40.47	41.24	41.51	38.93	40.60	42.87
CaO	0.01	0.00	0.00	0.01	0.02	0.00	0.00	0.00	0.01	0.03	0.01	0.01	0.02	0.00	0.01	0.01	0.01	0.02	0.01	0.01	0.00	0.01	0.01
Total	100.25	99.75	99.99	99.64	100.45	100.26	100.29	100.74	100.53	99.47	100.70	100.93	99.94	99.52	99.57	100.50	100.33	100.57	99.65	99.79	99.74	100.63	100.70
Cations (based on 4 oxygens)																							
Si	0.99	0.99	1.00	0.99	0.99	0.98	1.01	0.99	0.99	0.98	1.00	0.98	0.99	0.99	1.00	1.01	0.99	0.98	1.00	1.00	1.01	0.99	0.99
Fe	0.39	0.41	0.36	0.43	0.40	0.47	0.41	0.58	0.41	0.41	0.40	0.40	0.39	0.39	0.40	0.42	0.41	0.46	0.41	0.40	0.46	0.45	0.38
Mn	0.00	0.00	0.00	0.00	0.00	0.01	0.00	0.01	0.00	0.00	0.00	0.00	0.00	0.00	0.00	0.01	0.00	0.01	0.00	0.00	0.00	0.00	0.00
Ni	0.01	0.01	0.01	0.01	0.01	0.01	0.01	0.01	0.01	0.01	0.01	0.01	0.01	0.01	0.00	0.01	0.01	0.01	0.01	0.01	0.01	0.01	0.01
Mg	1.62	1.59	1.63	1.58	1.61	1.55	1.56	1.42	1.60	1.61	1.59	1.63	1.63	1.61	1.59	1.54	1.60	1.56	1.58	1.59	1.51	1.55	1.62
Ca	0.00	0.00	0.00	0.00	0.00	0.00	0.00	0.00	0.00	0.00	0.00	0.00	0.00	0.00	0.00	0.00	0.00	0.00	0.00	0.00	0.00	0.00	0.00
Total	3.01	3.01	3.00	3.01	3.01	3.02	2.99	3.01	3.01	3.02	3.00	3.02	3.01	3.01	3.00	2.99	3.01	3.02	3.00	3.00	2.99	3.01	3.01
Mg#	0.804	0.794	0.817	0.787	0.803	0.766	0.791	0.710	0.798	0.797	0.798	0.801	0.808	0.804	0.798	0.785	0.794	0.771	0.795	0.797	0.764	0.777	0.809
1 Standard deviation [wt%]																							
SiO2	0.20	0.23	0.13	0.21	0.08	0.14	0.23	0.11	0.11	0.10	0.05	0.11	0.14	0.13	0.14	0.21	0.20	0.04	0.04	0.16	0.15	0.11	0.22
FeO	0.28	0.25	0.46	0.27	0.49	0.52	0.09	0.21	0.29	0.12	0.30	0.03	0.34	0.25	0.19	0.24	0.18	0.25	0.09	0.32	0.23	0.19	0.41
MnO	0.01	0.02	0.01	0.01	0.01	0.01	0.00	0.00	0.01	0.01	0.03	0.01	0.01	0.01	0.01	0.01	0.01	0.01	0.01	0.01	0.01	0.01	0.01
NiO	0.03	0.04	0.03	0.02	0.01	0.03	0.01	0.02	0.04	0.04	0.01	0.01	0.03	0.03	0.03	0.01	0.01	0.01	0.02	0.03	0.02	0.02	0.03
MgO	0.20	0.34	0.17	0.36	0.09	0.43	0.21	0.14	0.25	0.14	0.20	0.07	0.35	0.28	0.19	0.09	0.23	0.16	0.48	0.28	0.19	0.15	0.10
CaO	0.01	0.00	0.00	0.01	0.01	0.01	0.00	0.01	0.00	0.00	0.01	0.01	0.01	0.00	0.00	0.00	0.01	0.00	0.01	0.01	0.00	0.00	0.01
Mg#	0.003	0.002	0.004	0.004	0.004	0.006	0.002	0.004	0.002	0.001	0.003	0.000	0.003	0.003	0.002	0.002	0.002	0.003	0.002	0.002	0.002	0.002	0.003
n	5	5	4	6	3	4	2	3	4	4	6	4	7	6	6	3	5	3	4	3	6	5	3

Chromite analyses: EK22 sequence

Sample	284.25	288.40 a	288.40 b	288.95	291.48	299.95	306.30	306.50 a	306.50 b	307.66	313.00	313.60 b
Rock type	#	*	.	.	*	*	#	*	#	+	+	*
[wt%]												
TiO2	0.68	1.59	2.21	2.28	0.74	2.74	1.15	0.87	1.87	0.95	2.03	1.68
Al2O3	17.28	15.38	10.69	9.03	10.94	5.86	13.58	12.81	10.77	8.22	10.64	12.12
Cr2O3	41.61	25.15	25.72	31.14	24.00	24.20	43.25	37.82	39.87	46.09	36.31	34.46
FeO(P)	29.33	49.46	53.90	50.55	56.83	60.58	32.69	41.03	40.06	39.00	42.68	45.06
FeO(C)	20.02	27.15	28.78	29.48	27.06	31.10	23.06	26.49	26.16	28.05	25.98	27.36
Fe2O3	10.34	24.79	27.91	23.41	33.09	32.75	10.70	16.16	15.46	12.17	18.56	19.67
MnO	0.31	0.37	0.41	0.46	0.34	0.39	0.33	0.35	0.35	0.35	0.33	0.30
NiO	0.09	0.37	0.31	0.32	0.34	0.40	0.27	0.32	0.35	0.16	0.21	0.33
MgO	9.70	4.97	3.78	3.07	4.23	1.88	7.42	4.82	5.56	3.48	5.69	4.89
Total(P)	99.00	97.29	97.02	96.84	97.43	96.04	98.69	98.02	98.83	98.25	97.89	98.85
Total(C)	100.03	99.77	99.81	99.19	100.74	99.33	99.76	99.64	100.38	99.47	99.75	100.83
Cations (based on 32 oxygens)												
Ti	0.13	0.32	0.47	0.49	0.15	0.60	0.23	0.18	0.38	0.20	0.42	0.34
Al	5.25	4.90	3.51	3.02	3.54	2.01	4.27	4.11	3.46	2.72	3.44	3.88
Cr	8.48	5.39	5.67	6.99	5.23	5.59	9.12	8.21	8.60	10.28	7.88	7.41
Fe2	4.32	6.17	6.73	7.02	6.27	7.60	5.14	6.07	5.97	6.62	5.97	6.22
Fe3	2.01	5.07	5.89	5.02	6.93	7.20	2.15	3.32	3.17	2.60	3.84	4.02
Mn	0.07	0.09	0.10	0.11	0.08	0.10	0.08	0.08	0.08	0.08	0.08	0.07
Ni	0.02	0.08	0.07	0.07	0.08	0.09	0.06	0.07	0.08	0.04	0.05	0.07
Mg	3.73	1.99	1.57	1.28	1.73	0.81	2.95	1.96	2.26	1.46	2.33	1.98
Mg#	0.463	0.244	0.189	0.153	0.216	0.097	0.365	0.244	0.275	0.181	0.281	0.242
Cr/Fe	1.250	0.452	0.439	0.548	0.405	0.361	1.165	0.816	0.877	1.051	0.751	0.674
Cr/Al	1.626	1.121	1.617	2.318	1.525	2.820	2.138	2.139	2.485	3.942	2.292	1.909
1 Standard Deviation [wt%]												
TiO2	0.14	0.13	0.53	0.58	0.15	0.62	0.10	0.30	0.24	0.40	0.23	0.44
Al2O3	1.31	2.41	1.78	0.48	3.31	1.06	0.27	2.76	0.36	1.93	0.50	0.47
Cr2O3	0.81	0.98	4.69	1.56	7.45	4.80	0.28	4.11	1.07	1.93	1.34	0.78
FeO(P)	1.02	4.16	6.85	3.83	11.02	5.25	0.46	2.07	0.96	3.17	1.63	0.75
FeO(C)	0.45	2.00	1.86	2.52	1.62	1.41	0.13	1.50	0.23	0.45	0.52	0.39
Fe2O3	0.80	2.66	5.62	1.49	10.82	5.21	0.40	2.61	0.90	3.03	1.52	0.42
MnO	0.03	0.02	0.05	0.01	0.04	0.02	0.04	0.04	0.03	0.01	0.02	0.03
NiO	0.02	0.04	0.06	0.03	0.10	0.05	0.03	0.04	0.05	0.02	0.03	0.04
MgO	0.38	1.53	1.26	2.10	1.49	0.70	0.06	0.25	0.09	0.37	0.40	0.03
Mg#	0.015	0.072	0.060	0.101	0.071	0.036	0.003	0.059	0.005	0.018	0.018	0.004
Cr/Fe	0.040	0.051	0.151	0.070	0.182	0.110	0.019	0.110	0.045	0.129	0.054	0.027
Cr/Al	0.145	0.158	0.169	0.134	0.338	0.517	0.044	0.746	0.046	0.768	0.080	0.061
n	30	5	6	5	6	5	7	8	6	4	8	6

Chromite analyses: IN sequence

Sample	817.50	817.68	863.12	866.40	866.67 Top	866.67 Seam	875.75
Rock type	.	.	.	x	+	#	+
[wt%]							
TiO2	0.71	0.91	1.01	0.82	1.21	1.16	1.20
Al2O3	5.45	8.57	12.36	17.20	14.63	15.04	9.03
Cr2O3	37.66	37.49	31.08	33.41	37.02	39.65	45.59
FeO(P)	50.01	48.07	49.77	40.95	39.77	34.13	39.94
FeO(C)	30.27	29.19	30.38	26.09	27.77	24.08	30.19
Fe2O3	21.94	20.99	21.55	16.51	13.33	11.17	10.84
MnO	0.67	0.44	0.51	0.35	0.39	0.34	0.39
NiO	0.11	0.25	0.27	0.14	0.19	0.16	0.09
MgO	0.97	2.79	2.11	5.74	4.29	6.66	2.40
Total(P)	95.57	98.52	97.11	98.60	97.49	97.14	98.63
Total(C)	97.77	100.63	99.27	100.26	98.83	98.26	99.72
Cations (based on 32 oxygens)							
Ti	0.16	0.19	0.21	0.16	0.25	0.24	0.25
Al	1.90	2.84	4.10	5.37	4.73	4.79	2.99
Cr	8.86	8.34	6.92	7.01	8.02	8.47	10.20
Fe2	7.53	6.87	7.16	5.79	6.37	5.44	7.14
Fe3	4.92	4.44	4.55	3.29	2.75	2.27	2.31
Mn	0.17	0.11	0.12	0.08	0.09	0.08	0.09
Ni	0.03	0.06	0.06	0.03	0.04	0.04	0.02
Mg	0.43	1.17	0.88	2.27	1.75	2.68	1.00
Mg#	0.054	0.145	0.109	0.282	0.216	0.330	0.123
Cr/Fe	0.671	0.688	0.552	0.720	0.819	1.026	1.006
Cr/Al	5.128	2.950	1.687	1.327	1.700	1.769	3.647
1 Standard deviation [wt%]							
TiO2	0.18	0.37	0.74	0.39	0.16	0.09	0.41
Al2O3	1.73	0.42	0.13	1.82	0.52	0.39	2.67
Cr2O3	3.63	3.13	1.44	1.86	0.21	0.65	1.66
FeO(P)	3.57	1.26	2.54	1.46	0.23	1.81	1.76
FeO(C)	0.34	1.19	0.46	0.82	0.32	1.23	1.29
Fe2O3	3.82	2.60	3.34	0.97	0.13	0.66	0.83
MnO	0.09	0.11	0.05	0.02	0.02	0.04	0.05
NiO	0.01	0.07	0.01	0.02	0.06	0.02	0.05
MgO	0.26	0.97	0.11	0.46	0.27	0.89	1.19
Mg#	0.014	0.049	0.002	0.022	0.012	0.042	0.058
Cr/Fe	0.107	0.075	0.054	0.056	0.003	0.064	0.028
Cr/Al	1.757	0.366	0.060	0.233	0.070	0.042	0.887
n	3	3	2	7	4	6	4

Chromite analyses: IM sequence

Sample	787.90	788.80	790.64	793.22 b	794.53	796.25	798.00	804.40	810.10	818.00	819.30	819.85	823.50	826.48	836.00 b	839.00	843.61	848.52	851.90	853.95	856.00	866.20 Seam	866.20
Rock type	.	.	.	.	o	.	x	.	.	.	.	x	o	.	.	.	o	o	+	+	.	#	o
[wt%]																							
TiO2	0.82	0.88	1.62	0.87	1.06	1.96	2.01	0.71	1.41	0.64	0.99	2.17	3.05	1.43	1.77	1.65	3.31	23.17	1.45	1.26	0.75	3.13	1.94
Al2O3	7.89	6.91	8.77	4.02	2.91	14.23	14.69	17.95	16.45	24.83	13.89	12.53	5.06	3.37	6.39	9.39	4.14	1.60	9.19	9.93	10.71	6.85	5.50
Cr2O3	42.50	41.07	39.19	26.33	20.73	30.00	31.28	40.39	40.59	35.01	44.25	33.89	26.78	20.15	36.35	41.29	20.74	4.77	43.78	45.01	48.15	35.76	31.16
FeO(P)	43.73	45.42	45.44	62.45	68.21	47.19	43.64	34.33	34.35	30.71	35.38	46.69	61.01	69.52	51.63	43.06	67.55	66.38	40.20	38.02	34.03	49.62	57.26
FeO(C)	29.46	29.31	30.77	30.00	31.15	28.52	26.30	26.28	26.53	23.91	28.49	31.35	33.52	32.03	32.08	31.14	33.68	51.39	30.36	29.30	27.82	32.07	32.25
Fe2O3	15.86	17.91	16.31	36.07	41.19	20.74	19.26	8.95	8.69	7.55	7.66	17.05	30.55	41.67	21.72	13.24	37.64	16.66	10.93	9.68	6.90	19.51	27.80
MnO	0.45	0.42	0.42	0.44	0.57	0.36	0.31	0.34	0.31	0.30	0.33	0.37	0.59	0.68	0.43	0.41	0.45	1.03	0.41	0.37	0.34	0.50	0.62
NiO	0.10	0.16	0.15	0.34	0.21	0.34	0.23	0.12	0.17	0.17	0.08	0.12	0.13	0.02	0.10	0.12	0.25	0.01	0.08	0.09	0.03	0.11	0.06
MgO	2.38	2.27	2.03	1.30	0.21	4.40	5.94	5.78	5.72	7.98	3.94	2.57	0.67	0.27	1.14	1.90	0.69	0.06	2.16	2.87	3.68	1.95	0.93
Total(P)	97.87	97.13	97.63	95.76	93.89	98.46	98.11	99.61	99.00	99.64	98.87	98.34	97.29	95.44	97.82	97.82	97.12	97.03	97.27	97.55	97.68	97.92	97.46
Total(C)	99.46	98.92	99.26	99.38	98.02	100.54	100.04	100.51	99.87	100.40	99.64	100.05	100.35	99.62	100.00	99.15	100.89	98.69	98.37	98.52	98.37	99.87	100.25
Cations (based on 32 oxygens)																							
Ti	0.18	0.19	0.35	0.19	0.24	0.40	0.41	0.14	0.28	0.12	0.20	0.46	0.67	0.32	0.39	0.35	0.73	5.28	0.31	0.27	0.16	0.68	0.42
Al	2.65	2.35	2.95	1.41	1.05	4.54	4.65	5.55	5.16	7.35	4.47	4.06	1.73	1.19	2.18	3.15	1.43	0.57	3.10	3.32	3.54	2.32	1.89
Cr	9.59	9.37	8.84	6.17	5.01	6.43	6.64	8.40	8.54	6.98	9.55	7.43	6.19	4.77	8.32	9.30	4.81	1.14	9.92	10.08	10.69	8.12	7.17
Fe2	7.03	7.08	7.35	7.43	7.95	6.47	5.91	5.78	5.91	5.04	6.50	7.30	8.21	8.02	7.77	7.42	8.26	12.99	7.27	6.94	6.53	7.70	7.85
Fe3	3.41	3.90	3.51	8.04	9.45	4.23	3.89	1.77	1.74	1.43	1.57	3.59	6.73	9.40	4.73	2.84	8.30	3.73	2.36	2.06	1.46	4.21	6.09
Mn	0.11	0.10	0.10	0.11	0.15	0.08	0.07	0.08	0.07	0.06	0.08	0.09	0.15	0.17	0.11	0.10	0.11	0.26	0.10	0.09	0.08	0.12	0.15
Ni	0.02	0.04	0.03	0.08	0.05	0.07	0.06	0.02	0.04	0.04	0.02	0.03	0.03	0.01	0.02	0.03	0.06	0.00	0.02	0.02	0.01	0.02	0.01
Mg	1.01	0.97	0.87	0.57	0.10	1.78	2.38	2.26	2.27	2.98	1.60	1.05	0.29	0.12	0.49	0.80	0.30	0.03	0.92	1.21	1.54	0.83	0.40
Mg#	0.126	0.121	0.105	0.072	0.012	0.215	0.287	0.281	0.278	0.372	0.198	0.125	0.034	0.015	0.059	0.098	0.035	0.002	0.112	0.149	0.191	0.098	0.049
Cr/Fe	0.856	0.796	0.759	0.371	0.268	0.560	0.631	1.036	1.040	1.004	1.101	0.639	0.386	0.255	0.620	0.844	0.270	0.063	0.959	1.042	1.245	0.634	0.479
Cr/Al	3.614	3.992	3.003	4.389	4.778	1.414	1.428	1.563	1.657	0.965	2.137	1.831	3.571	4.022	3.813	2.950	3.359	1.990	3.199	3.041	3.020	3.501	3.805
1 Standard deviation [wt%]																							
TiO2	0.33	0.25	0.76	0.22	0.69	0.92	0.01	0.50	0.51	0.02	0.23	1.38	2.33	0.65	0.31	0.61		7.29	0.22	0.17	0.04	0.26	0.59
Al2O3	0.74	1.09	2.03	0.58	1.38	0.94	0.18	2.74	1.55	2.47	0.26	4.70	2.02	1.05	0.66	1.08		0.24	1.02	0.22	1.06	0.53	1.14
Cr2O3	3.27	3.51	3.08	2.46	9.71	1.33	0.10	2.85	0.46	2.13	0.71	3.62	2.77	2.99	1.03	1.12		0.02	0.44	1.12	0.22	0.44	1.76
FeO(P)	3.44	4.05	4.45	2.96	12.29	3.01	0.11	0.51	0.94	1.45	0.32	7.82	5.23	4.98	0.85	0.96		8.31	0.16	0.17	0.12	0.72	2.57
FeO(C)	0.98	1.23	0.64	0.07	0.24	1.45	0.05	0.65	0.45	1.28	0.42	2.46	2.31	0.50	0.39	0.70		6.01	0.24	0.36	0.30	0.43	0.59
Fe2O3	2.87	3.39	5.09	3.21	13.92	2.01	0.17	0.76	0.55	0.62	0.20	6.00	6.24	5.81	1.00	1.42		15.92	0.09	0.59	0.46	0.49	2.20
MnO	0.05	0.06	0.09	0.02	0.02	0.05	0.01	0.03	0.03	0.05	0.02	0.07	0.19	0.15	0.08	0.09		0.13	0.04	0.03	0.03	0.03	0.12
NiO	0.01	0.05	0.08	0.02	0.06	0.02	0.00	0.02	0.01	0.02	0.06	0.04	0.05	0.02	0.03	0.05		0.01	0.00	0.00	0.01	0.02	0.00
MgO	0.69	0.99	0.61	0.12	0.19	0.98	0.03	0.72	0.11	1.15	0.36	1.27	0.72	0.18	0.53	0.78		0.01	0.08	0.33	0.13	0.17	0.16
Mg#	0.035	0.052	0.030	0.006	0.011	0.046	0.001	0.031	0.007	0.048	0.017	0.063	0.037	0.010	0.027	0.039		0.001	0.004	0.016	0.004	0.009	0.009
Cr/Fe	0.128	0.135	0.122	0.052	0.179	0.058	0.003	0.083	0.026	0.036	0.014	0.177	0.076	0.054	0.018	0.040		0.008	0.014	0.030	0.001	0.005	0.049
Cr/Al	0.458	0.745	0.518	0.229	0.026	0.107	0.022	0.351	0.183	0.190	0.073	0.480	1.107	0.981	0.442	0.279		0.291	0.394	0.142	0.315	0.324	0.596
n	3	3	2	3	3	4	5	3	3	3	3	5	3	3	3	3	2	2	5	6	4	6	3

Chromite analyses: LK7 sequence

Sample	1424.28 a	1578.43 c-Seam	1578.43 c-Base	1578.68 b-Top	1578.68 b-Seam	1578.68 b-Base	1579.20	1581.88 b	1582.70 a	1583.00 b	1583.25	1584.25 Top	1584.25 Base	1585.38	1585.85
Rock type	#	#	.	.	#	.	+	+	+	#	+	+	#	#	*
[wt%]															
TiO2	2.12	3.88	2.39	3.65	3.93	3.04	1.20	1.33	1.79	1.06	1.10	1.98	1.52	0.85	1.39
Al2O3	10.51	12.57	10.51	8.70	11.64	8.64	8.18	16.67	9.53	15.11	13.96	10.97	13.69	17.49	15.77
Cr2O3	38.92	39.87	44.16	38.67	36.89	40.69	47.46	36.98	44.76	43.30	43.17	41.98	44.15	42.81	31.89
FeO(P)	40.93	37.25	36.95	44.14	41.19	42.50	38.12	35.74	37.56	30.47	32.35	37.78	31.01	27.60	42.70
FeO(C)	28.00	29.90	28.82	32.79	30.27	31.51	30.48	25.28	29.26	23.17	24.19	27.53	23.21	20.61	26.86
Fe2O3	14.37	8.17	9.03	12.62	12.13	12.21	8.50	11.63	9.22	8.11	9.06	11.40	8.67	7.77	17.60
MnO	0.35	0.34	0.39	0.37	0.32	0.42	0.52	0.33	0.42	0.36	0.37	0.37	0.31	0.29	0.30
NiO	0.09	0.10	0.09	0.11	0.08	0.15	0.09	0.18	0.15	0.12	0.13	0.16	0.11	0.13	0.22
MgO	4.29	4.50	4.12	1.89	4.21	2.36	1.73	6.22	3.04	7.31	6.51	4.61	7.59	9.29	5.18
Total(P)	97.21	98.52	98.60	97.53	98.25	97.80	97.31	97.45	97.23	97.73	97.59	97.85	98.37	98.47	97.44
Total(C)	98.65	99.34	99.50	98.80	99.47	99.02	98.16	98.61	98.15	98.54	98.50	98.99	99.24	99.25	99.20
Cations (based on 32 oxygens)															
Ti	0.45	0.80	0.50	0.79	0.82	0.65	0.26	0.27	0.38	0.21	0.22	0.41	0.31	0.17	0.28
Al	3.46	4.06	3.43	2.94	3.79	2.90	2.79	5.27	3.19	4.77	4.46	3.59	4.31	5.35	5.02
Cr	8.61	8.65	9.68	8.77	8.06	9.18	10.84	7.84	10.07	9.17	9.25	9.21	9.33	8.79	6.82
Fe2+	6.55	6.86	6.69	7.86	6.99	7.52	7.37	5.67	6.97	5.19	5.48	6.39	5.19	4.48	6.08
Fe3+	3.03	1.69	1.89	2.72	2.52	2.62	1.85	2.35	1.98	1.64	1.85	2.38	1.74	1.52	3.59
Mn	0.08	0.08	0.09	0.09	0.08	0.10	0.13	0.07	0.10	0.08	0.08	0.09	0.07	0.06	0.07
Ni	0.02	0.02	0.02	0.03	0.02	0.03	0.02	0.04	0.03	0.03	0.03	0.04	0.02	0.03	0.05
Mg	1.79	1.84	1.70	0.81	1.73	1.00	0.75	2.49	1.28	2.92	2.63	1.91	3.02	3.60	2.08
Mg#	0.215	0.212	0.203	0.093	0.198	0.117	0.092	0.305	0.156	0.360	0.324	0.230	0.368	0.445	0.255
Cr/Fe	0.838	0.943	1.053	0.771	0.789	0.846	1.096	0.912	1.053	1.251	1.175	0.978	1.254	1.366	0.658
Cr/Al	2.492	2.127	2.823	2.992	2.128	3.228	3.905	1.489	3.176	1.922	2.075	2.570	2.170	1.642	1.368
1 Standard deviation [wt%]															
TiO2	1.29	2.38	0.21	0.77	0.93	0.68	0.12	0.10	0.26	0.06	0.13	0.32	0.08	0.03	0.16
Al2O3	0.58	0.22	0.41	0.53	0.32	1.34	0.45	0.52	0.90	0.29	0.09	0.34	0.58	0.13	1.28
Cr2O3	0.56	0.67	0.50	0.21	0.30	1.82	0.79	0.79	0.78	0.33	0.34	0.49	1.03	0.22	0.49
FeO(P)	1.15	1.38	0.91	0.57	0.86	2.24	0.51	1.08	2.21	0.62	0.44	0.65	0.43	0.25	1.68
FeO(C)	1.32	2.08	0.51	0.89	0.67	1.13	0.72	0.44	1.64	0.35	0.62	0.51	0.20	0.13	1.27
Fe2O3	2.39	3.82	0.48	1.37	1.69	1.34	0.50	0.91	0.79	0.44	0.33	0.28	0.45	0.16	0.55
MnO	0.04	0.03	0.01	0.02	0.03	0.05	0.07	0.02	0.05	0.03	0.04	0.03	0.04	0.02	0.04
NiO	0.02	0.01	0.01	0.02	0.02	0.03	0.02	0.02	0.02	0.03	0.03	0.01	0.02	0.02	0.02
MgO	0.39	0.05	0.27	0.16	0.11	0.94	0.42	0.28	1.07	0.23	0.45	0.17	0.18	0.08	0.98
Mg#	0.022	0.010	0.014	0.009	0.002	0.044	0.022	0.013	0.054	0.011	0.021	0.010	0.007	0.004	0.046
Cr/Fe	0.029	0.020	0.038	0.010	0.020	0.070	0.030	0.042	0.076	0.033	0.019	0.028	0.039	0.017	0.026
Cr/Al	0.124	0.030	0.088	0.172	0.073	0.466	0.261	0.060	0.258	0.030	0.024	0.071	0.143	0.020	0.138
n	6	5	3	3	4	4	4	10	6	6	7	5	8	7	6

Chromite analyses: H3 sequence

Sample	1054.10	1253.30 a Top	1253.30 a Seam	1253.30 a Seam	1253.30 a Base	1261.65
Rock type	o	.	#	#	.	+
[wt%]						
TiO2	0.84	1.29	1.26	1.43	1.57	1.61
Al2O3	6.33	12.29	12.28	11.66	9.35	7.14
Cr2O3	38.51	40.79	40.44	41.70	40.29	44.50
FeO(P)	46.81	36.04	37.12	36.23	40.34	41.17
FeO(C)	27.96	23.50	23.94	23.94	25.50	27.72
Fe2O3	20.95	13.94	14.65	13.65	16.50	14.95
MnO	0.43	0.37	0.35	0.38	0.42	0.39
NiO	0.18	0.14	0.18	0.13	0.20	0.19
MgO	2.82	7.03	6.83	6.84	5.48	4.15
Total(P)	95.91	97.95	98.45	98.37	97.65	99.17
Total(C)	98.01	99.35	99.92	99.74	99.30	100.66
Cations (based on 32 oxygens)						
Ti	0.18	0.26	0.26	0.29	0.33	0.34
Al	2.17	3.92	3.90	3.72	3.06	2.35
Cr	8.86	8.72	8.62	8.92	8.84	9.83
Fe2	6.81	5.31	5.40	5.42	5.92	6.48
Fe3	4.60	2.84	2.97	2.78	3.45	3.14
Mn	0.11	0.08	0.08	0.09	0.10	0.09
Ni	0.04	0.03	0.04	0.03	0.04	0.04
Mg	1.22	2.83	2.74	2.76	2.27	1.73
Mg#	0.15	0.35	0.34	0.34	0.28	0.21
Cr/Fe	0.73	1.00	0.96	1.01	0.88	0.95
Cr/Al	4.20	2.23	2.21	2.40	2.90	4.21
1 Standard deviation [wt%]						
TiO2	0.19	0.00	0.22	0.01	0.00	0.27
Al2O3	1.18	0.08	0.18	0.07	0.55	0.64
Cr2O3	1.96	0.05	0.09	0.01	0.01	0.55
FeO(P)	3.02	0.07	0.67	0.07	0.49	1.61
FeO(C)	0.73	0.05	0.36	0.05	0.22	0.87
Fe2O3	2.80	0.02	0.34	0.03	0.30	1.06
MnO	0.05	0.02	0.04	0.02	0.03	0.02
NiO	0.03	0.01	0.01	0.03	0.00	0.04
MgO	0.50	0.01	0.41	0.01	0.29	0.70
Mg#	0.027	0.000	0.017	0.001	0.012	0.033
Cr/Fe	0.080	0.001	0.015	0.002	0.011	0.046
Cr/Al	0.625	0.012	0.037	0.016	0.169	0.404
n	3	2	2	2	2	8

Chromite analyses: additional samples

Sample	"Boulder" Bou-2	"Boulder" BBBC	"Boulder" BBTC	UG2-Peg	IM 866.67 Seam	IM 866.67 Top	LK5 1488.26 A-Seam	LK5 1488.26 A-Inside	LK5 1488.26 B-Seam	BM277	Lone Chrome Seam INMCR	Lone Chrome Seam RS38	Lone Chrome Seam BBCR	Merensky Reef BSIM Above	Merensky Reef BSIM Seam
Rock type	*	*	+	#	#	#	#	+	#	#	#	#	#	*	#
[wt%]															
TiO2	1.53	2.95	1.29	0.98	1.16	1.21	1.28	1.14	1.51	0.82	0.88	1.74	1.70	1.65	1.17
Al2O3	15.56	17.67	12.08	14.86	15.04	14.63	10.37	11.78	8.07	16.94	17.81	10.99	16.54	18.71	19.54
Cr2O3	26.52	33.39	46.53	40.13	39.65	37.02	43.69	41.73	41.35	36.56	42.10	39.38	35.35	43.30	43.48
FeO(P)	46.94	38.32	33.32	33.19	34.13	39.77	37.07	39.89	43.66	34.98	28.70	38.47	37.13	28.95	27.94
FeO(C)	25.87	27.17	26.51	21.86	24.08	27.77	25.29	28.83	29.64	21.98	21.89	24.17	25.31	25.35	24.39
Fe2O3	23.41	12.39	7.56	12.59	11.17	13.33	13.08	12.28	15.58	14.45	7.57	15.89	13.14	3.99	3.95
MnO	0.33	0.38	0.39	0.33	0.34	0.39	0.39	0.45	0.42	0.30	0.29	0.33	0.30	0.33	0.32
NiO	0.18	0.19	0.06	0.22	0.16	0.19	0.14	0.13	0.17	0.24	0.14	0.14	0.19	0.10	0.08
MgO	5.83	6.38	5.20	8.12	6.66	4.29	5.80	3.47	2.65	8.24	8.48	6.73	6.47	7.09	7.53
Total(P)	96.89	99.28	98.87	97.83	97.14	97.49	98.73	98.6	97.83	98.08	98.40	97.77	97.69	100.13	100.07
Total(C)	99.24	100.52	99.63	99.09	98.26	98.83	100.04	99.83	99.39	99.53	99.16	99.36	99.01	100.53	100.46
Cations (based on 32 oxygens)															
Ti	0.31	0.58	0.27	0.20	0.24	0.25	0.26	0.24	0.32	0.16	0.17	0.36	0.34	0.32	0.23
Al	4.95	5.46	3.85	4.66	4.79	4.73	3.34	3.82	2.71	5.24	5.48	3.53	5.21	5.71	5.93
Cr	5.66	6.93	10.06	8.43	8.47	8.02	9.44	9.14	9.31	7.58	8.69	8.49	7.47	8.87	8.85
Fe2	5.85	5.96	6.07	4.86	5.44	6.37	5.78	6.69	7.06	4.82	4.78	5.52	5.66	5.49	5.25
Fe3	4.76	2.45	1.56	2.52	2.27	2.75	2.69	2.56	3.34	2.85	1.49	3.26	2.64	0.78	0.77
Mn	0.08	0.08	0.09	0.07	0.08	0.09	0.09	0.11	0.10	0.07	0.06	0.08	0.07	0.07	0.07
Ni	0.04	0.04	0.01	0.05	0.04	0.04	0.03	0.03	0.04	0.05	0.03	0.03	0.04	0.02	0.02
Mg	2.35	2.50	2.09	3.22	2.68	1.75	2.36	1.41	1.12	3.22	3.30	2.74	2.57	2.74	2.89
Mg#	0.287	0.295	0.256	0.398	0.330	0.216	0.290	0.175	0.136	0.40	0.41	0.33	0.313	0.333	0.355
Cr/Fe	0.499	0.767	1.231	1.064	1.026	0.819	1.038	0.923	0.836	0.92	1.29	0.90	0.838	1.317	1.373
Cr/Al	1.144	1.269	2.797	1.815	1.769	1.700	2.829	2.478	3.437	1.45	1.59	2.41	1.437	1.552	1.493
1 Standard deviation [wt%]															
TiO2	0.087	0.521	0.220	0.095	0.094	0.165	0.080	0.144	0.262	0.077	0.102	1.428	0.115		0.265
Al2O3	0.601	0.717	3.086	0.646	0.192	0.521	0.267	2.354	0.006	0.591	0.134	0.446	0.734		0.340
Cr2O3	0.827	0.308	2.433	0.422	0.646	0.206	0.257	1.312	0.507	0.626	0.130	0.468	0.442		0.710
FeO(P)	1.897	0.583	2.081	0.321	1.807	0.229	0.266	2.470	2.183	0.981	0.246	1.336	0.393		1.144
FeO(C)	0.459	0.537	1.875	0.155	1.235	0.316	0.035	2.319	1.858	0.491	0.201	1.416	0.158		1.035
Fe2O3	1.602	0.054	0.554	0.337	0.663	0.132	0.257	0.260	0.362	0.637	0.231	2.696	0.339		0.121
MnO	0.012	0.014	0.066	0.020	0.037	0.017	0.005	0.027	0.083	0.026	0.019	0.027	0.023		0.037
NiO	0.038	0.014	0.039	0.017	0.016	0.057	0.012	0.020	0.031	0.039	0.025	0.031	0.025		0.026
MgO	0.365	0.128	1.790	0.160	0.893	0.270	0.160	1.781	1.378	0.299	0.125	0.366	0.119		0.587
Mg#	0.016	0.008	0.080	0.006	0.042	0.012	0.005	0.086	0.069	0.014	0.005	0.021	0.003		0.028
Cr/Fe	0.035	0.019	0.048	0.014	0.064	0.003	0.014	0.036	0.052	0.034	0.009	0.035	0.018		0.074
Cr/Al	0.031	0.040	0.836	0.096	0.042	0.070	0.090	0.510	0.045	0.065	0.016	0.101	0.079		0.028
n	5	3	4	7	8	8	4	2	3	22	4	62	5	1	5

Chromite analyses: TF sequence

Sample	859.00	866.50	957.00	962.00	964.00
Rock type	o	*	+	+	+
[wt%]					
TiO2	1.12	2.00	1.12	1.60	2.14
Al2O3	11.84	14.76	12.30	11.69	11.25
Cr2O3	23.51	31.17	47.68	46.71	45.76
FeO(P)	55.96	42.83	31.02	32.25	32.67
FeO(C)	28.05	26.23	25.54	26.87	26.60
Fe2O3	31.01	18.45	6.10	5.98	6.74
MnO	0.34	0.35	0.36	0.37	0.33
NiO	0.31	0.17	0.09	0.15	0.15
MgO	3.77	5.77	5.60	4.76	5.25
Total(P)	96.85	97.05	98.16	97.55	97.56
Total(C)	99.96	98.90	98.78	98.13	98.24
Cations (based on 32 oxygens)					
Ti	0.23	0.41	0.23	0.33	0.45
Al	3.88	4.70	3.97	3.82	3.67
Cr	5.17	6.71	10.32	10.26	10.03
Fe2	6.52	5.97	5.84	6.24	6.17
Fe3	6.49	3.77	1.26	1.25	1.41
Mn	0.08	0.08	0.08	0.09	0.08
Ni	0.07	0.04	0.02	0.03	0.03
Mg	1.56	2.33	2.28	1.97	2.17
Mg#	0.193	0.281	0.281	0.240	0.260
Cr/Fe	0.370	0.643	1.353	1.276	1.233
Cr/Al	1.333	1.583	2.600	2.695	2.733
1 Standard deviation [wt%]					
TiO2	0.019	0.590	0.086	0.099	0.227
Al2O3	0.049	3.767	0.227	0.769	0.419
Cr2O3	0.486	4.639	0.189	0.608	0.349
FeO(P)	0.201	1.757	0.403	0.800	0.338
FeO(C)	0.046	1.505	0.294	0.671	0.436
Fe2O3	0.275	1.913	0.260	0.353	0.145
MnO	0.003	0.058	0.003	0.024	0.018
NiO	0.005	0.018	0.014	0.017	0.019
MgO	0.035	1.087	0.288	0.479	0.210
Mg#	0.001	0.051	0.013	0.023	0.011
Cr/Fe	0.009	0.107	0.023	0.030	0.008
Cr/Al	0.033	0.655	0.041	0.214	0.116
n	2	6	3	6	5

Clinopyroxene analyses: IM sequence

Sample	787.90	788.32	790.64	793.22 b	794.53	796.25	801.00	804.00	810.10	818.00	819.30	819.85	823.50	826.48	836.00 b	839.00	843.61	848.52
Rock type	.	.	.	.	.	.	.	.	.	.	.	x	o	.	.	.	o	o
[wt%]																		
SiO2	52.72	52.88	52.14	51.59	52.22	51.63	52.54	52.80	52.11	52.48	52.05	51.53	50.69	52.09	51.81	52.62	52.30	50.52
TiO2	0.35	0.36	0.43	0.51	0.51	0.45	0.42	0.33	0.22	0.30	0.32	0.36	0.23	0.33	0.24	0.36	0.22	0.22
Al2O3	1.74	1.51	1.60	1.88	2.01	2.43	1.89	1.60	1.85	2.10	1.75	2.02	1.75	1.38	1.23	1.36	0.94	1.19
Cr2O3	0.76	0.72	0.48	0.64	0.59	0.61	0.76	0.46	0.65	0.77	0.65	0.57	0.26	0.55	0.51	0.45	0.05	0.04
FeO	4.10	3.90	4.82	4.84	6.50	4.99	4.31	4.70	3.91	3.81	4.03	5.53	8.18	5.39	4.79	5.02	9.40	11.96
MnO	0.12	0.14	0.16	0.14	0.17	0.33	0.14	0.11	0.10	0.15	0.09	0.13	0.20	0.21	0.12	0.12	0.24	0.30
NiO	0.05	0.03	0.07	0.07	0.05	0.04	0.03	0.02	0.03	0.05	0.01	0.05	0.01	0.01	0.05	0.06	0.09	0.02
MgO	16.65	16.73	16.30	15.87	15.74	16.17	16.68	17.20	16.75	16.68	16.43	15.97	14.76	15.70	15.83	16.11	13.90	11.82
CaO	23.84	23.71	23.56	23.27	22.75	23.00	23.38	22.71	23.71	23.33	23.35	23.17	21.88	23.22	23.77	22.97	22.50	22.40
Na2O	0.32	0.33	0.34	0.34	0.33	0.35	0.30	0.28	0.33	0.33	0.30	0.30	0.25	0.29	0.27	0.26	0.23	0.22
Total	100.64	100.32	99.90	99.15	100.85	99.98	100.43	100.22	99.64	100.01	98.98	99.62	98.20	99.16	98.61	99.32	99.87	98.69
Cations (based on 6 oxygens)																		
Si	1.93	1.94	1.93	1.92	1.92	1.91	1.92	1.93	1.92	1.92	1.93	1.91	1.93	1.94	1.94	1.95	1.96	1.95
Ti	0.01	0.01	0.01	0.01	0.01	0.01	0.01	0.01	0.01	0.01	0.01	0.01	0.01	0.01	0.01	0.01	0.01	0.01
Al	0.07	0.07	0.07	0.08	0.09	0.11	0.08	0.07	0.08	0.09	0.08	0.09	0.08	0.06	0.05	0.06	0.04	0.05
Cr	0.02	0.02	0.01	0.02	0.02	0.02	0.02	0.01	0.02	0.02	0.02	0.02	0.01	0.02	0.02	0.01	0.00	0.00
Fe	0.13	0.12	0.15	0.15	0.20	0.15	0.13	0.14	0.12	0.12	0.12	0.17	0.26	0.17	0.15	0.16	0.29	0.39
Mn	0.00	0.00	0.01	0.00	0.01	0.01	0.00	0.00	0.00	0.00	0.00	0.00	0.01	0.01	0.00	0.00	0.01	0.01
Ni	0.00	0.00	0.00	0.00	0.00	0.00	0.00	0.00	0.00	0.00	0.00	0.00	0.00	0.00	0.00	0.00	0.00	0.00
Mg	0.91	0.91	0.90	0.88	0.86	0.89	0.91	0.94	0.92	0.91	0.91	0.88	0.84	0.87	0.88	0.89	0.78	0.68
Ca	0.93	0.93	0.93	0.93	0.90	0.91	0.92	0.89	0.94	0.92	0.93	0.92	0.89	0.93	0.95	0.91	0.90	0.93
Na	0.01	0.01	0.01	0.01	0.01	0.01	0.01	0.00	0.01	0.01	0.01	0.01	0.00	0.01	0.00	0.00	0.00	0.00
Total	4.01	4.01	4.01	4.01	4.01	4.01	4.01	4.01	4.02	4.00	4.01	4.02	4.02	4.01	4.01	4.00	4.00	4.01
Mg#	0.879	0.884	0.858	0.854	0.812	0.852	0.873	0.867	0.884	0.886	0.879	0.837	0.763	0.838	0.855	0.851	0.725	0.638
1 Standard deviation [wt%]																		
SiO2	0.07	0.24	0.50	0.09	0.04	0.51	0.07	0.23	0.29	0.31	0.47	0.73	1.23	0.29	0.39	0.17		0.23
TiO2	0.07	0.13	0.10	0.12	0.04	0.11	0.03	0.06	0.00	0.07	0.10	0.13	0.02	0.13	0.07	0.07		0.03
Al2O3	0.21	0.36	0.42	0.28	0.10	0.16	0.10	0.16	0.61	0.29	0.34	0.42	0.71	0.49	0.30	0.18		0.25
Cr2O3	0.04	0.02	0.22	0.06	0.09	0.07	0.07	0.04	0.22	0.12	0.09	0.15	0.04	0.13	0.18	0.04		0.03
FeO	0.38	0.17	0.25	0.07	0.16	0.43	0.08	0.13	0.18	0.13	0.16	0.30	0.45	0.37	0.10	0.40		0.28
MnO	0.02	0.02	0.02	0.01	0.00	0.26	0.00	0.02	0.02	0.01	0.01	0.01	0.01	0.02	0.01	0.02		0.01
NiO	0.01	0.03	0.01	0.02	0.02	0.03	0.02	0.00	0.01	0.01	0.01	0.02	0.01	0.00	0.01	0.02		0.01
MgO	0.16	0.01	0.23	0.12	0.12	0.73	0.05	0.03	0.26	0.30	0.13	0.33	0.02	0.39	0.31	0.10		0.03
CaO	0.27	0.00	0.22	0.37	0.16	0.35	0.08	0.32	0.28	0.08	0.45	0.29	0.94	0.50	0.01	0.41		0.17
Na2O	0.02	0.00	0.04	0.01	0.02	0.01	0.03	0.01	0.04	0.03	0.04	0.04	0.02	0.03	0.04	0.02		0.00
Mg#	0.011	0.004	0.005	0.002	0.003	0.017	0.002	0.003	0.006	0.002	0.005	0.010	0.010	0.013	0.004	0.011		0.006
n	3	3	3	3	3	3	3	3	3	3	3	3	3	3	3	3	1	3

Plagioclase zonation (cumulus plagioclase):

LK7 1562.25 (Fig.4.13a)

	rim									rim
[wt%]	1	2	3	4	5	6	7	8	9	10	11
SiO2	48.67	49.50	49.54	49.12	48.86	49.07	48.78	49.55	49.10	48.66	48.03
Al2O3	32.39	31.45	31.62	31.89	32.21	31.96	31.92	31.73	31.71	32.09	32.47
FeO	0.44	0.44	0.45	0.45	0.38	0.50	0.46	0.43	0.49	0.48	0.40
CaO	16.57	15.80	15.87	16.28	16.37	16.36	16.27	15.97	15.98	16.56	16.80
Na2O	2.50	2.87	2.86	2.69	2.57	2.62	2.60	2.82	2.78	2.53	2.36
K2O	0.11	0.15	0.15	0.15	0.11	0.13	0.12	0.16	0.14	0.12	0.09
Total	100.67	100.21	100.49	100.58	100.51	100.63	100.16	100.65	100.21	100.44	100.15
Cations (based on 32 oxygens)											
Si	8.89	9.06	9.05	8.97	8.93	8.96	8.95	9.04	9.00	8.91	8.83
Al	6.97	6.79	6.81	6.87	6.94	6.88	6.90	6.82	6.85	6.93	7.03
Fe	0.07	0.07	0.07	0.07	0.06	0.08	0.07	0.06	0.08	0.07	0.06
Ca	3.24	3.10	3.11	3.19	3.20	3.20	3.20	3.12	3.14	3.25	3.31
Na	0.88	1.02	1.01	0.95	0.91	0.93	0.92	1.00	0.99	0.90	0.84
K	0.03	0.03	0.03	0.04	0.02	0.03	0.03	0.04	0.03	0.03	0.02
Total	20.08	20.07	20.07	20.09	20.07	20.08	20.07	20.07	20.09	20.09	20.09
An	78.12	74.63	74.77	76.32	77.39	77.01	77.05	75.11	75.46	77.85	79.33

Plagioclase zonation (cumulus plagioclase):

LK7 1562.25 (Fig. 4.13b)

	rim							rim
[wt%]	1	2	3	4	5	6	7	8
SiO2	49.53	49.75	49.21	48.56	50.00	49.72	49.49	49.26
Al2O3	31.73	31.61	32.04	32.50	31.51	31.52	31.64	31.76
FeO	0.40	0.46	0.41	0.32	0.36	0.39	0.43	0.40
CaO	15.77	15.66	16.04	16.58	15.50	15.59	15.77	15.80
Na2O	2.93	2.99	2.84	2.53	3.06	3.00	2.99	2.91
K2O	0.12	0.14	0.12	0.05	0.10	0.12	0.11	0.09
Total	100.47	100.61	100.66	100.54	100.53	100.35	100.43	100.22
Cations (based on 32 oxygens)								
Si	9.04	9.07	8.98	8.88	9.11	9.08	9.04	9.02
Al	6.83	6.79	6.89	7.00	6.77	6.79	6.81	6.85
Fe	0.06	0.07	0.06	0.05	0.06	0.06	0.07	0.06
Ca	3.08	3.06	3.14	3.25	3.02	3.05	3.09	3.10
Na	1.04	1.06	1.01	0.90	1.08	1.06	1.06	1.03
K	0.03	0.03	0.03	0.01	0.02	0.03	0.03	0.02
Total	20.08	20.08	20.10	20.08	20.06	20.07	20.09	20.08
An	74.35	73.75	75.23	78.13	73.27	73.69	73.99	74.59

Plagioclase zonation (cumulus plagioclase):

LK7 1577.45 (Fig. 4.13c)

	rim															rim
[wt%]	1	2	3	4	5	6	7	8	9	10	11	12	13	14	15	16	17
SiO2	48.40	49.29	49.13	49.30	49.56	49.57	49.51	49.59	49.60	49.61	49.35	49.15	49.08	49.36	49.95	49.65	48.74
Al2O3	32.04	31.63	31.02	31.29	31.29	31.55	31.45	31.41	31.38	31.16	31.39	31.90	31.42	31.52	31.15	31.23	31.72
FeO	0.20	0.26	0.43	0.20	0.26	0.16	0.21	0.26	0.22	0.26	0.22	0.26	0.27	0.27	0.27	0.22	0.27
CaO	15.98	15.51	15.02	15.35	15.36	15.59	15.15	15.39	15.34	15.21	15.82	15.81	15.93	15.77	15.29	15.48	16.31
Na2O	2.48	2.90	2.95	2.92	3.01	2.98	2.89	2.99	3.07	3.06	2.94	2.85	2.83	2.93	3.19	3.14	2.61
K2O	0.09	0.15	0.25	0.15	0.15	0.13	0.13	0.12	0.12	0.12	0.14	0.11	0.12	0.11	0.13	0.11	0.11
Total	99.19	99.75	98.79	99.20	99.64	99.99	99.35	99.76	99.74	99.42	99.86	100.07	99.66	99.98	99.97	99.84	99.76
Cations (based on 32 oxygens)																	
Si	8.94	9.05	9.11	9.10	9.11	9.08	9.11	9.10	9.10	9.13	9.06	9.00	9.04	9.05	9.15	9.11	8.97
Al	6.98	6.85	6.78	6.80	6.78	6.81	6.82	6.79	6.79	6.76	6.79	6.89	6.82	6.81	6.72	6.75	6.88
Fe	0.03	0.04	0.07	0.03	0.04	0.03	0.03	0.04	0.03	0.04	0.03	0.04	0.04	0.04	0.04	0.03	0.04
Ca	3.16	3.05	2.98	3.03	3.02	3.06	2.99	3.03	3.02	3.00	3.11	3.10	3.14	3.10	3.00	3.04	3.22
Na	0.89	1.03	1.06	1.04	1.07	1.06	1.03	1.06	1.09	1.09	1.05	1.01	1.01	1.04	1.13	1.12	0.93
K	0.02	0.03	0.06	0.03	0.04	0.03	0.03	0.03	0.03	0.03	0.03	0.03	0.03	0.03	0.03	0.03	0.03
Total	20.02	20.06	20.06	20.04	20.06	20.06	20.01	20.05	20.06	20.05	20.08	20.07	20.07	20.07	20.07	20.09	20.07
An	77.67	74.08	72.75	73.78	73.17	73.74	73.76	73.50	72.94	72.81	74.26	74.94	75.18	74.37	72.08	72.69	77.08

Plagioclase zonation (cumulus plagioclase):

LK7 1577.45 (Fig. 4.13d)

	rim																							rim
[wt%]	1	2	3	4	5	6	7	8	9	10	11	12	13	14	15	16	17	18	19	20	21	22	23	24
SiO2	49.47	49.42	49.47	49.37	49.36	49.02	49.41	49.27	49.51	49.00	49.20	49.07	49.28	48.49	49.03	49.67	49.31	49.33	49.66	49.55	49.81	49.01	49.03	48.41
Al2O3	31.26	31.13	31.40	31.62	31.52	31.05	31.10	31.02	31.00	31.41	31.33	31.40	30.91	32.17	31.62	31.38	31.30	31.36	31.43	31.54	31.31	32.00	31.30	31.92
FeO	0.25	0.24	0.23	0.22	0.21	0.26	0.17	0.24	0.30	0.24	0.27	0.29	0.24	0.21	0.25	0.26	0.27	0.22	0.22	0.20	0.26	0.24	0.20	0.24
CaO	15.70	15.70	15.73	15.88	15.94	15.65	15.42	15.36	15.65	15.64	15.71	15.91	15.38	16.22	15.89	15.36	15.67	15.58	15.52	15.67	15.62	16.06	16.17	16.44
Na2O	3.05	3.11	3.03	2.89	2.92	3.00	3.13	3.11	3.04	2.99	2.89	2.91	3.15	2.36	2.76	2.92	2.88	2.78	2.94	2.82	2.96	2.60	2.61	2.48
K2O	0.12	0.12	0.12	0.10	0.11	0.11	0.08	0.10	0.10	0.13	0.11	0.12	0.15	0.11	0.16	0.16	0.16	0.15	0.15	0.10	0.13	0.12	0.11	0.11
Total	99.85	99.73	99.98	100.09	100.07	99.10	99.30	99.10	99.60	99.40	99.49	99.71	99.11	99.57	99.70	99.75	99.58	99.41	99.92	99.86	100.10	100.03	99.41	99.59
Cations (based on 32 oxygens)																								
Si	9.08	9.09	9.07	9.04	9.05	9.07	9.11	9.11	9.11	9.04	9.06	9.03	9.11	8.93	9.02	9.11	9.08	9.08	9.10	9.08	9.11	8.98	9.04	8.93
Al	6.76	6.75	6.79	6.83	6.81	6.77	6.76	6.76	6.72	6.83	6.80	6.81	6.74	6.98	6.85	6.78	6.79	6.81	6.79	6.81	6.75	6.91	6.80	6.94
Fe	0.04	0.04	0.04	0.03	0.03	0.04	0.03	0.04	0.05	0.04	0.04	0.05	0.04	0.03	0.04	0.04	0.04	0.03	0.03	0.03	0.04	0.04	0.03	0.04
Ca	3.09	3.09	3.09	3.12	3.13	3.10	3.05	3.04	3.09	3.09	3.10	3.14	3.05	3.20	3.13	3.02	3.09	3.07	3.05	3.08	3.06	3.15	3.19	3.25
Na	1.08	1.11	1.08	1.03	1.04	1.08	1.12	1.11	1.09	1.07	1.03	1.04	1.13	0.84	0.98	1.04	1.03	0.99	1.04	1.00	1.05	0.92	0.93	0.89
K	0.03	0.03	0.03	0.02	0.03	0.03	0.02	0.02	0.02	0.03	0.03	0.03	0.03	0.03	0.04	0.04	0.04	0.03	0.03	0.02	0.03	0.03	0.03	0.03
Total	20.09	20.11	20.09	20.07	20.08	20.09	20.08	20.08	20.08	20.10	20.06	20.09	20.10	20.01	20.06	20.03	20.06	20.03	20.05	20.02	20.05	20.04	20.03	20.06
An	73.53	73.12	73.67	74.80	74.63	73.79	72.82	72.80	73.57	73.77	74.59	74.64	72.37	78.64	75.41	73.72	74.40	74.97	73.86	75.05	73.93	76.85	76.93	78.11

Plagioclase zonation (cumulus plagioclase):

LK7 1577.45 (Fig. 4.13e)

	rim										rim
[wt%]	1	2	3	4	5	6	7	8	9	10	11
SiO2	48.49	49.03	49.67	49.31	49.33	49.66	49.55	49.81	49.01	49.03	48.41
Al2O3	32.17	31.62	31.38	31.30	31.36	31.43	31.54	31.31	32.00	31.30	31.92
FeO	0.21	0.25	0.26	0.27	0.22	0.22	0.20	0.26	0.24	0.20	0.24
CaO	16.22	15.89	15.36	15.67	15.58	15.52	15.67	15.62	16.06	16.17	16.44
Na2O	2.36	2.76	2.92	2.88	2.78	2.94	2.82	2.96	2.60	2.61	2.48
K2O	0.11	0.16	0.16	0.16	0.15	0.15	0.10	0.13	0.12	0.11	0.11
Total	99.57	99.70	99.75	99.58	99.41	99.92	99.86	100.10	100.03	99.41	99.59
Cations (based on 32 oxygens)											
Si	8.93	9.02	9.11	9.08	9.08	9.10	9.08	9.11	8.98	9.04	8.93
Al	6.98	6.85	6.78	6.79	6.81	6.79	6.81	6.75	6.91	6.80	6.94
Fe	0.03	0.04	0.04	0.04	0.03	0.03	0.03	0.04	0.04	0.03	0.04
Ca	3.20	3.13	3.02	3.09	3.07	3.05	3.08	3.06	3.15	3.19	3.25
Na	0.84	0.98	1.04	1.03	0.99	1.04	1.00	1.05	0.92	0.93	0.89
K	0.03	0.04	0.04	0.04	0.03	0.03	0.02	0.03	0.03	0.03	0.03
Total	20.01	20.06	20.03	20.06	20.03	20.05	20.02	20.05	20.04	20.03	20.06
An	78.64	75.41	73.72	74.40	74.97	73.86	75.05	73.93	76.85	76.93	78.11

Plagioclase zonation (cumulus plagioclase):

LK7 1446.2 (Fig. 4.13f)

	rim													rim
[wt%]	1	2	3	4	5	6	7	8	9	10	11	12	13	14
SiO2	49.33	48.84	49.49	49.45	49.69	49.65	49.49	49.24	49.23	49.32	49.41	49.40	49.20	48.06
Al2O3	32.14	31.86	31.65	31.52	31.80	31.31	31.71	31.63	31.76	31.57	31.53	31.87	31.85	32.68
FeO	0.31	0.27	0.32	0.26	0.30	0.29	0.33	0.31	0.33	0.27	0.29	0.38	0.37	0.31
CaO	16.23	16.07	15.78	15.75	15.86	15.34	15.83	15.87	15.86	15.68	15.45	15.53	15.85	16.67
Na2O	2.53	2.59	2.80	2.88	2.81	2.92	2.76	2.71	2.69	2.77	2.87	2.77	2.73	2.31
K2O	0.16	0.17	0.19	0.21	0.19	0.19	0.17	0.16	0.17	0.19	0.18	0.18	0.17	0.10
Total	100.70	99.79	100.23	100.07	100.65	99.70	100.29	99.92	100.04	99.79	99.73	100.12	100.15	100.13
Cations (based on 32 oxygens)														
Si	8.98	8.98	9.05	9.06	9.05	9.12	9.05	9.04	9.02	9.06	9.07	9.04	9.01	8.82
Al	6.90	6.90	6.82	6.81	6.83	6.78	6.83	6.84	6.86	6.83	6.82	6.87	6.87	7.07
Fe	0.05	0.04	0.05	0.04	0.05	0.05	0.05	0.05	0.05	0.04	0.04	0.06	0.06	0.05
Ca	3.17	3.16	3.09	3.09	3.09	3.02	3.10	3.12	3.12	3.08	3.04	3.04	3.11	3.28
Na	0.89	0.92	0.99	1.02	0.99	1.04	0.98	0.96	0.96	0.99	1.02	0.98	0.97	0.82
K	0.04	0.04	0.04	0.05	0.04	0.04	0.04	0.04	0.04	0.05	0.04	0.04	0.04	0.02
Total	20.03	20.05	20.06	20.07	20.05	20.04	20.05	20.04	20.04	20.04	20.05	20.04	20.06	20.06
An	77.28	76.69	74.87	74.27	74.91	73.58	75.28	75.73	75.77	74.93	74.06	74.84	75.50	79.52

Plagioclase zonation (cumulus plagioclase):

LK7 1446.2 (Fig. 4.13g)

	rim																				rim
[wt%]	1	2	3	4	5	6	7	8	9	10	11	12	13	14	15	16	17	18	19	20	21
SiO2	48.72	48.59	48.75	48.86	49.10	48.88	49.22	49.15	49.34	49.37	49.33	49.43	49.12	49.10	49.29	48.74	49.00	48.90	48.88	48.66	48.45
Al2O3	32.06	31.89	31.82	31.69	31.51	31.30	31.35	31.30	31.42	31.31	31.42	31.48	31.23	31.57	31.30	31.44	31.46	31.57	31.56	31.71	31.77
FeO	0.26	0.29	0.30	0.24	0.28	0.37	0.31	0.26	0.32	0.32	0.31	0.33	0.30	0.31	0.30	0.34	0.33	0.32	0.32	0.29	0.31
CaO	16.34	16.17	16.13	15.90	15.89	15.73	15.72	15.75	15.74	15.48	15.78	15.55	15.54	15.50	15.48	15.35	15.57	15.77	15.82	15.70	16.01
Na2O	2.49	2.55	2.71	2.69	2.74	2.84	2.82	2.79	2.90	2.90	2.92	2.90	2.86	2.88	2.81	2.80	2.78	2.67	2.75	2.66	2.54
K2O	0.15	0.15	0.16	0.15	0.18	0.18	0.18	0.18	0.21	0.21	0.19	0.21	0.18	0.20	0.17	0.20	0.16	0.16	0.18	0.18	0.17
Total	100.02	99.64	99.88	99.54	99.72	99.30	99.59	99.44	99.93	99.59	99.95	99.91	99.23	99.56	99.35	98.87	99.30	99.39	99.51	99.21	99.26
Cations (based on 32 oxygens)																					
Si	8.94	8.95	8.96	9.00	9.03	9.04	9.06	9.06	9.06	9.09	9.05	9.07	9.07	9.04	9.09	9.03	9.04	9.02	9.01	8.99	8.96
Al	6.94	6.92	6.90	6.88	6.83	6.82	6.80	6.80	6.80	6.79	6.80	6.81	6.80	6.85	6.80	6.87	6.84	6.86	6.86	6.91	6.92
Fe	0.04	0.04	0.05	0.04	0.04	0.06	0.05	0.04	0.05	0.05	0.05	0.05	0.05	0.05	0.05	0.05	0.05	0.05	0.05	0.05	0.05
Ca	3.21	3.19	3.18	3.14	3.13	3.12	3.10	3.11	3.10	3.05	3.10	3.06	3.08	3.06	3.06	3.05	3.08	3.12	3.13	3.11	3.17
Na	0.88	0.91	0.97	0.96	0.98	1.02	1.01	1.00	1.03	1.03	1.04	1.03	1.02	1.03	1.00	1.00	0.99	0.95	0.98	0.95	0.91
K	0.04	0.04	0.04	0.04	0.04	0.04	0.04	0.04	0.05	0.05	0.04	0.05	0.04	0.05	0.04	0.05	0.04	0.04	0.04	0.04	0.04
Total	20.05	20.06	20.09	20.06	20.06	20.09	20.06	20.06	20.08	20.06	20.09	20.07	20.06	20.07	20.03	20.06	20.05	20.04	20.07	20.05	20.05
An	77.74	77.13	75.98	75.89	75.43	74.60	74.76	74.94	74.11	73.83	74.12	73.88	74.27	74.01	74.57	74.36	74.92	75.88	75.32	75.77	76.93

Plagioclase zonation (cumulus plagioclase):

LK7 1577.45 (Fig. 4.13h)

	rim																					rim
[wt%]	1	2	3	4	5	6	7	8	9	10	11	12	13	14	15	16	17	18	19	20	21	22
SiO2	47.25	47.96	48.45	48.33	47.93	48.57	48.99	47.15	48.26	47.71	47.84	47.82	47.80	48.53	48.59	48.80	49.07	48.70	48.63	47.48	47.66	47.37
Al2O3	33.28	32.96	32.74	32.46	32.64	32.71	32.54	33.57	32.57	32.62	32.77	32.68	32.61	32.41	31.92	32.00	32.16	32.05	32.14	32.83	32.92	32.93
FeO	0.24	0.25	0.26	0.27	0.25	0.20	0.25	0.12	0.20	0.16	0.18	0.21	0.21	0.24	0.23	0.22	0.23	0.21	0.24	0.25	0.23	0.24
CaO	17.32	16.82	16.52	16.41	16.37	16.27	16.47	17.47	16.41	16.71	16.89	16.89	16.85	16.51	16.16	15.92	16.16	16.06	16.22	16.97	17.00	17.14
Na2O	2.27	2.54	2.70	2.75	2.46	2.66	2.89	2.24	2.76	2.76	2.72	2.60	2.55	2.82	3.04	3.05	3.07	3.05	3.00	2.59	2.52	2.43
K2O	0.07	0.08	0.11	0.09	0.49	0.32	0.08	0.04	0.14	0.10	0.09	0.11	0.10	0.12	0.15	0.16	0.14	0.15	0.14	0.11	0.09	0.10
Total	100.42	100.61	100.77	100.32	100.14	100.73	101.22	100.59	100.34	100.06	100.49	100.31	100.12	100.64	100.10	100.15	100.83	100.23	100.37	100.23	100.42	100.22
Cations (based on 32 oxygens)																						
Si	8.67	8.77	8.84	8.86	8.81	8.86	8.90	8.64	8.84	8.78	8.77	8.78	8.79	8.87	8.93	8.95	8.94	8.93	8.91	8.73	8.74	8.71
Al	7.20	7.11	7.04	7.01	7.07	7.04	6.96	7.25	7.04	7.08	7.08	7.07	7.07	6.98	6.91	6.92	6.91	6.93	6.94	7.12	7.12	7.14
Fe	0.04	0.04	0.04	0.04	0.04	0.03	0.04	0.02	0.03	0.02	0.03	0.03	0.03	0.04	0.04	0.03	0.04	0.03	0.04	0.04	0.04	0.04
Ca	3.41	3.30	3.23	3.22	3.22	3.18	3.21	3.43	3.22	3.30	3.32	3.32	3.32	3.23	3.18	3.13	3.16	3.16	3.18	3.35	3.34	3.38
Na	0.81	0.90	0.95	0.98	0.88	0.94	1.02	0.79	0.98	0.99	0.97	0.93	0.91	1.00	1.08	1.08	1.08	1.08	1.07	0.92	0.89	0.87
K	0.02	0.02	0.02	0.02	0.12	0.07	0.02	0.01	0.03	0.02	0.02	0.03	0.02	0.03	0.04	0.04	0.03	0.04	0.03	0.03	0.02	0.02
Total	20.14	20.13	20.13	20.13	20.14	20.13	20.14	20.14	20.14	20.19	20.18	20.16	20.14	20.15	20.18	20.15	20.16	20.17	20.17	20.18	20.16	20.16
An	80.54	78.20	76.72	76.32	76.48	75.81	75.56	81.03	76.10	76.56	77.07	77.73	78.08	75.88	73.97	73.62	73.85	73.82	74.35	77.91	78.47	79.13

Plagioclase zonation (cumulus plagioclase):

LK7 1577.45 (Fig. 4.13i)

	rim																										
[wt%]	1	2	3	4	5	6	7	8	9	10	11	12	13	14	15	16	17	18	19	20	21	22	23	24	25	26	27	28
SiO2	47.97	47.47	47.58	47.96	48.20	48.14	48.18	48.21	48.10	48.19	48.27	48.38	48.36	48.17	47.84	48.24	48.13	47.90	47.88	47.83	48.04	48.01	48.37	48.01	48.10	47.67	47.97	47.93
Al2O3	32.75	32.80	32.83	32.49	32.44	32.51	32.58	32.54	32.32	32.38	32.40	32.45	32.39	32.54	32.49	32.69	32.54	32.11	32.37	32.51	32.40	32.66	32.23	32.02	32.71	32.00	32.44	32.77
FeO	0.22	0.24	0.27	0.26	0.27	0.22	0.24	0.21	0.22	0.20	0.25	0.23	0.24	0.23	0.23	0.25	0.20	0.19	0.22	0.27	0.23	0.21	0.21	0.22	0.25	0.22	0.23	0.29
CaO	17.02	17.08	17.17	16.72	16.88	16.45	16.68	16.79	16.58	16.66	16.65	16.74	16.88	16.69	16.79	16.76	16.56	16.72	16.97	16.89	17.06	17.02	16.75	16.77	17.15	16.77	16.77	17.05
Na2O	2.51	2.41	2.46	2.72	2.75	2.78	2.68	2.66	2.61	2.58	2.60	2.62	2.59	2.64	2.58	2.56	2.60	2.56	2.55	2.63	2.58	2.60	2.64	2.55	2.60	2.52	2.64	2.62
K2O	0.08	0.08	0.09	0.12	0.10	0.10	0.13	0.11	0.12	0.14	0.13	0.13	0.13	0.11	0.10	0.10	0.11	0.12	0.12	0.11	0.13	0.12	0.13	0.12	0.12	0.13	0.11	0.10
Total	100.55	100.07	100.40	100.27	100.64	100.20	100.49	100.51	99.94	100.15	100.30	100.55	100.60	100.39	100.04	100.61	100.14	99.61	100.12	100.23	100.45	100.62	100.33	99.69	100.93	99.31	100.16	100.77
Cations (based on 32 oxygens)																												
Si	8.78	8.74	8.74	8.81	8.82	8.84	8.82	8.83	8.85	8.85	8.85	8.85	8.85	8.83	8.81	8.82	8.84	8.85	8.81	8.79	8.81	8.79	8.87	8.86	8.79	8.84	8.82	8.77
Al	7.07	7.12	7.10	7.03	7.00	7.03	7.03	7.02	7.01	7.01	7.00	7.00	6.99	7.03	7.05	7.05	7.04	6.99	7.02	7.04	7.01	7.05	6.97	6.97	7.04	6.99	7.03	7.07
Fe	0.03	0.04	0.04	0.04	0.04	0.03	0.04	0.03	0.03	0.03	0.04	0.04	0.04	0.03	0.04	0.04	0.03	0.03	0.03	0.04	0.04	0.03	0.03	0.03	0.04	0.03	0.03	0.04
Ca	3.34	3.37	3.38	3.29	3.31	3.24	3.27	3.29	3.27	3.28	3.27	3.28	3.31	3.28	3.31	3.28	3.26	3.31	3.35	3.33	3.35	3.34	3.29	3.32	3.36	3.33	3.30	3.34
Na	0.89	0.86	0.88	0.97	0.98	0.99	0.95	0.94	0.93	0.92	0.92	0.93	0.92	0.94	0.92	0.91	0.93	0.92	0.91	0.94	0.92	0.92	0.94	0.91	0.92	0.91	0.94	0.93
K	0.02	0.02	0.02	0.03	0.02	0.02	0.03	0.02	0.03	0.03	0.03	0.03	0.03	0.03	0.02	0.02	0.03	0.03	0.03	0.03	0.03	0.03	0.03	0.03	0.03	0.03	0.03	0.02
Total	20.14	20.14	20.16	20.17	20.18	20.15	20.15	20.15	20.12	20.12	20.12	20.13	20.13	20.14	20.14	20.12	20.12	20.13	20.15	20.17	20.16	20.16	20.13	20.12	20.17	20.13	20.15	20.17
An	78.56	79.31	79.02	76.79	76.79	76.19	76.97	77.27	77.31	77.52	77.42	77.36	77.71	77.24	77.76	77.93	77.39	77.76	78.09	77.58	77.97	77.84	77.25	77.91	77.96	78.06	77.34	77.81

Plagioclase zonation (cumulus plagioclase):

H3 1206.95 (Fig. 4.13j)

				rim		rim													rim
29	30	31	32		[wt%]	1	2	3	4	5	6	7	8	9	10	11	12	13
47.78	47.77	45.43	46.92		SiO2	48.76	49.87	49.55	49.57	49.18	49.44	49.54	49.73	49.79	49.62	50.17	49.84	49.41
32.67	32.80	34.50	33.34		Al2O3	31.80	31.47	31.43	31.45	31.67	31.01	31.42	31.40	31.27	31.54	31.33	31.48	31.86
0.24	0.20	0.26	0.20		FeO	0.36	0.34	0.31	0.37	0.35	0.31	0.29	0.29	0.32	0.27	0.35	0.37	0.33
16.88	16.95	19.10	17.42		CaO	16.21	15.68	15.40	15.71	15.57	15.53	15.57	15.60	15.71	15.47	15.59	15.58	15.98
2.59	2.51	1.46	2.18		Na2O	2.66	2.99	3.14	3.06	3.04	3.04	3.12	3.17	3.09	3.08	3.08	3.10	2.85
0.09	0.05	0.04	0.05		K2O	0.10	0.14	0.12	0.14	0.15	0.14	0.14	0.09	0.10	0.11	0.14	0.10	0.10
100.25	100.29	100.80	100.12		Total	99.89	100.49	99.96	100.30	99.95	99.47	100.08	100.27	100.29	100.08	100.66	100.47	100.54
					Cations (based on 32 oxygens)													
8.78	8.77	8.36	8.64		Si	8.97	9.10	9.08	9.07	9.03	9.11	9.08	9.09	9.10	9.08	9.13	9.09	9.02
7.07	7.10	7.48	7.24		Al	6.89	6.77	6.79	6.78	6.85	6.73	6.78	6.76	6.74	6.80	6.72	6.77	6.85
0.04	0.03	0.04	0.03		Fe	0.06	0.05	0.05	0.06	0.05	0.05	0.04	0.04	0.05	0.04	0.05	0.06	0.05
3.32	3.33	3.76	3.44		Ca	3.19	3.06	3.03	3.08	3.06	3.07	3.06	3.06	3.08	3.03	3.04	3.04	3.12
0.92	0.89	0.52	0.78		Na	0.95	1.06	1.12	1.08	1.08	1.09	1.11	1.12	1.09	1.09	1.09	1.10	1.01
0.02	0.01	0.01	0.01		K	0.02	0.03	0.03	0.03	0.03	0.03	0.03	0.02	0.02	0.02	0.03	0.02	0.02
20.16	20.14	20.17	20.14		Total	20.08	20.07	20.09	20.10	20.11	20.08	20.10	20.10	20.09	20.08	20.07	20.08	20.07
77.87	78.62	87.62	81.28		An	76.68	73.77	72.56	73.38	73.31	73.28	72.84	72.74	73.34	73.08	73.11	73.10	75.18

Plagioclase zonation (inclusions):

LK7 1395.60 (Fig. 4.15a)

	rim			
[wt%]	1	2	3	4
SiO2	48.50	48.90	48.68	48.94
Al2O3	32.04	31.81	31.95	32.02
FeO	0.53	0.38	0.38	0.40
CaO	16.31	15.92	16.03	16.05
Na2O	2.66	2.77	2.84	2.73
K2O	0.08	0.09	0.08	0.08
Total	100.11	99.88	99.96	100.23
Cations (based on 32 oxygens)				
Si	8.91	8.98	8.95	8.96
Al	6.94	6.89	6.92	6.91
Fe	0.08	0.06	0.06	0.06
Ca	3.21	3.13	3.16	3.15
Na	0.95	0.99	1.01	0.97
K	0.02	0.02	0.02	0.02
Total	20.10	20.08	20.11	20.07
An	76.91	75.66	75.40	76.16

Plagioclase zonation (inclusions):

H3 1250.35 (Fig. 4.15b)

	rim(opx)							rim(opx)
[wt%]	1	2	3	4	5	6	7	8
SiO2	48.98	49.23	49.80	49.75	49.51	49.12	48.86	48.77
Al2O3	32.42	32.20	31.63	31.65	31.54	31.80	32.12	32.43
FeO	0.53	0.43	0.41	0.38	0.32	0.38	0.44	0.54
CaO	16.71	16.39	15.75	15.78	15.94	16.33	16.61	16.82
Na2O	2.57	2.80	2.95	3.07	2.93	2.75	2.64	2.49
K2O	0.05	0.07	0.09	0.09	0.09	0.09	0.09	0.05
Total	101.27	101.11	100.63	100.72	100.32	100.47	100.75	101.10
Cations (based on 32 oxygens)								
Si	8.90	8.95	9.07	9.06	9.05	8.98	8.92	8.88
Al	6.94	6.90	6.79	6.79	6.80	6.85	6.91	6.96
Fe	0.08	0.06	0.06	0.06	0.05	0.06	0.07	0.08
Ca	3.25	3.19	3.07	3.08	3.12	3.20	3.25	3.28
Na	0.91	0.98	1.04	1.08	1.04	0.97	0.93	0.88
K	0.01	0.02	0.02	0.02	0.02	0.02	0.02	0.01
Total	20.09	20.10	20.06	20.10	20.08	20.09	20.10	20.09
An	77.98	76.11	74.31	73.57	74.67	76.31	77.31	78.67

Plagioclase zonation (inclusions):

H3 1250.35 (Fig. 4.15c)

	rim(opx)												rim(opx)
[wt%]	1	2	3	4	5	6	7	8	9	10	11	12	13
SiO2	48.04	48.47	49.22	48.94	49.24	49.17	49.33	49.86	49.36	49.43	49.32	49.36	48.82
Al2O3	32.39	31.89	31.83	31.43	31.38	31.52	31.49	31.55	31.47	31.78	32.06	32.03	32.63
FeO	0.37	0.29	0.34	0.36	0.30	0.30	0.27	0.32	0.33	0.36	0.43	0.43	0.58
CaO	17.13	16.24	16.07	16.03	15.98	15.85	16.06	15.77	15.94	16.06	16.18	16.23	16.66
Na2O	2.41	2.64	2.82	2.88	2.96	2.94	3.00	3.08	2.94	2.86	2.76	2.69	2.56
K2O	0.06	0.08	0.08	0.05	0.07	0.07	0.09	0.08	0.09	0.10	0.09	0.06	0.06
Total	100.40	99.61	100.36	99.70	99.94	99.84	100.24	100.65	100.12	100.59	100.84	100.82	101.31
Cations (based on 32 oxygens)													
Si	8.82	8.94	9.00	9.01	9.04	9.03	9.03	9.08	9.05	9.02	8.98	8.99	8.87
Al	7.00	6.93	6.86	6.82	6.79	6.82	6.80	6.77	6.80	6.83	6.88	6.87	6.98
Fe	0.06	0.05	0.05	0.06	0.05	0.05	0.04	0.05	0.05	0.05	0.07	0.07	0.09
Ca	3.37	3.21	3.15	3.16	3.14	3.12	3.15	3.08	3.13	3.14	3.16	3.17	3.24
Na	0.86	0.94	1.00	1.03	1.05	1.05	1.06	1.09	1.04	1.01	0.97	0.95	0.90
K	0.01	0.02	0.02	0.01	0.02	0.02	0.02	0.02	0.02	0.02	0.02	0.01	0.01
Total	20.12	20.08	20.08	20.10	20.10	20.09	20.11	20.08	20.09	20.08	20.08	20.06	20.10
An	79.47	76.97	75.59	75.25	74.61	74.56	74.40	73.58	74.64	75.20	76.04	76.64	77.96

Plagioclase zonation (inclusions):

LK7 1446.20 (Fig. 4.15d)

	rim			rim
[wt%]	1	2	3	4
SiO2	48.59	49.26	49.34	48.79
Al2O3	31.98	31.43	31.37	31.62
FeO	0.30	0.30	0.28	0.33
CaO	16.34	15.59	15.59	15.87
Na2O	2.66	2.96	2.98	2.74
K2O	0.16	0.16	0.16	0.15
Total	100.03	99.71	99.73	99.49
Cations (based on 32 oxygens)				
Si	8.93	9.06	9.07	9.00
Al	6.93	6.81	6.80	6.87
Fe	0.05	0.05	0.04	0.05
Ca	3.22	3.07	3.07	3.14
Na	0.95	1.06	1.06	0.98
K	0.04	0.04	0.04	0.03
Total	20.10	20.08	20.08	20.07
An	76.56	73.73	73.60	75.55

Plagioclase zonation (inclusions):

H3 1206.95 (Fig. 4.15e)

	rim(opx)					rim(opx)
[wt%]	1	2	3	4	5	6
SiO2	49.43	49.74	49.65	49.47	49.44	49.04
Al2O3	31.52	31.46	31.60	31.53	31.61	32.01
FeO	0.51	0.45	0.42	0.43	0.49	0.52
CaO	15.80	15.71	15.71	15.89	15.83	16.15
Na2O	2.91	3.01	3.01	2.91	2.94	2.69
K2O	0.10	0.11	0.12	0.11	0.10	0.08
Total	100.26	100.48	100.52	100.34	100.41	100.49
Cations (based on 32 oxygens)						
Si	9.05	9.08	9.06	9.05	9.04	8.96
Al	6.80	6.77	6.80	6.80	6.81	6.90
Fe	0.08	0.07	0.06	0.07	0.07	0.08
Ca	3.10	3.07	3.07	3.11	3.10	3.16
Na	1.03	1.06	1.07	1.03	1.04	0.95
K	0.02	0.03	0.03	0.03	0.02	0.02
Total	20.08	20.08	20.09	20.08	20.09	20.07
An	74.59	73.82	73.73	74.66	74.47	76.51

Plagioclase zonation (inclusions):

LK7 1446.2 (Fig. 4.15f)

	rim				rim
[wt%]	1	2	3	4	5
SiO2	49.19	49.07	49.19	49.27	49.10
Al2O3	31.69	31.59	31.46	31.76	31.72
FeO	0.37	0.35	0.33	0.32	0.48
CaO	15.90	15.90	15.73	15.81	15.69
Na2O	2.83	2.75	2.75	2.83	2.80
K2O	0.16	0.16	0.17	0.17	0.17
Total	100.15	99.82	99.64	100.15	99.96
Cations (based on 32 oxygens)					
Si	9.02	9.02	9.05	9.02	9.01
Al	6.85	6.84	6.82	6.85	6.86
Fe	0.06	0.05	0.05	0.05	0.07
Ca	3.12	3.13	3.10	3.10	3.09
Na	1.01	0.98	0.98	1.01	1.00
K	0.04	0.04	0.04	0.04	0.04
Total	20.08	20.07	20.05	20.07	20.07
An	74.95	75.46	75.19	74.82	74.83

Plagioclase zonation (inclusions):

LK7 1395.60 (Fig. 4.15g)

rim		rim				rim
5	[wt%]	1	2	3	4	5
49.23	SiO2	48.22	48.03	48.06	48.05	47.35
32.02	Al2O3	31.81	31.57	31.65	31.88	31.73
0.41	FeO	0.56	0.31	0.47	0.44	0.56
15.90	CaO	16.08	16.03	16.04	16.06	16.23
2.67	Na2O	2.60	2.67	2.63	2.61	2.46
0.10	K2O	0.11	0.13	0.13	0.14	0.11
100.33	Total	99.38	98.74	98.98	99.17	98.43
	Cations (based on 32 oxygens)					
9.00	Si	8.92	8.94	8.93	8.91	8.86
6.90	Al	6.94	6.92	6.93	6.96	6.99
0.06	Fe	0.09	0.05	0.07	0.07	0.09
3.11	Ca	3.19	3.20	3.19	3.19	3.25
0.95	Na	0.93	0.96	0.95	0.94	0.89
0.02	K	0.03	0.03	0.03	0.03	0.03
20.04	Total	20.09	20.10	20.10	20.10	20.11
76.26	An	76.89	76.28	76.52	76.70	78.02

Plagioclase zonation (inclusions):

H3 1250.35 (Fig. 4.15h)

	rim(opx)							rim(opx)
[wt%]	1	2	3	4	5	6	7	8
SiO2	48.44	48.75	48.45	48.85	49.11	49.08	48.95	48.58
Al2O3	32.35	32.17	32.13	32.01	31.94	32.04	32.27	32.13
FeO	0.59	0.50	0.46	0.38	0.41	0.37	0.40	0.50
CaO	16.68	16.64	16.64	16.36	16.26	16.25	16.33	16.72
Na2O	2.49	2.64	2.70	2.72	2.81	2.78	2.68	2.58
K2O	0.04	0.07	0.06	0.08	0.08	0.08	0.08	0.06
Total	100.59	100.76	100.44	100.41	100.60	100.61	100.71	100.59
Cations (based on 32 oxygens)								
Si	8.86	8.90	8.88	8.94	8.97	8.96	8.93	8.89
Al	6.98	6.92	6.94	6.91	6.87	6.89	6.94	6.93
Fe	0.09	0.08	0.07	0.06	0.06	0.06	0.06	0.08
Ca	3.27	3.26	3.27	3.21	3.18	3.18	3.19	3.28
Na	0.88	0.93	0.96	0.96	0.99	0.99	0.95	0.92
K	0.01	0.02	0.01	0.02	0.02	0.02	0.02	0.02
Total	20.09	20.11	20.13	20.10	20.10	20.09	20.09	20.11
An	78.52	77.41	77.07	76.57	75.86	75.99	76.75	77.88

Plagioclase zonation (inclusions):

H3 1250.35 (Fig. 4.15i)

	rim(opx)						rim(pl)
[wt%]	1	2	3	4	5	6	7
SiO2	45.83	46.53	46.72	47.12	46.27	46.95	48.56
Al2O3	34.47	34.30	33.69	33.60	34.25	33.76	32.79
FeO	0.42	0.38	0.35	0.32	0.20	0.25	0.30
CaO	18.81	18.48	17.85	17.77	18.64	17.98	16.83
Na2O	1.29	1.38	1.88	1.89	1.46	1.73	2.44
K2O	0.03	0.04	0.04	0.03	0.03	0.02	0.05
Total	100.85	101.09	100.52	100.74	100.87	100.69	100.97
Cations (based on 32 oxygens)							
Si	8.41	8.50	8.58	8.63	8.48	8.60	8.84
Al	7.45	7.38	7.29	7.25	7.40	7.29	7.04
Fe	0.06	0.06	0.05	0.05	0.03	0.04	0.05
Ca	3.70	3.62	3.51	3.49	3.66	3.53	3.28
Na	0.46	0.49	0.67	0.67	0.52	0.62	0.86
K	0.01	0.01	0.01	0.01	0.01	0.01	0.01
Total	20.09	20.06	20.11	20.09	20.09	20.07	20.08
An	88.81	87.92	83.85	83.70	87.40	85.04	79.01

Plagioclase zonation (inclusions):

H3 1250.35 (Fig. 4.15j)

	rim(opx)				rim(plag)
[wt%]	1	2	3	4	5
SiO2	48.28	48.25	48.84	48.11	48.82
Al2O3	32.63	31.69	32.09	31.70	32.15
FeO	0.46	0.45	0.41	0.47	0.52
CaO	16.68	16.39	16.47	16.24	16.50
Na2O	2.45	2.72	2.65	2.65	2.73
K2O	0.08	0.09	0.10	0.10	0.10
Total	100.57	99.60	100.57	99.26	100.81
Cations (based on 32 oxygens)					
Si	8.83	8.92	8.93	8.91	8.91
Al	7.03	6.90	6.91	6.92	6.92
Fe	0.07	0.07	0.06	0.07	0.08
Ca	3.27	3.25	3.23	3.22	3.23
Na	0.87	0.98	0.94	0.95	0.97
K	0.02	0.02	0.02	0.02	0.02
Total	20.09	20.13	20.09	20.11	20.12
An	78.69	76.50	77.03	76.80	76.53

Plagioclase zonation (intercumulus plagioclase):

UA 667.20 (Fig. 4.14a)

	rim										rim
[wt%]	1	2	3	4	5	6	7	8	9	10	11
SiO2	54.00	53.48	50.72	50.02	49.94	49.21	49.78	49.33	49.13	49.23	52.92
Al2O3	28.68	28.77	30.25	31.01	30.82	31.06	31.08	31.28	31.19	31.07	29.22
FeO	0.30	0.25	0.23	0.17	0.19	0.17	0.16	0.18	0.17	0.21	0.19
CaO	11.86	12.01	13.94	14.66	14.35	14.64	14.78	15.06	15.07	15.09	12.56
Na2O	4.97	4.94	3.76	3.48	3.44	3.28	3.29	3.10	3.16	3.10	3.29
K2O	0.22	0.25	0.23	0.15	0.15	0.12	0.14	0.14	0.12	0.12	0.13
Total	100.04	99.70	99.13	99.47	98.88	98.48	99.23	99.10	98.84	98.82	98.32
Cations (based on 32 oxygens)											
Si	9.78	9.73	9.34	9.19	9.22	9.13	9.17	9.11	9.10	9.12	9.71
Al	6.12	6.17	6.56	6.71	6.71	6.80	6.75	6.80	6.81	6.78	6.32
Fe	0.05	0.04	0.04	0.03	0.03	0.03	0.02	0.03	0.03	0.03	0.03
Ca	2.30	2.34	2.75	2.89	2.84	2.91	2.92	2.98	2.99	2.99	2.47
Na	1.75	1.74	1.34	1.24	1.23	1.18	1.18	1.11	1.14	1.11	1.17
K	0.05	0.06	0.05	0.03	0.04	0.03	0.03	0.03	0.03	0.03	0.03
Total	20.05	20.08	20.08	20.09	20.06	20.07	20.06	20.06	20.08	20.06	19.73
An	56.15	56.54	66.34	69.38	69.17	70.72	70.71	72.28	71.96	72.42	67.26

Plagioclase zonation (intercumulus plagioclase):

UA 669.6 (Fig. 4.14b)

	rim												rim				rim
[wt%]	1	2	3	4	5	6	7	8	9	10	11	12	13	14	15	16	17
SiO2	50.35	50.07	50.09	49.99	50.11	50.12	50.10	50.01	50.02	50.28	50.44	50.78	51.97	50.96	49.89	50.42	51.39
Al2O3	29.92	30.73	30.61	31.14	31.37	31.31	31.19	31.12	30.99	31.11	31.32	31.00	30.40	30.64	31.26	31.08	29.99
FeO	0.63	0.23	0.14	0.15	0.12	0.14	0.17	0.14	0.13	0.14	0.12	0.12	0.21	0.30	0.17	0.18	1.18
CaO	13.97	14.69	14.75	14.67	14.83	14.95	15.04	14.88	14.82	14.76	14.78	14.46	13.45	14.15	14.80	14.63	11.99
Na2O	3.79	3.52	3.38	3.33	3.40	3.31	3.32	3.41	3.41	3.46	3.40	3.63	4.17	3.80	3.34	3.48	4.02
K2O	0.05	0.14	0.09	0.09	0.09	0.12	0.12	0.10	0.10	0.11	0.10	0.10	0.12	0.11	0.10	0.08	0.73
Total	98.70	99.38	99.06	99.36	99.91	99.94	99.95	99.66	99.48	99.86	100.17	100.09	100.33	99.96	99.56	99.87	99.29
Cations (based on 32 oxygens)																	
Si	9.33	9.21	9.24	9.19	9.16	9.16	9.17	9.17	9.19	9.20	9.19	9.26	9.43	9.31	9.16	9.22	9.45
Al	6.53	6.67	6.65	6.74	6.76	6.75	6.73	6.73	6.71	6.71	6.73	6.66	6.50	6.59	6.76	6.70	6.50
Fe	0.10	0.04	0.02	0.02	0.02	0.02	0.03	0.02	0.02	0.02	0.02	0.02	0.03	0.05	0.03	0.03	0.18
Ca	2.77	2.90	2.91	2.89	2.90	2.93	2.95	2.92	2.92	2.89	2.89	2.82	2.61	2.77	2.91	2.86	2.36
Na	1.36	1.25	1.21	1.18	1.21	1.17	1.18	1.21	1.21	1.23	1.20	1.28	1.47	1.35	1.19	1.23	1.43
K	0.01	0.03	0.02	0.02	0.02	0.03	0.03	0.02	0.02	0.03	0.02	0.02	0.03	0.02	0.02	0.02	0.17
Total	20.10	20.10	20.05	20.05	20.07	20.06	20.07	20.08	20.08	20.07	20.05	20.07	20.07	20.08	20.07	20.06	20.10
An	66.90	69.23	70.35	70.56	70.31	70.92	70.99	70.27	70.18	69.81	70.21	68.38	63.62	66.88	70.60	69.57	59.58

Orthopyroxene zonation:

LK7 1446.20 (Fig. 4.16a)

	rim									rim
[wt%]	1	2	3	4	5	6	7	8	9	10
SiO2	55.45	55.37	55.24	55.02	54.83	55.20	54.54	54.86	54.74	54.55
TiO2	0.23	0.19	0.18	0.22	0.22	0.16	0.33	0.21	0.23	0.18
Al2O3	1.01	1.00	1.00	1.06	1.05	1.00	0.93	0.86	0.90	0.86
Cr2O3	0.40	0.38	0.35	0.34	0.38	0.40	0.28	0.25	0.25	0.28
FeO	12.64	12.54	12.50	12.39	11.80	12.28	14.67	14.79	14.97	15.37
MnO	0.30	0.34	0.29	0.32	0.31	0.27	0.28	0.27	0.31	0.29
NiO	0.04	0.08	0.03	0.08	0.08	0.09	0.09	0.06	0.09	0.05
MgO	29.77	30.01	29.79	29.81	28.95	29.87	28.30	28.49	28.64	28.50
CaO	0.98	0.83	0.83	0.86	2.24	0.87	1.21	1.44	1.21	0.84
Na2O	0.00	0.00	0.00	0.00	0.02	0.00	0.01	0.02	0.03	0.06
Total	100.81	100.75	100.19	100.10	99.86	100.13	100.63	101.25	101.36	100.98
Cations (based on 6 oxygens)										
Si	1.96	1.96	1.96	1.96	1.96	1.96	1.95	1.95	1.95	1.95
Ti	0.01	0.01	0.00	0.01	0.01	0.00	0.01	0.01	0.01	0.00
Al	0.04	0.04	0.04	0.04	0.04	0.04	0.04	0.04	0.04	0.04
Cr	0.01	0.01	0.01	0.01	0.01	0.01	0.01	0.01	0.01	0.01
Fe	0.37	0.37	0.37	0.37	0.35	0.36	0.44	0.44	0.45	0.46
Mn	0.01	0.01	0.01	0.01	0.01	0.01	0.01	0.01	0.01	0.01
Ni	0.00	0.00	0.00	0.00	0.00	0.00	0.00	0.00	0.00	0.00
Mg	1.57	1.58	1.58	1.58	1.54	1.58	1.51	1.51	1.52	1.52
Ca	0.04	0.03	0.03	0.03	0.09	0.03	0.05	0.06	0.05	0.03
Na	0.00	0.00	0.00	0.00	0.00	0.00	0.00	0.00	0.00	0.00
Total	4.01	4.01	4.01	4.01	4.01	4.01	4.02	4.02	4.02	4.02
Mg#	0.808	0.810	0.809	0.811	0.814	0.813	0.775	0.774	0.773	0.768

Orthopyroxene zonation:

LK7 1520.4 (Fig. 4.16b)

	rim									rim
[wt%]	1	2	3	4	5	6	7	8	9	10
SiO2	54.29	54.68	54.63	54.44	54.65	54.62	54.44	54.48	54.68	54.87
TiO2	0.29	0.21	0.14	0.12	0.13	0.14	0.18	0.19	0.22	0.26
Al2O3	0.91	0.99	1.11	1.19	1.17	1.05	1.07	1.00	0.98	0.88
Cr2O3	0.25	0.30	0.35	0.36	0.33	0.32	0.34	0.32	0.27	0.26
FeO	15.36	14.57	14.11	14.11	14.26	14.63	14.29	14.94	14.98	15.14
MnO	0.26	0.28	0.26	0.24	0.24	0.21	0.28	0.25	0.25	0.26
NiO	0.06	0.04	0.02	0.01	0.08	0.02	0.02	0.05	0.00	0.03
MgO	27.65	28.38	27.51	27.38	27.81	28.02	27.41	27.97	27.93	27.87
CaO	1.09	1.53	2.72	2.80	2.27	1.85	2.13	1.54	1.47	1.08
Na2O	0.03	0.02	0.03	0.05	0.04	0.03	0.03	0.02	0.02	0.01
Total	100.18	100.99	100.68	100.70	100.99	100.90	100.18	100.76	100.79	100.67
Cations (based on 6 oxygens)										
Si	1.96	1.95	1.95	1.95	1.95	1.95	1.96	1.95	1.96	1.96
Ti	0.01	0.01	0.00	0.00	0.00	0.00	0.00	0.01	0.01	0.01
Al	0.04	0.04	0.05	0.05	0.05	0.04	0.05	0.04	0.04	0.04
Cr	0.01	0.01	0.01	0.01	0.01	0.01	0.01	0.01	0.01	0.01
Fe	0.46	0.43	0.42	0.42	0.43	0.44	0.43	0.45	0.45	0.45
Mn	0.01	0.01	0.01	0.01	0.01	0.01	0.01	0.01	0.01	0.01
Ni	0.00	0.00	0.00	0.00	0.00	0.00	0.00	0.00	0.00	0.00
Mg	1.49	1.51	1.47	1.46	1.48	1.49	1.47	1.49	1.49	1.49
Ca	0.04	0.06	0.10	0.11	0.09	0.07	0.08	0.06	0.06	0.04
Na	0.00	0.00	0.00	0.00	0.00	0.00	0.00	0.00	0.00	0.00
Total	4.01	4.02	4.01	4.02	4.02	4.02	4.01	4.02	4.01	4.01
Mg#	0.762	0.776	0.777	0.776	0.777	0.773	0.774	0.769	0.769	0.766

Orthopyroxene zonation:

LK7 1520.4 (Fig. 4.16c)

	rim													rim
[wt%]	1	2	3	4	5	6	7	8	9	10	11	12	13	14
SiO2	54.69	54.24	54.82	54.60	54.85	54.55	55.22	55.16	55.34	55.36	54.50	54.85	54.41	55.07
TiO2	0.32	0.59	0.29	0.23	0.20	0.24	0.16	0.12	0.17	0.15	0.12	0.11	0.15	0.18
Al2O3	0.92	0.90	0.90	0.92	0.96	0.96	1.10	1.08	1.08	0.97	1.25	1.13	1.06	0.97
Cr2O3	0.29	0.32	0.28	0.27	0.30	0.30	0.40	0.37	0.41	0.38	0.43	0.42	0.44	0.34
FeO	14.82	15.43	14.36	14.52	14.71	14.58	12.23	12.50	12.06	12.39	11.94	12.29	12.31	12.51
MnO	0.30	0.34	0.34	0.34	0.31	0.30	0.29	0.29	0.28	0.31	0.27	0.26	0.29	0.24
NiO	0.05	0.09	0.08	0.10	0.11	0.05	0.02	0.01	0.05	0.04	0.06	0.08	0.10	0.07
MgO	27.91	28.22	28.40	28.40	28.43	28.41	29.76	29.95	29.66	30.04	28.73	29.43	29.24	29.58
CaO	0.94	0.83	1.28	1.13	1.42	1.67	1.21	0.78	1.46	0.90	2.26	1.34	1.62	0.91
Na2O	0.01	0.00	0.01	0.03	0.02	0.02	0.00	0.00	0.01	0.00	0.02	0.01	0.00	0.00
Total	100.25	100.96	100.76	100.55	101.30	101.07	100.39	100.26	100.51	100.54	99.58	99.92	99.61	99.87
Cations (based on 6 oxygens)														
Si	1.96	1.94	1.96	1.95	1.95	1.95	1.96	1.96	1.96	1.96	1.95	1.96	1.95	1.96
Ti	0.01	0.02	0.01	0.01	0.01	0.01	0.00	0.00	0.00	0.00	0.00	0.00	0.00	0.00
Al	0.04	0.04	0.04	0.04	0.04	0.04	0.05	0.05	0.05	0.04	0.05	0.05	0.04	0.04
Cr	0.01	0.01	0.01	0.01	0.01	0.01	0.01	0.01	0.01	0.01	0.01	0.01	0.01	0.01
Fe	0.45	0.46	0.43	0.43	0.44	0.44	0.36	0.37	0.36	0.37	0.36	0.37	0.37	0.37
Mn	0.01	0.01	0.01	0.01	0.01	0.01	0.01	0.01	0.01	0.01	0.01	0.01	0.01	0.01
Ni	0.00	0.00	0.00	0.00	0.00	0.00	0.00	0.00	0.00	0.00	0.00	0.00	0.00	0.00
Mg	1.49	1.51	1.51	1.52	1.51	1.51	1.57	1.58	1.57	1.58	1.53	1.56	1.56	1.57
Ca	0.04	0.03	0.05	0.04	0.05	0.06	0.05	0.03	0.06	0.03	0.09	0.05	0.06	0.03
Na	0.00	0.00	0.00	0.00	0.00	0.00	0.00	0.00	0.00	0.00	0.00	0.00	0.00	0.00
Total	4.00	4.02	4.01	4.02	4.02	4.02	4.01	4.01	4.01	4.01	4.01	4.01	4.02	4.01
Mg#	0.770	0.765	0.779	0.777	0.775	0.776	0.813	0.810	0.814	0.812	0.811	0.810	0.809	0.808

Orthopyroxene zonation:

LK7 1520.4 (Fig. 4.16d)

	rim										rim
[wt%]	1	2	3	4	5	6	7	8	9	10	11
SiO2	54.78	54.78	54.50	54.80	54.20	54.40	54.66	54.58	54.62	54.36	53.64
TiO2	0.28	0.28	0.24	0.21	0.24	0.25	0.23	0.30	0.37	0.27	0.20
Al2O3	0.91	0.88	0.98	0.97	0.98	0.92	0.92	0.88	0.87	0.95	1.36
Cr2O3	0.24	0.23	0.29	0.27	0.29	0.26	0.27	0.25	0.24	0.24	0.20
FeO	14.95	15.08	14.52	14.74	14.53	14.73	14.60	14.72	14.79	15.09	15.11
MnO	0.32	0.31	0.25	0.30	0.29	0.32	0.25	0.32	0.29	0.36	0.35
NiO	0.10	0.08	0.10	0.08	0.06	0.11	0.08	0.09	0.09	0.08	0.07
MgO	28.58	28.70	28.43	28.57	28.31	28.55	28.68	28.47	28.49	27.94	27.48
CaO	1.17	1.17	1.04	1.55	1.55	1.40	1.58	1.27	1.27	0.92	0.84
Na2O	0.09	0.08	0.09	0.09	0.17	0.09	0.09	0.07	0.09	0.01	0.05
Total	101.42	101.61	101.24	101.59	100.62	101.04	101.35	100.95	101.11	100.23	99.29
Cations (based on 6 oxygens)											
Si	1.95	1.95	1.94	1.95	1.94	1.94	1.94	1.95	1.95	1.96	1.95
Ti	0.01	0.01	0.01	0.01	0.01	0.01	0.01	0.01	0.01	0.01	0.01
Al	0.04	0.04	0.04	0.04	0.04	0.04	0.04	0.04	0.04	0.04	0.06
Cr	0.01	0.01	0.01	0.01	0.01	0.01	0.01	0.01	0.01	0.01	0.01
Fe	0.44	0.45	0.43	0.44	0.44	0.44	0.43	0.44	0.44	0.45	0.46
Mn	0.01	0.01	0.01	0.01	0.01	0.01	0.01	0.01	0.01	0.01	0.01
Ni	0.00	0.00	0.00	0.00	0.00	0.00	0.00	0.00	0.00	0.00	0.00
Mg	1.52	1.52	1.51	1.51	1.51	1.52	1.52	1.52	1.51	1.50	1.49
Ca	0.04	0.04	0.07	0.06	0.06	0.05	0.06	0.05	0.05	0.04	0.03
Na	0.00	0.00	0.00	0.00	0.00	0.00	0.00	0.00	0.00	0.00	0.00
Total	4.02	4.02	4.02	4.02	4.02	4.03	4.02	4.02	4.02	4.01	4.01
Mg#	0.773	0.772	0.777	0.776	0.776	0.775	0.778	0.775	0.774	0.767	0.764

Orthopyroxene zonation:

LK7 1520.4 (Fig. 4.16e)

	rim														rim
[wt%]	1	2	3	4	5	6	7	8	9	10	11	12	13	14	15
SiO2	53.59	54.43	54.56	54.58	54.53	54.74	54.42	54.51	54.61	54.53	54.52	54.59	54.35	54.37	54.33
TiO2	0.27	0.30	0.25	0.22	0.22	0.21	0.21	0.18	0.21	0.22	0.22	0.35	0.26	0.25	0.25
Al2O3	1.23	0.92	0.94	0.97	0.95	1.00	0.99	0.97	0.99	0.97	0.95	0.91	0.90	0.92	0.89
Cr2O3	0.21	0.21	0.23	0.28	0.29	0.29	0.30	0.24	0.25	0.24	0.25	0.24	0.23	0.23	0.21
FeO	14.71	14.95	14.77	14.21	14.40	14.19	14.29	14.66	14.75	14.40	14.76	14.82	15.27	15.43	16.27
MnO	0.33	0.29	0.28	0.32	0.27	0.30	0.28	0.28	0.25	0.38	0.31	0.33	0.32	0.35	0.36
NiO	0.02	0.08	0.08	0.08	0.07	0.08	0.04	0.09	0.04	0.05	0.04	0.08	0.10	0.09	0.04
MgO	27.89	28.18	28.42	28.06	27.97	28.14	28.09	28.20	28.35	28.02	28.10	28.23	27.90	27.59	27.36
CaO	0.87	1.09	0.87	1.64	1.69	1.35	1.63	1.39	1.44	1.84	1.78	1.35	1.24	1.07	0.83
Na2O	0.03	0.02	0.02	0.02	0.01	0.01	0.02	0.01	0.00	0.01	0.02	0.00	0.01	0.01	0.00
Total	99.14	100.46	100.43	100.38	100.41	100.30	100.28	100.54	100.90	100.65	100.95	100.91	100.57	100.30	100.55
Cations (based on 6 oxygens)															
Si	1.95	1.95	1.96	1.96	1.96	1.96	1.95	1.95	1.95	1.95	1.95	1.95	1.95	1.96	1.96
Ti	0.01	0.01	0.01	0.01	0.01	0.01	0.01	0.00	0.01	0.01	0.01	0.01	0.01	0.01	0.01
Al	0.05	0.04	0.04	0.04	0.04	0.04	0.04	0.04	0.04	0.04	0.04	0.04	0.04	0.04	0.04
Cr	0.01	0.01	0.01	0.01	0.01	0.01	0.01	0.01	0.01	0.01	0.01	0.01	0.01	0.01	0.01
Fe	0.45	0.45	0.44	0.43	0.43	0.43	0.43	0.44	0.44	0.43	0.44	0.44	0.46	0.46	0.49
Mn	0.01	0.01	0.01	0.01	0.01	0.01	0.01	0.01	0.01	0.01	0.01	0.01	0.01	0.01	0.01
Ni	0.00	0.00	0.00	0.00	0.00	0.00	0.00	0.00	0.00	0.00	0.00	0.00	0.00	0.00	0.00
Mg	1.51	1.51	1.52	1.50	1.50	1.50	1.50	1.51	1.51	1.50	1.50	1.50	1.49	1.48	1.47
Ca	0.03	0.04	0.03	0.06	0.06	0.05	0.06	0.05	0.06	0.07	0.07	0.05	0.05	0.04	0.03
Na	0.00	0.00	0.00	0.00	0.00	0.00	0.00	0.00	0.00	0.00	0.00	0.00	0.00	0.00	0.00
Total	4.02	4.02	4.01	4.01	4.01	4.01	4.02	4.02	4.02	4.02	4.02	4.02	4.02	4.01	4.01
Mg#	0.772	0.771	0.774	0.779	0.776	0.779	0.778	0.774	0.774	0.776	0.772	0.772	0.765	0.761	0.750

Orthopyroxene zonation:

LK7 1446.2 (Fig. 4.16f)

	rim																	rim
[wt%]	1	2	3	4	5	6	7	8	9	10	11	12	13	14	15	16	17	18
SiO2	54.97	55.30	55.31	55.19	55.32	55.74	55.25	55.07	55.37	55.40	55.37	55.31	55.32	55.37	55.35	55.40	55.14	55.49
TiO2	0.17	0.19	0.19	0.20	0.18	0.20	0.19	0.18	0.15	0.18	0.18	0.17	0.17	0.18	0.17	0.17	0.17	0.22
Al2O3	0.95	1.06	1.08	1.05	1.03	1.05	1.15	1.09	1.02	1.08	1.02	1.13	1.10	1.04	1.05	1.01	1.10	1.03
Cr2O3	0.41	0.44	0.42	0.38	0.39	0.38	0.45	0.43	0.41	0.42	0.38	0.36	0.38	0.35	0.37	0.40	0.37	0.37
FeO	12.62	12.06	12.13	12.23	12.20	11.77	11.78	11.91	11.94	11.66	11.78	12.36	12.60	12.47	12.64	12.50	12.81	12.66
MnO	0.29	0.27	0.24	0.29	0.26	0.28	0.30	0.29	0.30	0.27	0.27	0.27	0.26	0.31	0.28	0.26	0.27	0.24
NiO	0.07	0.02	0.09	0.07	0.08	0.06	0.06	0.04	0.07	0.08	0.03	0.05	0.07	0.05	0.08	0.05	0.11	0.04
MgO	30.09	29.79	29.77	30.06	29.95	29.68	29.30	30.05	30.02	29.81	30.12	29.51	29.94	29.98	30.25	30.39	30.23	30.15
CaO	0.72	0.90	0.95	0.93	1.01	1.66	2.04	1.47	1.00	1.28	0.98	1.24	1.03	0.99	0.81	0.84	0.82	0.72
Na2O	0.00	0.01	0.02	0.01	0.01	0.02	0.02	0.01	0.02	0.02	0.00	0.01	0.00	0.00	0.00	0.00	0.00	0.00
Total	100.29	100.06	100.21	100.42	100.44	100.83	100.55	100.55	100.30	100.20	100.12	100.41	100.84	100.76	100.99	100.99	101.05	100.91
Cations (based on 6 oxygens)																		
Si	1.95	1.96	1.96	1.96	1.96	1.96	1.96	1.95	1.96	1.96	1.96	1.96	1.95	1.96	1.95	1.95	1.95	1.96
Ti	0.00	0.01	0.01	0.01	0.00	0.01	0.01	0.00	0.00	0.00	0.00	0.00	0.00	0.00	0.00	0.00	0.00	0.01
Al	0.04	0.04	0.05	0.04	0.04	0.04	0.05	0.05	0.04	0.05	0.04	0.05	0.05	0.04	0.04	0.04	0.05	0.04
Cr	0.01	0.01	0.01	0.01	0.01	0.01	0.01	0.01	0.01	0.01	0.01	0.01	0.01	0.01	0.01	0.01	0.01	0.01
Fe	0.38	0.36	0.36	0.36	0.36	0.35	0.35	0.35	0.35	0.35	0.35	0.37	0.37	0.37	0.37	0.37	0.38	0.37
Mn	0.01	0.01	0.01	0.01	0.01	0.01	0.01	0.01	0.01	0.01	0.01	0.01	0.01	0.01	0.01	0.01	0.01	0.01
Ni	0.00	0.00	0.00	0.00	0.00	0.00	0.00	0.00	0.00	0.00	0.00	0.00	0.00	0.00	0.00	0.00	0.00	0.00
Mg	1.59	1.58	1.57	1.59	1.58	1.56	1.55	1.59	1.58	1.57	1.59	1.56	1.58	1.58	1.59	1.60	1.59	1.59
Ca	0.03	0.03	0.04	0.04	0.04	0.06	0.08	0.06	0.04	0.05	0.04	0.05	0.04	0.04	0.03	0.03	0.03	0.03
Na	0.00	0.00	0.00	0.00	0.00	0.00	0.00	0.00	0.00	0.00	0.00	0.00	0.00	0.00	0.00	0.00	0.00	0.00
Total	4.02	4.00	4.00	4.01	4.01	4.00	4.01	4.02	4.01	4.00	4.01	4.01	4.01	4.01	4.02	4.02	4.02	4.01
Mg#	0.809	0.815	0.814	0.814	0.814	0.818	0.816	0.818	0.818	0.820	0.820	0.810	0.809	0.811	0.810	0.812	0.808	0.809

Chromite zonation:

EK22 284.25

	rim								rim	rim					rim	rim							rim
[wt%]	1	2	3	4	5	6	7	8	9	1	2	3	4	5	6	1	2	3	4	5	6	7	8	9
TiO2	0.50	0.73	0.69	0.75	1.00	0.99	0.71	0.73	0.63	0.51	0.72	0.72	0.73	0.73	0.76	1.22	5.15	1.13	1.25	1.24	1.24	1.07	12.34	1.51
Al2O3	18.52	15.67	15.56	16.37	16.54	16.25	15.94	15.21	16.09	17.85	16.88	16.63	16.09	15.97	15.73	10.93	10.35	11.07	11.24	11.23	11.19	11.41	9.18	11.20
Cr2O3	40.57	41.64	43.21	42.67	41.52	42.26	42.43	43.19	40.22	42.28	41.86	42.18	42.53	42.58	42.59	39.50	40.20	39.78	39.56	39.51	39.52	39.55	37.43	39.32
FeO(P)	28.77	30.97	30.03	30.02	29.70	30.06	29.93	30.18	31.96	27.83	29.61	29.80	29.83	30.16	29.61	37.65	34.18	37.71	37.57	37.52	37.81	37.89	31.24	37.86
FeO(C)	19.33	20.60	20.54	20.70	20.36	20.81	20.20	20.64	20.43	19.34	19.89	20.28	20.37	20.37	20.18	23.28	27.08	23.28	23.22	23.14	23.42	23.19	34.25	23.57
Fe2O3	10.49	11.53	10.55	10.36	10.38	10.29	10.82	10.60	12.82	9.45	10.81	10.58	10.51	10.89	10.48	15.97	7.89	16.03	15.95	15.97	15.99	16.34	-3.35	15.87
MnO	0.34	0.33	0.33	0.34	0.29	0.33	0.32	0.32	0.33	0.27	0.33	0.31	0.34	0.30	0.30	0.32	0.32	0.34	0.32	0.32	0.34	0.33	0.29	0.35
NiO	0.09	0.08	0.09	0.10	0.06	0.07	0.10	0.12	0.06	0.12	0.12	0.13	0.10	0.09	0.11	0.13	0.11	0.14	0.19	0.13	0.17	0.09	0.10	0.11
MgO	10.15	9.10	9.22	9.29	9.56	9.33	9.43	9.05	9.22	10.10	9.82	9.54	9.35	9.45	9.37	6.74	6.50	6.79	6.91	6.96	6.77	6.96	5.72	6.90
Total(P)	98.94	98.52	99.13	99.55	98.67	99.29	98.87	98.80	98.52	98.97	99.33	99.31	98.97	99.28	98.46	96.49	96.82	96.96	97.04	96.90	97.04	97.32	96.29	97.23
Total(C)	99.99	99.67	100.18	100.59	99.71	100.32	99.95	99.86	99.80	99.91	100.41	100.37	100.03	100.37	99.51	98.09	97.61	98.56	98.64	98.50	98.65	98.96	95.96	98.82
Cations (based on 32 oxygens)																								
Ti	0.10	0.14	0.14	0.14	0.20	0.19	0.14	0.14	0.12	0.10	0.14	0.14	0.14	0.14	0.15	0.25	1.08	0.23	0.26	0.25	0.26	0.22	2.63	0.31
Al	5.58	4.83	4.77	4.98	5.06	4.96	4.88	4.69	4.95	5.40	5.12	5.06	4.93	4.88	4.84	3.55	3.39	3.58	3.63	3.63	3.62	3.67	3.07	3.61
Cr	8.20	8.61	8.89	8.71	8.52	8.65	8.72	8.94	8.29	8.58	8.51	8.61	8.73	8.72	8.80	8.62	8.82	8.64	8.57	8.57	8.57	8.53	8.39	8.50
Fe2	4.14	4.51	4.47	4.47	4.42	4.51	4.39	4.52	4.46	4.15	4.28	4.38	4.43	4.41	4.41	5.37	6.28	5.35	5.32	5.31	5.37	5.29	8.12	5.39
Fe3	2.02	2.27	2.07	2.01	2.03	2.00	2.12	2.09	2.51	1.82	2.09	2.05	2.06	2.12	2.06	3.32	1.65	3.31	3.29	3.30	3.30	3.36	-0.71	3.27
Mn	0.07	0.07	0.07	0.07	0.06	0.07	0.07	0.07	0.07	0.06	0.07	0.07	0.08	0.07	0.07	0.07	0.08	0.08	0.07	0.07	0.08	0.08	0.07	0.08
Ni	0.02	0.02	0.02	0.02	0.01	0.01	0.02	0.02	0.01	0.02	0.02	0.03	0.02	0.02	0.02	0.03	0.03	0.03	0.04	0.03	0.04	0.02	0.02	0.02
Mg	3.87	3.55	3.57	3.58	3.70	3.60	3.65	3.53	3.58	3.86	3.76	3.67	3.62	3.65	3.65	2.78	2.69	2.78	2.82	2.84	2.77	2.83	2.42	2.81
Mg#	0.483	0.440	0.444	0.444	0.456	0.444	0.454	0.439	0.446	0.482	0.468	0.456	0.450	0.453	0.453	0.341	0.300	0.342	0.347	0.349	0.340	0.349	0.229	0.343
Cr/Fe	1.241	1.183	1.267	1.251	1.231	1.237	1.248	1.260	1.108	1.337	1.245	1.246	1.255	1.243	1.266	0.924	1.035	0.929	0.927	0.927	0.920	0.919	1.055	0.914
Cr/Al	1.469	1.782	1.863	1.748	1.684	1.745	1.786	1.906	1.677	1.589	1.664	1.701	1.773	1.788	1.817	2.426	2.605	2.412	2.361	2.361	2.369	2.325	2.736	2.355

Chromite zonation:

RS38

	rim							rim	rim					rim
[wt%]	1	2	3	4	5	6	7	8	1	2	3	4	5	6
TiO2	1.58	1.37	1.24	1.11	1.36	1.46	1.55	1.28	1.52	1.64	1.67	1.65	1.61	1.50
Al2O3	10.98	11.10	11.21	11.41	11.15	10.95	11.13	11.29	10.98	11.08	10.98	10.96	11.04	11.24
Cr2O3	38.63	39.14	39.95	39.58	39.43	39.19	39.16	39.59	38.88	39.15	39.25	39.27	38.62	38.75
FeO(P)	38.80	38.00	37.19	38.13	40.07	39.04	39.52	38.29	39.15	39.09	38.82	39.30	38.91	39.04
FeO(C)	23.88	23.57	23.30	23.44	24.38	23.91	24.11	23.50	23.71	23.88	23.85	24.05	23.83	23.74
Fe2O3	16.58	16.03	15.44	16.33	17.45	16.82	17.12	16.43	17.16	16.91	16.64	16.96	16.76	17.01
MnO	0.33	0.34	0.33	0.34	0.30	0.38	0.30	0.33	0.28	0.38	0.37	0.34	0.34	0.34
NiO	0.19	0.13	0.15	0.17	0.16	0.12	0.11	0.09	0.09	0.12	0.18	0.12	0.10	0.11
MgO	6.68	6.71	6.83	6.81	6.71	6.75	6.92	6.99	7.02	7.00	6.95	6.95	6.84	6.96
Total	97.18	96.78	96.89	97.56	99.18	97.90	98.69	97.86	97.91	98.47	98.23	98.59	97.47	97.96
Total(C)	98.85	98.39	98.44	99.20	100.93	99.58	100.41	99.51	99.63	100.16	99.90	100.29	99.15	99.66
Cations (based on 32 oxygens)									based on 32 oxygen					
Ti	0.33	0.28	0.26	0.23	0.28	0.30	0.31	0.26	0.31	0.33	0.34	0.34	0.33	0.31
Al	3.55	3.60	3.63	3.67	3.53	3.52	3.54	3.61	3.52	3.53	3.51	3.49	3.56	3.60
Cr	8.38	8.51	8.67	8.53	8.38	8.44	8.35	8.50	8.35	8.37	8.41	8.39	8.34	8.32
Fe2	5.48	5.42	5.35	5.34	5.48	5.45	5.44	5.34	5.39	5.40	5.41	5.43	5.44	5.39
Fe3	3.42	3.32	3.19	3.35	3.53	3.45	3.48	3.36	3.51	3.44	3.40	3.45	3.44	3.47
Mn	0.08	0.08	0.08	0.08	0.07	0.09	0.07	0.07	0.06	0.09	0.09	0.08	0.08	0.08
Ni	0.04	0.03	0.03	0.04	0.04	0.03	0.02	0.02	0.02	0.03	0.04	0.03	0.02	0.02
Mg	2.73	2.75	2.79	2.77	2.69	2.74	2.78	2.83	2.84	2.82	2.81	2.80	2.79	2.81
Mg#	0.333	0.337	0.343	0.341	0.329	0.335	0.338	0.346	0.345	0.343	0.342	0.340	0.339	0.343
Cr/Fe	0.876	0.907	0.945	0.914	0.866	0.884	0.872	0.910	0.874	0.882	0.890	0.879	0.874	0.874
Cr/Al	2.359	2.366	2.391	2.326	2.373	2.400	2.359	2.353	2.375	2.371	2.399	2.403	2.346	2.312

Chromite zonation:

RS38

	rim																							rim
[wt%]	1	2	3	4	5	6	7	8	9	10	11	12	13	14	15	16	17	18	19	20	21	22	23	24
TiO2	0.50	0.73	0.69	0.75	1.00	0.99	0.71	0.73	0.63	0.51	0.72	0.72	0.73	0.73	0.76	1.22	5.15	1.13	1.25	1.24	1.24	1.07	12.34	1.51
Al2O3	18.52	15.67	15.56	16.37	16.54	16.25	15.94	15.21	16.09	17.85	16.88	16.63	16.09	15.97	15.73	10.93	10.35	11.07	11.24	11.23	11.19	11.41	9.18	11.20
Cr2O3	40.57	41.64	43.21	42.67	41.52	42.26	42.43	43.19	40.22	42.28	41.86	42.18	42.53	42.58	42.59	39.50	40.20	39.78	39.56	39.51	39.52	39.55	37.43	39.32
FeO(P)	28.77	30.97	30.03	30.02	29.70	30.06	29.93	30.18	31.96	27.83	29.61	29.80	29.83	30.16	29.61	37.65	34.18	37.71	37.57	37.52	37.81	37.89	31.24	37.86
FeO(C)	19.33	20.60	20.54	20.70	20.36	20.81	20.20	20.64	20.43	19.34	19.89	20.28	20.37	20.37	20.18	23.28	27.08	23.28	23.22	23.14	23.42	23.19	34.25	23.57
Fe2O3	10.49	11.53	10.55	10.36	10.38	10.29	10.82	10.60	12.82	9.45	10.81	10.58	10.51	10.89	10.48	15.97	7.89	16.03	15.95	15.97	15.99	16.34	-3.35	15.87
MnO	0.34	0.33	0.33	0.34	0.29	0.33	0.32	0.32	0.33	0.27	0.33	0.31	0.34	0.30	0.30	0.32	0.32	0.34	0.32	0.32	0.34	0.33	0.29	0.35
NiO	0.09	0.08	0.09	0.10	0.06	0.07	0.10	0.12	0.06	0.12	0.12	0.13	0.10	0.09	0.11	0.13	0.11	0.14	0.19	0.13	0.17	0.09	0.10	0.11
MgO	10.15	9.10	9.22	9.29	9.56	9.33	9.43	9.05	9.22	10.10	9.82	9.54	9.35	9.45	9.37	6.74	6.50	6.79	6.91	6.96	6.77	6.96	5.72	6.90
Total(P)	98.94	98.52	99.13	99.55	98.67	99.29	98.87	98.80	98.52	98.97	99.33	99.31	98.97	99.28	98.46	96.49	96.82	96.96	97.04	96.90	97.04	97.32	96.29	97.23
Total(C)	99.99	99.67	100.18	100.59	99.71	100.32	99.95	99.86	99.80	99.91	100.41	100.37	100.03	100.37	99.51	98.09	97.61	98.56	98.64	98.50	98.65	98.96	95.96	98.82
Cations (based on 32 oxygens)																								
Ti	0.10	0.14	0.14	0.14	0.20	0.19	0.14	0.14	0.12	0.10	0.14	0.14	0.14	0.14	0.15	0.25	1.08	0.23	0.26	0.25	0.26	0.22	2.63	0.31
Al	5.58	4.83	4.77	4.98	5.06	4.96	4.88	4.69	4.95	5.40	5.12	5.06	4.93	4.88	4.84	3.55	3.39	3.58	3.63	3.63	3.62	3.67	3.07	3.61
Cr	8.20	8.61	8.89	8.71	8.52	8.65	8.72	8.94	8.29	8.58	8.51	8.61	8.73	8.72	8.80	8.62	8.82	8.64	8.57	8.57	8.57	8.53	8.39	8.50
Fe2	4.14	4.51	4.47	4.47	4.42	4.51	4.39	4.52	4.46	4.15	4.28	4.38	4.43	4.41	4.41	5.37	6.28	5.35	5.32	5.31	5.37	5.29	8.12	5.39
Fe3	2.02	2.27	2.07	2.01	2.03	2.00	2.12	2.09	2.51	1.82	2.09	2.05	2.06	2.12	2.06	3.32	1.65	3.31	3.29	3.30	3.30	3.36	-0.71	3.27
Mn	0.07	0.07	0.07	0.07	0.06	0.07	0.07	0.07	0.07	0.06	0.07	0.07	0.08	0.07	0.07	0.07	0.08	0.08	0.07	0.07	0.08	0.08	0.07	0.08
Ni	0.02	0.02	0.02	0.02	0.01	0.01	0.02	0.02	0.01	0.02	0.02	0.03	0.02	0.02	0.02	0.03	0.03	0.03	0.04	0.03	0.04	0.02	0.02	0.02
Mg	3.87	3.55	3.57	3.58	3.70	3.60	3.65	3.53	3.58	3.86	3.76	3.67	3.62	3.65	3.65	2.78	2.69	2.78	2.82	2.84	2.77	2.83	2.42	2.81
Mg#	0.483	0.440	0.444	0.444	0.456	0.444	0.454	0.439	0.446	0.482	0.468	0.456	0.450	0.453	0.453	0.341	0.300	0.342	0.347	0.349	0.340	0.349	0.229	0.343
Cr/Fe	1.241	1.183	1.267	1.251	1.231	1.237	1.248	1.260	1.108	1.337	1.245	1.246	1.255	1.243	1.266	0.924	1.035	0.929	0.927	0.927	0.920	0.919	1.055	0.914
Cr/Al	1.469	1.782	1.863	1.748	1.684	1.745	1.786	1.906	1.677	1.589	1.664	1.701	1.773	1.788	1.817	2.426	2.605	2.412	2.361	2.361	2.369	2.325	2.736	2.355

Olivine zonation:

IN 844.00																		IN 844.00										
	rim																	rim	rim									rim
[wt%]	1	2	3	4	5	6	7	8	9	10	11	12	13	14	15	16	17	18	1	2	3	4	5	6	7	8	9	10	11
SiO2	39.27	39.11	38.90	38.98	39.04	38.99	38.99	38.77	38.74	38.46	38.38	38.87	38.50	38.59	38.79	39.04	38.62	38.31	38.51	38.89	38.73	38.94	38.75	38.71	38.81	38.89	38.75	38.87	38.65
FeO	19.30	19.27	19.63	19.42	19.46	19.64	19.57	19.50	19.46	19.23	19.48	19.20	19.34	19.32	19.57	19.48	19.42	18.97	19.19	18.93	19.25	19.54	19.34	19.26	19.31	19.25	19.04	19.24	19.01
MnO	0.19	0.22	0.20	0.18	0.20	0.21	0.19	0.17	0.21	0.18	0.18	0.20	0.18	0.16	0.19	0.20	0.19	0.18	0.17	0.25	0.24	0.22	0.22	0.23	0.23	0.22	0.22	0.22	0.20
NiO	0.37	0.38	0.38	0.38	0.42	0.39	0.39	0.36	0.42	0.36	0.33	0.42	0.41	0.38	0.34	0.38	0.42	0.35	0.40	0.37	0.37	0.39	0.37	0.33	0.35	0.32	0.35	0.35	0.37
MgO	41.13	41.48	41.33	41.59	41.47	41.56	41.30	41.14	41.60	40.95	41.78	42.04	42.02	41.96	41.94	42.11	41.31	42.17	41.65	41.39	41.79	41.54	41.62	41.52	41.35	41.54	41.41	41.68	41.76
CaO	0.00	0.00	0.00	0.01	0.00	0.00	0.00	0.00	0.00	0.00	0.00	0.00	0.00	0.00	0.00	0.00	0.00	0.00	0.00	0.00	0.00	0.00	0.00	0.00	0.00	0.00	0.00	0.00	0.00
Total	100.25	100.46	100.43	100.55	100.59	100.79	100.44	99.94	100.43	99.18	100.15	100.73	100.45	100.41	100.83	101.20	99.95	99.97	99.92	99.82	100.37	100.64	100.30	100.05	100.05	100.22	99.77	100.36	99.99
Cations (based on 4 oxygens)																													
Si	1.00	1.00	1.00	1.00	1.00	0.99	1.00	1.00	0.99	1.00	0.99	0.99	0.99	0.99	0.99	0.99	0.99	0.98	0.99	1.00	0.99	0.99	0.99	0.99	1.00	1.00	1.00	0.99	0.99
Fe	0.41	0.41	0.42	0.41	0.42	0.42	0.42	0.42	0.42	0.42	0.42	0.41	0.41	0.41	0.42	0.41	0.42	0.41	0.41	0.41	0.41	0.42	0.41	0.41	0.41	0.41	0.41	0.41	0.41
Mn	0.00	0.00	0.00	0.00	0.00	0.00	0.00	0.00	0.00	0.00	0.00	0.00	0.00	0.00	0.00	0.00	0.00	0.00	0.00	0.01	0.01	0.00	0.00	0.00	0.00	0.00	0.00	0.00	0.00
Ni	0.01	0.01	0.01	0.01	0.01	0.01	0.01	0.01	0.01	0.01	0.01	0.01	0.01	0.01	0.01	0.01	0.01	0.01	0.01	0.01	0.01	0.01	0.01	0.01	0.01	0.01	0.01	0.01	0.01
Mg	1.57	1.58	1.58	1.58	1.58	1.58	1.57	1.58	1.59	1.58	1.60	1.60	1.60	1.60	1.59	1.59	1.58	1.61	1.60	1.58	1.59	1.58	1.59	1.59	1.58	1.59	1.59	1.59	1.60
Ca	0.00	0.00	0.00	0.00	0.00	0.00	0.00	0.00	0.00	0.00	0.00	0.00	0.00	0.00	0.00	0.00	0.00	0.00	0.00	0.00	0.00	0.00	0.00	0.00	0.00	0.00	0.00	0.00	0.00
Total	3.00	3.00	3.00	3.00	3.00	3.01	3.00	3.00	3.01	3.00	3.01	3.01	3.01	3.01	3.01	3.01	3.01	3.02	3.01	3.00	3.01	3.01	3.01	3.01	3.00	3.00	3.00	3.01	3.01
Mg#	0.792	0.793	0.790	0.792	0.792	0.790	0.790	0.790	0.792	0.791	0.793	0.796	0.795	0.795	0.793	0.794	0.791	0.798	0.795	0.796	0.795	0.791	0.793	0.793	0.792	0.794	0.795	0.794	0.797

Olivine zonation:

EK22 296.90											EK22 296.90								EK22 296.90										
	rim									rim	rim								rim	rim									rim
[wt%]	1	2	3	4	5	6	7	8	9	10	1	2	3	4	5	6	7	8	1	2	3	4	5	6	7	8	9	10	11
SiO2	38.81	39.13	38.89	39.05	38.76	38.62	38.95	39.15	38.83	38.99	38.98	38.92	38.96	39.19	38.90	38.72	38.85	38.88	38.66	39.24	39.09	39.05	39.04	39.01	38.94	38.99	38.99	39.36	39.06
FeO	17.97	18.12	18.07	18.28	18.10	18.07	18.44	18.33	18.22	18.56	18.66	18.63	18.80	18.72	18.71	18.58	18.99	18.90	18.49	19.06	18.95	18 95	19.07	18.59	18.92	18.84	18.83	18.72	18.72
MnO	0.20	0.22	0.22	0.21	0.21	0.21	0.23	0.21	0.22	0.20	0.24	0.22	0.23	0.23	0.23	0.21	0.24	0.23	0.22	0.23	0.24	0.22	0.23	0.23	0.24	0.23	0.21	0.23	0.23
NiO	0.33	0.32	0.35	0.32	0.35	0.33	0.34	0.31	0.26	0.36	0.29	0.37	0.37	0.37	0.33	0.34	0.33	0.36	0.34	0.37	0.35	0.35	0.39	0.35	0.33	0.39	0.32	0.40	0.35
MgO	42.46	42.28	42.21	41.75	42.35	42.17	42.14	42.11	42.30	42.12	42.40	42.39	42.68	42.56	42.45	42.46	42.60	42.38	42.30	42.27	42.50	42.51	42.40	42.44	42.51	42.47	42.48	42.42	42.61
CaO	0.00	0.00	0.00	0.00	0.00	0.00	0.00	0.01	0.01	0.00	0.01	0.01	0.02	0.02	0.02	0.03	0.02	0.02	0.02	0.03	0.02	0.02	0.02	0.01	0.02	0.02	0.00	0.01	0.01
Total	99.77	100.07	99.74	99.61	99.78	99.40	100.10	100.11	99.84	100.23	100.57	100.55	101.06	101.08	100.64	100.33	101.03	100.77	100.03	101.21	101.15	101.10	101.15	100.63	100.95	100.93	100.84	101.14	100.98
Cations (based on 4 oxygens)																													
Si	0.99	1.00	1.00	1.00	0.99	0.99	0.99	1.00	0.99	1.00	0.99	0.99	0.99	0.99	0.99	0.99	0.99	0.99	0.99	0.99	0.99	0.99	0.99	0.99	0.99	0.99	0.99	1.00	0.99
Fe	0.38	0.39	0.39	0.39	0.39	0.39	0.39	0.39	0.39	0.40	0.40	0.40	0.40	0.40	0.40	0.40	0.40	0.40	0.40	0.40	0.40	0.40	0.40	0.40	0.40	0.40	0.40	0.40	0.40
Mn	0.00	0.00	0.00	0.00	0.00	0.00	0.00	0.00	0.00	0.00	0.01	0.00	0.00	0.00	0.00	0.00	0.01	0.00	0.00	0.00	0.00	0.00	0.00	0.00	0.01	0.00	0.00	0.00	0.00
Ni	0.01	0.01	0.01	0.01	0.01	0.01	0.01	0.01	0.01	0.01	0.01	0.01	0.01	0.01	0.01	0.01	0.01	0.01	0.01	0.01	0.01	0.01	0.01	0.01	0.01	0.01	0.01	0.01	0.01
Mg	1.62	1.61	1.61	1.59	1.62	1.62	1.60	1.60	1.61	1.60	1.61	1.61	1.61	1.61	1.61	1.62	1.61	1.61	1.61	1.60	1.60	1.61	1.60	1.61	1.61	1.61	1.61	1.60	1.61
Ca	0.00	0.00	0.00	0.00	0.00	0.00	0.00	0.00	0.00	0.00	0.00	0.00	0.00	0.00	0.00	0.00	0.00	0.00	0.00	0.00	0.00	0.00	0.00	0.00	0.00	0.00	0.00	0.00	0.00
Total	3.01	3.00	3.00	3.00	3.01	3.01	3.01	3.00	3.01	3.00	3.01	3.01	3.01	3.01	3.01	3.01	3.01	3.01	3.01	3.01	3.01	3.01	3.01	3.01	3.01	3.01	3.01	3.00	3.01
Mg#	0.808	0.806	0.806	0.803	0.807	0.806	0.803	0.804	0.805	0.802	0.802	0.802	0.802	0.802	0.802	0.803	0.800	0.800 M	0.803	0.798	0.800	0.800	0.798	0.803	0.800	0.801	0.801	0.802	0.802

APPENDIX V

XRF Operating Conditions

All whole-rock analyses were executed at Rhodes University on a Phillips PW 1410 semi-automatic X-ray fluorescence spectrometer. Samples of intersection AE are from Field, (1987) and analyses of intersection UA were made available by W.J. de Klerk. Trace elements Co, Cr, V, Zn, Cu, and Ni in cores $7E^3$ and $60E^3$ were analysed by B. M. Walters in 1981.

Sample preparation methods and analytical techniques are those compiled by Marsh (1979). A number of international and in-house standards were used for calibration:

Major elements: NIM-N, BCR, GSP, AGV, G-2, DTS
Na: PCC, BCR, GSP, AGV, G-2, NIM-G
Zn, Cu, Ni: BCR, BHVO, PCC, DTS, SCO
Sc: NIM-N, BCR, SDC, GSP
Co, Cr, V: BHVO, SDC, S-15
Rb, Sr, Zr, Y, Nb: BCR, AGV, S-12, BHVO, SDC

Major elements, excluding Na, were analysed in duplicate on fusion discs, according to the method of Norrish & Hutton (1969). Trace elements and Na were analysed on 5 g pressed powder tablets. Corrections were made for background and matrix effects, spectral line and tube interferences, instrumental drift and dead time. Data reduction was done on the Rhodes University Cyber Main Frame, using programmes by Marsh (1979). Sample compositions were normalized to 100 wt% L.O.I.-free (including Cr_2O_3 and NiO) and a constant FeO/Fe_2O_3 ratio of 10 has been assumed. Values for L.O.I., H_2O^-, and original totals are tabulated as well. The latter were not obtainable for two samples of core EK22 (analysed by Ellis, 1989), one sample of core UA (analysed by de Klerk, 1991), and all samples of core AE (analysed by Field, 1987). The operating conditions, with the K_α emission line for each element, and the tube being run at 55 kV and 40 mA, are summarized below.

ELEMENT	TUBE	CRYSTAL	TIME	COUNTER	COLLIMATOR
Si	Cr	PET	40	FLOW	COARSE
Ti	Cr	LIF(200)	10	FLOW	FINE
Al	Cr	PET	40	FLOW	COARSE
Fe	Cr	LIF(200)	20	FLOW	FINE
Mn	Cr	LIF(200)	20	FLOW	COARSE
Mg	Cr	TLAP	100	FLOW	FINE
Ca	Cr	LIF(200)	10	FLOW	FINE
Na	Cr	TLAP	100	FLOW	FINE
K	Cr	LIF(200)	10	FLOW	FINE
P	Cr	GE	40	FLOW	COARSE
Sr	W	LIF(220)	200	SCINT	FINE
Rb	W	LIF(220)	200	SCINT	FINE
Zr	W	LIF(220)	200	SCINT	FINE
Y	W	LIF(220)	200	SCINT	FINE
Nb	W	LIF(220)	200	SCINT	FINE
Co	W	LIF(220)	100	FLOW	FINE
Cr	W	LIF(220)	100	FLOW	FINE
V	W	LIF(220)	100	FLOW	FINE
Zn	Mo	LIF(220)	100	FLOW + SCINT	FINE
Cu	Mo	LIF(220)	100	FLOW + SCINT	FINE
Ni	Mo	LIF(220)	100	FLOW + SCINT	FINE
Sc	Cr	LIF(200)	200	FLOW	FINE

The abbreviations and symbols used in the tables are listed in Appendix IV except for H_2O, which represents the loss of atmospheric water after initial heating of the sample to 120°C. MgO and FeO are divided by their molecular weights to calculate the Mg# of whole-rock compositions.

CIPW normative compositions have been calculated for all whole rock samples, using a Rhodes University computer program, based on the method by Kelsey (1965). The abbreviations used are listed below:

Ap = apatite
Cm = chromite
Il = ilmenite
Or = orthoclase
Ab = albite
An = anorthite
C = corundum
Ru = rutile
Mt = magnetite

DiEn = diopside - enstatite
DiFs = diopside - ferrosilite
DiWo = diopside - wollastonite
HyEn = hypersthene - enstatite
HyFs = hypersthene - ferrosilite
Q = quartz
Fo = forsterite
Fa = fayalite
Ne = nepheline

Precision of Trace Element Determination

The precision of trace element determination is a function of two variables (Marsh, 1979):

- sample reproducibility techniques
- X-ray counting statistics

The precision of the analysis is expressed by two parameters:

(1) the counting error
(2) the lower limit of detection

whereby the counting error (c.e.) is:

$$\text{c.e.} = \sqrt{\frac{\frac{R_P}{T_P} - \frac{R_B}{T_B}}{R_P - R_B}} * \text{concentration of element in sample}$$

wherein the upper part of the fraction is the standard deviation of the net peak count rate with

R_P, R_B = count rates at peak and background positions
T_P, T_B = counting times at peak and background positions

Counting errors are large when the counting time is short and when the peak / background ratio is low. Under these circumstances, one has to determine the detection limit (DL). The DL can be calculated if one takes into account that count rates for X-rays behave within Gaussian distribution laws. Hence, the background fluctuation will lie within ± 3 standard deviations of the mean background count rate. A peak must thus have an intensity of the mean background count rate plus 3 standard deviations:

$$\text{Detection limit (DL)} = 3 * \sqrt{\frac{R_B}{T_B}}$$

and in terms of concentration:

$$DL = \frac{3}{M} * \sqrt{\frac{R_B}{T_B}} \qquad \text{where } M = \text{counts / sec / unit concentration}$$

At the detection limit counting errors are large and thus, the lower limit of detection (LLD) is expressed as 2 * DL.

Counting errors and detection limits can be reduced by increasing the ratio of peak / background concentration or by increasing the counting times.

A range of typical counting errors and lower limits of detection for the various trace elements are listed below (from Marsh, 1979). Counting times are 200s at peak positions and 100s at background positions.

Element	Counting error (ppm)	LLD (ppm)	Concentration
Nb	.6	1.6	150 ppm level
Zr	.5	1.4	100 "
Y	.5	1.5	60 "
Sr	.6	1.4	100 "
Rb	.6	1.4	100 "
Zn	.8	1.7	100 "
Cu	1.0	2.4	100 "
Ni	1.3	3.1	100 "
Co	.8	3.0	40 "
Cr	1.3	2.7	350 "
V	.8	2.8	60 "

WHOLE-ROCK XRF-ANALYSES: UA sequence

Sample	642.80	644.00	645.70	646.70	647.70	647.90	649.40	651.30	652.30	652.60	652.90	654.10	654.90	655.50	656.10	661.30	662.70	664.30	665.70	667.20	668.90	669.60	670.20
Rock type	o	o	o	o	o	.	.	.	.	.	o	.	.	-	.	+	-	+	+	+	+	+	+
[wt%]																							
SiO2	48.42	48.99	49.40	49.13	48.65	49.20	49.21	50.06	49.46	49.55	49.28	49.44	51.42	52.72	51.99	54.32	51.81	53.98	53.84	54.85	53.65	53.45	49.67
TiO2	0.05	0.07	0.07	0.08	0.08	0.07	0.06	0.08	0.09	0.09	0.06	0.05	0.08	0.15	0.14	0.27	0.10	0.19	0.22	0.24	0.26	0.13	0.19
Al2O3	31.71	30.05	29.28	30.24	30.56	28.30	28.84	24.80	25.69	25.45	28.86	25.95	19.07	11.11	12.70	4.67	16.44	5.00	4.74	4.09	4.59	6.06	3.95
Fe2O3	0.08	0.15	0.17	0.16	0.11	0.18	0.18	0.30	0.29	0.29	0.18	0.26	0.46	0.71	0.66	0.99	0.62	1.02	1.00	1.04	1.06	0.96	1.28
FeO	0.79	1.52	1.66	1.65	1.11	1.85	1.80	2.95	2.90	2.91	1.81	2.56	4.63	7.08	6.58	9.91	6.21	10.18	10.04	10.40	10.55	9.60	12.84
MnO	0.01	0.03	0.03	0.02	0.02	0.03	0.03	0.06	0.05	0.05	0.03	0.05	0.10	0.15	0.15	0.21	0.12	0.22	0.23	0.22	0.22	0.20	0.22
MgO	0.83	1.87	1.70	1.85	1.64	3.75	3.54	7.21	6.21	6.17	3.30	6.36	12.68	19.96	18.34	24.36	14.46	24.46	24.21	24.20	24.10	24.04	28.05
CaO	15.43	14.77	15.11	14.56	15.19	14.19	13.93	12.35	13.11	13.05	14.00	13.05	9.69	6.53	7.65	3.85	8.87	3.67	4.32	3.66	3.69	4.21	2.55
Na2O	2.51	2.39	2.34	2.10	2.36	2.24	2.19	1.88	1.92	2.26	2.12	2.03	1.43	1.11	1.31	0.66	0.69	0.68	0.77	0.59	0.67	0.54	0.37
K2O	0.16	0.14	0.16	0.16	0.17	0.12	0.14	0.14	0.15	0.15	0.27	0.14	0.17	0.06	0.09	0.15	0.09	0.03	0.04	0.04	0.06	0.02	0.10
P2O5	0.00	0.00	0.06	0.03	0.00	0.00	0.02	0.06	0.03	0.03	0.03	0.00	0.02	0.02	0.00	0.01	0.01	0.04	0.00	0.00	0.07	0.01	0.00
Cr2O3	0.00	0.01	0.01	0.01	0.01	0.05	0.06	0.11	0.09	0.02	0.04	0.10	0.21	0.35	0.34	0.52	0.50	0.46	0.52	0.52	0.94	0.69	0.61
NiO	0.00	0.00	0.00	0.00	0.00	0.01	0.01	0.02	0.02	0.01	0.01	0.02	0.04	0.06	0.06	0.08	0.08	0.08	0.07	0.15	0.15	0.09	0.16
TOTAL	100.00	100.00	100.00	100.00	100.00	100.00	100.00	100.00	100.00	100.00	100.00	100.00	100.00	100.00	100.00	100.00	100.00	100.00	100.00	100.00	100.00	100.00	100.00
Mg#	0.650	0.686	0.646	0.667	0.724	0.784	0.778	0.813	0.793	0.791	0.765	0.816	0.830	0.834	0.832	0.814	0.806	0.811	0.811	0.806	0.803	0.817	0.796
LOI	0.37	0.25	0.45	0.32	0.39	0.41	0.26	0.43	0.39	0.43	0.52	0.43	0.51	0.22	0.54	-0.21		-0.31	-0.12	-0.28	-0.27	0.88	2.60
H2O	0.09	0.09	0.09	0.03	0.07	0.06	5.61	0.05	0.00	0.00	0.00	0.04	0.10	0.04	0.07	0.04		0.02	0.04	0.07	0.05	0.05	0.10
Total	99.19	98.62	99.50	104.53	98.74	98.51	100.20	100.58	99.95	99.98	99.97	97.91	100.56	97.55	98.28	97.29		96.75	97.80	98.07	97.28	100.37	97.26
Trace elements [ppm]																							
Sr	354	458	464	452	454	426	425	368	387	446	429	400	317	178	247	54	67	73	68	58	56	80	43
Rb	1	2	5	5	5	2	0	3	3	4	5	4	4	2	0	6	3	2	3	2	4	0	6
Zr	2	7	9	8	8	8	3	6	9	3	6	4	2	9	8	13	6	7	8	10	9	5	13
Y	0	1	2	1	2	0	2	4	5	2	2	2	1	3	5	6	5	6	10	7	6	4	4
Co	4	9	6	9	7	14	14	25	21	8	12	20	43	59	55	86	82	82	90	88	87	92	122
Cr	19	58	66	75	90	356	379	766	625	144	289	652	1466	2412	2320	3574	3447	3139	3553	3590	6523	4759	4190
V	8	36	19	20	13	22	20	33	32	16	21	26	46	76	72	117	105	102	126	125	142	99	91
Zn	7	13	13	13	10	15	15	23	22	10	15	21	33	53	50	80	79	84	77	164	159	69	88
Cu	12	9	13	10	10	13	15	13	17	12	10	13	28	38	55	29	33	36	33	58	75	23	30
Ni	11	26	29	28	28	75	78	153	148	41	72	135	278	481	455	636	601	603	543	1171	1210	743	1242
Sc	2	8	4	4	3	6	5	9	9	4	6	9	15	23	22	31	33	29	32	32	31	26	22
CIPW-norm [wt%]																							
AP	0.00	0.00	0.14	0.07	0.02	0.00	0.05	0.14	0.07	0.07	0.14	0.00	0.05	0.05	0.00	0.02	0.02	0.09	0.00	0.00	0.17	0.02	0.00
CM	0.00	0.01	0.01	0.01	0.01	0.07	0.09	0.16	0.13	0.03	0.06	0.15	0.31	0.52	0.50	0.77	0.74	0.68	0.77	0.77	1.38	1.02	0.90
IL	0.09	0.13	0.13	0.15	0.15	0.13	0.11	0.15	0.17	0.17	0.11	0.09	0.15	0.28	0.26	0.51	0.19	0.36	0.41	0.45	0.49	0.24	0.36
OR	0.95	0.83	0.95	0.95	1.00	0.71	0.83	0.83	0.89	0.89	1.60	0.83	1.00	0.35	0.53	0.89	0.53	0.18	0.24	0.24	0.35	0.12	0.59
AB	19.96	20.22	19.80	17.77	19.97	18.95	18.53	15.91	16.24	19.12	17.94	17.18	12.10	9.39	11.08	5.58	5.84	5.75	6.51	4.99	5.67	4.57	3.13
AN	74.79	70.86	68.92	72.04	72.57	66.81	68.45	58.82	61.04	58.86	68.44	61.29	45.12	25.16	28.51	9.34	41.50	10.50	9.36	8.39	9.34	14.05	8.82
C	0.00	0.00	0.00	0.21	0.00	0.00	0.00	0.00	0.00	0.00	0.00	0.00	0.00	0.00	0.00	0.00	0.00	0.00	0.00	0.00	0.00	0.00	0.00
MT	0.12	0.22	0.25	0.23	0.16	0.26	0.26	0.43	0.42	0.42	0.26	0.38	0.67	1.03	0.96	1.44	0.90	1.48	1.45	1.51	1.54	1.39	1.86
DIEN	0.43	0.61	1.35	0.00	0.73	1.03	0.15	0.61	1.10	1.64	0.18	1.03	0.85	2.16	2.86	2.88	0.72	2.20	3.57	2.87	2.50	2.02	1.11
DIFS	0.27	0.34	0.91	0.00	0.33	0.35	0.05	0.17	0.36	0.54	0.07	0.29	0.22	0.53	0.71	0.81	0.21	0.64	1.03	0.86	0.75	0.56	0.36
DIWO	0.74	1.01	2.36	0.00	1.14	1.50	0.22	0.86	1.59	2.37	0.26	1.44	1.18	2.97	3.94	4.05	1.02	3.11	5.04	4.08	3.55	2.83	1.60
HYEN	0.00	2.76	2.88	4.61	1.00	5.78	7.55	16.45	11.69	7.53	7.73	10.33	30.11	42.78	34.79	57.01	35.29	56.67	52.80	57.40	56.33	56.01	43.22
HYFS	0.00	1.54	1.94	2.80	0.45	1.96	2.64	4.66	3.77	2.48	2.93	2.90	7.69	10.55	8.69	16.00	10.45	16.46	15.20	17.21	16.84	15.49	13.85
Q	0.00	0.00	0.36	1.16	0.00	0.00	0.00	0.00	0.00	0.00	0.00	0.00	0.00	0.00	0.00	0.00	2.59	0.00	0.00	1.23	0.00	0.00	0.00
FO	1.15	0.90	0.00	0.00	1.65	1.77	0.79	0.63	1.88	4.34	0.22	3.14	0.43	3.34	5.62	0.54	0.00	1.43	2.74	0.00	0.83	1.29	17.88
FA	0.81	0.55	0.00	0.00	0.82	0.66	0.30	0.20	0.67	1.57	0.09	0.97	0.12	0.91	1.55	0.17	0.00	0.46	0.87	0.00	0.27	0.39	6.31
NE	0.69	0.00	0.00	0.00	0.00	0.00	0.00	0.00	0.00	0.00	0.00	0.00	0.00	0.00	0.00	0.00	0.00	0.00	0.00	0.00	0.00	0.00	0.00
TOTAL	100.00	99.98	100.00	100.00	100.00	99.98	100.02	100.02	100.02	100.03	100.03	100.02	100.00	100.02	100.00	100.01	100.00	100.01	99.99	100.00	100.01	100.00	99.99

WHOLE-ROCK XRF-ANALYSES: AE sequence

Sample	26	28	29	30	31	32	32	33	34	35	36	37	38	39	40	41	42	43	44	44	45	46	47	48	48	49	50	51	52	53	54	55	56
Rock type	+	o	o	o	o	o	.	.	.	o	.	.	.	.	*	+	.	o	o	o	o	o	o	o	*	+	+	+	+	+	+	+	+
[wt%]																																	
SiO2	53.53	49.09	49.71	49.76	49.23	49.68	49.79	49.30	51.29	48.92	50.80	50.00	50.74	51.23	44.11	42.54	49.15	48.86	48.83	49.06	49.31	49.00	49.21	47.74	42.80	54.21	53.57	54.87	54.74	53.73	51.46	49.05	54.45
TiO2	0.25	0.09	0.09	0.09	0.08	0.11	0.09	0.07	0.12	0.10	0.10	0.08	0.10	0.14	0.13	0.17	0.09	0.06	0.06	0.07	0.06	0.06	0.06	0.06	0.03	0.16	0.20	0.26	0.27	0.23	0.29	0.20	0.25
Al2O3	5.31	30.41	29.55	29.86	31.03	31.48	28.09	29.36	21.87	30.69	21.58	24.31	18.53	11.67	4.18	5.31	27.87	31.42	31.89	30.35	30.88	29.59	29.68	29.21	5.66	6.23	5.74	5.54	4.89	6.12	6.60	5.10	4.75
Fe2O3	1.04	0.16	0.16	0.18	0.12	0.12	0.20	0.17	0.40	0.12	0.42	0.34	0.59	0.77	1.25	1.32	0.24	0.11	0.09	0.15	0.12	0.15	0.16	0.23	1.37	0.90	0.94	0.94	1.01	0.95	1.08	1.21	1.03
FeO	10.44	1.64	1.61	1.75	1.19	1.16	2.04	1.68	4.03	1.24	4.20	3.36	5.90	7.65	12.45	13.19	2.42	1.11	0.88	1.49	1.15	1.52	1.61	2.26	13.71	9.05	9.39	9.48	10.10	9.49	10.81	12.11	10.28
MnO	0.23	0.03	0.05	0.03	0.03	0.02	0.04	0.03	0.09	0.03	0.09	0.08	0.16	0.16	0.22	0.22	0.06	0.03	0.03	0.04	0.03	0.03	0.04	0.06	0.23	0.20	0.21	0.21	0.22	0.23	0.22	0.24	0.23
MgO	23.47	1.67	2.08	2.27	1.27	1.51	3.95	3.06	9.30	1.53	9.99	7.79	15.56	19.81	32.70	32.50	4.22	1.41	0.95	2.21	1.62	2.66	2.69	4.31	29.89	23.35	23.29	22.63	23.55	22.76	23.89	26.88	22.90
CaO	3.96	14.44	14.33	13.87	14.06	13.99	13.54	14.00	10.89	14.93	10.84	12.16	8.56	6.60	4.03	3.18	13.29	14.63	14.90	14.31	14.49	14.07	14.26	13.94	2.60	4.39	3.65	4.46	3.54	4.75	3.95	3.55	4.48
Na2O	0.80	2.23	2.18	1.97	2.20	1.71	1.96	2.04	1.62	2.16	1.60	1.55	1.33	1.27	0.55	0.59	2.07	2.09	2.08	2.05	2.05	2.03	1.99	1.76	2.31	0.77	2.17	0.78	0.81	0.74	0.59	0.51	0.85
K2O	0.15	0.17	0.17	0.19	0.20	0.19	0.18	0.17	0.16	0.20	0.14	0.13	0.13	0.11	0.11	0.17	0.16	0.15	0.16	0.14	0.15	0.16	0.16	0.19	0.09	0.10	0.26	0.22	0.32	0.14	0.08	0.09	0.11
P2O5	0.05	0.06	0.05	0.02	0.02	0.01	0.06	0.06	0.05	0.08	0.05	0.05	0.05	0.06	0.05	0.05	0.05	0.05	0.05	0.05	0.05	0.05	0.05	0.05	0.02	0.05	0.03	0.05	0.06	0.12	0.05	0.06	0.05
Cr2O3	0.63	0.01	0.01	0.02	0.50	0.02	0.06	0.05	0.15	0.01	0.17	0.12	0.29	0.44	0.23	0.59	0.35	0.09	0.08	0.09	0.09	0.08	0.09	0.17	0.64	0.52	0.48	0.50	0.52	0.66	0.87	0.87	0.54
NiO	0.15	0.00	0.00	0.01	0.07	0.00	0.01	0.01	0.03	0.00	0.03	0.02	0.05	0.10	0.00	0.19	0.04	0.00	0.00	0.01	0.01	0.01	0.01	0.03	0.43	0.07	0.07	0.07	0.07	0.07	0.10	0.14	0.07
TOTAL	100.00	100.00	100.00	100.00	100.00	100.00	100.00	100.00	100.00	100.00	100.00	100.00	100.00	100.00	100.00	100.00	100.00	100.00	100.00	100.00	100.00	100.00	100.00	100.00	100.00	100.00	100.00	100.00	100.00	100.00	100.00	100.00	100.00
Mg#	0.800	0.645	0.697	0.698	0.655	0.699	0.775	0.765	0.804	0.687	0.809	0.805	0.825	0.822	0.824	0.815	0.757	0.694	0.658	0.726	0.715	0.757	0.749	0.773	0.795	0.821	0.816	0.810	0.806	0.810	0.798	0.798	0.799
Trace elements [ppm]																																	
Sr	59	449	444	447	6	452	413	416	315	456	317	346	213	157	60	92	339	450	459	435	443	437	430	445	76	83	79	75	61	74	78	69	66
Rb	6	1	4	4	3	5	4	4	3	2	5	2	4	1	2	5	4	4	3	1	1	3	4	4	0	1	9	9	11	4	2	6	2
Zr	15	7	9	10	10	10	12	7	14	6	10	7	6	8	11	8	8	6	5	6	6	8	10	8	7	6	14	21	27	17	9	11	14
Y	7	5	3	3	4	4	3	3	7	5	5	2	3	6	5	6	2	3	5	4	5	0	1	0	3	4	4	5	6	8	4	2	8
Co	113	11	12	13	91	9	19	14	40	9	42	33	58	81	160	168	25	8	7	12	9	14	14	26	182	90	90	91	93	90	105	126	96
Cr	4357	87	99	114	3429	144	435	324	1050	37	1141	848	1975	3006	1583	4081	2392	597	573	588	600	563	603	1180	4434	3561	3324	3427	3596	4521	6000	6000	3743
V	146	25	23	27	125	16	29	22	48	20	49	35	67	89	58	85	42	17	16	20	19	21	21	22	56	120	129	102	143	138	220	155	145
Zn	93	0	14	14	76	8	19	14	29	9	33	25	45	54	0	58	26	8	7	12	11	13	14	23	84	79	74	75	82	77	95	94	80
Cu	600	0	25	25	33	13	21	13	20	19	21	22	49	130	0	52	65	18	18	19	18	19	23	71	719	37	32	34	34	35	63	42	21
Ni	1151	0	39	40	553	35	81	65	210	33	237	189	369	760	0	1500	279	34	29	55	42	66	63	245	3413	566	550	545	556	573	810	1091	590
Sc	27	0	5	6	27	5	8	7	13	6	12	10	17	18	0	9	0	5	5	6	5	6	6	4	8	24	26	28	29	29	27	21	29
CIPW-norm [wt%]																																	
AP	0.12	0.14	0.12	0.05	0.05	0.02	0.14	0.14	0.12	0.19	0.12	0.12	0.12	0.14	0.12	0.12	0.12	0.12	0.12	0.12	0.12	0.12	0.12	0.12	0.05	0.12	0.07	0.12		0.28	0.12	0.14	0.12
CH	0.00	0.00	0.00	0.00	0.00	0.00	0.00	0.00	0.00	0.00	0.00	0.00	0.00	0.00	0.00	0.00	0.00	0.00	0.00	0.00	0.00	0.00	0.00	0.00	0.00	0.00	0.00	0.00		0.00	0.00	0.00	0.00
IL	0.47	0.17	0.17	0.17	0.15	0.21	0.17	0.13	0.23	0.19	0.19	0.15	0.19	0.26	0.24	0.32	0.17	0.11	0.11	0.13	0.11	0.11	0.11	0.11	0.15	0.30	0.38	0.49		0.43	0.54	0.38	0.47
OR	0.89	1.00	1.00	1.12	1.18	1.12	1.06	1.00	0.95	1.18	0.83	0.77	0.77	0.65	0.65	1.00	0.95	0.89	0.95	0.83	0.89	0.35	0.95	1.12	0.53	0.59	1.54	1.30		0.83	0.47	0.53	0.65
AB	6.85	18.87	18.44	16.67	18.70	14.47	16.58	17.26	13.71	18.28	13.54	13.11	11.25	10.83	4.65	4.99	17.60	17.68	17.60	17.34	17.34	17.18	16.84	14.89	12.05	6.51	18.44	6.60		6.35	5.08	4.40	7.28
AN	10.52	71.25	70.37	68.73	70.02	69.34	66.83	69.11	52.04	73.49	51.40	59.10	38.92	25.94	8.64	11.46	65.65	72.30	73.64	70.72	71.61	69.53	70.47	68.98	4.84	13.36	5.19	11.05		13.06	15.27	11.45	8.86
C	0.00	0.46	0.00	1.23	1.70	3.06	0.20	0.51	0.00	0.00	0.00	0.00	0.00	0.00	0.00	0.00	0.25	1.35	1.34	0.94	1.13	0.74	0.44	0.89	0.00	0.06	0.00	0.00		0.00	0.00	0.00	0.00
NT	1.52	0.23	0.23	0.26	0.17	0.17	0.29	0.25	0.58	0.17	0.61	0.49	0.86	1.12	1.81	1.93	0.35	0.16	0.13	0.22	0.17	0.22	0.23	0.33	2.02	1.32	1.38	1.38		1.39	1.56	1.77	1.51
DIEN	2.61	0.00	0.10	0.00	0.00	0.00	0.00	0.00	0.51	0.02	0.63	0.29	1.04	1.98	3.31	1.21	0.00	0.00	0.00	0.00	0.00	0.00	0.00	0.00	2.45	2.46	3.80	3.21		2.93	1.22	1.73	3.84
DIFS	0.82	0.00	0.05	0.00	0.00	0.00	0.00	0.00	0.16	0.01	0.19	0.09	0.28	0.54	0.90	0.35	0.00	0.00	0.00	0.00	0.00	0.00	0.00	0.00	0.80	0.68	1.08	0.95		0.86	0.39	0.55	1.21
DIWO	3.74	0.00	0.16	0.00	0.00	0.00	0.00	0.00	0.73	0.03	0.90	0.42	1.45	2.76	4.62	1.71	0.00	0.00	0.00	0.00	0.00	0.00	0.00	0.00	3.54	3.44	5.35	4.55		4.14	1.75	2.49	5.51
HYEN	52.35	4.16	5.08	5.65	3.19	3.76	9.84	7.62	22.67	3.79	24.29	19.13	29.72	34.22	10.60	7.58	10.40	3.51	2.37	5.50	4.03	6.62	6.70	7.71	0.00	55.46	34.50	53.47		53.13	48.14	38.07	53.54
HYFS	16.42	2.79	2.72	2.98	2.03	1.89	3.51	2.89	6.91	2.06	7.20	5.84	8.04	9.35	2.87	2.18	4.17	1.91	1.50	2.57	1.97	2.63	2.80	2.85	0.00	15.24	9.84	15.74		15.65	15.30	12.15	16.96
Q	0.00	0.94	1.54	3.17	2.82	5.96	1.39	1.08	1.38	0.62	0.11	0.50	0.00	0.00	0.00	0.00	0.00	1.97	2.25	1.64	2.62	2.41	1.35	0.00	0.00	0.00	0.00	1.17		0.00	0.00	0.00	0.08
FO	2.77	0.00	0.00	0.00	0.00	0.00	0.00	0.00	0.00	0.00	0.00	0.00	5.69	9.40	47.46	51.01	0.11	0.00	0.00	0.00	0.00	0.00	0.00	2.14	51.02	0.41	14.05	0.00		0.74	7.52	19.49	0.00
FA	0.96	0.00	0.00	0.00	0.00	0.00	0.00	0.00	0.00	0.00	0.00	0.00	1.70	2.83	14.15	16.15	0.05	0.00	0.00	0.00	0.00	0.00	0.00	0.87	18.38	0.12	4.41	0.00		0.24	2.63	6.85	0.00
NE	0.00	0.00	0.00	0.00	0.00	0.00	0.00	0.00	0.00	0.00	0.00	0.00	0.00	0.00	0.00	0.00	0.00	0.00	0.00	0.00	0.00	0.00	0.00	0.00	4.20	0.00	0.00	0.00		0.00	0.00	0.00	0.00
TOTAL	100.04	100.01	99.98	100.03	100.01	100.00	100.01	99.99	99.99	100.03	100.01	100.01	100.03	100.02	100.02	100.00	100.02	100.00	100.01	100.01	99.99	99.91	100.01	100.01	100.03	100.01	100.03	100.03		100.03	100.01	100.00	100.03

WHOLE-ROCK XRF-ANALYSES: 7E3 sequence

Sample	393.25	393.75	394.57	395.56	396.50	397.37	398.05	398.67	399.50	400.50	402.30	404.30	406.50
Rock type	.	.	.	+	+	+	o	o	o	o	o	.	.
Trace elements [ppm]													
Sr	329	302	243	96	70	81	112	423	455	435	440	393	417
Rb	2	2	1	4	6	4	8	1	2	2	1	0	1
Zr	8	6	6	20	23	17	33	5	5	5	4	8	8
Y	4	5	5	9	10	8	7	3	3	2	2	3	3
Co	38	44	59	89	98	100	103	14	13	16	12	24	19
Cr	444	601	956	2017	2066	2744	1460	98	70	87	59	295	207
V	50	63	79	125	122	123	172	21	21	23	19	27	23
Zn	34	38	48	75	75	73	81	11	14	13	9	18	14
Cu	95	115	163	305	374	302	579	54	27	28	25	21	24
Ni	291	363	542	955	1135	1063	1554	76	51	71	44	115	91
Sc	12	14	18	30	30	29	26	3	3	5	4	9	6

Sample	432.50	433.50	434.13
Rock type	+	+	*
Trace elements [ppm]			
Sr	50	56	62
Rb	5	6	4
Zr	12	12	11
Y	8	10	8
Co	97	109	119
Cr	9902	57140	2701
V	142	158	78
Zn	83	86	60
Cu	39	45	35
Ni	595	757	1097
Sc	30	13	14

Sample	407.50	408.51	409.25	410.50	412.15	412.15	413.40	414.50	415.50	416.40	417.40	418.45	419.45
Rock type	.	.	o	.	.	.	*	*	*	*	o	o	.
Trace elements [ppm]													
Sr	382	356	463	364	205	282	347	334	46	347	240	274	418
Rb	1	2	3	3	2	2	1	2	6	2	1	1	1
Zr	10	8	2	4	7	7	4	5	10	5	4	3	5
Y	2	3	2	3	4	3	2	2	3	3	3	2	2
Co	25	32	9	28	63	-	144	163	162	185	11	16	14
Cr	338	464	38	379	1280	-	1840	509	635	1201	426	372	347
V	30	38	12	31	67	-	67	48	52	46	17	18	20
Zn	20	21	4	21	46	-	69	85	91	90	10	10	9
Cu	27	24	16	31	44	-	160	58	59	672	50	36	29
Ni	136	187	31	168	404	-	1806	1858	1920	3619	73	113	79
Sc	8	9	1	8	18	-	12	11	13	10	2	3	-

Sample	420.50	421.50	422.50	423.50	424.41	425.08	425.56	426.40	427.50	428.50	429.50	430.50	431.50
Rock type	.	.	.	.	.	.	*	+	+	+	+	+	+
Trace elements [ppm]													
Sr	451	450	73	125	374	417	491	559	525	189	85	51	41
Rb	3	4	0	1	2	6	12	4	14	0	3	3	3
Zr	7	5	3	4	4	3	6	7	15	28	11	9	8
Y	3	2	0	2	2	3	3	4	5	15	9	9	7
Co	14	14	13	15	24	22	126	96	92	93	94	94	96
Cr	374	329	355	342	344	317	548	2866	2701	2586	2688	3003	3119
V	20	18	18	19	19	16	152	141	118	119	125	127	127
Zn	11	9	10	10	10	9	85	77	72	77	75	76	80
Cu	32	25	28	29	29	31	347	52	36	27	30	38	36
Ni	78	64	75	75	73	92	2199	771	674	631	612	605	586
Sc	3	3	3	4	3	2	27	32	28	30	31	30	30

WHOLE-ROCK XRF-ANALYSES: EK22 sequence

Sample	271.75	272.25	280.65	282.80 a	285.80 a	286.20	288.40	288.95 b	291.30	291.40 a	293.60 a	296.90	300.27	300.60 b	303.90	307.66	310.58	313.60 a	315.90
Rock type	o	.	.	.	o	.	.	+	X	.	.	*	o	o	.	+	+	+	.
[wt%]																			
SiO2	49.04	49.93	50.70	52.76	49.01	48.87	49.23	49.54	50.09	48.59	50.01	44.49	49.36	48.00	49.43	53.33	53.68	50.25	48.73
TiO2	0.04	0.09	0.07	0.15	0.03	0.06	0.04	0.19	0.07	0.08	0.07	0.12	0.03	0.10	0.06	0.17	0.31	0.14	0.07
Al2O3	31.35	25.97	23.37	13.17	32.00	27.59	28.68	6.14	20.08	19.12	21.26	3.89	31.44	29.20	27.96	6.57	4.71	5.50	22.00
Fe2O3	0.09	0.29	0.34	0.65	0.08	0.25	0.19	1.03	0.45	0.49	0.41	1.29	0.08	0.13	0.20	0.89	0.96	1.04	0.38
FeO	0.94	2.91	3.42	6.53	0.79	2.55	1.88	10.29	4.54	4.79	4.07	12.86	0.76	1.28	2.01	8.93	9.57	10.44	3.77
MnO	0.00	0.04	0.05	0.14	0.00	0.04	0.02	0.20	0.07	0.10	0.06	0.24	0.06	0.04	0.09	0.22	0.26	0.23	0.12
MgO	1.04	6.00	8.42	17.60	0.76	5.24	3.91	27.54	12.65	12.66	11.58	33.78	0.79	2.65	4.38	24.42	24.05	27.61	9.47
CaO	14.54	12.34	11.26	7.11	14.61	13.06	13.50	3.47	10.02	9.70	10.45	2.61	14.54	15.02	13.42	3.77	4.14	3.46	10.91
Na2O	2.75	2.15	2.06	1.35	2.52	2.01	2.32	0.46	1.63	2.15	1.68	0.35	2.71	2.15	2.20	0.91	0.83	0.55	4.17
K2O	0.20	0.14	0.14	0.17	0.17	0.16	0.13	0.19	0.13	0.13	0.20	0.10	0.22	0.10	0.17	0.20	0.47	0.06	0.11
P2O5	0.00	0.00	0.00	0.00	0.00	0.00	0.00	0.00	0.00	0.00	0.00	0.00	0.00	0.06	0.00	0.00	0.00	0.00	0.00
Cr2O3	0.01	0.10	0.14	0.31	0.03	0.14	0.10	0.82	0.20	0.04	0.18	0.18	0.00	0.04	0.06	0.50	0.96	0.57	0.23
NiO	0.00	0.02	0.02	0.05	0.00	0.03	0.01	0.12	0.04	0.00	0.03	0.21	0.00	0.00	0.01	0.09	0.07	0.13	0.03
TOTAL	100.00	100.00	100.00	100.00	100.00	100.00	100.00	100.00	100.00	100.00	100.00	100.00	100.00	100.00	100.00	100.00	100.00	100.00	100.00
Mg#	0.665	0.786	0.815	0.828	0.633	0.786	0.787	0.827	0.832	0.825	0.835	0.824	0.648	0.787	0.796	0.830	0.817	0.825	0.817
LOI	1.08	1.24	0.61	0.47	0.63	0.60	0.65	1.61	0.29		1.88	2.51	1.07		0.83	0.10	0.19	0.22	0.27
H2O	0.16	0.20	0.19	0.15	0.10	0.14	0.18	0.40	0.22		0.20	0.73	0.18		0.20	0.19	0.18	0.18	0.14
Total	98.40	99.95	99.11	98.91	99.72	98.56	98.76	99.43	99.70		99.10	101.30	100.57		99.59	101.60	99.36	100.25	104.84
Trace elements [ppm]																			
Sr	462	400	329	179	467	585	417	76	282	535	330	61	484	491	405	73	51	61	318
Rb	0	5	7	5	4	6	0	9	3	3	4	5	3	3	4	5	18	4	2
Zr	0	0	1	8	0	0	1	10	2	3	2	4	1	3	3	12	54	2	1
Y	2	7	4	5	0	3	5	5	3	0	0	0	9	0	7	0	4	0	7
CO	10	30	37	71	8	35	21	133	47	10	40	172	6	9	21	102	186	134	43
Cr	60	686	960	2162	179	981	674	5685	1399	257	1249	1234	27	290	431	3417	6640	3894	1581
V	12	38	44	97	10	28	22	117	49	10	45	55	8	12	38	131	298	113	54
ZN	7	21	22	53	4	26	5	84	35	13	32	96	7	10	17	72	78	82	33
Cu	15	23	15	33	8	28	7	22	16	14	18	24	7	11	15	41	37	23	14
NI	23	141	183	431	15	272	101	975	343	64	250	1614	17	59	87	730	552	1060	246
Sc	3	9	10	20	2	6	5	21	12	–	11	14	2	–	5	26	32	24	12
CIPW-norm [wt%]																			
AP	0.00	0.00	0.00	0.00	0.00	0.00	0.00	0.00	0.00	0.00	0.00	0.00	0.00	0.00	0.00	0.00	0.00	0.00	0.00
CM	0.01	0.15	0.21	0.46	0.04	0.21	0.15	1.21	0.29	0.06	0.27	0.27	0.00	0.06	0.09	0.74	1.41	0.84	0.34
IL	0.08	0.17	0.13	0.28	0.06	0.11	0.08	0.36	0.13	0.15	0.13	0.23	0.06	0.19	0.11	0.32	0.58	0.26	0.13
OR	1.18	0.83	0.83	1.00	1.00	0.95	0.77	1.12	0.77	0.77	1.18	0.59	1.30	0.59	1.00	1.24	2.78	0.35	0.65
AB	23.24	18.19	17.43	11.42	21.32	17.01	19.63	3.89	13.79	18.19	14.21	2.96	22.93	18.19	18.61	7.70	7.02	4.65	21.19
AN	72.13	60.80	54.11	29.38	72.48	64.79	66.98	14.13	47.09	42.14	49.88	8.75	72.13	69.73	65.92	13.22	7.74	12.36	40.99
C	0.17	0.00	0.00	0.00	1.11	0.37	0.18	0.00	0.00	0.00	0.00	0.00	0.31	0.00	0.00	0.00	0.00	0.00	0.00
MT	0.13	0.42	0.49	0.94	0.12	0.36	0.28	1.49	0.65	0.71	0.59	1.87	0.12	0.19	0.29	1.29	1.39	1.51	0.55
DIEN	0.00	0.12	0.52	1.78	0.00	0.00	0.00	0.93	0.79	1.79	0.60	1.11	0.00	1.39	0.19	1.66	3.84	1.44	3.91
DIFS	0.00	0.04	0.15	0.46	0.00	0.00	0.00	0.24	0.20	0.48	0.15	0.30	0.00	0.45	0.06	0.42	1.03	0.38	1.09
DIWO	0.00	0.17	0.73	2.46	0.00	0.00	0.00	1.29	1.09	2.50	0.82	1.55	0.00	2.00	0.28	2.29	5.34	2.01	5.48
HYEN	0.00	12.86	18.24	39.04	1.89	9.78	7.13	40.54	21.62	11.38	19.90	18.48	1.50	2.64	8.62	50.41	49.93	42.25	0.00
HYFS	0.00	4.41	5.13	10.06	1.31	3.29	2.34	10.41	5.41	3.04	4.85	5.06	1.06	0.85	2.82	12.87	13.38	11.21	0.00
Q	0.00	0.00	0.00	0.00	0.66	0.00	0.00	0.00	0.00	0.00	0.00	0.00	0.00	0.00	0.00	0.00	0.00	0.00	0.00
FO	1.81	1.37	1.55	2.11	0.00	2.29	1.83	19.00	6.37	12.86	5.84	45.23	0.33	1.80	1.47	6.13	4.29	17.57	13.79
FA	1.22	0.52	0.48	0.60	0.00	0.85	0.66	5.38	1.76	3.78	1.57	13.64	0.25	0.64	0.53	1.72	1.27	5.14	4.23
NE	0.02	0.00	0.00	0.00	0.00	0.00	0.00	0.00	0.00	0.00	0.00	0.00	0.00	0.00	0.00	0.00	0.00	0.00	7.64
TOTAL	99.99	100.05	100.00	99.99	99.99	100.01	100.03	99.99	99.96	97.85	99.99	100.04	99.99	98.72	99.99	100.01	100.00	99.97	99.99

WHOLE-ROCK XRF-ANALYSES: 60E3 sequence

Sample	117.55	118.55	119.66	120.75	121.70	123.30	124.65	125.15	125.70	126.50	127.55	128.25	128.92
Rock type	.	.	.	.	+	o	.	.	.	.	.	o	.
Trace elements [ppm]													
Sr	370	339	329	167	86	415	396	395	380	357	314	454	295
Rb	3	2	0	0	3	1	2	3	1	2	0	6	2
Zr	4	4	3	7	10	4	5	3	6	5	5	2	5
Y	3	3	2	4	7	3	4	2	3	2	3	2	2
Co	20	30	31	78	109	67	60	29	32	29	46	11	43
Cr	209	315	356	1205	29376	200	5398	274	390	379	656	88	869
V	31	38	41	94	151	20	54	27	36	33	34	13	51
Zn	14	27	25	61	94	10	37	26	20	20	30	6	29
Cu	61	75	108	349	754	1603	1058	117	25	28	20	16	32
Ni	151	224	265	869	1739	3215	2061	348	142	161	331	48	258
Sc	0	4	11	24	26	4	6	4	10	9	9	5	14

Sample	129.70	130.60	131.60	132.55	133.76	134.70	136.50	136.80	138.20	139.15	140.51	141.55	142.55
Rock type	.	.	.	.	.	X	X	X	X	X	X	X	X
Trace elements [ppm]													
Sr	365	312	225	232	352	300	258	309	258	289	317	328	318
Rb	1	2	0	1	0	2	1	2	3	0	2	1	0
Zr	4	3	6	7	5	4	8	6	5	6	7	6	6
Y	3	2	5	4	1	2	4	3	3	4	2	2	4
Co	27	40	64	61	56	73	40	42	86	58	45	47	43
Cr	346	637	1347	1330	1071	4649	698	632	670	754	733	1057	775
V	31	45	73	75	61	45	34	46	23	35	33	40	38
Zn	17	31	46	49	41	40	25	30	45	37	29	30	31
Cu	22	27	42	33	93	22	18	26	26	16	20	17	21
Ni	149	248	421	435	598	698	241	250	885	486	331	341	293
Sc	8	12	20	20	16	6	9	15	6	9	10	10	11

Sample	143.45	144.65	145.80	146.65	147.55	148.65	149.60	150.85	152.35	153.50	154.50	155.55	157.70
Rock type	X	X	X	X	X	X	X	X	X	X	X	X	X
Trace elements [ppm]													
Sr	339	315	282	223	305	539	330	311	285	294	306	293	292
Rb	2	2	1	2	3	2	2	1	2	1	1	2	1
Zr	4	6	8	6	3	10	9	4	5	6	4	0	5
Y	4	3	3	2	2	6	4	3	4	3	2	6	3
Co	42	54	67	74	60	56	49	55	59	62	51	53	56
Cr	692	734	812	517	637	681	616	596	794	653	751	750	701
V	34	36	38	24	32	35	40	30	38	37	36	36	35
Zn	26	32	35	44	34	36	34	33	34	36	31	31	32
Cu	18	31	24	22	20	18	23	17	14	20	19	18	42
Ni	330	423	543	710	515	449	389	463	481	525	395	414	503
Sc	11	9	8	7	9	11	9	9	10	9	3	3	3

Sample	158.70	159.80	161.15	162.45	163.60	164.50	165.00	165.53	166.52	167.70	168.90	170.28	171.56
Rock type	X	X	.	o	o	+	.	.	o	o	o	o	+
Trace elements [ppm]													
Sr	271	313	420	470	457	79	143	398	417	392	474	431	178
Rb	2	1	2	2	4	0	1	1	6	11	3	11	1
Zr	3	3	4	4	5	3	4	4	3	3	4	11	22
Y	3	3	2	2	2	0	3	0	2	3	2	4	14
Co	67	60	18	18	12	73	30	32	16	15	20	12	35
Cr	792	817	501	479	590	1662	870	648	410	632	565	498	1334
V	34	30	18	21	17	33	29	20	17	20	18	26	198
Zn	35	32	16	8	11	21	15	13	12	9	15	17	38
Cu	17	25	45	72	32	160	153	120	68	47	79	22	93
Ni	551	514	182	154	104	930	339	371	186	176	214	101	117
Sc	4	2	2	2	3	2	6	4	3	3	3	3	28

Sample	172.70	173.80	175.05	176.52	177.82	178.70	180.80	182.90	183.26	183.40	184.08	185.00	186.80
Rock type	+	+	+	+	+	+	+	*	+	+	+	+	.
Trace elements [ppm]													
Sr	88	54	45	54	55	64	76	62	13	46	15	38	357
Rb	4	4	4	6	7	5	3	1	1	1	1	3	1
Zr	12	9	10	11	11	11	8	8	6	12	4	7	3
Y	8	8	9	10	9	8	6	6	6	6	5	7	3
Co	89	97	99	95	94	97	113	126	276	124	262	141	31
Cr	2562	2813	2568	2998	3116	14605	10744	5160	2955	6109	14480	2620	499
V	165	149	146	145	138	152	117	98	4815	667	4947	279	35
Zn	75	99	93	100	86	86	81	73	603	159	596	101	23
Cu	48	59	42	41	43	47	36	40	44	212	109	18	13
Ni	557	582	553	573	574	625	967	1326	1326	911	1278	1076	169
Sc	32	33	33	34	34	32	26	21	35	36	34	34	10

WHOLE-ROCK XRF-ANALYSES: IN sequence

Sample	806.92	811.78	817.10	817.68	820.55	826.00	837.86	844.00	850.73	858.55	863.12	866.40	869.60	872.50	877.28	880.50	883.14
Rock type	o	.	.	.	o	.	X	X	X	X	X	x	o	+	+	+	.
[wt%]																	
SIO2	49.34	50.11	51.46	52.26	49.35	50.86	50.83	50.09	49.11	49.80	49.35	46.72	49.25	53.44	52.24	53.89	51.12
TIO2	0.08	0.07	0.11	0.12	0.04	0.07	0.08	0.06	0.06	0.07	0.06	0.04	0.05	0.23	0.31	0.18	0.06
AI203	29.40	26.45	15.70	12.78	31.30	21.96	20.72	23.40	21.39	20.24	20.49	27.15	29.51	3.68	3.81	1.73	23.55
Fe203	0.23	0.26	0.58	0.70	0.08	0.39	0.44	0.36	0.45	0.46	0.47	0.34	0.19	1.10	1.12	1.14	0.34
FeO	2.31	2.65	5.80	7.03	0.77	3.88	4.45	3.61	4.47	4.59	4.66	3.44	1.87	10.96	11.21	11.38	3.40
MnO	0.00	0.01	0.11	0.15	0.01	0.08	0.06	0.09	0.26	0.09	0.08	0.06	0.04	0.67	0.22	0.26	0.09
MgO	1.76	5.39	15.72	18.30	0.77	9.67	11.44	8.62	11.72	12.54	12.87	6.88	2.36	24.59	25.05	27.48	7.61
CaO	14.48	12.75	8.74	7.19	15.37	11.09	10.49	11.81	10.54	10.30	10.25	13.16	14.46	4.16	4.32	2.95	11.84
Na2O	2.21	2.05	1.35	1.10	2.28	1.80	1.24	1.80	1.69	1.59	1.44	1.78	2.19	0.39	0.46	0.13	1.69
K2O	0.00	0.15	0.08	0.00	0.01	0.00	0.00	0.00	0.11	0.09	0.09	0.00	0.01	0.00	0.07	0.00	0.00
P2O5	0.00	0.00	0.00	0.00	0.01	0.00	0.00	0.00	0.00	0.00	0.00	0.01	0.02	0.00	0.00	0.00	0.05
Cr203	0.02	0.08	0.28	0.31	0.01	0.17	0.21	0.14	0.17	0.19	0.21	0.33	0.05	0.67	1.09	0.77	0.22
NIO	0.18	0.01	0.05	0.06	0.00	0.03	0.04	0.03	0.04	0.04	0.04	0.07	0.01	0.11	0.10	0.08	0.03
TOTAL	100.00	100.00	100.00	100.00	100.00	100.00	100.00	100.00	100.00	100.00	100.00	100.00	100.00	100.00	100.00	100.00	100.00
Mg#	0.575	0.784	0.829	0.823	0.640	0.816	0.821	0.810	0.824	0.829	0.831	0.781	0.693	0.800	0.799	0.811	0.800
LOI	0.54	0.41	0.26	0.26	0.36	0.33	0.31	0.48	0.44	0.38	0.79	0.51	0.19	-0.22	0.61	0.26	0.24
H20	0.26	0.21	0.18	0.29	0.24	0.30	0.25	0.37	0.17	0.22	0.18	0.35	0.17	0.32	0.28	0.31	0.29
TOTAL	99.72	99.27	100.56	100.02	99.48	100.87	99.45	100.11	99.92	99.31	100.38	100.09	99.87	99.14	99.13	99.99	100.32
Trace elements [ppm]																	
Sr	423	381	222	184	447	320	287	344	297	278	283	383	426	37	35	10	332
Rb	3	4	3	4	2	4	2	2	2	3	2	3	4	5	3	4	2
Zr	0	2	0	0	0	1	0	0	0	0	0	0	3	4	9	3	0
Y	0	3	5	0	49	4	2	4	6	0	0	3	1	5	2	6	6
CO	36	28	55	68	-	41	46	38	15	53	58	46	13	101	108	99	34
Cr	111	564	1933	2125	61	1132	1415	981	1136	1307	1420	2288	314	4639	7440	5279	1515
V	22	0	86	92	12	46	57	39	39	46	40	27	26	200	283	203	41
ZN	18	24	44	63	10	31	35	28	37	36	36	32	13	85	96	79	26
CU	789	16	83	48	9	13	14	12	11	12	13	216	15	163	92	64	17
NI	1433	114	432	445	19	225	289	245	332	315	356	578	50	852	815	603	208
SC	4	8	20	30	1	11	11	9	10	14	12	2	3	35	35	37	10
CIPW-norm [wt%]																	
AP	0.00	0.00	0.00	0.02	0.00	0.00	0.00	0.00	0.00	0.00	0.02	0.05	0.00	0.00	0.00	0.00	0.12
CM	0.03	0.12	0.41	0.46	0.01	0.25	0.31	0.21	0.25	0.28	0.31	0.49	0.07	0.99	1.61	1.13	0.32
IL	0.15	0.13	0.21	0.23	0.08	0.13	0.15	0.11	0.11	0.13	0.11	0.08	0.09	0.43	0.58	0.34	0.11
OR	0.00	0.89	0.47	0.00	0.06	0.00	0.00	0.00	0.65	0.53	0.53	0.00	0.06	0.00	0.41	0.00	0.00
AB	18.70	17.34	11.42	9.31	19.29	15.23	10.49	15.23	14.30	13.45	12.18	15.06	18.53	3.30	3.89	1.10	14.30
AN	70.31	62.53	36.55	29.94	75.15	51.84	50.97	55.77	50.46	47.83	49.18	65.16	70.67	8.29	8.13	4.14	56.68
C	0.00	0.00	0.00	0.00	0.00	0.00	0.00	0.00	0.00	0.00	0.00	0.34	0.00	0.00	0.00	0.00	0.00
MT	0.33	0.38	0.84	1.01	0.12	0.57	0.64	0.52	0.65	0.67	0.68	0.49	0.28	1.59	1.62	1.65	0.49
DIEN	0.32	0.21	2.06	1.70	0.26	0.94	0.32	0.83	0.55	0.99	0.49	0.00	0.27	3.58	3.91	3.11	0.51
DIFS	0.31	0.07	0.53	0.46	0.18	0.26	0.09	0.25	0.15	0.25	0.12	0.00	0.15	1.15	1.18	0.89	0.16
DIWO	0.64	0.30	2.85	2.37	0.46	1.33	0.45	1.18	0.77	1.37	0.67	0.00	0.45	5.16	5.56	4.38	0.73
HYEN	4.06	13.21	31.61	40.69	1.65	22.66	28.17	18.42	16.21	20.47	20.82	4.62	5.60	55.78	50.37	63.10	18.44
HYFS	3.92	4.44	8.11	10.94	1.12	6.35	7.59	5.44	4.53	5.25	5.27	1.60	3.09	17.95	15.18	18.09	5.74
Q	1.24	0.36	0.00	0.00	1.62	0.00	0.82	0.00	0.00	0.00	0.00	0.00	0.72	0.00	0.00	0.00	2.41
FO	0.00	0.00	3.84	2.23	0.00	0.33	0.00	1.55	8.71	6.85	7.53	8.77	0.00	1.31	5.68	1.56	0.00
FA	0.00	0.00	1.08	0.66	0.00	0.10	0.00	0.50	2.68	1.94	2.10	3.34	0.00	0.47	1.89	0.49	0.00
NE	0.00	0.00	0.00	0.00	0.00	0.00	0.00	0.00	0.00	0.00	0.00	0.00	0.00	0.00	0.00	0.00	0.00
TOTAL	100.01	99.98	99.98	100.02	100.00	99.99	100.00	100.01	100.02	100.01	100.01	100.00	99.98	100.00	100.01	99.98	100.01

WHOLE-ROCK XRF-ANALYSES: IN sequence

Sample	787.90	788.80	790.64	797.25	801.00	810.10	818.00	819.30	823.00	827.65	836.00 a	839.00	843.60	847.50	851.90 a	853.95	854.84 b	856.00	859.22
Rock type	-	-	-	-	-	-	-	-	o	-	-	-	o	o	+	+	+	-	-
[wt%]																			
SiO2	52.13	52.38	50.82	47.48	50.12	51.53	50.39	50.94	49.00	49.64	49.53	49.61	48.91	48.61	51.94	51.83	52.55	49.70	48.36
TiO2	0.14	0.17	0.09	0.08	0.07	0.10	0.10	0.08	0.05	0.09	0.08	0.07	0.04	0.04	0.47	0.39	0.31	0.06	0.04
Al2O3	14.28	12.85	22.79	23.98	21.72	18.42	17.54	21.17	31.64	26.29	27.90	27.69	31.71	30.94	5.40	4.21	5.27	25.79	29.27
Fe2O3	0.65	0.69	0.40	0.45	0.42	0.50	0.53	0.41	0.10	0.30	0.23	0.23	0.10	0.15	1.38	1.36	1.14	0.27	0.19
FeO	6.53	6.92	3.96	4.49	4.16	4.98	5.29	4.12	1.05	2.97	2.27	2.27	1.00	1.53	13.79	13.58	11.41	2.69	1.88
MnO	0.16	0.17	0.10	0.07	0.12	0.11	0.08	0.08	0.00	0.05	0.00	0.00	0.00	0.00	0.24	0.27	0.21	0.05	0.01
MgO	16.36	17.69	8.40	9.83	10.46	13.00	15.19	10.32	0.58	5.51	3.83	4.05	0.76	1.18	21.23	22.76	23.16	5.92	4.05
CaO	7.95	7.61	11.41	11.87	11.08	9.57	9.10	10.89	14.86	13.06	13.57	13.78	15.15	15.36	4.12	3.93	4.60	13.14	13.06
Na2O	1.23	1.11	1.81	1.54	1.61	1.48	1.40	1.77	2.51	1.91	2.28	2.19	2.30	2.15	0.73	0.57	0.71	2.19	2.70
K2O	0.00	0.00	0.00	0.01	0.00	0.01	0.13	0.00	0.05	0.00	0.17	0.00	0.00	0.00	0.26	0.11	0.12	0.06	0.37
P2O5	0.00	0.01	0.02	0.00	0.01	0.00	0.00	0.00	0.00	0.02	0.00	0.00	0.00	0.00	0.00	0.13	0.00	0.00	0.00
Cr2O3	0.52	0.34	0.16	0.15	0.18	0.24	0.22	0.20	0.16	0.13	0.13	0.10	0.02	0.02	0.44	0.81	0.46	0.12	0.08
NiO	0.05	0.05	0.03	0.07	0.04	0.04	0.05	0.02	0.00	0.03	0.01	0.01	0.00	0.02	0.06	0.05	0.07	0.01	0.01
TOTAL	100.00	100.00	100.00	100.00	100.00	100.00	100.00	100.00	100.00	100.00	100.00	100.00	100.00	100.00	100.00	100.00	100.00	100.00	100.00
Mg#	0.817	0.820	0.791	0.796	0.817	0.82	0.837	0.817	0.496	0.767	0.751	0.760	0.576	0.579	0.733	0.749	0.783	0.797	0.794
LOI	0.52	0.60	0.72	2.00	0.83	0.57	0.73	0.52	0.71	0.78	0.60	0.60	0.57	0.65	-0.12	-0.36	-0.15	0.39	2.74
H2O	0.17	0.20	0.18	0.24	0.17	0.15	0.43	0.15	0.15	0.16	0.31	0.12	0.12	0.13	0.37	0.12	0.31	0.15	0.27
Total	100.67	100.01	98.96	99.83	99.32	98.59	99.89	99.35	99.53	98.15	98.57	98.28	99.78	98.66	99.99	98.63	99.70	99.40	99.39
Trace elements [ppm]																			
Sr	206	205	343	357	311	258	244	301	459	384	389	388	443	446	69	42	71	395	478
Rb	2	5	3	4	2	3	3	3	1	4	18	3	2	2	10	3	4	1	6
Zr	8	15	8	9	7	8	4	7	4	9	4	5	2	2	19	17	18	5	2
Y	0	5	3	3	2	2	2	3	2	3	0	3	0	3	14	13	8	2	0
Co	108	70	39	52	44	51	61	39	9	29	22	21	9	12	111	206	104	26	18
Cr	3594	2334	1068	1000	1255	1652	1532	1366	1123	917	886	688	121	133	3014	5562	3117	801	542
V	146	92	52	32	45	64	56	45	22	39	33	31	11	19	161	296	143	43	27
Zn	55	61	26	40	192	37	50	29	3	23	21	17	7	10	121	92	93	15	25
Cu	34	43	21	11	14	0	21	33	13	43	34	24	34	80	83	30	34	10	13
Ni	381	429	240	518	307	304	367	190	19	214	109	108	43	132	475	364	566	121	89
Sc	20	21	11	4	9	15	15	11	2	7	6	5	1	4	45	41	36	8	6
CIPW-norm [wt%]																			
AP	0.02	0.02	0.05	0.00	0.02	0.02	0.00	0.00	0.00	0.05	0.00	0.00	0.00	0.00	0.00	0.28	0.00	0.00	0.00
CM	0.77	0.50	0.24	0.22	0.27	0.35	0.32	0.29	0.24	0.19	0.19	0.15	0.03	0.03	0.65	1.19	0.68	0.18	0.12
IL	0.26	0.32	0.17	0.15	0.13	0.19	0.19	0.15	0.09	0.17	0.15	0.13	0.08	0.08	0.88	0.73	0.58	0.11	0.08
OR	0.00	0.00	0.00	0.00	0.00	0.06	0.77	0.00	0.30	0.00	1.00	0.00	0.00	0.00	1.54	0.65	0.71	0.35	2.13
AB	10.41	9.39	15.31	13.03	13.62	12.52	11.85	14.98	21.24	16.16	19.29	18.53	19.46	18.19	6.18	4.82	6.01	18.53	21.85
AN	33.45	30.08	54.06	58.52	52.04	43.59	41.19	49.82	73.72	63.17	65.40	65.73	75.16	74.78	10.69	8.60	10.84	60.37	64.79
C	0.00	0.00	0.00	0.00	0.00	0.00	0.00	0.00	0.44	0.00	0.00	0.00	0.38	0.00	0.00	0.00	0.00	0.00	0.69
MT	0.94	1.00	0.58	0.65	0.61	0.72	0.77	0.59	0.14	0.43	0.33	0.33	0.14	0.22	2.00	1.97	1.65	0.39	0.28
DIEN	1.77	2.27	0.70	0.11	0.85	1.15	1.20	1.25	0.00	0.42	0.53	0.74	0.00	0.31	2.63	2.79	3.43	1.40	0.00
DIFS	0.49	0.62	0.23	0.03	0.24	0.31	0.29	0.35	0.00	0.16	0.21	0.28	0.00	0.27	1.17	1.13	1.17	0.44	0.00
DIWO	2.48	3.18	1.01	0.15	1.20	1.60	1.65	1.76	0.00	0.62	0.80	1.10	0.00	0.60	4.07	4.22	5.00	2.01	0.00
HYEN	38.37	40.31	20.22	10.76	21.72	31.01	26.16	23.34	1.44	13.30	7.81	9.35	1.89	2.63	44.23	48.19	46.91	9.79	0.00
HYFS	10.51	10.96	6.67	3.46	6.10	8.27	6.34	6.46	1.63	4.94	3.07	3.52	1.67	2.36	19.74	19.62	15.96	3.07	0.00
Q	0.00	0.00	0.76	0.00	0.00	0.00	0.00	0.00	0.76	0.39	0.00	0.15	1.17	0.54	0.00	0.00	0.00	0.00	0.00
FO	0.42	1.03	0.00	9.54	2.44	0.15	7.33	0.78	0.00	0.00	0.84	0.00	0.00	0.00	4.21	4.00	5.14	2.48	7.07
FA	0.13	0.31	0.00	3.38	0.75	0.05	1.96	0.24	0.00	0.00	0.36	0.00	0.00	0.00	2.07	1.79	1.93	0.86	2.47
NE	0.00	0.00	0.00	0.00	0.00	0.00	0.00	0.00	0.00	0.00	0.00	0.00	0.00	0.00	0.00	0.00	0.00	0.00	0.54
TOTAL	100.02	99.99	100.00	100.00	99.99	99.99	100.02	100.01	100.00	100.00	99.98	100.01	99.98	100.01	100.06	99.98	100.01	99.98	100.02

WHOLE-ROCK XRF-ANALYSES: LK7 sequence

Sample	1389.70	1401.95	1414.80	1421.10 a	1430.90 a	1441.25 a	1457.35	1464.56	1476.10	1487.00 c	1500.95 a	1511.10 b	1539.10	1552.25 a	1556.56	1562.20	1569.80 a	1577.45	1578.70	1587.50
Rock type	.	.	.	.	.	.	.	.	.	.	.	.	.	o	.	o	.	o	+	.
[wt%]																				
SiO2	50.73	52.47	49.45	49.78	52.88	50.89	51.38	53.19	51.56	51.64	51.33	50.84	50.50	49.63	49.81	50.59	49.31	49.76	54.40	52.89
TiO2	0.08	0.13	0.06	0.05	0.17	0.08	0.10	0.17	0.12	0.12	0.12	0.10	0.10	0.10	0.06	0.13	0.09	0.06	0.25	0.13
Al2O3	23.17	15.75	28.94	27.38	14.33	22.15	20.22	12.45	20.92	19.94	21.45	23.60	24.73	29.52	27.70	28.22	28.56	28.83	6.22	12.85
Fe2O3	0.35	0.58	0.16	0.23	0.67	0.40	0.46	0.74	0.44	0.49	0.44	0.37	0.33	0.17	0.22	0.21	0.22	0.19	1.10	0.68
FeO	3.47	5.81	1.62	2.27	6.73	3.98	4.62	7.45	4.44	4.91	4.43	3.67	3.27	1.74	2.22	2.13	2.23	1.91	10.98	6.84
MnO	0.04	0.10	0.00	0.00	0.09	0.04	0.05	0.11	0.04	0.05	0.04	0.01	0.01	0.00	0.00	0.00	0.01	0.00	0.17	0.09
MgO	8.13	14.46	2.62	4.02	15.11	8.84	10.61	16.68	9.37	10.42	8.85	6.96	5.86	1.65	3.62	1.88	2.82	2.33	20.54	17.26
CaO	11.92	8.35	14.72	13.93	7.94	11.44	10.41	7.44	10.81	10.18	11.02	12.09	12.75	14.58	13.98	14.06	14.22	14.27	4.73	7.45
Na2O	1.81	1.44	2.21	2.12	1.27	1.85	1.80	1.27	1.94	1.85	1.96	2.04	2.09	2.36	2.18	2.45	2.36	2.42	0.91	1.35
K2O	0.14	0.19	0.16	0.13	0.18	0.15	0.14	0.16	0.18	0.20	0.20	0.19	0.24	0.21	0.16	0.29	0.15	0.14	0.20	0.07
P2O5	0.00	0.00	0.01	0.00	0.01	0.01	0.00	0.01	0.00	0.02	0.00	0.00	0.00	0.02	0.00	0.02	0.00	0.00	0.02	0.00
Cr2O3	0.14	0.26	0.04	0.07	0.57	0.15	0.16	0.27	0.14	0.13	0.14	0.10	0.09	0.01	0.04	0.02	0.03	0.03	0.43	0.33
NiO	0.02	0.45	0.01	0.01	0.04	0.02	0.03	0.05	0.03	0.03	0.02	0.02	0.02	0.00	0.01	0.00	0.01	0.01	0.06	0.05
TOTAL	100.00	100.00	100.00	100.00	100.00	100.00	100.00	100.00	100.00	100.00	100.00	100.00	100.00	100.00	100.00	100.00	100.00	100.00	100.00	100.00
Mg#	0.807	0.816	0.743	0.759	0.800	0.799	0.804	0.800	0.790	0.791	0.781	0.772	0.761	0.628	0.744	0.611	0.693	0.685	0.770	0.818
LOI	0.37	0.16	0.09	0.32	0.18	0.20	0.04	-0.18	0.01	-0.03	0.05	0.12	0.26	0.50	0.23	0.19	0.46	0.24	-0.14	-0.21
H2O	0.40	0.32	0.24	0.21	0.31	0.22	0.12	0.25	0.24	0.32	0.31	0.33	0.23	0.33	0.26	0.21	0.16	0.86	0.44	0.34
TOTAL	101.05	100.33	100.24	100.37	100.10	99.86	99.52	99.80	100.34	100.67	100.27	100.16	100.16	99.67	100.06	100.56	99.04	100.24	98.54	99.93
Trace elements [ppm]																				
Sr	334	226	431	407	200	321	285	174	300	284	313	346	361	424	400	426	410	419	82	180
Rb	4	8	2	4	9	5	3	29	7	7	6	5	7	5	3	9	7	2	10	3
Zr	3	13	4	0	14	4	5	16	8	10	10	7	7	12	1	17	1	0	12	1
Y	3	4	5	0	9	5	1	6	0	1	3	4	4	0	2	11	3	9	4	5
Co	38	59	15	23	130	41	47	71	43	24	43	34	31	13	23	17	18	18	102	71
Cr	983	1800	274	483	3917	100	1115	1850	965	906	936	683	586	92	308	118	191	189	2960	2270
V	49	80	21	30	192	50	56	100	59	68	60	48	47	24	30	38	36	25	150	114
Zn	34	47	13	57	52	48	35	58	64	38	35	48	26	34	19	16	22	16	119	52
Cu	13	14	10	8	16	9	11	17	12	12	18	19	19	14	19	18	19	16	43	43
Ni	196	351	50	85	354	200	235	389	211	232	193	150	129	35	81	43	55	47	468	428
Sc	11	18	4	6	23	12	13	23	12	15	13	10	10	4	6	5	8	5	33	23
CIPW-norm [wt%]																				
AP	0.00	0.00	0.02	0.02	0.02	0.02	0.00	0.02	0.00	0.05	0.00	0.00	0.00	0.05	0.00	0.05	0.00	0.00	0.05	0.00
CM	0.21	0.38	0.06	0.10	0.84	0.22	0.24	0.40	0.21	0.19	0.21	0.15	0.13	0.01	0.06	0.03	0.04	0.04	0.63	0.49
IL	0.15	0.24	0.11	0.09	0.32	0.15	0.19	0.32	0.23	0.23	0.23	0.19	0.19	0.19	0.11	0.24	0.17	0.11	0.47	0.24
OR	0.83	1.12	0.95	0.77	1.06	0.89	0.83	0.95	1.06	1.18	1.18	1.12	1.42	1.30	0.95	1.77	0.89	0.83	1.18	0.41
AB	15.31	12.18	18.70	17.94	10.75	15.65	15.23	10.75	16.41	15.65	16.58	17.26	17.68	19.97	18.44	20.73	19.97	20.48	7.70	11.42
AN	54.69	35.95	68.58	64.81	32.87	51.70	46.68	27.80	47.85	45.52	49.14	54.68	57.39	69.31	65.33	65.12	66.90	67.39	12.30	28.80
C	0.00	0.00	0.00	0.00	0.00	0.00	0.00	0.00	0.00	0.00	0.00	0.00	0.00	0.00	0.00	0.00	0.00	0.00	0.00	0.00
MT	0.51	0.84	0.23	0.33	0.97	0.58	0.67	1.07	0.64	0.71	0.64	0.54	0.48	0.25	0.32	0.30	0.32	0.28	1.59	0.99
DIEN	1.31	1.61	1.20	1.18	1.90	1.46	1.46	2.64	1.67	1.40	1.58	1.50	1.64	0.68	1.10	1.03	0.93	0.86	3.11	2.44
DIFS	0.39	0.48	0.50	0.45	0.57	0.45	0.44	0.82	0.54	0.46	0.54	0.54	0.62	0.48	0.46	0.78	0.50	0.48	1.15	0.67
DIWO	1.86	2.28	1.83	1.77	2.70	2.09	2.07	3.78	2.41	2.03	2.31	2.21	2.45	1.21	1.68	1.88	1.52	1.42	4.61	3.41
HYEN	18.93	34.40	5.32	8.83	35.73	20.18	24.16	38.90	21.66	24.54	20.46	15.83	12.95	3.43	7.91	3.65	4.67	4.94	48.04	39.13
HYFS	5.56	10.26	2.23	3.40	10.71	6.26	7.27	12.04	7.06	7.99	7.02	5.70	4.92	2.41	3.32	2.74	2.51	2.76	17.75	10.71
Q	0.26	0.22	0.27	0.30	1.56	0.00	0.00	0.52	0.24	0.03	0.11	0.27	0.11	0.73	0.31	1.69	0.00	0.35	1.43	0.00
FO	0.00	0.00	0.00	0.00	0.00	0.26	0.56	0.00	0.00	0.00	0.00	0.00	0.00	0.00	0.00	0.00	1.00	0.00	0.00	0.99
FA	0.00	0.00	0.00	0.00	0.00	0.09	0.19	0.00	0.00	0.00	0.00	0.00	0.00	0.00	0.00	0.00	0.59	0.00	0.00	0.30
NE	0.00	0.00	0.00	0.00	0.00	0.00	0.00	0.00	0.00	0.00	0.00	0.00	0.00	0.00	0.00	0.00	0.00	0.00	0.00	0.00
TOTAL	100.01	99.96	100.00	99.99	100.00	100.00	99.99	100.01	99.98	99.98	100.00	99.99	99.98	100.02	99.99	100.01	100.01	99.94	100.01	100.00

WHOLE-ROCK XRF-ANALYSES: M3 sequence

Sample	1054.10 b	1062.50	1071.05 a	1078.80	1082.10	1088.65	1089.65	1090.20 a	1110.05	1135.35	1156.45	1175.80	1191.50	1211.85	1219.05	1231.35	1252.08	1256.75	1263.60	1266.28
Rock type	-	-	-	o	o	-	-	-	-	-	-	-	-	-	-	-	-	+	+	-
[wt%]																				
SiO2	49.89	52.54	50.36	48.96	49.18	50.34	52.57	51.82	51.51	51.66	51.83	51.15	50.72	50.66	50.61	49.07	49.49	54.63	54.88	52.35
TiO2	0.07	0.11	0.10	0.04	0.05	0.05	0.12	0.10	0.11	0.11	0.12	0.11	0.10	0.09	0.09	0.04	0.08	0.24	0.30	0.11
Al2O3	27.34	15.26	26.29	31.46	29.71	24.27	15.25	17.52	21.20	20.16	20.30	21.39	24.33	24.98	24.65	30.21	29.36	5.46	3.18	16.52
Fe2O3	0.22	0.61	0.28	0.09	0.16	0.33	0.63	0.55	0.43	0.47	0.46	0.43	0.34	0.30	0.32	0.13	0.17	1.04	1.09	0.59
FeO	2.25	6.12	2.81	0.87	1.57	3.30	6.28	5.52	4.26	4.70	4.63	4.27	3.36	3.04	3.21	1.34	1.74	10.50	11.02	5.87
MnO	0.00	0.07	0.01	0.00	0.00	0.02	0.09	0.08	0.06	0.07	0.05	0.05	0.03	0.03	0.01	0.00	0.00	0.17	0.20	0.08
MgO	4.36	15.34	4.63	0.61	2.21	7.42	14.67	13.28	9.44	10.17	10.04	9.23	6.42	5.88	6.31	1.94	2.03	21.84	23.86	13.68
CaO	13.60	8.23	13.08	15.45	14.73	12.28	8.68	9.25	10.82	10.39	10.44	11.13	12.43	12.65	12.59	14.91	14.62	4.37	3.24	8.92
Na2O	2.05	1.29	2.27	2.34	2.22	1.70	1.31	1.50	1.85	1.85	1.74	1.88	2.04	2.12	1.97	2.19	2.21	0.77	0.54	1.44
K2O	0.13	0.09	0.16	0.15	0.13	0.13	0.10	0.10	0.16	0.22	0.20	0.18	0.16	0.16	0.13	0.13	0.18	0.27	0.32	0.12
P2O5	0.00	0.00	0.00	0.00	0.00	0.00	0.00	0.00	0.00	0.01	0.00	0.01	0.00	0.00	0.00	0.00	0.00	0.00	0.01	0.00
Cr2O3	0.08	0.28	0.08	0.02	0.03	0.13	0.27	0.23	0.15	0.16	0.16	0.15	0.05	0.08	0.09	0.02	0.12	0.68	1.33	0.27
NiO	0.01	0.05	0.01	0.00	0.01	0.02	0.04	0.04	0.03	0.03	0.03	0.03	0.02	0.02	0.02	0.01	0.01	0.10	0.10	0.04
TOTAL	100.00	100.00	100.00	100.00	100.00	100.00	100.00	100.00	100.00	100.00	100.00	100.00	100.00	100.00	100.00	100.00	100.00	100.00	100.00	100.00
Mg#	0.776	0.817	0.746	0.558	0.715	0.800	0.806	0.811	0.798	0.794	0.794	0.794	0.773	0.775	0.778	0.721	0.676	0.787	0.794	0.806
LOI	0.40	0.03	0.29	0.29	0.36	0.77	0.18	0.39	0.03	0.07	0.35	0.19	0.25	0.29	0.57	0.12	0.29	0.08	-0.45	-0.30
H2O	0.35	0.24	0.37	0.41	0.31	0.37	0.23	0.24	0.22	0.28	0.30	0.22	0.21	0.25	0.22	0.26	0.24	0.30	0.22	0.38
Total	100.34	100.05	100.03	101.01	100.65	98.65	99.53	100.58	100.11	99.80	100.13	99.82	100.17	99.70	99.70	99.64	98.89	97.97	98.77	100.24
Trace elements [ppm]																				
Sr	402	218	387	469	435	342	217	245	304	284	291	308	357	370	357	433	429	71	22	235
Rb	4	1	3	4	2	1	3	2	5	5	6	5	4	4	3	3	2	11	16	3
Zr	4	4	10	3	2	0	0	0	4	7	8	7	6	5	3	0	4	22	48	1
Y	6	2	9	2	5	2	6	3	4	5	1	2	2	2	5	0	2	7	12	57
Co	24	62	27	7	14	35	63	57	44	48	48	42	33	30	32	14	16	97	105	60
Cr	523	1920	562	119	237	917	1852	1606	1014	1083	1082	1001	315	577	648	173	793	4643	9095	1876
V	30	82	41	13	20	39	89	75	58	60	64	57	47	39	41	16	30	156	225	86
Zn	19	47	21	9	10	22	48	44	30	35	36	58	27	26	28	11	13	85	94	46
Cu	12	16	15	10	13	8	14	14	13	13	13	15	16	14	18	13	17	33	34	18
Ni	103	376	98	17	47	161	342	305	207	235	234	214	146	131	141	45	46	597	600	332
Sc	5	19	8	2	3	9	19	17	12	14	15	12	10	8	9	3	4	32	36	18
CIPW-norm [wt%]																				
AP	0.00	0.00	0.02	0.00	0.00	0.00	0.00	0.00	0.00	0.02	0.02	0.02	0.02	0.00	0.00	0.00	0.00	0.00	0.05	0.00
CM	0.12	0.41	0.12	0.03	0.04	0.19	0.40	0.34	0.22	0.24	0.24	0.22	0.07	0.12	0.13	0.03	0.18	3.95	0.48	0.40
IL	0.13	0.21	0.19	0.08	0.09	0.09	0.23	0.19	0.21	0.21	0.23	0.21	0.19	0.17	0.17	0.08	0.15	0.45	0.56	0.21
OR	0.77	0.53	0.95	0.89	0.77	0.77	0.59	0.59	0.95	1.30	1.18	1.06	0.95	0.95	0.77	0.77	1.06	0.59	0.00	0.71
AB	17.34	10.91	19.21	19.80	18.78	14.38	11.08	12.69	15.65	15.65	14.72	15.91	17.26	17.94	16.67	18.53	18.70	6.51	4.57	12.18
AN	65.02	35.58	61.08	74.90	70.72	58.21	35.44	40.78	49.07	46.06	46.99	49.40	56.76	58.18	58.04	72.22	69.66	11.04	6.20	38.26
C	0.00	0.00	0.00	0.00	0.00	0.00	0.00	0.00	0.00	0.00	0.00	0.00	0.00	0.00	0.00	0.00	0.00	0.00	0.00	0.00
MT	0.32	0.88	0.41	0.13	0.23	0.48	0.91	0.80	0.62	0.68	0.67	0.62	0.49	0.43	0.46	0.19	0.25	1.51	1.58	0.86
DIEN	0.70	1.56	1.03	0.37	0.62	0.79	2.25	1.51	1.34	1.57	1.38	1.67	1.37	1.30	1.26	0.46	0.72	3.05	2.76	1.76
DIFS	0.24	0.43	0.42	0.35	0.30	0.24	0.67	0.44	0.42	0.50	0.44	0.53	0.49	0.46	0.44	0.22	0.41	0.97	0.94	0.52
DIWO	1.02	2.19	1.57	0.73	0.98	1.13	3.18	2.13	1.92	2.26	1.98	2.40	2.02	1.91	1.85	0.73	1.20	4.38	4.03	2.50
HYEN	10.16	36.64	10.50	1.15	4.88	17.69	34.29	31.17	22.16	23.75	23.63	20.92	14.62	13.34	14.45	4.37	4.33	50.94	56.21	32.30
HYFS	3.54	10.10	4.31	1.09	2.36	5.42	10.16	8.99	6.91	7.61	7.50	6.67	5.28	4.75	5.02	2.07	2.43	16.25	19.18	9.58
Q	0.63	0.53	0.30	0.48	0.21	0.59	0.82	0.00	0.54	0.14	1.05	0.00	0.48	0.46	0.74	0.33	0.92	2.17	2.11	0.71
FO	0.00	0.00	0.00	0.00	0.00	0.00	0.00	0.27	0.00	0.00	0.00	0.27	0.00	0.00	0.00	0.00	0.00	0.00	0.00	0.00
FA	0.00	0.00	0.00	0.00	0.00	0.00	0.00	0.09	0.00	0.00	0.00	0.10	0.00	0.00	0.00	0.00	0.00	0.00	0.00	0.00
NE	0.00	0.00	0.00	0.00	0.00	0.00	0.00	0.00	0.00	0.00	0.00	0.00	0.00	0.00	0.00	0.00	0.00	0.00	0.00	0.00
TOTAL	99.99	99.97	100.11	100.00	99.98	99.98	100.02	99.99	100.01	99.99	100.03	100.00	100.00	100.01	100.00	100.00	100.01	101.81	98.67	99.99

WHOLE-ROCK XRF-ANALYSES: KR2 sequence

Sample	1146.85	1155.45	1160.40	1168.55	1174.10	1181.20	1185.90 a	1191.20	1192.10 a	1194.20	1203.75	1219.75	1227.15	1236.20	1251.90	1260.30	1287.25	1289.65	1297.40	1300.90
Rock type	o	.	.	o	.	.	.	.	+	.	.	.	.	.	.	.	.	+	+	.
[wt%]																				
SiO2	49.52	51.84	50.05	50.04	50.04	50.83	49.91	50.26	52.54	49.93	50.59	51.21	51.55	50.75	48.33	51.14	50.94	54.07	50.12	51.87
TiO2	0.05	0.12	0.05	0.09	0.06	0.15	0.06	0.06	0.12	0.06	0.08	0.11	0.13	0.09	0.10	0.12	0.11	0.21	0.32	0.14
Al2O3	31.44	13.89	26.14	27.77	27.68	20.64	26.72	22.22	11.14	25.54	24.97	21.61	19.79	24.17	23.28	22.79	21.19	5.50	4.58	13.70
Fe2O3	0.10	0.63	0.25	0.24	0.21	0.52	0.26	0.39	0.76	0.28	0.30	0.40	0.48	0.32	0.50	0.40	0.42	1.02	1.12	0.68
FeO	0.97	6.33	2.51	2.38	2.09	5.18	2.62	3.91	7.60	2.78	3.04	3.97	4.75	3.20	4.95	4.01	4.23	10.20	11.23	6.79
MnO	0.05	0.18	0.08	0.06	0.06	0.13	0.08	0.12	0.19	0.08	0.10	0.12	0.15	0.11	0.17	0.13	0.13	0.26	0.29	0.19
MgO	0.96	17.66	6.07	3.28	4.11	10.91	5.13	10.00	20.11	6.53	6.55	9.68	10.88	7.10	11.72	9.35	9.92	23.42	24.31	17.27
CaO	13.56	7.73	12.61	13.60	13.35	10.08	12.90	10.99	6.27	12.54	12.26	10.74	10.22	11.78	8.90	10.50	10.54	4.14	3.50	7.36
Na2O	3.06	1.18	2.01	2.33	2.20	1.42	2.10	1.77	0.82	2.03	1.81	1.84	1.78	2.17	1.83	1.30	2.07	0.58	0.58	1.45
K2O	0.28	0.07	0.10	0.15	0.12	0.08	0.12	0.09	0.05	0.12	0.17	0.14	0.11	0.18	0.06	0.09	0.14	0.07	0.06	0.10
P2O5	0.00	0.00	0.00	0.00	0.00	0.00	0.00	0.00	0.00	0.00	0.00	0.00	0.00	0.00	0.00	0.00	0.00	0.00	0.00	0.00
Cr2O3	0.01	0.32	0.11	0.05	0.07	0.04	0.08	0.17	0.35	0.10	0.10	0.14	0.12	0.10	0.14	0.15	0.29	0.47	3.81	0.39
NiO	0.00	0.05	0.02	0.01	0.01	0.03	0.01	0.02	0.05	0.02	0.02	0.03	0.02	0.02	0.03	0.03	0.02	0.06	0.08	0.05
Total	100.00	100.00	100.00	100.00	100.00	100.00	100.00	100.00	100.00	100.00	100.00	100.00	100.00	100.00	100.00	100.00	100.00	100.00	100.00	100.00
Mg#	0.637	0.833	0.812	0.711	0.778	0.790	0.777	0.820	0.825	0.807	0.794	0.813	0.803	0.798	0.808	0.806	0.807	0.804	0.794	0.819
LOI	1.32	1.08	1.22	0.86	0.63	2.46	0.93	0.74	1.43	0.97	1.44	0.93	0.85	1.16	0.89	4.13	5.53	0.99	-0.50	0.11
H2O	0.35	0.33	0.30	0.27	0.23	0.61	0.31	0.33	0.30	0.27	0.36	0.37	0.37	0.38	0.31	0.84	0.57	0.41	0.24	0.28
Total	99.51	99.34	99.94	98.85	100.48	100.44	99.75	99.04	101.61	99.80	99.37	101.49	101.11	99.48	102.62	99.96	98.09	101.56	100.27	99.91
Trace elements [ppm]																				
Sr	501	228	398	410	413	276	395	321	147	387	361	314	332	427	335	301	267	64	39	202
Rb	8	2	2	4	3	2	4	3	2	4	3	3	3	5	4	3	2	5	5	3
Zr	3	2	2	7	4	8	1	0	2	0	1	6	6	0	2	5	0	11	8	4
Y	0	1	0	0	3	7	1	4	2	3	4	8	4	0	1	3	3	12	3	0
Co	9	66	28	22	22	49	26	43	82	33	33	43	38	33	44	44	43	102	107	74
Cr	44	2198	758	355	451	2697	558	1132	2364	708	692	968	845	668	970	1052	1991	3192	26039	2342
V	17	90	32	39	26	82	33	49	110	36	43	55	53	40	56	57	71	152	374	91
Zn	8	52	21	22	16	45	22	31	67	22	24	34	32	23	34	31	32	85	119	53
Cu	8	17	10	12	12	11	9	10	7	8	10	12	10	11	14	9	18	32	35	14
Ni	20	378	127	59	83	218	103	197	426	136	136	202	186	145	210	201	181	500	603	395
Sc	5	21	8	7	7	16	8	17	26	9	9	14	12	10	12	11	44	52	30	22
CIPW-norm [wt%]																				
AP	0.00	0.00	0.00	0.00	0.00	0.00	0.00	0.00	0.00	0.00	0.00	0.00	0.00	0.00	0.00	0.00	0.00	0.00	0.00	0.00
CM	0.01	0.47	0.16	0.07	0.10	0.06	0.12	0.25	0.52	0.15	0.15	0.21	0.18	0.15	0.21	0.22	0.43	0.69	5.61	0.57
IL	0.09	0.23	0.09	0.17	0.11	0.28	0.11	0.11	0.23	0.11	0.15	0.21	0.24	0.17	0.19	0.23	0.21	0.39	0.60	0.26
OR	1.65	0.41	0.59	0.89	0.71	0.47	0.71	0.53	0.30	0.71	1.00	0.83	0.06	1.06	0.35	0.53	0.83	0.41	0.35	0.06
AB	25.89	9.98	17.01	19.71	18.61	12.01	17.77	14.98	6.94	17.18	15.31	15.57	15.06	18.36	15.48	11.00	17.51	4.91	4.91	12.27
AN	67.27	32.40	62.01	64.88	65.30	49.71	63.13	52.42	26.57	60.23	59.51	50.30	45.98	55.68	44.15	52.09	48.12	12.20	9.72	30.85
C	1.45	0.00	0.00	0.00	0.00	0.00	0.00	0.00	0.00	0.00	0.00	0.00	0.00	0.00	4.02	1.46	0.00	0.00	0.00	0.00
MT	0.14	0.91	0.36	0.35	0.30	0.75	0.38	0.57	1.10	0.41	0.43	0.58	0.70	0.46	0.72	0.58	0.61	1.48	1.62	0.99
DIEN	0.00	1.80	0.16	0.68	0.26	0.09	0.25	0.63	1.36	0.58	0.38	0.88	1.38	0.80	0.00	0.00	1.23	2.44	2.28	1.69
DIFS	0.00	0.45	0.05	0.34	0.09	0.03	0.09	0.17	0.36	0.17	0.12	0.25	0.42	0.25	0.00	0.00	0.36	0.74	0.62	0.46
DIWO	0.00	2.48	0.23	1.08	0.39	0.12	0.36	0.88	1.89	0.83	0.55	1.25	1.97	1.15	0.00	0.00	1.74	3.48	3.19	2.37
HYEN	1.06	36.78	14.95	7.49	9.97	27.08	12.53	20.11	46.24	13.69	15.93	23.22	25.71	15.94	20.83	23.28	19.61	55.88	49.68	35.08
HYFS	0.75	9.24	4.36	3.77	3.54	9.07	4.51	5.55	12.25	4.10	5.22	6.68	7.90	5.07	6.25	7.00	5.77	16.99	13.58	9.61
Q	0.00	0.00	0.02	0.57	0.60	0.32	0.04	0.00	0.00	0.00	1.23	0.02	0.27	0.00	0.00	3.61	0.00	0.38	0.00	0.00
FO	0.93	3.79	0.00	0.00	0.00	0.00	0.00	2.92	1.74	1.40	0.00	0.00	0.00	0.66	5.86	0.00	2.71	0.00	6.01	4.37
FA	0.73	1.05	0.00	0.00	0.00	0.00	0.00	0.89	0.51	0.46	0.00	0.00	0.00	0.23	1.94	0.00	0.88	0.00	1.81	1.32
NE	0.00	0.00	0.00	0.00	0.00	0.00	0.00	0.00	0.00	0.00	0.00	0.00	0.00	0.00	0.00	0.00	0.00	0.00	0.00	0.00
TOTAL	99.97	99.99	99.99	100.00	99.98	99.99	100.00	100.01	100.01	100.02	99.98	100.00	99.87	99.98	100.00	100.00	100.01	99.99	99.98	99.90